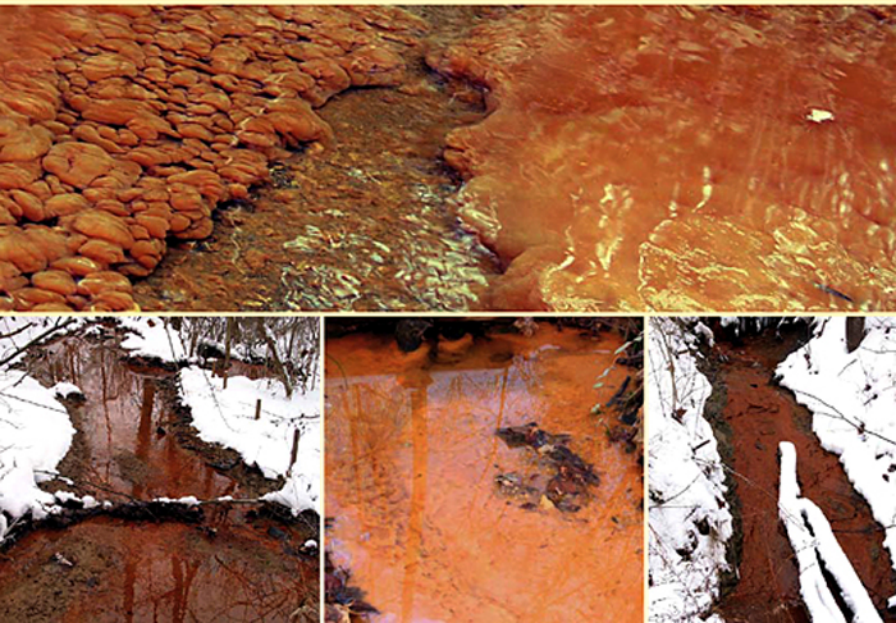
ELSEVIER

ATLASES IN GEOSCIENCE 2

ATLAS OF MICROBIAL MAT FEATURES PRESERVED WITHIN THE SILICICLASTIC ROCK RECORD

Edited by J. SCHIEBER, P.K. BOSE, P.G. ERIKSSON, S. BANERJEE, S. SARKAR, W. ALTERMANN, O. CATUNEANU



ATLASES IN GEOSCIENCE, 2

Atlas of Microbial Mat Features Preserved within the Siliciclastic Rock Record

This page intentionally left blank

ATLASES IN GEOSCIENCE, 2

Atlas of Microbial Mat Features Preserved within the Siliciclastic Rock Record

Edited by Juergen Schieber, Pradip K. Bose, Patrick G. Eriksson, Santanu Banerjee, Subir Sarkar, Wladyslaw Altermann and Octavian Catuneanu



ELSEVIER

Amsterdam – Boston – Heidelberg – London – New York – Oxford – Paris
San Diego – San Francisco – Singapore – Sydney – Tokyo

Elsevier
Radarweg 29, PO Box 211, 1000 AE Amsterdam, The Netherlands
Linacre House, Jordan Hill, Oxford OX2 8DP, UK

First edition 2007

Copyright © 2007 Elsevier B.V. All rights reserved

No part of this publication may be reproduced, stored in a retrieval system or transmitted in any form or by any means electronic, mechanical, photocopying, recording or otherwise without the prior written permission of the publisher

Permissions may be sought directly from Elsevier's Science & Technology Rights Department in Oxford, UK: phone (+44) (0) 1865 843830; fax (+44) (0) 1865 853333; email: permissions@elsevier.com. Alternatively you can submit your request online by visiting the Elsevier web site at http://elsevier.com/locate/permissions, and selecting *Obtaining permission to use Elsevier material*

Notice
No responsibility is assumed by the publisher for any injury and/or damage to persons or property as a matter of products liability, negligence or otherwise, or from any use or operation of any methods, products, instructions or ideas contained in the material herein. Because of rapid advances in the medical sciences, in particular, independent verification of diagnoses and drug dosages should be made

Library of Congress Cataloging-in-Publication Data
A catalog record for this book is available from the Library of Congress

British Library Cataloguing in Publication Data
A catalogue record for this book is available from the British Library

ISBN: 978-0-444-52859-9
ISSN: 1574-1966

For information on all Elsevier publications
visit our website at books.elsevier.com

Printed and bound in Italy

07 08 09 10 11 10 9 8 7 6 5 4 3 2 1

Working together to grow
libraries in developing countries
www.elsevier.com | www.bookaid.org | www.sabre.org
ELSEVIER BOOK AID International Sabre Foundation

List of Editors

N.B. Note that the *order* of the editors for the book is as follows (the list below is alphabetically arranged for convenience): Juergen Schieber, Pradip K. Bose, Patrick G. Eriksson, Santanu Banerjee, Subir Sarkar, Wladyslaw Altermann and Octavian Catuneanu.

Wladyslaw Altermann, Department of Earth and Environmental Sciences, Geology and GeoBioCenter^{LMU}, Ludwig-Maximilians-University Munich, Luisenstrasse 37, D-80333 Munich, Germany; tel.: +49 089 21806552; fax: +49 089 21806514; e-mail: wlady.altermann@iaag.geo.uni-muenchen.de

Santanu Banerjee, Department of Earth Sciences, IIT Bombay, Powai, Mumbai-400076, India; tel.: +91 22 25768282; fax: +91 22 25767253; e-mail: santanu@iitb.ac.in

Pradip K. Bose, Department of Geological Sciences, Jadavpur University, Kolkata-700032, India; tel.: +91 33 24146366; fax: +91 33 24146781; e-mail: jugeopkb@vsnl.net

Octavian Catuneanu, Department of Earth and Atmospheric Sciences, University of Alberta, 1-26 Earth Sciences Building, Edmonton, Alberta, Canada T6G 2E3; tel.: +1 780 4926569; fax: +1 780 4927598; e-mail: octavian@ualberta.ca

Patrick G. Eriksson, Department of Geology, University of Pretoria, Pretoria 0002, South Africa; tel.: +27 12 4202238; fax: +27 12 3625219; e-mail: pat.eriksson@up.ac.za

Subir Sarkar, Department of Geological Sciences, Jadavpur University, Kolkata-700032, India; tel.: +91 33 24146366; fax: +91 33 24146781; e-mail: ssarkar@geology.jdvu.ac.in

Juergen Schieber, Department of Geological Sciences, Indiana University, Bloomington, IN 47405, USA; tel.: +1 812 8564740 (lab), +1 812 8555322 (office); fax: +1 812 8557899; e-mail: jschiebe@indiana.edu

This page intentionally left blank

List of Authors

Wladyslaw Altermann, Department of Earth and Environmental Sciences, Geology and GeoBioCenter^{LMU}, Ludwig-Maximilians-University Munich, Luisenstrasse 37, D-80333 Munich, Germany; tel.: +49 089 21806552; fax: +49 089 21806514; e-mail: wlady.altermann@iaag.geo.uni-muenchen.de

Santanu Banerjee, Department of Earth Sciences, IIT Bombay, Powai, Mumbai-400076, India; tel.: +91 22 25768282; fax: +91 22 25767253; e-mail: santanu@iitb.ac.in

Kevin M. Bohacs, ExxonMobil Upstream Research Company, 3120 Buffalo Speedway, Houston, TX 77096, USA; tel.: +1 713 4317799; fax: +1 713 4316310; e-mail: kevin.m.bohacs@exxonmobil.com

El Hafid Bouougri, Department of Geology, Faculty of Sciences Semlalia, Cadi-Ayyad University, P.O. Box 2390, Marrakech 40000, Morocco; tel.: +212 24 434649; fax: +212 24 437411; e-mail: bouougri@ucam.ac.ma

Pradip K. Bose, Department of Geological Sciences, Jadavpur University, Kolkata-700032, India; tel.: +91 33 24146366; fax: +91 33 24146781; e-mail: jugeopkb@vsnl.net

David J. Bottjer, Department of Earth Sciences, University of Southern California, 3651 Trousdale Parkway, Los Angeles, CA 90089-0740, USA; tel.: +1 213 7406100; e-mail: dbottjer@usc.edu

Adam J. Bumby, Department of Geology, University of Pretoria, Pretoria 0002, South Africa; tel.: +27 12 4203316; fax: +27 12 3625219; e-mail: adam.bumby@up.ac.za

Octavian Catuneanu, Department of Earth and Atmospheric Sciences, University of Alberta, 1-26 Earth Sciences Building, Edmonton, Alberta, Canada T6G 2E3; tel.: +1 780 4926569; fax: +1 780 4927598; e-mail: octavian@ualberta.ca

Snehasis Chakraborty, Department of Geological Sciences, Jadavpur University, Kolkata-700032, India; tel.: +91 33 24146366; fax: +91 33 24146781

Asru K. Chaudhuri, Department of Geological Sciences, Indian Statistical Institute, Kolkata-700108, India; fax: +91 33 25773026; e-mail: asru41@rediffmail.com

Jeffrey R. Chiarenzelli, Department of Geology, St. Lawrence University, 147 Brown Hall, Canton, NY 13617, USA; tel.: +1 315 2295202; fax: +1 315 2295804; e-mail: jchiarenzelli@stlawu.edu

John Allan Donaldson, Ottawa–Carleton Geoscience Centre, Carleton University, Colonel By Drive, Ottawa, ON K1S 5B6, Canada; tel.: +1 613 2256427; e-mail: donaldson6427@rogers.com

Stephen Q. Dornbos, Department of Geosciences, Lapham Hall, University of Wisconsin–Milwaukee, P.O. Box 413, Milwaukee, WI 53201, USA; tel.: +1 414 2296630; fax: +1 414 2295452; e-mail: sdornbos@uwm.edu

Patrick G. Eriksson, Department of Geology, University of Pretoria, Pretoria 0002, South Africa; tel.: +27 12 4202238; fax: +27 12 3625219; e-mail: pat.eriksson@up.ac.za

Gisela Gerdes, Senckenberg Research Institute, Department of Marine Science, postal address: Research Centre Terramare, Schleusenstrasse 1, D-26382 Wilhelmshaven, Germany; tel.: +49 4421 944188; fax: +49 4421 944299; e-mail: ggerdes@icbm.terramare.de

J. Ghergut, Department of Applied Geology, Geowissenschaftliches Zentrum Göttingen, Universität Göttingen, Goldschmidtstrasse 3, D-37077 Göttingen, Germany; tel.: +49 551 399707; fax: +49 551 399379; e-mail: ighergu@gwdg.de

Mihaela Glamoclija, Department of Geological Sciences, Indiana University, 1001 East 10th Street, Bloomington, IN 47405, USA; e-mail: mglamocl@indiana.edu

James W. Hagadorn, Department of Geology, Amherst College, Amherst, MA 01002, USA; tel.: +1 413 5422714; fax: +1 413 5422713; e-mail: jwhagadorn@amherst.edu

Christopher K. Junium, Department of Geosciences, Pennsylvania State University, State College, PA 16801, USA

Nora Noffke, Old Dominion University, Ocean, Earth & Atmospheric Sciences, 4600 Elkhorn Avenue, Norfolk, VA 23529, USA; tel.: +1 757 6833313; fax: +1 757 6835303; e-mail: nnoffke@odu.edu

Sarbani Patranabis-Deb, Department of Geological Sciences, Indian Statistical Institute, Kolkata-700108, India; tel.: +91 33 25753158; fax: +91 33 25773026; e-mail: sarbani@isical.ac.in

Hubertus Porada, Department of Applied Geology, Geowissenschaftliches Zentrum Göttingen, Universität Göttingen, Goldschmidtstrasse 3, D-37077 Göttingen, Germany; tel.: +49 551 397917; fax: +49 551 399379; e-mail: hporada@gwdg.de

Subir Sarkar, Department of Geological Sciences, Jadavpur University, Kolkata-700032, India; tel.: +91 33 24146366; fax: +91 33 24146781; e-mail: ssarkar@geology.jdvu.ac.in

Juergen Schieber, Department of Geological Sciences, Indiana University, Bloomington, IN 47405, USA; tel.: +1 812 8564740 (lab), +1 812 8555322 (office); fax: +1 812 8557899; e-mail: jschiebe@indiana.edu

Sohini Sur, School of Geology and Geophysics, The University of Oklahoma, Norman, OK 73019, USA; tel.: +1 405 2277493; e-mail: ssur@ou.edu

Acknowledgements

Octavian Catuneanu acknowledges research support from the Natural Sciences and Engineering Research Council of Canada (NSERC) and the University of Alberta. **Gisela Gerdes** wishes to thank the following colleagues and institutes for help in digitising photographs: Rolf Kiene, Niedersächsisches Landesinstitut für historische Küstenforschung Wilhelmshaven; Fritz Riedinger, Jens Kahle, Research Centre Terramare, Wilhelmshaven. Plate figures are in part from projects supported financially by the Deutsche Forschungsgemeinschaft (DFG): grant GE 64/1, GE 64/6-1, Kr 333/22-1, 2. **Santanu Banerjee** acknowledges IIT Bombay and the Department of Science and Technology, Government of India, for research support. **Subir Sarkar and Pradip Bose** acknowledge financial help from the Department of Science and Technology, Government of India, and from Jadavpur University, Kolkata. **Pat Eriksson** thanks the University of Pretoria for financial support, Mrs. M. de Swardt for logistical help and Mrs. M. Geringer for her considerable assistance with images. **Pat Eriksson and Adam Bumby** thank Igor Tonzetic for his very valuable help during fieldwork in the Waterberg Group, South Africa and for his photographic expertise. **Juergen Schieber** acknowledges support from a range of organisations that sponsored research involving microbial mats in terrigenous clastics. These organisations include the National Science Foundation (grants EAR-9117701, EAR-9706178, EAR-0073995, EAR-0318769, EAR-0308921), the Petroleum Research Fund (grants 25134-AC2, 33941-AC8, 38523-AC8), NASA (EXB04-0017-0111), Anaconda Minerals Co., Exxon Production Research Labs., and ChevronTexaco.

The following referees are acknowledged for their contributions: Patrick G. Eriksson (Univ. of Pretoria, South Africa), Gisela Gerdes (Senckenberg Research Institute, Wilhelmshaven, Germany), Juergen Schieber (Indiana Univ., Bloomington, USA), Juergen Schneider (Göttingen Univ., Germany) and Bruce Simonson (Oberlin College, USA). Editing duties were distributed amongst the chapters as follows: Juergen Schieber and Patrick Eriksson (Chapters 1, 9 and 10), Wladyslaw Altermann (Chapter 2), Juergen Schieber (Chapters 3 and 7), Octavian Catuneanu (Chapter 4), Patrick Eriksson (Chapter 5), Subir Sarkar (Chapter 6), Santanu Banerjee (Chapter 8 and reference list).

This page intentionally left blank

Contents

List of Editors v

List of Authors vii

Acknowledgements ix

1. Prologue: An Introduction to Microbial Mats 1
J. Schieber, P.K. Bose, P.G. Eriksson, S. Banerjee, S. Sarkar, W. Altermann, O. Catuneanu

2. Structures Left by Modern Microbial Mats in Their Host Sediments 5
G. Gerdes

3. Classification of Structures Left by Microbial Mats in Their Host Sediments 39
P.G. Eriksson, J. Schieber, E. Bouougri, G. Gerdes, H. Porada, S. Banerjee, P.K. Bose, S. Sarkar

4. Mat Features in Sandstones 53

4(a). Mat Growth Features 53
D. Bottjer, J.W. Hagadorn

4(b). Diagenetic Features Related to Mat Metabolism and Decay 72
J. Schieber

4(c). Mat-Destruction Features 76
P.G. Eriksson, H. Porada, S. Banerjee, E. Bouougri, S. Sarkar, A.J. Bumby

4(d). Mat-Decay Features 106
S.Q. Dornbos, N. Noffke, J.W. Hagadorn

4(e). Diagenetic Mat Features 111

4(f). Complex Structures Associated with Siliciclastic Biolaminites 111
E. Bouougri, H. Porada

5. Microbial Mats on Muddy Substrates – Examples of Possible Sedimentary Features and Underlying Processes 117
J. Schieber

6. Discussion of Some Problems: Unusual Features and the Importance of Terminology 135

6(a). 'Wrinkle Structures' – A Critical Review 135
H. Porada, E. Bouougri

6(b). Some Unusual and/or Problematic Inferred Mat-Related Features 145
S. Sarkar, S. Banerjee

6(c). Inherent Problems of Terminology: Definition of Terms Frequently Used in Connection with Microbial Mats 145
E. Bouougri, G. Gerdes, H. Porada

7. Examples of Stratigraphic Units Bearing Outstanding Mat Features 153

7(a). Microbially-Induced Sedimentary Structures (MISS) of Early and Middle Archaean Ages – Moodies Group, Pongola Supergroup, Witwatersrand Supergroup (South Africa) 153
N. Noffke

7(b). Microbial Mat Features in Terrigenous Clastics of the Belt Supergroup, Mid-Proterozoic of Montana, USA 158
J. Schieber

7(c). Microbial Mat Features in Mudstones of the Mesoproterozoic Somanpalli Group, Pranhita-Godavari Basin, India 171
S.P. Deb, J. Schieber, A.K. Chaudhuri

7(d). Mat-Related Features from Sandstones of the Vindhyan Supergroup in Central India 181
P.K. Bose, S. Sarkar, S. Banerjee, S. Chakraborty

7(e). Benthic Microbial Mats in Black Shale Units from the Vindhyan Supergroup, Middle Proterozoic of India: The Challenges of Recognising the Genuine Article 189
J. Schieber, S. Sur, S. Banerjee

7(f). Mat-Related Features from the Neoproterozoic Tizi n-Taghatine Group, Anti-Atlas Belt, Morocco 198
E. Bouougri, H. Porada

7(g). Microbial Mat Sedimentary Structures and Their Relation to Organic-Carbon Burial in the Middle Neoproterozoic Chuar Group, Grand Canyon, Arizona, USA 208
K.M. Bohacs, C.K. Junium

7(h). Mat-Related Features from the Terminal Ediacaran Nudaus Formation, Nama Group, Namibia 214
E. Bouougri, H. Porada

7(i). Ripple Patches in the Cretaceous Dakota Sandstone Near Denver, Colorado, a Classical Locality for Microbially Bound Tidal Sand Flats 222
J. Schieber

7(j). Benthic Microbial Mats as an Oil Shale Component: Green River Formation (Eocene) of Wyoming and Utah 225
J. Schieber

8. New Developments in Research on Microbial Mats 233

8(a). Microbial Mats Built by Iron Bacteria: A Modern Example from Southern Indiana 233
J. Schieber, M. Glamoclija

8(b). Disruption of Mats by Seismic Events 245
J.A. Donaldson, J.R. Chiarenzelli

8(c). Flume Experiments on the Durability of Sandy Microbial Mat Fragments During Transport 248
J. Schieber

8(d). Hydraulic Conditions and Mat-Related Structures in Tidal Flats and Coastal Sabkhas 258
H. Porada, E. Bouougri, J. Ghergut

Appendix A 262

9. Palaeoenvironmental and Chronological Relationships of Mat-Related Features, and Sequence Stratigraphic Implications of Microbial Mats 267

9(a). Palaeogeography of Microbial Mats in Terrigenous Clastics – Environmental Distribution of Associated Sedimentary Features and the Role of Geologic Time 267
J. Schieber, P.K. Bose, P.G. Eriksson, S. Sarkar

9(b). Sequence Stratigraphic Context of Microbial Mat Features 276
O. Catuneanu

10. Conclusions 285
J. Schieber, G. Gerdes, P.G. Eriksson, S. Sarkar, P.K. Bose, S. Banerjee, O. Catuneanu, W. Altermann

Reference List 289

Subject Index 307

Atlas of Microbial Mat Features Preserved within the Siliciclastic Rock Record
Edited by J. Schieber et al.
© 2007 Elsevier B.V. All rights reserved
DOI: 10.1016/S1574-1966(07)02001-9

CHAPTER 1

Prologue: An Introduction to Microbial Mats

Paracelsus (approx. 1519) is on record as having been among the first to have taken note of the substrate-altering and rock-generating properties of biofilms (Krumbein, 1994). Yet, he simply was so far ahead of his time that his perfectly modern sounding descriptions were soon forgotten. Subsequently, scientists have discovered, forgotten, and re-invented the significance of biofilms and microbial mats many times (Krumbein, 1994). Today, the importance of microbial life and microbial mats for multiple aspects of Earth processes is undisputed, and a 3.5 billion year fossil record affirms that these oldest known ecosystems are also crucial for understanding Earth history (Margulis and Dolan, 2002). Photosynthetic microbial mats figure prominently because sunlight has long powered the bulk of global primary productivity, and, through interaction with the hydrosphere and non-photosynthetic microbial ecosystems, has profoundly influenced the evolution of the Earth's atmosphere–ocean system (e.g., Lovelock, 1988). Microbial life, geochemical processes, and the sedimentary rock record are intimately and complexly entangled. Reading the rock record for its presence and its influences is not without peril, but there is no alternative if we are to make progress in understanding Earth history.

It was a simpler world half a century ago, when Francis Pettijohn's classic text "Sedimentary Rocks" (1957) was the standard reference for the majority of sedimentary geologists. Pettijohn's text was firmly grounded in physics and chemistry, and the main role of organisms appeared to be the production of useful particles for carbonate rocks and complicating the observation of primary sedimentary structures. A tremendous amount of research into the processes that control the formation of sedimentary rocks was conducted in the following decades. Especially trace fossil studies (Seilacher, 1964; Bromley, 1990) and dissemination of the idea that carbonate stromatolites were the constructs of microbial mats (Black, 1933; Logan et al., 1964), made clear that biological influences on sedimentation were profound. Today, rather than simply being tombs for the creatures that palaeontologists enjoy studying, sedimentary rocks are the place where physics, chemistry, and biology meet and are the most closely intertwined in the rock record.

Yet, whereas major biological influences in the formation of carbonate rocks are by now largely taken for granted (Altermann et al., 2006), many still consider terrigenous clastic sediments a product primarily of physics and chemistry. For example, none of three relatively recent and influential textbooks in sedimentary geology (Füchtbauer, 1988; Blatt, 1992; Boggs, 1995) list the terms 'microbial' or 'microbial mat' in their indexes. That the latter may actually occur in terrigenous clastics is at best noted as an aside among more weighty matters. In the widely referenced book "Sedimentary Environments", edited by H.G. Reading, the term microbial mat finally shows up in the third edition (Reading, 1996), but in a general discussion animals and plants are still considered to have the most important impact on sedimentary and diagenetic processes (Reading and Levell, 1996).

Nonetheless, microbial mat deposits in sandstones and mudstones were first identified several decades ago (e.g., Davis, 1968; Schieber, 1986). Growing interest in microbial mats in siliciclastic sediments was stoked by a rising awareness that microbes play a vital role in their accretion and diagenesis (Krumbein et al., 1994; Hagadorn et al., 1999; Riding and Awramik, 2000), and by the importance of the microbial biomass for biogeochemical cycles throughout Earth history (Madigan and Martinko, 2006). Our new atlas illustrates the presence of a wide range of mat-induced sedimentary structures in the siliciclastic rock record, and the progress in this new field of sedimentological studies is gathering momentum and gradually entering the mainstream of geological debate. Our main purpose with this project was to provide a basic visual reference for both students and professionals, in order to more broadly disseminate our current understanding on how microbial mats in terrigenous clastics might be recognised, and to stimulate further research into the ways by which microbial mats influence physical, chemical and biotic characteristics of sandstones and shales.

Chapter 2 of this atlas details structures attributed to living/modern microbial mats in their host clastic sediments. It describes the path from initial biofilm (clusters of micro-organisms attached to a surface and commonly embedded in extracellular polymeric substances – EPS) to microbial mat, and outlines how cyanobacteria, due to their wide inventory of adaptive responses and capacity for biostabilisation of illuminated clastic surfaces, became the

most successful group of mat builders. Experimental work stresses the temporal component of mat evolution. For example, laboratory cultivations indicate that the transition from a thin and fragile biofilm to the durable fibrillar meshworks of a mat requires several weeks of non-burial (Gerdes and Klenke, 2003). This is a valuable piece of information to keep in mind for sedimentary facies-modelling. Cyanobacteria and other micro-organisms leave subtle traces and hints of their former presence in clastic (as well as other) sediments, with the chance thus of preservation in the rock record, particularly that of the Precambrian era. Modern examples of the continuum from biofilms to microbial mats are found most commonly within marine shallow water and tidal environments, right through to supratidal and sabkha settings. Yet, mat-forming cyanobacteria are not restricted to peritidal settings, and also occur in lake, river and other deposits (see Table 2-1 and Chapter 9(a)). They may also thrive in mixed clastic-chemical sediments, such as for example in hypersaline lagoons. This general trend of wide palaeoenvironmental adaptation is largely mirrored in the rock record (e.g., Chapter 7), with examples known even from Earth's oldest deserts (Eriksson et al., 2000). Thus, in a generic sense, microbial mat features are non-facies-specific. Only a careful evaluation of mat-produced features with regard to underlying processes (such as desiccation, erosion, gas development, etc.) allows the determination of environmental parameters. With these limitations in mind, microbial mat features can provide yet another perspective for the analysis of sedimentary facies, complementing information derived from other sedimentary structures.

Terminology and classification can be (and often is) a contentious issue irrespective of the subject matter. The evolution of sandstone classifications, from Krynine (1948) to Dickinson (1970), can serve as an example of the process, and illustrates how a prevailing philosophy of classification becomes established (Pettijohn et al., 1987). This also holds true for the relatively young discipline of 'microbial mat sedimentology'. Issues of terminology are addressed in both Chapter 2 and Chapter 6(a) and (c). The photographic material that makes up the bulk of this book was organised within the framework of a process–response organisational scheme devised by Schieber (2004). Main subdivisions are by lithology (sandstone or mudstone; Chapters 4 and 5 respectively), and secondary subdivisions are by the process that is predominantly responsible for a given feature (growth, metabolism, physical destruction, decay, and diagenetic overprint). While this scheme forms the organisational backbone of this book, it was adopted because it is visually appealing and has a consistent internal logic (Chapter 3; Figures 3-1 and 3-2), not because we believe it will be the final word in this regard. The discussion of alternative schemes in Chapter 3 makes clear that we are still in the process of defining what the salient features of microbial mats in terrigenous clastics might be, and that any attempt at classification is necessarily a work in progress. By the same token, there will most likely always be problematic features that elude ready categorisation.

In terrigenous clastic sedimentary rocks, features directly attributable to the constructing organisms are either rare or very localised. Proxy structures, however, resulting from interaction with the sediment, such as mat-induced sediment binding, grain agglutination, and chemical compartmentalisation of the sediment, are common in shallow marine sandstones and offshore shales, especially those of Precambrian affinity. To a large degree these proxy structures owe their formation to extracellular polymer substances (EPS) secreted by cyanobacteria and other microorganisms (Decho, 1990, 2000). Binding by EPS and microbial filaments makes sand and watery mud cohesive, and enables trapping and binding of particles. Originally granular and non-cohesive, sand will then respond differently to stress, often behaving more like mud, and forming a host of features generally not expected in sands/sandstones, such as desiccation cracks, sand-curls, and pebble-sized, flat or rolled-up fragments upon erosion (Chapter 4). Microbially colonised mud surfaces analogously exhibit a range of features incompatible with the expected behaviour of a watery mixture of clay minerals and silt grains. In addition to unexpected cohesiveness, such stabilised mud surfaces are also characterised by lamina textures that suggest microbial growth, and are associated with authigenic minerals that reflect sub-mat decay of organic matter (Schieber, 2004; Chapter 5).

More than 50 individual mat-related features are detailed within Chapter 4 (sandstone-hosted) and Chapter 5 (mudstone-hosted). Features preserved within muddy siliciclastics tend to be more subtle, and often require microscopic or even electron microscopic observations, whereas those preserved in sandstones are more readily observed in outcrop and hand specimen. Yet even there, certain features, such as diagenetic cements related to mat metabolism and decay, require microscopic examination. Chapter 2 complements Chapters 4 and 5, by providing large numbers of illustrations of modern and laboratory-cultivated microbial mat features in clastic environments. Although it is comparatively easy to understand genetic processes in observations of modern mats, when working on the rock record this exercise becomes rather involved. Quite a few of the microbial mat-related features illustrated and discussed in this book can have multiple origins, not all of them microbial. For example, microbial mat features in sandstones can be recognised with a good deal of confidence as long as we are looking at amalgamated, well-sorted sandstone beds, where evidence for cohesiveness would be unexpected. The presence of mudstone interbeds tends to complicate matters, because then cohesion-indicative features in a sandstone bed may actually

be due to the cohesive behaviour of an overlying mudstone bed. Rather than basing a microbial mat interpretation solely on outcrop studies, it is generally good practise to also examine suspected mat features in thin section. In that way the details of the contact relationship of successive sediment layers can be used to confirm (or refute) a microbial mat origin.

Microbial mat-related structures in sandstones and mudstones that range in age from Archaean to Tertiary are illustrated in Chapter 7. The oldest example is from the Moodies Group (ca. 3.2 Ga) of the Barberton greenstone belt in South Africa, and the majority of examples are from Proterozoic strata. Among the latter, the Mesoproterozoic Belt Basin of North America and the Palaeo- to Neoproterozoic Vindhyan basin of India provide classic examples of sandstone- and mudstone-hosted mat features that occur in a wide range of depositional palaeoenvironments. The youngest example is from the Eocene Green River Formation in the USA and underscores the continuity of mat-induced features within the siliciclastic rock record. Although the advent of metazoan grazers in the Phanerozoic has changed the natural niches occupied by microbial mats, and despite their decreased importance compared to the Precambrian sedimentary record, the range of features that occur in lithified sands and muds remains essentially unchanged. Microbial mats thus exemplify the general applicability of uniformitarianism to the Precambrian sedimentary record (cf. Donaldson et al., 2002a).

In Chapter 8 of this volume, emerging new research is discussed, with subjects as diverse as bacterial mats produced by iron bacteria (which has important connotations for models of Precambrian BIF evolution), seismic disruption of mat-bound sands, hydraulic influences on mats within tidal flats and coastal sabkhas, to flume experiments with living and 'dead' mat fragments. As more geologists become familiar with the spectrum of structures that may result from the interaction of microbial mats with terrigenous clastic sediments, the study of microbial mat features is rapidly becoming indispensable for modern sedimentological studies. It is the purpose of this book to ease the transition for the broader geologic community. Continued expansion of the knowledge base will bring to light structures that are still unknown, as well as generating better comprehension of microbial mat influence on physical, chemical and biotic characteristics of siliciclastic depositional environments and deposits.

Juergen Schieber
Pradip K. Bose
Patrick G. Eriksson
Santanu Banerjee
Subir Sarkar
Wladyslaw Altermann
Octavian Catuneanu
The Editors

This page intentionally left blank

Atlas of Microbial Mat Features Preserved within the Siliciclastic Rock Record
Edited by J. Schieber et al.
© 2007 Elsevier B.V. All rights reserved
DOI: 10.1016/S1574-1966(07)02002-0

CHAPTER 2

Structures Left by Modern Microbial Mats in Their Host Sediments

Gisela Gerdes

INTRODUCTION

Microbial mats can generally be seen as 'larger biofilms' (Costerton and Stoodley, 2003). Biofilms, i.e. closely related clusters of micro-organisms attached to a surface and often embedded in extracellular polymeric substances (EPS), embrace all metabolic pathways that ever emerged on Earth (Krumbein et al., 2003). Modern biofilm substrates are rock surfaces and deep cracks and fissures, soils, sedimentary granular systems of lacustrine, riverine and marine environments, and they occur from inside Antarctic ice to the walls of deep sea hydrothermal vents (Costerton and Stoodley, 2003). Biofilms are thus ubiquitous, microbial mats with the proviso that ecological conditions allow for the succession from biofilm to mat. Most successful in the enlargement of biofilms are cyanobacteria because of their great morphologic variability and biostabilisation capacity on sun-lit sedimentary surfaces. In combination with anoxygenic phototrophs, anaerobic and aerobic chemotrophs, organic and inorganic respiration and fermentation, cyanobacteria-dominated microbial mats successfully leave records in sediments, and thus, concomitantly and to a lesser degree, in the sedimentary rock record. Increasing interest in modern microbial mat features formed in siliciclastic sediments is complemented by a growing body of sedimentary features that are being found in Precambrian clastic sedimentary rocks, pointing to the important impact of such mats during Earth's earlier sedimentation record.

Generally speaking, microbial mats and their initial biofilms *per se* are relatively uncharacteristic in terms of facies, although shallow water and tidal environments composed of siliciclastic sediments host microbial mats across a broad spectrum of successional stages from cryptic biofilms to prolific mats, the latter being able to overgrow bedding planes by thicknesses of several centimetres. Yet, mat structures may appear also in lacustrine, riverine and other settings (Table 2-1), as do biofilms; they are even known from the oldest palaeo-deserts on Earth, ca. 1.8 Ga as will be shown in this volume.

Undoubtedly important within a facies framework are structures left by mat-forming micro-organisms when interacting with physical conditions of the depositional environment. A facies criterion in this respect is the time span available to create topographically heterogeneous laminae which may help to identify sedentary organic layers. From experimental mat cultivations, it has become known that a transition from a thin and fragile biofilm to condensed fibrillar meshworks of mat consistency needs several weeks of non-burial (Gerdes and Klenke, 2003). Lee-side shallow water environments of unusual salinity, rarely disturbed by sedimentation, are particularly successful in bringing out living three-dimensional surface layers. The term 'living surface' illustrates well all dynamic processes constantly at work in mats: cell growth/replication, EPS production, motility/immotility, aggregation/dispersal, etc. During life, such dynamic systems overprint sedimentary surfaces, and after burial may leave behind uneven lamination which, in rocks, may provide a proxy for sedentary microbial life rather than for transported organic matter.

ORGANISATION OF PHOTOGRAPHIC MATERIAL

The photographic presentation of the following series of mat-related sedimentary structures is based on Schieber's (2004) process-related classification scheme, subdividing features according to (i) growth, (ii) metabolism, (iii) physical destruction and (iv) decay. This scheme is adopted as a framework throughout this book, and is discussed in detail in the next chapter.

Growth-related features and structures

Structures and fabrics related to the abundance and interaction of the main morphotypes (cyanobacterial filaments and unicells)

Figure 2-1-1: Biolaminites (single layer view);
Figure 2-1-2: Growth bedding;
Figure 2-1-3: Jelly forms, nodules, biscuits.

Structures generated from a change in growth direction

Figure 2-1-4: Pinnacles, tufts, microstromatolites;
Figure 2-1-5: Reticulate surface patterns;
Figure 2-1-6: Polygonal bulges, involute structures.

Features and fabrics related to trapping and binding of sediment

Figure 2-1-7: Microbial binding structures.

Microbial overprints of physically preformed bedding planes

Figure 2-1-8: Overgrowth, fixation and nivellement of ripples.

Features derived from metabolic effects

Figure 2-2-1: Mat-confined bubbles;
Figure 2-2-2: Layered iron enrichment;
Figure 2-2-3: Patterns resembling *Kinneyia*.

Features derived from physical mat destruction

Figure 2-3-1: Shrinkage cracks;
Figure 2-3-2: Jelly rolls, flip-overs;
Figure 2-3-3: Erosional edges, mat chips;
Figure 2-3-4: Ripple patches, *Astropolithon*-like features (sand volcanoes).

Features derived from mat decay and post-burial effects

Figure 2-4-1: *In situ* calcium carbonate precipitates in evaporite microbial mats;
Figure 2-4-2: Fenestral fabrics;
Figure 2-4-3: Gas domes;
Figure 2-4-4: Petee variations.

Structures owing their patterns to microbial growth (Figures 2-1-1 to 2-1-8) are closely related to the five subdivisions in the alternative classification scheme of 'microbially induced sedimentary structures' (MISS), proposed by Noffke et al. (2001a), and reflecting: (i) biostabilisation, (ii) levelling, (iii) baffling, trapping and binding, (iv) imprinting, (v) microbial grain separation (see also Chapter 3). Structures owing their patterns to mat metabolism (Figures 2-2-1 to 2-2-3) also relate to biostabilisation phenomena of sedimentary surfaces. Biostabilisation is also an important factor to explain structures owing their patterns to physical mat destruction (Figures 2-3-1 to 2-3-4). Finally the mat-related structures owing their patterns to the interplay of mat growth and mat decay in the subground are closely related to the biostabilisation potential of surface mats, as can be seen particularly in Figures 2-4-2, 2-4-3 and 2-4-4.

TERMINOLOGY

As is the case in many scientific fields, a plethora of terminology for microbial mats and their related features has emerged over the past several decades (see more discussion in Chapter 6(c)). Many terms reflect similar features. Hofmann (2000) used the term stromatolite for "all morphologically circumscribed accretionary growth structures with primary lamination that is, or may be, biogenic". Krumbein (1983) suggested the term 'potential stromatolite' if structures are modern. Burne and Moore (1987) related the term 'microbialite' to both laminated and unlaminated accumulations of microbial origin. Earlier terms like 'cryptalgal fabrics' (Aitken, 1967), 'algal mats', 'algal skin' or 'algal carpet' (Black, 1933; Walter, 1976) have largely fallen away since the group of so-called 'blue-green algae' has been revised taxonomically into gram-negatively reacting photosynthetic cyanobacteria.

For tufts and pinnacles (Figure 2-1-4), the terms microstromatolite or microdome were also used. Reticulate ornaments, shown in Figure 2-1-5 and observed on various other mat surfaces, may give rise to wrinkle structures. Yet, there is no unifying use of this term. Hagadorn and Bottjer (1999) assume that wrinkle structures may occur in various modifications in the presence of microbial growth. Noffke et al. (2002, 2003a) interpreted fossil wrinkle marks to represent load marks of buried mats. Abiotic genesis of '*Runzelmarken*' was experimentally studied by Reineck (1969). Sarkar et al. (2004) argued that wrinkle structures observed in certain Precambrian sandstones developed due to sand flow around synaeresis cracks protected by a mat. The complexity of wrinkle marks and their possible genetic influences will be explored in Chapter 6(a).

Bulges and involute structures (Figure 2-1-6) are also termed 'compression double bulges' by Noffke (2000). Ripple overprints (Figure 2-1-8) may also generate 'palimpsest ripples' (Schieber, 2004, his Figure 7.9-1a). Shrinkage cracks (Figure 2-3-1) are also named desiccation cracks, sun cracks (Fischer, 1964, p. 114; cited in Fagerstrom, 1967), or contraction cracks (Fairbridge and Bourgeois, 1978). Other terms for mat chips (Figure 2-3-3) are microbial sand chips, organosedimentary fragments, or eroded mat fragments. Ripple patches (Figure 2-3-4) are also termed erosion pockets (Gerdes et al., 1993). *In situ* carbonate precipitates in microbial mats (Figure 2-4-1) are summarised under the term 'biominerals' (Flügel, 2004). Another term for fenestral fabrics (Figure 2-4-2) is 'sponge pore sand' (Noffke et al., 1997b; ancient analogues: Noffke et al., 2003a). Flügel (2004) refers to laminoid fenestral fabrics.

ENVIRONMENTAL ASSOCIATIONS

Microbial mat-related structures and features in this chapter are from modern transitional areas between land and sea (Table 2-1). Considering the settings according to their degree of exposure, the sequence follows from permanently water-filled shallow lagoons, transitional areas between lagoon and adjacent areas, intertidal flats, intertidal–supratidal transitions and finally supratidal flats and sabkhas (Table 2-1). Sediments bearing these structures and features are partly pure siliciclastic (e.g., Figure 2-1-1), or siliciclastics mixed with evaporites (Figure 2-1-3F), detrital carbonate grains (Figure 2-1-2H), or *in situ* carbonates (Figure 2-4-1).

Krumbein et al. (2003) argued that microbial mats and their products may occur "at any place offering biologically available water and temperatures. . . which comprises the whole geomorphologic range from approximately 10 km above to 10 km below NN. . .". Yet modern planar forms as presented in this contribution are prevalent at low energy levels (Sami and James, 1993; Schieber, 2004). Further, experience with modern microbial mats from settings indicated in Table 2-1 suggests that photoautotrophic biofilms following a succession towards thick mature microbial mats need sufficient time spans of non-burial. Transient biofilms can form rapidly (within 20 minutes) and usually disperse shortly before or after the tidal exposure period ends (Paterson et al., 1998, 2003). Yet, thick multi-laminated surface carpets need time spans of several weeks, if not of several months (Gerdes and Klenke, 2003) of exposure. Thus, on closer examination of fossil microbial carpets on bedding surfaces it would be worth thinking about the kind of environment which could have ensured longer time spans of non-burial.

Several sedimentary structures grouped in Table 2-1 may occur also in a variety of other settings, including subaqueous marine and non-marine facies, since mat-forming cyanobacteria are not by any means restricted to peritidal settings. Particularly, structures related to metabolic activity (Figures 2-2-1 to 2-2-3) or post-burial decay of mats (Figures 2-4-1 to 2-4-4) may occur in subaqueous environments. Even cracks and incomplete polygons may be subaqueous phenomena (Donovan and Foster, 1972), although facies relationships have been a matter of debate (Astin and Rogers, 1991, 1993; Barclay et al., 1993). Fossil roll-up structures were described from shelf deposits below wave base (Simonson and Carney, 1999), although the authors assume that the microbial mats involved may

Table 2-1
Environmental settings for structures and features illustrated in this chapter

Environmental settings
Temperate-humid tidal flats of Mellum Island, southern North Sea (Germany): Intertidal–supratidal transitions. Between 70 and 20% of all high tides on yearly average reach or cross mat habitats. Sediments: fine to medium siliciclastic sand. Mats benefit from low-rate sedimentation, but become occasionally buried by landward-directed sedimentation of storm sands (see Figure 2-1-2C). General salinity in the study area 30–32 psu. (Figures 2-1-1 (A–D); 2-1-2 (A–C); 2-1-7 (B–F); 2-1-8 (C–E); 2-2-1 (H); 2-2-2 (D); 2-3-1 (A); 2-3-3 (A, B); 2-3-4 (A, B); 2-4-2 (A–D)) Selected references: Aigner (1985); Gerdes et al. (1985); Reineck and Gerdes (1997)
Hypersaline sea-marginal ecosystems, Gulf of Aqaba coast (Egypt): Water-covered lagoon; salinity 100–200 psu. Strong seasonal evaporation causes water level changes which have an effect on light intensity, salinity and temperature within shallow hypersaline water overlying mat surfaces. (Figures 2-1-2 (D, G); 2-2-1 (D, L); 2-4-1 (A, E)) Saline mud flats inundated by trickling water films; salinity 60–100 psu. (Figure 2-1-3 (C)) Higher-lying sabkha plains. (Figure 2-4-4 (G)) Selected references: Friedman and Krumbein (1985); Gerdes and Krumbein (1987)
Southern Tunisia coastal bays and sabkhas: Lower supratidal shallows and impondments of 5–25 cm depth filled with concentrated seawater (salinity 60–200 psu); mineral sediments consist of clay and silt mixed with fine to medium-grained quartz sands, oolitic bioclastic sand and evaporites (mainly gypsum). (Figures 2-1-2 (H); 2-1-3 (B); 2-1-4 (A, D); 2-1-5 (E, F); 2-1-6 (B); 2-1-7 (A); 2-1-8 (F); 2-2-1 (J); 2-2-2 (C); 2-3-3 (C, E); 2-4-2 (E); 2-4-3 (A–C)) Higher-lying supratidal sabkhas; ground water from sea and hinterland (see Chapter 8(h) in this volume), evaporative pumping sensu Hsü and Siegenthaler (1969). (Figures 2-1-3 (F); 2-2-1 (F, G); 2-2-2 (E); 2-2-3 (A–E); 2-3-1 (F–H); 2-3-2 (A, B)) Extended coastal plains composed of damp brown clay and silt mixed with numerous mm-sized gypsum crystals (only southern Tunisia study areas). (Figures 2-3-2 (E–G); 2-3-3 (D)) Selected reference: Noffke et al. (2001)
Saltworks at Bretagne coast (France), on Lanzarote, Canary Islands (Spain) and Formentera, Balearic Islands (Spain): Ponds for evaporation of seawater, in which precipitation of evaporites is less remarkable. Light intensity, temperature and salinity fluctuating in seasonal rhythm with water depth; salinity 60–120 psu. Mineral sediments: clay and silt providing the base for the mats. (Figures 2-1-2 (E, F); 2-1-4 (C, F); 2-1-6 (A); 2-2-1 (K); 2-3-1 (C); 2-4-1 (B–F)) Crystallisation ponds; intermittent flooding and exposure of mats, increasing salinity,evaporite precipitation. (Figures 2-1-6 (C–F); 2-2-2 (A, B); 2-3-1 (B); 2-4-3 (D–F, H); 2-4-4 (A–F)) Abandoned ponds, air-exposed, progressive shrinkage of surface mats and underlying sediments due to evaporation. (Figures 2-1-6 (F); 2-3-1 (D, I); 2-3-2 (C, D); 2-4-3 (G)) Selected references: Gerdes et al. (1993); Reineck et al. (1990); Schneider (1995); Schneider and Herrmann (1980)

Table 2-1
(continued)

Environmental settings
Lab-cultured system simulating shallow hypersaline lagoonary conditions: Mats inundated by some cm deep hypersaline water; light intensity, temperature and salinity fluctuating with evaporation-related changes of water depths; salinity 60–120 psu; mineral base of mats: clay–silt mixture. (Figures 2-1-3 (A, D–F, E); 2-1-4 (B, E); 2-1-5 (A–D); 2-2-1 (A–C, I)) Selected reference: Gerdes and Klenke (2003)
Tidal flats and beaches, NE Brazil: Icapui intertidal flats, fine- to medium-grained siliciclastic sediments and bioclasts. (Figure 2-1-8 (A, B)) Icapui mangals. (Figure 2-2-1 (E)) Jericoacoara intertidal beach, medium-grained siliciclastic sediments. (Figure 2-3-4 (C–D)) Selected reference: Maia (1998)

not have been based on photosynthesis. These authors apply the term roll-up structures to features from depositional environments below wave base, and refer to 'jelly rolls' if peritidal shallow-water features are described (such as in Figure 2-3-2). Source areas of mat chips may be shallow peritidal lakes, lagoons and their adjacent flats (Figure 2-3-3); on the other hand, accumulation areas may be subaqueous (Schieber, 1999; his Figure 12H). Photosynthetically produced oxygen bubbles may cause flotation of thin, loosely attached crusts (Fagerstrom, 1967; a similar example is illustrated in Figure 2-3-2G). According to Flügel (2004), aligned fenestral cavities caused by the interplay of post-burial processes and sealing effects of mats (Figure 2-4-2) may develop in both subaqueous and subaerial settings (as do cyanobacterial mats). Domes (Figure 2-4-3) may be characteristic of periodically subaerially exposed hypersaline lagoons; yet gas doming is not restricted to arid areas but occurs also on tidal flats of the temperate humid climate zone, as well as in various other environments. Theoretically, gas-doming may also occur subaquatically, although forming mainly under intertidal to lower supratidal conditions (Bouougri and Porada, 2002). To seal their surfaces well, thick cohesive mats may need repeated phases of submersion, e.g., during a seasonal cycle (Figure 2-4-3G). Finally, *Kinneyia* may be subaqueous phenomena, although modern structures resembling *Kinneyia* may occur on peritidal evaporative flats, where surface sediments are enriched in watery gels by dominance of coccoid cyanobacteria (Figures 2-1-6 and 2-2-3).

INFERRED SEDIMENTARY AND BIOLOGIC PROCESSES, IDEAS ON GENESIS

Sedimentary features and structures related to growth

Structures related to the local abundance of different morphotypes (Figures 2-1-1 to 2-1-3) Sedimentary structures shown in this section relate to cell growth and replication, production of extracellular polymers (EPS), mat growth and layered biomass condensation in time and space. Most important are physio-ecological responses to physical triggers, e.g., light meeting a mat surface, depth of overstanding water, and shading. Growth bedding of the biovarvite type (Figures 2-1-2D to -1-2G) is common in protected peritidal lagoons affected by higher evaporation and salinity (Gerdes et al., 2000b). Seasonally changing water depths corresponding to fluctuations in light intensities trigger the stacked buildup of sets of dark/light laminae. The dark horizontal layers are products of local abundance of filamentous cyanobacteria. The often more extensive light layers are made of coccoid cyanobacteria, large amounts of protective EPS, and often are interspersed by authigenic mineral precipitates. Light surface laminae provide shading for low-light filaments which remain beneath the translucent mats in summer. In winter, filamentous species benefit from decreasing light intensities and a higher water level, and over-ride the coccoid mats. Thus, a seasonal rhythm is indicated by the sets of hydroplastic and filamentous layers (Gerdes et al., 1994b). Such slowly growing sequences store high amounts of organic matter and enhance upward movement of fronts of sulphate-reducing bacteria and H_2S.

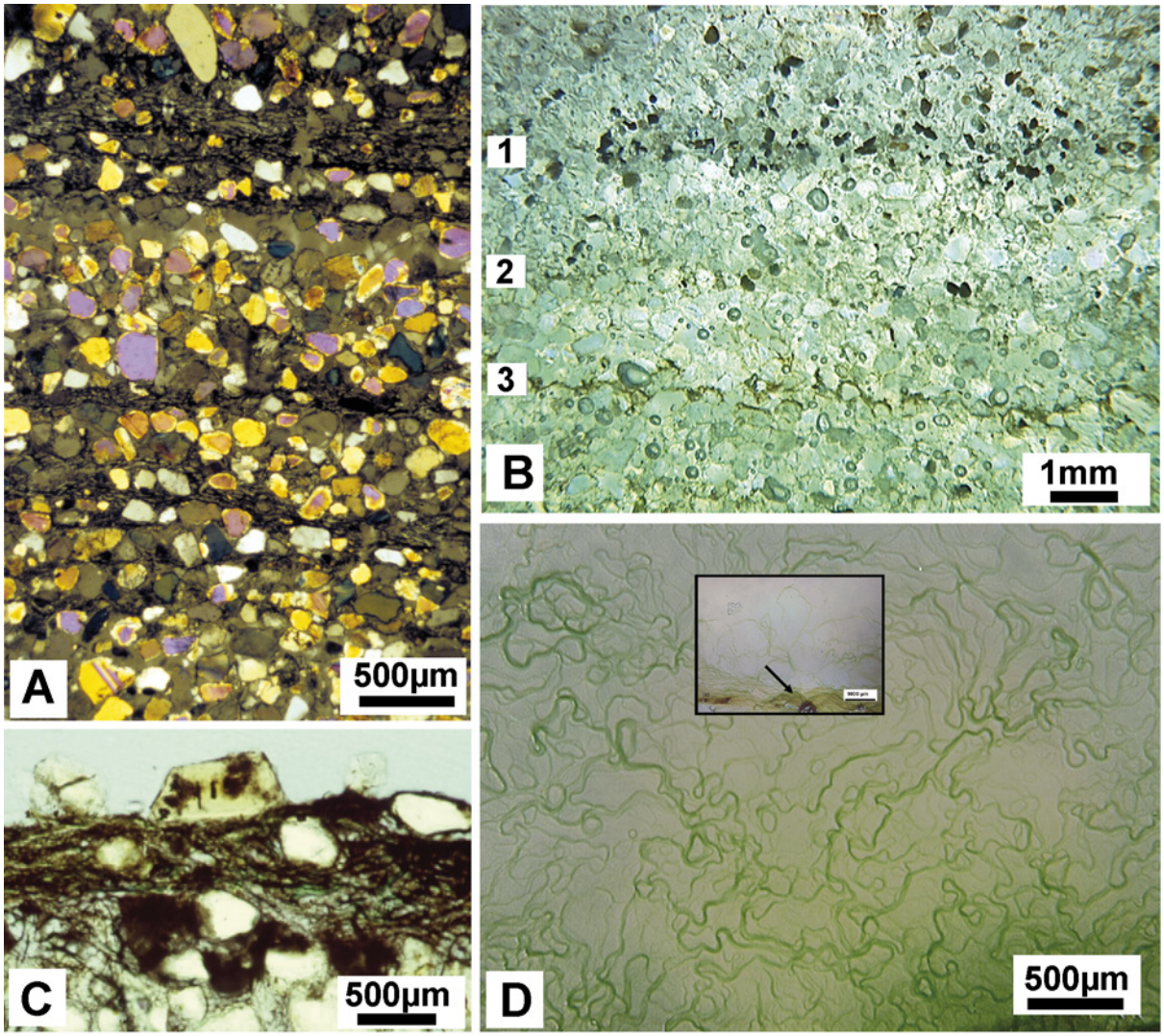


Figure 2-1-1: Biolaminites (single layer view).
(A) Single filamentous mats embedded in quartz-sandy tidal flat deposits. Photo: T. Klenke. (B) Faint indications of microbial films in quartz-sandy sediment mimicked by lamina-specific heavy mineral grains (lamina no. 1) and iron oxides (laminae nos. 2 and 3). Photo: Gisela Gerdes; modified after photo published in Gerdes et al. (2000a). (C) Vertical section through living microbial network (biodyction) made of filamentous cyanobacteria penetrating pore spaces of siliciclastic sediments. Photo: Gisela Gerdes; modified after photo published in Gerdes et al. (1993). (D) Filaments of *Phormidium* sp., a common mat-forming cyanobacterium, spreading on an agar plate. Small inserted photo: inoculum from where spreading started (arrow). Large photo: 10 days-old stage, filaments amalgamated into bundles and tangles. Succession to coherent mat would need additional time. Photo: modified after one taken by K. Bröhldick. *Locality of photos*: A to C – Mellum Island, southern North Sea coast (Germany); D – experimental set-up.

On intertidal flats, high levels of light intensity meeting surface mats lead to a productivity increase some millimetres beneath sedimentary surfaces (Garcia-Pichel and Castenholz, 1994). However, as long as surface sediments are damp to ensure water availability necessary for life processes, growth bedding can also rise above subaerial surfaces. Repeated low-rate sedimentation serves as a trigger that forces buried filamentous cyanobacteria to move upwards and over-ride the new sediment surface, producing the type of growth bedding driven with the aid of mineral sedimentation (Figures 2-1-2A to -1-2C).

The relief cast in Figure 2-1-2C exemplifies how environment-specific frequency and rates of sedimentation can control the interposition of mats within a sedimentary sequence. In the lower part, two cross-stratified sediment layers, each separated by a monolayered microbial mat, represent storm sand layers which irreversibly buried underlying mats and left behind single biolaminites. A sequence of closely stacked mats in the middle part of the

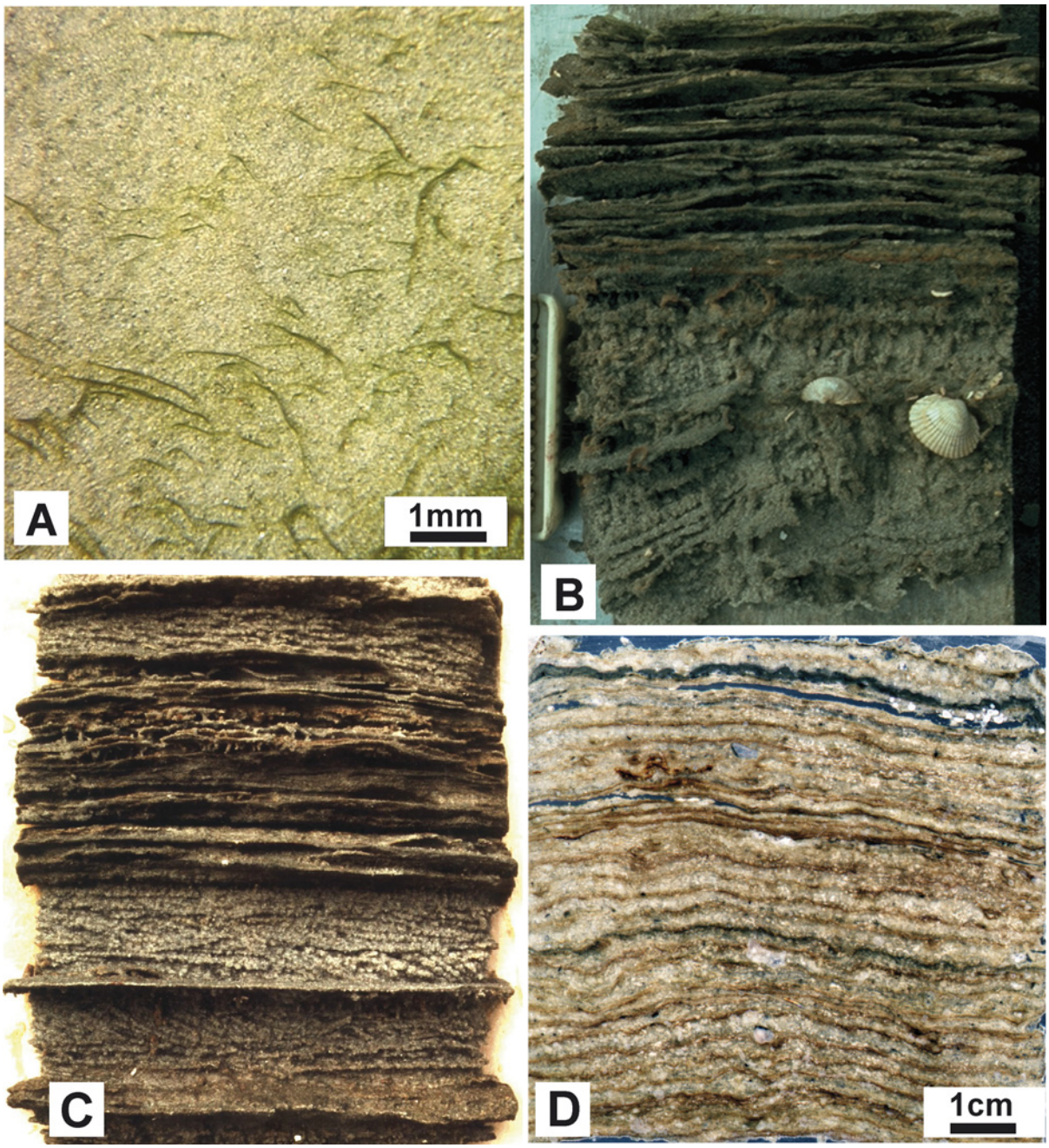


Figure 2-1-2: Growth bedding.

(A) Recolonisation of a quartz-sandy surface layer from a pre-existing mat underneath, by filaments of the pioneer species *Microcoleus chthonoplastes*. Photo modified after one taken by K. Bröhldick. (B) Experimental over-sedimentation revealed a stack of twelve mat generations (sharply projecting laminae) that originated from a basic mat, cored on top of tidal flat deposits (lower part). Experiment showing the importance of intermittent low-rate sedimentation (relief cast 20 cm high). Photo: Gisela Gerdes; modified after photo published in Gerdes and Krumbein (1987). (C) Relief cast showing stacks of microbial mats in the middle part, similar to (B), underlain and overlain by cross-stratified sediments (relief cast 30 cm high). Photo: Gisela Gerdes; modified after photo published in Gerdes and Krumbein (1987). (D) Direct scan of thin section showing shallow water growth-bedding, developed from seasonal over-riding between filamentous cyanobacteria (dark laminae, winter generations) and coccoids (light laminae, summer generations). Type of growth-bedding without the aid of sedimentation (biovarvites). Photo: R. Kiene.

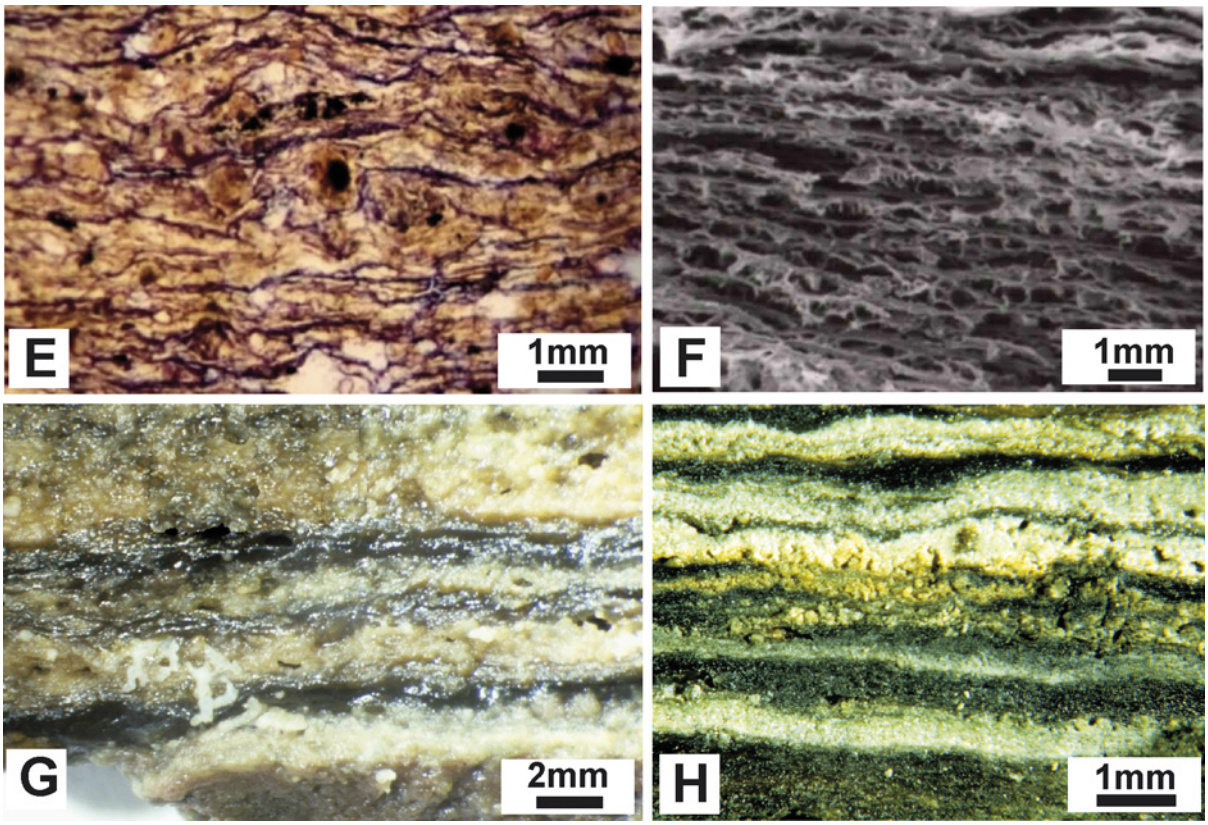


Figure 2-1-2: ***Continued.***
(E) Thin section of biovarvites showing sequence of filamentous (blue stained) and coccoid mats (yellow interlayers) growing independently from sedimentation. Photo: Gisela Gerdes; modified after photo published in Gerdes et al. (1991). (F) SEM view of the same material as in E: Filamentous mats visible, intercalated water-enriched coccoid mats destroyed by critical point drying. Photo: Gisela Gerdes; modified after photo published in Gerdes et al. (1993). (G) Vertical section through biovarvites showing white laminae overlying thin filamentous mats (dark). Extension of white laminae indicates arid climate influence: surface populations dominated by coccoids excrete large amounts of slime in which carbonates and gypsum precipitated. Dark laminae: winter mats. Photo: Gisela Gerdes. (H) Vertical section showing biovarvites mixed with subtidal ooid sands (centre) from a nearby lagoon. Yellow colour of grains may indicate weathering products of pyrite. Photo: Nora Noffke. *Locality of photos*: A, B – Laboratory-cultured microbial mat; C – Mellum Island, southern North Sea coast (Germany); D – Solar Lake, Gulf of Aqaba (Egypt), hypersaline sea-marginal ecosystem; E, F – saltworks, Lanzarote, Canary Islands (Spain); G – Gavish Sabkha, Gulf of Aqaba (Egypt); H – Bahar Alouane, southern Tunisia.

relief cast indicates calmer conditions associated with low-rate sedimentation. These common summer conditions induce the type of growth bedding modelled in the experimental build-up in Figure 2-1-2B.

Sufficient time for growth is an important factor influencing the characters of biolaminites as they appear in vertical sequences. Initial propagation of mat-forming organisms on a bedding surface, the essential construction zone of mat formation, often is not linear. To amalgamate into bundles and tangles (a prerequisite of mat formation), trichomes need time (Figure 2-1-1D). A coherent mat which homogeneously covers the substrate may need several weeks of almost zero deposition (Gerdes and Klenke, 2003).

Single buried mats of lower thickness within sedimentary sequences may indicate pioneer stages which, after short periods of non-deposition, became buried again (Figures 2-1-1A, -1-1B). Increasing biomass condensation, and the buildup of three-dimensional networks (biodyction; Krumbein et al., 2003) are hints for sediment starvation (Figure 2-1-1C).

Coccoidal surface populations are dominant components of hypersaline shallow water and dessication-endangered arid settings. The more physical harshness increases in these habitats, the more coccoids persist in increasing abundance. Large amounts of EPS, viscous polysaccharide solutions and protective pigmentation are attributes that

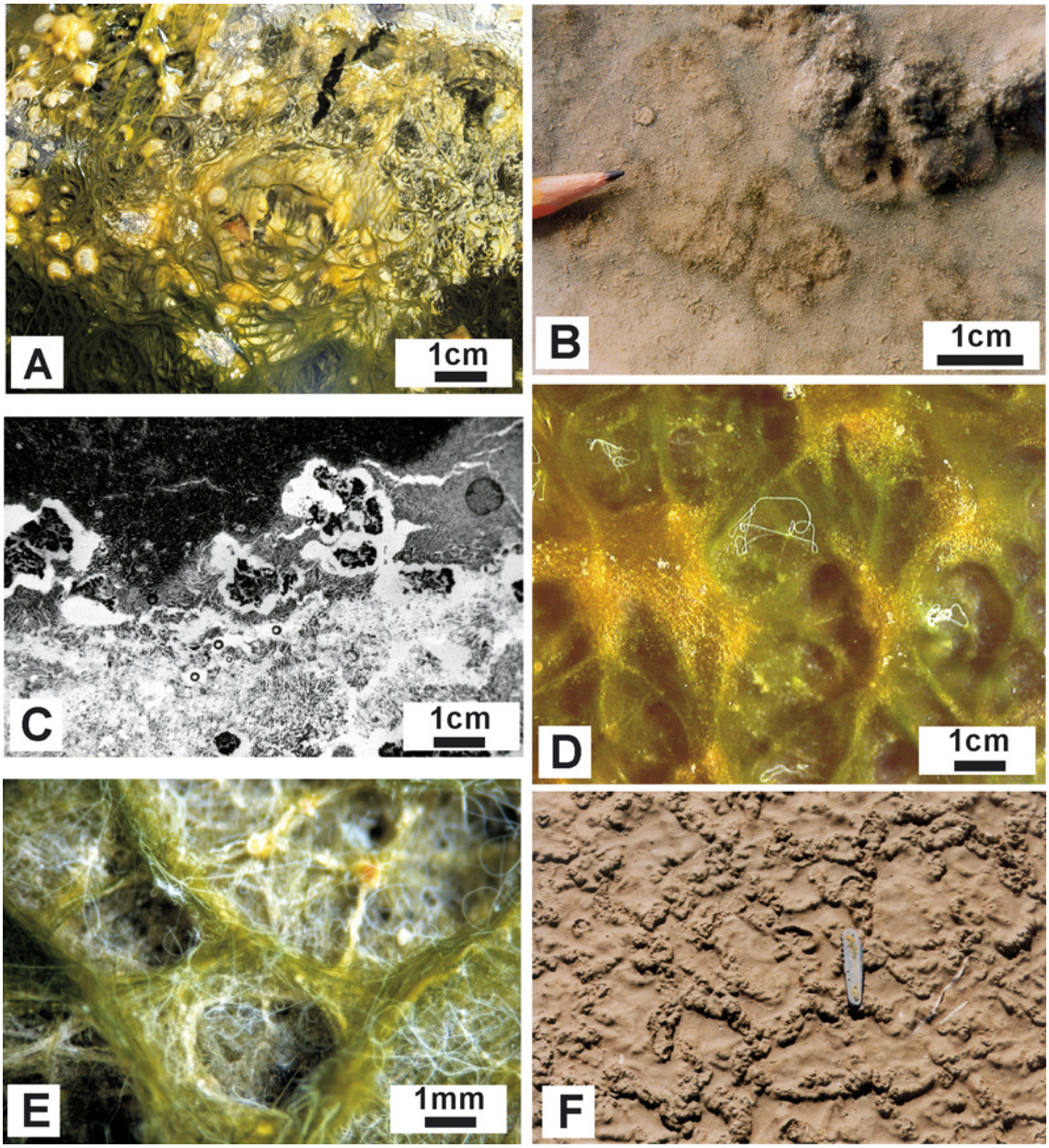


Figure 2-1-3: Jelly forms, nodules, biscuits.
(A) Surface view of a laboratory cultured mat illustrating the over-riding phenomenon; yellow ground: populations of coccoids coloured by photoprotective pigments enriched in EPS; dark green network: filamentous cyanobacteria competing with the coccoids for the most optimal light position. Photo: K. Bröhldick. (B) Nodular to biscuit-like surface structures produced by local dominance of coccoids. Photo: Nora Noffke. (C) Internal view of nodular structures made by dominance of coccoids (*Pleurocapsa* sp.), embedded in a fabric of carbonate-coated filamentous sheaths. Photo: Gisela Gerdes; modified after photo published in Gerdes and Krumbein (1987). (D) Surface view of jelly cushion-like bulges produced by dominance of coccoids, yellow-pigmented slime running into the valleys. Photo: K. Bröhldick. (E) Nodular surface structures of a shallow water mat surrounded by a network of filamentous cyanobacteria (*Lyngby*a sp.). White filaments: *Beggiatoa*-type chemolithoautotrophic bacteria marking a shift of the O_2-/H_2S chemocline from the inner mat to the mat surface. Photo: Gisela Gerdes. (F) Salt-encrusted cauliflower-like nodules made by dominance of coccoids projecting over polygonal ridges, about 0.5 to 2 cm high. Knife is 8 cm long. Photo: Nora Noffke; modified after photo published in Noffke et al. (2001a). *Locality of photos*: A, D, E – Laboratory-cultured microbial mat; B – Bou Jemel, southern Tunisia; C – Gavish Sabkha, Gulf of Aqaba coast (Egypt), hypersaline sea-marginal ecosystem; F – Bahar Alouane, southern Tunisia.

allow for inhabiting environments of extreme light radiations (Figure 2-1-3). Also, processes of space competition may be facies-relevant (Figures 2-1-2D to -1-2H). The overriding phenomenon is well visualised in Figure 2-1-3A showing filamentous cyanobacteria in space competition with coccoids for the most optimal light position.

The dominance of coccoid cyanobacteria is often indicated by a characteristic irregular surface topography including mammillate, jelly, cushion-like or cauliflower-like patterns (Figure 2-1-3). Mammillate surface patterns may also originate from nodules in which unicellular cyanobacteria with multiple fission such as *Pleurocapsalean* taxa are involved (see intrasedimentary nodules in Figure 2-1-3C). Nodule formation may indicate changing levels of salinity and water cover (schizohaline conditions; Gerdes et al., 1985a). Nodular salt crusts (Figure 2-1-3F) form on higher sabkha flats where microbial growth and slime production interfered with salt precipitation from hypersaline groundwater transported to the surface by evaporative pumping (Noffke et al., 2001a). As is the case for quartz sands, gypsum crystals are ideal in light channelling.

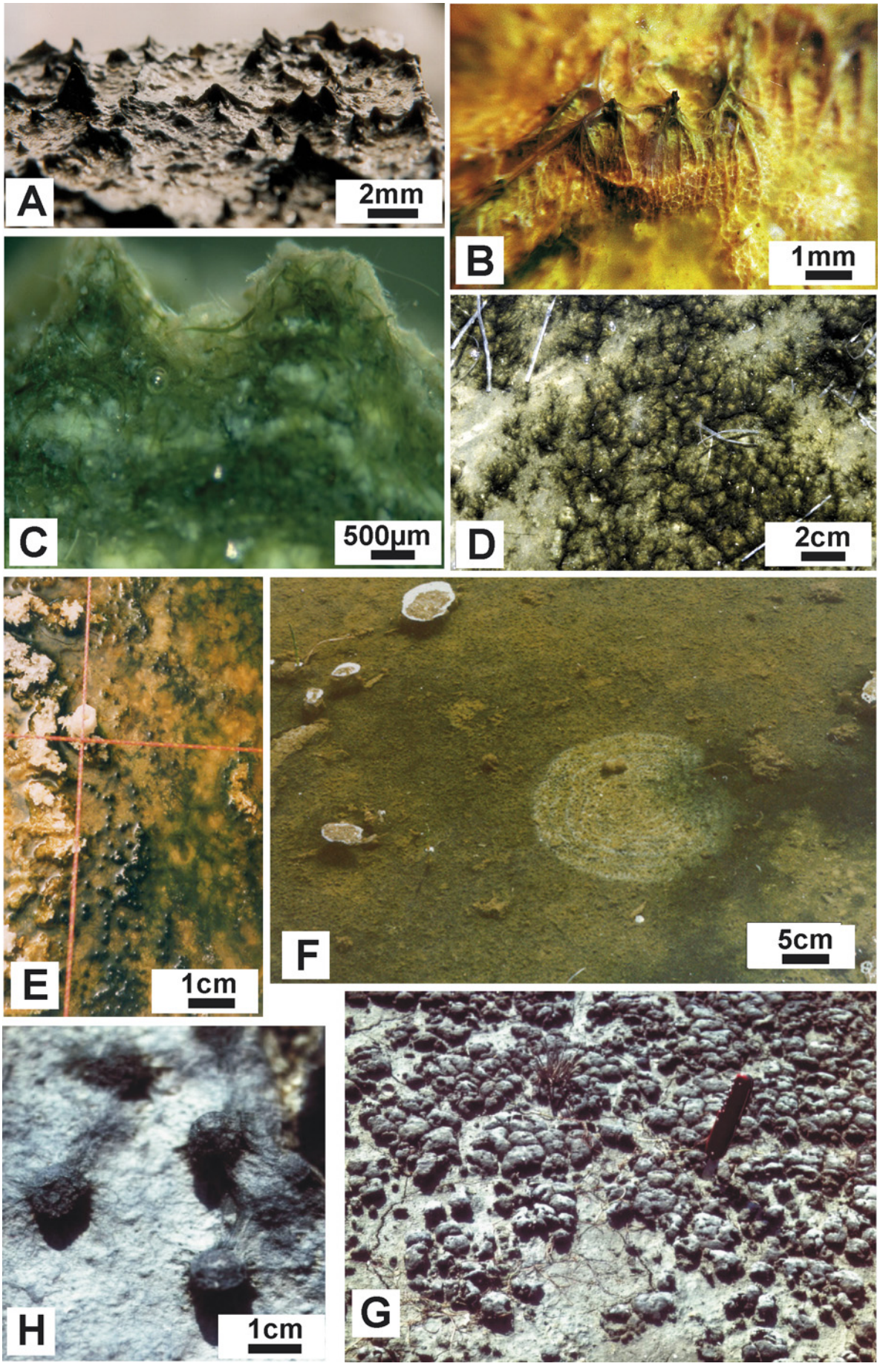
Structures generated from a change in growth direction (Figures 2-1-4 to 2-1-6) Filamentous cyanobacteria, which originally contribute to the basic mat, are able to change their growth direction into a vertical position and rise above the mat base. Results are tufts and cone-shaped pinnacles some millimetres high. When stabilised by EPS, initially soft and flexible tufts change into rigid pinnacles. Different filamentous species are able to initiate pinnacle formation. Examples are *Microcoleus chthonoplastes* (Figures 2-1-4A, -1-4C to -1-4F), and *Lyngbya aestuarii* (Figures 2-1-4B, -1-4G and -1-4H). The knotty structures result from a combination of growth and movement of filaments in response to environmental factors such as light, ionic composition of interstitial and surface water, or oxygen supply. The outer form and size depends largely on the presence of the respective species morphotype. Raised tufts and pinnacles formed by *M. chthonoplastes* are usually smaller than those of *Lyngbya* ssp. The knotty surface structures of *L. aestuarii* in Figures 2-1-4G and -1-4H protrude up to 20 mm out of the sediment. They resemble structures at Shark Bay made by the same species, forming radiating bunchlets (Golubic, 1976). Such relatively permanent structures may also benefit from the participation of other filamentous genera, e.g., *Schizothrix* (Golubic, 1992).

Distribution patterns of pinnacles (Figures 2-1-4D to -1-4F, see also Figure 2-3-1H) seem not to be random, but may reflect oriented behaviour probably triggered by small-scale differences in nutrient concentrations, shading, or even space competition. The curious concentric arrangement of pinnacles in the so-called ‘fairy rings’ (Figure 2-1-4F) may be a sign of oriented behaviour of pinnacle-forming organisms. Although no sufficient explanation exists until now, one idea was that concentric micro-waves initiated by gas bubbling through small exit points within mat surfaces propagate nutrient fronts which may trigger chemotactic responses (Gerdes et al., 1994a).

Pinnacles combined with reticulated patterns are shown in Figures 2-1-5A to -1-5C. Particularly thick elongated bulges are shaped by dominance of *Lyngbya aestuari* (Figure 2-1-5D). Browne et al. (2000) describe similar reticulate mats from Shark Bay composed of ridges dominated by *Lyngbya* sp. These authors assume that filaments have greater advantage of upwards growth and thickening of bulges where O_2 is more available. In Figure 2-1-5A,

---

Figure 2-1-4: Pinnacles, tufts, microstromatolites.
(A) Oblique view showing filament tufts of *M. chthonoplastes* standing about 1 mm above the basic mat. Photo: Nora Noffke. (B) Pinnacles projecting through the mat surface. Basic mat coloured by yellow pigmented slimes. Pinnacles made by dominance of filamentous cyanobacteria (*Lyngbya* sp., *M. chthonoplastes*). Photo: K. Bröhldick (colour-adapted). (C) Vertical section through basic mat and pinnacles, both made by dominance of *M. chthonoplastes*. Photo: Gisela Gerdes; modified after photo published in Gerdes and Klenke (2003; courtesy of Assoc. Geoaustria). (D) Local tuft cluster of *M. chthonoplastes* projecting through a flocculous surface mat. Photo: Nora Noffke. (E) Irregular distribution of pinnacles. Basic mat enriched in yellow pigmented slimes. The photo visualises polarity change of *M. chthonoplastes* from prostrate-growing filaments (below right) to vertically-erected pinnacles (below left). Laboratory-cultured microbial mat. Photo: K. Bröhldick. (F) Ring-shaped structures on the surface of a shallow water mat, ring crests crowned by pinnacles. Photo: W.-E. Krumbein. (G) Knotty surface made by dominance of filamentous cyanobacteria (*Lyngbya aestuarii*?) which protrude out of the sediment. Knife for scale: 8 cm. Photo by courtesy of J. Schneider. (H) Individual knots protruding up to 20 mm out of the leathery surface mat. Major species in both the stratiform surface mat and the blister-like knots is the rigid sheath-forming filamentous cyanobacterium *L. aestuarii*. Photo by courtesy of J. Schneider. *Locality of photos*: A, D – Bahar Alouane, southern Tunisia; B, E – Laboratory-cultured microbial mat; C, F – saltworks, Bretagne coast (France); G, H – saltworks of Sečovlje (Gulf of Piran, Slovenia).


A
2mm
B
1mm
C
500µm
D
2cm
E
1cm
F
5cm
G
H
1cm

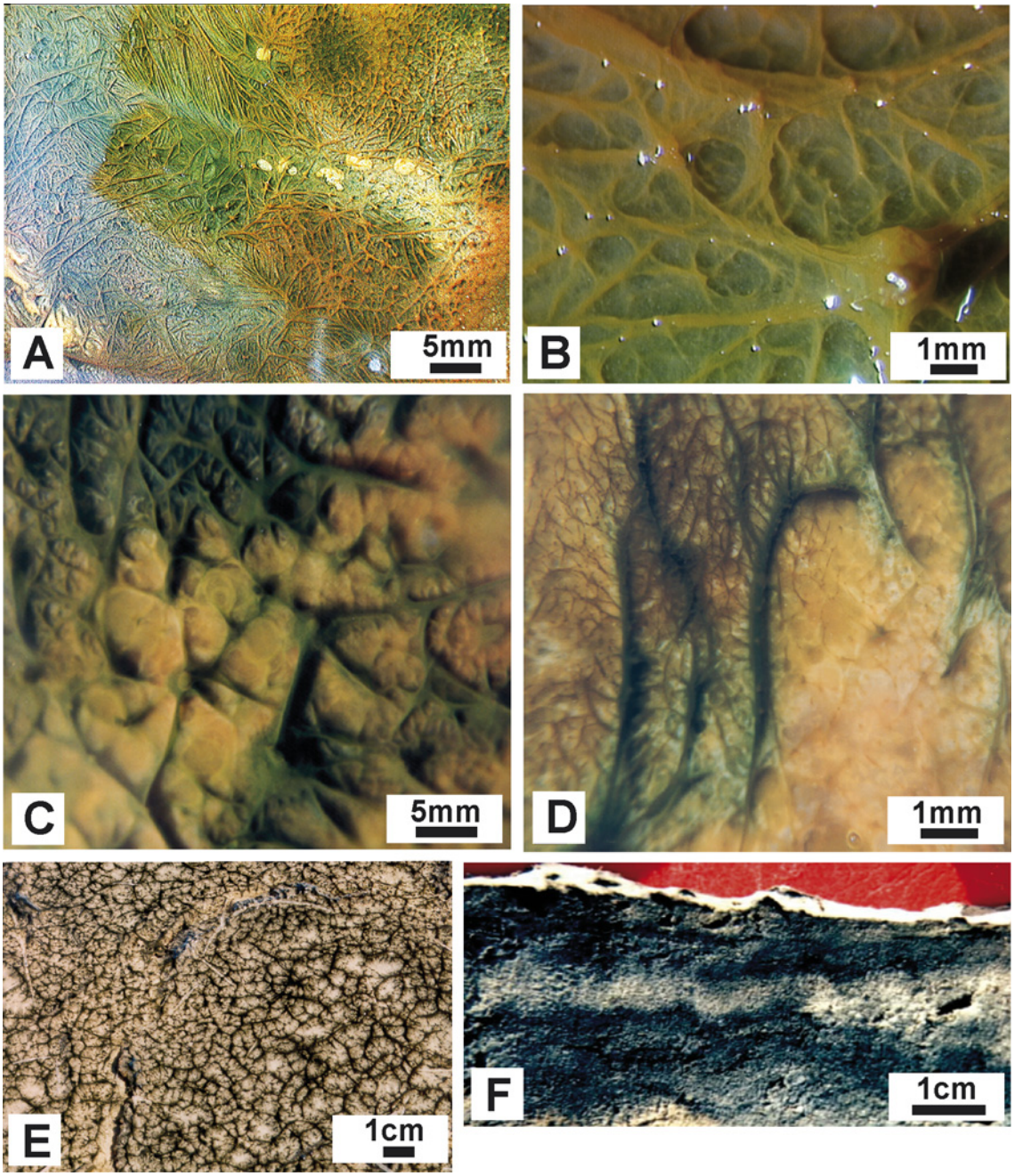


Figure 2-1-5: Reticulate surface patterns.
(A) Reticulated patterns made of intersecting bulges and pinnacles established on a microbial mat surface. Photo: K. Bröhldick (colour-adapted); modified after photo published in Gerdes and Klenke (2003; courtesy of Assoc. Geoaustria). (B) Close-up of A: Pinnacles form the focus of radial bulges. Photo: K. Bröhldick; modified after photo published in Gerdes and Klenke (2003; courtesy of Assoc. Geoaustria). (C) Small-scale reticulated mat surface produced by lateral dominance changes between coccoids (jelly cushion-like features) and filaments (tufts, pinnacles, bulges). Photo: K. Bröhldick. (D) Thick bulges made by the filamentous cyanobacterium *Lyngbya* sp. and smaller reticulated veins stretching over a yellow layer of slime-embedded coccoids. Photo: K. Bröhldick. (E) Macroscopic surface view of a reticulated microbial mat resembling 'elephant skin'. Photo: Nora Noffke; modified after photo published in Gerdes et al. (2000b). (F) Vertical section revealing counterparts of reticulated surface mat (top) and wavy-crinkly bounding planes in the sediment below. Photo: Nora Noffke. *Locality of photos*: A to D – Laboratory-cultured microbial mat; E, F – Bahar Alouane, southern Tunisia.

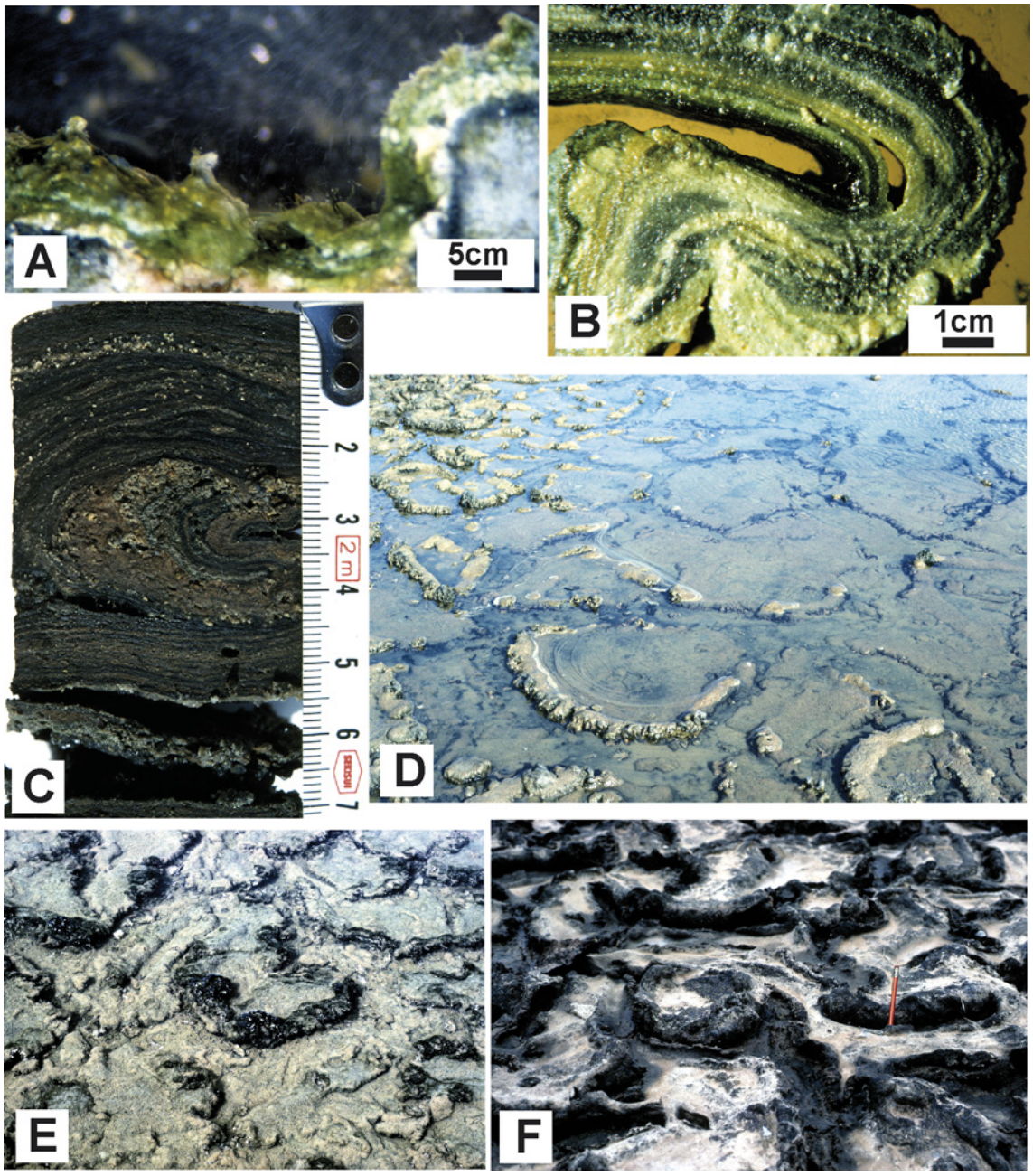


Figure 2-1-6: Polygonal bulges, convoluted structures.
(A) Microbial mat growing into a shrinkage crack. Pinnacles on the base of the crack (left). Dominant genera: *Microcoleus, Oscillatoria*. Photo: Gisela Gerdes. (B) Vertical section through a pocket-like multilayered crack tapestry produced by microbial mats that grew from the surrounding mat into a shrinkage crack. Photo: Nora Noffke; modified after photo published in Gerdes et al. (2000a). (C) Sectional view of sediment core showing involute growth bedding. Photo: K. Dunajtschik-Piewak; modified after photo published in Gerdes et al. (1994a). (D) Water-covered microbial bulges marking polygonal cracks. Photo: K. Dunajtschik-Piewak. (E) Irregular surface patterns due to the bulging growth of mats as a reaction to cracking and subsequent flooding. Some individual mat fragments partly flipped-over. Photo: K. Dunajtschik-Piewak. (F) Extraordinarily thick polygonal bulges within abandoned salina basin. Prolonged periods of overstanding calm and warm seawater alternating with shorter periods of drying may have produced these growth structures (pencil 17 cm long). Photo: K. Dunajtschik-Piewak. *Locality of photos*: A – saltworks, Bretagne coast (France); B – Bahar Alouane, southern Tunisia; C to F – saltworks Lanzarote, Canary Islands (Spain).

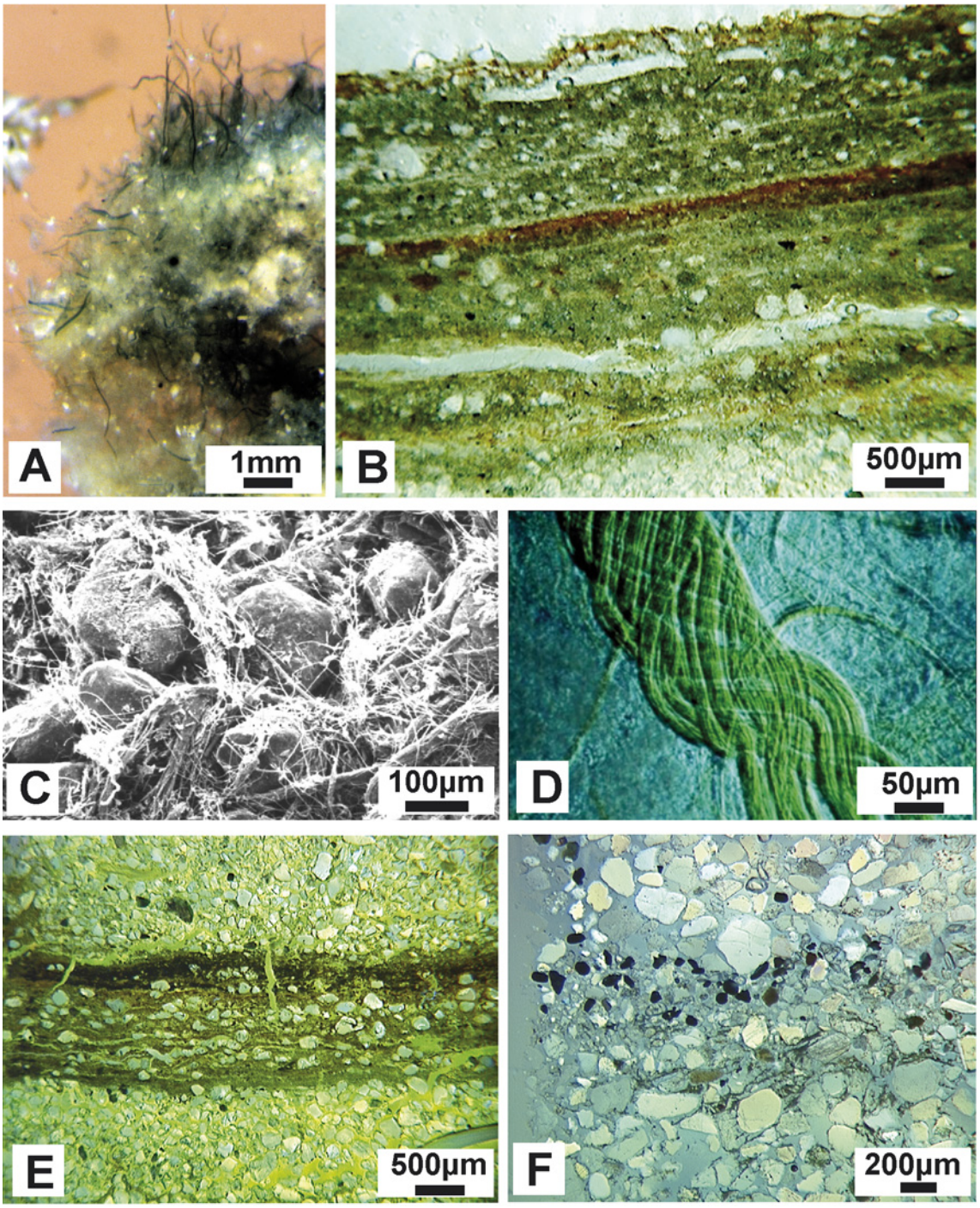


Figure 2-1-7: Microbial binding structures.
(A) White amorphous carbonate cluster enriched in microbial fabrics due to baffling effects of upright colonies of filamentous cyanobacteria. Photo: Nora Noffke. (B) Vertical section of a thick multilayered surface mat overlying a quartz-sandy layer. A few sand grains are bound internally and on top of the mat surface. Photo: Gisela Gerdes. (C) SEM view of quartz grains bound by filamentous microbial surface mat. Photo: Gisela Gerdes. (D) Light microscopy showing an elongated, twisted sheath bundle of *M. chthonoplastes*, a species particularly capable of sediment binding. Photo: Gisela Gerdes; modified after photo published in Gerdes and Klenke (2003; courtesy of Assoc. Geoaustria). (E) Biolaminite within quartz sandy tidal flat sediments, containing matrix-supported sediment grains arranged with their long axes parallel to the bounding plane. Photo: Gisela Gerdes. (F) Microbial lamina-bound heavy mineral grains within siliciclastic tidal flat sediments. Photo: Gisela Gerdes. *Locality of photos*: A – Bahar Alouane, southern Tunisia; B to F – Mellum Island, southern North Sea coast (Germany).

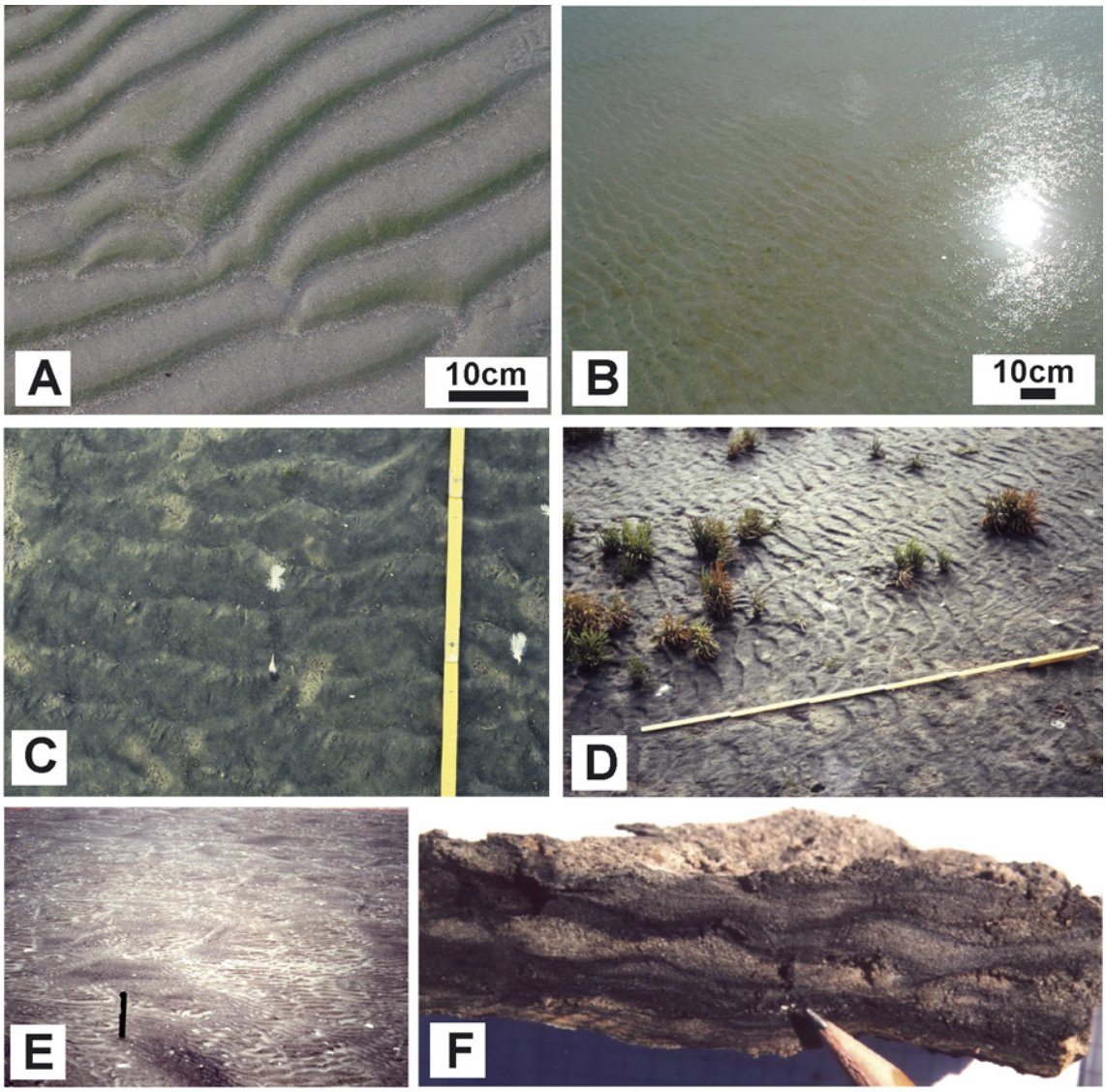


Figure 2-1-8: Overgrowth, fixation and nivellement of ripples.
(A) Surface of intertidal beach sand. Thin microbial biofilms cover the flanks of asymmetric oscillation ripples. Photo: B. Petzelberger. (B) Surface of an intertidal sand flat. Small asymmetric current ripples covered by a slightly increasing microbial biofilm. Photo: B. Petzelberger. (C) Advanced microbial growth overprinting asymmetric ripples. Photo: Nora Noffke. (D) Rippled surface of high-lying tidal flats completely overprinted and stabilised by a highly productive microbial mat. Photo: Nora Noffke; modified after photo published in Noffke (1997b). (E) Multidirectional ripple marks generated from changes between physical sedimentation and microbial colonisation and fixation of ripple marks. Photo: Nora Noffke; modified after photo published in Gerdes et al. (2000a) and Noffke (1998a). (F) Cross-section through surface sediments showing structures resembling lenticular bedding. Mats of different thickness have overgrown ripple crests, flanks and valleys indicating that the microtopography of ripples is of ecologic importance (tip of pencil is 1 cm long). Photo: Nora Noffke. *Locality of photos*: A, B – Icapui tidal flats, NE Brazil; C to E – Mellum Island, southern North Sea coast (Germany); F – Zarzis beach, southern Tunisia.

distinct microbial populations contribute to individual parts of the surface texture (Gerdes and Klenke, 2003): green reticulate strips and pinnacles can be traced back to *M. chthonoplastes*, species of *Spirulina* are abundant within yellow brown strips and pinnacles, and coccoids (e.g., *Synechococcus* sp.) form the yellow cushions in between.

Macroscopically, the reticulate patterns resemble ‘elephant skin’ (Figure 2-1-5E; Gehling, 1991). Striking similarity exists between these patterns and wrinkle structures described by Hagadorn and Bottjer (1997). The studies illustrated in Figure 2-1-5 confirm the suggestion of Gehling (1999) that reticulate mat textures are characteristic of thick (mature) microbial mats. Experiments using lab-cultured mats have shown that the development of a retic-

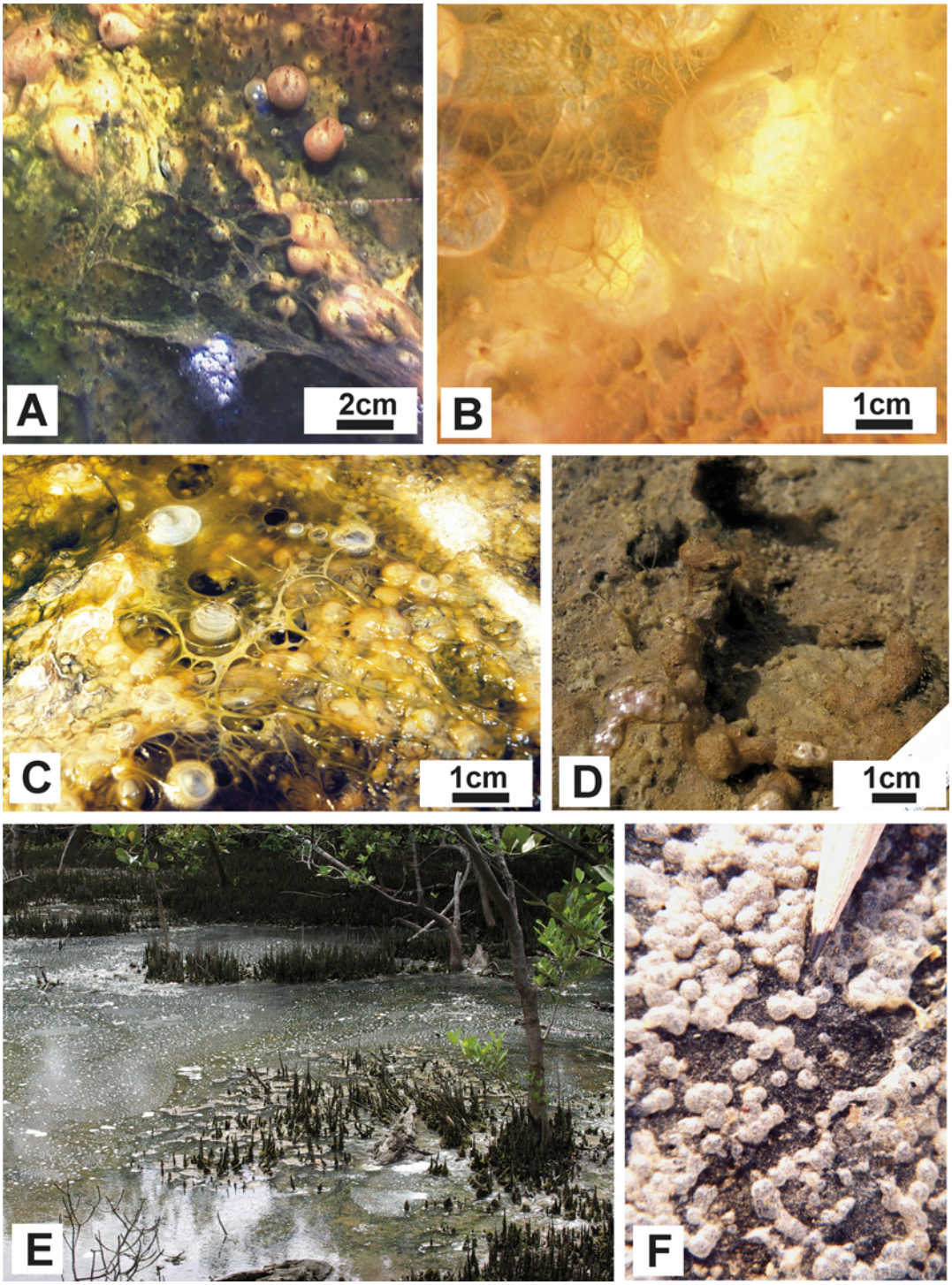


Figure 2-2-1: Mat-confined gas bubbles.
(A) Surface of a shallow water mat built-over by slime threads and bubbles. Bubbles coated by biofilms. Pinnacles grow on bubble surfaces and the basic mat. Photo: K. Bröhldick (colour-adapted). (B) Close-up of bubbles captured by biofilm. In the thin radial ridges and small pinnacles growing on bubble surfaces, small filamentous species (*Spirulina* sp.) are abundant. Photo: E. Ahrensfeld (colour-adapted); modified after photo published in Gerdes and Klenke (2003; courtesy of Assoc. Geoaustria). (C) Three-dimensional scum expanding from the surface of a shallow water mat into the surficial water. Slime-enriched threads, films and bubbles provide various interfaces and three-dimensional spaces for the bacterial front to move into the pelagic realm. Photo: E. Ahrensfeld (colour-adapted); modified after photo published in Gerdes and Klenke (2003; courtesy of Assoc. Geoaustria). (D) Similar three-dimensional structures building over the surface of hypersaline shallow water mats. In biofilms coating bubbles, diatoms are abundant. Reticulate patterns cover bubble surfaces. Deeper holes (centre) favour growth of green-pigmented filamentous mats. Photo: W.-E. Krumbein.

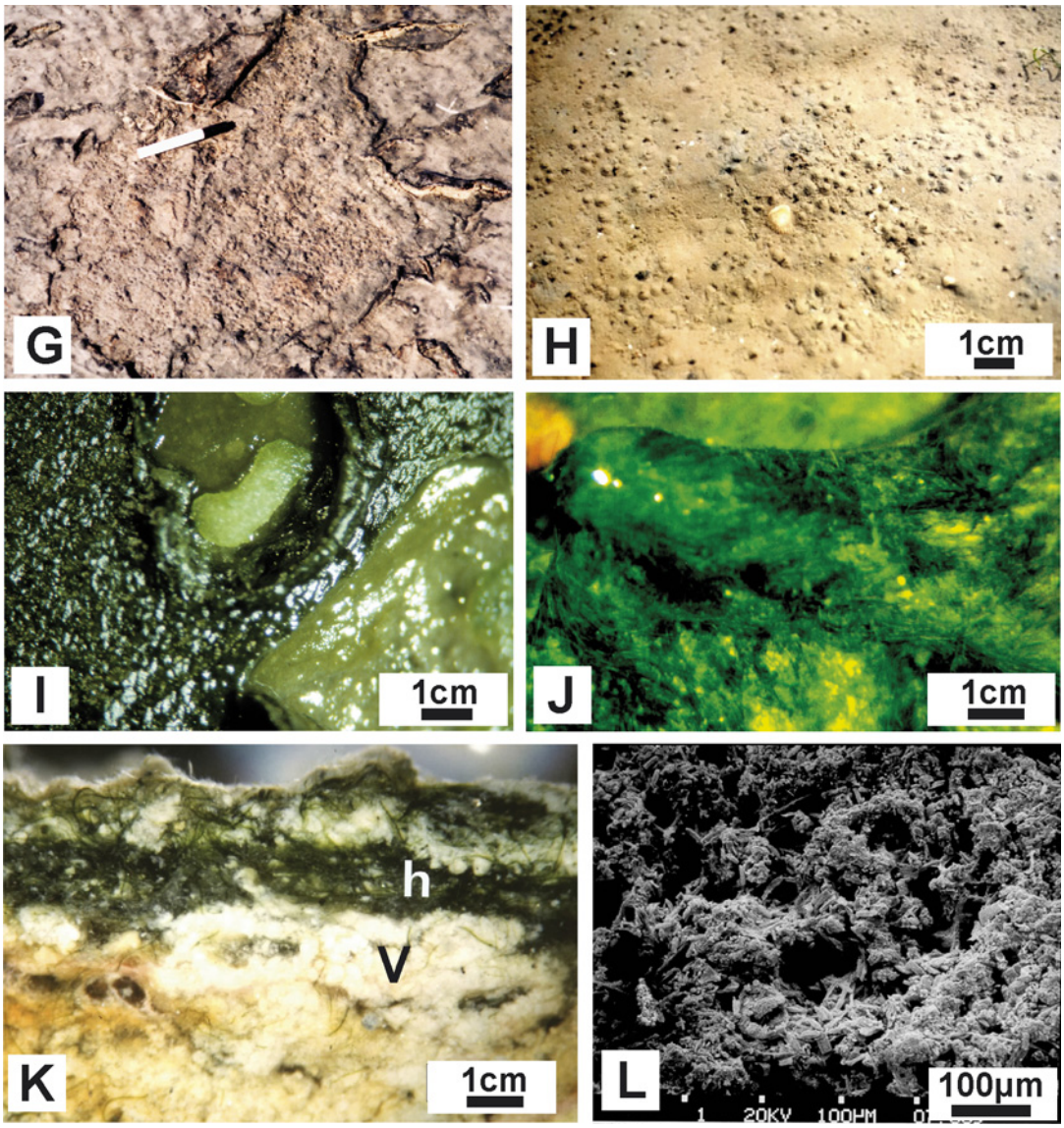


Figure 2-2-1: ***Continued.***

(E) Benthic microbial mats projecting into the water column of a mangal pool using their own metabolic products (bubbles, scums, slimes, flocs) as interfaces for colonisation. Photo: B. Petzelberger. (F) Froth on a dark mat surface left behind after complete evaporation of shallow water stands. Bubbles are 'frozen' by biofilm-coatings. Pencil tip is 1 cm long. Photo: Nora Noffke. (G) Surface of a widely cracked desiccating mat. Blistered crack-bottom indicating subsurface metabolic effects. Mat remains at left and right. Photo: Nora Noffke. (H) Blisters 0.5 to 1 mm high project above a thin cohesive sand layer. Photo: H.-E. Reineck. (I) Blister including a dumbbell-shaped gypsum precipitate embedded in polysaccharide slime (bubble punctured to look inside). Blisters formed by gypsum precipitates are described by Golubic (1973). Photo: Gisela Gerdes. (J) Bubbles producing filamentous meshworks giving rise to pinnacle formation. Photo: Nora Noffke. (K) Cross-section through multilaminated mat surface including horizontally oriented filamentous (h) and vertically extended mat horizons (v). Various bubbles dispersed in the white amorphous organic layer. Photo: Gisela Gerdes. (L) SEM view of internal microbial fabric, containing a small hollow sphere (probably a bubble), surface coated by diatoms, and bacteria producing stabilising slime coating the surface of the sphere. Photo: W.-E. Krumbein; modified after photo published in Gerdes et al. (1994b). *Locality of photos*: A to C – Laboratory-cultured microbial mat; D – Gavish Sabkha, Gulf of Aqaba coast (Egypt), hypersaline sea-marginal ecosystem; E – Icapui mangals, NE Brazil; F – Sabkha Bou Jemel, southern Tunisia; G, J – Bahar Alouane, southern Tunisia; H – Mellum Island, southern North Sea coast (Germany); I – Laboratory-cultured microbial mat; K – saltworks, Bretagne coast (France); L – Solar Lake, Gulf of Aqaba coast (Egypt), hypersaline sea-marginal ecosystem.

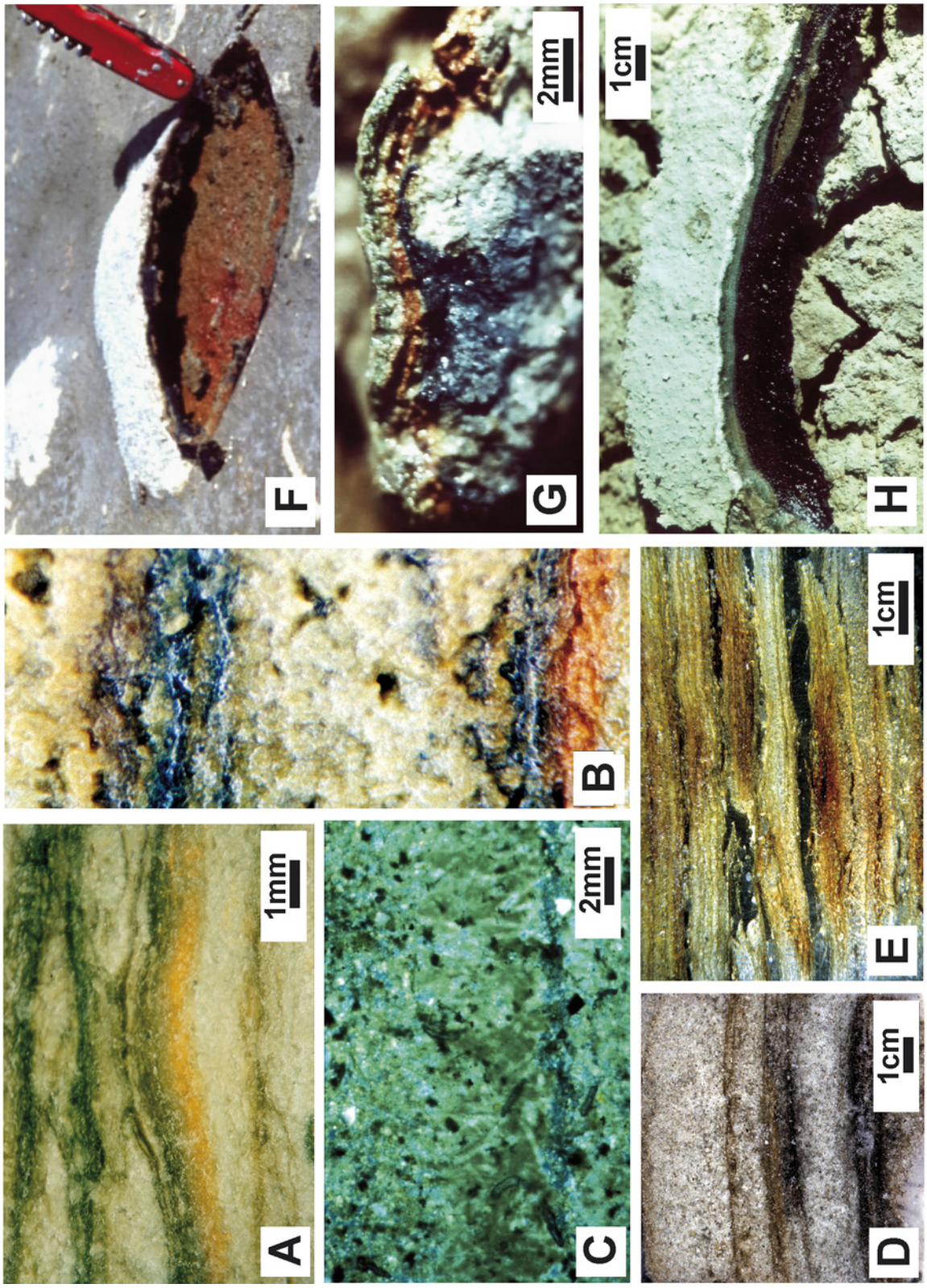

A
1mm
B
C
2mm
D
1cm
E
1cm
F
G
2mm
H
1cm

Figure 2-2-2: Layered iron enrichment.
(A) Cross-section through a filament-dominated surface mat (*M. chthonoplastes* dominant). Iron hydroxide horizon developed below the filamentous photosynthetic mat. Photo: Gisela Gerdes. (B) Deeper core section 5 to 10 cm below aerial surface. Mats enriched in organic matter appear black from ferrous iron (FeS). Lower mat horizon underlain by a ferric iron horizon. Photo: Gisela Gerdes. (C) Thin section microphotograph showing lamina-bound pyrite below a horizon of vertically to diagonally oriented microbial sheaths. Pyrite is also distributed between the sheaths. Photo: Nora Noffke; modified after photo published in Noffke et al. (2003b). (D) Direct scan of a thin section of quartz-sandy tidal flat sediments prepared from deeper core material about 15 cm below aerial surface. Strongly reduced mat horizons (below) reveal metabolic activity of sulphate-reducing bacteria, brownish iron horizons of hydrous iron oxides mimic former microbial mats (above). Photo: R. Kiene. (E) Cross-section through core material showing heterogeneous nucleation sites for metal oxide deposition within biolaminites mixed with clay minerals, ooid grains, microbial cells, sheaths and capsules. Photo: Nora Noffke. (F) Vertical section through an aragonite-covered gas dome developed in a surface mat. The opening allows the view onto the subsurface layer which is coloured by rusty-brown iron-oxide-hydrate. According to the model of iron mobilisation in microbial mats (Schneider and Herrmann, 1980), Fe^{++} (aqu) is able to migrate upwards from pore water within anoxic mats and anaerobic clay, underneath the redox-discontinuity-layer (RDL) and precipitates as Fe^{+++} above the RDL. Photo by courtesy of J. Schneider. (G) Vertical section through wavy microbial mat which covers organics and a clay- like carpet (also termed 'petola' by the salt workers). Blue-green top mat dominated by *M. chthonoplastes*. Rusty-brown layer between top mat and anoxic sediment underneath indicates Fe^{+++} formation above RDL-layer. Salt workers take care to keep the petola intact (for techniques to avoid Fe^{+++} discolouration of NaCl precipitating from brines, see Schneider and Herrmann, 1980). Photo by courtesy of J. Schneider. (H) Parts of the surface (top and below) surrounding a fresh crack (middle) in microbial mat. Note the black reduced material made visible by the crack reaching up to the blue-green cyanobacterial top mat. White cover: aragonite, freshly precipitated from surficial seawater. Photo by courtesy of J. Schneider. *Locality of photos*: A, B – saltworks, Bretagne coast (France); C – Bahar Alouane, southern Tunisia; D – Mellum Island, southern North Sea coast (Germany); E – lagoon of Bou Grara, southern Tunisia; F to H – saltworks, Sečovlje, Gulf of Piran, Slovenia (increasing hypersalinity from F to H).

---

ulated mat texture necessitates time spans in the range of several months during which mats are not disturbed by burial (Gerdes and Klenke, 2003). Knowledge of the tendency of filamentous cyanobacteria to amalgamate into bundles and tangles, to change their growth direction and to produce non-linear growth patterns may help to explain often topographically heterogeneous bounding planes in internal sequences (Figure 2-1-5F).

Involute structures (Figure 2-1-6) may be products of complex interconnected processes which include tactic responses of mat-forming cyanobacteria to surface cracking, increasingly confined space and self-shading due to continual growth (Noffke, 2000). Multilayered crack tapestries may indicate repeated wetting which supplies the micro-organisms with essential water (Figure 2-1-6B). Mats finally protruding above the filled cracks form bulges which mark the former polygonal crack patterns (Figures 2-1-6D to -1-6F).

Features and fabrics related to trapping and binding of sediment (Figure 2-1-7) In life, erect cyanobacterial tufts function as binders and bafflers, providing a trap for sediments, organic debris or calcium carbonate precipitates in the water column (Figure 2-1-7A). Of sedimentological importance is the 'fly paper effect' of sticky mat surfaces which provide traps for detrital grains. Grains providing favourable solids are bound by filaments and thick filament clusters and incorporated into the microbial laminae. Grains trapped and bound by microbial mats aid the upward-directed growth of multilaminated mat sequences (Figure 2-1-7B). The reduction of mechanical friction within the soft matrix surrounding the quartz grains aids the rotation of the grains to an energetically suitable position, resulting in grains orientated with their long axes parallel to the biolaminite (Figure 2-1-7E). In closely packed sediments, gravity-related orientation is not possible (Noffke et al., 1997a). Another effect of trapping and binding is the selection of heavy mineral grains by microbial mat surfaces (Figures 2-1-1B, 2-1-7F).

Ripple overgrowth and nivellement (Figure 2-1-8) In open intertidal flats or beaches, surficial biofilms may relatively rapidly overgrow rippled surfaces during stages of sediment starvation. Preferred sites for initial growth are leeward faces of ripples (Figures 2-1-8A, -1-8B). Such biofilms are not coherent enough to modify the primary physical structures, although stabilisation effects may be possible. At topographically higher or more protected sites, mats are able to increase their surface-modifying productivity. This is depicted in the sequence of photographs in Figures 2-1-8A to -1-8F, from thin initial biofilms to the increase of surficial biomass and finally completely overprinted ripple marks.

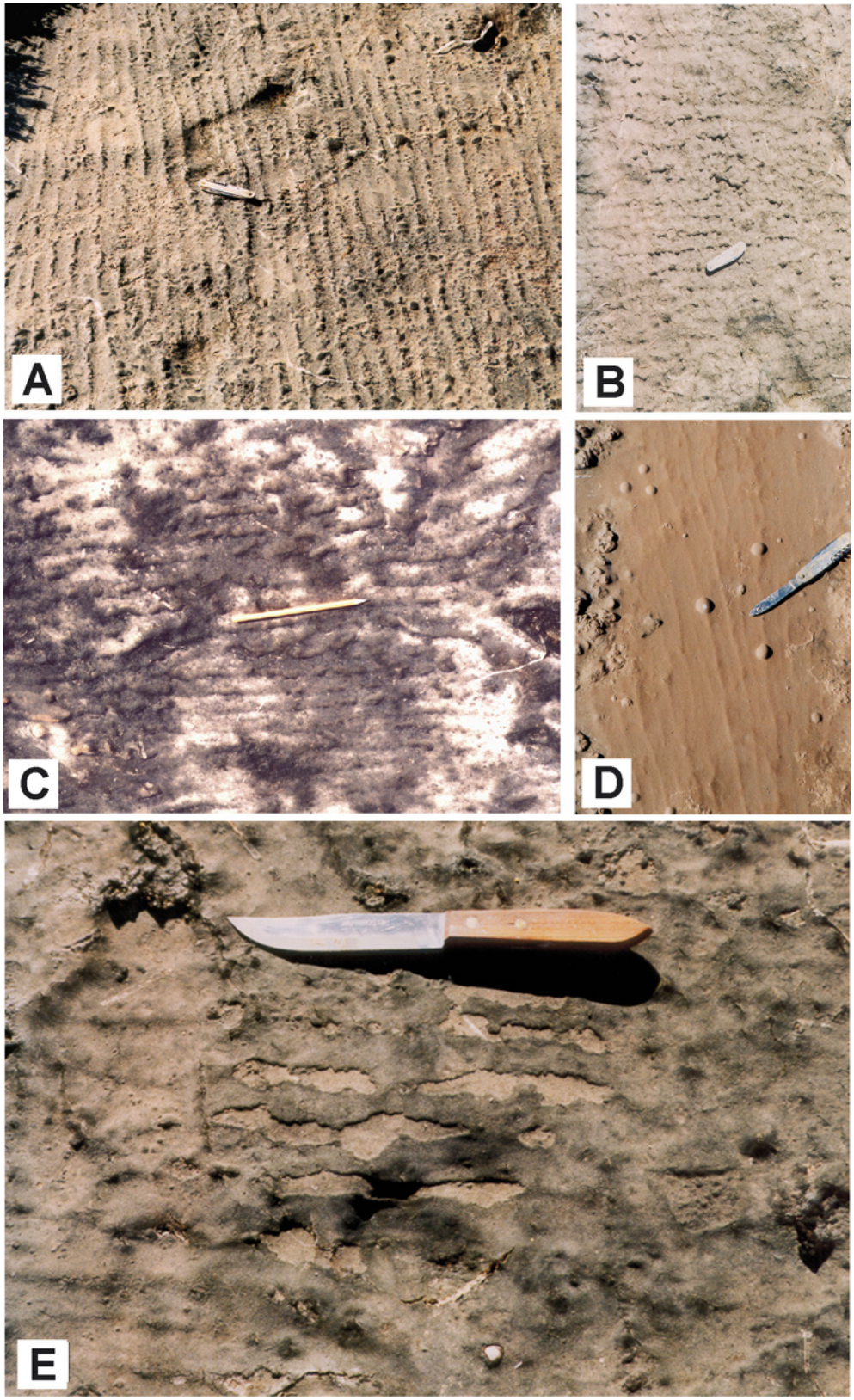


Figure 2-2-3: Patterns resembling '*Kinneyia*'.

(A) Plane surface view of small elongated parallel ridges 0.5 to 1 cm wide, forming a regular pattern. Blisters line the crests. Knife is 8 cm long. Photo: Nora Noffke. (B) Small ridges only a few centimetres in length running only partly parallel to each other, some are curved and merge with adjacent ridges. Trapped blisters again correspond to the crests. Photo: Nora Noffke. (C) Slightly damp surface conditions favour buried mat organisms to overgrow ripples from below. Photo: Nora Noffke. (D) From gently elevated margins occupied by coccoids forming character-

istic cauliflower-like nodules (example at left), microbial slimes moved into the shallow topographic low (centre). Mat extension or slow gravity gliding of the sluggish surface composed of bacteria, slime-agglutinated clay and gypsum may have caused fine elongated folds similar to disturbed table cloths. Gas bubbles from metabolic activities of the mat below are captured by the sluggish surface. Photo: Nora Noffke; modified after photo published in Gerdes et al. (2000a). (E) Cracking taking place along crests of the hollow ridges after drying. Photo: Nora Noffke. *Locality of photos*: A to E – Bahar Alouane, southern Tunisia.

Microbial effects (biostabilisation, trapping, binding sediments) interfering with mechanical reworking are able to produce chaotic ripple patterns (Noffke, 1998a). Sinoidal structures evolving from microbial drapes of ripple troughs and leeward faces are described by Noffke et al. (1997b). Ripple levelling proceeds during longer-lasting periods of non-deposition or non-erosion, in which the mats have the possibility to overprint the surface with thick condensed biomass. Baffling/binding may be a favourable process for ripple levelling (Noffke et al., 2003b).

Features derived from metabolic effects

Closely linked metabolic and decay processes (Figure 2-2-1) Well developed, highly diverse microbial mats represent ecosystems in which both the upward directed primary growth and the degradation of the organic matter are closely linked via biochemicals which are excreted by the one group, used and transformed by the other (Stal, 1994). In dealing with product–process relationships, it is thus not easy to make a clear separation between features/structures related to metabolic effects, and those related to mat decay. An example is the precipitation of calcium carbonate in microbial mats, which may be seen in relation to cyanobacterial taxa controlling calcification processes directly (Merz, 1992), or in relation to autotrophic CO_2 depletion, or to heterotrophic pathways in which numerous bacterial groups through degradation of the organic substrates passively create the chemical milieu for carbonate precipitation (Castanier et al., 2000; Schneider and Le Campion-Alsumard, 1999). Friedman et al. (1992) stated that a sedimentary product "itself might not convey information pointing to a single specific process". This should be kept in mind when looking only for a single explanation of structures, such as the bubbles shown in Figure 2-2-1, but also almost throughout the other figures shown in this contribution.

Bubbles may be encountered with various metabolic activities. Processes concerning carbon and sulphur metabolism take place even in the topmost few millimetres of mats, photosynthesis occurring simultaneously with respiratory reactions. Sulphate reduction occurs at high rates in close proximity to, or even within, the phototrophic zone of microbial mats (Skyring et al., 1989). Even oxygen and hydrogen sulphide can coexist in high concentrations for extended periods of time, probably caused by the low diffusivity of gases through cyanobacterial slimes (Krumbein et al., 1979b). Bubbles resulting from the activity of various physiologic groups may thus contain O_2, CO_2, H_2S or CH_4.

In shallow water environments, photic conditions are also modified by diffusion processes across the sediment–water interface making the overstanding water viscous and 'sticky' (Jørgensen, 1994). Slime-captured bubbles, threads and flocs contribute to shading which may support pelagic propagation of biofilms above the benthic mats (Figures 2-2-1A to -2-1E). The heterogeneous three-dimensional structures may contribute to topographically heterogeneous microbial laminae within internal sediments.

Subaerially exposed surfaces generate bubbles if surface sediments are sludgy from microbial slimes which slow down diffusion of gases. Sludgy sediments or gypsum mush glued together by microbial slimes also capture bubbles, giving rise to blistered sedimentary surfaces (Figure 2-2-1F). Sulphate nodules embedded in microbial mats may result from metabolic activity of chemolithotrophs or sulphur bacteria (Figure 2-2-1I). Internal bubbles may also provide nuclei for carbonate precipitation.

Iron precipitation in mats (Figure 2-2-2) Black iron sulphide deposits are particularly significant in coastal microbial mats in which sulphate-reducing bacteria are active (Figure 2-2-2H). Cores taken from microbial sediments usually show the dark colours of reduction almost up to the surface, eventually topped by red and green zones indicating anoxygenic and oxygenic photosynthesis. Immediately below mats dominated by *Microcoleus chthonoplastes*, sharp layers of iron hydroxides are sometimes obvious (Figure 2-2-2A, see also Figure 2-1-7B). According to Stal (1994), *M. chthonoplastes* is capable of binding iron to the polysaccharide sheaths where the iron is reduced concomitant with its binding. This same author reports advantages of this process for the organisms: (i) binding and reduction of iron makes this element available for metabolic processes; (ii) since ferrous iron reacts rapidly

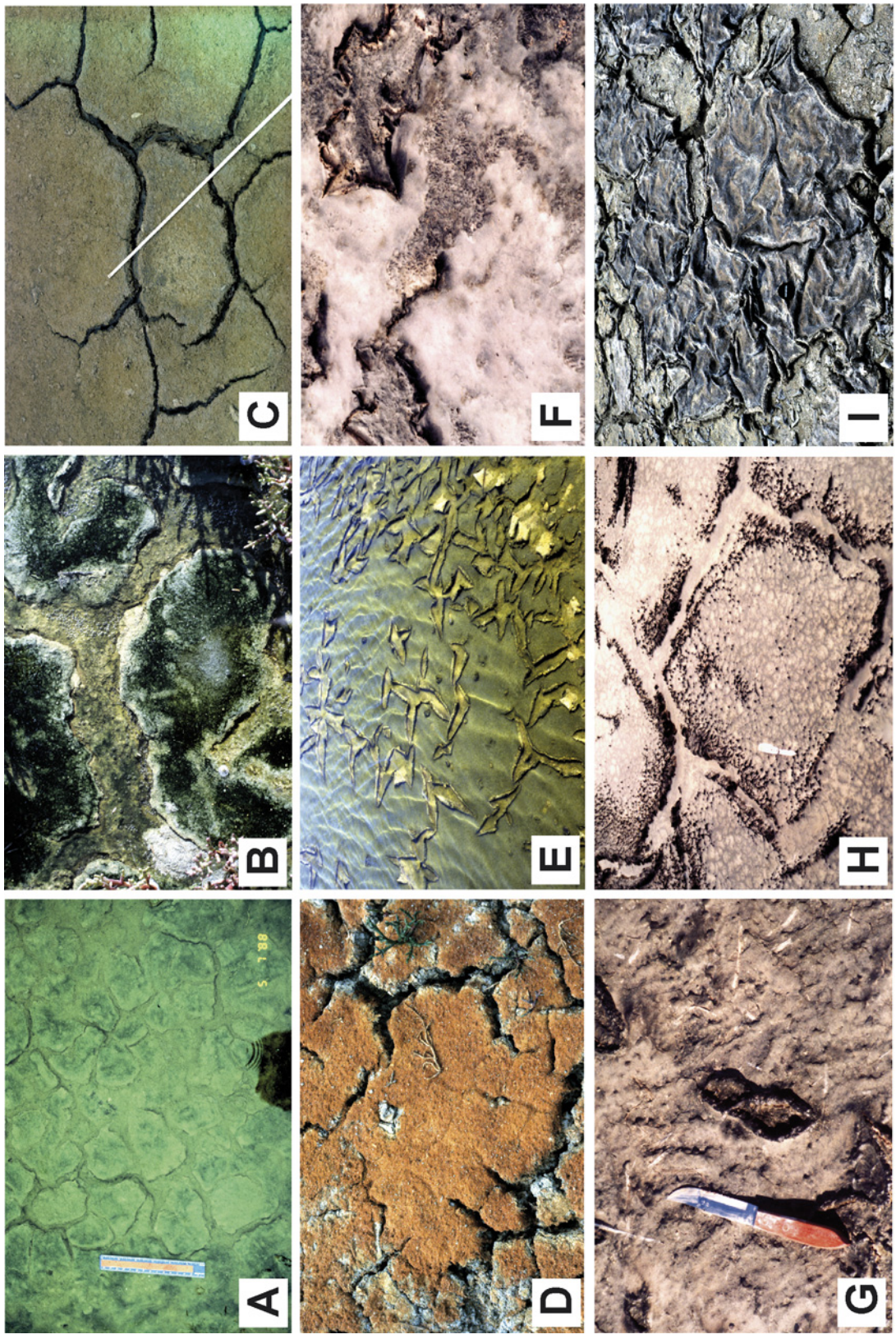

A
B
C
D
E
F
G
H
I

Figure 2-3-1: Shrinkage cracks.
(A) Polygonal cracks in a thin microbial mat growing on quartz-sandy tidal flats. Sand base exposed by widely spaced cracks, clefts re-colonised by microbial films after re-wetting. Photo: H.-E. Reineck. (B) Polygonal cracks in a thin microbial mat growing on a mixture of clay and gypsum mush. Widely spaced cracks expose the underlying sediment. Oxygen bubbles in the cracks indicate photosynthetic activity of biofilms after flooding. Photo: J. Gifford. (C) Cracks within a thick microbial mat growing on clay. Compare deep-reaching cracks and narrow clefts with wide shallow cracks in thin mats – B. Photo: J. Gifford. (D) Partly incomplete cracks within a thick microbial mat, polygon surfaces covered by filaments coated by iron oxides during drying. Filamentous meshwork triggered crack patterns, similar to tearing blotting paper. Photo: J. Gifford. (E) Subaqueous clay and gypsum sediment covered by a thin mat loosely attached to the substrate. Spindle-like cracks caused by bird traces. Photo: J. Gifford. (F) Unusual kind of non-orthogonal, incomplete cracks formed in a mixture of terrestrial mud and gypsum glued together by microbial slimes (surface sediments are white smooth areas). Crack resembles a bird's foot; note the curled-up edges. Photo: Nora Noffke. (G) Crack morphology resembling a bird's foot, developed in pseudo-rippled and blistered surface patterns of a mat (table cloth-like features, see Figure 2-2-3). Knife is 20 cm long. Photo: Nora Noffke. (H) Widely spaced polygonal cracks, margins elevated due to microbial bulges (see Figure 2-1-6) and contoured by pinnacles (Figure 2-1-4) confined to polygon edges. Reticulate patterns (Figure 2-1-5) shimmer through a mixture of salt crystals and microbial slimes covering polygon surfaces. Knife is 15 cm long. Photo: Nora Noffke; modified after photo published in Gerdes et al. (2000a). (I) Surface of a desiccated and cracked mat, with shrinkage exposing the clay mineral substrate marked by orthogonal cracks, while the overlying mat shows unusual crack morphologies, incomplete fissures, folds and upcurled margins. Abandoned salina basin (lens cap = 5 cm in diameter). Photo: H.-E. Reineck. *Locality of photos*: A – Mellum Island, southern North Sea coast (Germany); B to E – saltworks, Bretagne coast (France); F, G – Bahar Alouane, southern Tunisia; H – Sabkha Bou Jemel, southern Tunisia; I – saltworks, Lanzarote, Canary Islands (Spain).

---

with oxygen, the accumulation of ferrous iron in the immediate vicinity of the cell may keep oxygen partial pressure low. This enhances the efficiency of CO_2 fixation and limits photorespiration; (iii) in the view of community metabolism, ferric hydroxides underneath the cyanobacterial layer may function as barriers protecting the overlying cyanobacteria from sulphide which is produced in the deeper anoxic layers, as well as preventing oxygen from reaching the anaerobic microbial community.

Physio-ecologic processes in mats certainly interact with physico-chemical dynamics proceeding across sharp redox gradients which are characteristic of multilayered microbial mats. Schneider and Herrmann (1980) developed the model of iron mobilisation from underlying anoxic layers giving rise to sharp layers of iron hydroxides below photosynthetic active mats (Figures 2-2-2F and -2-2G). Evaporation pumping may support upwards-directed pore water flows, whereas strongly entangled meshworks dominated by *M. chthonoplastes* or similar morphotypes may slow down the pore water flow so that iron hydroxide can precipitate below.

Finally it should be noted that rusty-brown iron hydroxide horizons may also develop after cross-cutting of fresh material which opens oxygen windows. The ferrous iron enriched in buried microbial mats reacts rapidly with the oxygen. Therefore, it cannot be excluded that the rusty-brown iron hydroxide horizons in Figures 2-2-2B, -2-2D and -2-2E might be preparative artefacts.

Sulphate-reduction starts immediately within decaying mats, giving rise to lamina-specific pyrite arrangements (Figures 2-2-2B and -2-2C). Also, ferric iron reacting with sulphide may result in the formation of stable pyrite (Stal, 1994).

Wind-derived ripples in microbial slime-sediment sludge (Figure 2-2-3) Ripples are characteristic features of sabkha sediments agglutinated by microbial slimes and precipitating salts. The structures in Figure 2-2-3 were observed on higher-lying parts of coastal sabkhas where coccoid cyanobacteria (*Aphanocapsa* sp., *Gloeothece* sp.) dominated the surface mats. Gavish et al. (1985) described hollow ripple structures folded like table cloths by wind. Locally also, subsidence of the slushy sediment down a gentle slope may produce similar folds. Photosynthetic gas bubbles captured in the slime are aligned by the ripples. Gas from decay also may be involved since decay may start already within the uppermost centimetres of a mat (Stal, 1994). Pflüger (1999) mentioned that '*Kinneyia*'-style ripples may reflect gas-trapping beneath flat mats. Yet the aligned bubbles in Figure 2-2-3 mark ripple crests, while Pflüger (1999) indicates that trapped bubbles correspond to the troughs of '*Kinneyia*'.

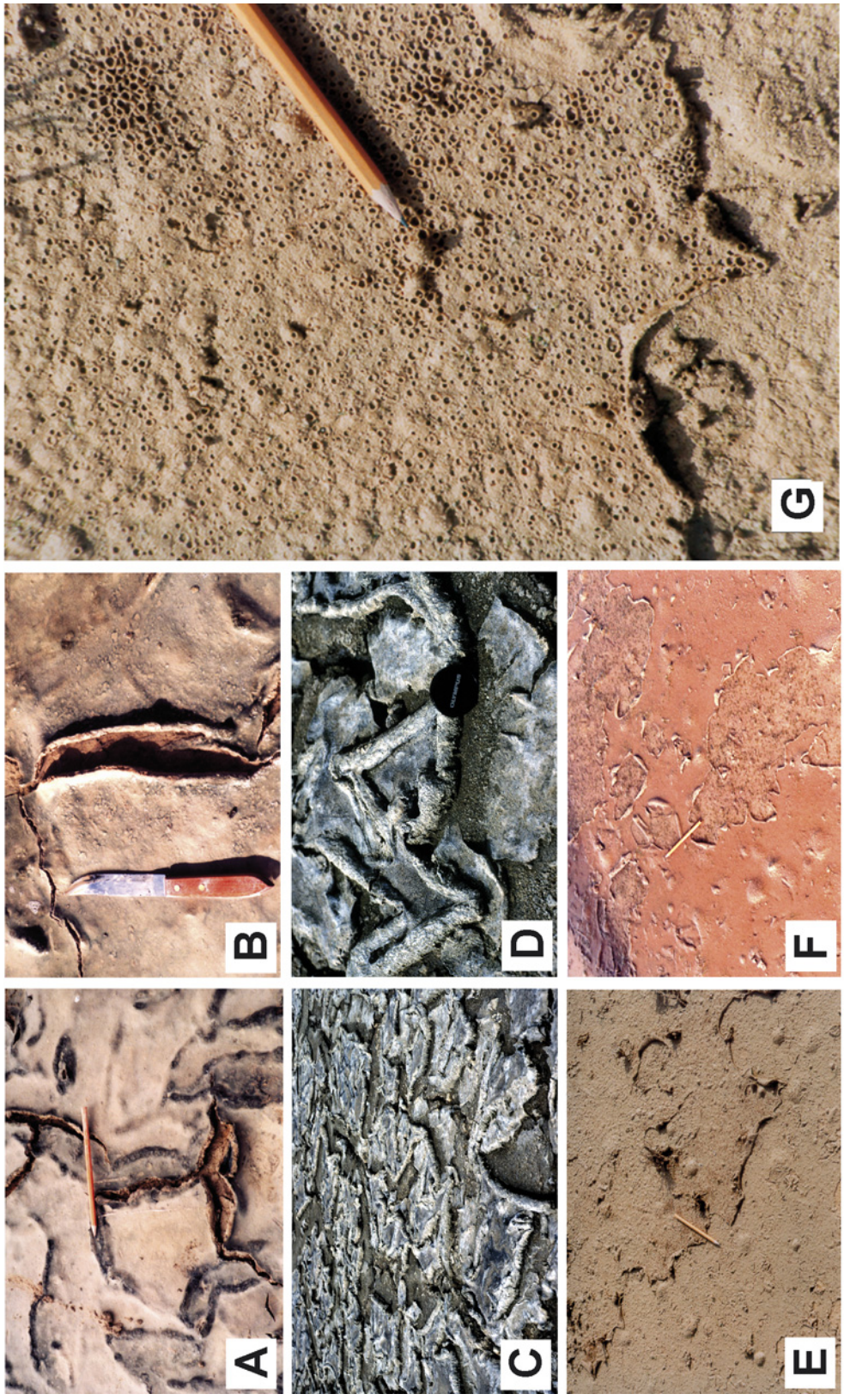

A
B
C
D
E
F
G

Figure 2-3-2: Jelly-rolls, flip-overs.
(A) Healed-up and new spindle-like cracks in jelly mats dominated by coccoids and enriched in slime-agglutinated gypsum (white areas). Note healed-up cracks guiding new crack directions. Crack margins roll up tightly as they dry. The rusty red colour underneath may be due to the precipitation of iron hydroxides above the RDL layer. Pencil = 17 cm in length. Photo: Nora Noffke. (B) Close-up of elongated spindle-like crack, margins rolled-up (knife is 20 cm long). Photo: Nora Noffke. (C) Surface patterns of a desiccated and widely cracked microbial mat loosely attached to the substrate, polygon margins rolled-up after drying (lens cap = 5 cm in diameter). Photo: H.-E. Reineck. (D) Close-up of C: crack margins giving rise to mat curls. Photo: H.-E. Reineck; modified after photo published in Gerdes et al. (1993). (E) Jelly surficial biofilm has cracked due to drying; gas bubbles indicate metabolic activity of mat-forming organisms (similar occurrences revealed contents of CO_2 and CH_4 within the bubbles; J. Schneider, personal comm., 2006). Pencil in E–G = 17 cm in length. Photo: Nora Noffke. (F) Similar biofilm as in E. Gas bubbles aerating the jelly mat from below may support mat detachment. Upcurled margins producing jelly-rolls, some on top of the mat. Photo: Nora Noffke. (G) Edges of loosely attached biofilm partly flipped-over and rolled up. Flip-over exposing mat underside, the jelly material being occupied by various burst-open bubbles supporting detachment processes. Photo: Nora Noffke. *Locality of photos*: A, F – Sabkha Amchoun, southern Tunisia; B – Sabkha Bou Jemel, southern Tunisia; C, D – saltworks of Lanzarote, Canary Islands (Spain); E, G – Sidi Slim, Djerba, southern Tunisia.

Features derived from physical mat destruction

Presence of mats changes the rules (Figure 2-3-1) The rule that cracks do not form in pure sand does not hold true where microbial mats are abundant. Thus, fossil records of shrunken sand layers must have had an additional component that could shrink during dehydration, a microbial substrate being the most likely candidate (Schieber, 2004). Also, the rule that large cracks develop in thick and smaller cracks in thin surface beds does not hold true where microbial mats are abundant. Thin microbial mats are able to produce extraordinarily wide cracks (Figures 2-3-1A to -3-1E).

The presence of a mat may be indicated by multiple incomplete sub-fracturing of crack margins, imparting cauliflower-like patterns (Figure 2-3-1D). The fibrillar network of filamentous cyanobacteria controls irregular and incomplete sub-fracturing, giving rise to blotting paper effects (Gerdes et al., 1993). Viscous microbial mats experience particularly high reduction of surface volume owing to dehydration or desiccation (Figure 2-3-1E, see also Figures 2-4-4B, -4-4C).

Slippery sediments effectively prevent attachment. Mats easily scour and tear, or are moved due to wind or water stress. In quartz sand, on the other hand, characteristic biodyctions develop (Figure 2-1-1C) which effectively intertwine with the sand grains and are far less removable than mats on slippery clay (Figure 2-4-4B) or evaporites (Figure 2-3-1E, see also Figures 2-3-2E to -3-2G and Figure 2-4-4C).

The bottom of an abandoned salina basin shows well the difference between crack morphologies in clay and microbial mats. In the underlying clay, cracks are orthogonal, while volume reduction in the elastic surface mat has left behind irregular and partly incomplete polygons showing folds and upcurled margins (Figure 2-3-1I).

In higher parts of a supratidal setting, unusual crack morphologies have been observed supported by the flexible behaviour of surface sediments made viscous and sticky by microbial slimes (Figures 2-3-1F, -3-1G, see also Figures 2-3-2A, -3-2B). Mats naturally include various defects and local thickness variations which may also explain unusual rupturing. Also, healed-up former cracks provide such local unevenness (Figure 2-3-2A).

Specific milieu conditions within the cracks attract organisms from adjacent mats to invade the cracks where they benefit from damp conditions and additional space for attachment. Results are rounded edges and pillow structures (Figure 2-1-6).

Desiccation and curling-up edges of cracks, jelly rolls (Figure 2-3-2) Figure 2-3-2 reflects the cohesive behaviour of soft and jelly-like surfaces of microbial origin. Schieber (1999) emphasises the flexible behaviour of soft mats when rolled up and transported by currents. Such overfolded rolled up fragments also help to distinguish cohesion due to microbial binding from cohesion caused by synsedimentary cementation (Schieber, 1999). The patterns in Figure 2-3-2 may belong to a similar category of features known as ‘jelly-roll’ structures, which

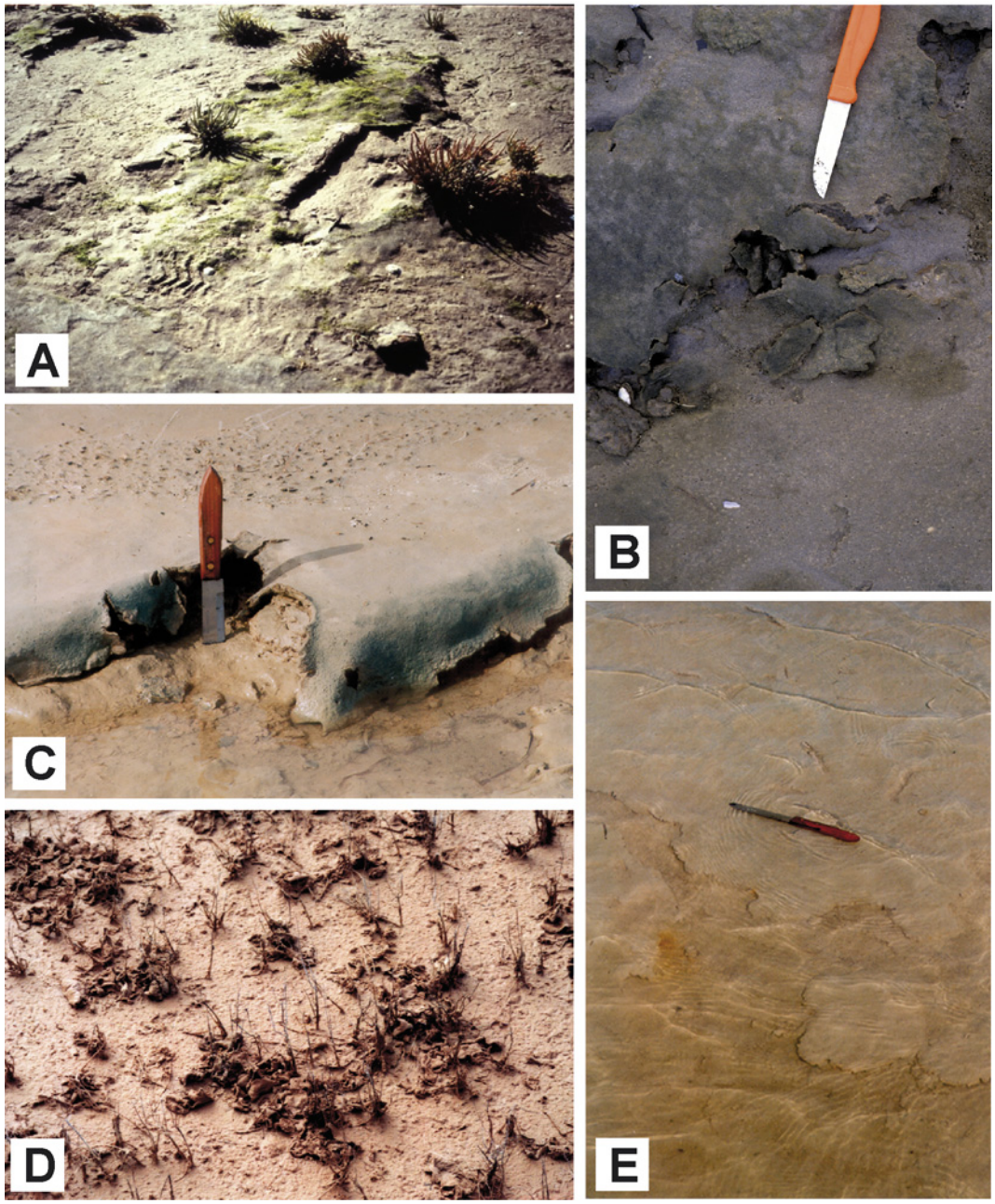


Figure 2-3-3: Erosional edges, mat chips.
(A) Microbial mat hanging over the edge of an erosional depression (right) giving rise to the genesis of mat chips (biostabilised quartz-sandy tidal flats). Photo: Nora Noffke. (B) Microbial sand chips drop off the undermined mat (knife is 20 cm long). Photo: Nora Noffke. (C) Coherent mat made of coccoidal and filamentous cyanobacteria hangs over a small terraced cliff undermined by water agitation. Structure marking the shoreline of a hypersaline lagoon. Some mat chips lie upside down on muddy substrate of the lower terrace. Photo: Nora Noffke. (D) Microbial mat chips accumulating behind stands of halophytes. Photo: Nora Noffke. (E) Subaqueous erosion-edge of mat, and reworking of mat; loose and thin mats growing on soft muddy sediments producing fragile mat chips. Photo: Nora Noffke. *Locality of photos*: A, B – Mellum Island, southern North Sea coast (Germany); C – Sabkha Bou Jemel, southern Tunisia; D – Sidi Slim, Djerba, southern Tunisia; E – Sabkha Bou Jemel, southern Tunisia.

have been described from Phanerozoic carbonates (Demicco and Hardie, 1994, cited in Simonson and Carney, 1999).

Variety of conditions involved in chip production (Figure 2-3-3) Cohesiveness of advanced stages of microbial mats is particularly obvious at erosional edges (Figure 2-3-3). Margins undermined by currents tear and become

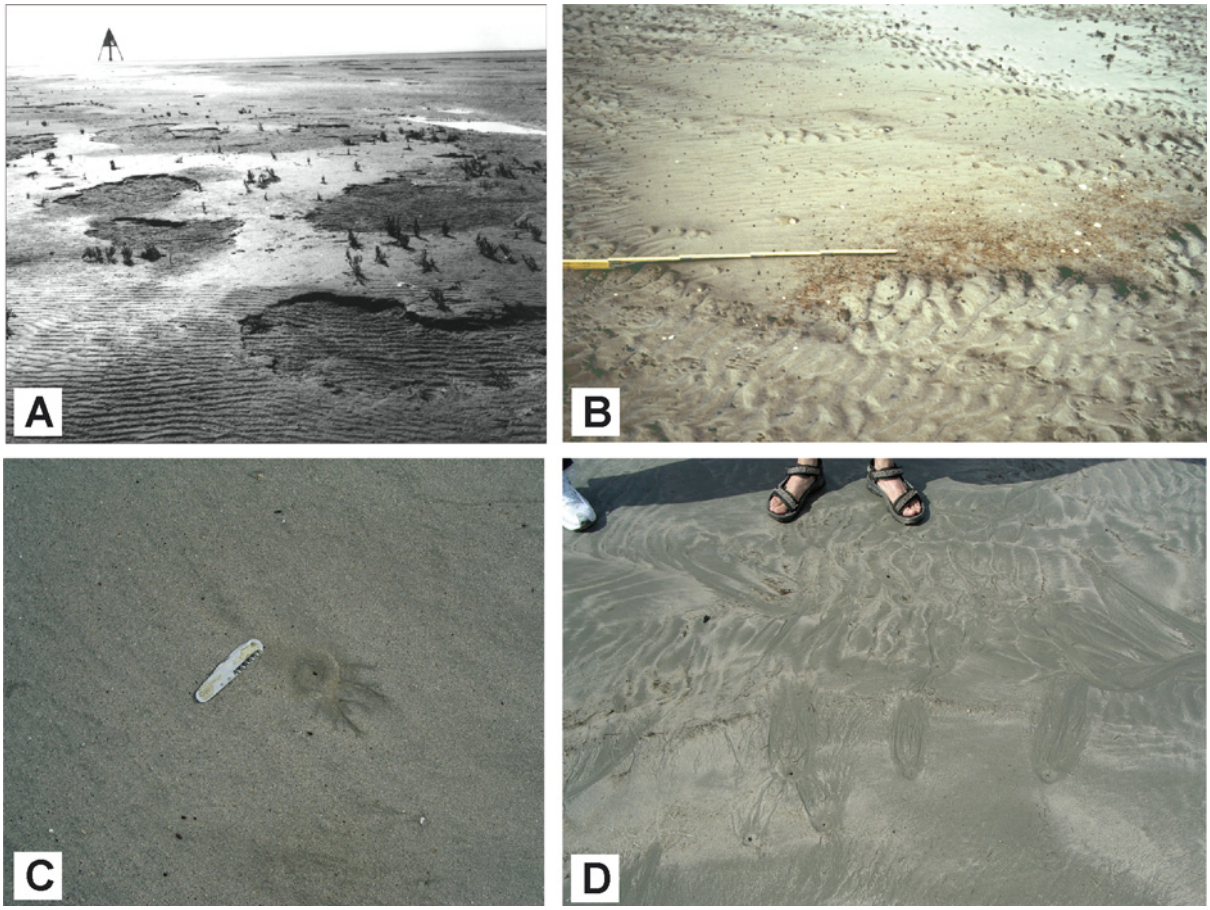


Figure 2-3-4: Ripple patches, '*Astropolithon*'-like features.
(A) Slightly rounded, rippled depressions of about 10 to 50 cm diameter on microbial mat-stabilised siliciclastic tidal flats. Photo: H.-E. Reineck; modified after photo published in Reineck (1979). (B) Transition from the non-eroded biostabilised surface into a ripple patch; ripple crests merge laterally with the non-eroded surface. Eroded worm tubes at the margins. Photo: Nora Noffke. (C) Individual '*Astropolithon*'-like feature on the surface of an intertidal beach: flat bulge rising on top of beach sand, central vertical pipe and dykes radiating from the central pipe. Host sediments are medium-grained quartz-sandy beach sands bound by a thin biofilm (knife is 8 cm long). Photo: B. Petzelberger. (D) Similar locality to that shown in C, but slightly different morphology of a series of sand volcanoes across a steeper part of the intertidal beach, showing radiating dykes closer together than in C. Photo: B. Petzelberger. *Locality of photos*: A, B – Mellum Island, southern North Sea coast (Germany); C, D – Jericoacoara beach, NE Brazil.

fringed (Figures 2-3-3A to -3-3C). Such conditions, but also mat cracking (Figure 2-3-1), jelly rolls (Figure 2-3-2) or gas from the subsoil may give rise to the genesis of mat chips. Chip characters depend on (i) mat types, (ii) substrate types, (iii) forces which release the chips, (iv) source area, (v) depositional areas. Main *mat types* as presented here include fibrillar microbial meshworks strongly entangled with the subsediment (Figure 2-1-1C), or loose, often monolayered mats enriched in hydroplastic gel (Figure 2-3-2). During decay, single-layered, often scummy mats get peeled-off piece by piece from the substrate, by moving water. The *substrate* determines the efficiency of entanglement of biofilm organisms with the subsoil. Entanglement seems to be less effective in clay or slippery gypsum mush (Figure 2-3-2). *Forces* which release mats from the subground include erosion by currents or wind, desiccation and subsequent erosion, or gas pressing from below on to the surface mats. *Source areas* of chips can be various (as are formational sites of cyanobacterial mats). Finally *depositional areas* of chips may be far away from source areas, e.g., towards deep subtidal zones. Particularly flake-like chips are easily transported. Wind transport of dry chips also provides 'meteor paper' (Krumbein et al., 2003).

Erosive forces acting upon biostabilized sediment surfaces (Figure 2-3-4) Ripple patches in microbial mat-stabilised sand flats (Figure 2-3-4A) are caused by tide-controlled waves and currents which act upon the sedimentary surface. Although microbial films and mats attenuate the effects of erosive forces, the protective biofilm

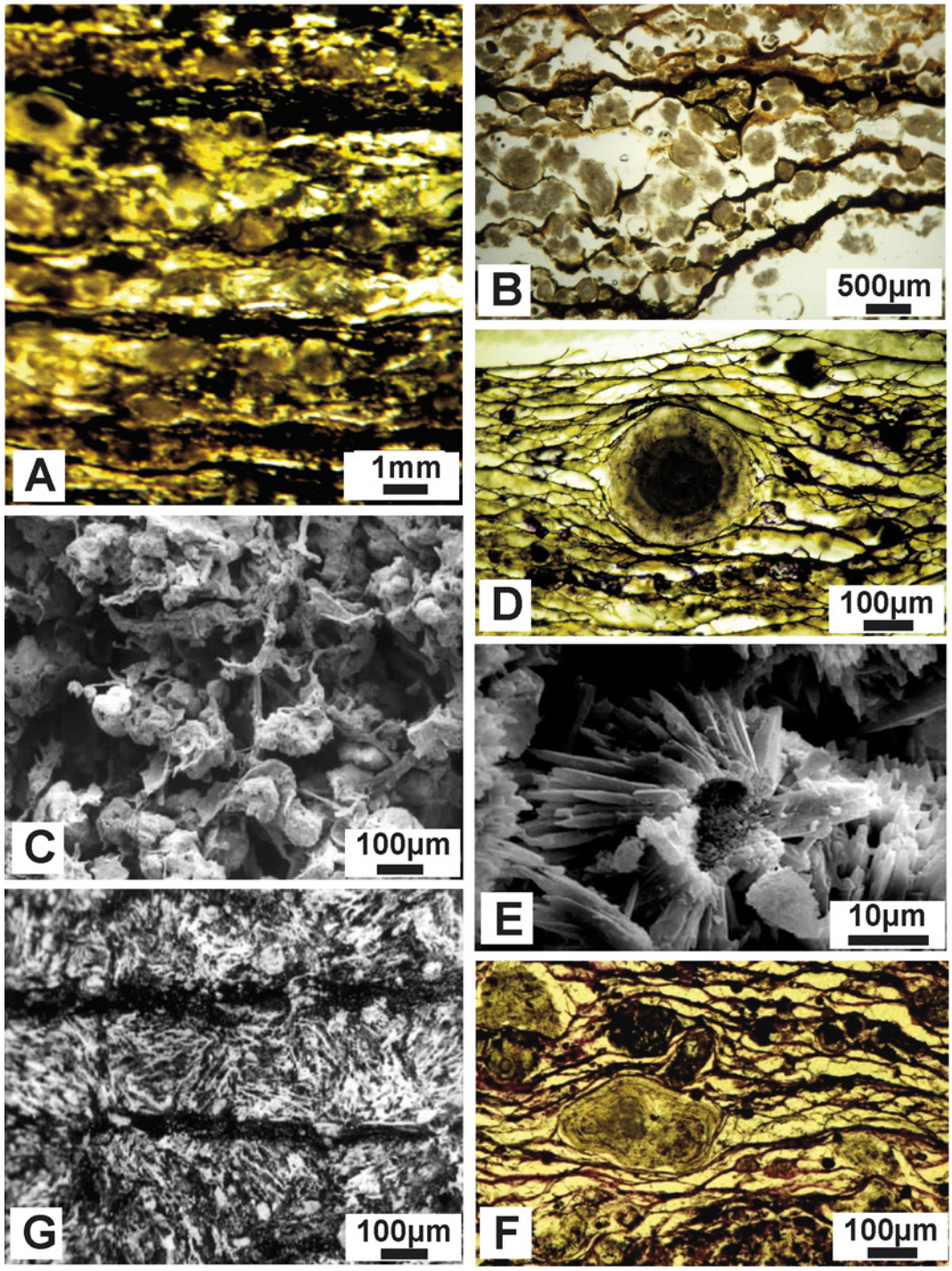


Figure 2-4-1: *In situ* carbonate precipitation in evaporite microbial sediments.

(A) Cross-section through growth-bedding (see Figure 2-1-2) containing lamina-specific arrangements of carbonate grains, biogeochemically formed *in situ*. Photo: Gisela Gerdes. (B) Banded arrangement of granular carbonate inclusions in plastic microbial mats. Photo: Gisela Gerdes; modified after photo published in Gerdes et al. (2000b). (C) SEM view of grape-like peloids attached to fragments of microbial mats. Photo: Gisela Gerdes; modified after photo published in Gerdes et al. (1994b). (D) Section across cortoid-like particle showing opaque nucleus and translucent rim made of fibrous cement, organic matter scattered between aragonite crystals. Particle growth within elastic microbial meshwork gives rise to 'sedimentary augen structure' (indications of compressed laminae at top and bottom of the particle and strained laminae to left and right). Photo: K. Dunajtschik-Piewak. (E) SEM view of internal mat fabric showing hollow nucleus surrounded by radial aragonite. Photo: W.-E. Krumbein. (F) Cross-section showing filamentous meshwork containing carbonate particles of various shapes and sizes. Centre: composite grain showing inclusions of microbial lumps or non-finished particles surrounded by a superficial coating,

similar to botryoidal lumps. Photo: K. Dunajtschik-Piewak. (G) Vertical section showing extended light laminae (summer generations, see Figure 2-1-2) interspersed with sheaths in diagonal to vertical orientation coated by calcium carbonate ('frozen' filaments). Photo: Gisela Gerdes; modified after photo published in Gerdes and Krumbein (1987). *Locality of photos*: A, E – Solar Lake, Gulf of Aqaba coast (Egypt), hypersaline sea-marginal ecosystem; B to D, F – saltworks of Lanzarote, Canary Islands (Spain); G – Gavish Sabkha, Gulf of Aqaba coast (Egypt), hypersaline sea-marginal ecosystem.

---

may be destroyed locally where obstacles (e.g., skeletal hard parts) lying in the path of currents, or storm surges cause vortices and small-scale rip currents (Gerdes et al., 1993; Noffke, 1999). Where microbial binding is lacking, the unsecured sand becomes rippled. Ancient examples have been reported from the Cretaceous Dakota Sandstone (Reineck, 1979) and from various units in the Belt Supergroup (Schieber, 1998a). The shape of such ripple patches is strikingly different from obstacle marks, which occur in sediments lacking biofilms or mats. The features cannot readily be confused with weathering of a fossil bedding plane through which a lower rippled layer is laid free (Schieber, 1999). In case of such 'windows', there will be a sharp break between the rippled subground and the remaining cover. In contrast, ripple patches evolving from partial mat erosion exhibit smooth transitions between the ripples and the margins of the remaining surface mat (Figure 2-3-4B).

Sediment volcanoes ('*Astropolithon*'; Dawson, 1878) are associated with the expulsion of water from sediment as a result of slumping, very rapid sedimentation, or agitation of freshly deposited sediment (Reineck and Singh, 1980). According to Pflüger (1999) and Seilacher and Goldring (1996), such structures can only form in cohesive host sediment, e.g., microbially bound sand (Figures 2-3-4C, -3-4D).

Features derived from mat decay and post-burial effects

In situ carbonates (Figure 2-4-1) Against the background of the introductory remarks in this chapter, it seems acceptable to subsume carbonate precipitates in Figure 2-4-1 under features derived from mat decay and post-burial effects. Genesis, form, size and arrangement of carbonate precipitates are strongly influenced by the members of the mat community and internal heterogeneous micro-textures. Various studies have associated *in situ* calcium carbonate precipitation in mats with degradation of biomass in zones containing purple bacteria and heterotrophic bacteria (Kühl et al., 2003, for discussion). The distribution of precipitates seems not to be random, and features evolving from microbial coating of mineral particles indicate active growth response of microbial inhabitants to interfaces (Gerdes et al., 1994a). Granular carbonates in plastic gel (Figure 2-4-1D) form around nuclei which may have been cells or cell clusters, liquid or gaseous bubbles, or tissue remains of mats. Growth-bedding confines particles into a layered appearance (Figure 2-4-1A). Different particle types coexist in microbial mats, including peloids, ooids or botryoidal lumps (Figures 2-4-1B to -4-1F). The term 'sedimentary augen structure' (Dahanayake et al., 1985) denotes fabrics owing their structures to interaction of particle growth and elastic response of filamentous mats (Figure 2-4-1D). Ooids are common where individual nucleation centres are isolated in the viscous gel or between filamentous laminae. Metabolic vesicles or bubbles may also provide adequate interfaces for bacterial attachment and subsequent carbonate precipitation (Figure 2-4-1E). Botryoidal forms (Figure 2-4-1F) reflect amalgamation of carbonate precipitates in close proximity, surrounded by microbially active biogenic substrates. Over-riding processes triggered by seasonal cycles of environmental variables are recorded in the vertical section in Figure 2-4-1G. The vertically to diagonally oriented filaments demonstrate active movements of filamentous cyanobacteria, encrustation in life position and death with progressing mineralisation.

In situ carbonate precipitates of biogeochemical origin usually reveal heterogeneous distribution patterns within the mat fabrics (Figures 2-4-1A to -4-1G). On the other hand, inorganic carbonate crystallisation from brines is also possible (Schneider and Herrmann, 1980). Results are homogeneous white layers covering the mat surfaces as indicated in Figures 2-2-2F to -2-2H.

Surface sealing by mats interacting with post-burial gas production (Figures 2-4-2 and 2-4-3) Fenestral fabrics (Figure 2-4-2) are closely related to the deformation of primary fabrics and cohesive bedding planes owing to the pressure of gas released from deeper buried organic matter. Gas pressure greater than the resistance of the sediment grains results in the formation of secondary voids (Noffke et al., 1997b). Fenestrae arranged concordant to biolaminites (Figures 2-4-2A, -4-2C, -4-2D) are a consequence of the sealing effect of buried mats, connected with compaction of subspherical gas bubbles (Flügel, 2004). Interactive gas pressure from decaying organic material and surface sealing by mats also cause lifting and separation of mat surfaces from the adjacent sediment (Figures 2-4-2E and 2-2-2F; Logan et al., 1974).

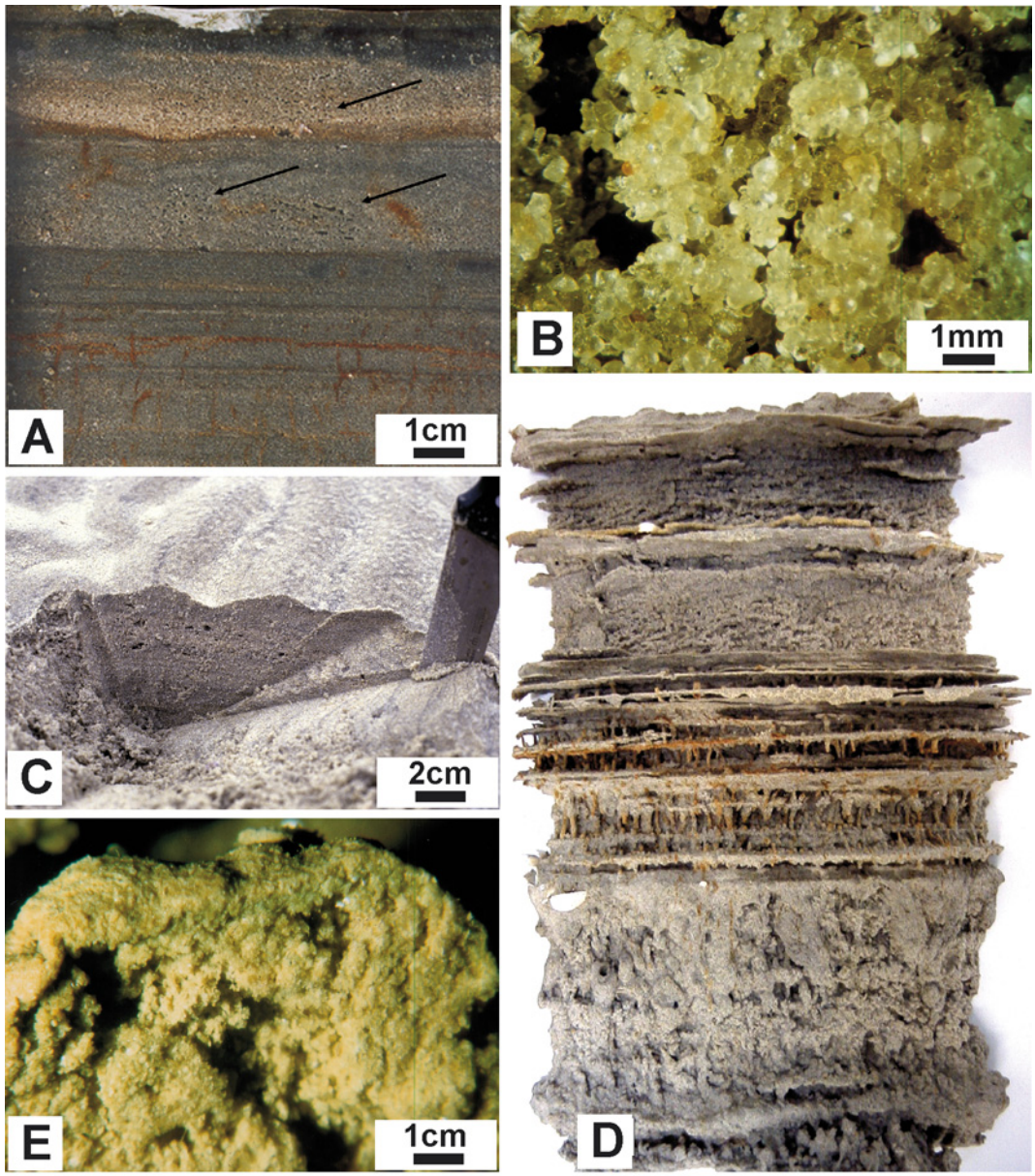


Figure 2-4-2: Fenestral fabrics.
(A) Vertical section through biolaminites embedded in siliciclastic sediments. Arrows pointing to fenestral cavities caused by gas from the lower organic decay zone migrating towards the surface, captured by the sealing mats. Iron oxides mark sub-recent mats and root channels of salt marsh plants. Photo: Nora Noffke; modified after photo published in Gerdes et al. (2000a). (B) Close-up of quartz sands, secondary voids being produced by degassing of decaying organic material in the subground. Photo: Nora Noffke; modified after photo published in Gerdes et al. (2000a). (C) Oblique view and cross-section of rippled sand, elongated secondary pores caused by gas from lower organic decay zone and fixed by sealing mat layers. Photo: Nora Noffke. (D) Relief cast showing fenestral fabrics in the two topmost layers, each bordered by sharply projecting mats overprinting ripples (see slightly curved morphologies and cross-stratification in the layers underlying the mats). Middle part marked by growth-bedding penetrated by tubes of polychaetes and small amphibian crustaceans characteristic of higher-lying tidal flat areas (same as those visible in Figure 2-3-4B). Lower part: strongly bioturbated intertidal sediments. Iron oxides confined to mats and worm tubes (organic influence). Relief = 30 cm thickness. Photo: H.-E. Reineck. (E) Cross-section of a gas dome forming in muddy sediments, gas from the lower organic decay zone producing large voids. Thin green mat on top. Photo: Nora Noffke. *Locality of photos*: A to D – Mellum Island, southern North Sea coast (Germany); E – Bahar Alouane, southern Tunisia.

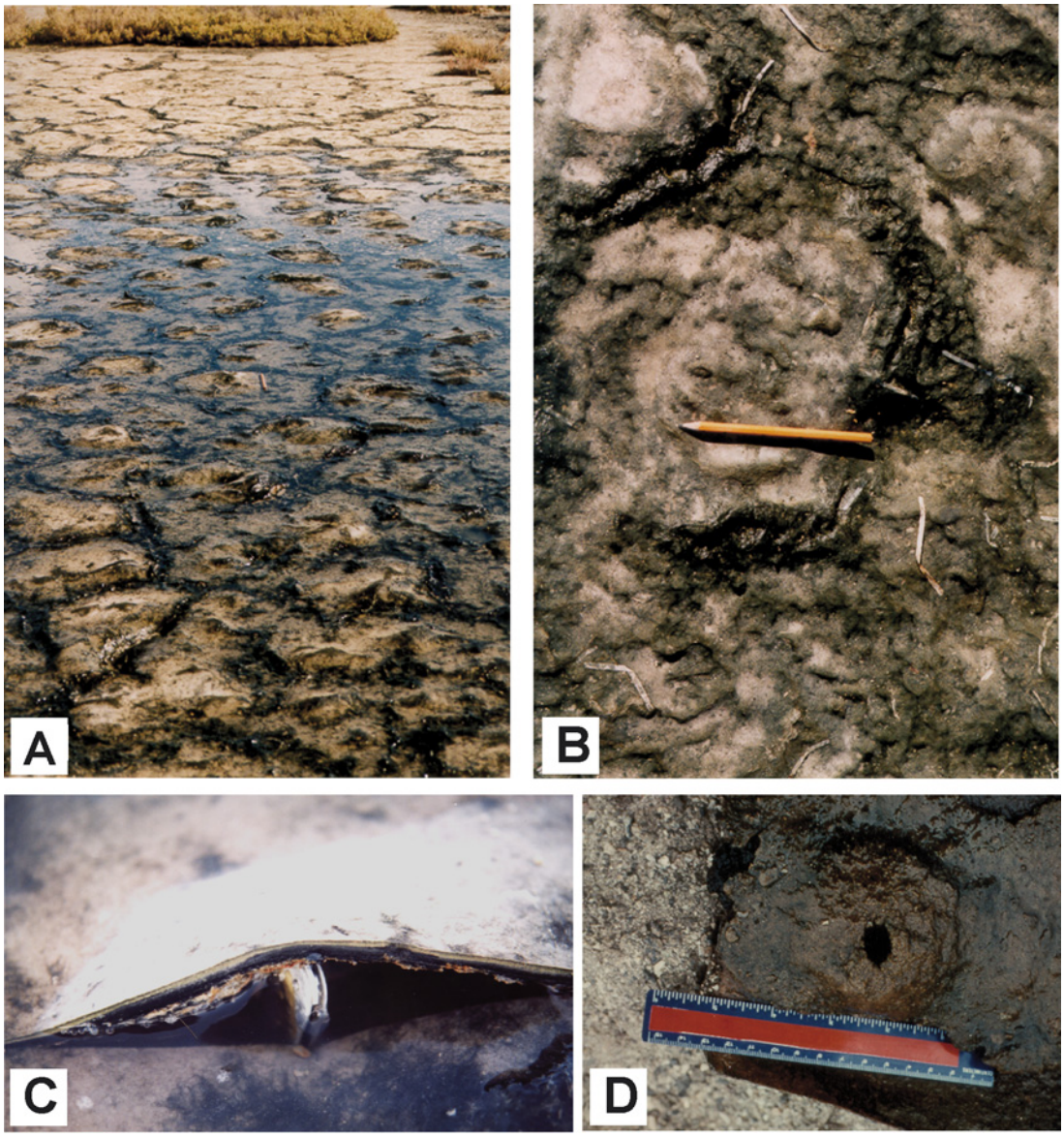


Figure 2-4-3: Gas domes (figures showing bedding plane structures; ground planes about 30 cm in diameter).
(A) Gas domes in hypersaline shallow-water mats; yellow pencil for scale in middle of photograph. Photo: Nora Noffke; modified after photo published in Gerdes et al. (2000a). (B) Soft-sediment dome partly collapsed, surrounding cracks re-colonised by microbial mats. Photo: Nora Noffke. (C) Surface mat in shallow water artificially detached from the subground to show empty space below. Knife hindering collapse of the soft dome. Photo: Nora Noffke. (D) Punctured gas dome. Gypsum crystals stabilising the organic surface tissue prevented collapse. Photo: H.-E. Reineck; modified after photo published in Reineck et al. (1990).

In Figure 2-4-3, mats are flooded and non-mineralised prior to and during deformation due to gas pressure. Gas diffuses from deeper buried organic deposits or mats toward the surface where cohesive microbial tissues retard the exchange through the mat–water interface. Hummocks may rise up convexly over selective vents (Figures 2-4-3A to -4-3D). Subaerial exposure supports gypsum and halite encrustation, possibly also forced by evaporative pumping (Figures 2-4-3D to -4-3H). If domes do not experience salt encrustation, continuous gas concentration beneath the surface mat may increase the tension along weak zones, establishing circular cracks at transitions from the planar to the domed mat (Figure 2-4-3B).

Well-known ‘cabbage-head’ structures (Figure 2-4-3G) are products of intermittent flooding associated with domal mat overgrowth, and subaerial exposure associated with mineral encrustations.

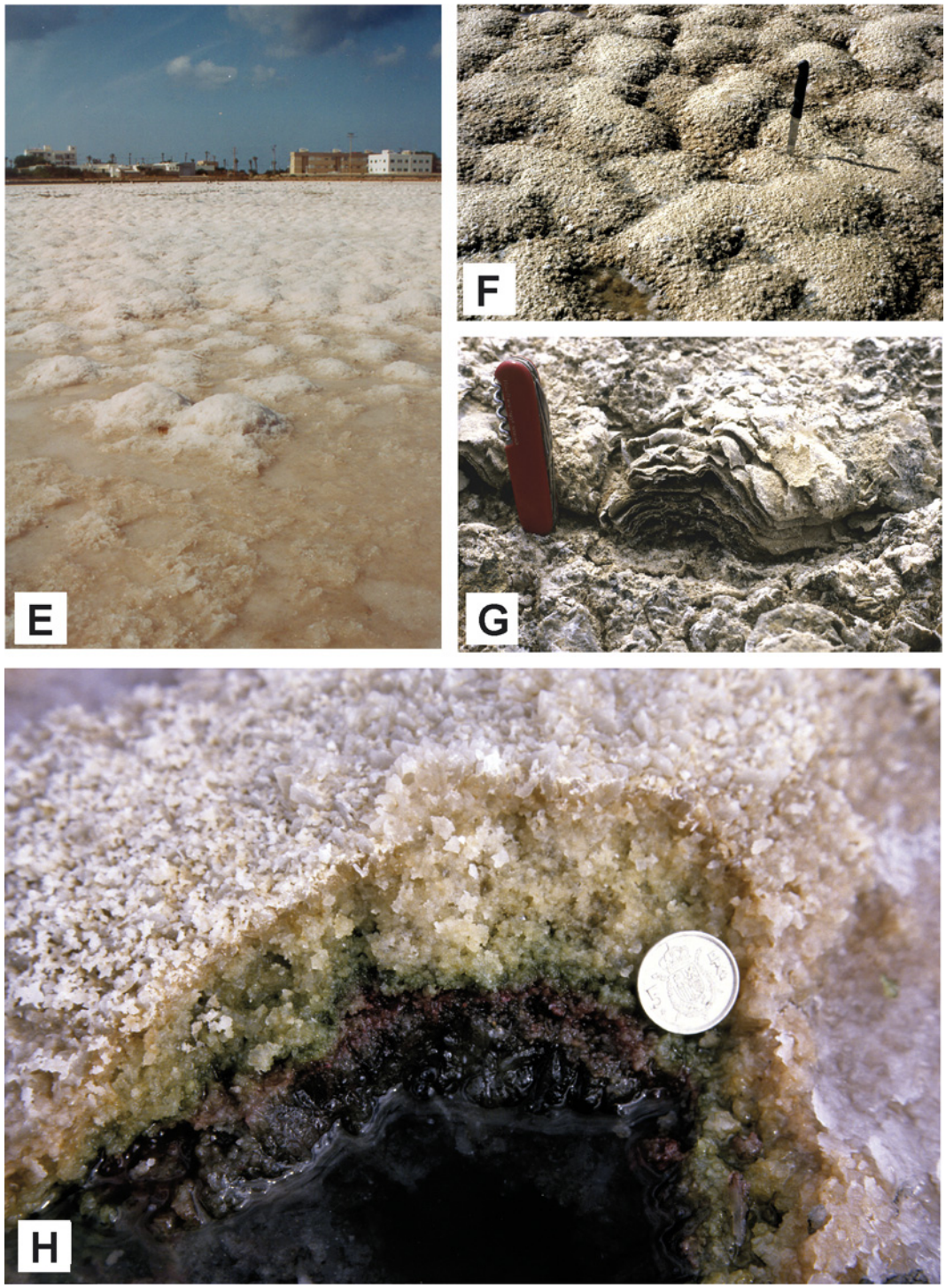


Figure 2-4-3: ***Continued.***
(E) 'Mole-hill'-like gas domes distributed on the bottom of a gypsum- and halite-encrusted salina basin. Photo: Gisela Gerdes. (F) Closer view of evaporite-encrusted gas domes. Photo: H.-E. Reineck; modified after photo published in Gerdes et al. (1993). (G) Typical cabbage-head structure within abandoned salina basin. Photo: H.-E. Reineck; modified after photo published in Gerdes et al. (1993). (H) Salt-encrusted gas dome cut vertically to show the hollow centre. Reduced slushy ooze (black) was forced in when the dome became opened (protuberance structures; Gerdes et al., 1993). Gypsum crust displaying colourful zonation of blue-green, purple phototrophs (dominant *Chromatium* sp.) and black sulphate-reducing zone. Photo: H.-E. Reineck. *Locality of photos*: A, B – Sabkha Amchoun, southern Tunisia; C – Bahar Alouane, southern Tunisia; D, F to H – saltworks of Lanzarote, Canary Islands (Spain); E – saltworks, Formentera, Balearic Islands (Spain).

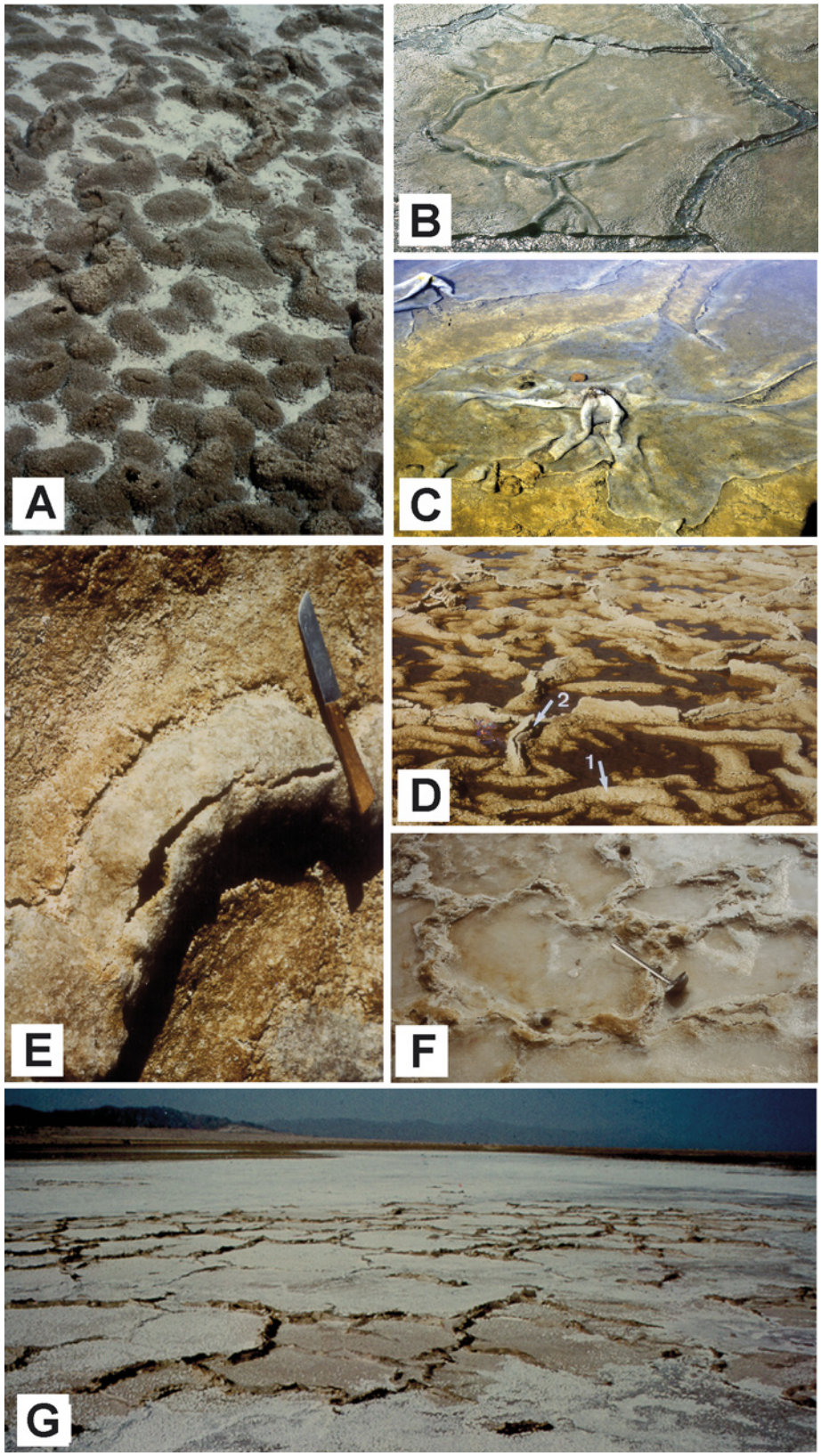


Figure 2-4-4: Petee variations (with reference to Reineck et al., 1990).
(A) Transitions from gas domes to elongated folds may be established by gas concentrated beyond the formerly non-encrusted, elastic and easily deformable mats. Photo: H.-E. Reineck; modified after photo published in Reineck et al. (1990). (B) Monolayered soft microbial mat growing on a substrate enriched in clay minerals. Folding and tearing may be due to wind and/or water friction influencing the monolayered mat which shows low capacity to integrate into the subsoil (different to sandy sediments, see Figure 2-1-1C). Photo: J. Gifford; modified after

photo published in Reineck et al. (1990). (C) Similar monolayered soft microbial mat growing on a mixture of subaquatic gypsum and bacterial EPS. Mats are scouring on the slippery substrate due to wind drift, causing folds and tears. Wide tears and exposure of subsoil due to the non-sticking nature of the mat. Photo: H.-E. Reineck. (D) Folds in initially elastic biogenic matrix of microbial mats subsequently gypsum-encrusted. Note rounded (1) and ruptured (2) crests. Photo: H.-E. Reineck; modified after photo published in Reineck et al. (1990). (E) Close-up of elongated petee with ruptured crest. Rounded form of the crust, although ruptured, is initiated by elastic microbial mat. Photo: H.-E. Reineck; modified after photo published in Reineck et al. (1990). (F) Polygonal overthrust structures in gypsum-encrusted microbial mats, crests ruptured (beta-petee). Photo: H.-E. Reineck; modified after photo published in Reineck et al. (1990). (G) Polygonal overthrust structures in halite-encrusted terrigenous sabkha sediments (tepees and gamma petees. Polygon diameter increasing to 50 cm and more). Photo: W.-E. Krumbein; modified after photo published in Reineck et al. (1990). *Locality of photos*: A, C to F – saltworks of Lanzarote, Canary Islands (Spain); B – saltworks, Bretagne coast (France); G – Gavish Sabkha, Gulf of Aqaba (Egypt), sea-marginal hypersaline ecosystem.

'Petee' variations (Figure 2-4-4) Reineck et al. (1990) subsumed domes, folds and their transitions (Figure 2-4-4A) under the term 'petee' and defined petees as overthrust structures in biogenic matrix. Initially, the term 'petee' was created by Gavish et al. (1985) to contrast biogenically rounded positive structures (petees) from abiogenic sharp-edged triangular 'tepees'. Reineck et al. (1990) termed domes and folds in soft mats 'alpha-petees' and related these structures to subsurficial gas pressure caused by post-burial decay of buried mats. These authors termed gypsum-encrusted stages of initially soft-ground domes and folds in arid climates 'beta-petees' and related these still to post-burial decay and gas production of buried mats (Figures 2-4-4A, -4-4B). Circular tearing of soft monolayered mats and circular subsoil exposure may form due to particularly strong gas pressure from below (Figure 2-4-4B). Repeated changes between wetting and exposure favour the formation of massive gypsum. Wetting encourages populations of microbial coccoids to colonise outer petee surfaces. Tan colour in Figures 2-4-4D and -4-4E indicates slime coatings produced by numerous coccoid cyanobacteria which protect themselves against phototoxic reactions by carotenoids and EPS.

However, folding supported by wind and water friction (Figure 2-4-4C), and expansion of gypsum-encrusted surface mats also produce overthrust structures. Reineck et al. (1990) termed the latter 'gamma-petees' (Figure 2-4-4F) and defined them as intermediate between petees and tepees due to the same underlying process. Expansion of surface crusts may also cause cracking and subsequent movement of the cracked crusts against each other (Figure 2-4-4F). In vertical section these structures show the characteristic tent (tepee) form (Assereto and Kendall, 1977; Reineck et al., 1990). Gamma-petees evolve from the same processes, but in the presence of biogenic matrices which smooth sharp-edged overthrust structures. Tepee and gamma-petee structures may be characteristic of higher-lying sabkha flats (Figure 2-4-4G).

Atlas of Microbial Mat Features Preserved within the Siliciclastic Rock Record
Edited by J. Schieber et al.
© 2007 Elsevier B.V. All rights reserved
DOI: 10.1016/S1574-1966(07)02003-2

CHAPTER 3

Classification of Structures Left by Microbial Mats in Their Host Sediments

P.G. Eriksson, J. Schieber, E. Bouougri, G. Gerdes, H. Porada, S. Banerjee, P.K. Bose, S. Sarkar

INTRODUCTION

We view the structures and features described in this atlas as *sedimentary structures*, albeit of a complex organo-physico-chemical origin. Just like their physical sedimentary structure counterparts (e.g., Pettijohn and Potter, 1964), they can be of great assistance in unravelling depositional palaeoenvironments inferred for ancient rock successions. Pettijohn and Potter (1964) included stromatolites in their well known classification of primary physical sedimentary structures, under their class 2E structures, as positive growth features upon bedding planes (Noffke et al., 2001a). The combination of microbial construction, accretion of detrital grains, and biochemical precipitation implicit in stromatolite formation (e.g., Walter, 1976) was originally thought to be endemic to carbonate-forming settings (e.g., Awramik, 1984; Walter et al., 1992; Altermann, 2002). There is a growing recognition, however, that surficial microbial communities interacted with physical agents of erosion, sedimentation and even deformation (Noffke et al., 2001a) in ancient clastic sedimentary settings (e.g., Schieber, 1986, 1998a, 1999, 2004; Hagadorn et al., 1999; Gehling, 1999; Pflüger, 1999). A large array of modern examples of resultant features, both microbial and clastic-sedimentary, has been presented in Chapter 2 of this book.

Classification of stromatolites has a long and contentious history (see recent summary in Altermann, 2004), with the best result likely having been achieved by Hofmann (1973, updated 2000). Hofmann proposed a pyramidal diagram, in which each of the four corners represented one of the four main genetic processes, namely biological non-skeletal, biological skeletal, mechanical clastic, and chemical. Classification of the infinitely more complex set of microbial mat features preserved in sandstones and mudrocks, as presented in this atlas, is a much more challenging task. As for carbonates, genetically-based approaches seem to enjoy the broadest acceptance.

Three main genetic classification schemes have appeared in recent years. Gerdes et al. (2000a) examined modern textural signatures of microbial activity in two chosen study areas of siliciclastic sediments along the peritidal coastlines of the North Sea and Tunisia. They recognised six types of biogenically mediated clastic sedimentary fabrics, those due to:

(1) intrinsic biofactors – i.e., essentially the morphology and behaviour of biofilms and their more robust counterparts, microbial mats;
(2) biological response to physical disturbances;
(3) trapping and binding of clastic sediment;
(4) mechanical deformation of biologically stabilised clastic sediment surfaces;
(5) post-burial processes;
(6) bioturbation processes.

Although Gerdes et al. (2000a) clearly recognised that this scheme was a catalogue of microbial signatures in modern peritidal clastic settings, the potential fossilisation of these fabrics/features meant that it also could provide the basis for a genetic classification scheme. This same team of authors, with the addition of Krumbein (Noffke et al., 2001a) published a formal classification scheme for what they termed 'microbially-induced sedimentary structures' (MISS), arguing logically in favour of these forming a fifth category in the well-known Pettijohn and Potter (1964) classification scheme for primary (physical) sedimentary structures. Once again, this was a scheme based on genetic factors. Noffke et al. (2001a) proposed two classes of MISS: (class A) structures atop bedding planes, and (class B) those within beds:

(1) Class A:
   (a) levelled depositional surfaces and wrinkle marks;
   (b) microbial mat chips;
   (c) erosional remnants and pockets;
   (d) multidirectional or palimpsest ripples;
   (e) mat curls, shrinkage cracks.
(2) Class B:
   (a) sponge pore fabrics, gas domes, fenestrae structures;
   (b) sinoidal laminae;
   (c) oriented grains, benthic ooids;
   (d) biolaminites, mat-layer-bound grain sizes.

The third classification scheme for microbial mat features preserved in the siliciclastic rock record is that of Schieber (2004), who emphasised that microbial mats influence the depositional fabric of clastic deposits across a wide range of physical, chemical and biological processes. He further stressed that these mat-related structures and features are in many ways analogous to trace fossils, and that the influence and thus former presence of mats can be inferred from observations suggesting sediment properties that would be uncharacteristic for a purely physically deposited sand or mud. Useful features are those that indicate original sediment cohesiveness, tensile strength, and erosion-resistance during deposition, and those that allow deduction of original permeability and geochemical behaviour during early diagenesis. His classification scheme encompassed a set of features that spans the process continuum from active mat growth, through mat metabolism, and on to mat destruction, and finally, mat decay and diagenesis (Figures 3-1 and -2). He presented separate, yet basically analogous schemes for mat-related features from sandstones and mudrocks (Figures 7.9-1 and 7.9-2 in Schieber, 2004). Schieber (op. cit.) also stressed that several of the observed features could have multiple origins (e.g., *'Astropolithon'* gas or fluid escape structures in Chapter 4(a) and (d), or ripple patches in Chapter 4(a) and (c)), something already implicit if not always fully apparent, from earlier classification schemes. This scheme is discussed in some detail below as it is the classification followed in this book. Some minor adaptations have been made to this published scheme here, and an additional short section illustrating complex structures resulting from microbial mats has been added.

SCHIEBER'S (2004) CLASSIFICATION

Microbial mat features preserved in sandstones (see Chapter 4)

Figure 3-1 summarises features that have been observed in sandstones subject to microbial mat influences during deposition or diagenesis. Genetic processes inferred to be responsible for these biogenic sedimentary structures are shown on a clockwise-arranged continuum, from mat growth to final destruction and diagenesis (cf. Schieber, 2004).

Features formed under conditions of mat growth (see Chapter 4(a)) Biostabilisation of clastic sediment (cf. Gerdes et al., 2000a) encompasses binding, trapping, and baffling. Thin biofilms comprising intermingled sand grains and microbial filaments tend to stabilise sediment surfaces following physical reworking processes. Any surface morphology from such sediment layers can then be 'frozen'; *multiple-directed ripple marks* (Noffke, 1998a) may form during further reworking, or, if new sediment is introduced (Pflüger, 1999), *palimpsest ripples* ('a' in Figure 3-1) may develop. If reworking has sufficient energy, ripple crests may partially be removed, with *narrow ridges* ('b', Figure 3-1; see also cracked and eroded ripple crests in Figures 4(a)-17 and -18) surviving to attest to erosion-resistance provided by mat growth and concomitant cohesion (Pflüger, 1999). As with many mat features, those described in this paragraph also reflect a combination of factors. Some physical modification, or even partial destruction, is inherent apart from the initial mat growth influences. Pliable spheroidal sand clasts, reflecting non-sorted, sticky sand clasts which deform each other, are an additional feature to those detailed by Schieber (2004) and are illustrated in Figures 4(a)-3 and -4.

Analogous binding and trapping of sediment grains can also result in characteristic laminar features. These comprise evidence for microbial mats preserved in single laminae as well as in biolaminated deposits (cf. biolaminites). In some modern environments, laminae of *horizontally oriented mineral grains* alternate with graded laminae ('c', Figure 3-1) – the former are ascribed to mat formation which either trapped grains horizontally, or rotated them to that orientation during mat-decomposition and compaction, while the latter laminae reflect short-lived depositional events (Noffke et al., 1997a). No examples have yet been identified from the rock record, and such features

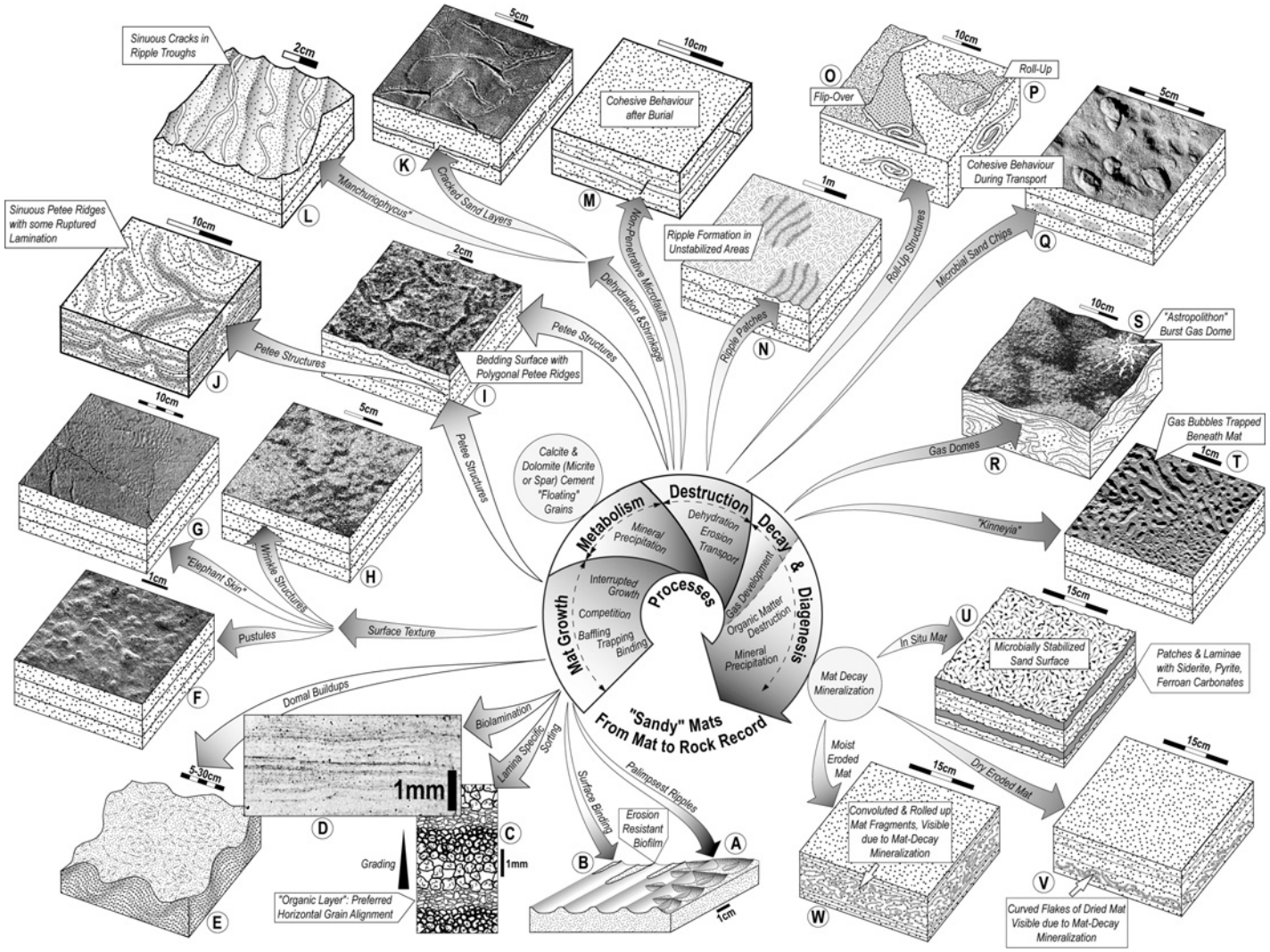


Figure 3-1: Features found in sandstones where microbial mats flourished in the past.

Genetic processes are arranged clockwise along a continuum from active growth of mats to final destruction during diagenesis. Modified after Schieber (2004; his Figure 7.9-1).

are problematic to differentiate from non-biogenic compaction-related grain fabrics. Other fabrics indicating evidence for microbial mats can include *lamina-specific mineral enrichment*, in either heavy minerals ('d', Figure 3-1; Gerdes et al., 2000a) or micas (Garlick, 1981, 1988).

Positive bed-top features resulting from mat growth are relatively common and display a wide range of morphologies and sizes, varying from *tufts, pinnacles and pustules* ('f' in Figure 3-1), to *bulges* and *reticulate ornamentation* (cf. '*elephant skin*'; Gehling, 1999; 'g' in Figure 3-1); a range of *wrinkle structures* ('h', Figure 3-1; Hagadorn and Bottjer, 1997, 1999; Schieber, 1998a, 1999; see also Chapter 6(a)) may also result. *Dome-like features* ('e', Figure 3-1; see also 'sand stromatolites' in Figures 4(a)-11 to -13) are reported from several Precambrian and younger sandstone occurrences (Davis, 1968; Garlick, 1981, 1988; Schieber, 1998a). They are ascribed to higher levels of wave or current energy (which favour more rapid synsedimentary lithification), with *planar forms* resulting from lower energy levels (Hoffman, 1976; Sami and James, 1993).

Mat growth can be disturbed by currents, winds, the development of gas, or by intermittent desiccation. These processes lead to buckling, doming and rupturing of microbially bound surficial sand layers. Modern examples (Reineck et al., 1990; Gerdes et al., 1993) and ancient analogues (Gehling, 1999) of these antiformal structures are termed *petees*. Within this framework, and depending on intensity of the disruption to mat-bound sand layers, either more simple networks or more complex sinuous *petee ridges* may result, the latter commonly encompassing rupture of the microbial surfaces (respectively, 'i' and 'j' in Figure 3-1).

Features formed due to metabolic effects of growing mat (see Chapter 4(b)) In modern mats, metabolic processes like photosynthesis have been observed to shift carbonate solubility enough to cause precipitation of carbonate minerals between and along filaments within the growing mats (Krumbein, 1974, 1986; Gerdes and Krumbein, 1987; Chafetz and Buczynski, 1992; Chafetz, 1994). These *mineral precipitation effects* can be preserved within the rock record as: irregular ooids (Gerdes and Krumbein, 1987), disseminated carbonate grains (e.g., Kropp et al., 1997), micritic cement between terrigenous grains, and highly lamina-specific carbonate cementation within laminated sandstones. Another metabolic effect would be the formation of *very early diagenetic dolomite* (Gebelein and Hoffman, 1973) from high Mg concentrations in sheaths of living filamentous cyanobacteria. If mat-internal carbonate precipitation is voluminous enough, detrital grains of quartz and mica may be encased in a carbonate matrix and form '*floating grains*' upon lithification. In ancient examples, a '*coated grain*' *fabric* denotes sand- and silt-sized grains that are surrounded by fine-grained sericitic material (Bouougri and Porada, 2002; Draganits and Noffke, 2004). Modern analogues have been described by various authors (e.g., Gerdes et al., 2000a; Noffke et al., 2001a, 2003b). Coated grain fabrics have been related to the presence of intergranular coccoidal bacteria and their mucilages (e.g., Noffke et al., 2001a). Clays transported through the grain fabric by uprising or circulating groundwater are trapped on grain surfaces by mucilage coatings and may later form sericite. Alternatively, biogeochemical processes within the microbial mat itself (Krumbein and Werner, 1983) may allow clay accumulation.

Forming in inherently permeable sandstones, syngenetic signatures, such as lamina-specific carbonate cementation, are easily overprinted by subsequent diagenetic processes. Certain textural features, however, like '*floating*' *terrigenous grains* in a carbonate matrix, suggest precompactional and possibly syngenetic carbonate formation (Garlick, 1988; Schieber, 1998). In addition, highly *lamina-conformable distribution of pyrite* may reflect the metabolic activity of sulphate-reducing bacteria beneath the photosynthetic surface layer of a mat (Schieber, 1989a).

Features formed by physical mat destruction (see Chapter 4(c)) Physical destruction of microbially bound sediments generates a wide range of sedimentary features that may occur at the original mat location, or may be observed in redeposited materials. Because physically deposited sand layers are grain-supported, they can not shrink upon desiccation. Thus, if sand layers are found to contain shrinkage cracks, an additional component that shrinks upon desiccation must originally have been present between the sand grains. Clays, for example, can function in this role. Yet, because the resulting rock could readily be identified as a clay-rich sandstone, contraction upon desiccation would be expected. In the absence of a clay matrix, however, a water-rich matrix of microbial filaments and extracellular polymer substance (EPS) would be the most likely cause for shrinkage upon desiccation. The resulting *sand crack patterns* vary from incomplete networks to polygonal patterns, and may even form complexly superimposed sets of spindle-shaped cracks (Bouougri and Porada, 2002; Schieber, 2004; Sarkar et al., 2004, 2006) that can themselves become filled with sand (e.g., 'k', Figure 3-1).

In this book, the spectrum of shrinkage-related features is expanded by adding features observed at crack margins in modern sandy mats, such as *curled crack margins, overgrown*, and *upturned crack margins* (see Chapter 4(c)). The latter have not yet been described explicitly from ancient sandy mat deposits.

Sinuous to circular sand cracks restricted to ripple troughs form a special case, known as '*Manchuriophycus*' ('l' in Figure 3-1), probably formed due to thickened mat layers within ripple troughs (Pflüger, 1999; Gehling, 2000). Microbial mats may also maintain a measure of cohesiveness for some time after burial. Deformation of such microbially-bound sand layers may result in contrasting behaviour to over- and underlying layers of loose, non-bound sand. *Non-penetrative microfaults* ('m', Figure 3-1) in sandstones have been interpreted to reflect cohesive behaviour of buried mat layers in sandy deposits (Pflüger, 1999; Gehling, 1999).

Binding of sand surfaces by microbial mats significantly enhances their resistance to erosion (e.g., Neumann et al., 1970), but erosion, tearing, and transport of mat fragments will commence once strong currents are active. Erosion of mat-bound sands leads to sedimentary features that are distinctively different from those that form during the erosion and reworking of a loose and unbound sand substrate. Whereas in the latter case we can expect to see scouring and the formation of wave and current ripples over wide expanses of the sand bed, mat erosion tends to produce localised erosional 'windows' where the protective mat is removed. These exposed areas can then be remoulded into a rippled surface by wave and current action, forming *rippled patches* in an otherwise smooth sandy surface ('n', Figure 3-1). This feature is known from both modern tidal flats (Reineck, 1979; Gerdes et al., 1985b), and the rock record (McKenzie, 1972; Reineck, 1979; Schieber, 1998a). It is important to note that a smooth transition results between purported mat surface and rippled sandstones in these features (see also Chapter 7(i)).

The inherent cohesiveness of mat-bound sand surfaces also leads to the formation of *flipped-over edges* ('o' in Figure 3-1) of partially eroded mat surfaces, as well as to the redeposition of deformed and *rolled-up mat fragments*, also called 'roll-ups' ('p' and 'w', Figure 3-1). Modern examples are reported by Reineck (1979) and Gerdes et al. (2000a), and inferred ancient equivalents by Schieber (1998a, 1999), Garlick (1981, 1988), Simonson and Carney (1999), and Eriksson et al. (2000). A subclass of the eroded mat fragments is comprised by *microbial sand chips* (Pflüger and Gresse, 1996; Bouougri and Porada, 2002; Sarkar et al., 2006; 'q' in Figure 3-1). These probably reflect a longer transport history than roll-ups, resulting in a measure of sorting and abrasion. What sets microbial sand chips apart from irregular and rolled-up mat fragments are their typically smaller dimensions (a few centimetres at most), similar sizes within a given occurrence, plastic deformation, and commonly observed current-alignment (Pflüger and Gresse, 1996). In places they may even show imbrication (Bouougri and Porada, 2002).

Desiccation of microbially-bound sand surfaces results in many instances in polygonal crack patterns (see above) and a surface that is covered by rigid, *curved sand chips* (several centimetres across; 'v', Figure 3-1). Upon erosion, the latter can be transported as intraclasts and become incorporated into high energy sandstone deposits. Fossil examples are reported by Garlick (1988) and Schieber (1998a). In the absence of textural differences (grain size, lamination), these sand chips may be difficult to distinguish from their sandstone matrix. In that case diagenetic effects, such as mat decay mineralisation related to the organic content of the chips (Garlick, 1988; Schieber, 1999), may be the only means for their recognition in the rock record (see below also).

Features resulting from mat decay and diagenesis (see Chapter 4(b) and (d)) Once mat decay begins, decay gases can disturb the sediment beneath the mats as well as disrupting the mats themselves, forming *gas domes, convoluted internal lamination* ('r', Figure 3-1; Gerdes et al., 2000a), and *ruptured gas domes* known as '*Astropolithon*' (Pflüger, 1999; 's', Figure 3-1). The substrate cohesiveness implicit in the radial ruptures of '*Astropolithon*' domes also provides a supporting argument for the former presence of a mat. Gas development related to may decay also helps form the more severely disturbed and ruptured *petee* structures ('j' in Figure 3-1). The steep slopes of the troughs and the flat tops associated with '*Kinneyia*' *style ripples* ('t' in Figure 3-1) led Pflüger (1999) to propose that these formed due to gas trapping beneath a mat. However, *'Kinneyia'* can easily be confused with wrinkled mat surfaces ('g' and 'h', Figure 3-1) (see also Chapter 6(a)), and many '*Kinneyia*' described in the literature rather resemble the round-crested microbial wrinkle marks described by Hagadorn and Bottjer (1999).

The permeability of sand results in rapid microbial metabolisation of buried organic matter. This circumstance largely obviates survival of organic matter as an indicator of microbial mats in sandstones. However, mats constitute sharply defined geochemical boundaries (Bauld, 1981), and anaerobic decay beneath them favours formation of 'anoxic' minerals such as pyrite, siderite, and ferroan dolomite. These authigenic minerals can locally cement the sand, occlude porosity, and result in '*mat-decay mineralisation*' (Schieber, 1998a). The 'ghosts' of filaments may be preserved in these cements. Preservation of thin, stratiform horizons of mat decay minerals ('u', Figure 3-1) in shallow water sandstones suggests the former presence of microbial mats (Gerdes et al., 1985b; Garlick, 1988). Different minerals are favoured depending whether water chemistry is marine or fresh (e.g., respectively, pyrite versus siderite). The burial of rigid ('v', Figure 3-1) or soft fragments ('q' and 'w', Figure 3-1) of re-sedimented

mat can induce similar cementation once decay sets in and can preserve a ghost outline of the transported mat fragments (Garlick, 1988; Pflüger and Gresse, 1996; Schieber, 1998a).

Microbial mat features preserved in shales (see Chapter 5)

Figure 3-2 summarises features that have been observed in shales that were subject to microbial mat influences during deposition or diagenesis. Genetic processes inferred to be responsible for these biogenic sedimentary structures are shown on a clockwise-arranged continuum, from mat growth to final destruction and diagenesis (cf. Schieber, 2004).

Features formed as a result of mat growth Because of the high degree of compaction that surface muds are subjected to upon burial, surface features formed due to binding, trapping, and baffling by microbial mats on muddy substrates is preserved as a much more subtly defined surface relief in the rock record (Schieber, 2004). Despite this, *wavy-crinkly laminae* ('a' in Figure 3-2) form, that are distinctively different from the parallel laminae that form in mudstones from suspension settling during physical sedimentation processes (Schieber, 1986; Fairchild and Herrington, 1989; O'Brien, 1990; Goth, 1990; Wuttke and Radtke, 1993; Goth and Schiller, 1994). Colonisation of irregular sediment surfaces (such as an intraclast conglomerate) by mats can result in *bed-smoothing* ('b', Figure 3-2). In non-mat mudstones, compactional effects above comparable relief are generally detectable for a greater distance upward from the underlying surface irregularities. Differences in the *behaviour* of shales under conditions of *soft sediment loading* (Schieber, 1986) also provides evidence for bed-surface stabilisation by a mat cover. As an example, where silt layers have been deposited on mat-bound mudstone surfaces, only minor load features result ('d', Figure 3-2), whereas miniature ball-and-pillow structures tend to form on non-mat mudstones ('c', Figure 3-2).

In contrast to the wavy-crinkly carbonaceous laminae discussed above, which are reported mainly from inferred subtidal and shelf settings (Schieber, 1986; Fairchild and Herrington, 1989; Logan et al., 1999a), *domal buildups* of variable amplitude and spacing have been observed in near-shore mudstones ('e' and 'f', Figure 3-2; Schieber, 1998a). The inherent rapid weathering of mudstones has likely hampered recognition and preservation of a variety of other, similar occurrences in the rock record.

Event sedimentation such as caused by floods and storms, will bury growing mats under a sudden influx of sediment, thereby causing interruption of mat growth. Such intermittent events can then lead to '*striped shales*' with alternating mat and event layers ('g', Figure 3-2; Schieber, 1986; Logan et al., 1999a; see Chapter 7(b) and (c)). As mat cover expands over a muddy substrate, intermittent deposition of thin clay drapes can lead to a feature called *false cross-lamination* ('h', Figure 3-2) at the edge of the expanding mat patches. This feature reflects the rapid re-establishment of mats (via vertical movement of buried filaments) on top of the recently deposited clay drapes, followed by their lateral expansion (Schieber, 1986).

Although fossil *petee structures* formed on muddy substrates have not yet been identified in the rock record, petee formation is independent of substrate calibre (e.g., Reineck et al., 1990; Gerdes et al., 2000a). Analogous structures, at a smaller scale, are known in modern mud puddles.

Lamina-specific grain selection, as evinced by mat laminae enriched in mica flakes ('i' in Figure 3-2) has been observed in mud-based microbial mats (Schieber, 1998a). As for their sandy microbial mat equivalents, the underlying causes for this type of grain enrichment are not well understood (Gerdes et al., 2000a).

Features formed as a consequence of mat metabolism Syngenetic carbonate precipitation can be associated with mats growing on a muddy substrate, as analogously found for sandy sediments above (Schieber, 2004). Such syngenetic carbonate deposition is for example suggested by *randomly oriented mica flakes* in conformable carbonate-rich laminae (Schieber, 1998a) or by *terrigenous grains floating in a carbonate matrix*. In the first case, partial rotation of the flakes to more horizontal orientations may occur during cementation later in the burial history, as compaction begins to play a role. Examples from the rock record are illustrated in Chapter 7(b).

Where *bituminous substances* can still be extracted from suspected fossil mat deposits, determination of carbon isotopes, biomarkers, and sulphur isotopes, can suggest likely metabolic pathways operating at the time of deposition (Brassell, 1992; Logan et al., 1999a). Such *biomarkers* may help to indicate which bacteria dominated in the living mats, such as cyanobacteria (oxygenic photosynthesis), photosynthetic sulphur bacteria (anaerobic photosynthesis), or sulphide-oxidising bacteria (chemoautotrophy) (Gallardo, 1977; Williams and Reimers, 1983).

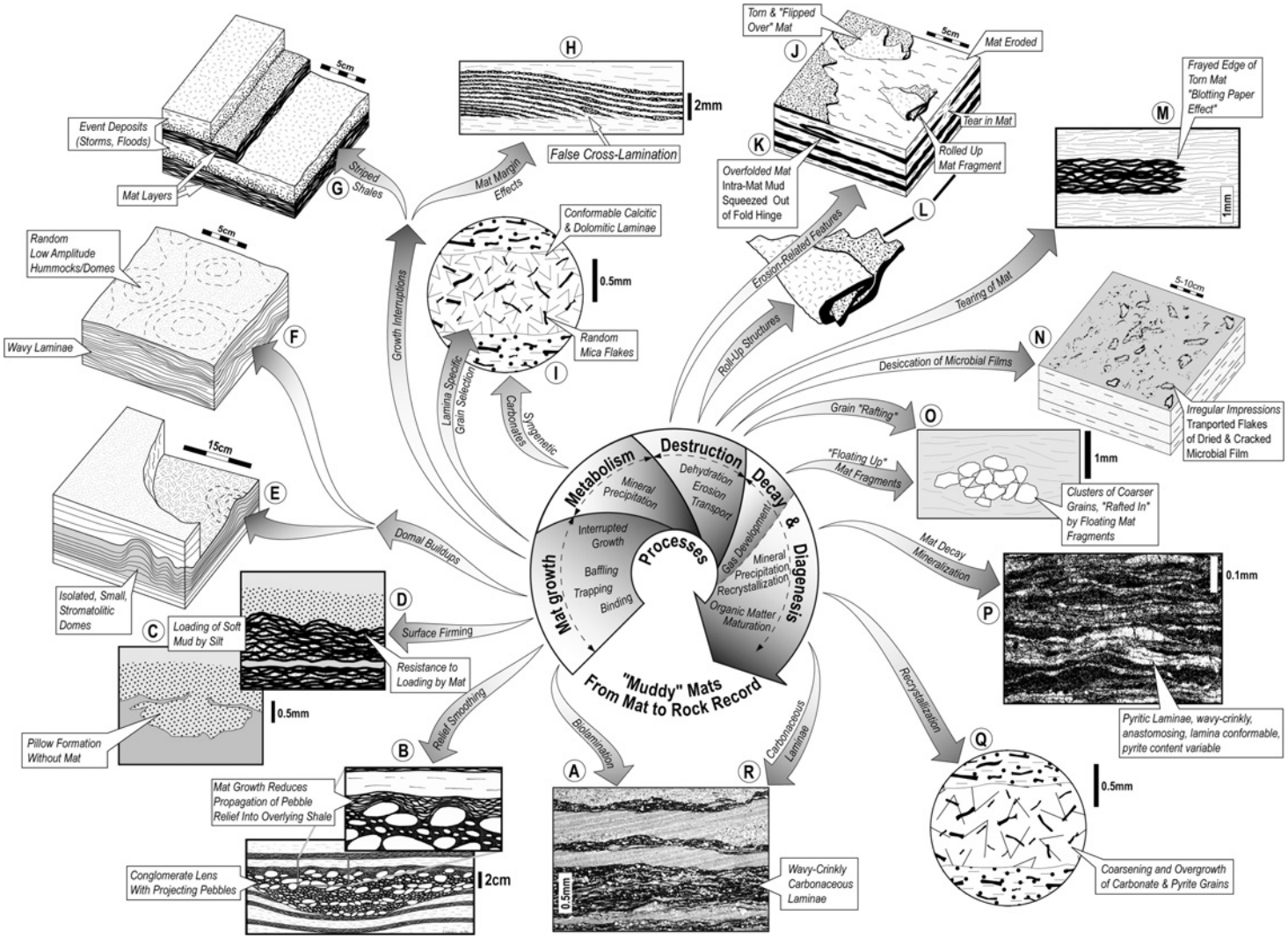


Figure 3-2: Features found in mudstones where microbial mats flourished in the past.
Genetic processes are arranged clockwise along a continuum from active growth of mats to final destruction during diagenesis. Modified after Schieber (2004; his Figure 7.9-2).

Features produced by physical mat destruction In general, features resulting from erosion of mat-bound muddy surfaces have close analogues in those formed by erosion of microbially-bound sandy sediments. Mat-bound mud layers display 'within layer' cohesiveness when eroded and transported ('l' in Figure 3-2) as well as a different rheological quality (firm-doughy, less compactible) when compared to 'normal' mud layers (which are soft-fluid- and yoghurt-like; 'k' in Figure 3-2) (Schieber, 1986). *Flipped-over mat edges* ('j' in Figure 3-2), *overfolded mat layers* ('k', Figure 3-2), and variably-sized '*roll-up*' *structures* are all known from ancient mudstone examples (Schieber, 1986, 1998a, 1999). *Torn mats and mat fragments* commonly display frayed edges ('m', Figure 3-2), sometimes called the 'blotting paper effect' in modern mats (Gerdes et al., 1993). This feature is also found in ancient examples (Schieber, 1999).

Analogous to sandy mat deposits, desiccation and shrinkage of muddy microbial mats produces cracks and dried out mat chips. Yet, because muddy substrates would, due to their water content, show these features anyway, the discrimination of palaeo-desiccation features in suspected muddy mat deposits (such as cracks and dried-out mat chips) remains problematic. In modern muddy settings, mats will cause modifications of crack morphology and crack-edges (Gerdes et al., 1993); however, comparable features from the rock record have not yet been reported.

Desiccation of thin biofilms on mudflats causes cracking and curling upon drying, and these paper-thin fragments can then be transported by either water (Fagerstrom, 1967) or wind (Trusheim, 1936). Being desiccated, they resist compaction when re-deposited and can then produce *irregular impressions* if they come to rest on a semi-dried muddy surface of stiff consistency ('n', Figure 3-2). An ancient example has been described by Horodyski (1982, 1983).

Dried-out mat fragments may also float, and can then carry detrital near-shore grains to deeper parts of a water body (Fagerstrom, 1967). Such rafting processes are inferred for *clusters of coarser grains* ('o', Figure 3-2) found in otherwise 'pure' mudstones (Olsen et al., 1978; Schieber, 1999). In Phanerozoic-age sedimentary rocks, analogous raft deposition may occur through floating plant debris or animal carcases, as well as by fecal pellets. Thus, distinguishing coarse grain-clusters due to the latter processes from those formed through mat-rafting is very difficult in Phanerozoic mudrocks (Schieber, 2004).

Features formed under conditions of mat decay and diagenesis Gas formation in submerged mats, due to either photosynthesis or decay processes, may cause rupturing and detachment of mat fragments that can then float to the surface (Fagerstrom, 1967). Any attached coarse grains can then be rafted offshore, forming *coarse-grain-clusters* in a mudstone matrix upon deposition (Schieber, 2004; 'o', Figure 3-2). This feature is analogous to that described immediately above, and highlights the polygenetic nature of many mat-related sedimentary structures.

When anaerobic decay of organic matter occurs beneath a growing mat, favourable conditions occur for *precipitation of* '*anoxic*' *minerals like pyrite, siderite, and ferroan dolomite*. Within marine settings, hydrogen sulphide commonly forms beneath the mat, and pyrite will crystallise (Berner, 1984). Depending on the amount of iron available in the environment, manifestations in the rock record may range from *carbonaceous laminae dusted with tiny pyrite grains* to *strongly pyritic laminae* ('p', Figure 3-2) that essentially mimic the wavy-crinkly mat lamination ('a' in Figure 3-2; Schieber, 1989a; see also Chapter 7(b) and (e)). During early diagenesis, pyrite overgrowth and cementation of the original fine-grained pyrite may occur (Strauss and Schieber, 1990; Chapter 7(b)). Analogous *recrystallisation and enlargement of carbonate minerals* takes place in layers with syngenetic carbonate accumulations ('q', Figure 3-2). As further burial leads to maturation of organic matter and reduction of organic content (hydrocarbon formation), biomarkers and kerogens are gradually destroyed. However, the low inherent permeability of mudstones prevents complete organic matter destruction (in contrast to most permeable sandstones) and *anastomosing carbonaceous laminae* may be preserved ('r', Figure 3-2; Schieber, 2004).

COMPLEX STRUCTURES

Because of its all-embracing nature, the organisational scheme presented by Schieber (2004) is used to order the manifold structures illustrated in this book in a process–response context. Not all mat-related structures observable in modern environments are explicitly included in this scheme, in part due to their lacking descriptions and due to a lack of ancient equivalents. A variety of 'complex structures' are briefly introduced to complement the range of features summarised in Figures 3-1 and -2.

As stated in the introduction, the structures and features in this atlas are considered sedimentary structures that can be used as tools for unravelling depositional palaeoenvironments, analogous to their physical sedimentary

counterparts. However, even features due to physical forces on mat-bound sedimentary surfaces cannot always be subsumed under the rules of sedimentation formulated by Stokes' Law (Krumbein and Schellnhuber, 1990). Observations of modern microbial mats in stressed environments (e.g., intertidal and supratidal flats of arid coasts) have shown that physical damage to surfaces overgrown by mats immediately prompts complex physiological strategies of the community members to again find their most optimal ecological niches after the disturbance has passed.

Observation of a 'living' mat surface also provides insight into the history of the mat which often undergoes changes within hours. Many structures are not simple results of 'events', but rather reflect a series of reactions of the microbiota to 'events', even more so as combinations of different life styles are involved rather than only one. Each variation of irradiation, each rain drop, each grain of sediment deposited on the surface is an 'event' triggering a reaction. All these 'events' are a source for energy input into the system. It is not necessary to think only of 'catastrophic events' like sudden burial, flooding and destruction, etc. Synergistic reactions of the system, possibly in a kind of feedback, are able to produce meso-/macroscopic structures. This could also explain why many structures are so similar in appearance and may thus be classified, e.g., as 'bulges', 'petees', etc. (see Chapter 6(c)). The effect of a cause may not be uniform across the area occupied by a mat. Mat destruction and mat growth may occur directly adjacent to each other.

Zavarzin (2003) stated that cyanobacteria-dominated mats are a highly sustainable biotic system that dominated Earth from the early Proterozoic to the end of the Neoproterozoic, and still survive in habitats where successor organisms (seaweeds, etc.) and metazoans are excluded. To understand such spatial and temporal sustainability of mats in spite of often unpredictable disturbances by physical processes (e.g., cracking, tearing, transport, scouring), the approach of 'parahistology' seems to be particularly important. In terms of structure, cohesion, and distribution of tasks of individual cells, biofilms and microbial mats are compared to tissues (Krumbein et al., 2003) which are similar to cells of living plants or to animal tissues, and which start immediately with protective actions against injuries. Some patterns of self-healing are illustrated in Figures 3-3A and -3B (see also mat growth concurrent with desiccation and cracking in Chapter 4(f)). Another aspect to understand is why these systems flourish particularly well in intertidal and supratidal flats of arid coasts in spite of an immense physical stress, due to the cooperative growth of different morphological and metabolic types in well-protected biofilms and microbial mats (Wachendörfer et al., 1994; Costerton and Stoodley, 2003).

Patterns of self-healing, the successful protection of biofilm organisms against water-loss and UV irradiation, or the textural and geometric similarity of mats in spite of the diversity of habitats (Zavarzin, 2003) cannot be explained by linear processes. As Krumbein and Schellnhuber (1990, 1992) stated, the processes apparently are not thermodynamic but follow laws governing dissipative or dynamic systems. These are attributes of complex structures resulting from self-organised processes, controlled by 'complex fractal system physics' (Krumbein and Schellnhuber, 1990).

Features observed in complex structures

Figures 3-3 to -5 illustrate examples of complex structures that reflect growth responses of mats that were triggered by external forces. All these structures cannot be linearly classified according to physical deformation or destruction, but rather indicate concomitant vital dynamics and 'parahistology' attributes of biofilms and microbial mats following non-linear laws in their growth and extension behaviour.

Under thin water cover (a few centimetres), small surface elevations such as ripple crests, PS (photosynthetic) domes (Chapter 6(c)) or gas domes may become sites of localised microbial growth of filamentous cyanobacteria, e.g., *Lyngbya* sp. (Figures 3-3A to -3D). In such cases, growth patterns may deviate from the normally reticulate arrangement of crests (see Figure 3-3A).

On sand deposited by wind or currents and concomitantly agglutinated and stabilised by coccoidal biofilms (e.g., *Synechococcus* sp.), photosynthetic (PS) domes resulting from metabolic processes of the filamentous mat below are overgrown, thus expanding the biofilm substrates (Figure 3-4A). The processes are combined when induced growth on ripple crests leads to development of coalescing PS domes which in turn are overgrown (Figure 3-4B). Growth and expansion of biofilm substrates (see also Figures 3-4C to -4H) is stimulated by physical factors, such as slight topographic elevations.

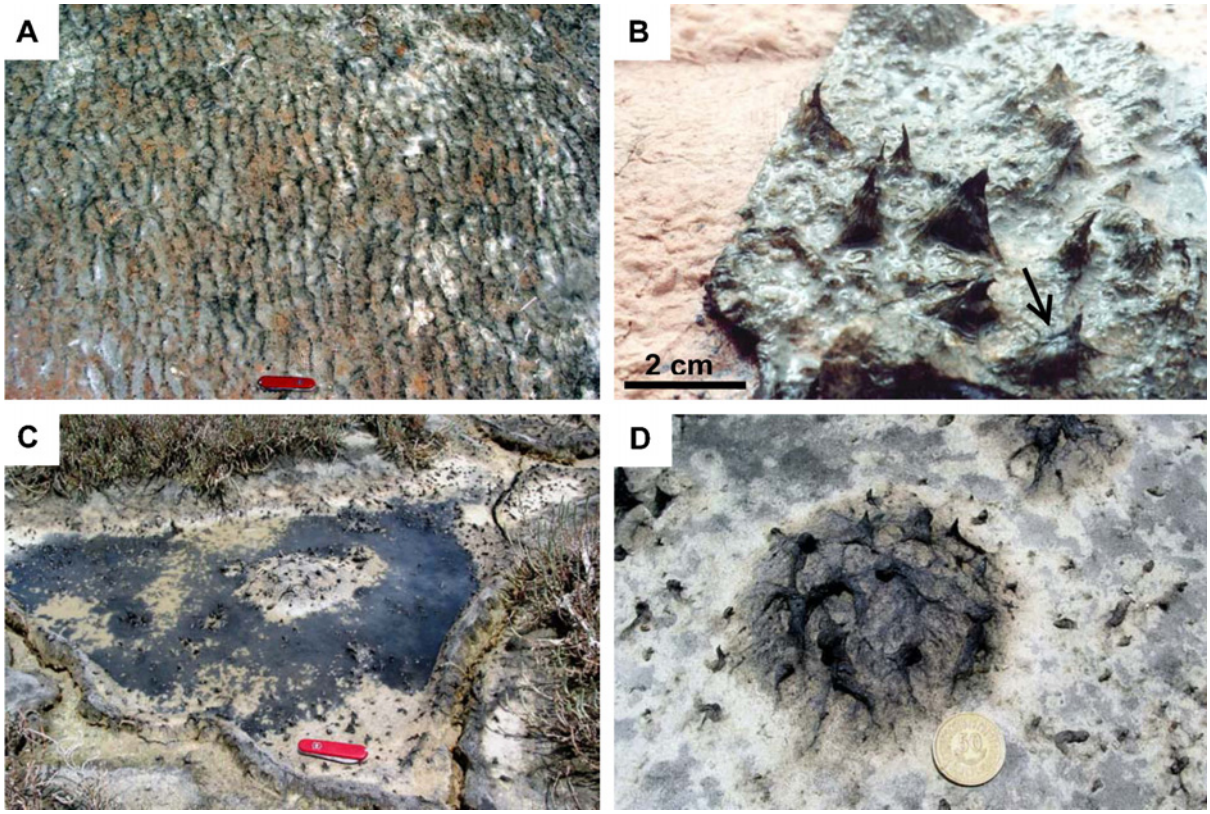


Figure 3-3: Structures resulting from 'induced growth' at small topographic elevations on mat surfaces. (A) Selective growth of filamentous cyanobacteria (*Lyngbya* sp.) along small-scale current ripple crests after temporary marine inundation. Lower supratidal zone, Bhar Alouane, southern Tunisia. Scale (knife) is 8 cm. (B) Shows a piece of a mat cut from the surface of a living mat for photographic documentation. Filamentous cyanobacteria (*Lyngbya* sp.) form isolated tufts upon photosynthetic domes (PS domes – see Chapter 6(c)). Note partly exposed PS dome (black arrow) at tuft close to lower image border. The black *Lyngbya* filaments were carefully removed with a knife to expose the milky-white membrane consisting of coccoid cyanobacteria and strongly cohesive EPS material comprising the upper surface of the PS dome. Upper intertidal zone, Bou Ghrara, southern Tunisia. (C) Supratidal puddle partly filled with sulphide-rich water, and with central gas dome, formed by trapped uprising gas from decaying mats. Note isolated *Lyngbya* tufts on gas dome and along elevated margins of puddle. Lower supratidal zone, Bhar Alouane, southern Tunisia. Scale (knife) is 8 cm. (D) Gas dome in dried-up portion of lower supratidal puddle, with reticulate growth pattern and tufts produced by *Lyngbya* sp. The structure may be interpreted as an 'escape structure' documenting escape of motile cyanobacteria from hostile, sulphide-rich water in the puddle. It should be noted that, for varying day/night conditions within an active mat community, many photosynthetic cyanobacteria can tolerate reducing and sulphidic conditions; however, in this case, the sulphide-rich water provides permanent reducing and sulphidic conditions. Supratidal zone, Bhar Alouane, southern Tunisia. Scale (coin) is 25 mm. All photos: Hubertus Porada.

Striking complex structures can, for example, result from a succession starting with the production of gas bubbles, their trapping and stabilisation by EPS, and microbial overgrowth using the interfaces of bubbles. Bursting of these bubbles produces characteristic lizard-skin textures (Figure 3-4G). These, as well as the overgrown and stabilised rims of burst bubbles (Figure 3-4H), may become preserved and appear as more or less distinct microstructures on ancient bedding surfaces.

Shrinkage cracks developed in microbial mats after extended subaerial exposure may become sites of localised 'induced growth' (see definition of terms in Chapter 6(c)), because of uprising water due to hydraulic 'upward pressure' in the sedimentary mat substratum. The emerging groundwater which in sabkhas is often well enriched in dissolved inorganic nutrients, e.g., phosphates (Javor, 1989), offers a liquid medium for biofilms/microbial layers to grow and expand within the cracks and may produce flat (Figure 3-5A) or bulge-like expansion structures (Figure 3-5B) completely spanning the cracks.

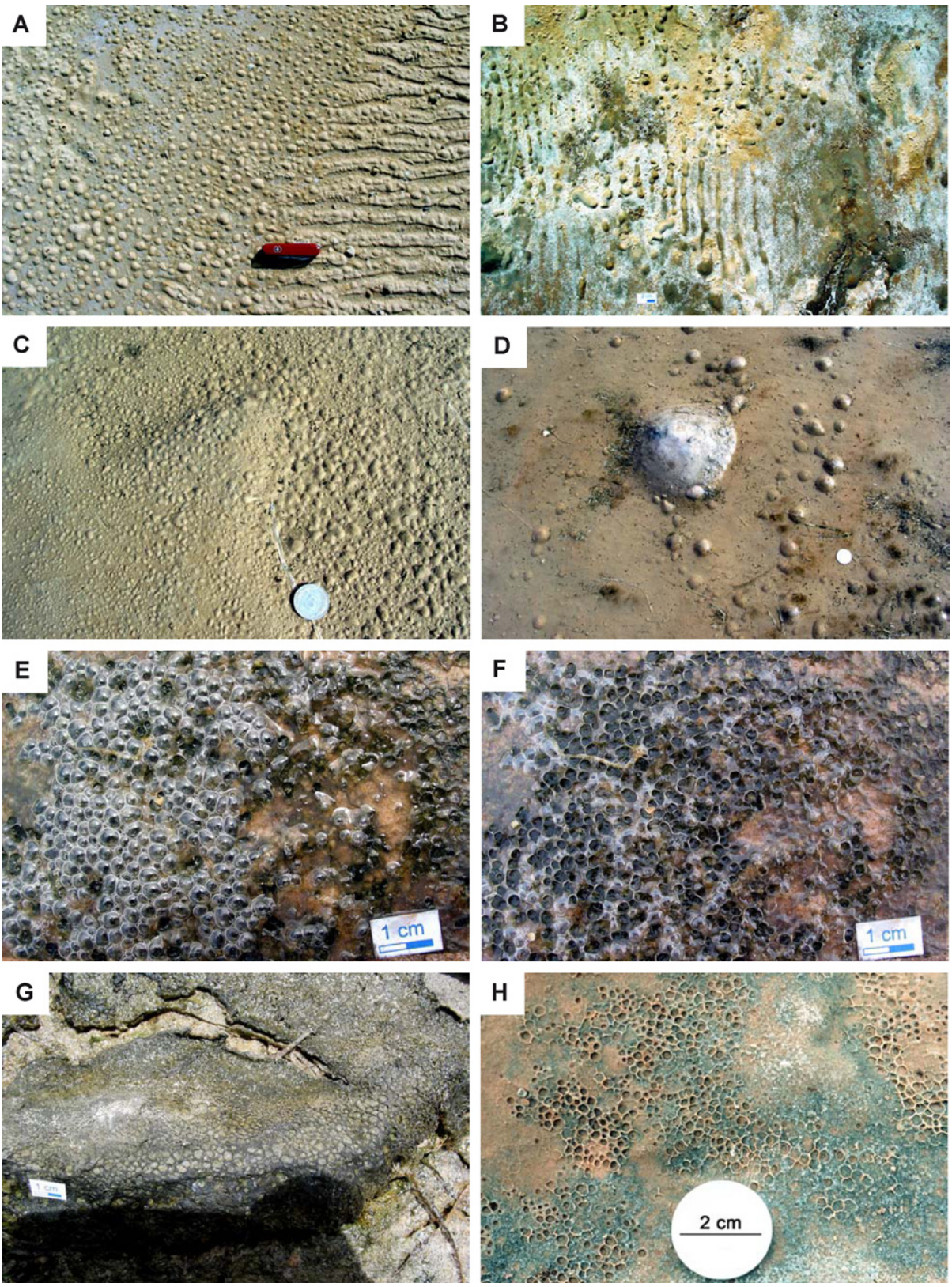


Figure 3-4: Structures reflecting 'induced growth' related to photosynthetic bubbles and PS domes.
(A) Congregation of overgrown PS domes in flat area of a shallow depression (left side), reflecting prolonged microbial activity of coccoidal cyanobacteria under a thin cover of residual water. Note isolated PS domes on ripple crests (right side) produced at higher water levels in the depression. Scale (knife) is 8 cm. Supratidal zone, Bhar Alouane, southern Tunisia. (B) Stabilised and overgrown small-scale current ripples; ripple crests partly associated with isolated PS domes and small elongate bulges, resulting from coalescence of domes. Ripple crests were pre-

ferred sites of microbial activity and localised accretion of biomass. Scale is 2 cm. Supratidal zone, Bhar Alouane, southern Tunisia. (C) Sediment surface with overgrown PS domes of various sizes in relation to microtopographic features. Large PS domes indicate prolonged activity of coccoidal cyanobacteria under thin cover of residual water in microtopographic lows. Scale (coin) is 25 mm. Supratidal zone, Bhar Alouane, southern Tunisia. (D) Isolated PS domes on fresh flat mat of mainly coccoidal cyanobacteria. The domes are stabilised by EPS and partly overgrown. Note large gas dome, about 10 cm in diameter and stabilised by EPS, in centre of photo. The large gas dome likely originated from uprising gases of buried, decaying mats. Scale (coin) is 25 mm. Shallow supratidal pond, Bhar Alouane, southern Tunisia. (E) View of active microbial community and freshly produced photosynthetic bubbles. The bubbles are stabilised by EPS and may merge to form larger units. Lower supratidal puddle, Bhar Alouane, southern Tunisia. (F) Same surface as in Figure 3-4E, after artificial destruction of gas bubbles. Note EPS formerly stabilising bubbles, now forming light, circular, nutrient-rich rims, and interstitial patches around dark hollows. Lower supratidal puddle, Bhar Alouane, southern Tunisia. (G) 'Lizard-skin' texture on microbial mat surface, reflecting structures left behind after bursting of photosynthetic gas bubbles. The microbial mat, developed along the margin of a supratidal puddle, has developed a bulge-like termination towards the puddle. Note shrinkage crack with upturned and slightly curled margins. Scale is 1 cm. Lower supratidal puddle, Bhar Alouane, southern Tunisia. (H) Circular to hexagonal pattern, possibly resulting from burst photosynthetic gas bubbles; partly overgrown and almost disappearing (left side). Rims may have been sites of first overgrowth or internal growth, using nutrient-rich EPS that once stabilised the bubbles. Margin of supratidal pond, El Gourine, southern Tunisia. All photos: Hubertus Porada.

Upon subaerial exposure, small elevated areas on the surface of thin mats may become sites of accelerated desiccation, shrinkage and initial cracking at the crests or peaks (Figure 3-5C). If the desiccating mat still possesses sufficient elasticity, involution or 'curling' of the crack margins may occur (Figure 3-5D). If hydraulic 'upward pressure' in the mat substratum is still sufficient to cause ascent of groundwater, the 'curled margins' may be overgrown and preserved as linear, bulge-like features on the mat surface (Figure 3-5E). Cracking starting at the peaks of domal features in a thin mat frequently leads to circular/subcircular 'curled margin' structures (Figure 3-5F). These may also be overgrown by further microbial expansion.

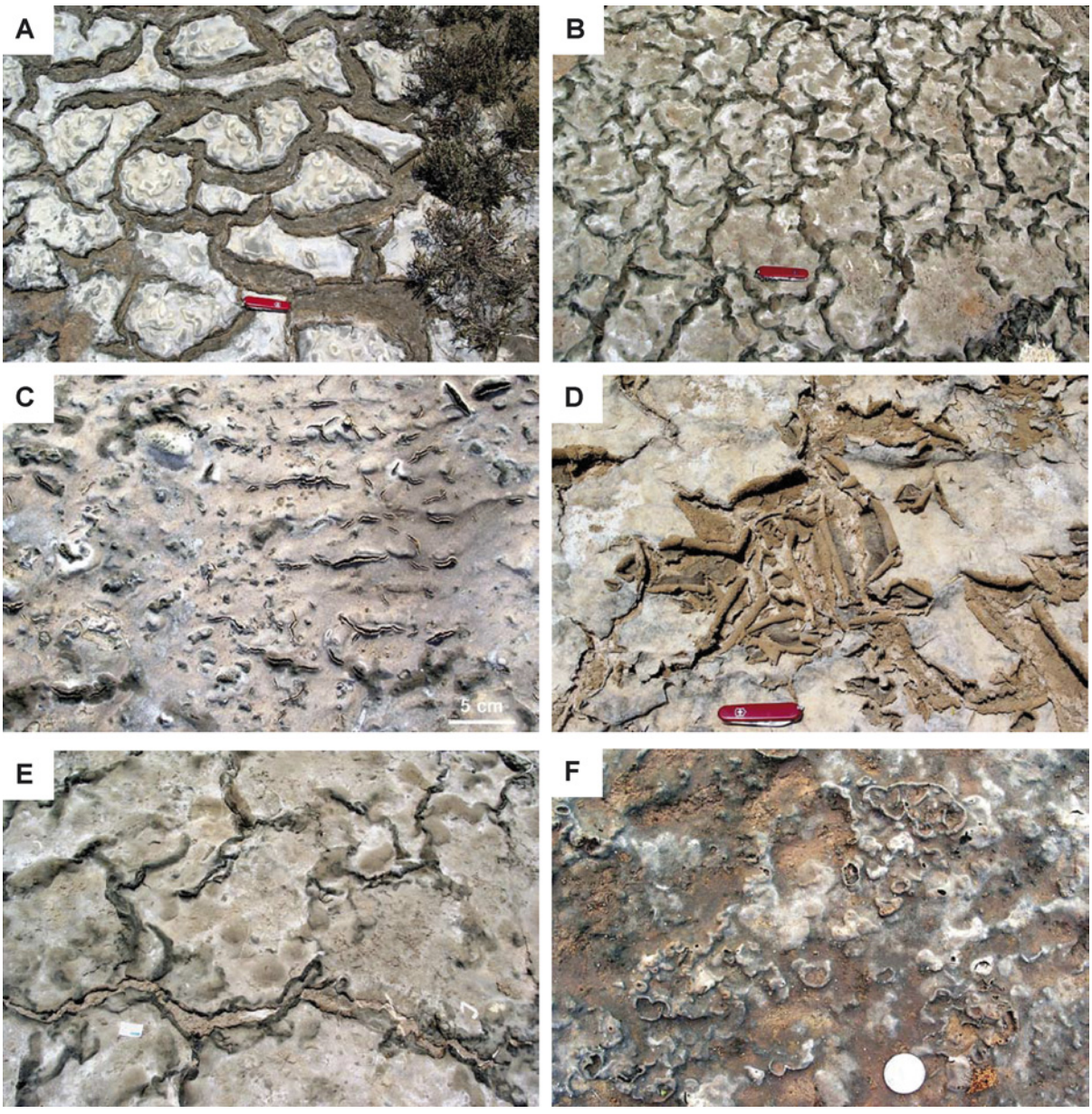
Impressive examples of the intimate interplay of physical processes and vital dynamics in thick biolaminites, modern and ancient, are seen in Figures 4(f)-1 and -2. These 'complex structures' reflect incremental upturning of

Figure 3-5: Structures reflecting 'induced growth' related to mat shrinkage and cracking.
(A) Network of wide shrinkage cracks developed in microbial mat after prolonged subaerial exposure. Crack margins are upturned and locally curled. Crack openings and margins are overgrown by new, flat biofilm/mat layers, microbial growth being induced by ascending groundwater due to hydraulic "upward pressure" in the sedimentary mat substratum. Scale (knife) is 8 cm. Upper intertidal zone, El Jellabia; southern Tunisia. (B) Polygonal network of narrow shrinkage cracks in mature microbial mat. Cracks are overgrown by bulge-like mat expansion structures resulting from localised excessive microbial growth and biomass accretion, induced by uprising groundwater in the crack openings. Scale (knife) is 8 cm. Lower supratidal zone, Bhar Alouane, southern Tunisia. (C) Thin microbial mat with small linear shrinkage cracks located preferably along crests of overgrown ripples, initial cracking being induced by more advanced desiccation and shrinkage on small microtopographic elevations. Note dark zones in lower and upper left part of photo, representing sites of uprising groundwater and induced microbial activity. Supratidal zone, Bhar Alouane, southern Tunisia. (D) Thin microbial mat with wide, irregular shrinkage cracks and curled crack margins. Involution or 'curling' of crack margins may occur if a 'contractional force' emanates from the shrinking but still elastic surface layer, involving adhering mat layers below. Scale (knife) is 8 cm. Supratidal zone, El Gourine, southern Tunisia. (E) Thin microbial mat exhibiting various generations of cracking and microbial overgrowth. First generation, narrow shrinkage cracks in upper and left part of photo are overgrown by bulging mat expansion structures; second generation, wider cracks in central part of photo have developed curled margins and are overgrown by flat mat layers; a youngest, third generation crack in the lower part of the photo partly follows second generation cracks, rupturing flat mat layers and inheriting overgrown crack margins. Scale is 2 cm. Supratidal zone, Bhar Alouane, southern Tunisia. (F) Thin microbial mat of mainly coccoid cyanobacteria, with numerous domal features on the surface. Initial cracking at peaks of domal features frequently leads to circular/subcircular 'curled margin' structures which subsequently may be overgrown. Scale (coin) is 25 mm. Supratidal zone, El Gourine, southern Tunisia. All photos: Hubertus Porada.

a crack margin and microbial growth during repeated tidal cycles with periods of subaerial exposure and inundation, respectively.

CONCLUSIONS

As with most scientific fields, the various classification schemes proposed for microbial mats in terrigenous clastic sediments have advantages and disadvantages when applied to specific case studies, and it can seldom be argued that one scheme is intrinsically superior. In Chapter 2 of this book, Gerdes points out that microbial growth-related structures (in Schieber's 2004 organisational scheme) can easily be related to the five processes implicit in the MISS scheme of Noffke et al. (2001a), namely biostabilisation, levelling, baffling–trapping–binding, imprinting, and microbial grain separation. Analogously, she notes that the mat metabolism-, mat destruction- and mat decay-related structure groupings of Schieber (2004) also relate to biostabilisation. While in many ways, the differences between the various classification schemes discussed may hinge on semantics, the scheme that proves to be most practical in everyday application and is most widely adopted will eventually prevail. It is also likely that the best aspects of each scheme will ultimately be combined into a standard classification as research proceeds. The history of sandstone classifications in sedimentary petrology provides an example how this may play out eventually.



Other, less well-known classification schemes make use of physical properties of preserved mat-induced features in clastic sedimentary rocks (e.g., Sarkar et al., 2004). Due to its combination of simplicity and inclusion of a wide range of interacting genetic factors, we have elected to adopt the Schieber (2004) scheme in this book. This decision is not meant to detract from other classification systems.

Atlas of Microbial Mat Features Preserved within the Siliciclastic Rock Record
Edited by J. Schieber et al.
© 2007 Elsevier B.V. All rights reserved
DOI: 10.1016/S1574-1966(07)02004-4

CHAPTER 4

Mat Features in Sandstones

INTRODUCTION

This chapter deals with biofilm- or microbial mat-mediated sedimentary structures which are preserved in sandstones within the rock record. The arrangement of the sections within the chapter follows the classification scheme of Schieber (2004) adopted for this book (Chapter 3): (a) mat growth features; (b) mat metabolism features; (c) mat destruction features; (d) mat decay features; (e) diagenetic mat features; with an additional short section (f) on complex features.

Mat decay features discussed under (d) are predominantly those resulting from the escape of gases or liquids resulting from decay of organic matter buried beneath cohesive biofilms. The diagenetic mat features, classified under (e) in the Schieber (2004) scheme, encompass most commonly microscopic features (as opposed to the much larger structures discussed under (d)) related to *in situ* mat decay. As the decay of one bacterium may well be the metabolism of another, it makes sense to examine features classified under (b) and (e) within a single context of related genesis (J. Schieber, personal comm., 2006). Within the chapter that follows, features classified under (b) and (e) are thus treated together by Schieber under a single heading, namely Section 4(b).

A detailed and more formal description of each mat-related feature to be found in sandstones is provided here. This contrasts with the companion Chapter 5, dealing with microbial mat features formed in muddy sediments and preserved in mudrocks. The latter features are generally microscopic in scale and much less studied than their larger sandstone-related counterparts, justifying a more general discussion of the mat-related structures in the single-authored Chapter 5.

4(a). MAT GROWTH FEATURES

D. Bottjer, J.W. Hagadorn

Introduction

Because sandy siliciclastic subaqueous environments are not typically characterised by mineral precipitation, their microbially mediated sedimentary structures have more subtle vertical relief when compared with microbial structures produced in mineral-precipitating carbonate environments. For a long time sedimentologists and palaeobiologists only worked on the more obvious stromatolites and associated carbonate structures, and microbial mat features from siliciclastic rocks were overlooked. But, in the past decade close examination of siliciclastic sedimentary rocks, particularly those from Precambrian and early Phanerozoic marine strata, has revealed a plethora of structures, largely formed due to growth of microbial mats at the sediment-water interface or the interaction of physical processes with biofilm- or mat-bound sediment surfaces.

There are numerous relevant references to these structures, which are listed in this book and referred to in many of the other chapters. We draw readers' attention to certain critical references: Hagadorn and Bottjer (1997), Hagadorn et al. (1999), Gerdes et al. (2000a), Noffke et al. (2001a) and Schieber (2004).

Definition and genesis of mat growth features

When a microbially-bound sandy surface is subjected to current and wave action, the surface may tear and break apart into cohesive fragments that can range from having a pliable consistency to being relatively rigid (Figures 4(a)-1, -2, -3A). A variety of evidence can indicate the original pliable nature of such clasts, including deformation of adjacent clasts (Figures 4(a)-1, -2). Sand chips indicate the possible influence of both microbial binding and mineral precipitation (Figure 4(a)-3A).

Increased cohesiveness of sandy substrates imparted by the presence of microbial mat binding is also indicated by the stabilisation of ripples on seafloors that are overlain by a subsequent generation of ripples (Figures 4(a)-3B to -3D). In these cases the underlying rippled surface can show no evidence for erosion from deposition of the overlying rippled sand, indicating that the underlying surface was stabilised by microbial binding. Evidence for loading of the underlying rippled surface can also be used to demonstrate increased cohesiveness due to presence of a microbial mat (Figures 4(a)-3C, -3D).

A variety of patterned bedding plane structures have been termed wrinkle structures and include such features as wrinkle marks (also known as 'runzelmarken'), 'old elephant skin' (OES), and '*Kinneyia*' (Figures 4(a)-4 to -8). Wrinkle structures (Figures 4(a)-4A to -4E) may have multiple origins. When they occur at sandstone bed interfaces in which mud is demonstrably absent, the corrugated surface of the underlying sand bed likely reflects the original surface topography of a microbial mat, and/or micro-scale loading of these microbially-bound sediments (see also discussion in Chapter 6(a)). For example, 'old elephant skin' (Figures 4(a)-5 to -7) is caused by small-scale loading due to deposition of a thin sand bed upon a microbially-bound sandy seafloor. '*Kinneyia*' (Figure 4(a)-4F) is a surface of reticulated flat-topped ridges that are interpreted to form by gas bubble buildup beneath a biofilm, which inhibits cementation. When such features form in a series of successive beds, the phenomenon of exfoliating sand laminae may present itself in outcrop (Figure 4(a)-8).

In sandy siliciclastic settings, significant topography may build up on the seafloor in the form of domal sand buildups or 'sand stromatolites' (Figures 4(a)-9 to -11). Patterns in these structures can include clusters with larger domes in the middle surrounded by smaller domes (Figures 4(a)-9, -10A, -10C, -10D), while other associations are not clustered and show no preferential size distribution (Figures 4(a)-10B, -11). Clustered and non-clustered associations of domes can occur on the same bedding surface (Figure 4(a)-10). The low synoptic relief of these domal sand buildups, in contrast with stromatolites, is likely due to the lack of carbonate precipitation in sandy siliciclastic environments, which aids in buildup of microbialites with greater vertical relief in carbonate settings.

In environments where sand stromatolites have formed, current action may transport sand across the seafloor, leading to the development of sand shadow structures (Figure 4(a)-12). Ripples can also develop differentially on seafloors where the coverage by microbial mats was patchy, either due to original growth patterns or because mats were partially ripped-up by waves and/or currents (Figures 4(a)-13, -14). Ripples with cracked crests are also found (Figure 4(a)-15), most likely formed by fluid expulsion through the crests of the microbially-bound ripples. Such cracking of microbially-bound ripple crests can then lead to significant erosion of crests (Figure 4(a)-16).

A variety of other features associated with microbial mat growth has also been described and is outlined in other sections of this book. Sand 'roll-ups' and petees also form during mat growth; in common with many of the microbial mat-related features in this book, these features may also be associated with genetic processes other than mat growth, and mat destruction-related examples are examined in Section 4(c) of this chapter. Although we have made great progress over the past decade in identifying microbial mat growth features in sandy siliciclastic environments, we still have much to learn about what controls the morphology and distribution of microbial structures in siliciclastic environments – especially in ancient settings for which there are no modern comparative analogues.

Formal description of mat growth features

Spheroidal pliable sand clasts: Figures 4(a)-1, -2, -3A

Name of structure: spheroidal pliable sand clasts.

Other terms used: 'algal balls', 'sand balls', 'sand ooids' .

Description of structure: sphere-shaped clasts of sandstone showing no internal evidence for either clay or internal concentric lamination when examined through slabs, X-rays and thin sections. Clasts commonly deformed or deform one another; show no tendency towards sorting into ripple troughs or (palaeo-)topographic depressions. May deform overlying or underlying sandstone beds, or be preserved as impressions in either of these bounding sandy beds.

Associated sedimentary structures: (1) ripple marks; (2) trace fossils.

Palaeoenvironment: intertidal to very shallow subtidal marine.

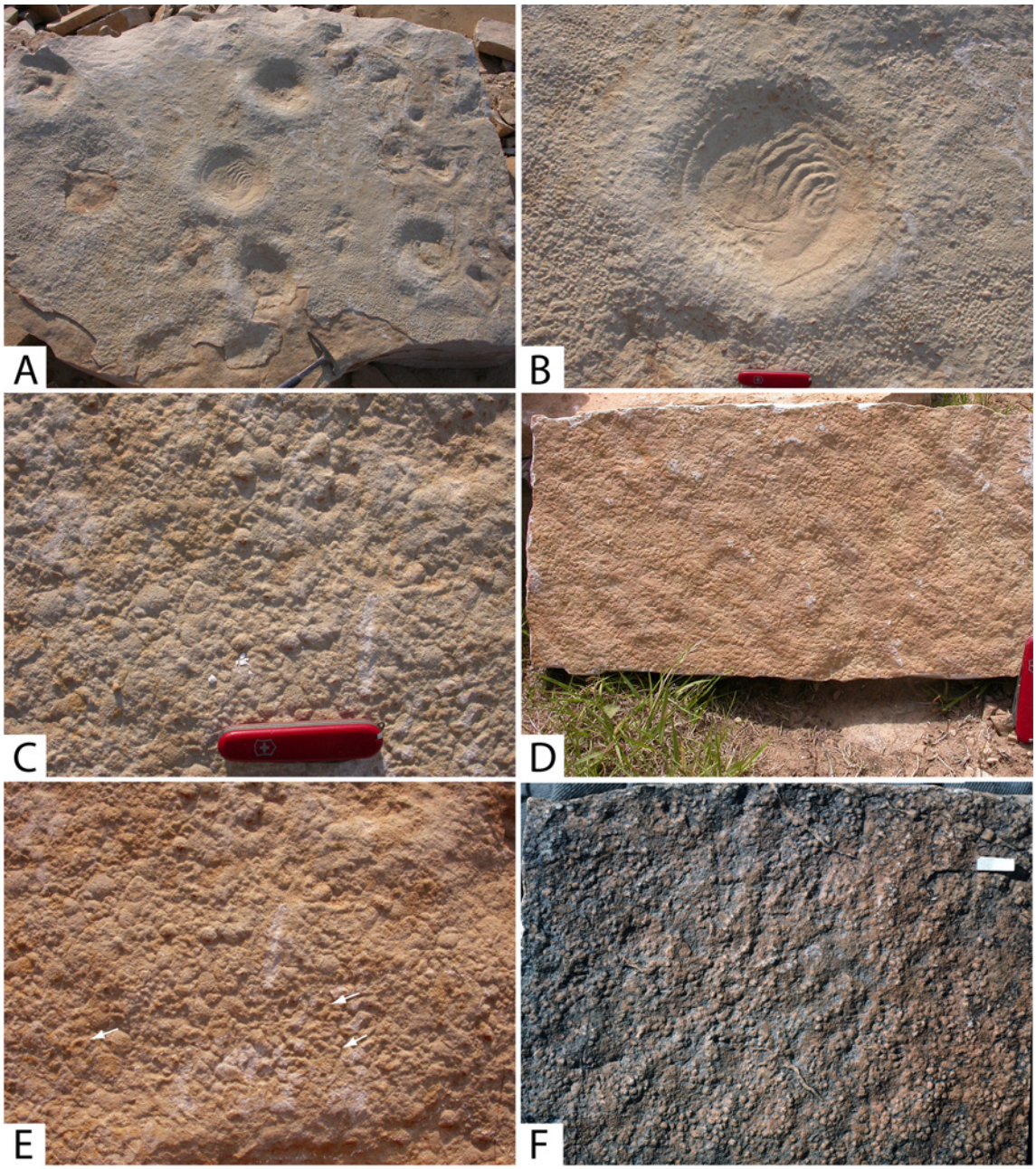


Figure 4(a)-1: Spheroidal pliable sand clasts, also known as 'algal balls', 'sand balls', or 'sand ooids', in quartz arenites of the Late Cambrian Elk Mound Group, Wisconsin, USA (A–E), and of the Cambrian Fish River Formation, Namibia (F).

Images (A)–(E) are bed-soles; (A), (B) bear scyphomedusae impressions. All surfaces are overlain and underlain by very fine- to medium-grained quartz arenites. (B) is a close-up of the centre of (A), and (C) is a close-up of the lower right portion of (B). (E) is a close-up of the upper left portion of (D). Spheroidal clasts in (A)–(C) are preserved in convex hyporelief (figured) and convex epirelief (not figured; but on reverse side of exfoliating sand veneer near hammer in A). Note the deflated/compressed clasts in (E), some of which are arrowed. Slab, X-ray, and petrographic examination of serially sectioned spheroidal sand clasts in (A)–(C) revealed no concentric internal lamination, clay, or evidence for non-quartzose cements. Together with the fact that these clasts deform one another, yet are not preferentially sorted into ripple troughs or topographic depressions, these properties suggest that they were likely pliable and possibly also sticky – properties consistent with fecal pellets or microbially bound sand spheres. Pliability of clasts and deformation of overlying and underlying beds (implying that all three were unlithified) diminishes the possibility that these clasts could be weathered beach rock fragments. Specimen in (F) is from P. Pflüger, Tubingen University. Hammer head in (A) is 17.5 cm long; Swiss army knife in (B)–(D) is 8.3 cm long; scale in (F) is 1 cm long. All photos: J.W. Hagadorn.

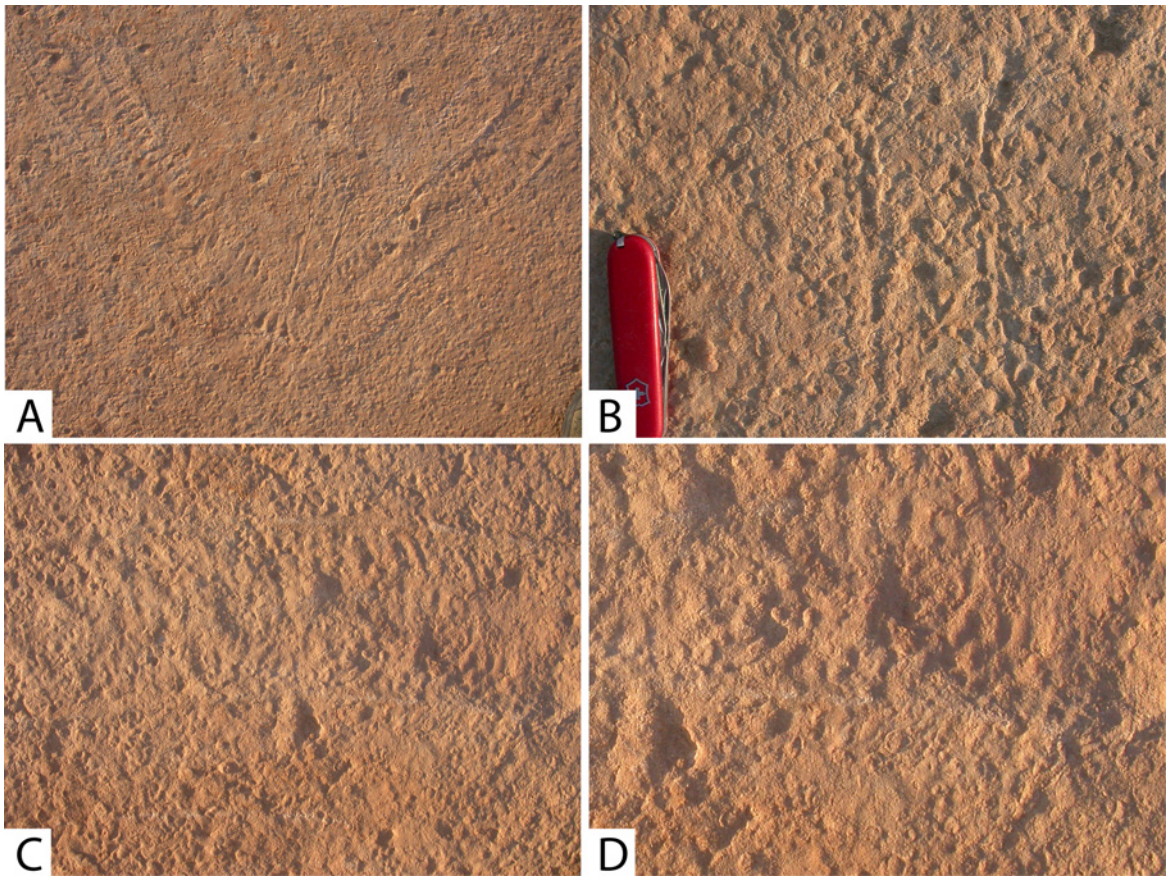


Figure 4(a)-2: Spheroidal pliable sand clasts in quartz arenites of the Late Cambrian Elk Mound Group, Wisconsin, USA.
All images are of the same bed surface, that bears *Climactichnites* (A, C, D) and *Diplichnites*-like (A, B) trackways, which have pliable sand clasts superimposed atop and impressed into them. (B) is a close-up of the centre of (A), and (D) is a close-up of the right-centre portion of (C). In (B) and (D), note where trace fossils have been pliably deformed by the sand clasts, and that where clasts have been removed, crater-like features remain. Exfoliation of the bed overlying this surface reveals that spheroidal sand clasts are sandwiched between medium-grained quartz arenite beds, but create convex impressions in both overlying and underlying beds. Note that clasts exhibit evidence of folding, mutual deformation, and partial deflation. In petrographic and X-radiographic analyses of thin-sectioned clasts, no concentric internal lamination, clay, or evidence for non-quartzose cements is present. *Climactichnites* trails in (A), (C), (D) are 12 cm wide, Swiss army knife in (B) is 8.3 cm long. All photos: J.W. Hagadorn.

Ideas on genesis: growth of a mat which is subject to high energy wave and current action in shallow water (largely marine) settings can result in cohesive fragments of mat-bound sand which are then able to become rounded and pliable during their transport and deposition; deformation of these clasts and unlithified under- and overlying beds may then easily result. Spheroidal sandy fecal pellets can have similar shapes, sizes, and textures in Phanerozoic marginal marine settings; at present it is unknown how/if one can distinguish between such pellets and microbially-mediated sand spheroids.

Palimpsest ripples and loaded ripples:* *Figures 4(a)-3B to -3D

Name of structure: palimpsest ripples, and loaded ripples.

Other terms used: none.

Description of structure: preservation of successive sets of ripples in sandy sediments, with crests of each set being relatively sharp and un-reworked. An absence of mud between such successive rippled sandy beds is essential to their identification; non-amalgamation of two rippled sandstone beds suggests the presence of a mat or biofilm

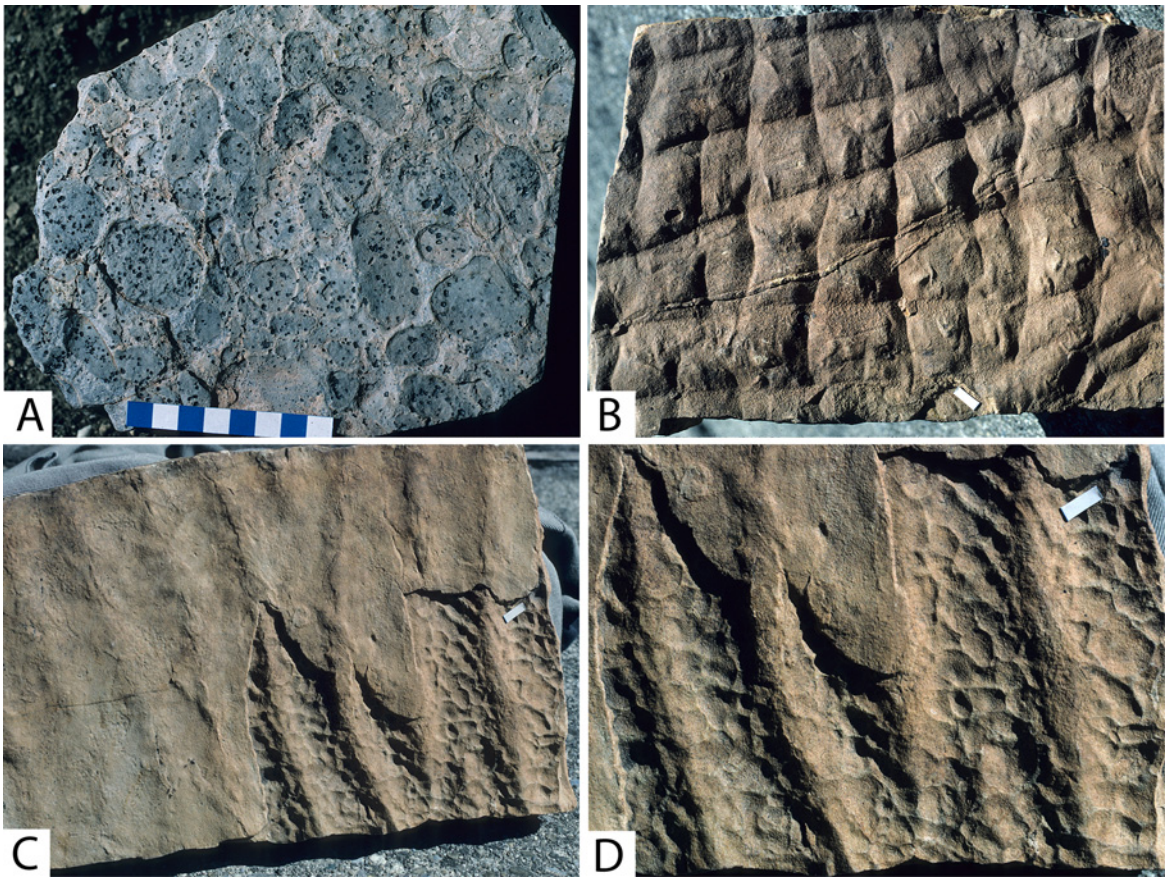


Figure 4(a)-3: Sand chips (A), palimpsest ripples (B) and loaded ripples (C, D).
(A) is from the Neoproterozoic Nudaus Formation, Namibia (Pflüger and Gresse, 1996). (B)–(D) are from the Mesoproterozoic Chorhat Sandstone, India. (A), (C), (D) are bed surfaces, (B) is a bed-sole. Note preferential pyritisation of quartz arenite sand chips in (A), and preservation of older ripple crests and younger ripple crests in (B). Both the rounding and transport of unlithified quartz sand in (A), and the lack of erosional scouring of older sharp ripple crests (by the younger set) in (B) suggest that organically-mediated sand stabilisation occurred – possibly resulting from microbial binding of older surfaces. In (C) and (D), note the loading of oscillation ripple-marked sand by a thin veneer of overlying sand. The absence of clay at this bed interface, together with the absence of amalgamation of the two lithologically identical layers suggests that there must have existed some type of biofilm or other veneer which inhibited amalgamation, but was flexible enough to allow plastic deformation at the time of burial of the underlying rippled surface. Specimens from P. Pflüger, Tubingen University. Scale bar increments in (A) are 1 cm, and bars in (B)–(D) are 1 cm long. All photos: J.W. Hagadorn.

providing organically-mediated sand stabilisation. For loaded ripples, the rippled sandstone surface is marked by loading features related to a thin veneer of overlying sandstone.

Associated sedimentary structures: palimpsest and loaded ripples can occur together.

Palaeoenvironment: intertidal marine.

Ideas on genesis: the preservation of underlying ripples despite deposition of an overlying sandy, rippled bed argues for the presence of a microbial mat separating the two successive sandy beds, protecting the earlier ripples from reworking. For loaded ripples, the evidence for soft sediment deformation of the lower sandy bed and the lack of amalgamation of the two sandy beds argues for the presence of a mat to provide flexibility and cohesiveness of the lower, deformed bed.

Wrinkle structures:* *Figures 4(a)-4A to -4E

Name of structure: wrinkle structures.

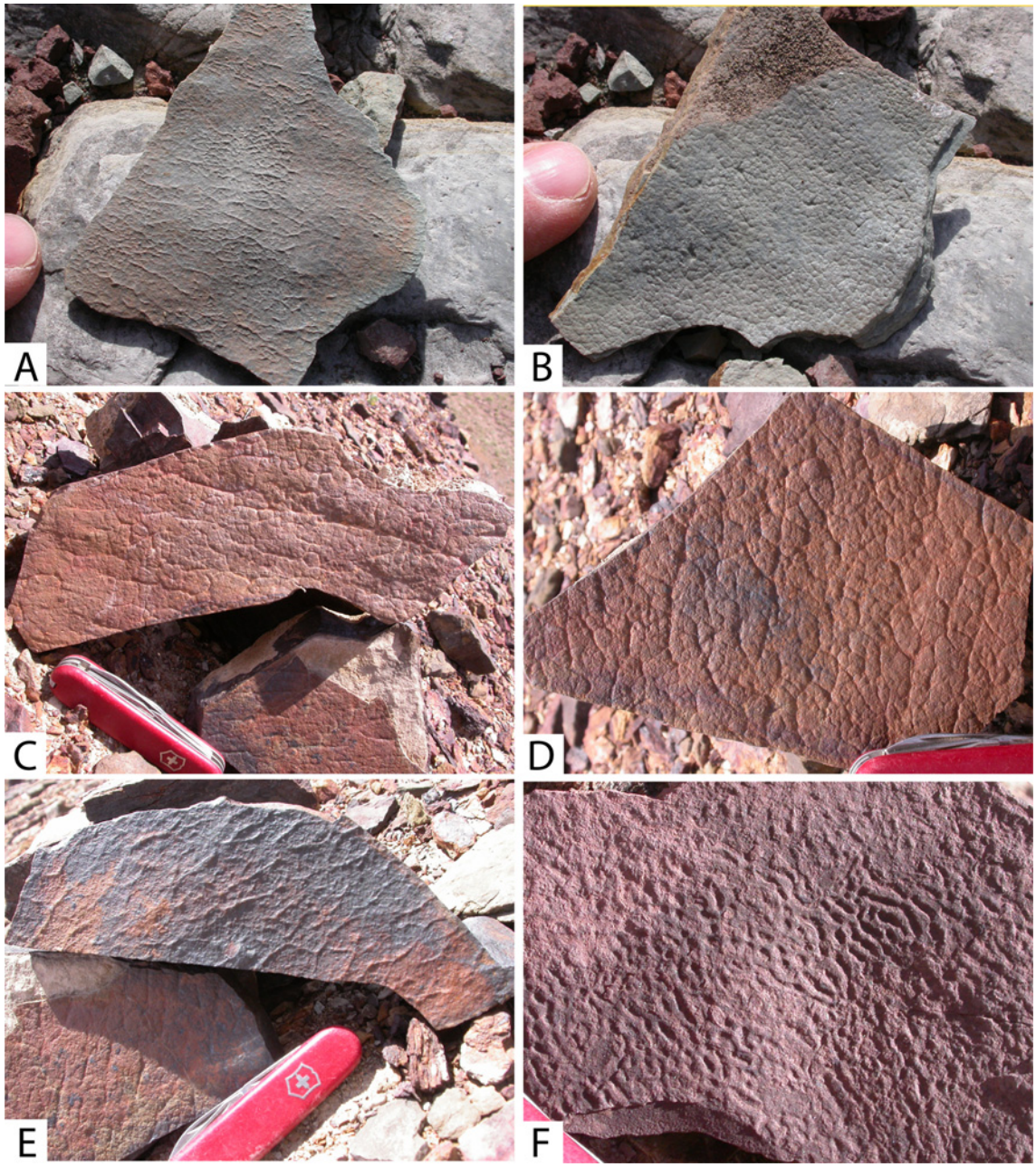


Figure 4(a)-4: Wrinkle structures, including 'runzelmarken'/wrinkle marks (A–E) and '*Kinneyia*' (D) in fine-grained sandstones. (A, B) Carbon Canyon Member, and (C–E) Jupiter Member, Neoproterozoic Chuar Group, Grand Canyon, USA. (F) Neoproterozoic Nankoweap Formation, Grand Canyon, USA.
(A, B) Freshly split fragments of part–counterpart wrinkle-bearing surfaces; upper surface at left. (C, D) Bed-soles of oxidised (limonitic?) wrinkled surfaces; counterpart (bed surface) to this horizon is in (E). Note raised reticulate pattern on bed tops in (A), (E), and bed-soles that display what look like small-scale loading features or 'old elephant skin' (OES) in (B)–(D) (see also Figures 4(a)-5 to -8 for additional examples of OES). Wrinkle structures are poorly understood, but in sandstones in which mud is absent between sandstone bed interfaces, may be formed by purely microbial processes or a combination of biofilm-mediated physical loading processes. (F) '*Kinneyia*', characterised by an irregular mosaic-pattern of flat-topped microripple-like crests. Such structures originally were thought to be biogenic (*sensu Kinneyia*), were then assigned to physically produced structures, and have recently been found to form through gas bubble buildup inhibiting cementation beneath a sandy mat (Pflüger, 1999). Thumbnail in (A), (B) is ~2 cm wide; Swiss army knife in (C)–(F) is 8.3 cm long. All photos: J.W. Hagadorn.

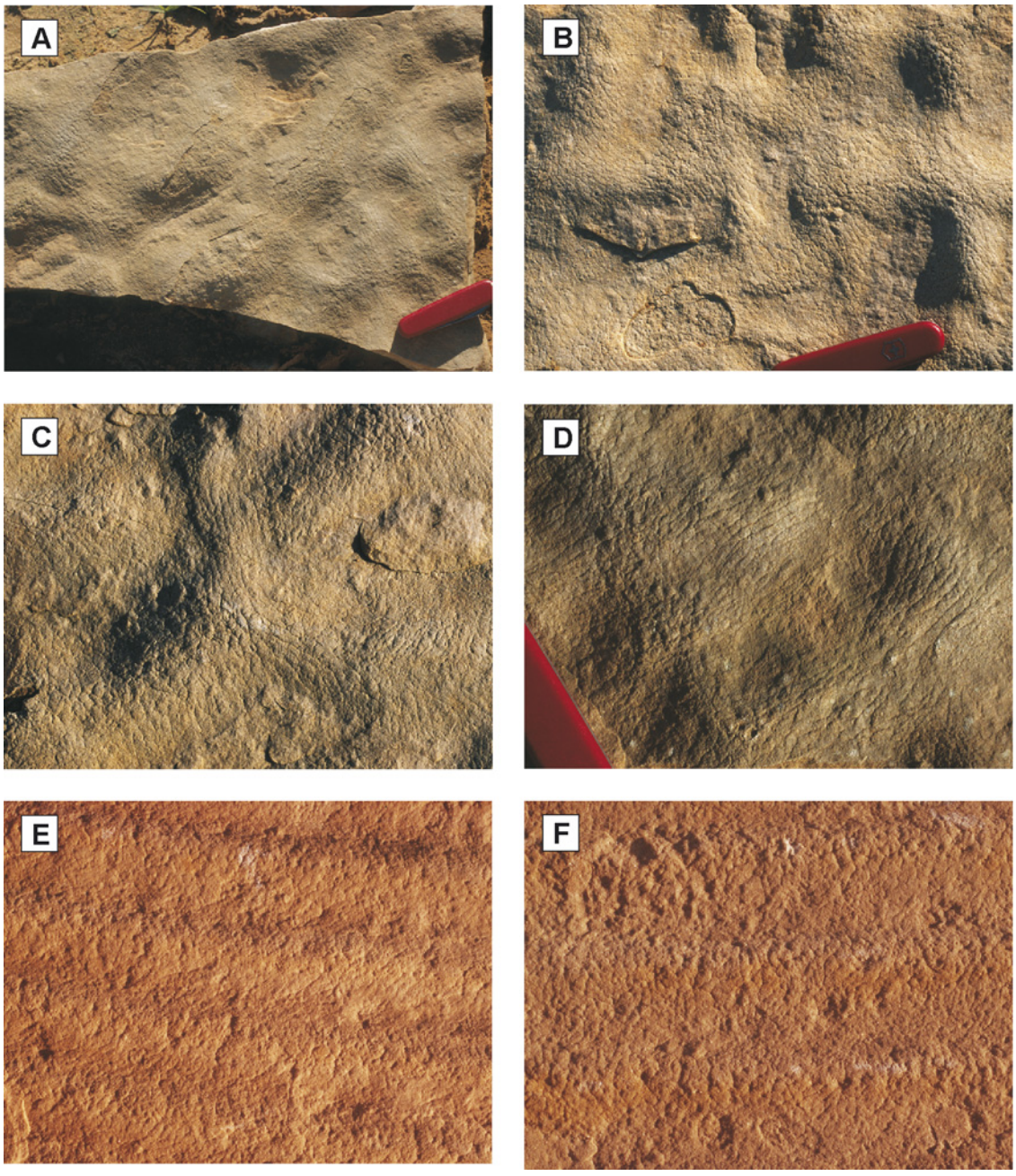


Figure 4(a)-5: 'Old elephant skin', also known as OES, a type of wrinkle structure visible on bed-soles at sand–sand bed interfaces; all images are of quartz arenites of the Late Cambrian Elk Mound Group, Wisconsin, USA.

This quasi-polygonal texture may form when biofilms provide a veneer between beds upon which loading occurs, yet in which the biofilm keeps the overlying and underlying beds (which are lithologically identical) from amalgamating. Modern mats have also been observed to produce a similar surface corrugation, and sand deposited atop such mats may cast this mat-produced surface sculpture. Many OES-bearing surfaces are also characterised by exfoliating sand laminae (compare A, B to Figures 4(a)-6A, -6D, -8). Given the very thin nature of overlying sand laminae (visible at bottom of B), where <0.5 mm thick quartz laminae are superimposed on top of one another, yet each have different and non-overlapping surface patterns, it seems plausible that this texture represents a primary surface-produced feature. (B–D) Close-up views of the ripple-marked bed-sole in (A), viewed with different lighting. (E) and (F) are part–counterpart slabs of a straight-crested oscillation ripple-marked bed interface. Swiss army knife in (A), (B), (D) is 8.3 cm long, scale bars in (C), (E), (F) are ~3 cm long. All photos: J.W. Hagadorn.

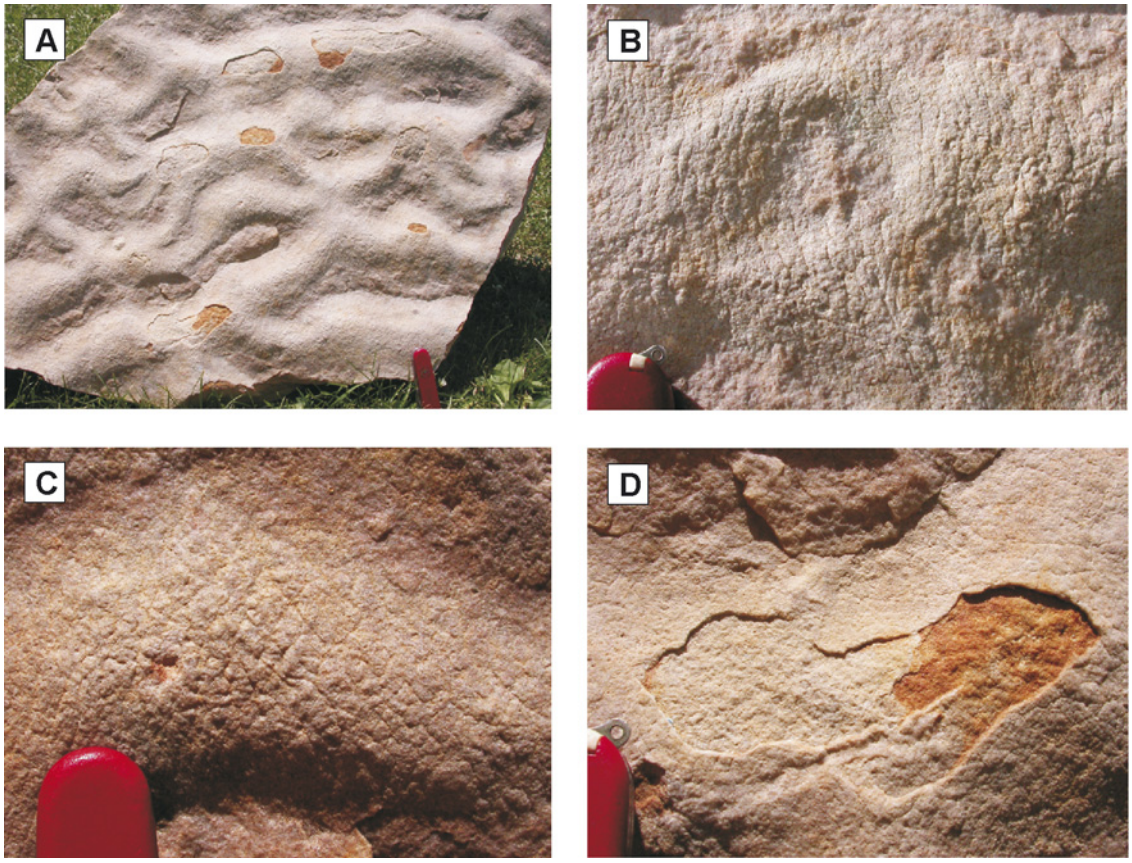


Figure 4(a)-6: 'Old elephant skin', or OES, on bed-soles in quartz arenites of the Late Cambrian Elk Mound Group, Wisconsin, USA.
This quasi-polygonal texture may form when biofilms provide a veneer between beds upon which loading processes can operate, yet in which the biofilm kept the overlying and underlying beds (which are lithologically identical) from amalgamating. On many freshly parted surfaces, an oxidised veneer or limonitic coating is visible at or between sand–sand bed interfaces (e.g., orange-coloured regions visible in A, D, where underlying layer has been removed; for comparison see freshly removed areas between sand laminae in Figure 4(a)-8). Gehling (1999) hypothesised that this coating represents oxidised remnants of bacterially mediated pyrite precipitated in/around a decomposing biofilm. (B–D) These are close-ups of the ripple-marked bed-sole in (A), viewed with different lighting. Swiss army knife in (A)–(D) is 8.3 cm long. All photos: J.W. Hagadorn.

Other terms used: 'runzelmarken', wrinkle marks.

Description of structure: wrinkled sandstone or muddy sandstone surfaces, either as bed-tops or bed-soles, showing a reticulate pattern of small raised ridges.

Associated sedimentary structures: '*Kinneyia*'.

Palaeoenvironment: intertidal to subtidal marine.

Ideas on genesis: wrinkle structures are thought to form due to either purely microbial processes or a combination of these with biofilm-mediated physical loading processes (see also discussion in Chapter 6(a)). Wrinkle structures may reflect original topography of a microbial mat growing on a sandy substrate, or such microbially-bound sediment affected by micro-scale loading or shear stresses.

'Old elephant skin': Figures 4(a)-5 to -7

Name of structure: 'old elephant skin'.

Other terms used: abbreviated as OES.

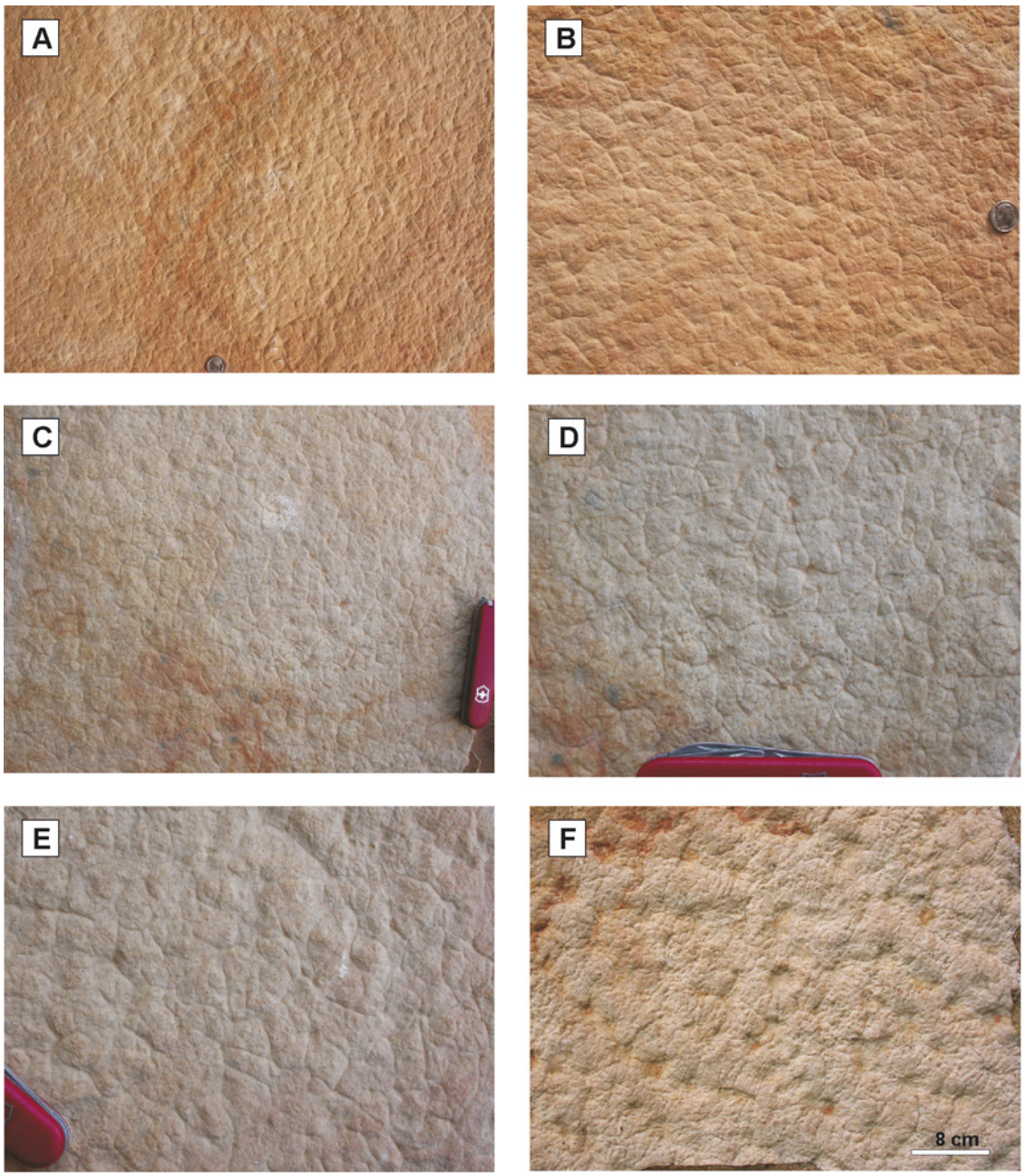


Figure 4(a)-7: Large OES ('old elephant skin') textures, a type of wrinkle structure visible on bed-soles at sand–sand bed interfaces. (A)–(E) are from quartz arenites of the Late Cambrian Elk Mound Group, Wisconsin, and (F) is from the Late Cambrian Gunter Sandstone, Missouri, USA.
Unlike smaller-sized OES, this type of large 0.5–2 cm scale wrinkle structure is not well known, and is not always associated with exfoliation of thin sand laminae; investigations of how it is manifested in vertical section have not been conducted. (B) is close-up of (A), and (D), (E) are close-ups of (C), lit from different angles. Note wicking and quasi-radial patterns to OES forming on ripple crests and troughs in (F). Coin in (A), (B) is 1.8 cm wide; Swiss army knife in (C)–(E) is 8.3 cm long; scale in (F) is 8 cm long. All photos: J.W. Hagadorn.

Description of structure: a surface corrugation of a sandstone bed which provides a quasi-polygonal texture in the rock record. Bed-top OES usually bears concave bulbous depressions and sharp convex crests, and bed-bottom OES bears convex-to-bulbous textures with sharp concave depressions.

Associated sedimentary structures: (1) oscillation ripples; (2) exfoliating sand laminae.

Palaeoenvironment: intertidal to subtidal marine.

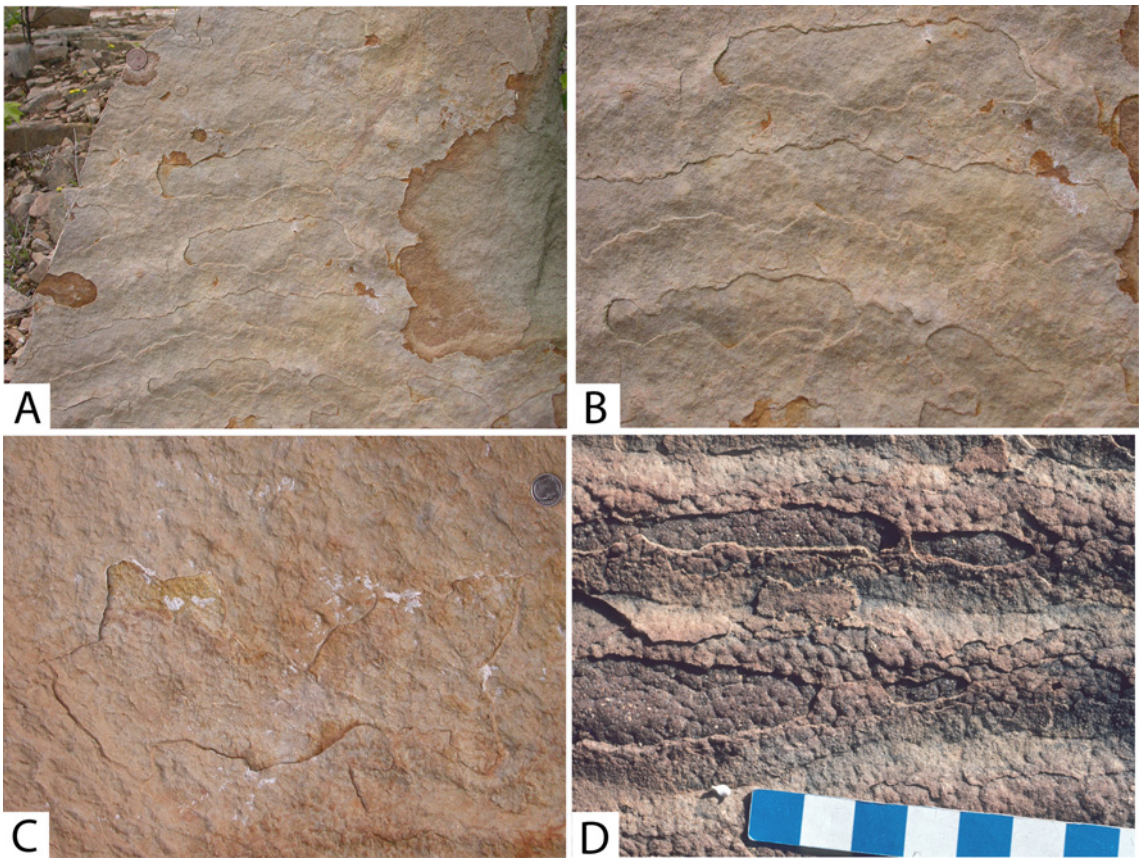


Figure 4(a)-8: Exfoliating sand laminae visible on bed-soles of rippled quartz arenites. (A)–(C) are from the Late Cambrian Elk Mound Group, Wisconsin, USA; (D) is from the Neoproterozoic Rawnsley Quartzite, South Australia.

(B) is a close-up of the central area in (A). Note the successive ⩽1 mm thick veneers of medium-grained sand spalling off the rock surface; no mud occurs between these laminae, and reticulate elephant skin structure occurring in overlying layers is not superimposed on or through underlying layers. Thus, wrinkled OES textures on each underlying layer differ in their arrangement from those of the overlying layer. Together, these features suggest that each veneer was resistant to erosion, loading, and imprinting by the overlying burial layer – and did not become amalgamated into or adhere to the compositionally identical overlying non-muddy layer. Such behaviour is consistent with the presence of a biofilm on each layer, which inhibited amalgamation of the underlying layer into the newly deposited overlying layer. A limonite coating is often visible between the two layers (orange areas where laminae have been freshly removed), and could result from oxidation of bacterially mediated pyrite beneath each biomat (*sensu* Gehling, 1999). Coin in (A), (C) is 1.8 cm wide; scale bar units in (D) are cm. All photos: J.W. Hagadorn.

Ideas on genesis: thought to reflect biofilms separating thin sandstone beds subject to soft sediment loading processes – the biofilm keeps the two beds separate and prevents their amalgamation, and also provides cohesiveness to the lower sandy bed to allow its deformation.

'Kinneyia': Figure 4(a)-4F

Name of structure: '*Kinneyia*'.

Other terms used: flat-topped 'runzelmarken' or wrinkle marks.

Description of structure: irregular mosaic-like pattern of flat-topped ovate pits or grooves. Walls of pits or grooves are steep sided and occur on sandstone or muddy sandstone bed-tops or flat tops between truncated ripple crests.

Associated sedimentary structures: (1) wrinkle structures; (2) large ripple troughs.

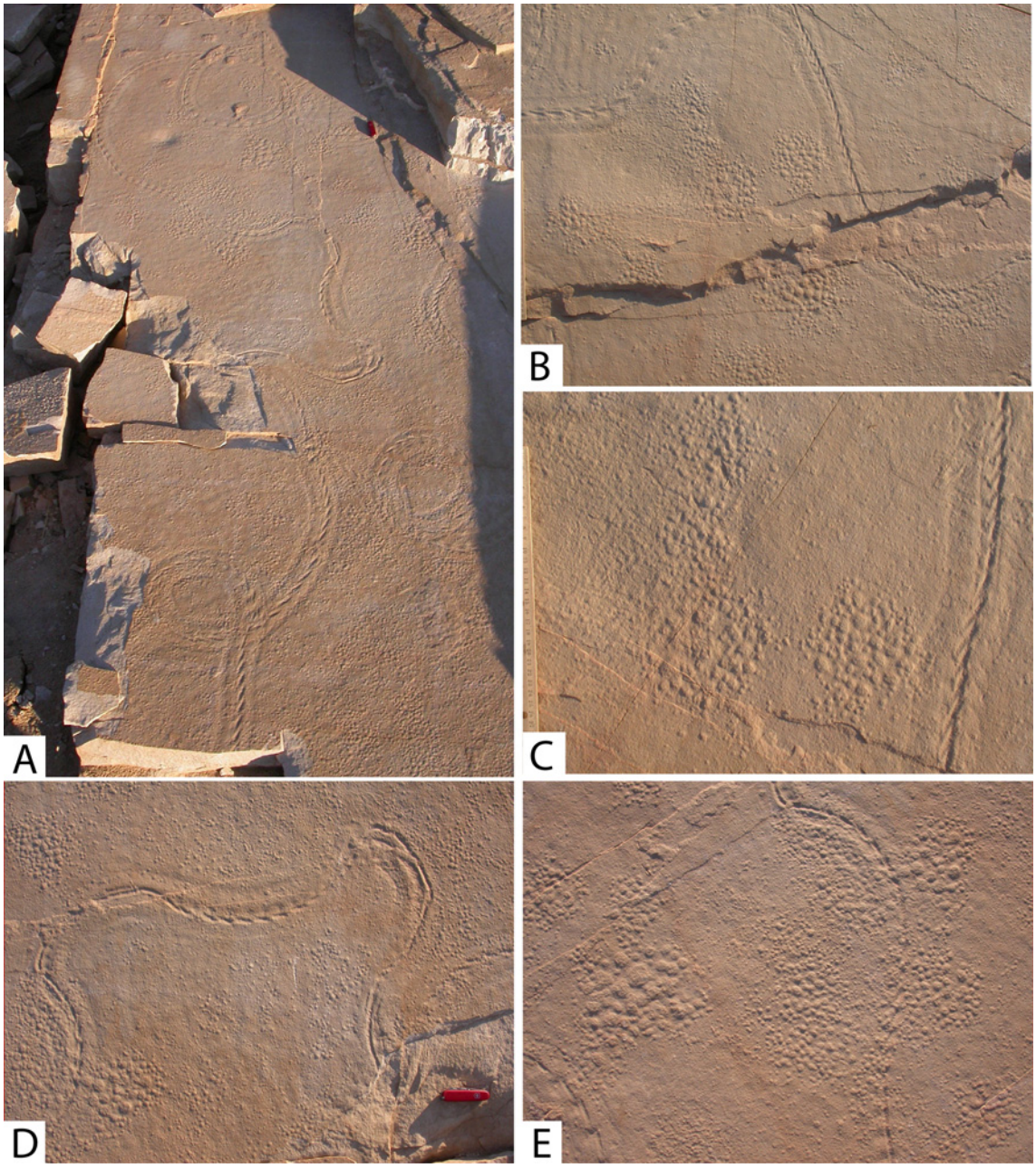


Figure 4(a)-9: Domal sand buildups, also known as 'sand stromatolites' on a bed surface characterised by *Protichnites* trackways in quartz arenites of the Late Cambrian Elk Mound Group, Wisconsin, USA. These low mound-like structures often occur in clusters, with larger heads toward their centre and smaller heads toward their exterior. Similar cauliflower-like growth morphologies are exhibited by stromatolites in carbonate settings, except that the sand stromatolite heads have significantly lower vertical relief – probably owing to the lack of bacterially mediated carbonate precipitation in heads – the latter normally facilitates upward growth of heads and physical resistivity to waves, wind, and tides. Images (B)–(E) are close-ups of surface in (A), and (E) is a close-up of left portion of (D), where track cross-cuts or is grown-over/-through by sand stromatolite clusters. Swiss army knife in (A), (D) is 8.3 cm long. All photos: J.W. Hagadorn.

Palaeoenvironment: intertidal to shallow marine.

Ideas on genesis: thought to form through buildup of gas bubbles in sandy sediments immediately underlying a biofilm or mat. Gas may be generated by decomposition of organic matter. Bubbles trapped on the underside of the biofilm may coalesce; sand between bubbles becomes cemented, and with subsequent decomposition of the overlying mat and compaction, overlying sediments infill the bubble pits.

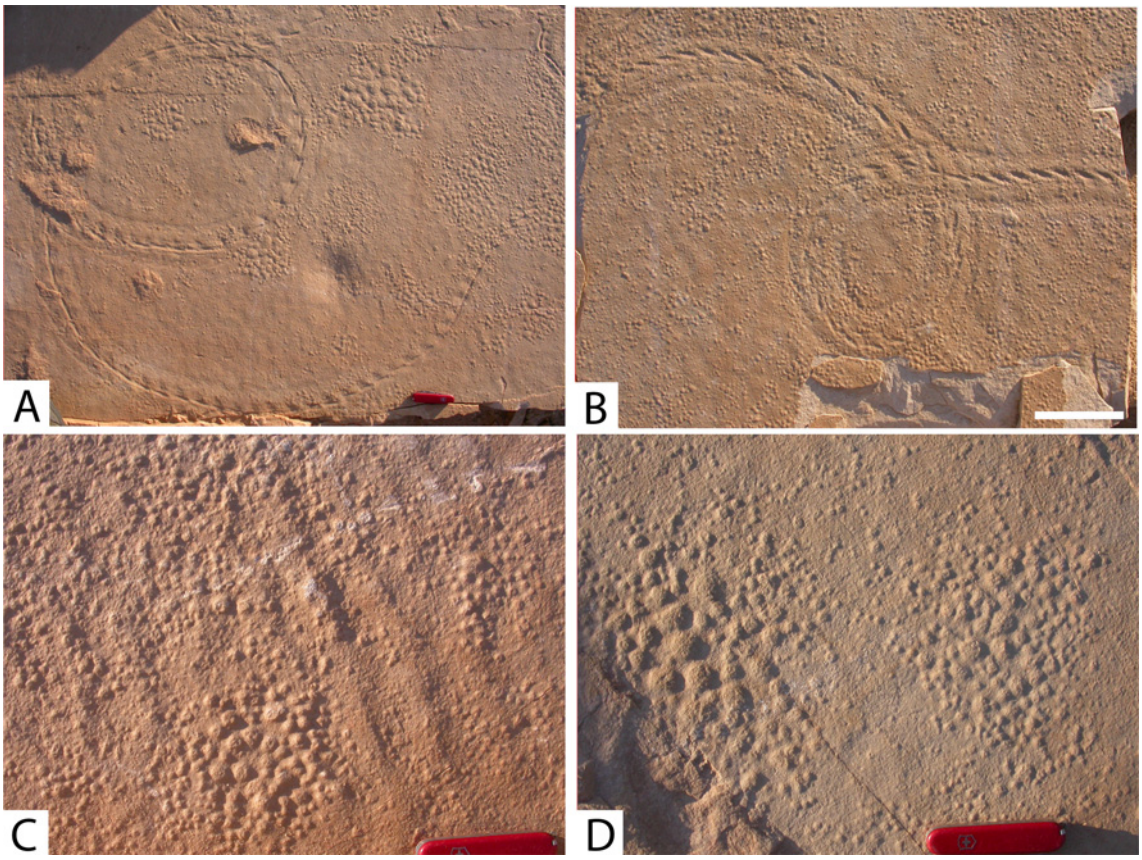


Figure 4(a)-10: Domal sand buildups, also known as 'sand stromatolites' on quartz arenite bed surfaces of the Late Cambrian Elk Mound Group, Wisconsin, USA.
(A) and (B) are from the same surface, and are characterised by looping *Protichnites* trackways. The area shown in (A) has well clustered heads, yet (B) is dominated by non-clustered small pea-sized sand stromatolites; together these indicate that both forms may exist under the same environmental conditions. The different morphologies thus may represent different life histories, biological affinities, and/or histories of interaction with the physical environment. Clustered sand stromatolites can also grow over rippled (C) and unrippled (D) surfaces, and together with the mixture of unclustered and clustered forms in (C), suggest that perhaps clustered sand stromatolites may represent an older or faster-growing region than the unclustered heads. Although it is possible that large sand stromatolites (Figure 4(a)-11) represent the oldest, fastest-growing, and/or most resistant components of such microbial communities, it is unclear how one could confidently falsify or constrain these hypotheses. Swiss army knife in (A), (C), (D) is 8.3 cm long; scale in (B) is ~12 cm long. All photos: J.W. Hagadorn.

Exfoliating sand laminae: Figure 4(a)-8

Name of structure: exfoliating sand laminae.

Other terms used: none.

Description of structure: successive, very thin (⩽1 mm) veneers of sandstone which spall off a preserved rock surface.

Associated sedimentary structures: (1) 'old elephant skin'; (2) petees; (3) domal sand buildups.

Palaeoenvironment: intertidal to subtidal marine.

Ideas on genesis: The lack of any mud separating such sandstone veneers as well as variable OES textures on each of the underlying layers suggest that each thin sandy layer was resistant to erosion, loading, and overprinting by the succeeding thin sand veneer due to the presence of a biofilm upon each sandy layer.

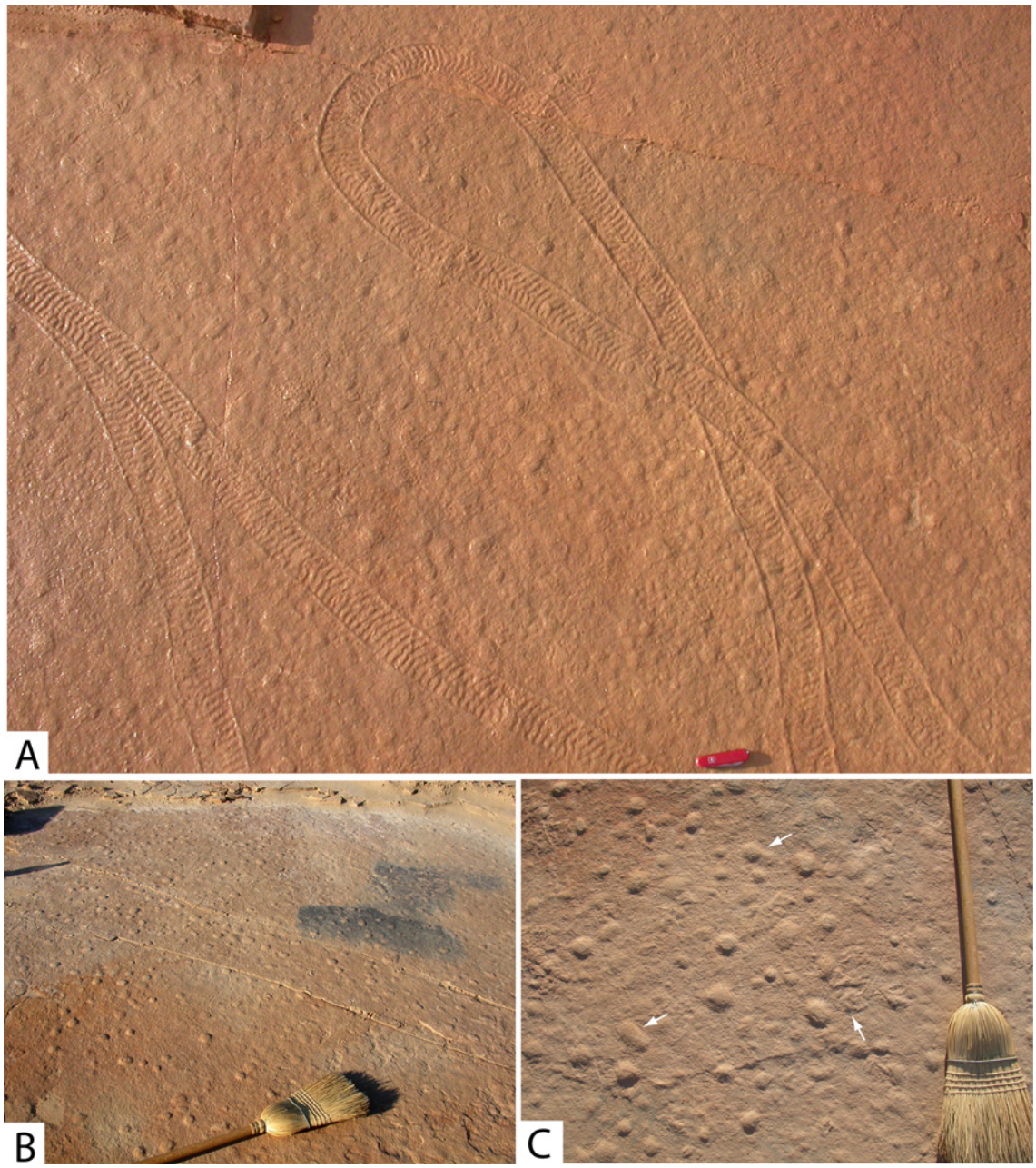


Figure 4(a)-11: Large non-clustered domal sand buildups, also known as 'sand stromatolites', on quartz arenite bed surfaces of the Late Cambrian Elk Mound Group, Wisconsin, USA.

These heads are relatively evenly distributed on these surfaces, and range from 0.1–2.5 cm high and 0.2–10 cm wide. Occasionally heads have grown/merged together (arrowed in C), but unliked clustered forms, smaller sand stromatolites do not occur on the periphery of larger heads. Upward-oriented arrow indicates where the tops of two joined stromatolite heads have been removed, revealing the amalgamation of two larger heads into one elongate barbell-shaped head. Structures exhibit evidence of having synoptic relief (note sand shadows in Figure 4(a)-12), yet are soft enough to be deformed by trace-making animals (e.g., the trackways that cross over and cross-cut domes in (A) and in Figures 4(a)-9, -10, -12). Study of cross-cutting relationships on the 200 m^2 surface in (A) revealed that sand stromatolites grew both before and after production of the surface-produced *Climactichnites* traces. Together with analyses of part–counterpart specimens that falsify an inorganic origin (e.g., as a concretion, nodule, sub-mat gas bubble) for all of the surfaces shown in Section 4(a), this information suggests that these structures might form by the vertical accretion and/or binding of quartz sand by localised biofilms. Serial slab, X-ray CT, and petrographic thin-section analyses of these structures reveal no internal structure, although in muddier sands (*sensu* the Cambro-Ordovician Nepean Formation sand stromatolites – see Chapter 8(b)), weak domal laminations are visible in cross-sectioned sand stromatolites. (C) is close-up of (B). Swiss army knife in (A) is 8.3 cm long, broom handle is 4 cm wide in (B) and (C). All photos: J.W. Hagadorn.

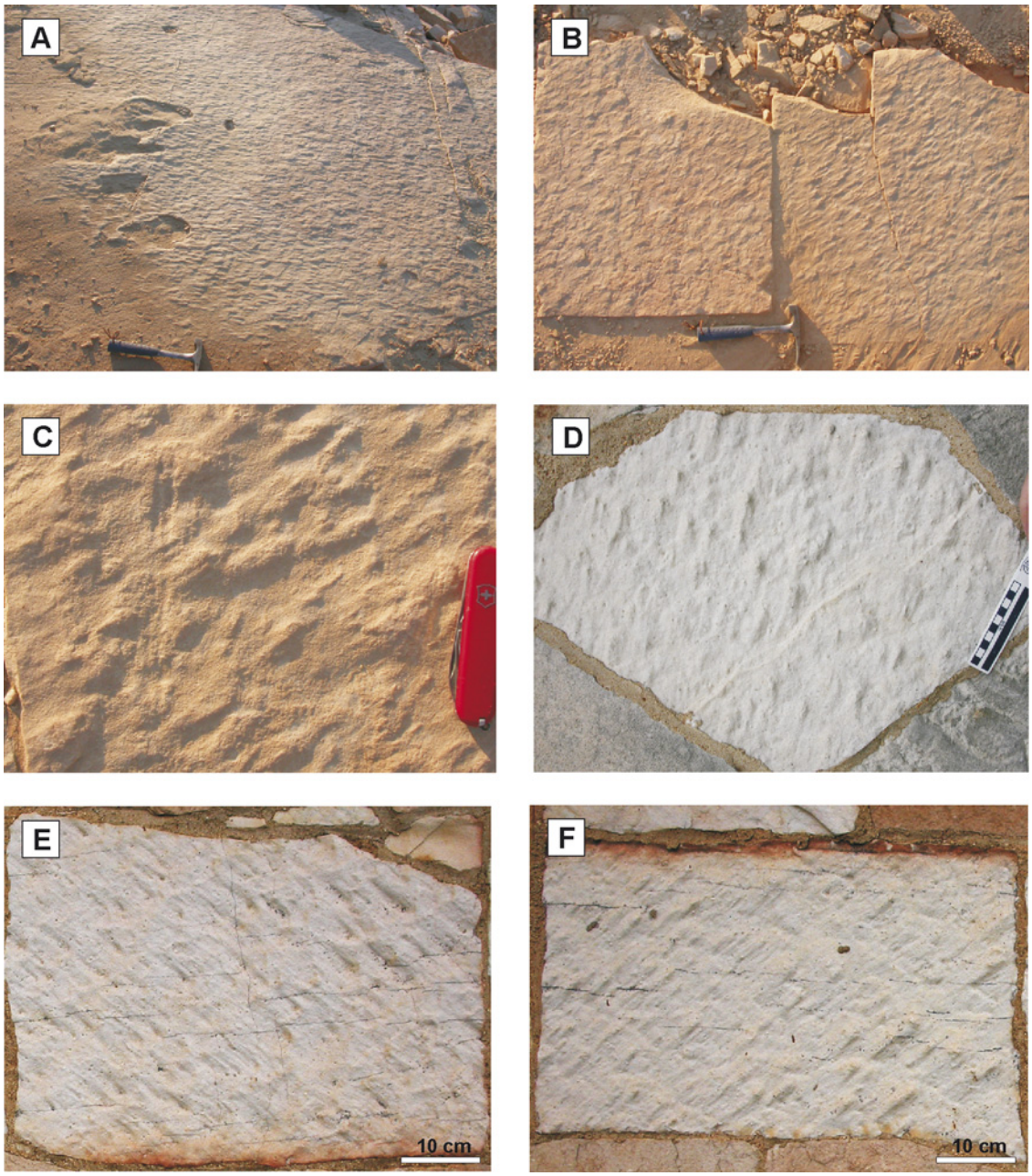


Figure 4(a)-12: Sand shadow structures, also known as 'inverted flutes', in quartz arenites of the Late Cambrian Elk Mound Group, Wisconsin (A–C), and Gunter Sandstone, Missouri (D–F), USA.
Images (A)–(E) are bed-tops; (F) is a bed-sole and is the counterpart to (E). (A) illustrates a surface pavement in which sand has accumulated in the downcurrent direction of surface bumps, forming drumlin-shaped sand shadows. Although serial sectioning of part–counterpart slabs from this surface reveals no internal lamination in the upcurrent end of the bumps, these bumps exhibit deformational features suggesting that they were cohesive, yet pliable – unlike nodules or concretions. For example, in the close-up of this surface (B, C) the stoss and leeward portions of sand stromatolite-like surface bumps are commonly cross-cut by *Cruziana* (arrowed in B, *Gordia, Helminthoidichnites*, and *Protichnites*), indicating that at the time of deposition, the core of the sand shadow was still pliable. Sand bumps are similar in size and shape to sand stromatolite heads, and are not expressed below bed surfaces. Given the absence of clay in these lithofacies, microbial binding provides one explanation for the cohesive, yet pliable rheology which mediated formation of sand bumps, followed by sand shadows. Fallout of wind- or water-borne grains led to buildup of leeward tails of sediment behind sand bumps. Hammer head in (A), (B) is 17.5 cm long; Swiss army knife in (C) is 8.3 cm long; scales in (D)–(F) are 10 cm long. All photos: J.W. Hagadorn.



Figure 4(a)-13: Patchy ripples, on oscillation rippled quartz arenite from the Upper Cambrian Elk Mound Group, Wisconsin, USA.
See close-ups of this surface in Figure 4(a)-14. Because the surface is nearly perfectly flat, the hypothesis that rippled patches could be forming on topographic highs within a tide-pool can be falsified. Instead, ripples are thought to form in regions where biofilms and biomats have either been ripped up or were not present (*sensu* Noffke et al., 1997b). In areas where ripples are absent, abundant sand stromatolite heads are present. Note also the '*Astropolithon*' (A), a probable sub-mat gas blister structure, in the zone characterised by unrippled sand stromatolite-laden sand. Also note the *Teichichnus*-like trace fossils (arrowed) on the surface – these cross-cut both ripple patches and sand stromatolite-laden patches, demonstrating that the sediment was pliable enough to be burrowed. Dark areas at top of photo are wet. Field of view is ~3 m. Photo: J.W. Hagadorn.

Domal sand buildups:* *Figures 4(a)-9 to -11

Name of structure: domal sand buildups.

Other terms used: 'sand stromatolites'.

Description of structure: clustered and non-clustered low mound-shaped structures on upper sandstone bed surfaces; clustered ones may locally amalgamate. Cauliflower-like patterns form where clustered buildups occur, resembling carbonate stromatolites, but with much lower relief. Can be deformed by trace-making animals. Show no internal structure except for sandstones with relatively higher mud content, where convex laminae may be visible. Various sizes occur and these as well as clustered and non-clustered forms may occur on the same sandstone bedding surface; also preserved in concave hyporelief on the soles of overlying sandstone beds.

Associated sedimentary structures: (1) various trace fossils; (2) sand shadow structures; (3) oscillation and interference ripples; (4) '*Astropolithon*'.

Palaeoenvironment: intertidal to shallow subtidal marine.

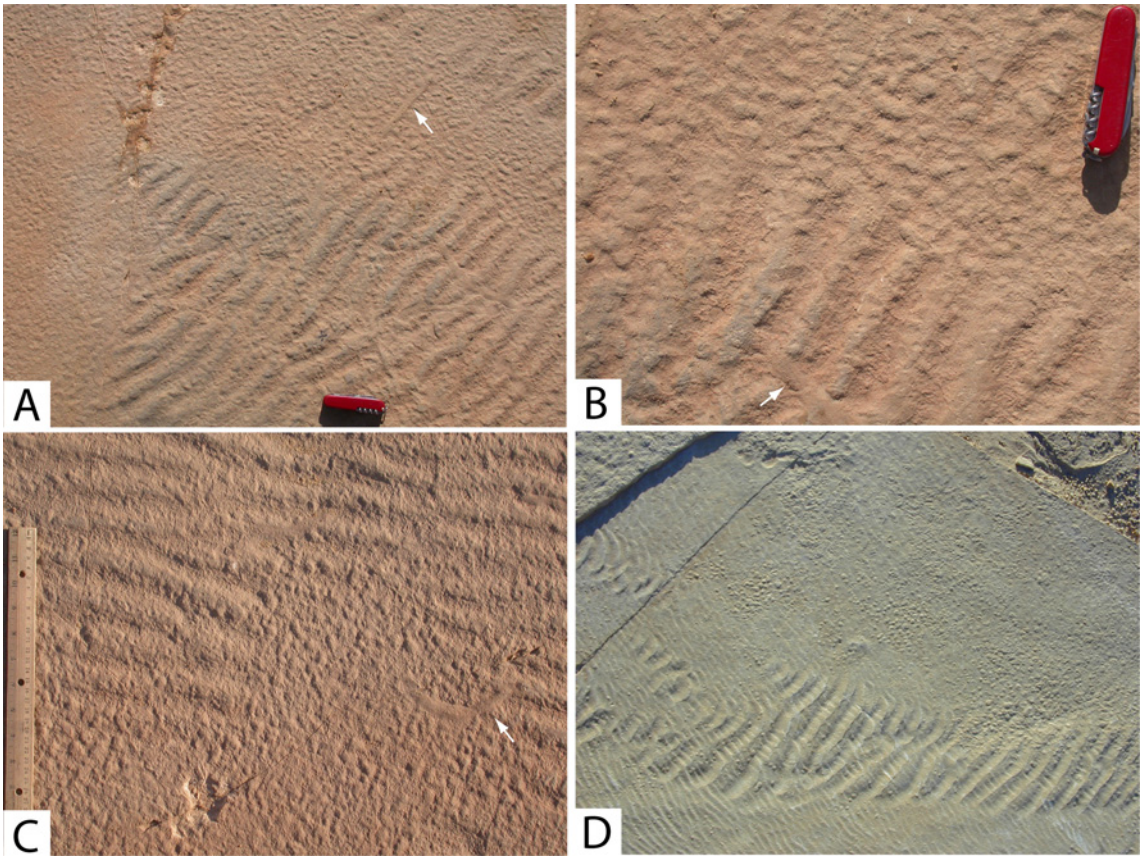


Figure 4(a)-14: Patchy ripples from the Late Cambrian Elk Mound Group, Wisconsin, USA. Surfaces in (A)–(C) are close-ups of surface in Figure 4(a)-13. Note pustulose, sand stromatolite-laden nature of unrippled regions in (A)–(C). Some of the ripple crests and troughs in (C), and on another surface in (D) have been colonised by biofilms after ripple formation, suggesting that at least two generations of microbial development occurred prior to burial. Isolated horizontal trace fossils are arrowed; note cluster of burrows above knife in (A). The surface in (D) is similar to (A)–(C), but is characterised by patches of clustered sand stromatolites in non-rippled regions. The second set of ripples on this surface is migrating over the top of the first ripple set and the sand stromatolite-covered region; crests of the second set are oriented from the upper left to lower right of the photo. Swiss army knife in (A), (B) is 8.3 cm long; ruler in (C) is 31 cm long; field of view in (D) is 2 m. All photos: J.W. Hagadorn.

Ideas on genesis: it is thought that localised development of biofilms on sandy surfaces enable vertical accretion and/or binding of the quartz sand grains.

Sand shadow structures: Figure 4(a)-12

Name of structure: sand shadow structures.

Other terms used: 'inverted flutes'.

Description of structure: these bed-top and bed-sole features resemble sand stromatolites in their size and shape, but additionally have a drumlin-like sand shadow accumulated in a downcurrent direction from the sand bed surface bumps. They lack any internal lamination, but have evidence of cohesiveness such as being cross-cut by trace-making animal trails.

Associated sedimentary structures: (1) various trace fossils; (2) sand stromatolites.

Palaeoenvironment: supratidal to shallow subtidal marine.

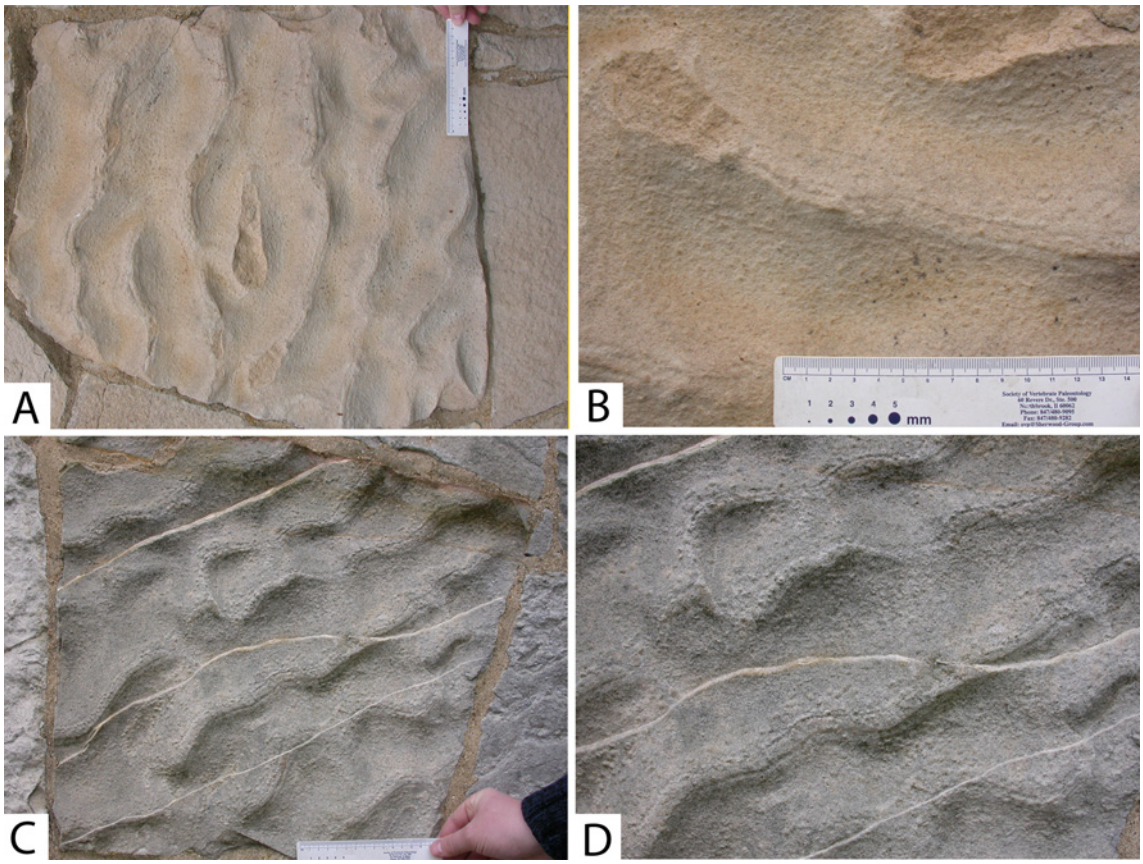


Figure 4(a)-15: Cracked ripple crests, with incipient sand stromatolites coating ripples in quartz arenites from the Late Cambrian Gunter Sandstone, Missouri, USA.
(B) and (D) are close-ups of (A) and (C), respectively. These structures are poorly understood, but examination of part–counterpart specimens and their occurrence at sand–sand bed interfaces suggests that linear ridge-crest features could form when exposed tops of organically-bound ripples crack when dewatering. Whether this occurs subaerially or subaqueously is unknown. Abundant small (incipient) sand stromatolites are visible in (D), and seem to be concentrated on ripple crests. The presence of microbial indicators elsewhere on these surfaces is consistent with the interpretation that biofilms are involved in the production of parallel sets of cracks along ripple crests, perhaps due to dehydration of bound sand. Although cracks occur at sand–sand bed interfaces, serially sectioned specimens have not been examined, and thus the origin and subsurface characteristics of these structures are still not well constrained. See also Figure 4(c)-4B in this chapter. Scale bar units are 1 cm. All photos: J.W. Hagadorn.

Ideas on genesis: microbial binding of sand may have produced these pliable yet cohesive surface bumps on sandy bed surfaces, with fallout of wind- or water-borne sand particles forming leeward tails behind these positive features.

Patchy ripples: Figures 4(a)-13, -14

Name of structure: patchy ripples.

Other terms used: none.

Description of structure: flat sandstone surfaces in which patches are marked by ripples of various types, and where the ripples grade into the surrounding sandstone surfaces.

Associated sedimentary structures: (1) domal sand buildups; (2) various trace fossils; (3) '*Astropolithon*'.

Palaeoenvironment: intertidal marine.

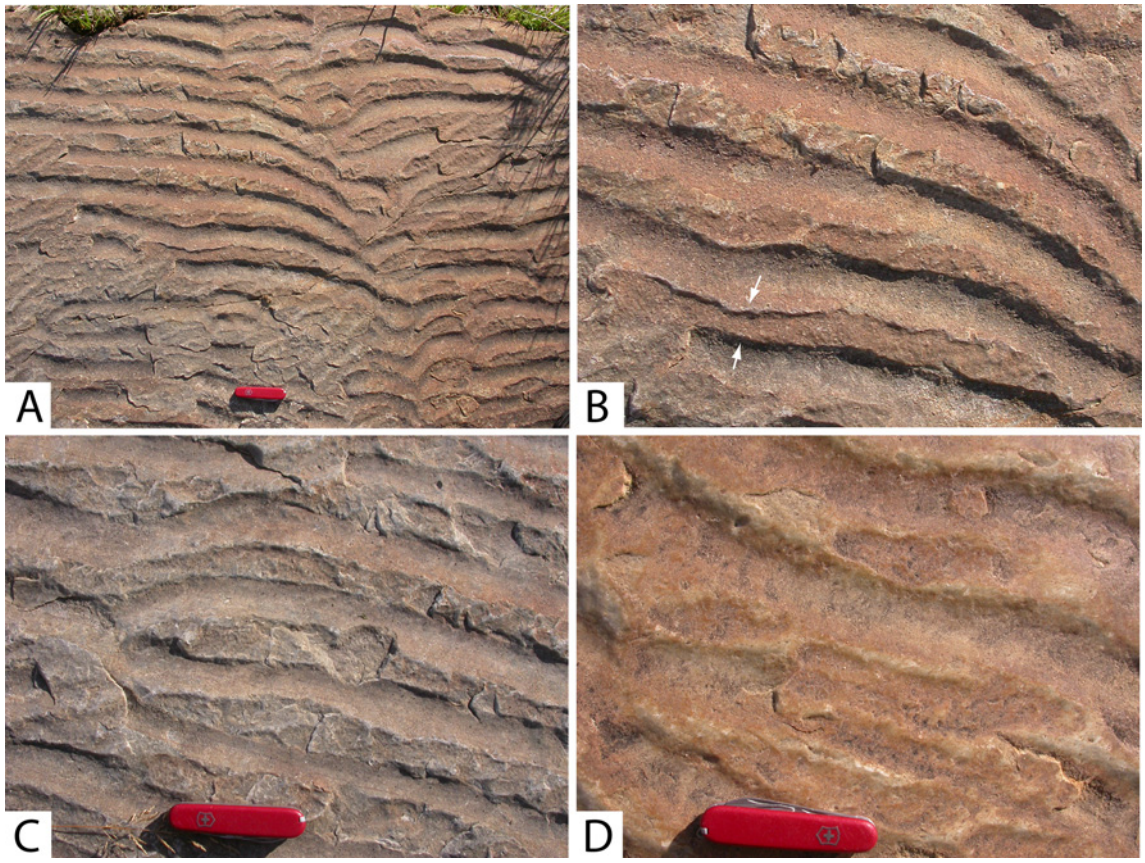


Figure 4(a)-16: Concave eroded ripple crests on bed surfaces of quartz arenites in the Late Cambrian Potsdam Group, New York, USA.
(B) is a close-up of central area in (A). Prior to or concomitant with burial of this layer by the veneer of sand above the pocket knife, the ripple crests were eroded and reworked. However, rather than forming flat-topped ripple crests, crests are excavated deeper than the adjacent stoss/lee sides of ripples, forming in some cases a cavity beneath the stoss and lee ripple surfaces. The margins of these cavities have a distinct lip (see close-ups in B and C; and arrowed example in B), as if the stoss and lee surfaces of the ripples were cohesive or more resistant to erosion during the erosive phase of reworking. One possible explanation for this phenomenon is that the surface of ripples had been stabilised prior to being buried and having their tops scoured. After their crests were plucked off, turbulent flow regimes could entrain unbound grains in the ripple crest, including grains that lay adjacent to and obliquely underneath a biofilm veneer that coated ripple surfaces. Similar features have been noted in Neoproterozoic sandstones by Pflüger (1999). However, diagenetic or other predepositional scenarios to account for these unusual ripple crest cavities are also possible, and sectioning is needed to evaluate all of these hypotheses. Swiss army knife is 8.3 cm long. All photos: J.W. Hagadorn.

Ideas on genesis: ripples are able to form due to current, wave or wind action in patches within a mat-stabilised sandstone bed surface where the mat is either absent or has been removed by reworking processes (*sensu* Noffke et al., 1997b).

Cracked ripple crests: Figure 4(a)-15

Name of structure: cracked ripple crests.

Other terms used: ripple-top sand cracks (see Figure 4(c)-4B).

Description of structure: parallel sets of cracks along ripple crests in rippled sandstone bed surfaces.

Associated sedimentary structures: (1) sand stromatolites; (2) a range of mat-related features.

Palaeoenvironment: supratidal to shallow subtidal marine.

Ideas on genesis: biofilms are inferred to have covered sandy rippled surfaces and when these dewatered or even desiccated, the cracks formed preferentially along ripple crests where lateral stress may have been maximised.

Concave eroded ripple crests: Figure 4(a)-16

Name of structure: concave eroded ripple crests.

Other terms used: broached ripples.

Description of structure: ripples are eroded in the sense that a shallow cavity is excavated in the ripple crests, rather than displaying either rounded or flat-topped crests that are the normal result of reworking of rippled sands. A distinct lip is also associated with these cavities.

Associated sedimentary structures: (1) ripple marks; (2) trace fossils.

Palaeoenvironment: intertidal to shallow subtidal marine.

Ideas on genesis: a rippled sandy surface stabilised by a microbial mat is envisaged. When high energy reworking processes remove both ripple crest mat and underlying loose sand, the rest of the ripple form remains relatively stable, enabling excavation of the shallow cavities in the crests, with formation of the lips due to microbial binding. May be genetically related to cracked ripple crests (above).

4(b). DIAGENETIC FEATURES RELATED TO MAT METABOLISM AND DECAY

J. Schieber

Microbes can influence mineral precipitation in a mat by: (a) changing the pore water chemistry in a mat via metabolic activity, such as photosynthesis, or (b) by nucleation of minerals on their cell walls and (c) within the extra cellular polysaccharides (EPS) that surround them. Given the right water chemistry, syngenetic carbonate precipitation due to photosynthesis (a) is considered a viable process (e.g., Thompson and Ferris, 1997; Pratt, 2001) and can occur in terrigenous clastic environments just as well as in carbonate dominated settings. Evidence for carbonate precipitation on cell walls (b) has been presented by a variety of authors (e.g., Krumbein, 1974; Gerdes and Krumbein, 1987; Chafetz, 1994), and EPS mediated microbial calcium carbonate precipitation (c) was, for example, reported by Arp et al. (2001) from biofilms in an alkaline lake. Cell wall nucleation of calcium carbonate by sulphate reducing bacteria has been examined by Van Lith et al. (2003).

Krumbein and Cohen (1977), in a study of modern cyanobacterial mats, concluded that not metabolic CO_2 uptake, but rather biogeochemical reactions during bacterial degradation of the mat were responsible for carbonate (calcite, aragonite) precipitation. The carbonates mimicked filament structures and formed onkoidal structures of 1–2 mm diameter, yet less than 1% of the modern mat volume was transformed into preservable carbonate matter (Cohen et al., 1977). The above observations on carbonate formation during decay in cyanobacterial mats were confirmed in a study by Gerdes and Krumbein (1987), which found micrite accumulation along cyanobacterial sheaths, micrite encapsulation of coccoidal cells, as well as formation of concentrically coated carbonate ooids. The latter authors also documented that with increasing burial depth and carbonate precipitation, original structures (filaments, coccoids) become increasingly unrecognisable. Thus, whereas it is difficult to determine with certainty whether a given carbonate grain in a modern mat is due to photosynthesis-induced precipitation, there is good observational evidence that decay of microbial filaments, cells, and EPS fosters abundant carbonate precipitation.

Examples of ancient microbial mat deposits in siliciclastics that show evidence for early lithification through mat-associated carbonate precipitation include the Mesoproterozoic of the Belt Basin (Chapter 7(b)), the Cambrian of Israel (Soudry and Weissbrod, 1995) and Minnesota/USA (Davis, 1968), the Carboniferous of North Africa (Bertrand-Sarfati, 1994), the Permian of New Mexico/USA (Harwood, 1990), and the Miocene of Spain (Martin et al., 1993; Braga and Martin, 2000). The common thread for all these deposits is the alternation of laminae that are enriched in carbonate minerals (usually calcite or dolomite) with laminae that consist largely of siliciclastic grains. Carbonate bearing laminae may be largely carbonate with small additions of siliciclastic grains, but may also contain in excess of 50% siliciclastics. Textural features in carbonate-rich laminae include fenestrae (Figure 4(b)-1B), calcified filaments, micritic laminae (Figures 4(b)-1A, -1B), peloidal and clotted micrite (Figures 4(b)-1A, -1C), siliciclastic grains with thin oolitic coatings, and 'floating' siliciclastic grains within micrite (Figures 4(b)-1A, -1C, -1D). In most of these examples, early lithification via carbonate precipitation allowed for the accretion and preservation of dome-shaped and laminated microbial buildups (see Chapter 7(b)).

In modern day mats, there is typically not enough calcite precipitation to preserve original mat structures via early lithification (Cohen et al., 1977). Thus, judging from the comparatively low number of reported sandy microbial mat deposits with carbonate enriched laminae in the rock record, conditions conducive to this type of mat preservation may only have occurred intermittently through geological time. A possible control may have been the interplay between dissolved CO_2 and calcium concentrations in basin waters (Arp et al., 2001).

Probably since at least the Mesoproterozoic (Johnston et al., 2005), many shallow marine microbial mats likely accumulated beneath oxygen-bearing seawater. Considering the interconnected pore spaces and high permeability of sandy sediments, one would expect to find minerals that require reducing conditions for precipitation (e.g., pyrite, ferroan carbonates) at some depth below the sediment-water interface. Under these conditions, lateral variability of permeability and irregular distribution of organic matter would probably preclude stratiform distribution of these 'reducing' minerals.

The presence of a microbial mat at the surface, however, makes a significant difference in this regard. Microbial mats typically define a sharp geochemical boundary. In photosynthetic cyanobacterial mats for example, the very surface layer of the mat may produce oxygen. Directly below this layer, however, in the region where anaerobic bacteria degrade original mat material, the sediment tends be strongly reducing (Bauld, 1981; Gerdes et al., 1985b). In such a geochemical environment conditions are favourable for the precipitation of 'anoxic' minerals, such as

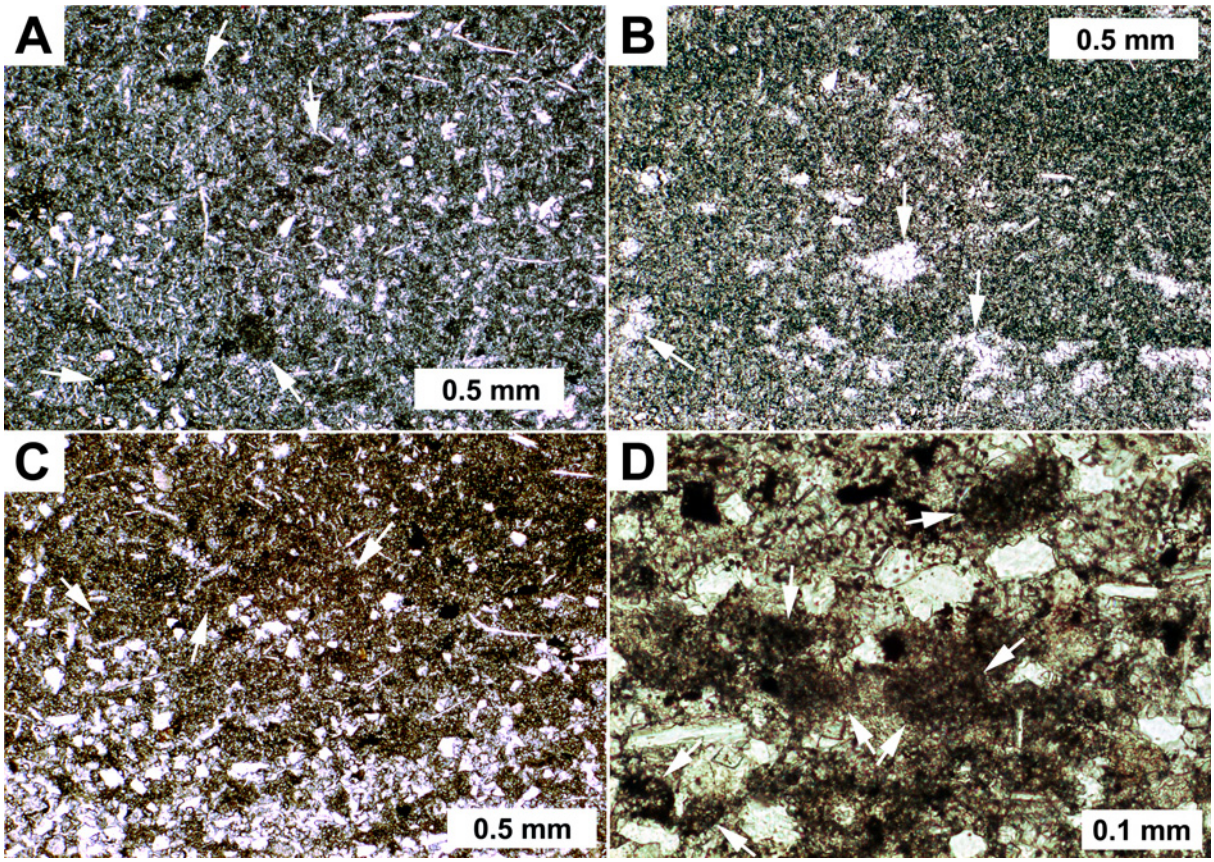


Figure 4(b)-1: Photomicrographs of calcite- and/or dolomite-rich laminae in sandy microbial mat deposits from the Revett Formation, Belt Supergroup, Middle Proterozoic of Montana, USA.
(A) Fine crystalline dolomitic lamina (originally micrite?) with scattered 'floating' grains of quartz and mica. Note relict peloidal texture (arrows point to peloids). (B) Dolomitic lamina with fenestrae (arrows) that are filled with dolomite spar. (C) Dolomite-rich lamina with peloids in a (originally micritic?) fine crystalline dolomite matrix; it contains a higher proportion of terrigenous clastic grains. (D) Peloidal texture in dolomite-rich lamina of sandy microbial mat deposit. Arrows point to clearly visible peloids.

pyrite, siderite (Figures 4(b)-2B, -2D), ankerite, and ferroan dolomite, in addition to calcium carbonate. The lowering of pore water sulphate concentrations by sulphate reducing bacteria also promotes the precipitation of early diagenetic dolomite (Baker and Kastner, 1981).

The comparatively high permeability of sandstones allows for microbial metabolisation of most co-deposited organic matter very early in burial history, and microbially mediated reactions between buried organic matter and migrating formation waters most likely will remove the remainder. Thus, in sandstones, carbonaceous horizons due to microbial mat colonisation most likely will not make it into the rock record as such. Aside of morphological features in the sandstone host, such as domal buildups (see Chapter 7(b)), cementation of sandstones by the above-mentioned 'anoxic' minerals may be the only remaining indicator of the former presence of microbial mats (Figure 4(b)-2A). Just as the bulk of calcium carbonate deposition in mats appears to be largely due to decay processes (Krumbein and Cohen, 1977; Cohen et al., 1977; Gerdes and Krumbein, 1987), these cements of 'reducing' minerals are considered 'mat decay mineralisation'. Mat decay mineralisation produces thin, well defined, and laterally extensive horizons of calcium carbonate and/or 'reducing' minerals, such as ferroan carbonates or pyrite. Conversely, if a sandstone layer contains *disseminated* carbonate, ferroan carbonate, or pyrite cement, a mat origin is unlikely.

Photomicrographs in Figure 4(b)-2 illustrate mat decay mineralisation features from the Revett Formation, Mesoproterozoic Belt Supergroup of Montana, USA (Schieber, 1998a, 1999). These sandstones formed in a fluviodeltaic setting (Boyce, 1973; Bowden, 1977; Mumma et al., 1982; White et al., 1984), and thus the pore waters contained in the original deposits were either fresh or brackish. This implies, in comparison to seawater, a shortage of dissolved sulphate and consequently low concentrations of sulphide in the anoxic sediments beneath mats.

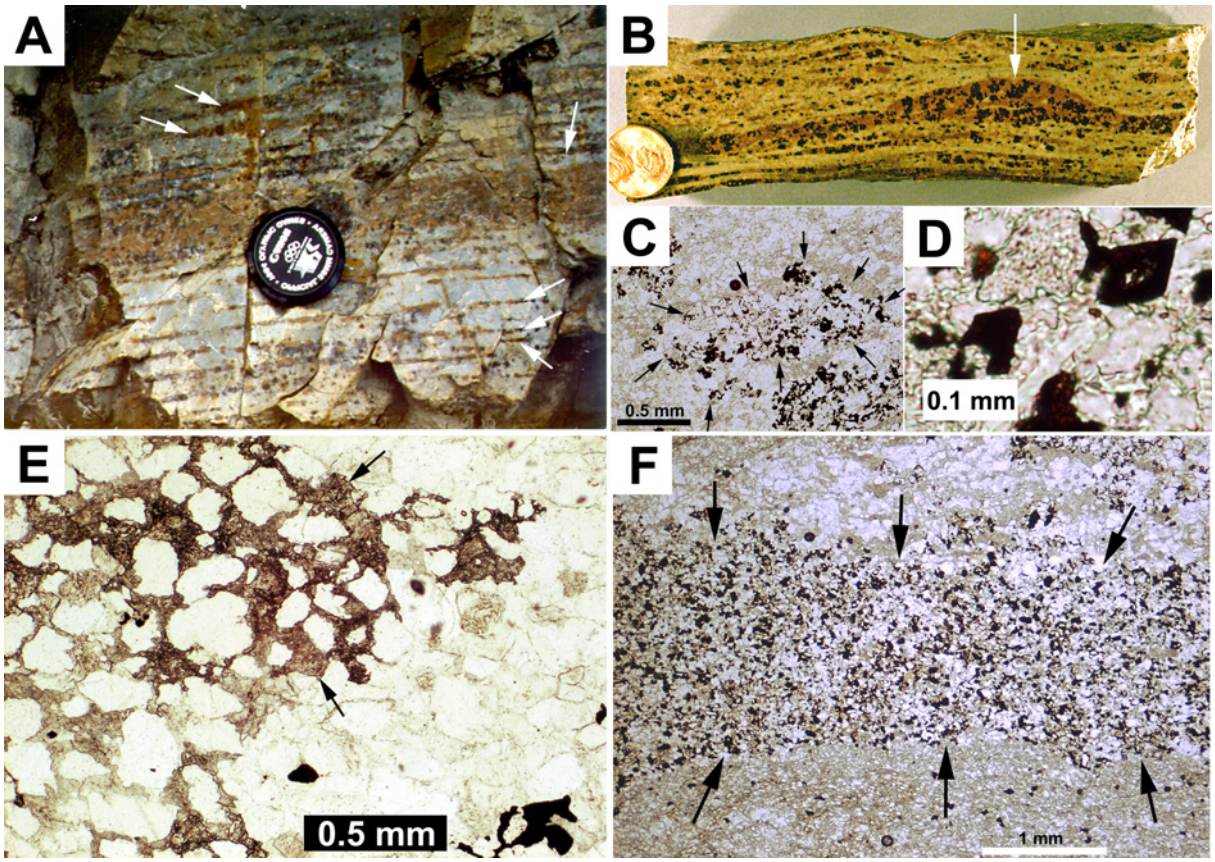


Figure 4(b)-2: Iron carbonate cements in microbial mat deposits from the Revett Quartzite, Belt Supergroup, Middle Proterozoic of Montana, USA.

(A) Outcrop photo that shows bedding-parallel brownish horizons (arrows) that are interpreted as the location of former microbial mats. Lens cap is 45 mm in diameter. (B) Hand specimen of Revett Formation sandstone with iron-stained (limonitic) laminae. The arrow points to a layer with asymmetric domal thickening, probably an incipient domal stromatolite. The very dark patches are oxidised patches of siderite cement. The brownish-orange coloured laminae mark the presence of ankerite and ferroan dolomite. (C) Oval patch of iron-stained sandstone (marked with arrows) within a matrix of non-stained sandstone. Detailed comparison of the matrix material with the detrital components of the patch shows that the matrix is finer grained and has a substantially larger content of clays and shale clasts. This observation suggests that the patch outlined with arrows was an eroded fragment of a prior sediment. Because sand itself is not cohesive, the sand grains might have been held together by microbial filaments during transport. (D) Oxidised siderite rhombs in sandstone. (E) Sandstone with patchy siderite cement (dark-brownish, upper left, arrows). Sandstone at lower right is quartz-cemented. Note floating grains in siderite patch. (F) Photomicrograph of an iron-stained lamina as seen in B. The black arrows point to the margins of the lamina, and the scattered opaque spots are largely iron oxides (variably hydrated) that resulted from oxidation of iron-bearing interstitial carbonates. Note that the under- and overlying layers contain comparatively small amounts of iron oxides.

This is probably the underlying reason for the preponderance of ferroan carbonates in the microbial mat layers of the Revett Formation. Garlick (1988) was the first to realise that the ferroan minerals in the Revett sandstones were probably the diagenetic imprint of former microbial mats. Had these sandstones been deposited in a setting dominated by marine waters, cementation by pyrite might have occurred instead of ferroan carbonates.

If minerals related to mat decay were originally deposited in a mat with abundant organic matter and EPS, siliciclastic grains were probably originally surrounded by an organic matrix. Once this organic matrix is gradually replaced by decay-related minerals (carbonates, ferroan carbonates, pyrite), 'floating' quartz and mica grains are to be expected (Figure 4(b)-2E).

If the mat simply gets buried by more sand, stratiform layers of decay-related minerals may result (Figures 4(b)-2A, -2B, -2F). If erosion of mat-bound sand occurs, fragments may be reworked and reburied, and then undergo re-

ducing diagenesis because of their contained organic matter (Figure 4(b)-2C). Desiccated eroded mat fragments may produce curved features once buried in more sand. On weathering, these curved features may be marked by carbonate cement and even iron stains from 'reducing' cement minerals (see Chapter 3, Chapter 7(b)). If the mat is still soft when erosion occurs, reworking may produce buried contorted fragments that again can be seen due to their cementation and/or iron stain (see Chapter 3, Chapter 7(b)).

4(c). MAT-DESTRUCTION FEATURES

P.G. Eriksson, H. Porada, S. Banerjee, E. Bouougri, S. Sarkar, A.J. Bumby

Introduction

In this section, sedimentary features preserved in sandstones due to mat-destruction processes (largely physical) are detailed. The sedimentary features which result in modern sandy settings or are preserved in ancient sandstone beds encompass:

(1) microbial shrinkage cracks within modern mats, which may also penetrate into underlying sandy bed surfaces to form sand cracks;
(2) sand cracks of all types, including "*Manchuriophycus*"/"*Rhysonetron*"; also, crack-marginal features such as: curled crack margins, and overgrown, upturned crack margins; filled sand crack features, including petee ridges; ripple-top sand crack features;
(3) flipped-over (mat) edges, and rolled-up mat fragments (cf. 'jelly-rolls', 'roll-ups');
(4) mat chips and sand chips;
(5) (destructive) wrinkle structures;
(6) ripple patches, and patchy reworking of ripples;
(7) non-penetrative micro-faults.

The reader is referred to Chapter 3, where classification schemes of mat-related features are discussed in detail; the above features are based on Schieber's (2004, and later modifications thereof) scheme, with some minor refinements. The descriptions and discussions presented below rely also to a large extent on a set of critical references on the mat destruction features in sands/sandstones: Astin and Rogers (1991); Bloos (1976); Bouougri and Porada (2002); Clemmey (1978); Eriksson et al. (2000); Garlick (1981, 1988); Gavish et al. (1985); Gehling (1999, 2000); Gerdes et al. (1985b, 1993, 2000a); Hagadorn and Bottjer (1997, 1999); Häntzschel (1975); Hofmann (1967, 1971); Noffke et al. (2001a, 2003a, 2003b); Parizot et al. (2005); Porada and Löffler (2000); Pflüger (1999); Pflüger and Gresse (1996); Reineck (1979); Reineck et al. (1990); Schieber (1998a, 1999, 2004); Simonson and Carney (1999).

Definition and genesis of mat destruction features

In modern mats, various crack features can be observed (Figure 4(c)-1), including leaf-shaped or spindle-shaped incipient tears that are not yet connected to each other; once they do thus connect, often, triradiate or 'triple junction' crack patterns result; however, triradiate cracks can also form as incipient structures on their own. In other cases a more polygonal or reticulate crack pattern may emerge as increasing numbers of cracks join up. Other more complex crack patterns observed include sinuously curved, to sigmoidal, circular or even, locally, figure-8 shaped features (Figure 4(c)-1). All of these features may also be found preserved in ancient sandstone beds (Figures 4(c)-2 to -4). It is possible that these more complex curved crack patterns develop from the simpler spindle-shaped incipient tears and triradiate cracks (see also Figure 4(c)-2 for ancient examples of this possible progression), and that mat thickness plays a role in determining the detailed crack patterns that result.

Once cracks occur in a microbial mat growing above an unconsolidated sandstone bed, they may penetrate into the underlying sand layer, provided with cohesiveness by the mat, or the cracks within the living/desiccating/decaying mat may become filled by sand, either from above or below. If filled from above, it is likely (although not axiomatic) that the crack-fill material will differ from the sand of the bed originally beneath the mat. In contrast, if microbial shrinkage cracks within a mat are filled from below, by sand driven into the cracks under pressure from overlying beds or over-standing water, or due to tidal water depth changes, then the crack-fill has the same composition as the bed below, and there will also be soft-sediment deformation features preserved below the resulting petee ridges *sensu lato* (filling the cracks) (note discussion on the meaning and use of the term 'petees' below), which disturbs the upper few laminae of sand(stone) (Figures 4(c)-8 to -10). It should be noted that petees (*sensu stricto*) may also form from growth-expansion of the mat or due to escaping gas from decaying buried mats, resulting in deformation of the mat surface and concomitant sinuous to polygonal surface ridge patterns (Gehling, 1999).

The appearance of preserved sandy crack-fills, whether 'petee's' (petee ridges, filled from below) or formed from above, is very similar, and they generally require detailed study of a sawn section or even of a microscopic thin section cut across the bedding at the top of such a sandstone layer, to discriminate them; examples of both types

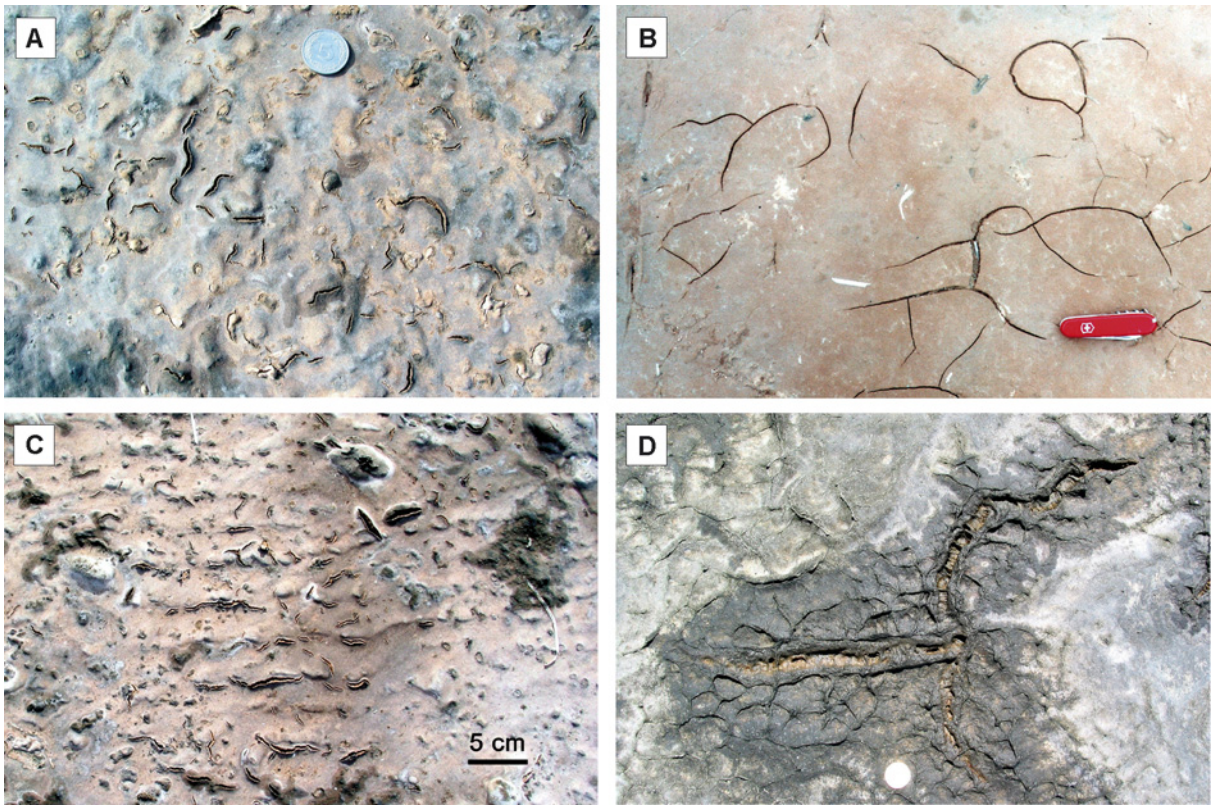


Figure 4(c)-1: Microbial shrinkage cracks in modern mats.
(A) Microbial shrinkage cracks (term proposed by Porada and Löffler, 2000) in surface of thin, modern microbial mat. Note isolated lenticular, curved, spindle-shaped, and triradiate shrinkage cracks; note also tapering ends of the cracks. Cracks may extend downward into sediment layer below mat. Dark areas around some cracks indicate that groundwater may be rising up from sediment below. Scale (coin): 24 mm. Locality: Bhar Alouane, Mediterranean coast of southern Tunisia; environment: upper intertidal to lower supratidal zones of tidal flat. (B) Microbial shrinkage cracks in thin, modern, flat mat (*Synechococcus*-type?) with simple, triradiate, curved to sinuously curved, and subcircular crack forms. Note that near centre of photo, curved cracks may join to form a figure-8-shaped pattern. Swiss army knife for scale: 8 cm. Locality: Bahirat Boughrara, Mediterranean coast of southern Tunisia; environment: lower supratidal zone of tidal flat. (C) Irregular surface of modern thin mat (*Synechococcus*-type?) with linear, lenticular to sigmoidal cracks, following the linear trends of shallow bulges. Locality: Bhar Alouane, Mediterranean coast of southern Tunisia; environment: upper intertidal to lower supratidal zones of tidal flat. (D) Close-up view of modern mat surface with shrinkage cracks. Margins and openings of the cracks show active growth of cyanobacterial filaments forming bridge-like structures between margins, and thus favouring progressive closure of the cracks and preservation of sediment filling the cracks. Note groundwater rising up along cracks. Scale (coin): 23 mm. Locality: Salins du Midi, Réserve Nationale Camargue, Southern France; environment: preconcentration basin of 'Salins de Midi' saltern. All photos: H. Porada and E. Bouougri.

are shown in Figures 4(c)-7 to -10. What is also noticeable in many ancient examples is the similarity of such positive sandstone ridges to the negative crack patterns (see Figure 4(c)-3 for good examples); all combinations of curvilinear, parallel, spindle-shaped and circular to figure-8 forms may be seen, and this supports the inferred link between initial crack (in the mat overlying the sand surface) and its later filling by sand from above or below (e.g., compare Figures 4(c)-1 and 4(c)-2 to -4 with Figures 4(c)-7 to -10). As shown in Figure 4(c)-9, negative sand cracks and positive petee ridges, with similar complex geometrical forms, may occur together in one sample; a modern example of sand cracks passing into petee ridges is shown in Figure 4(c)-8D. Filled sand cracks and petee ridges thus also imply the presence of an original crack, either in the living mat, or in the sand beneath. We here differentiate between *preserved* negative features (sand cracks) and positive features (either petee (*s.l.)* ridges or filled sand cracks), noting also that they often occur together (e.g., Figure 4(c)-3).

The term 'petees' was introduced by Gavish et al. (1985) where it referred exclusively to modern mats. In this earliest study, these authors addressed tepee-like structures which they considered, however, to be of biogenic origin and related to microbial mats. They found that undulation and wrinkling of microbial mat surfaces resulted

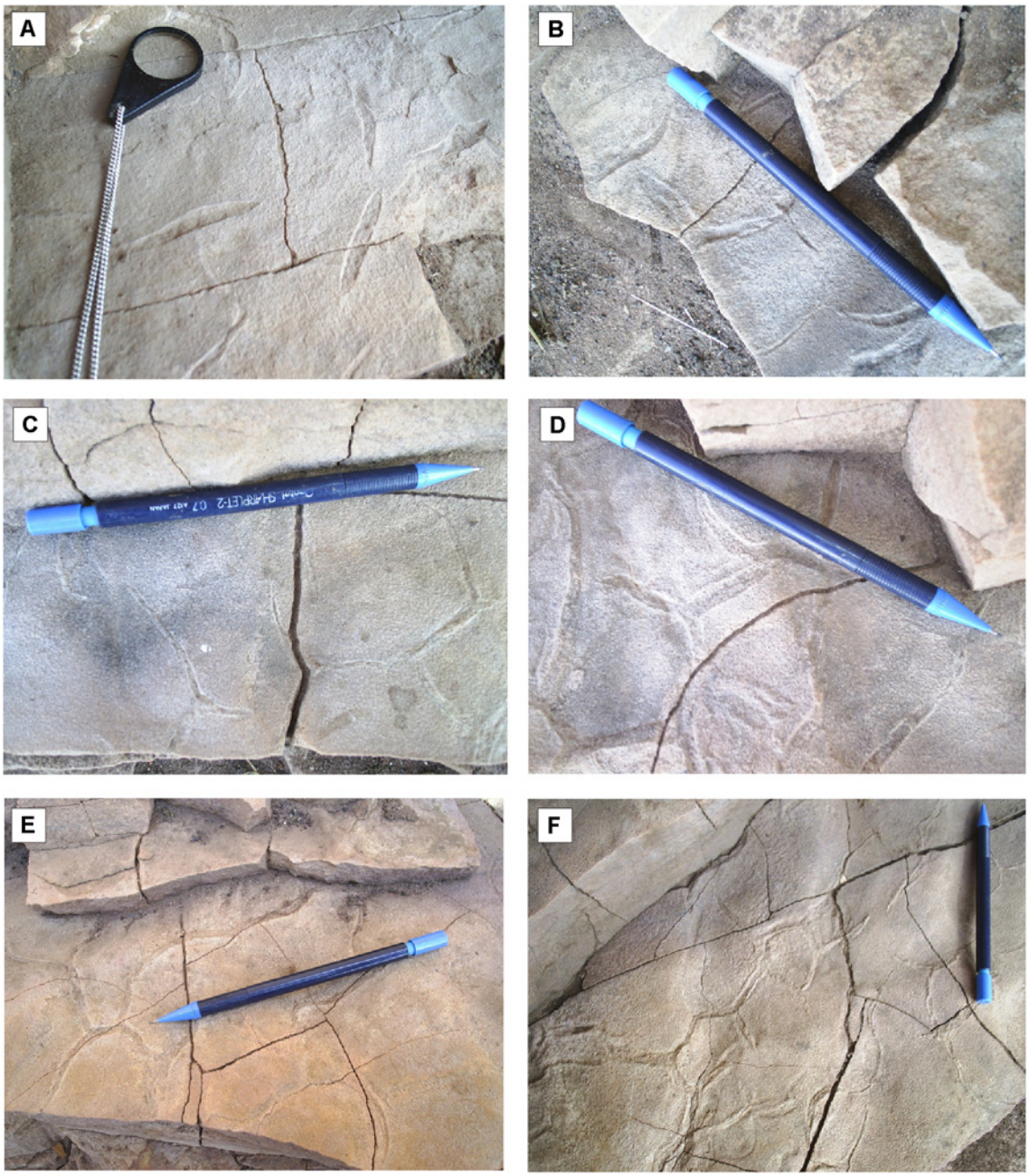


Figure 4(c)-2: Sand cracks.

(A) Single incipient tears (inferred from an ancient mat and preserved as cracks within underlying sandstone bed) at relatively high angle orientations to each other. (B) Two incipient tears joining up, to form two parts of a 'triple junction' (triradiate) crack pattern. Note also, below this, an incipient tear passing laterally into a narrow, sinuous sand crack. (C) Sand crack pattern formed from 'triple junction' incipient cracks with as-yet incomplete intersection of incipient cracks. (D) Sand crack mosaic formed by relatively complete intersection of 'triple junction' incipient cracks. (E) Curved crack patterns showing a development from 'triple junction' incipient cracks. (F) Crack patterns formed by intersection of 'triple junction'-type features in centre of photograph; in lower part of photograph is a series of curved cracks which may be secondary after the straighter 'triple junction' types. Note 'triple junction' crack feature just left of the base of the pen, where the three arms have a bead-like morphology; this may reflect joining-up of much smaller incipient tears. All structures in this figure are from planar and rippled (sinuous-crested ripples) sandstone beds within a playa lake lens, enclosed within predominant aeolian sandstones of the Makgabeng Formation (ca. 2.0–1.8 Ga), Makgabeng Plateau, Limpopo Province, South Africa. All photos: I. Tonzetic.

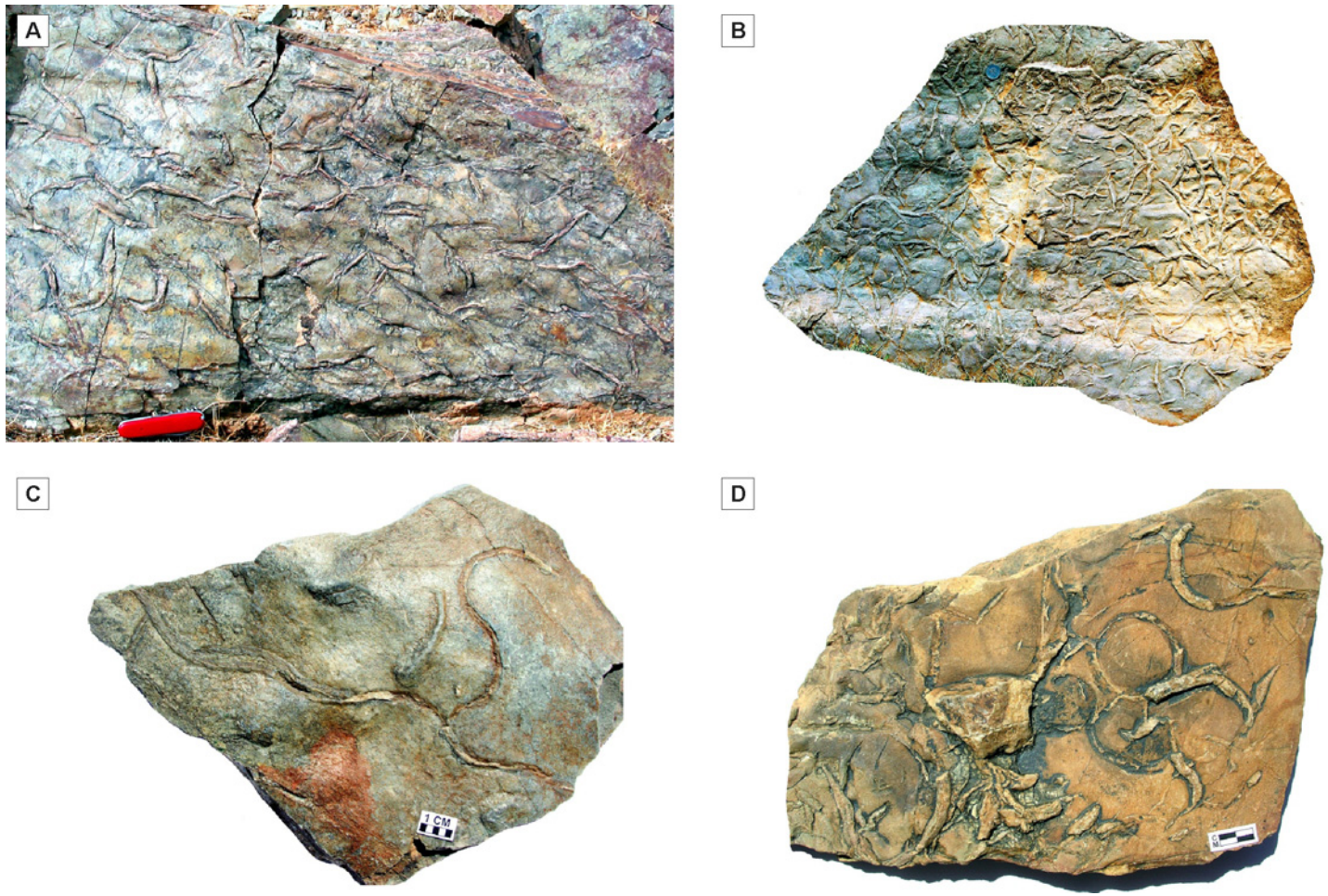


Figure 4(c)-3: Sand cracks.

(A) Upper sandstone bedding surface with spindle-shaped, lenticular, triradiate, and sinuous sand cracks. (B) Network of sand cracks, consisting of two superimposed crack generations (right side of photo). In the sandstone layer below (left side of photo) only one generation of cracks is developed. (C) Upper sandstone bedding surface with sigmoidal to sinusoidal, and sinuous sand cracks. (D) Upper sandstone bedding surface with spindle-shaped, curved, and figure-8-like sand cracks. All structures within this figure are from: Morocco, Anti-Atlas, Agoummy area; Neoproterozoic Imi n-Tizi Formation, n-Tizi n-Taghatine Group; palaeoenvironment: intertidal to lower supratidal zones of a peritidal coastal plain. All photos: H. Porada and E. Bouougri.

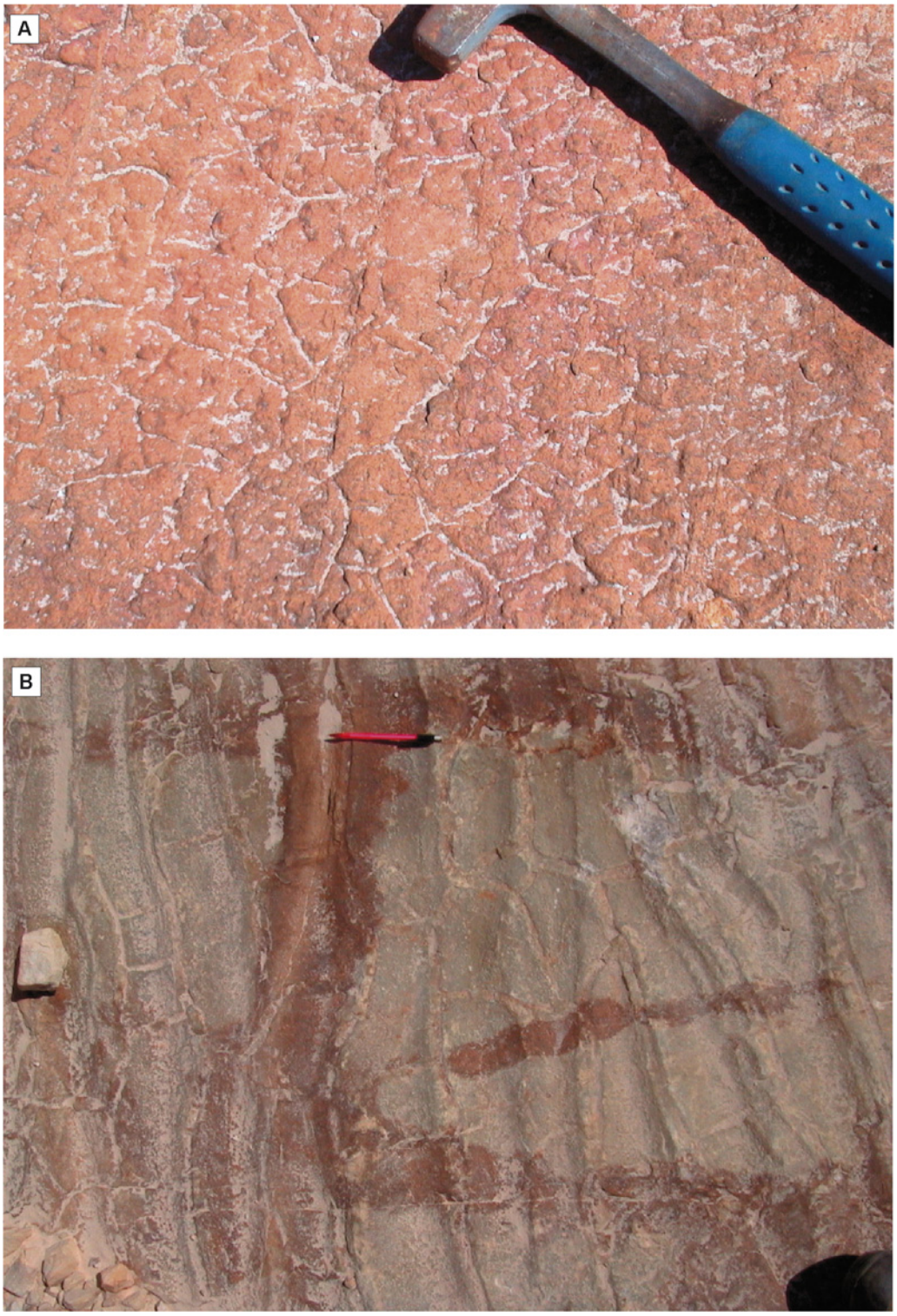


Figure 4(c)-4: Sand cracks, and ripple-top sand cracks.
(A) Well-developed first-order sand cracks (filled by modern windblown sand) with poorly developed second-order cracks visible locally. Locality: ca. 2.1 Ga Magaliesberg Formation (Pretoria Group, Transvaal Supergroup), B and E Silica Mine, ca. 50 km east of Pretoria, South Africa; palaeoenvironment: tidally reworked braid-deltaic epeiric marine coastline. Photo: M. Parizot. (B) Sand cracks developed preferentially on wave ripple crests, with crack orientation predominantly parallel with these crests and with lesser cracks at approximately right angles to this, joining ripple-crest cracks across ripple troughs. Note bifurcation of ripple-crest cracks (detailed discussion in Parizot et al., 2005). Compare with Figure 4(a)-15. Locality: ca. 2.1 Ga Magaliesberg Formation (Pretoria Group, Transvaal Supergroup), B and E Silica Mine, ca. 50 km east of Pretoria, South Africa; palaeoenvironment: tidal flat – braid-delta setting on an epeiric sea coastline. Pen is 8 mm wide. Photo: M. Parizot.

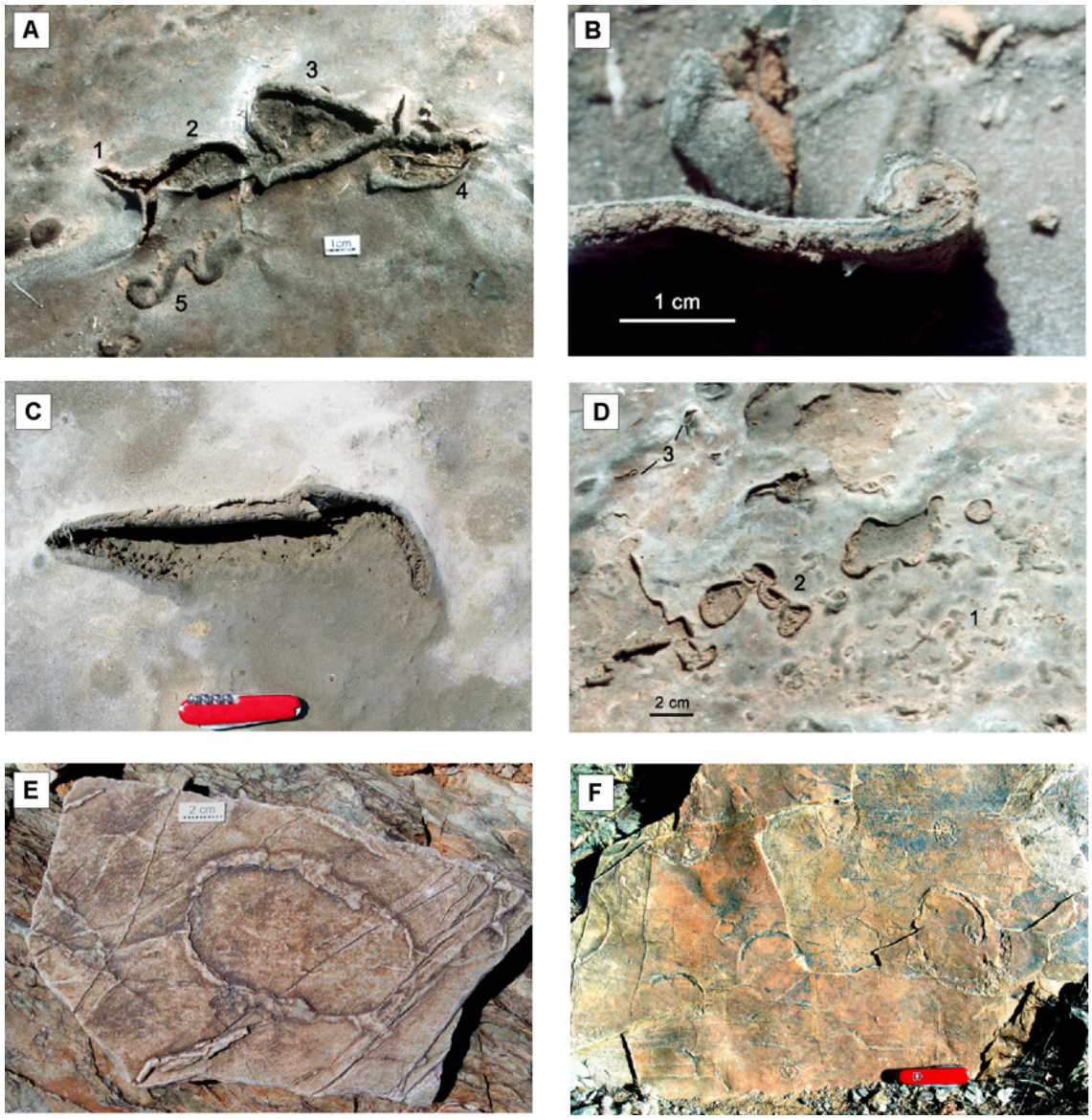


Figure 4(c)-5: Curled crack margins.

(A) Modern mat surface with shrinkage cracks. Various stages of crack margin evolution are recognised: (1) incipient crack with simple shape and slightly upturned margins; (2) two opposite margins, one curved and upturned, the other almost straight and curled; (3) three opposing curled margins surround a subcircular opening in the mat surface; (4) old curled margin, partly overgrown by a new mat layer; (5) relic old overgrown curled crack margins. Locality: Bhar Alouane, Mediterranean coast of southern Tunisia; environment: upper intertidal to lower supratidal zones of tidal flat. (B) Section across curled crack margin in modern mat, showing sediment layer below mat to be entangled in the involute margin. Green peripheral band is a new mat layer overgrowing the curled margin. Locality: Bhar Alouane, Mediterranean coast of southern Tunisia; environment: upper intertidal to lower supratidal zones of tidal flat. (C) Modern mat surface with large shrinkage crack showing only one margin to be curled, the other being flat and biostabilised. Locality: Salins du Midi, Réserve Nationale Camargue, southern France; environment: preconcentration basin of 'Salins de Midi' saltern. (D) Mat surface showing several generations of lenticular and irregular to circular, curled margins surrounding cracks and openings in a thin, modern microbial mat: (1) relics of first generation curled margins, completely overgrown; (2) second generation curled margins and openings, partly overgrown by new mat layers; (3) new, third generation, upturned crack margins. Locality: Bhar Alouane, Mediterranean coast of southern Tunisia; environment: upper intertidal to lower supratidal zones of tidal flat. (E) Upper surface of fine-grained quartzite layer showing subcircular and linear, irregular ridges. The subcircular one is distinctly flattened, whereas the linear ridge (near lower side of photo) exhibits a composite structure of two superimposed ridges. The structures are interpreted as curled margins of a narrow linear crack (two ridges) and a subcircular opening in a thin microbial mat that previously covered a sandy sediment surface. Locality:

Morocco, Anti-Atlas, Agoummy area; Neoproterozoic Wanimzi Formation, Tizi n-Taghatine Group; palaeoenvironment: peritidal (intertidal to supratidal) coastal plain. (F) Upper quartzite bedding surface with mainly circular to curved ridges, interpreted as curled crack margins partly surrounding circular and subcircular openings in a thin microbial mat that previously covered a sandy sediment surface. Note linear and triradiate ridges at lower left of photo. The diameters of the circular structures vary between 2 and 8 cm. Scale (knife): 8 cm. Locality: Morocco, Anti-Atlas, Agoummy area; Neoproterozoic Im n-Tizi Formation, Tizi n-Taghatine Group; palaeoenvironment: peritidal (intertidal to supratidal) coastal plain. All photos: H. Porada and E. Bouougri.

---

from either wind or gravity, and they termed these features ‘petees’. Subsequently, Reineck et al. (1990) suggested a classification of petees into alpha-, beta- and gamma-petees, and considered petees in general to be biologically modified overthrust structures, including single domes, multitudes of buckles and transitions of the latter into domes; in all cases in these two original definitions, the dome-like crests were closed and rounded, reflecting the cohesiveness of the microbial mats. Reineck et al. (1990) interpreted genesis of petees as due to either (1) subsurface gas concentration which deformed the overlying cohesive mat, or (2) wind or water friction, or gravity, leading to deformation of soft biogenic surface tissues.

The petees observed in modern mats by these early workers were positive deformation features in the mats themselves and obviously stood little chance of preservation, other than as vague irregularities on sandstone bed upper surfaces, once decay set in. However, modern mats from Tunisia do in some cases show positive features of analogous geometry in the sandy substrate, which are thought to have formed by upward movement of sediment filling the ‘open space’ beneath the buckles in the mat. In terms of the original and strict definition of the term petees, these are secondary structures reflecting the existence of the petees in the overlying mats themselves.

Thus, according to the original definition of Gavish et al. (1985) and the subsequent remarks by Reineck et al. (1990), petees are clearly denoted as domes, buckles and folds developed on a flexible mat surface. These earlier workers did not see any relation of petees to mat-cracks or filled cracks, even if the domes, buckles and folds may occasionally have undergone some cracking under desiccation. Later workers (e.g., Gehling, 1999, 2000), however, did bring in a possible association with cracks formed in a microbial mat, thereby expanding the original definition. At the same time, Gehling (1999) also discusses petees *sensu stricto*, which he related to genesis through mat growth expansion and gas pressure from underlying mat decay. In his 2004 classification scheme, also that adopted as the basis for this book, Schieber similarly encompassed this broader definition and genetic association of petees with mat-cracking – he uses the term ‘petee ridges’ to denote positive petee-like features related to this rupturing of microbial mat surfaces, and notes that simple polygonal petee ridge networks or more complex sinuous ridge patterns may result. Implicit in this more modern and expanded definition of the term ‘petee’ is that petee ridge patterns may often resemble the geometry of desiccation cracks in the microbial mats that aided their formation. Following on the discussion above and also based partly on the usage of Noffke et al. (2001a) we use the term ‘petee’ or ‘petee ridge’ in a loose and generalised sense to denote positive epirelief on mat surfaces; strictly speaking one should then differentiate between petees *sensu stricto*, related to the original definitions of Gavish et al. (1985) and Reineck et al. (1990) and the usage of Gehling (1999), and petees *sensu lato*, which have a relation to cracks in microbial mats.

‘*Manchuriophycus*’ (cf. ‘*Rhysonetron*’) represents a special type of microbial shrinkage crack, developed within thicker mats found within the troughs between ripples – various examples of ancient occurrences are shown in Figures 4(c)-11 and -12, together with one example of a living mat surviving reworking by currents within the relatively protected hollows between ripple crests. Some deviations from characteristic ‘*Manchuriophycus*’ cracks have been observed, including such cracks developed preferentially on ripple crests, and a more reticulate pattern of the normal trough-located cracks (Figure 4(c)-13). In contrast to these ripple-trough features, ripple crest sand cracks also occur; those shown form a reticulate pattern of sand cracks, where longer negative cracks tend to follow wave ripple crests, and are connected by shorter ‘cross-cracks’ across the intervening troughs (Figure 4(c)-4B; see also Figure 4(a)-15).

It is most important to emphasise that all of the cracks discussed here can easily be confused for non-biogenically formed features in the ancient sandstone record. It is thus of critical importance that any cracks and crack-like features are studied *in cross-section*, to ensure that no mudstone is present between the apparently cracked lower sandstone bed and that overlying it (see also caption to Figure 4(c)-7). If only one bed surface, the lower, is studied and carries sand cracks of any type, the possibility that mud(stone) was indeed present upon the sandy crack-laden surface of the lower bed cannot be disproved and the cracks cannot be assigned a microbial mat genesis with any

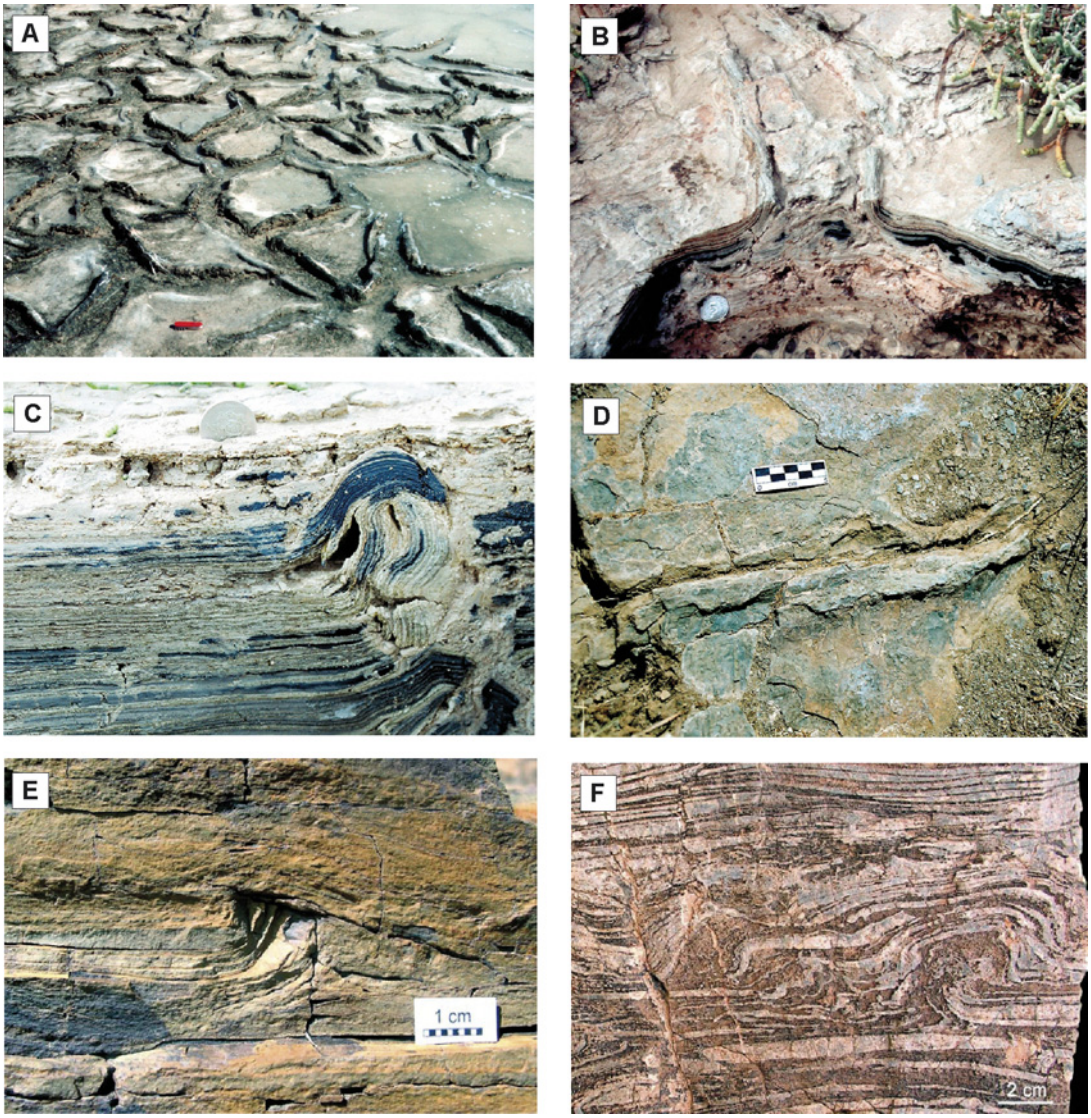


Figure 4(c)-6: Overgrown, upturned crack margins.
(A) View of surface of decimetre-scale polygonal network of shrinkage cracks within modern biolaminite. The edges of the polygons are upturned, overturned and partly overfolded. In the crack openings, a new thin mat has formed, partly overgrowing the polygons' edges. Note high tide water flooding the polygonal network from the right side. Scale (Swiss army knife): 8 cm. (B) Section across two symmetrical upturned crack margins in thin layer of modern biolaminite. The margins are upturned into a vertical attitude and have a thickness of 2 cm. On the bedding surface, they are slightly sinuous or curved. The crack opening is filled with sediment which is partly trapped beneath the upturned margins. Scale (coin): 24 mm. (C) Section across a single upturned crack margin developed on one side of a shrinkage crack in modern biolaminite. The margin is upturned into a vertical attitude and partly overgrown by new mat layers. Sand- to silt-sized sediment is accumulated on both sides of the overgrown upturned crack margin, thus fossilising the structure. Scale (coin): 25 mm. Photos (A) to (C) from the intertidal zone, Bhar Alouane, Mediterranean coast of southern Tunisia; environment: intertidal zone. (D) Upper sandstone bedding surface showing upturned crack margins forming inverted 'V' or antiformal structures along both sides of a shrinkage crack. Upturned margins are up to 3 cm high. Locality: Namibia, Haruchas area; Vingerbreek Member, Nudaus Formation, Schwarzrand Subgroup, Nama Group; Terminal Proterozoic; palaeoenvironment: intertidal to supratidal shallow back-barrier setting, with small tidal channels and few high energy storm deposits. (E) Cross-sectional view of an asymmetric upturned crack margin formed at one side of a shrinkage crack preserved within sandstone; laminae are upturned into a vertical attitude. Locality and palaeoenvironment, as for (D). (F) Section across an upturned margin of a shrinkage crack preserved in sandstone. The margin is overturned and completely overgrown. Towards the top of the photo, the structure is fossilised by continuous, normal lamination. Locality: Morocco, Anti-Atlas, Nqob area; Neoproterozoic Wanimzi Formation, Tizi n-Taghatine Group; palaeoenvironment: intertidal zone of a peritidal coastal plain. All photos: H. Porada and E. Bouougri.

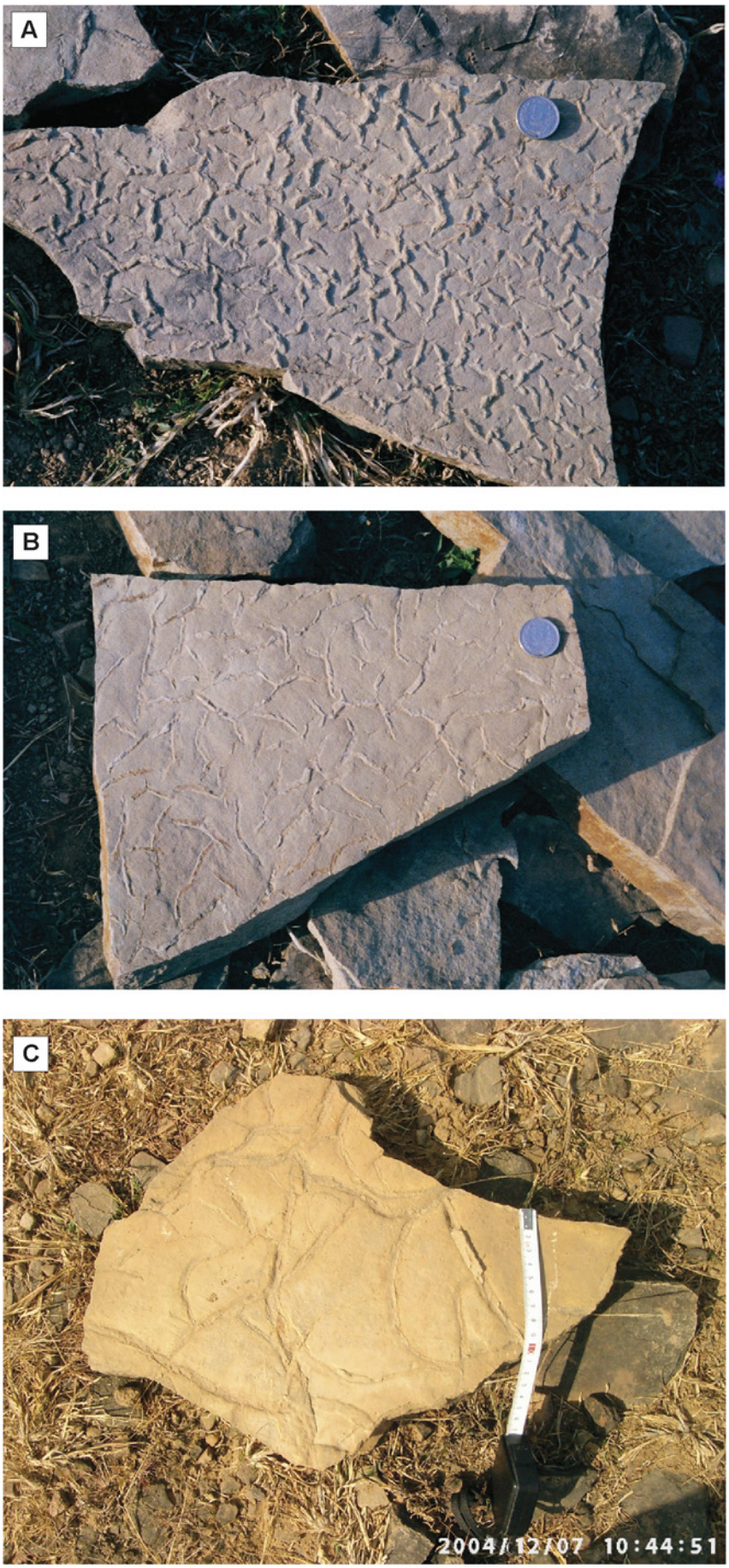

A
B
C
2004/12/07 10:44:51

Figure 4(c)-7: Filled sand cracks.
(A) Positive ridges on bed upper surface, which have a cross-cutting pattern (including 'triple junctions') and form an incipient network. Note also weak development of second-order ridges between well-developed first-order features. Resemble analogous sets of (negative) sand cracks with very similar geometrical pattern (compare with Figure 4(c)-2), but their positive nature is analogous to petee ridges. However, the latter generally comprise sandstone from the lower bed, are related to disturbance of laminated sands in lower bed and are separated by concave-upward segments between the ridges. In the example illustrated (and in B and C), none of these criteria are met and the composition of the ridges is that of the overlying sandstone bed. (B) Positive ridges on bed upper surface, which have a cross-cutting pattern (including 'triple junctions') and form an incipient network (first-order features only). Note also that many of these ridges are partially flattened, including a few that appear to have been pushed sideways and then flattened (see broader flattened ridge to left of coin). Resemble analogous sets of (negative) sand cracks with very similar geometrical pattern (compare with Figure 4(c)-2), but their positive nature is analogous to petee ridges. Note that some of these reticulate features change from being ridges to being shallow (negative) cracks, in the bottom left part of the slab. It must be emphasised, however, that a cracked mud layer, between the two sand layers in (A) and (B) may also have produced these crack-fill features, and these two examples cannot thus be taken as unequivocal evidence for desiccation of a mat growing on a sandy substrate. (C) Sinuous cracks which form irregular curved patterns, and which are filled by a later (coarser and more granular) sandy material, different to the underlying sandstone bed; much of this secondary crack-fill material has been erosively removed, the largest remnant being situated to the left of the measuring tape. The negative nature of the original sand cracks in the bed's top surface is clear. These crack-fills would thus appear not to be petee ridges, as also evidenced by undisturbed sandstone laminae in the upper part of the underlying sandstone bed (as seen in section) and the lack of concave-upwards segments between the crack features. For all three photos, locality: Chorhat Sandstone Member (Kheinjua Formation, Semri Group) (ca. 1600 Ma), Vindhyan Supergroup, central India, at Chopan; palaeoenvironment: intertidal setting. All photos: S. Banerjee.

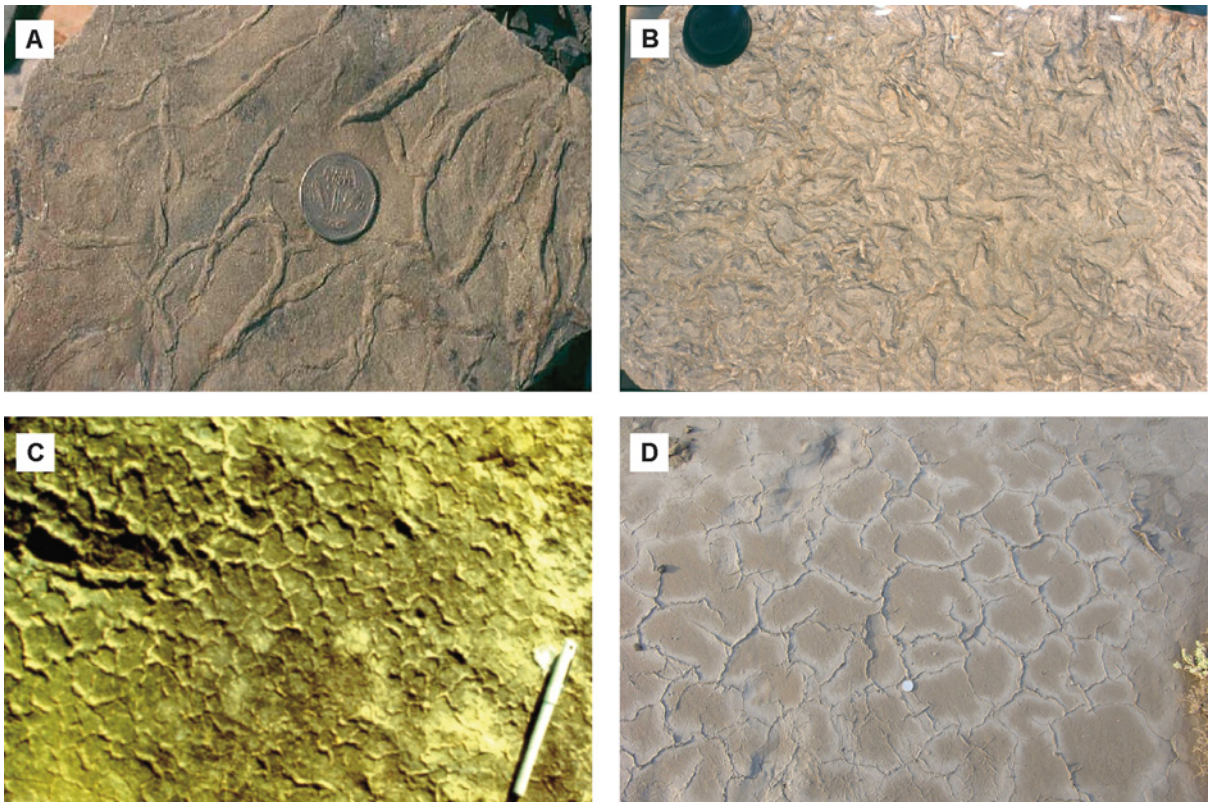


Figure 4(c)-8: Petees/petee ridges.
(A) Petee ridges showing both spindle-shaped forms and longer, more sinuous shapes. Presumably these formed initially as incipient tears and sinuous cracks in a mat covering a sandstone bed, and were then filled from below by that same sandstone to form the positive petee ridges. Locality: Chorhat Sandstone Member (Kheinjua Formation, Semri Group) (ca. 1600 Ma), Vindhyan Supergroup, central India, at Amjhore; palaeoenvironment: intertidal setting. (B) Dense pattern of at least two orders of petee ridges (filled by same sandstone as that comprising underlying bed, with deformation of sandstone laminae in that sandstone, and with upward-concave segments between petees). An impression is gained from this photo, that the densely packed petee ridges may have been deformed, possibly owing to a still-living mat between them which was subject to shortening, due to something like movement of mat and petees under the influence of a strong current. Locality and palaeoenvironment: as for (A). (C) More pervasive, reticulate-polygonal pattern of petee ridges; note ridges cutting across each other in several places, suggesting pervasive development, probably by synaeresis origin. Locality and palaeoenvironment: intertidal–supratidal zone of the 0.6 Ga Sonia Sandstone, Jodhpur Group, Rajasthan, India. (D) Reticulate, polygonal pattern of petee ridges, from modern sands along the Indian coast at Mumbai, in the intertidal zone. Note incomplete connection of many of the ridges; also, locally, sand cracks can be observed passing laterally into petee ridges – left of the coin, and in the middle of the top margin of the photo. Photos (A), (B) and (D): S. Banerjee. Photo (C): S. Sarkar.

confidence at all. If part–counterpart specimens of a lower, cracked sandstone bed and its immediately overlying successor sandstone bed are not available, at the very least, close to the site of an exposed, single (lower) cracked sandstone bed, the overlying sandstone bed must be observable, *in situ*, forming part of the outcropping succession of sandy beds. In Figures 4(c)-2A, -2D, -2E and -2F, for example, the undisturbed overlying sandstone bed (without mudstone between the two sandy beds) can be observed within centimetres of the lower, cracked sandy bed. Non-application of this very basic principle to investigations of any inferred microbial mat-related features in sandstones would essentially negate any such possible biological interpretations. It is emphasised that all examples shown in this book have been subject to this important test of potential 'bio-validity'.

Microbial shrinkage cracks in modern mats can locally develop curled crack margins, which may also be preserved in ancient sandstone beds (Figure 4(c)-5). These features form the first step in a continuum: curled crack margins – flipped-over mat edges – rolled-up mat fragments; in all cases, when the lower, sediment-rich part of the mat remains attached to these desiccating and partly reworked mat margins, these features are preserved in the clastic sedimentary rock record. Curled crack margins can also become overgrown by renewed mat growth, forming



Figure 4(c)-9: Petee ridges and related sand cracks.
Irregular network of petee ridges, composed of the same sandstone as the bed in whose top they occur; this underlying bed also has sandstone laminae which are disturbed, when seen in section, and the ridges are separated by concave-upward segments. Note, however, the presence of negative cracks in parts of this bed upper surface: particularly the two clearly negative features (which resemble incipient mat-tears – see Figure 4(c)-2) immediately above the two prominent ridges adjacent to the coin, and also several, more sinuous cracks in the right-lower part of the field of view. This suggests that the cracks were likely primary and were later filled from underneath by liquefied sand which, under pressure (gas expulsion or dewatering; or from overlying beds or due to loading with changes in tidal height) formed the petee ridges (see also Figure 4(c)-8D). Locality: Chorhat Sandstone Member (Kheinjua Formation, Semri Group) (ca. 1600 Ma), Vindhyan Supergroup, central India, at Amjhore; palaeoenvironment: intertidal setting. Photo: S. Banerjee.

'overgrown upturned margins', modern and ancient (Figure 4(c)-6). Flipped-over mat edges, also commonly termed 'flip-overs', reflect a complete inversion of a mat-edge, while rolled-up mat fragments (Figures 4(c)-14 and -15) form when more extreme mat desiccation, normally allied to sedimentary reworking, leads to breakup of the mat or at least parts thereof and the formation of rolled-up mat portions wherein several complete 360° revolutions often occur. These rolled-up mat fragments (often termed just 'roll-ups' or 'jelly-rolls') often occur together with variously shaped and sized mat fragments, such as mat chips and sand chips, discussed below.

Schieber (2004) notes that sand chips are a particular sort of eroded mat fragment, which form an end-member of the continuum mentioned in the previous paragraph. They tend to be smaller ($\leqslant$ few cm) than rolled-up mat fragments (or their sandy ancient versions) and tend to have rounded and plastically deformed shapes (Figure 4(c)-17). Like rolled-up mat fragments, current alignment (Figure 4(c)-15 for roll-ups) or even imbrication of sand chips may occur (Pflüger and Gresse, 1996; Bouougri and Porada, 2002). Microbial mats provide cohesiveness for these deformed sand chips to form and to survive sedimentary transport. When a microbial mat dries out, curved, rigid mat chips will result, which are then also subject to potential transport and reworking – in sub-Recent sandy sediments they can be preserved as carbonaceous clasts, and in ancient examples, the sediment associated with the basal portions of the mat will be preserved within these chips. In the example shown from the ca. 1.8 Ga Waterberg Group (South Africa), hematitic siltstone – very fine-grained sandstone forms these chips, and they are associated with roll-ups (Figure 4(c)-16).

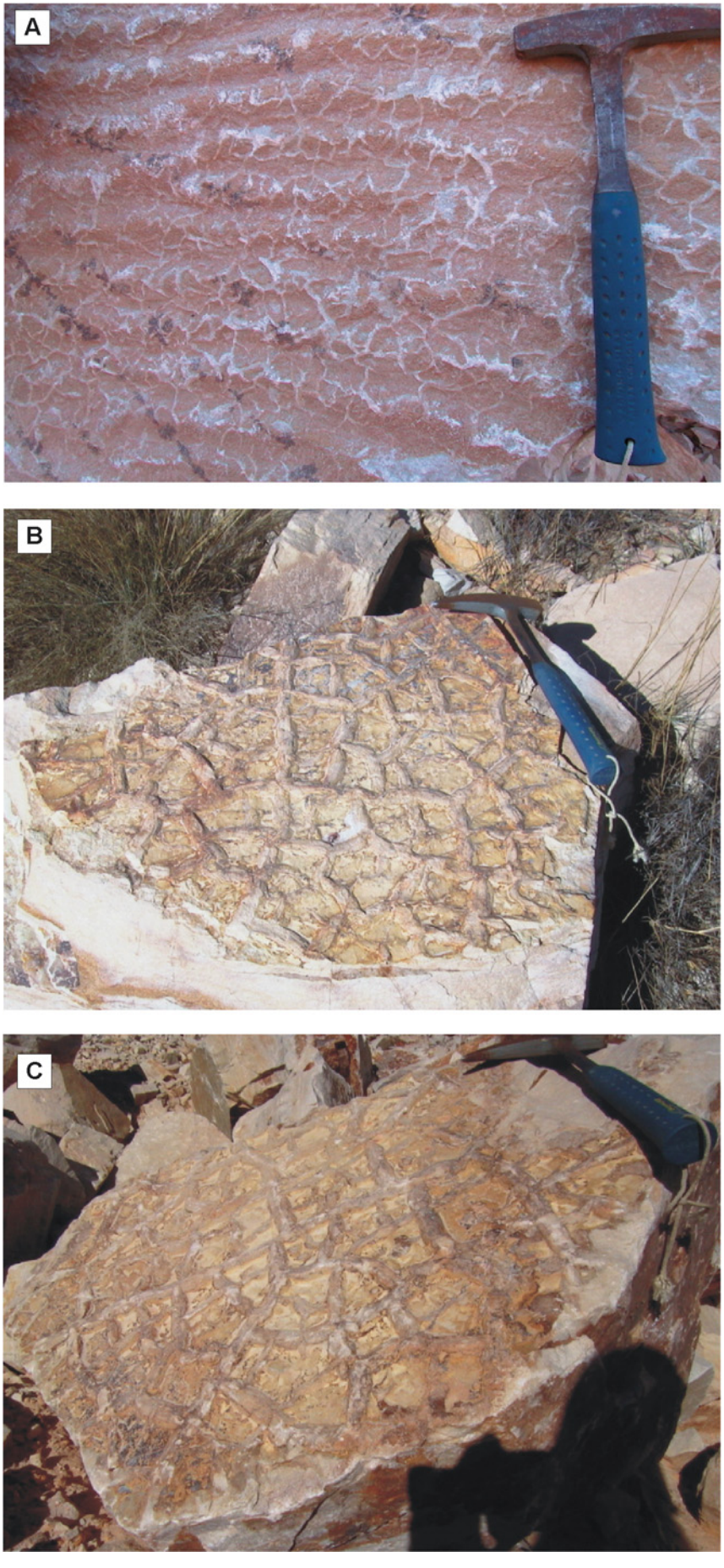

A
B
C

Figure 4(c)-10: Petees/petee ridges.
(A) Reticulate pattern of flattened petee ridges (mainly first-order with few second-order ridges) developed on earlier wave ripples. (B and C) Note three orders of petee ridges in both examples. Both are from loose blocks of partially recrystallised quartzites quarried in a small opencast working. Thin sections through these petee ridges showed clearly a lower medium-grained sandstone, overlain along an irregular contact (soft sediment deformation) by an upper fine-grained sandstone layer; the latter also makes up the petee ridges (detailed discussion in Parizot et al., 2005). For all three photos, locality: ca. 2.1 Ga Magaliesberg Formation (Pretoria Group, Transvaal Supergroup), B and E Silica Mine, ca. 50 km east of Pretoria, South Africa; palaeoenvironment: tidal flat – braid-delta setting on an epeiric sea coastline. All photos: M. Parizot.

Wrinkle marks, *sensu lato*, represent a problematic group of microbial mat-related features as they can just as easily form and be preserved from mat-growth settings (e.g., Figure 4(a)-4) as from mat-destruction settings, and because they can easily be confused with features formed from soft sediment deformation processes or even tectonically-formed structures (see Chapter 6(a)). In Section 4(a) of this chapter, wrinkle marks related to mat growth settings are detailed, but the continuum from such features to wrinkles related to mat destruction makes it difficult to draw a definitive line between these two groups. In this section, we consider only wrinkle marks which show evidence of significant detachment of the mat from its sandy substrate to fall within the destruction-related features (e.g., Figure 4(c)-18). In Chapter 6(a), a more comprehensive discussion of the wrinkle mark problem is provided by Porada and Bouougri.

Ripple patches (see also Figures 4(a)-13 and -14) will form when a mat-protected sandy bed is exposed locally due to removal of the mat in certain patches, leaving the exposed sand amenable to sedimentary reworking with the concomitant formation of ripple marks within those patches; such ripple patches tend to have margins marked by a smooth gradation of the ripples into the surrounding featureless sandstone bed-top (Figure 4(c)-19). Analogously, patchy reworking of a rippled sandstone bed suggests that a microbial mat protected the areas where the original ripple set is preserved (Figure 4(c)-19).

The cohesion given to sandy beds by microbial mats growing on them can also remain for some time after burial, and this can enable unique behaviour of such beds under deformation (Schieber, 2004); an example of this is non-penetrative micro-faults (Pflüger, 1999; Gehling, 1999). The various microbial mat-related features associated with mat destruction, discussed above in brief, are detailed below and illustrated in the accompanying figures.

Formal description of mat destruction features

Microbial shrinkage cracks (modern): Figure 4(c)-1

Name of structure: Microbial shrinkage cracks.

Other terms used: Synaeresis cracks, desiccation cracks, '*Manchuriophycus*', '*Rhysonetron*'.

Description of structure: Surface of thin microbial mat marked with isolated lenticular, sinuously curved and even subcircular cracks, spindle shaped and triradiate shrinkage cracks; ends of cracks generally taper; locally, figure-8 patterns occur. Cracks may extend downward into sediment layer below mat. In other cases, crack patterns comprise linear, lenticular to sigmoidal cracks, following the linear trends of shallow bulges. Active growth of cyanobacterial filaments can occur along margins and openings of cracks, forming bridge-like structures between margins, thus favouring progressive closure of the cracks and preservation of sediment filling the cracks.

Associated sedimentary structures: (1) small current ripples (2 cm wavelength, 3 to 5 mm amplitude) within organo-sedimentary layers; (2) interbedding of microbial mat layers and event layers of a few millimetres-scale; horizons of gypsum; (3) desiccation cracks; (4) burrowing (mainly by gastropods).

Environment: Upper intertidal to lower supratidal zones of tidal flat. Preconcentration basin of a saltern.

Ideas on genesis: Subaerial shrinkage and related cracking of thin mats may lead to a wide range of structures depending on the maturity and cohesiveness of the mat, and on the position in the intertidal–supratidal zones. Within these zones, limited shrinkage and formation of isolated and rarely interconnected cracks of various shapes

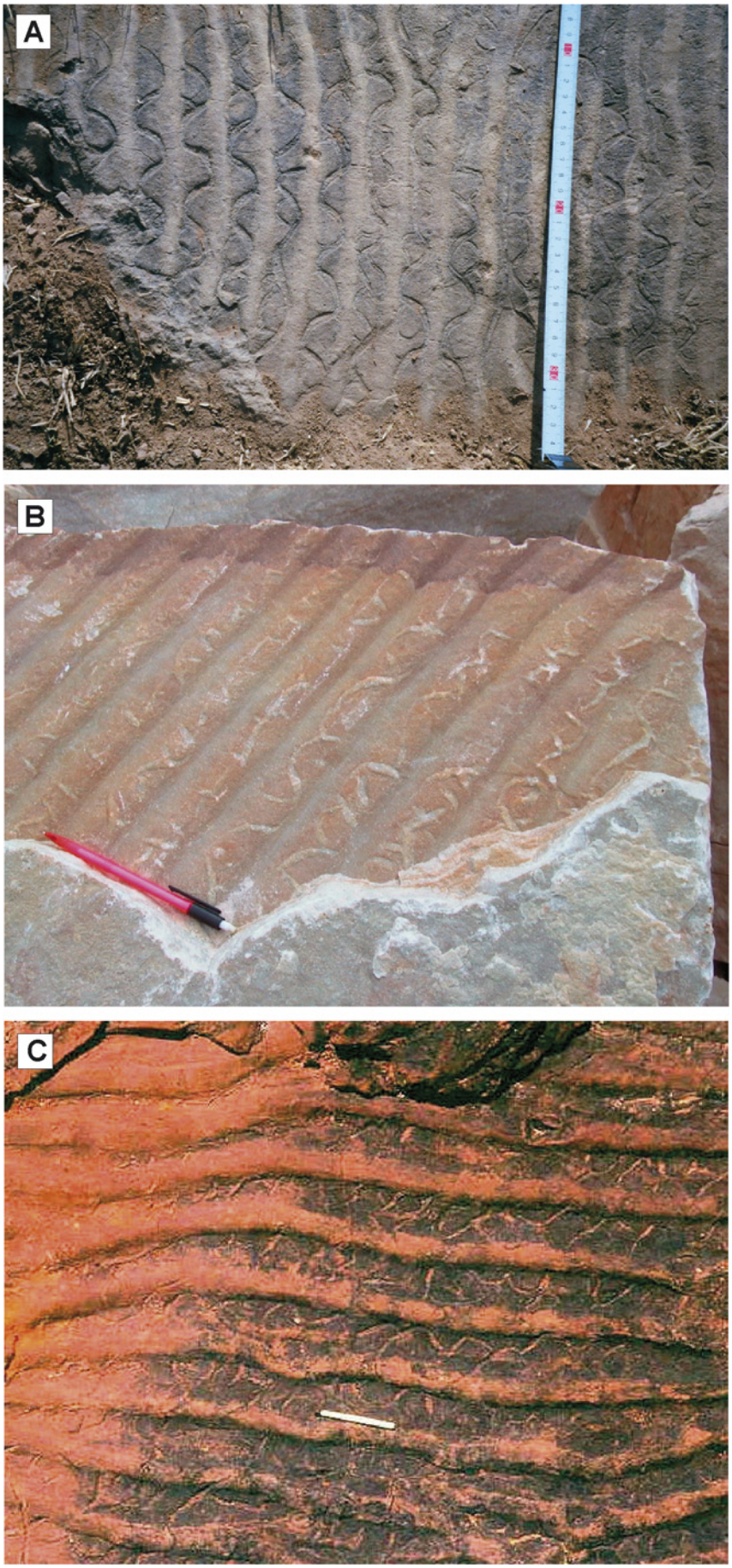

A
B
C

Figure 4(c)-11: '*Manchuriophycus*'.
(A) Sinuous cracks confined to troughs between wave ripples ('*Manchuriophycus*') on sandstone bed upper surface; note uncommon, smaller connecting cracks which do cross ripple crests. Locality: Chorhat Sandstone Member (Kheinjua Formation, Semri Group) (ca. 1600 Ma), Vindhyan Supergroup, central India, at Chorhat; environment: intertidal setting. Photo: S. Banerjee. (B) '*Manchuriophycus*' structures preserved on the sole of a sandstone bed overlying that on which they originally formed. Note that inverted wave ripple crests between these cracks are flattened off, most probably due to tidal reworking (detailed discussion in Parizot et al., 2005). Pen is 8 mm wide. Locality: ca. 2.1 Ga Magaliesberg Formation (Pretoria Group, Transvaal Supergroup), B and E Silica Mine, ca. 50 km east of Pretoria, South Africa; palaeoenvironment: tidal flat – braid-delta setting on an epeiric sea coastline. Photo: M. Parizot. (C) Sinuous cracks confined to troughs between wave ripples in sandstone ('*Manchuriophycus*'). Note that ripples bifurcate at left of photograph, and that the cracks grow in dimension as spacing between ripple crests widens. Note also a later generation of cracks (long cracks below and above pencil; also lower left of photograph) which cut across ripple crests and cracked troughs at an orientation approximately perpendicular to the ripple crests. Locality and palaeoenvironment: as in (A). Photo: S. Banerjee.

---

and sizes are the main shrinkage features of cohesive mats strongly attached to the substrate. Cracks formed are filled by sand- to silt-sized sediment transported by tidal currents and/or wind. The filling stage is accompanied and followed by active growth of bacterial filaments in and on the cracks leading to their sealing, preservation, and separation from sediment layers above. Cracks may also be filled by deposition of sands from the overlying bed, before sealing is complete.

Sand cracks: Figures 4(c)-2 to -4A

Name of structure: Sand cracks (compare with modern equivalents above, the microbial shrinkage cracks).

Other terms used: Synaeresis cracks, desiccation cracks, '*Manchuriophycus*', '*Rhysonetron*', microbial shrinkage cracks.

Description of structure: Upper bedding surface with isolated, lenticular and spindle-shaped microbial shrinkage cracks; sigmoidal to sinusoidal, curved, circular and sinuous ('wriggly') microbial shrinkage cracks; minor figure-8 forms. The isolated spindle-shaped cracks may possibly join up into triradiate cracks (however, 'triple junctions' are often incipient structures themselves, similar to isolated spindle-shaped cracks) or the beginnings of reticulate crack patterns, and these may be linked, locally, with the more sinuous crack forms. Polygonal/reticulate networks as well as complex interference patterns of more sinuous cracks occur commonly, and superimposed crack generations on sequential sandstone beds are found.

Associated sedimentary structures: (1) heterolithic deposits with centimetre-scale interbedded sandstone and organo-sedimentary sericitic layers; (2) event deposits related to fluvial sheet floods or storms; millimetre- to centimetre-scale alternation of sedimentary sandstone event layers of storm or fluvial origin, and organo-sedimentary laminated layers of siltstone and sericitic argillite; (3) few small fluvial/tidal channels; (4) mud clasts; (5) oscillation, interference and current ripples, and wave and current ripple laminations; (6) desiccation cracks; (7) adhesion warts; (8) small-scale load structures.

Palaeoenvironment: Intertidal to lower supratidal zones of a peritidal coastal plain; playa lake or saline pan lenses within thick aeolian palaeodesert succession.

Ideas on genesis: Isolated spindle-shaped cracks are thought to be incipient tears, the first cracks to form; these then link up, commonly in 'triple junction' or triradiate intersections of incipient cracks, and these may in their turn form complex intersections of either essentially straight crack patterns (polygonal to reticulate patterns) or, less commonly, curved crack patterns (some of these have a bead-like morphology and may have formed from linked, small incipient tears). Finally, there appears to be a second generation of more complex curved cracks, with smaller widths, which show no relationship to 'triple junction' features. All these crack features are inferred to reflect mat desiccation and subaerial shrinkage, with concomitant cohesiveness provided by the mat to underlying sands which then preserve these same features. By comparison with modern situations, incomplete, limited shrinkage appears to be controlled by the maturity and strong cohesiveness of 'inactive' thin mats in environmental settings like the upper intertidal to supratidal zones. Opened cracks are filled by sediment particles transported during exceptionally high tide, storm and rainfall, or by wind. In contrast, 'active' thin mats of lower to middle intertidal settings and around

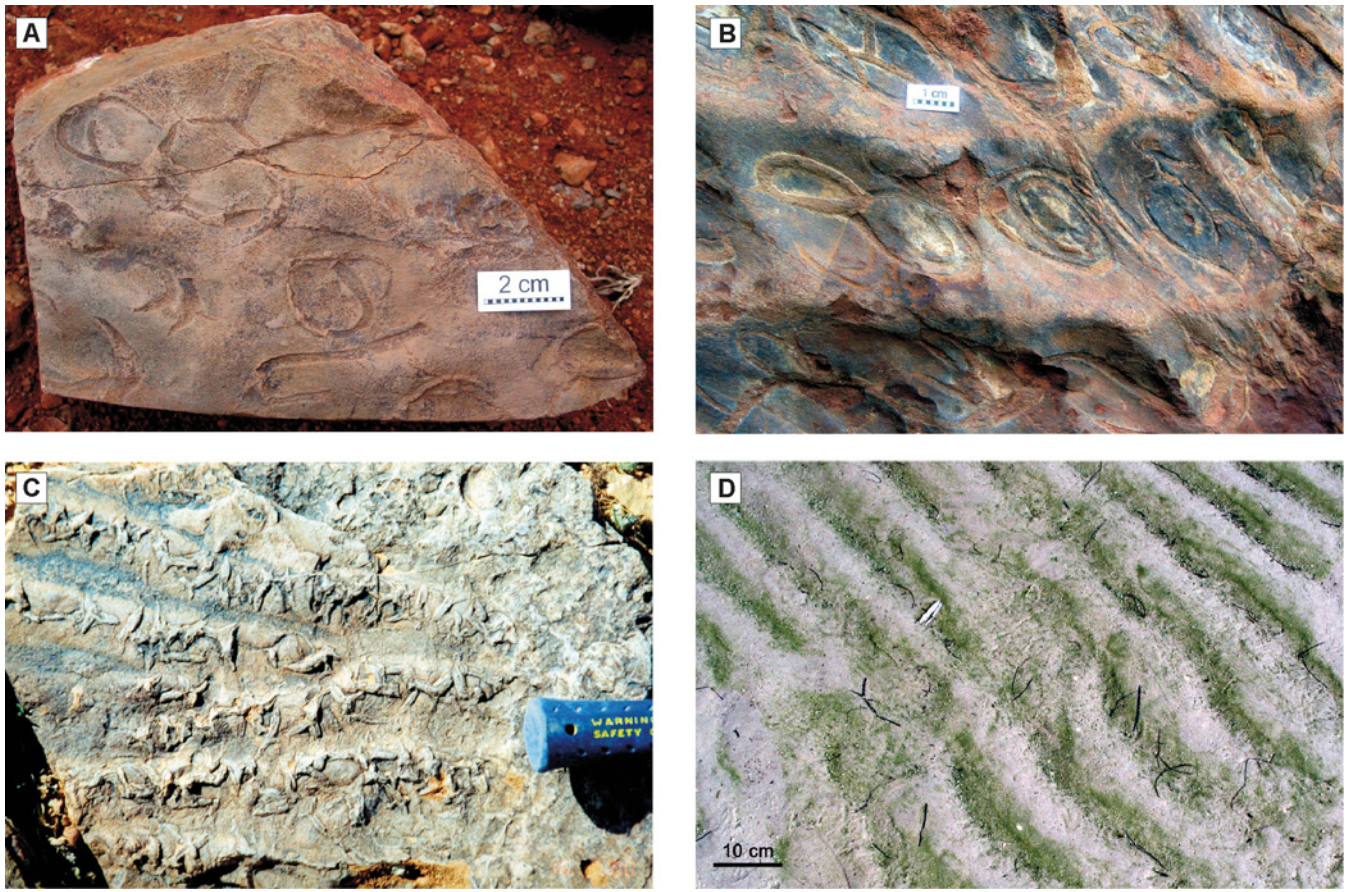


Figure 4(c)-12: '*Manchuriophycus*'.

(A) Sandstone upper bedding surface with interference ripples. In troughs, sinuous, circular and triradiate cracks ('*Manchuriophycus*') are developed. Note that cracks largely follow the edges of the troughs. Locality: Morocco, Anti-Atlas, Ifni inlier, Larbâa n-Sahel area; Neoproterozoic Tizi n-Taghatine Group; palaeoenvironment: coastal plain of lacustrine or shallow marine environment, fringing alluvial braid-delta system. (B) Upper bedding surface of sandstone with interference ripples and shrinkage cracks. In the troughs, figure-8-like cracks ('*Manchuriophycus*') occur. Locality and environment: as for (A). (C) Lower bedding surface of sandstone with spindle-shaped, lenticular and triradiate microbial shrinkage cracks in troughs of oscillation ripples. Locality: Morocco, Anti-Atlas, Agoummy area; Neoproterozoic Imi n-Tizi formation, Tizi n-Taghatine Group; palaeoenvironment: intertidal to lower supratidal zones of a peritidal coastal plain. (D) Modern sediment surface with current ripples and concentration of cyanobacteria in troughs and on lee sides of ripples. Locality and environment: shallow outlet of temporary pond in upper intertidal zone of tidal flat, Amrum island, North Sea coast of Germany. All photos: H. Porada and E. Bouougri.

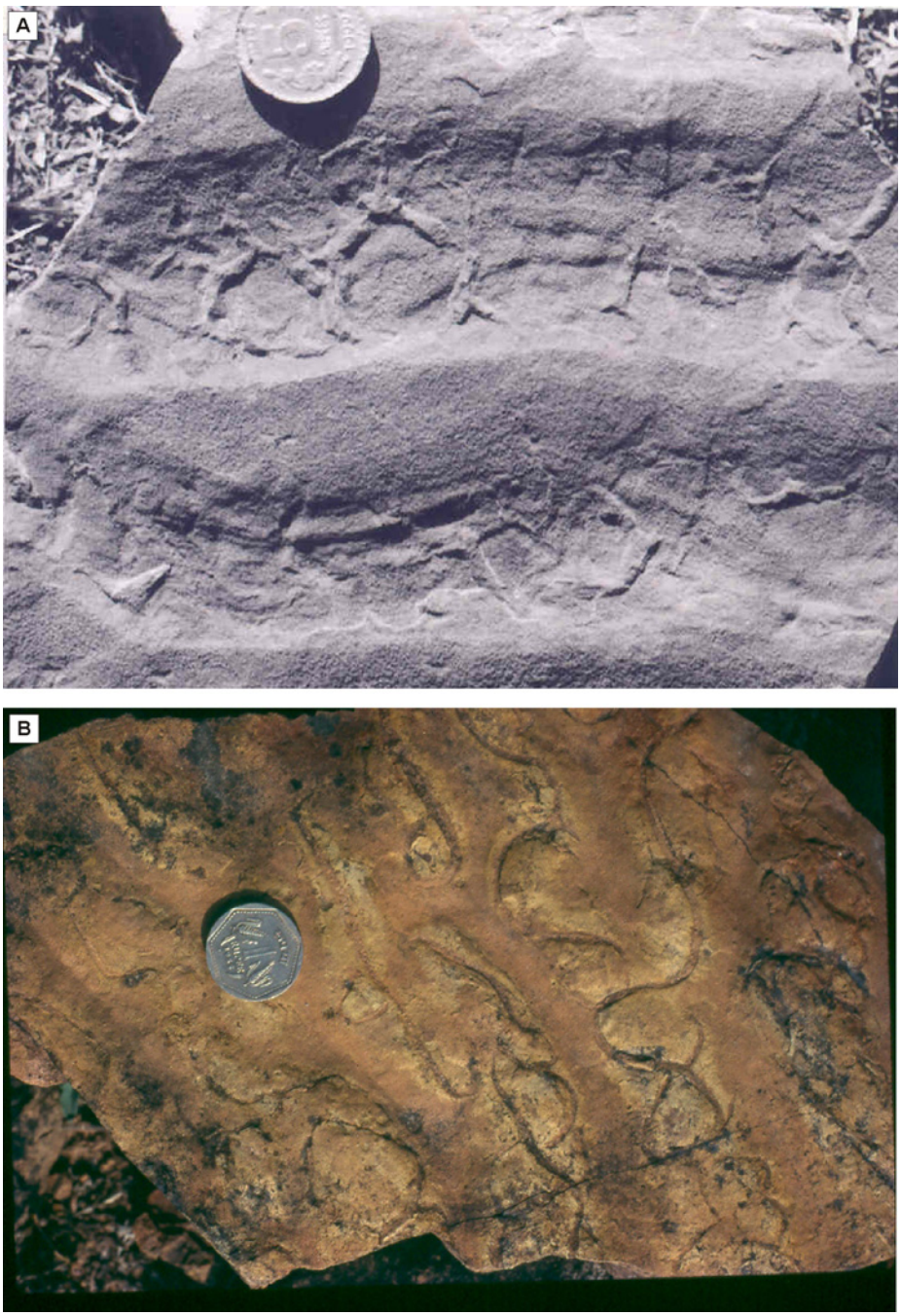


Figure 4(c)-13: '*Manchuriophycus*' oddities.
(A) Reticulate pattern of ridges, reflecting petee-type crack fills, where the primary cracks formed in the troughs between slightly sinuous ripples within sandstone. An origin similar to '*Manchuriophycus*' may thus be assumed, with thicker mat within ripple troughs cracking, but instead of the sinuous patterns typical of '*Manchuriophycus*', a reticulate assemblage of short, straight cracks formed, later filled from below by liquefied sand to form petee-type ridges. Locality: Chorhat Sandstone Member (Kheinjua Formation, Semri Group) (ca. 1600 Ma), Vindhyan Supergroup, central India, at Chopan; palaeoenvironment: intertidal setting. (B) Top surface of a rippled sandstone bed, with sinuous cracks developed only on ripple crests. Note that ripples form complex bifurcating patterns; also note the very well-developed sinuous crack which follows one such ripple crest subdivision in the top right part of the photograph. This pattern is effectively the opposite of that shown in Figure 4(c)-11 and can be described as an 'inverse *Manchuriophycus* feature'. Locality: Chorhat Sandstone Member (Kheinjua Formation, Semri Group) (ca. 1600 Ma), Vindhyan Supergroup, central India, at Amjhore; palaeoenvironment: intertidal setting. Both photos: S. Banerjee.

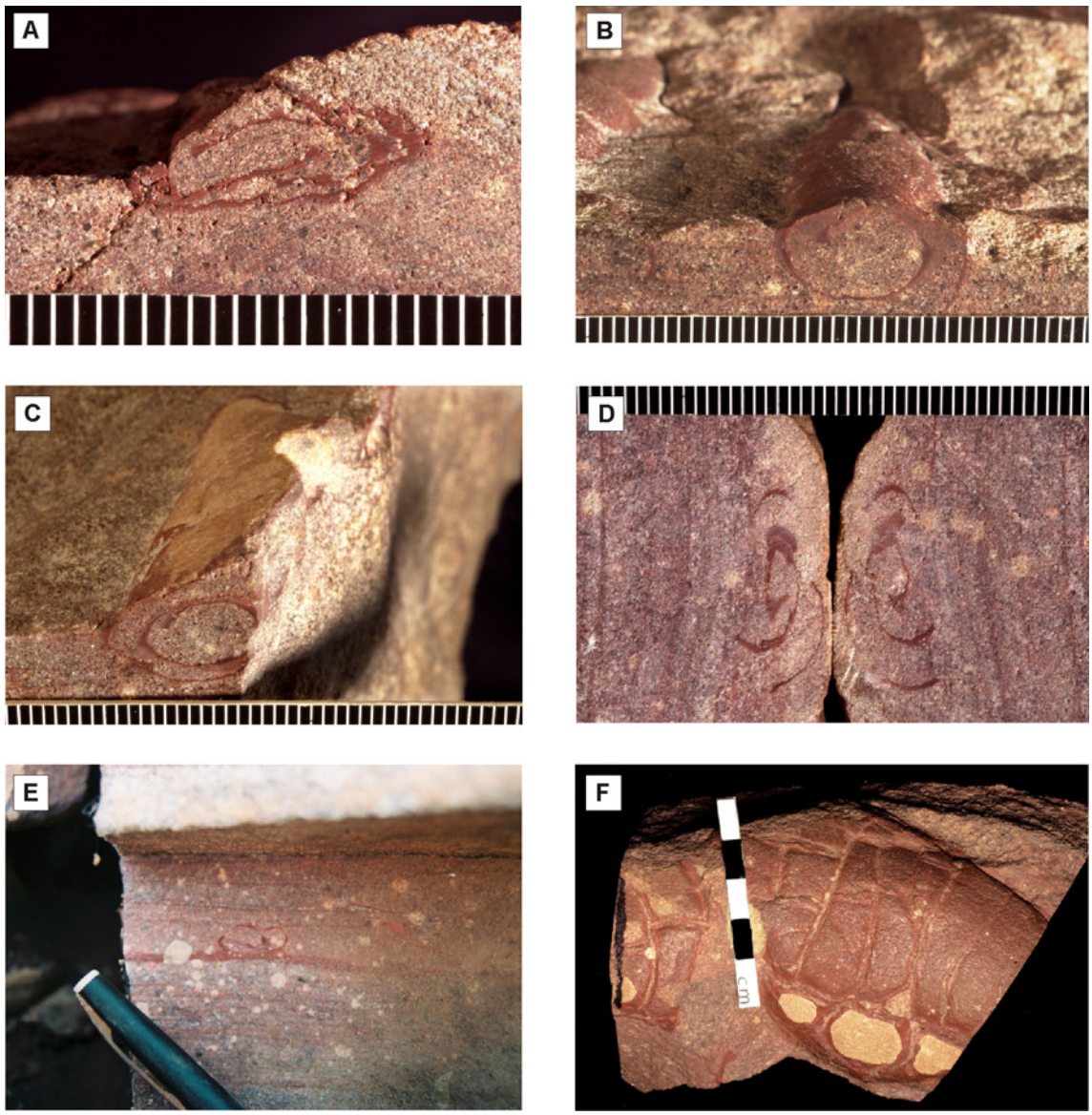


Figure 4(c)-14: Rolled-up mat fragments.
Various 'roll-up' structures from sandstones from a playa lake lens within predominant aeolian sandstones of the Makgabeng Formation (ca. 2.0–1.8 Ga), Makgabeng Plateau, Limpopo Province, South Africa. In all cases the roll-ups consist of strongly ferruginous mudrock, rolled up within thinly bedded (upper flow regime), flash-flood reworked playa and/or aeolian fine-grained sands. The individual roll-ups occur either within a part of or within the full thickness of a single such upper flow regime plane bed. (A) Slightly flattened concentric roll-up, shown in cross-section – roll-up extends several centimetres into the rock, having thus a cigar-like overall geometry. Millimetric scale. (B) Unflattened concentric roll-up, illustrating three-dimensional cigar-like geometry; almost two full concentric circles are preserved in the roll-up. Millimetric scale. (C) Unflattened concentric roll-up, with elongated cigar-like geometry and more than two full concentric revolutions preserved; right edge of roll-up partly destroyed in sampling. Millimetric scale. (D) Section sliced through a cigar-like roll-up, showing mirror-image geometry; note almost three complete concentric circles. Millimetric scale. (E) Two roll-ups, with opposite sense of rotation, forming a scroll-like feature. Note that the large light coloured spots within the sandstone are reduction spots, not coarse-grained sand particles. (F) Close-up detail of outer wall of a ferruginous rolled-up mat fragment. Note cracks in the mudrock forming the preserved roll-up, analogous to mud cracks. Under the microscope, such cracks have a typical V-shaped sectional geometry, and are filled with secondary, fine sand grains. The mud was thus able to form the roll-ups due to an inferred microbial mat providing cohesion for several concentric rotations to form a 'cigar', and then, upon desiccation (of inferred mat and mud), the rolled-up mud dried and cracked. Centimetric scale. All photos: A.J. Bumby; material collected in field by A.J. Bumby, I. Tonzetic and P.G. Eriksson.

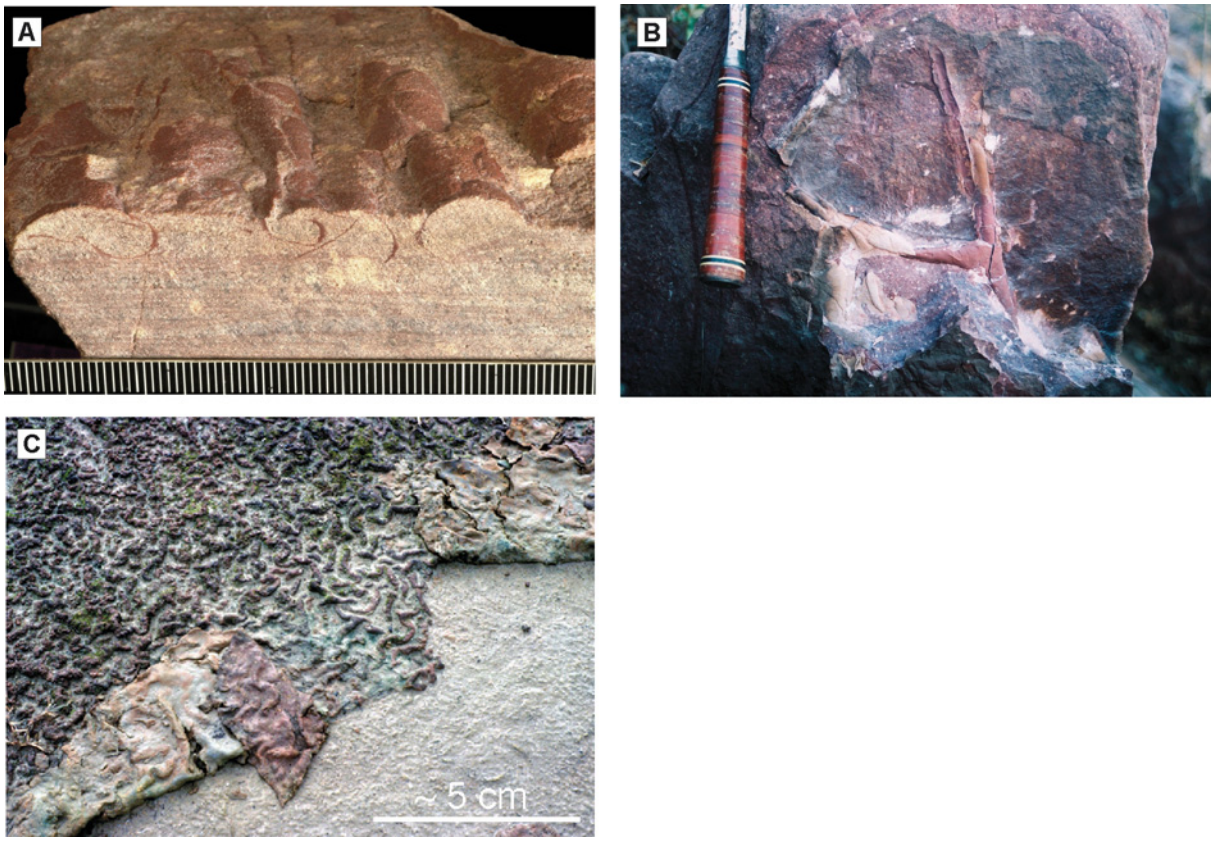


Figure 4(c)-15: Rolled-up mat fragments and flipped-over mat fragments.
(A) Large cut sandstone slab showing several preserved rolled-up mat fragments (comprised of ferruginous mudrock), each with cigar-like three-dimensional geometry; note parallel orientation of long axes of 'cigars', possibly due to high energy flash-flood fluvial current action. Millimetric scale. Locality: Makgabeng Formation (ca. 2.0–1.8 Ga), Makgabeng Plateau, Limpopo Province, South Africa; palaeoenvironment: playa lake lens within predominant aeolian sandstones, all subject to flash-flood reworking. (B) Upper surface of sandstone bed containing several large, linked rolled-up and flipped-over mat fragments. These suggest localised physical destruction of a microbial mat and formation of flip-over and roll-up features without complete detachment of the mat from its sandy substrate. Locality and palaeoenvironment: as for (A). Photos (A) and (B): A.J. Bumby. (C) Modern, wrinkled microbial mat, developed on loose quartz sand, showing segment of mat flipped over by wind when the area was flooded during a rainstorm, and subsequently dried up. Location: transient excavation, Ottawa, Canada. Photo: J.A. Donaldson.

ponds tend to develop cracks with 'curled margins'. Preservation of thin shrunken mat layers from erosion by the next sedimentary event may be explained by incomplete shrinkage and a high degree of attachment (adhesion) to the substrate below.

Curled crack margins:* *Figure 4(c)-5

Name of structure: Curled crack margins (new term additional to Schieber, 2004 classification).

Other terms used: none.

Description of structure: Mat surface (modern) with shrinkage cracks, in which crack margins show curling. The latter encompasses various stages of crack margin evolution, from slightly upturned margins (straight or curved in themselves, seen from above), to complex forms surrounding subcircular openings in the mat surface; old curled margins may become partly or, locally, even fully overgrown by a new mat layer. In ancient preserved examples, irregular subcircular or linear ridges occur which are distinctly flattened, and may be inferred to reflect the curled margins of a subcircular opening in a thin microbial mat that previously covered a sandy sediment surface, or a narrow linear crack with curling edges, respectively. May occur in biolaminites.



Figure 4(c)-16: Microbial mat chips.
Upper surface of sandstone bed containing numerous smaller to larger mat fragments and mat chips. Note that some of these have curled up to form roll-ups, while others are curved microbial mat chips. Some of the larger fragments have cracked surfaces; presumably, these became desiccated and cracked after becoming fragmented from a primary mat. All these mat destruction features consist of iron-pigmented mudrocks. Lens-cap for scale. Locality: Makgabeng Formation, Waterberg Group (ca. 2.0–1.8 Ga), Makgabeng Plateau, Limpopo Province, South Africa; palaeoenvironment: flash-flood deposited sandstones which reworked interdune-playa lacustrine deposits within an overall palaeodesert setting. Photo: A.J. Bumby.

Associated sedimentary structures: (1) small current ripples (2 cm wavelength, 3 to 5 mm amplitude) within organo-sedimentary layers; small-scale current, oscillation and interference ripples; wave and current ripple laminations; (2) interbedding of microbial mat layers and event layers of few millimetre-scale; horizons of gypsum; (3) millimetre- to centimetre-scale alternation of sedimentary sandstone event layers of storm or fluvial origin, and organo-sedimentary laminated layers of siltstone and sericitic argillite; (4) desiccation cracks; (5) burrows (mainly by gastropods); (6) small-scale load structures; (7) small tidal channels; (8) mud clasts; (9) wavy and lenticular bedding.

Environment: Upper intertidal to lower supratidal zones of tidal flat/coastal plain. Preconcentration basin of salterns. Intertidal to supratidal shallow back-barrier setting, with small tidal channels and few high energy storm deposits.

Ideas on genesis: The structures form subaerially in a thin mat that undergoes shrinkage and cracking. Initial linear or triradiate cracks may evolve into irregular to subcircular openings with progressive curling of the crack margins. If the sediment-rich lower part of the mat remains attached to the curling margin, sediment may be entangled in the involute structure. Overgrowth of the curled margins by new mat layers leads to their preservation.

Overgrown, upturned crack margins:* *Figure 4(c)-6

Name of structure: Overgrown upturned crack margin (new term additional to Schieber, 2004 classification).

Other terms used: ‘pillow-like bulges at crack margins’ (Noffke et al., 2003a). They are sometimes confused with petees.

Description of structure: The polygonal network of shrinkage cracks (in other examples, cracks are curved to sinuous) within a modern biolaminite will be marked by upturned, overturned and partly overfolded polygon edges; in the crack openings, a new thin mat forms, partly overgrowing the polygon edges. The cracks may also be partly filled by sediment before mat overgrowth occurs. In ancient examples antiformal, inverted-V shaped structures occur parallel to and along both margins of shrinkage cracks in preserved biolaminites; in other cases, upturned crack margins are preserved within polygonal crack networks. In cross-sections of ancient examples, a vertical (subvertical) attitude of the upturned margins is seen; these can become totally overgrown by further biolaminite deposits.

Associated sedimentary structures: (1) heterolithic succession of interlaminated (sericitic) siltstone/fine-grained sandstone and argillite; (2) storm event sandstone layers, 8–15 cm thick; (3) desiccation cracks; (4) mud chips and mat chips; (5) shallow tidal channels; (6) burrows, mainly by gastropods, in modern examples; (7) wavy and lenticular bedding/lamination; (8) small-scale oscillation and interference ripples.

Environment: Intertidal zone of a peritidal coastal plain, regularly flooded during high tide. Intertidal to supratidal shallow back-barrier setting, with small tidal channels and few high energy storm deposits.

Ideas on genesis: The structure occurs in the upper 2–3 cm of a biolaminite covered by an active microbial mat that underwent subaerial shrinkage. As a result, wide cracks with upturned margins develop, partly involving the underlying biolaminite. Cyclic, tidally controlled processes of mat growth and overgrowth, alternating with progressive upturning of crack margins, form the structure.

Ripple-top sand cracks: Figure 4(c)-4B

Name of structure: ripple-top sand cracks.

Other terms used: sand cracks, cracked ripple crests (see Figure 4(a)-15 in this chapter).

Description of structure: these are negative sand crack features that show variable degrees of association with wave ripple crests. Essentially parallel, elongated cracks (with wide bases and steep, slightly curved sides), parallel and mostly coincident with the crests of straight to slightly sinuous wave- and wind-formed ripples; shorter cracks link the elongated features across ripple troughs; both cracks and ripple crests tend to bifurcate.

Associated sedimentary structures: (1) wave, oscillation, current and wind ripples; (2) sand cracks; (3) '*Manchuriophycus*'; (4) tidal channels; (5) petee ridges; (6) wrinkle structures.

Environment: Braid-deltaic – tidally controlled epeiric marine coastline.

Ideas on genesis: Shrinkage of a desiccating mat draped over rippled sands is inferred; tensile stress was maximised across ripple crests, leading to a preferential crack occurrence there.

Filled sand cracks: Figure 4(c)-7

Name of structure: filled sand cracks.

Other terms used: petees/petee ridges, sand cracks.

Description of structure: These structures resemble the sand cracks discussed above, in all their variability, but instead of being negative features, they are in the form of positive ridges. They are differentiated from petees (petee ridges) by a noticeable difference in sandstone composition/type between the crack-fill (= ridge) and that in the bed within which the cracks formed; also, unlike petees, there is no observable deformation of the upper few sandstone laminae within the cracked bed. Some flattening of these sandstone ridges can be observed.

Associated sedimentary structures: sand cracks.

Environment: Braid-deltaic – tidally controlled epeiric marine coastline; intertidal settings generally.

Ideas on genesis: Based on the description above, these features are interpreted as reflecting filling of cracks within microbial mats growing/desiccating on a sandy surface from above, by other sands brought in either by

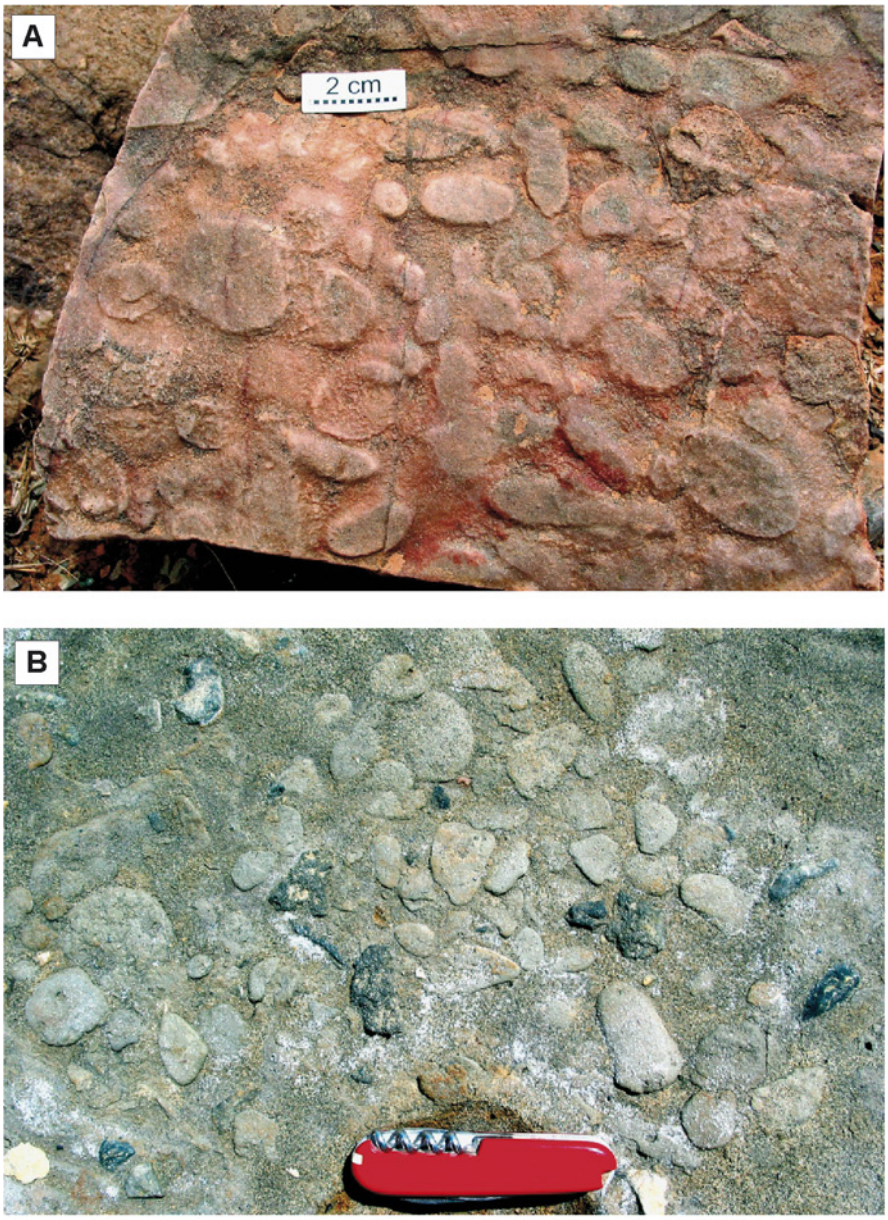

A
2 cm
B
C

Figure 4(c)-17: Microbial sand chips.
(A) Upper surface of fine-grained sandstone layer, about 5 cm thick, showing rounded and elongate, flat sand clasts. Size of clasts varies between 1 and 2 cm (long axis); thickness is less than 2 mm. Clasts are slightly oriented and some of them overlap. Locality: Morocco, Anti-Atlas, Agoummy area; Neoproterozoic Wanimzi Formation, Tizi n-Taghatine Group; palaeoenvironment: intertidal zone of a peritidal coastal plain. (B) Modern sandy–pebbly sediment surface with subrounded to rounded microbial sand chips. The chips consist of black organic material with enclosed fine-grained sand- to silt-sized grains, vary in size between 1 and 2 cm (long axis), are up to 3 mm thick, and partly show overlapping relationships. Surrounding sediment is biostabilised. Scale (knife): 8 cm. Locality: Salins du Midi, Réserve Nationale Camargue, Southern France; environment: shoreline of preconcentration basin of 'Salins du Midi' saltern. (C) Sand chips with obvious deformation, indicating flexible binding between sand grains. Extracellular polymeric substances and microbial filaments presumably provided the cohesion needed to produce the chips from granular sand. Locality: 0.6 Ga Lower Bhander Sandstone, Vindhyan Supergroup, central India; palaeoenvironment: coastal playa. Photos (A) and (B): H. Porada and E. Bouougri; photo (C): S. Sarkar.

---

aqueous currents or aeolian action. If the mat then decays or is eroded away, these crack-fills will remain behind as positive ridges, with the same plan-form geometry as the original microbial shrinkage cracks. Alternatively, the mats, with their sandy crack-fills may become buried beneath later sediments, and then the mat will, in time, decay and disappear and the crack-fill ridges will become flattened beneath the weight of overlying beds, which is commonly seen in ancient examples, including some of those shown here. It is distinctly possible that crack-fill and immediately overlying sandstone bed will have the same composition, reflecting a single sedimentation event, laid down on top of the original, cracked mat. This would appear to be relatively common.

Petees/petee ridges: Figures 4(c)-8 to -10

Name of structure: petees or petee ridges.

Other terms used: sinuous antiformal ridges.

Description of structure: Normally in the form of large numbers of ridges, which display polygonal, reticulate-polygonal and sinuous patterns in plan-view; spindle-shaped ridges are also common, and elongated, parallel forms occur also. Local flattening of ridges is seen quite often, and the more polygonal patterns commonly have multiple orders of ridges, up to three orders being recorded in some instances. Petees/petee ridges *sensu stricto* should be associated with concave-upward segments between the ridges, when seen in cut cross-sections of occurrences, as well as being associated with soft sediment deformation of thin planar beds underlying the mat/petee surface; in addition, the sand/sandstone making up the petee ridges should be the same material as that comprising the bed immediately beneath the mat/previous mat. If these features (last sentence) are not observed, it is likely that the observed structures are 'filled sand cracks' (above) and not proper petees.

Associated sedimentary structures: (1) tidal channel-fills; (2) oscillation, current, wave and aeolian ripples (petees may also occur on ripples); (3) sand cracks; (4) '*Manchuriophycus*'; (5) destructive wrinkle marks.

Environment: Braid-deltaic – tidally controlled epeiric marine coastline; intertidal settings generally. Less common in supratidal settings; few examples known from the lower shoreface setting.

Ideas on genesis: The evidence for soft sediment deformation and for the source of petee ridge sand in the bed immediately underlying the mat supports either a synaeresis-like origin (due to overlying beds' pressure causing post-burial movement of sand into cracks in the mat) for these features, or that the liquefied sand moved laterally into the cracks within the microbial mat from beneath, under pressure from overstanding water or even (spring) tidal oscillation. In all cases, inferred crack-filling is from the unconsolidated sand bed *beneath* the mat. In the case of the few shoreface examples of petees, a synaeresis-style origin would appear to be the most logical. Some dense networks of petees appear to be bunched up against each other, suggesting that the mat allowing ridge formation was also subject to (partial) detachment and wrinkling (see Figure 4(c)-9). Petees may also form under mat growth conditions, as well as due to mat destruction. In the former case, updoming and even rupturing of the mat due to wind, current action and gas development will allow petee ridge formation; their genesis during mat destruction is related to a high level of mat-cracking and desiccation and forms the latter part of a genetic continuum of petee origins.

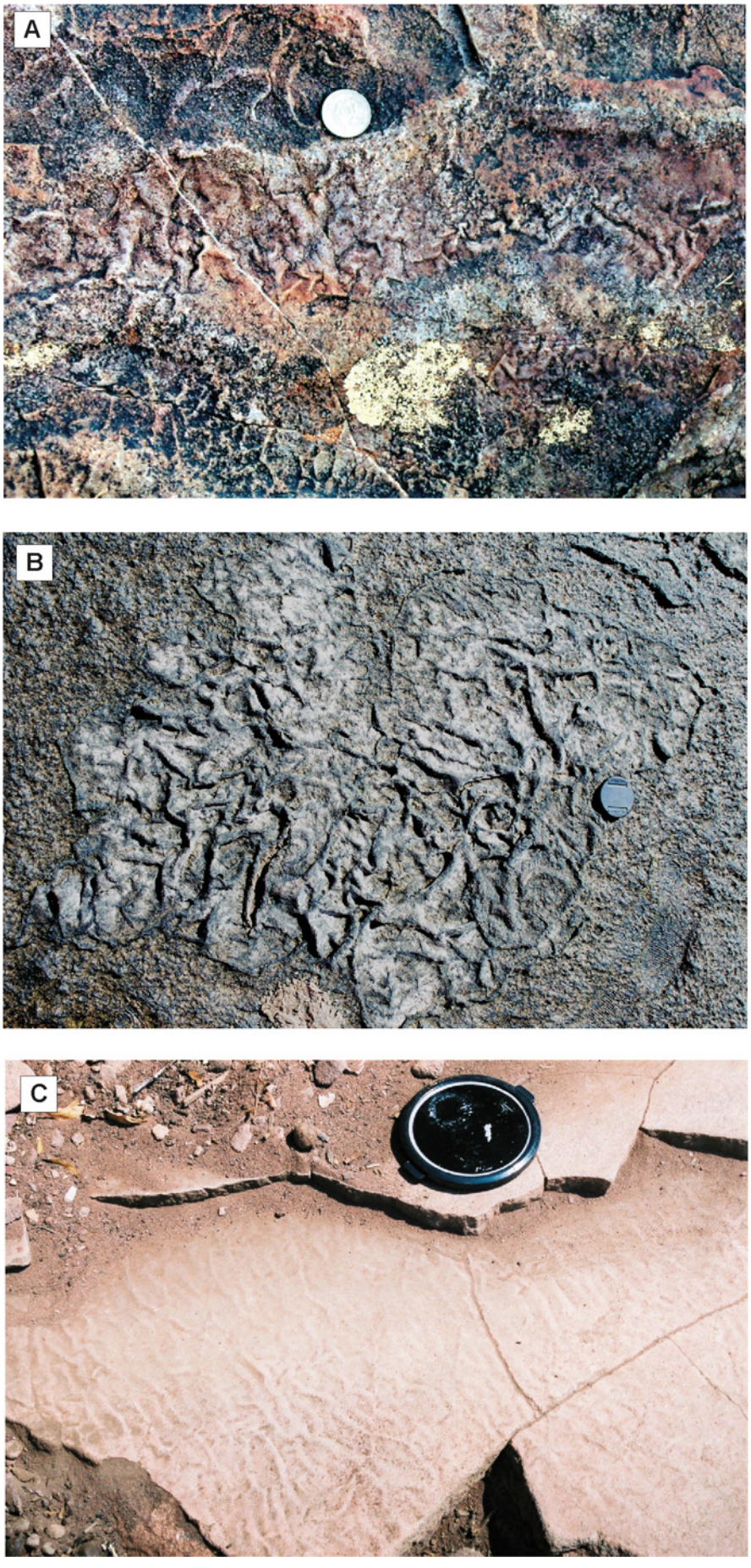

A
B
C

Figure 4(c)-18: Wrinkle structures (destructive).
Upper sandstone bedding surface with centimetre-sized, sinuous to curved, irregular, round to sharp-crested bulges (wrinkles). The deformation is restricted to a thin sandy layer. The underlying, undeformed sandstone layer exhibits a reticulate pattern of 'elephant skin' (see Figures 4(a)-5, -6, -7) type (lower left part of the photo), developed on a surface from which the mat has apparently been removed by tractional forces. Scale (coin): 24 mm. Locality: Morocco, Anti-Atlas, Tirsal area; Neoproterozoic Wanimzi Formation, Tizi n-Taghatine Group; palaeoenvironment: intertidal zone of a peritidal coastal plain. (B) Detached and previously floating mat fragment which has come to rest on sandy bed; note irregular, round to sharp-crested bulges (wrinkle structures), induced by successive tractional events affecting a thin, loosely attached microbial mat. The mat fragment underwent local cracking after a new mat had formed on the exposed sandy surrounding surface. Locality: Mediterranean coast of southern Tunisia, between Gabes and Skhirat; environment: upper intertidal zone surrounding a wide tidal channel plain. (C) Inferred wrinkle marks developed on a sandstone bed upper surface, presumably due to shortening of partially loose mat under the influence of a current. Found associated spatially and temporally with many mat destruction features such as flip-overs, roll-ups, and sand cracks. Note approximately parallel orientation of wrinkles in upper right part of photograph, contrasting with irregular patterns in lower foreground – these suggest the possibility that shortening of a loose mat was greater in the latter part of the sand bed upper surface. This photo illustrates the inherent problems associated with a continuum of wrinkle structures developed within both mat-growth and mat-destruction frameworks (see discussion in Chapter 6(a)). Locality: Makgabeng Formation, Waterberg Group (ca. 2.0–1.8 Ga), Makgabeng Plateau, Limpopo Province, South Africa; palaeoenvironment: flash-flood reworked interdune-playa lake lenticular deposit contained within aeolianites. Photos (A) and (B): H. Porada and E. Bouougri; photo (C): A.J. Bumby.

'Manchuriophycus': Figures 4(c)-11 to -13

Name of structure: '*Manchuriophycus*'.

Other terms used: '*Rhysonetron*' (Hofmann, 1967, 1971; see also Häntzschel's "Treatise on Invertebrate Paleontology, Part W", 1975). Essentially a specific type of microbial shrinkage crack; sand cracks (ancient examples).

Description of structure: Within the upper, rippled (or interference rippled) surface of sandstone beds, within the ripple troughs, complex crack patterns with curved, circular, spiral, triradiate or even figure-8 forms occur, and may follow the edges of these troughs. In other examples, more lenticular or spindle shaped cracks occur, with triradiate intersections thereof; all '*Manchuriophycus*' cracks can also be preserved on the sole of overlying beds.

Unusual forms: in a few cases, a more reticulate crack pattern is observed, marked by petee ridge-like, positive features, and one case, illustrated here (Figure 4(c)-13), is known where typical '*Manchuriophycus*'-type cracks occur preferentially on the preserved sandy ripple *crests* instead of in the troughs. Both these unusual forms occur within the ca. 1.6 Ga Vindhyan Supergroup, India.

Associated sedimentary structures: (1) wavy and lenticular bedding; (2) wave and current ripple laminations; (3) small-scale current, oscillation, wave, wind and interference ripples; (4) lenticular fluvial and/or tidal channels; (5) desiccation cracks; (6) mud clasts; (7) desiccation warts and adhesion warts; (8) heterolithic deposits with centimetre-scale interbedded sandstone and organo-sedimentary sericitic layers; (9) event deposits related to fluvial sheet floods or storms.

Environment: Coastal plains of lacustrine or shallow marine (including epeiric) environments, fringing alluvial braid-delta systems; may also be associated with significant tidal action within such settings; intertidal to lower supratidal zones of a peritidal coastal plain.

Ideas on genesis: Shrinkage (sand) cracks within rippled sandstone, confined to ripple troughs, may form if microbial mats selectively grow, or attain a greater thickness in ripple troughs, where eroded cyanobacteria settle from currents, and where supply of water is greatest and more long-lasting. Possibly, in a few cases, once cracks have occurred within a trough-located mat, petee ridges could occur. The one noted occurrence of 'inverse-*Manchuriophycus*', situated on ripple crests, may reflect a very thick mat cover within which optimal desiccation conditions for crack formation happened to occur above ripple crests rather than the deeper-lying ripple troughs.

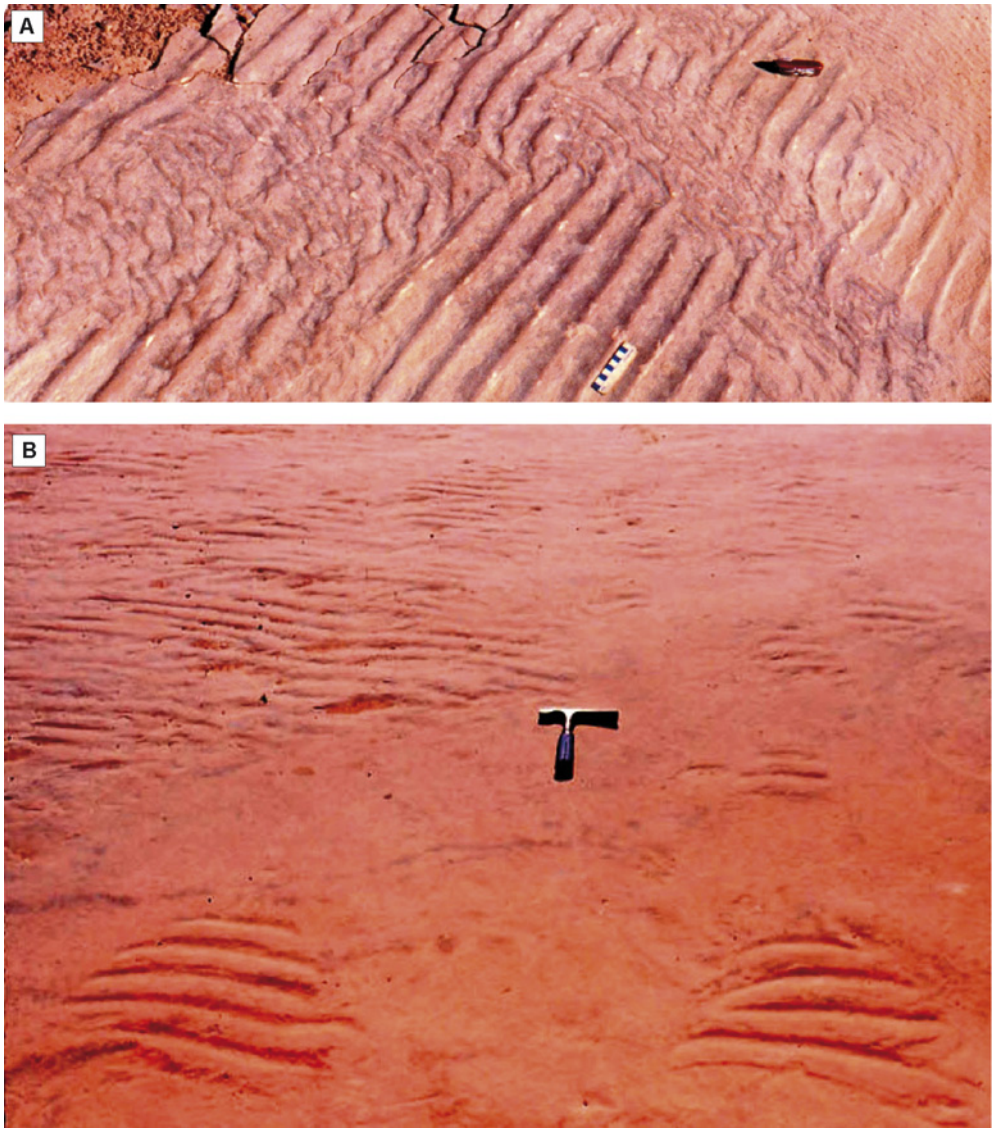


Figure 4(c)-19: Ripple patches.
(A) A first generation of ripples on a sandstone bed has been reworked only in certain places by a second generation of ripples, but is perfectly retained where it was presumably protected by a microbial mat cover. (B) Ripples preserved only in patches, where an inferred microbial mat providing the necessary protection from erosion had been removed locally. Note gradational contacts between ripple patches and surrounding smooth sandstone. Locality: 0.6 Ga Sonia Sandstone, Jodhpur Group, Rajasthan, India; palaeoenvironment: intertidal–supratidal zone. Photos: S. Sarkar.

Flipped-over (mat) edges, and rolled-up mat fragments (cf. 'jelly-rolls', 'roll-ups'): Figures 4(c)-14 and -15

Name of structure: Flipped-over mat edges; rolled-up mat fragments.

Other terms used: 'flip-overs'; 'roll-ups' or 'jelly-rolls'.

Description of structure: Flipped-over mat edges are relatively small to larger (centimetres to >10 cm in longest dimensions) portions of the edge of a mat that are inverted locally, due to current action (water, possibly occasionally, wind). They are very easy to identify in modern examples, but may be more difficult to define in ancient examples where compression has occurred. Rolled-up mat fragments, in contrast, are easy to discriminate at all ages; in longest dimension they are up to several tens of centimetres. Their modern versions are literally portions of a mat (either broken-off fragments or mat edges) that have begun to desiccate and whose edges have begun to curl up. This initial stage in the process can be greatly enhanced by current action (again water rather than wind), which

commonly results in several full revolutions of rolling-up – 720° are commonly observed in ancient examples. In cross-section, roll-ups resemble jelly-rolls or the rolled up tobacco leaves in a cigar, and in longitudinal view, the resemblance to a cigar is more apparent. Current reworking often results in a parallel orientation of several elongated roll-ups, and in certain cases mat fragments of all sizes and shapes (including mat chips) can be bunched up with several rolled-up fragments. In ancient examples the sandy sediment from immediately beneath the mat, or even muddy sediment trapped by the surface of the mat, becomes rolled up as well, and it is this sediment that is preserved to mark these structures.

Associated sedimentary structures: (1) current, wind, combined-flow and wave ripples; (2) suspension deposits; (3) upper flow regime plane bed deposits; (4) aeolian dune deposits and their structures, with evaporite pseudomorphs; also evaporate casts; (5) structures indicative of efflorescent salt crusts; (6) mud cracks.

Environment: Palaeodesert saline pan deposits and interdune deposits (including flash-flood reworking thereof). Also form due to currents in marine coastal settings.

Ideas on genesis: Microbial mats provide enough cohesion to sandy sediments immediately underlying the mats to form either flipped-over or rolled-up sediment-bearing mat fragments. Most of the inversion and rolling implicit in the formation of these features can be ascribed to sedimentary reworking by relatively strong, directed currents, generally due to water rather than wind, as supported also by the common parallel alignment of elongated fragments and roll-ups noted in many occurrences. It is likely that some initial curling is due to desiccation, to be followed by greater rolling-up through current action.

Microbial sand chips and mat chips: Figures 4(c)-16 and -17

Name of structure: Microbial sand chips; microbial mat chips.

Other terms used: Microbial sand clasts; spheroidal pliable sand clasts, also known as ‘algal balls’, ‘sand balls’, or ‘sand ooids’ (see Figures 4(a)-1 and -2).

Description of structure: Microbial sand chips (see also Figure 4(a)-3) reflect a feature which is analogous to ‘flip-overs’ and ‘roll-ups’ (e.g., Schieber, 2004), but were subject to longer sedimentary reworking, transport and abrasion. They are smaller than the previous class of feature, and generally comprise rounded, plastically deformed, often current-aligned sand clasts (shapes vary from rounded to elongated to partially flattened); they may even locally be imbricated. Mat chips reflect strongly desiccated mat-bound sandy sediment surfaces that form rigid and curved clasts, several centimetres in their longest dimensions; they are not as rounded as roll-ups and resemble dried-up mudclasts formed when a thin mud layer desiccates and breaks up. The well-known example described by Pflüger and Gresse (1996), from the ca. 2.7 Ga Ventersdorp Supergroup of South Africa, consists of formerly microbially-bound fine-grained volcanic ash; although this specific example is often described in literature as microbial sand chips, they are in reality mat chips (e.g., Donaldson et al., 2002a; their Figure 2(a)) in the Schieber (2004) terminology system used in this book (see Chapter 3).

Associated sedimentary structures: (1) heterolithic deposits with centimetre-scale interbedded sandstone and organo-sedimentary laminated layers; (2) a few event layers related to storms; (3) few small fluvial/tidal channels; (4) wave ripple-formed cross-lamination; (5) oscillation, interference, current and wind ripples; (6) desiccation cracks; (7) load structures; (8) erosional pockets; (9) suspension deposits; (10) upper flow regime plane bed deposits; (11) aeolian dune deposits and their structures, with evaporite pseudomorphs; also evaporate casts; (12) structures indicative of efflorescent salt crusts; (13) mud cracks.

Environment: Intertidal zone of a peritidal coastal plain; along shoreline of preconcentration basins of salterns; interdune and saline playa environments within a palaeodesert; playa lakes within a semi-arid volcanic-sedimentary setting.

Ideas on genesis: Physical erosion of a thin, microbially-bound sand layer and reworking of fragments by relatively high energy wave, current or even wind action. Can also be related to mat growth conditions (Figures 4(a)-1 to -3).

Wrinkle structures (destructive): Figure 4(c)-18

Name of structure: Wrinkle structures (related to mat destruction).

Other terms used: Wrinkle structures (Hagadorn and Bottjer, 1997, 1999) can be confusing (see also Chapter 6(a)), as these features are also associated with mat growth as easily as with mat destruction; as with many of the microbial mat-related structures (e.g., also sand chips, above), there is a continuum of these features, from mat growth to mat destruction associations. The reader is thus referred here also to Sections 4(a) and 4(f) in this chapter. H. Porada and E. Bouougri (personal comm., 2006) suggest the term 'warped mat' for mat destruction-related examples.

Description of structure: Upper bedding surface with millimetre- to, more commonly, centimetre-sized, sinuous to curved, irregular, round to sharp-crested bulges. The deformation is restricted to a thin sandy layer. The underlying, undeformed layer may exhibit a reticulate pattern of 'elephant skin' (see also 'old elephant skin', Figures 4(a)-5 to -7) type developed on a surface from which the mat has been removed by tractional forces. In more extreme cases of mat destruction, detached and floating mat fragments may result, with irregular, round to sharp-crested bulges, induced by successive tractional events affecting a thin, loosely attached microbial mat. Such mat fragments can undergo local cracking after a new mat forms on the exposed surface surrounding it.

Associated sedimentary structures: (1) heterolithic deposits with centimetre-scale interbedded sandstone and organo-sedimentary sericitic layers; (2) event deposits related to fluvial sheet floods or storms; (3) few small fluvial/tidal channels; (4) wave ripple-formed cross-lamination; (5) oscillation, interference and current ripples; (6) desiccation cracks; (7) mud clasts; (8) mat chips; (9) possible examples associated with palaeodesert saline pans and interdune settings with *their* typical associations of sedimentary structures.

Environment: Intertidal zone of a peritidal coastal plain; upper intertidal zone surrounding a wide tidal channel plain. Uncommonly from palaeodesert pan-interdune settings.

Ideas on genesis: Structure reflecting deformation by wind or current action of a detached or loosely attached, flexible, thin mat. In more extreme cases of mat destruction, mat fragments originate from a floating or loosely attached mat that has been broken up into pieces by wind/water traction. These fragments may be deformed by wind traction, when floating on water uprising from below or originating from tidal incursion.

Ripple patches (and patchy reworking of ripples; palimpsest ripples): Figure 4(c)-19

Name of structure: Ripple patches.

Other terms used: Patchy ripples; related terms are patchy reworking of ripples, and palimpsest ripples (see also Figures 4(a)-3, -13, -14).

Description of structure: Ripple patches are relatively smooth bedding planes within which localised patches exhibit various possible kinds of ripples, generally of an aqueous rather than an aeolian origin. For positive identification, it is important that there be a *smooth transition* from the ripple patches to the surrounding bedding planes (e.g., Schieber, 1998a). Related features would be ripple fields (also generally aqueous rather than aeolian in origin) with localised patches of reworked ripples. Palimpsest ripples reflect inherited features such as ripples which are still visible beneath later structures such as other ripples.

Associated sedimentary structures: (1) a wide range of inferred mat-related features: petees, sand cracks, 'elephant skin', wrinkle structures and '*Manchuriophycus*'; (2) current, wave, oscillation and minor aeolian ripples; (3) relatively small fluvial and tidal drainage channels; (4) planar bedding.

Environment: Epeiric marine to open-coastline tidally-influenced marine settings.

Ideas on genesis: Ripple patches develop when a smooth sandy bed surface covered by a microbial mat is subject to local erosion under relatively high energy (probably tractional) conditions; the exposed sandy patches resulting from this may then form ripples from the active currents, waves, tides, etc. causing the erosion. The smooth transition from ripple patch to surrounding smooth bed surface demonstrates the contemporaneity of the ripple patches and the sand-based mat. Patchy reworking of existing ripple fields is analogous: in this case where a mat covering rippled sands is removed locally by erosion, reworking will occur. In palimpsest ripples, a mat covering an existing rippled sandy bed allows partial preservation of the older structures when a new ripple field develops on top.

Non-penetrative micro-faults

Name of structure: Non-penetrative micro-faults.

Other terms used: Concentric micro-faults, micro-faults.

Description of structure: Occur as micro-faults restricted to a single sand(stone) bed. On flat upper surface of sand bed, examples are known which show concentric microfaults, with millimetric vertical displacement along the curved faults. Downthrows at individual faults accumulate towards the centre of the structure.

Associated sedimentary structures: (1) heterolithic succession of siltstone and argillite; (2) wavy and lenticular bedding; (3) thin storm deposits (fine-grained to medium-grained sandstone); (4) sand cracks, petees, and mat chips; (5) horizons of dolomite and anhydrite.

Environment: Intertidal zone fringed by sabkha.

Ideas on genesis: Cohesion of relatively thin sand bed underlying microbial mat can be retained for some time after burial, and compaction may then result in non-penetrative micro-faults restricted to that bed. Curved concentric micro-faults may reflect differential compaction; the elliptic shape of the structure suggests deposition of an event bed on an irregular microbial mat surface with elongate domes that resisted erosion.

4(d). MAT-DECAY FEATURES

S.Q. Dornbos, N. Noffke, J.W. Hagadorn

Introduction

Destructive features created by physical processes, such as mat chips, shrinkage cracks, and rolled up mat fragments, are the focus of Section 4(c). The suite of structures in this section is hypothesised to result from the decay of organic material, often mat-derived, buried underneath mat surfaces. Of particular interest are features resulting from the escape of gases or fluids produced by decay of buried organic matter beneath cohesive biofilms. These structures include:

(1) Radial gas or fluid escape structures, sometimes called '*Astropolithon*';
(2) Gas or fluid escape structures without radial forms.

The descriptions and discussions presented below rely also to a large extent on a set of critical references: Dawson (1878); Draganits and Noffke (2004); Gerdes et al. (2000a); Noffke et al. (1996, 1997a, 1997b, 2001a, 2001b, 2003b); Pickerill and Harris (1979).

Definition and genesis of mat-decay features

The decay releases gases or fluids that escaped through the upper mat surface, creating distinctive structures termed 'gas domes' (see also Chapter 6(c)). Some of these structures have radial morphologies and were first described as animal trace fossils and named *Astropolithon hindii* (Dawson, 1878). '*Astropolithon*' was considered a Cambrian index trace fossil, but was later reinterpreted as an escape structure (Pickerill and Harris, 1979) (Figure 4(d)-1). Other gas or fluid escape structures lack the radial morphology of '*Astropolithon*' and consist of conical mounds that are roughly circular in shape (Figures 4(d)-2, -3).

The structures discussed and figured here should not be confused with the structures commonly termed 'sand volcanoes', which are purely physically-formed structures that occur commonly in impure sands along the high water line of the lower supratidal zone. They are temporary in nature, and only form during the rising flood. These sand volcanoes form from gas pressure that is pushed upward by tidal flood water in the sediment. This gas has the same composition as the atmosphere. In contrast, 'gas domes' are thought to form in the presence of microbial mats when decaying microbial mat mass underneath the topmost microbial mat generates upward-rising gas pressure. These gases are typically richer in methane, CO_2, CO, H_2, and H_2S than the atmosphere (e.g., Gerdes et al., 2000a; Noffke, 2000; Noffke et al., 1996, 1997a, 1997b, 2001a, 2001b, 2003a, 2003b; Draganits and Noffke, 2004).

Formal description of mat-decay features

Radial gas or fluid escape structures: Figures 4(d)-1A to -1F

Name of structure: Radial gas or fluid escape structures.

Other terms used: '*Astropolithon*', 'gas domes'.

Description of structure: Roughly circular conical mound with a central or subcentral depression, or aperture, and radiating structures than can appear as ridges or grooves. The radial structures extend from the central depression to the edge of the mound and range from straight and continuous to sinuous and bifurcating. The mound is a surface expression of a vertical inverted-cone structure that extends downward into the sedimentary layers and contains a core linked to the central depression. The edges of the mound are typically indistinct as they grade into the surrounding sediment.

Associated sedimentary structures: (1) sand stromatolites; (2) thinly bedded laminated quartz arenites; (3) oscillation ripples.

Environment: Typically, intertidal.

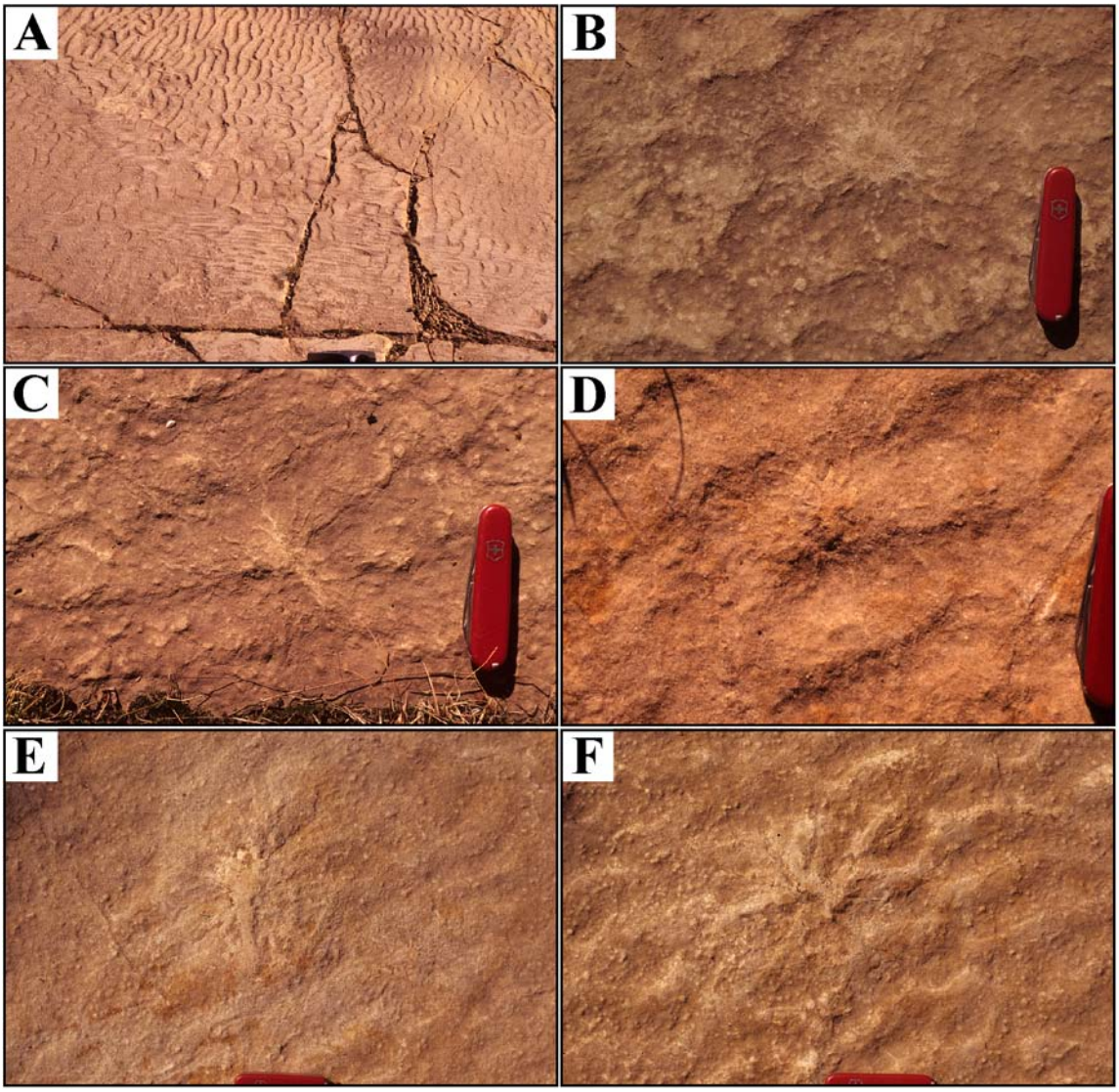


Figure 4(d)-1: Radial gas or fluid escape structures (‘*Astropolithon*’) in quartz arenites, Late Cambrian Elk Mound Group, Wisconsin, USA.

All images are from a ripple-marked bed surface (partially illustrated in A), which exhibits evidence of oscillation ripple washouts from tidal retreat, as well as ridge and runnels. Surface is characterised by small sand stromatolites (raised pustules in B–F, and at lower left in A), and is underlain and overlain by thinly bedded laminated quartz arenites. Locations of several of the escape structures on this surface are arrowed. (B)–(D) illustrate the typical raised boss with radiating cracks, thought to form when gas or fluid pressure from underlying layer(s) arches overlying sediment upward, cracking it. Radiating cracks are often filled with sand, either from below, or from surface transported grains. When minimal sand is ejected from below, the raised boss and cracks are the only evidence for gas/fluid escape. Stringers of ejected sediment are sometimes visible in the downcurrent direction (E) and overlap small sand stromatolites (E, F), but can be cross-cut by surface trails, such as the *Helminthoidichnites* in (E). Together, these features demonstrate the presence of a microbially-bound cohesive sandy surface layer that was arched upward and cracked prior to deposition of the overlying layer. Hammer head in (A) is 17.5 cm long; knife in (B)–(F) is 8.3 cm long. All photos: J.W. Hagadorn.

Ideas on genesis: These structures are interpreted as resulting from the escape of pressurised gas or fluid through a cohesive microbial mat surface. The gas or fluid was produced during the decay of buried mat material. As decay progressed, the gas or fluid pressure underneath the mat increased to the point of rupture when the trapped gas or fluid erupted through the mat surface, depositing a conical mound of sediment on the mat’s upper surface. The central depression in these mounds is the zone through which the gas or fluid and sediment flowed. Once the pressure was released, this central zone collapsed and created the depression. The radial structures were likely

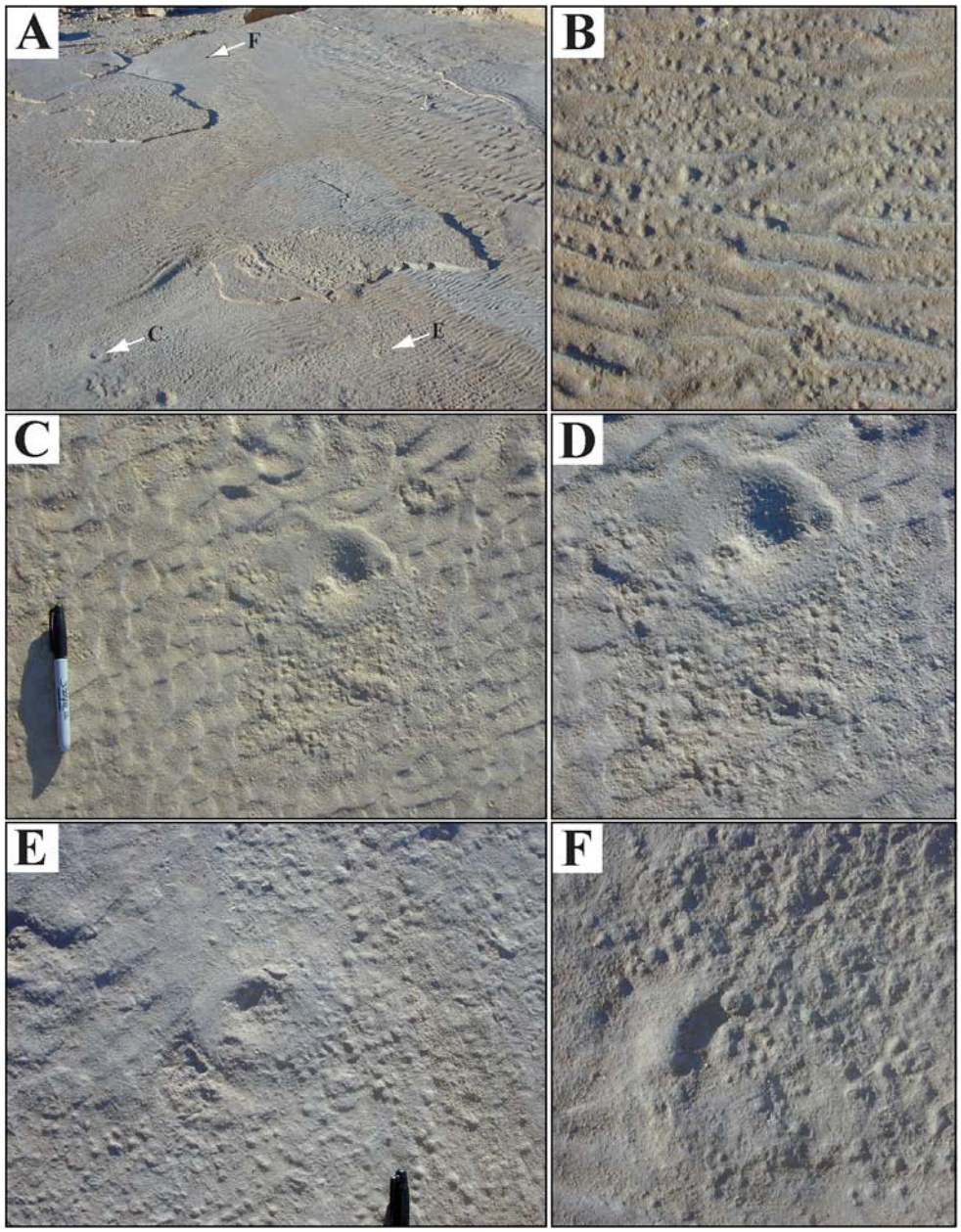


Figure 4(d)-2: Gas or fluid escape structures in quartz arenites, Late Cambrian Elk Mound Group, Wisconsin, USA.

All images are from the oscillation and combined flow ripple-marked bed surface in (A), which is characterised by patchy ripples, swaley topography, and is underlain and overlain by thinly bedded laminated to ripple cross-laminated quartz arenites. Three of the escape structures on this surface are arrowed. Sand stromatolites (B) that also occur in non-rippled patches (A, C, D, F), are often over-run by oscillation ripples. (B) is from the lower right corner of surface in (A). (D) is a close-up of (C), and bears the hallmark central depression characterised by a raised but flattened mound of adjacent sediment, which overlaps adjacent ripple crests and is in turn overlain by the margin of a cluster of sand stromatolites. (E) illustrates more asymmetric sediment expulsion, and overlap of this sediment mound by non-clustered sand stromatolites. (F) is similar to (D), but only a portion of the central cavity and marginal sediment mound remain. Together, these features demonstrate the presence of microbially-bound surfaces before, during, and after ripple formation, and that gas- or fluid-driven evulsion of sand occurred after ripple formation but before the final episode of microbial sealing. Width of field of view is (A) 2.5 m; (B) 25 cm; (F) 17 cm; pen is 13 mm wide. All photos: J.W. Hagadorn.

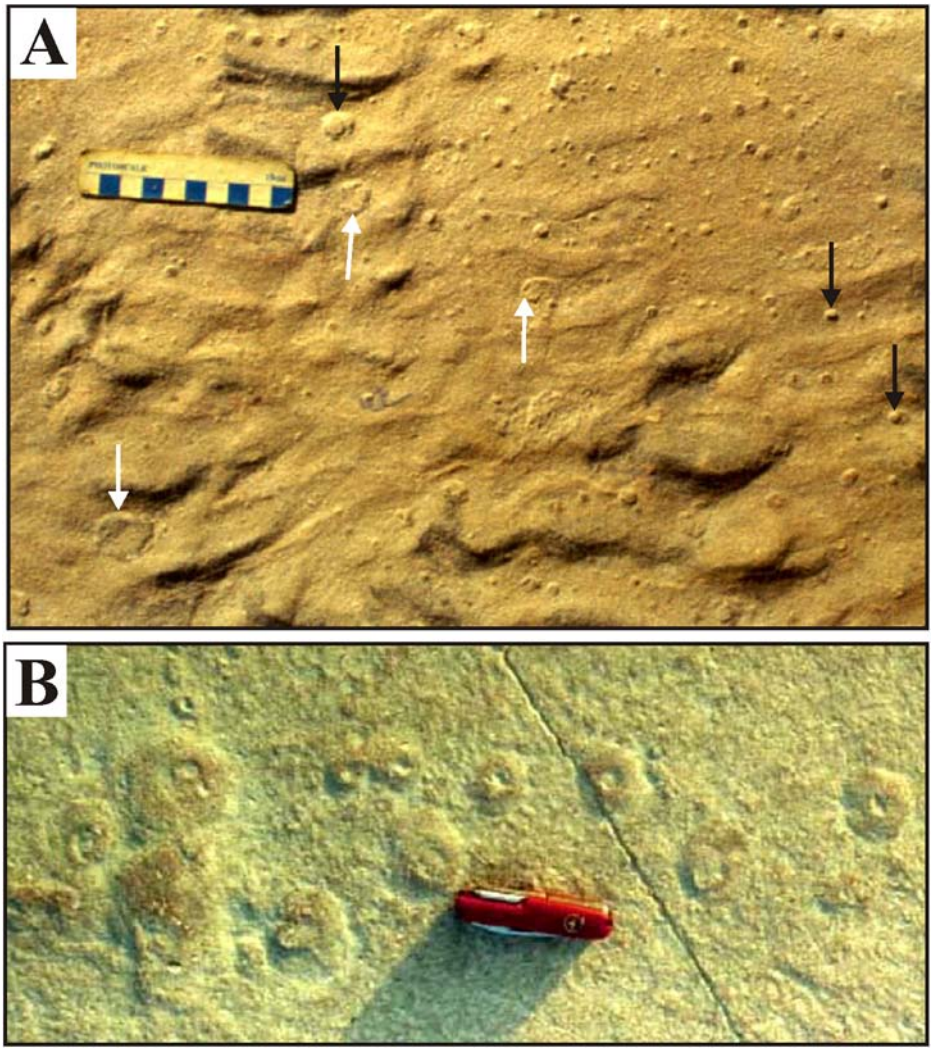


Figure 4(d)-3: Mat decay features from the Neoproterozoic of India.
(A) Small bulges (black arrows) on a sandstone bed surface in the intertidal–supratidal 0.6 Ga Sonia Sandstone, Jodhpur Group, Rajasthan, India. Note association with minute gas domes with craters at their centres (white arrows). (B) Bulges with craters at their centres in the same Sonia Sandstone. Gas entrapped under a mat and filling of the space thus created underneath the mat by sand, created the bulges. On the other hand, the gas domes formed where the upcoming gas could rupture through the mat cover. Decay of mat at its base presumably generated the gas pressure.

zones through which the sediment flowed as it spilled onto the mat upper surface, as they can occasionally extend beyond the margin of the mound itself (Pickerill and Harris, 1979).

Non-radial gas or fluid escape structures: ***Figures 4(d)-2A to -2F; Figures 4(d)-3A, -3B***

Name of structure: Non-radial gas or fluid escape structures.

Other terms used: 'Gas domes'.

Description of structure: Roughly circular conical mound with a central or subcentral depression or aperture. Unlike in '*Astropolithon*', there are no radial structures visible on the surface of the mound, although internal radial structures have been noted in some forms (Pickerill and Harris, 1979). In these structures, the mound is also a surface expression of a vertical inverted-cone structure that extends downward into the sedimentary layers and contains a core linked to the central depression. The edges of the mound are typically indistinct as they grade into the surrounding sediment, although they may be overgrown by microbial structures such as sand stromatolites.

Associated sedimentary structures: (1) sand stromatolites; (2) oscillation ripples (see also Chapter 7(a)); (3) combined flow ripples; (4) thinly bedded laminated to ripple cross-laminated quartz arenites.

Environment: Supratidal to intertidal.

Ideas on genesis: These structures are also interpreted as resulting from the escape of pressurised gas or fluid through a cohesive microbial mat surface. The gas or fluid was produced during the decay of buried mat material. As decay progressed, the gas or fluid pressure underneath the mat increased to the point of rupture when the trapped gas or fluid erupted through the mat surface, depositing a conical mound of sediment on the mat's upper surface. The central depression in these mounds is the zone through which the gas or fluid and sediment flowed. Once the pressure was released, this central zone collapsed and created the depression. The mounds may later be flattened by overlying layers, or overtop adjacent primary surface structures such as ripples. These features lack the radial structures found in '*Astropolithon*', perhaps because the sediment flowed out of the rupture in a more uniform manner, or because the mounded sediment has buried such fractures.

4(e). DIAGENETIC MAT FEATURES

As discussed in the Introduction to this chapter, these features are presented together with mat metabolism features in Section 4(b). Further details and examples are given in Chapter 7.

4(f). COMPLEX STRUCTURES ASSOCIATED WITH SILICICLASTIC BIOLAMINITES

E. Bouougri, H. Porada

Siliciclastic biolaminites result from biosedimentary accretion due to interaction of mat growth and siliciclastic sediment deposition. They are characterised by millimetre-scale alternating layers of microbial mat material and fine-grained sand- to silt-sized sediment, reflecting repeated cycles of mat growth, sediment deposition and burial, and renewed mat growth *sensu* Gerdes et al. (2000a). Siliciclastic biolaminites usually develop flat, parallel laminations, but excursions to more domal structures and wavy-crinkly laminations occur.

Upon subaerial exposure, the surface mat layers of biolaminite successions may undergo desiccation and shrinkage and develop *shrinkage cracks* of variable size and shape, ranging from isolated, lenticular and spindle-shaped types to networks of decimetre-scale polygonal cracks with upturned and overgrown margins (Figure 4(c)-6A). Within a package of biolaminite, shrinkage cracks may be observed at several levels indicating multiple repetitions of mat growth, shrinkage and cracking during biosedimentary accretion. When, at wide cracks, desiccation and shrinkage advance from the crack margins into the top portion of the biolaminite succession, thick packages of biolaminite may be upturned, forming an *upturned margin* (Figure 4(c)-6B).

Microbial growth, triggered by uprising groundwater in wide cracks may span the crack opening and encroach upon the margins, leading to *overgrown margins*. Alternating mat growth and upturning of crack margins, for example during tidal high and low water, respectively, may lead to *complex structures* along the crack margins. Depending on the rates of the processes involved, resulting structures may range from rather simple (Figure 4(c)-6C) to highly irregular (Figures 4(f)-1, -2) examples. Complex structures reflect a non-equilibrium system of quasi-concomitant growth, destruction by desiccation, deformation by repeated upturning, and renewed overgrowth.

When compared to modern examples, identification of ‘complex structures’ in ancient laminated siliciclastic successions may argue for: (1) the biogenicity of the deposits; (2) an intertidal environment, where continuous/episodic shrinkage and growth closely accompanied cyclic accretion of mat–sediment doublets; (3) processes involving continuous and repeated occurrences of shrinkage, upturning and overgrowth until the margin structure is completely sealed by new and continuous mat layers.

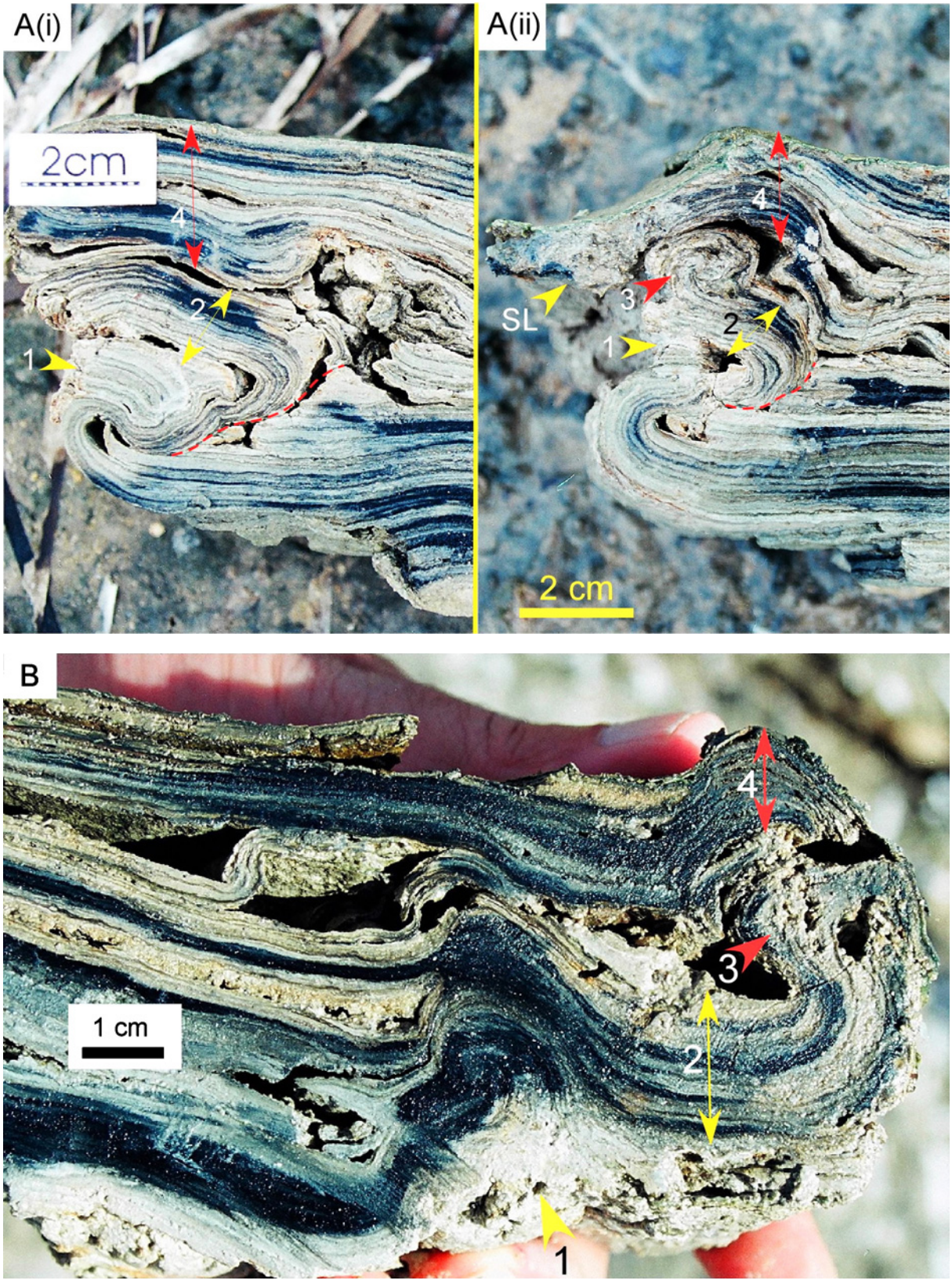

A(i)
2cm
4
2
1
A(ii)
4
SL
3
1
2
2 cm
B
4
3
2
1
1 cm

Figure 4(f)-1: Complex features resulting from continuous/episodic cracking, upturning of crack margins and concomitant mat growth; modern example from Tunisia.

(A) Sections across overgrown crack margins as developed along polygonal cracks in biolaminite (see Figure 4(c)-6A). Photos A(i) and A(ii) show internal structures resulting from cracking, upturning of crack margins and concomitant mat growth. Continuous overgrowth and overfolding of evolved upturned polygon edges may develop complex structures distinct from the rather simple structures of upturned and overgrown incipient margins as presented in Figure 4(c)-6C. Dashed lines indicate discontinuity of the flat lamination against the overturned evolved structure. A(i) is a section across the edge of a biolaminite polygon showing rolled-up structures related to continuous processes of microbial growth, shrinkage and overgrowth around the crack-edge. Note initial upturned margin (1) overgrown by a first generation of microbial layers (2). The resulting structure of the edge is Z-shaped and overfolded to a horizontal attitude. Overlying microbial layers (4) form the next step of overgrowth and fossilise the structure. A(ii) shows two superposed generations of upturned and overgrown edges developing a vertical meandering structure. The first upturned and overgrown edge (1 and 2) is overturned into a horizontal attitude before formation of the new edge (3). The overgrowing microbial layers (2) undergo shrinkage themselves and a second short upturned margin is formed (3), again overgrown by microbial layers (4), which completely seal the structure and which adjoin laterally to a sedimentary layer (SL) deposited between the polygon edges. (B) Section across the edge of a polygonal shrinkage crack in biolaminite. The structure shows lateral and vertical transitions between two successive overgrown crack-edges. The first (1) is completely overgrown by a stack of continuous microbial layers (2) which themselves undergo a new stage of shrinkage, upturning (3) and overgrowth by new microbial layers (4), leading to the formation of a new upturned margin structure. Repeated cracking, upturning and overgrowth may lead to successive and superimposed 'antiformal structures' which may be confused with tectonic folding or soft-sediment deformation (i.e., due to slumping or dewatering). Locality: Bhar Alouane, Mediterranean coast of southern Tunisia; environment: intertidal zone, regularly flooded during high tide. Photos: E. Bouougri and H. Porada.

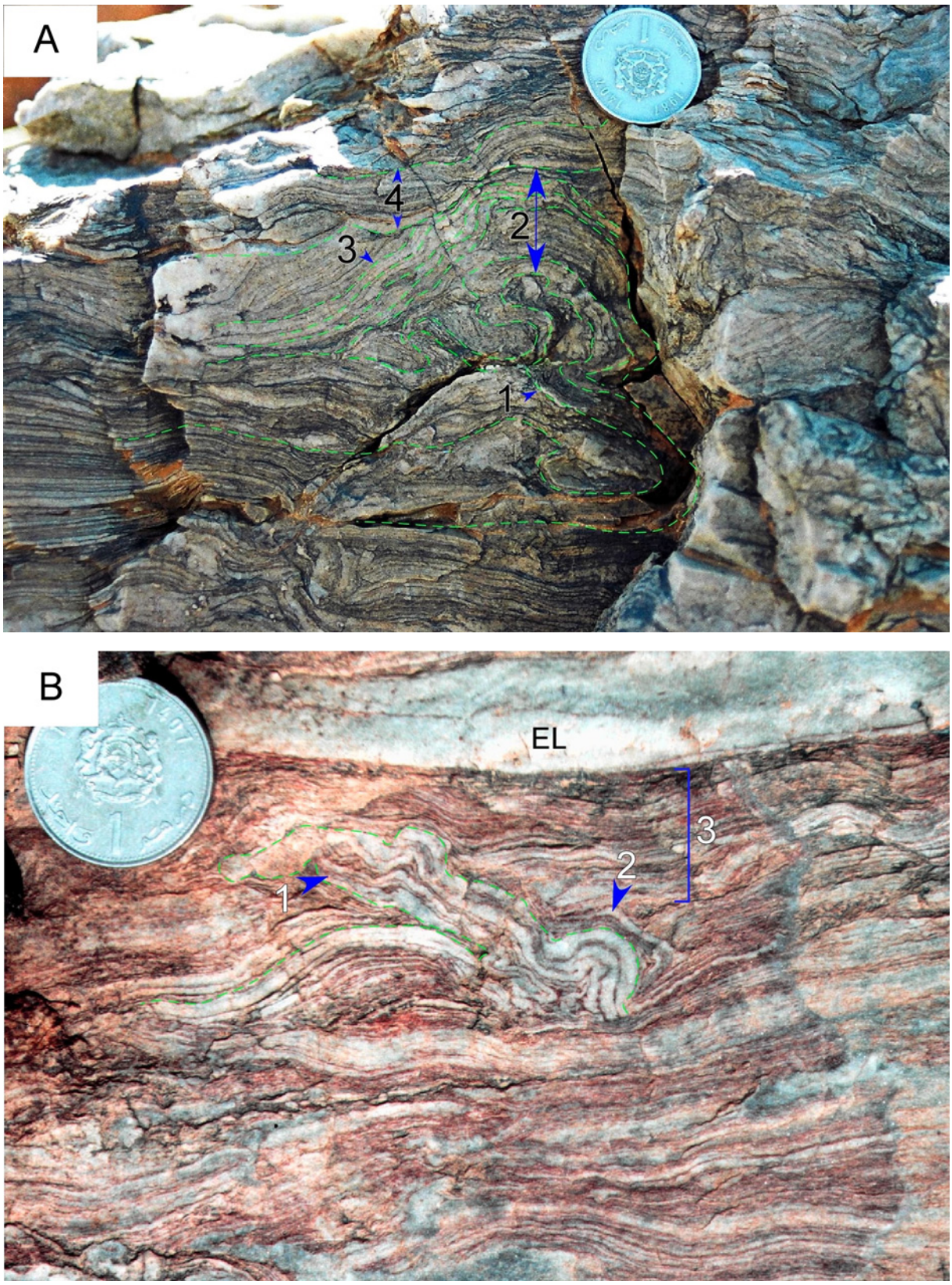

A
4
3
2
1
B
EL
3
2
1

Figure 4(f)-2: Complex features in biolaminites resulting from shrinkage, upturning of crack margins, concomitant mat growth and deformation during burial; ancient example from the Neoproterozoic of the Anti-Atlas.

(A) Internal organisation of structure resulting from shrinkage and overgrowth within biolaminite deposits. The geometry and organisation of the laminae record multiple stages of overgrowth and crack-margin upturning. Thus, the structure comprises: (1) an upturned crack margin resulting from shrinkage of the biolaminite layer; (2) a first interval of microbial layers overgrowing the margin, and in which the first overgrowth laminae are deformed behind the margin due to a high rate of overturning (and later compaction?), while the laminae above are continuous; (3) discontinuous laminae not continuing past the crack-edge which is again upturned, thus creating a depression behind; (4) continuous overgrowth laminae covering the whole structure. (B) Laminated siltstone/argillite (biolaminite) with interbeds of fine-grained quartzite (event layers: EL) showing internal fold structure (green dashed line) which records a high degree of flattening under burial and compaction. The structure is interpreted as resulting from shrinkage, cracking and overgrowth of the upturned crack margin, undergoing the following sequence of events: (a) shrinkage of biolaminite layers and formation of an upturned crack-margin developing an asymmetric S-like shape (1); (b) the margin is overgrown by new laminae with progressive onlap towards the stabilised overgrowth edge (2); (c) the whole structure is progressively sealed by growth of new biolaminite layers (3); (d) burial and compaction cause gliding between internal and surrounding (overgrowth) laminae; overgrowth layers are torn and the margin is strongly compacted; biolaminite layers below are disrupted forming a 'convex-up' structure in the left-hand part of the feature. Locality: Tirsal section, Tamgarda Formation, Tizi n-Taghatine Group, Anti-Atlas, Morocco. Scale (coin) is 24 mm. Palaeoenvironment: intertidal zone. Photos: E. Bouougri and H. Porada.

This page intentionally left blank

Atlas of Microbial Mat Features Preserved within the Siliciclastic Rock Record
Edited by J. Schieber et al.
© 2007 Elsevier B.V. All rights reserved
DOI: 10.1016/S1574-1966(07)02005-6

CHAPTER 5

Microbial Mats on Muddy Substrates – Examples of Possible Sedimentary Features and Underlying Processes

Juergen Schieber

INTRODUCTION

In modern environments where environmental parameters, such as low oxygen conditions or high salinity, restrict metazoan grazing, microbial mats tend to prosper. Examples are the Beggiatoa mats in the depths of the Santa Barbara Basin offshore of California (low oxygen), and the famous stromatolites of Sharks Bay in Western Australia (high salinity). Regardless of substrate, microbial mats can produce unique surface morphologies, display textures related to lateral expansion and grain capture, cause resistance to loading, enhance cohesion of surface layers, and upon erosion form flexible fragments with properties that contrast strongly from those of a simple sediment. Yet, whereas in carbonate rocks and sandstones the resulting sedimentary features might be recognised by their resemblance to features observed in modern environments, microbial mat features in mudstones are quite subtle and often overlooked (Schieber, 1999).

Nonetheless, the presence of microbial mats changes the rheology of the surface muds, and the organic material that they produce impacts mudstone diagenesis upon decay and burial. Whereas the organic mat texture, such as the original surface morphology (e.g., smooth, wrinkled, ridged, pinnacled) and the arrangement of filaments within the mat may largely be lost upon decay and compaction, the impact that the mat had on physical and chemical sediment properties (e.g., erodability, cohesion, redox conditions and authigenic minerals) can still be detected upon careful examination. In a sense these impacts are analogous to trace fossils in that they record the mat induced changes in the mechanical and chemical behaviour of the mud substrate. An overview of these features was given by Schieber (2004) and is summarised in Chapter 3 of this book. In the following paragraphs examples from the rock record are discussed and illustrated with the accompanying figures.

FEATURES RELATED TO MAT GROWTH

In addition to the continued growth of microbial filaments and clumps, microbial mats typically produce copious amounts of sticky extracellular polymer substances (EPS). Cumulatively, this organic production results in the trapping, agglutination, baffling, and binding of sediment particles that rain down on the mat surface or are transported across it (Gerdes et al., 2000a). As is true for sandy and carbonate environments, sedimentation in muddy environments is episodic, reflecting sediment pulses due to storms, floods, dust storms, and other short-lived disturbances (Schieber, 1998b). These sediment pulses will intermittently blanket microbially stabilised muddy surfaces, and this sediment blanket will be resurfaced by microbial mats once normal conditions return. The thin clay drapes that accentuate laminae in carbonaceous shale beds of the Newland Formation (Belt Supergroup, Montana; Figure 5-1A) are interpreted to be of such origin (Schieber, 1986), and the thicker graded silt/mud couplets of Proterozoic striped shales (Figure 5-1D; see also Chapter 7(b) and (c)) can be viewed as simply reflecting more voluminous or more proximal sedimentation events (Schieber, 1986).

When colonising muddy substrates, microbial mats provide a sharp geochemical interface beneath which the sediment is reducing and prone to better preservation of organic matter (Krumbein and Cohen, 1977). Thus, in mudstones the former presence of microbial mats may be indicated by laminated carbonaceous shale beds. Not all lamination in carbonaceous shales, however, is of microbial mat origin. Many non-mat carbonaceous shales are laminated as well (Figures 5-1B, -1C). Yet, while laminae in the latter are typically even and parallel (Figures 5-1B, -1C) in the absence of differential compaction effects, microbial mat-produced carbonaceous laminae tend to be more wavy-crinkly in nature (Figure 5-1A).

Although wavy-crinkly anastomosing carbonaceous laminae appear to be a characteristic feature of several examples of microbial mats in the rock record (Schieber, 1986; Sur et al., 2006; Patranabis-Deb et al., Chapter 7(c))

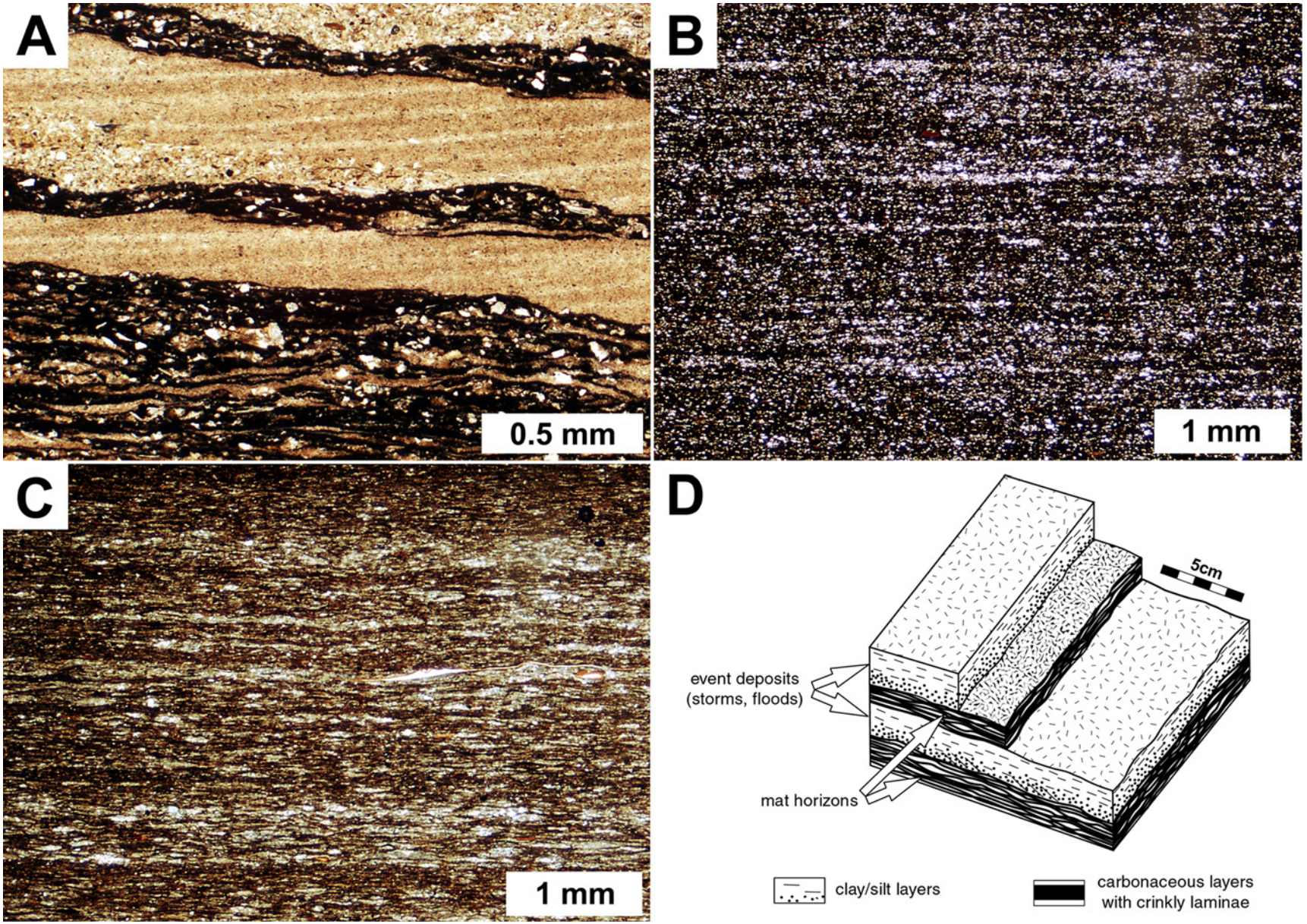

A
0.5 mm
B
1 mm
C
1 mm
D
5cm
event deposits
(storms, floods)
mat horizons
clay/silt layers
carbonaceous layers
with crinkly laminae

Figure 5-1: Comparison of microbial mat lamination with lamina styles typical in laminated Phanerozoic carbonaceous shales.
(A) Striped shale, Newland Formation, Belt Supergroup, Middle Proterozoic of Montana, USA. Note wavy-crinkly carbonaceous laminae that are interpreted as having been produced by a benthic microbial mat (Schieber, 1986; Chapter 7(b)). Light coloured layers are graded silt–mud couplets that are interpreted as event layers, possibly due to storms or floods. (B) Laminated black shale from Dowelltown Member of the Chattanooga Shale. The silt laminae are even and parallel and interpreted as due to seafloor reworking by storm waves (Schieber, 1998c). (C) Even parallel laminated Posidonia Shale from southwest Germany. The lighter laminae consist of tiny carbonate grains and fecal pellets. Although A, B, and C are all carbonaceous shales, the microbial mat laminae in A differ distinctly from the bottom current- and wave-produced even parallel laminae in B and C. (D) Graded silt/mud couplets in Proterozoic striped shales (see also Chapter 7(b)) reflect intervals of mat growth interrupted by brief sedimentation events (Schieber, 1986). From Schieber (1999); reproduced with permission of SEPM (Society for Sedimentary Geology).

---

and probably are an 'afterglow' of the once wrinkled irregular surface of a microbial mat, the presence of this lamina style should not be considered as diagnostic of surface colonisation by microbial mats. The reason for this cautionary note is that differential compaction around microconcretions, fecal pellets, silt lenses, etc. can produce a comparable style of lamination (Schieber, 1999). For example, mat-colonised muds of the Santa Barbara Basin (Beggiatoa mats) contain between 80 and 90% water (personal observations). Compaction will therefore tend to not only cause a severe reduction of original surface relief, but also produce waviness due to compaction around denser particles and sediment regions.

Presumed microbial mat laminae in Green River Formation oil shales (see Chapter 7(j)) differ from the above Middle Proterozoic examples by being smooth-wavy in appearance rather than wavy-crinkly (Figure 5-2A). The reason behind this difference is uncertain. The mat-forming communities could for example have formed a very even surface film that did not have many wrinkles to start with. Alternatively, terrigenous influx during times of optimal mat development could have been so small as not to produce thickness variations in the mat layer due to sediment trapping.

In more energetic shallow water environments, a combination of competition for light and sediment trapping by microbial mat surfaces (agglutination) tends to promote the formation of domal buildups in sandstone and carbonate environments (Schieber, 1999). Domal buildups of various amplitude and spacing have for example been observed in shallow water mudstones of the Belt Supergroup (Schieber, 1998a, 1999; see also Chapter 7(b)). These domal features (Figures 5-2B, -2C) may have developed because better lighting conditions allowed slightly elevated areas to grow more biomass and EPS, and as a consequence were also more efficient in trapping and binding sediment that moved across the sea floor by currents and waves. Domal features of this type have so far only been reported from mudstone units in the Middle Proterozoic Belt Supergroup (Schieber, 1998a), but potentially could occur in other Proterozoic shale successions as well. The paucity of observations may not so much reflect their actual rarity, but equally well might indicate that these features rarely survive outcrop weathering.

As pointed out above, sudden sedimentation events (storms, floods) can 'bury' a growing mat and cause an interruption of growth. If these even layers are of the thickness of millimetres to centimetres they give the shales a unique striped appearance (Figure 5-1D), such as also illustrated in Chapter 7(b) and (c). In the case of an incomplete but expanding mat cover, occasional deposition of thin clay drapes may lead to false cross-lamination (Figure 5-3A) as outward movement of mat margins is intermittently interrupted by deposition of clay drapes (Schieber, 1986). Depending on the regularity with which the growth-interrupting sedimentation events occur, the resulting false cross-lamination may look quite a bit more irregular than depicted in Figure 5-3A.

When micas are transported by currents across a microbial mat they are likely to be trapped in random orientation on a surface covered by a tangle of microbial filaments and sticky EPS. For mats growing on a muddy substrate, however, an initial random mica fabric will typically be obscured by later burial compaction. Thus, although random micas can be a growth related fabric element, this feature is only preserved in cases where mineral precipitation (Figure 5-3D) significantly reduces compaction (see below).

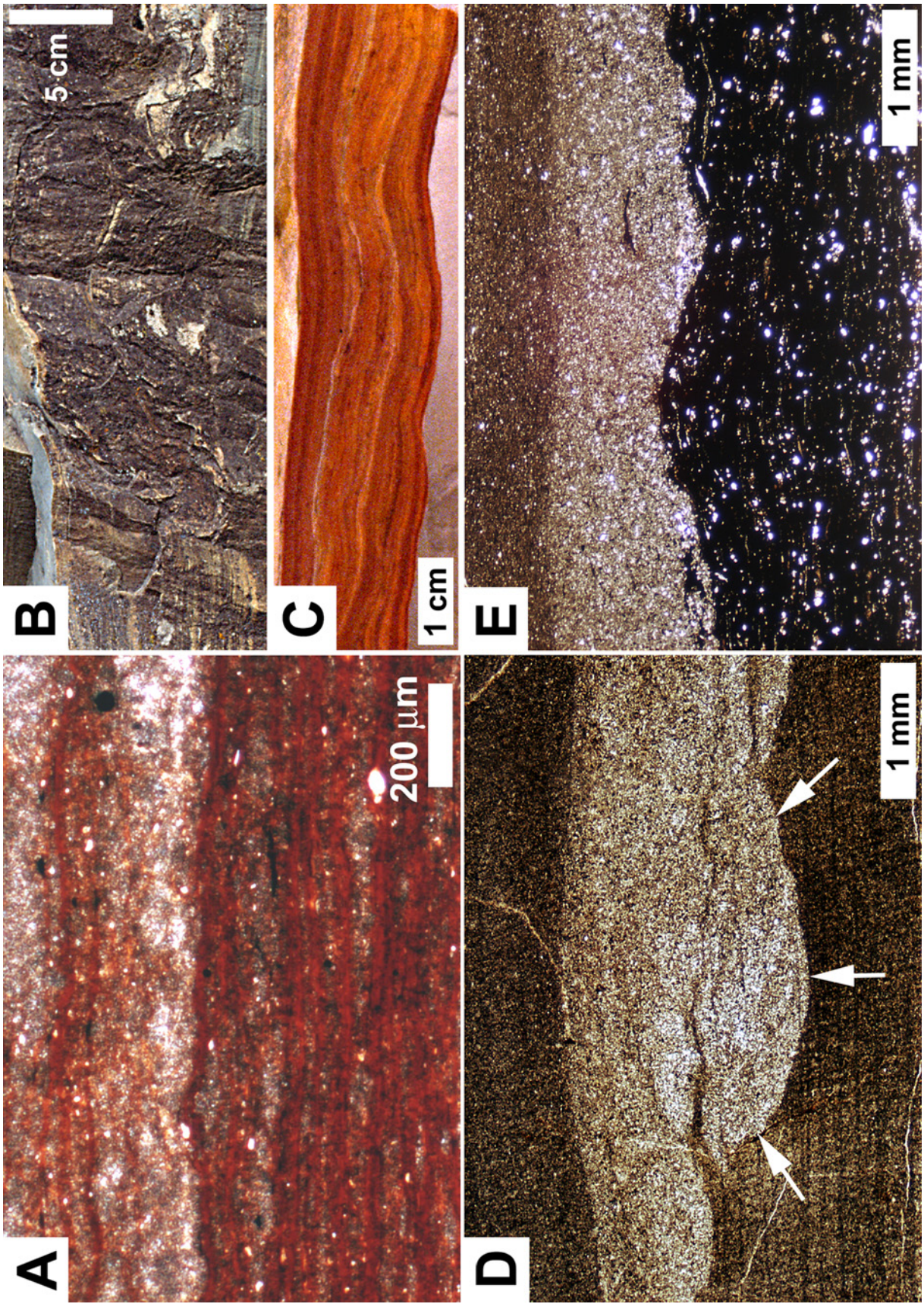

A
200 µm
B
5 cm
C
1 cm
D
1 mm
E
1 mm

Figure 5-2:
(A) Undulating continuous organic laminae (reddish brown) in lacustrine oil shale (Green River Formation). Laminae are not wavy-crinkly like in Proterozoic carbonaceous shales of microbial mat derivation (Chapter 7(b)), but instead are gently undulating. They are interpreted as remains of a contiguous organic film that covered the lake bottom (Chapter 7(j)). (B) Formation of positive relief buildups (small domes) in greenish grey laminated mudstones of the Mt. Shields Formation (Belt Supergroup, Middle Proterozoic of Montana; Chapter 7(b)). (C) Low amplitude domes in reddish mudstones of the Mt. Shields Formation (Belt Supergroup, Middle Proterozoic of Montana; Chapter 7(b)). In both cases the domes contain dolomitic laminae that are interpreted as microbial (Schieber, 1998a; Chapter 7(b)). Buildups may reflect upwards growth towards sunlight. (D and E) Comparing loading behaviour of silt layer on non-microbial mud layer with loading behaviour on microbial mat layer. In D the silt is able to sink into the underlying mud and forms small pillows (arrows), whereas in E the mat layer resists loading and the silt only forms shallow depressions. Images D and E are from shales of the Newland Formation, Belt Supergroup, Middle Proterozoic of Montana (see Chapter 7(b)).

FEATURES RELATED TO PHYSICAL FORCES ACTING ON MAT STABILISED MUD LAYERS

Generally speaking, surface muds are of low density because they contain abundant (70 to 90%) water. If covered with a layer of denser sediment, such as silt or sand, the loading of these hydroplastic mud layers results in subsidence of sand and silt in the form of lobes and to upwards movement of mud in the form of tongues. The resulting sedimentary structures are commonly known as load casts, flame structures, and ball-and-pillow structures (Reineck and Singh, 1980). In Figure 5-2D a thin silt layer overlying a bed of grey shale is visible, with a subsided silt pillow projecting into the underlying mud. The structure implies that the underlying mud behaved like a viscous fluid. In Figure 5-2E a silt layer of the same thickness on top of a wavy-crinkly laminated carbonaceous shale layer can be seen. Instead of sinking in and forming pillows, the silt layer only produces shallow depressions in the underlying mud. Comparing the two images suggests that the carbonaceous shale layer offered more resistance to loading than the grey shale layer. Both images are from the same Middle Proterozoic shale unit, and the carbonaceous layer has wavy-crinkly internal laminae that are suggestive of a microbial mat origin (Figure 5-1A). If the carbonaceous layer simply had originated as an organic muck it would have behaved very similarly to a clay–water mixture and shown sunk-in pillows like those seen in Figure 5-2E. The load resistance of the carbonaceous layer suggests internal cohesion, a property that is consistent with a surface-stabilising microbial mat.

The shales pictured in Figures 5-3B and -3C show soft sediment deformation of alternating layers of grey and carbonaceous shale (striped shales; see Chapter 7(b) and (c)). These shales were unconsolidated when rupturing and folding occurred, and carbonaceous shale layers behaved like cohesive sheets, whereas the interbedded grey shales flowed into gaps (Figure 5-3B) and were squeezed out of fold hinges (Figure 5-3C). In essence, the grey shales behaved like a thick fluid that in viscosity probably compared well to stirred yoghurt, and the carbonaceous layers possessed internal cohesion. These observations are testament to considerable original rheological differences between grey shales and carbonaceous shales, and are consistent with a microbial mat origin for the carbonaceous beds. If the latter had originally been a simple mixture of terrigenous material and organic particles (an organic muck), a fluid-like rather than a cohesive behaviour should be expected. Thus, whenever mechanical behaviour indicates that a given mudstone layer had considerably more internal cohesion than what could be expected of a simple mixture of its components, a microbial mat interpretation should be entertained.

Although microbial mats act to bind and stabilise the surface sediment (e.g., Neumann et al., 1970; Yallop et al., 1994; Paterson et al., 1994; Paterson, 1997), once eroding currents are too strong, holes will be eroded into the mat, and we may see features like ‘flipped over’ mat edges, overfolded mat layers, and ‘roll-up’ structures (Figure 5-4A). Eroded and deformed mat fragments may be several millimetres thick (Figures 5-3B and -3C) or may just be thin films (Figures 5-4B, -4C, -4D, -4E and -4F). In both cases, however, these fragments will exhibit high ‘within-lamina or -layer’ cohesiveness. On bedding planes of shales, carbonaceous fragments like those in Figures 5-4B, -4C, -4D, -4E and -4F will appear as irregularly shaped dark flakes that range in size from a few millimetres to centimetres.

The fragmentation of microbial mats during erosion and transport is analogous to the tearing of a fibrous fabric, and mat fragments may show frayed edges as a result. The phenomenon is also known as ‘blotting paper effect’ from the study of modern microbial mats (Gerdes et al., 1993), and is illustrated in Figure 5-5 with various examples from the rock record.

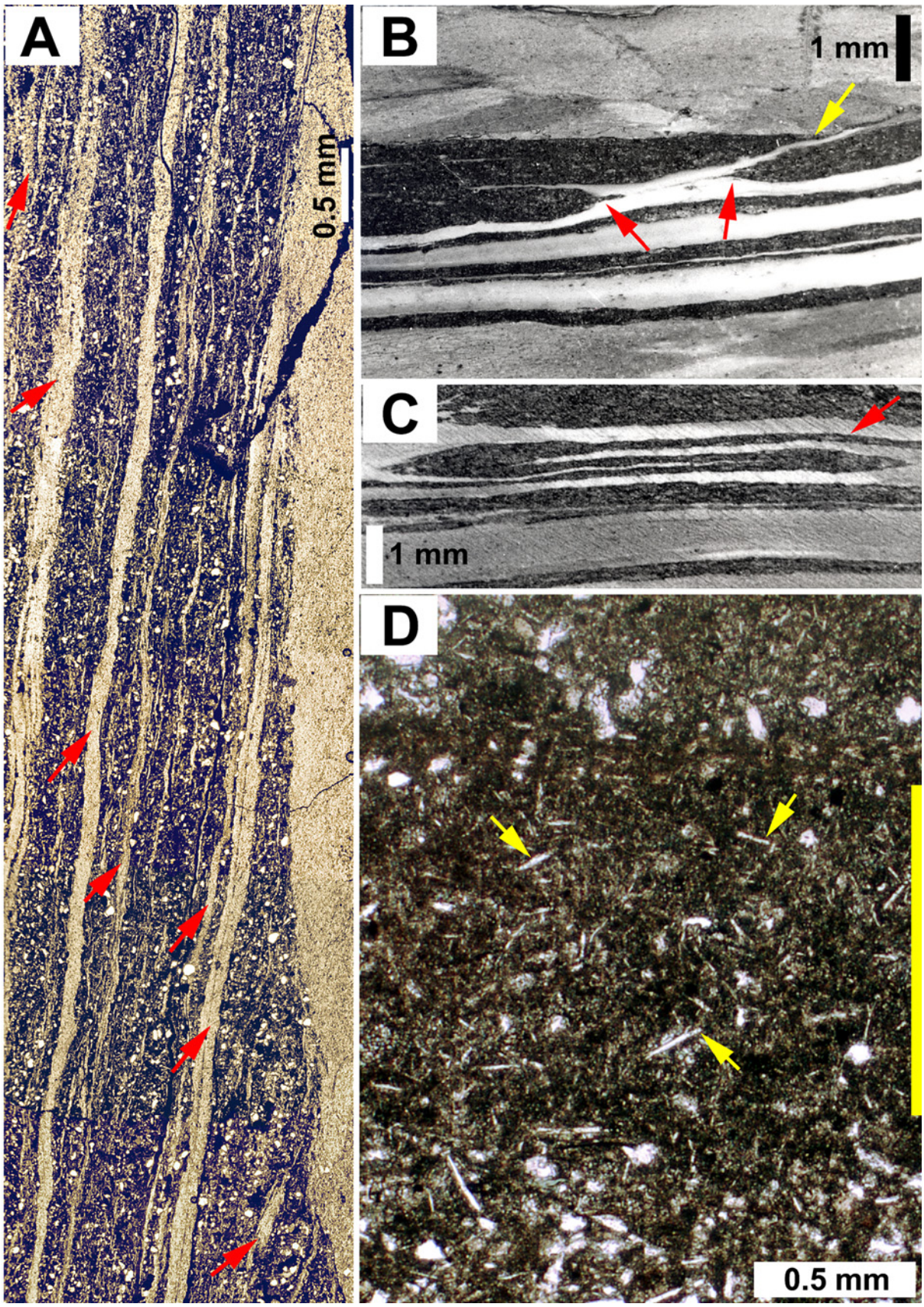

A
0.5 mm
B
1 mm
C
1 mm
D
0.5 mm

Figure 5-3:
(A) 'False cross-lamination' at the base of a carbonaceous silty shale bed from striped shale in the Newland Formation (Belt Supergroup, Middle Proterozoic of Montana). Internal drapes of clay (red arrows) range from 0.01 to 0.1 mm in thickness. The clearly visible thicker shale drapes form an angle of about 5 degrees with the base of the carbonaceous silty shale bed and continue into the underlying bed of clayey shale. The feature is interpreted as the result of the step-wise lateral expansion of a pioneer mat that was interrupted by deposition of clay drapes (Schieber, 1986). Stratigraphic 'up' is to the left. (B) Ruptured bed (red arrows) of carbonaceous silty shale in striped shales of the Newland Formation. The left part of this bed has been overfolded and thickened during early soft sediment deformation. The outer hinge of the overfolded portion is marked with a yellow arrow. Note that the intervening clay layer has been squeezed out of the hinges. These observations indicate that the clay layers were of a semi-liquid or yoghurt-like consistency, whereas the carbonaceous layers behaved like a cohesive, leathery membrane (see also C). (C) Overfolded (red arrow) but intact bed of carbonaceous silty shale (dark) interbedded with clayey shale (light). Most of the light clay-rich material has been squeezed out of the fold noses and limbs. This indicates that the dark beds were considerably more cohesive than beds of clayey shale, and that the latter behaved more like a highly viscous fluid during soft sediment deformation (Newland Formation, Belt Supergroup, Middle Proterozoic of Montana). (D) Photomicrograph of dolomitic lamina attributed to microbial mat growth (marked at right with yellow bar). The latter are common in domal features observed in the Mt. Shields Formation of the Belt Supergroup (see Chapter 7(b)). Characteristic for these laminae is a random orientation of mica flakes (muscovite). Some large mica flakes are pointed out by yellow arrows.

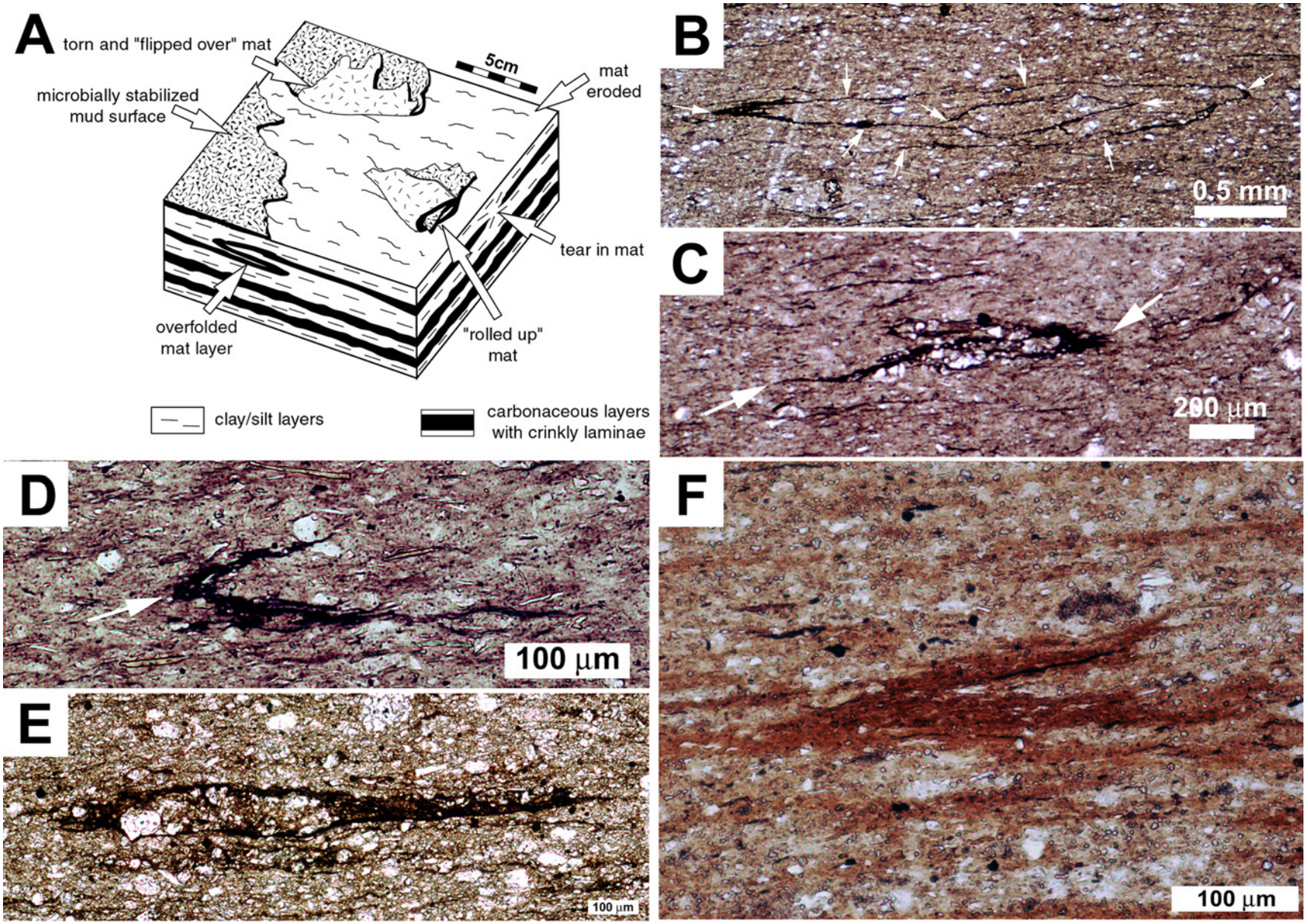

A
torn and "flipped over" mat
5cm
mat eroded
microbially stabilized mud surface
tear in mat
overfolded mat layer
"rolled up" mat
clay/silt layers
carbonaceous layers with crinkly laminae
B
0.5 mm
C
200 µm
D
100 µm
E
100 µm
F
100 µm

Figure 5-4:
(A) Examples of the erosion, transport, and deformation of microbial mat stabilised muds. (B) Eroded and transported microbial mat fragment from the Newland Formation, Belt Supergroup, Middle Proterozoic of Montana (see also Chapter 7(b)). The fragment is now a thin carbonaceous film (arrows) that originally was approximately 10 mm in diameter. It has been rolled up by transport over the sediment surface. (C) Another microbial mat fragment (arrows) in shales of the Newland Formation. It has attached silt grains and appears to be overfolded with fold hinge at right. (D) Folded-over carbonaceous flake of probable microbial mat origin (Newland Formation, Belt Supergroup, Middle Proterozoic of Montana). (E) Carbonaceous flake with attached silt grains from the Rampur Shale, Vindhyan Supergroup, Middle Proterozoic of India. (F) Folded-over carbonaceous fragment in Green River Formation oil shale (Eocene of Wyoming). From Schieber (1999); reproduced with permission of SEPM (Society for Sedimentary Geology).

In carbonates, the very early diagenetic cementation of microbial mat layers can preserve remains of the mat-constructing microbes and provide a supporting argument for the microbial mat origin of ancient examples. In mudstones such preservation rarely occurs, and the postulation of a microbial mat origin based on the observation of wavy-crinkly carbonaceous laminae alone is tenuous. Observing, however, that the alleged mat layers and laminae are erosion-resistant and appear to have internal cohesiveness strongly improves the odds that one is indeed looking at microbially bound surfaces. In mudstones evidence for the cohesive behaviour of microbial mats is one of the most useful indicators of their former presence (Schieber, 1999).

The integrity of microbial mats can also be destroyed through desiccation, and personal observations of modern sediments suggest that mudcracks in clay substrates do differ from those observed in mat bound muddy substrates. There is, however, to date no formal study of desiccation effects in ancient mat-bound sediments. Drying-out of mat-bound surfaces can produce fragments that are able to float out into open water bodies (Fagerstorm, 1967) and which can transport detrital grains from near-shore areas to deeper and mud-dominated portions of a basin. Clusters of coarser grains (Figure 5-6B) in a much finer mudstone matrix may be of such origin, being 'rafted in' by mat fragments and then buried collectively once a mat-fragment had detached and sunk to the bottom (Olsen et al., 1978; Schieber, 1999). Benthic microbial mats may also be torn apart because some portions are so strongly buoyed by attached gas bubbles that they detach from the substrate and float to the surface (Figure 5-6A). These could then conceivably be carried deeper into the basin and there deposit out-of-place coarse grains. Wave agitation, however, will tend to sink dried 'rafts' and will shake lose air bubbles from buoyed mat fragments. Thus, this rafting process is most likely restricted to lakes during tranquil weather periods. Ice is of course another potent rafting agent, but in that case we can probably expect to find a larger grain size range (up to pebble size) and distinct horizons with rafted material. Furthermore, for the Phanerozoic time period other factors aside of microbial mats have to be considered for grain rafting, such as floating plant debris (root attached material), animal carcasses (buoyed by decay gases), and fecal pellets.

FEATURES RELATED TO MAT METABOLISM

For carbonate stromatolites, microbial photosynthetic carbon assimilation is generally considered the cause of calcification, and modern cyanobacteria are known to induce precipitation of gypsum, calcite, and magnesite from alkaline lake waters (Thompson and Ferris, 1990; Thompson et al., 1997). Calcification of cyanobacterial filaments has also been proposed as a source of carbonate micrite in the Phanerozoic (Pratt, 2001), but the underlying details of calcification of microbial sheaths and EPS are still a matter of some debate (Arp et al., 2001). It has also been suggested that magnesium concentrated in microbial sheaths is released upon decomposition and leads to dolomite formation in the micro-environment of microbial mat layers (Gebelein and Hoffman, 1973).

In mudstones, conformable laminae enriched in calcite or dolomite can in principle have multiple origins. They could for example simply be due to carbonate mud that was washed off adjacent carbonate banks by storms and then settled through the water column and blanketed the pre-existing mud surface. Alternatively they might also be the deposits of lutite flows that originated from a shallow water carbonate bank. In both cases, however, we would expect these deposits to be of uniform thickness at the thin section and hand specimen scale, to possibly show a sharp base and normal grading, and also to be largely devoid of terrigenous material. Carbonate laminae in the Mt. Shields Formation of the Middle Proterozoic Belt Basin (Chapter 7(b)), found as parts of domal buildups (Figures 7(b)-9 and -10) and in places exhibiting fenestral texture (Figure 7(b)-9D), have been interpreted as microbial (Schieber, 1998a). They are used here (see below) to illustrate likely differences between carbonate-rich

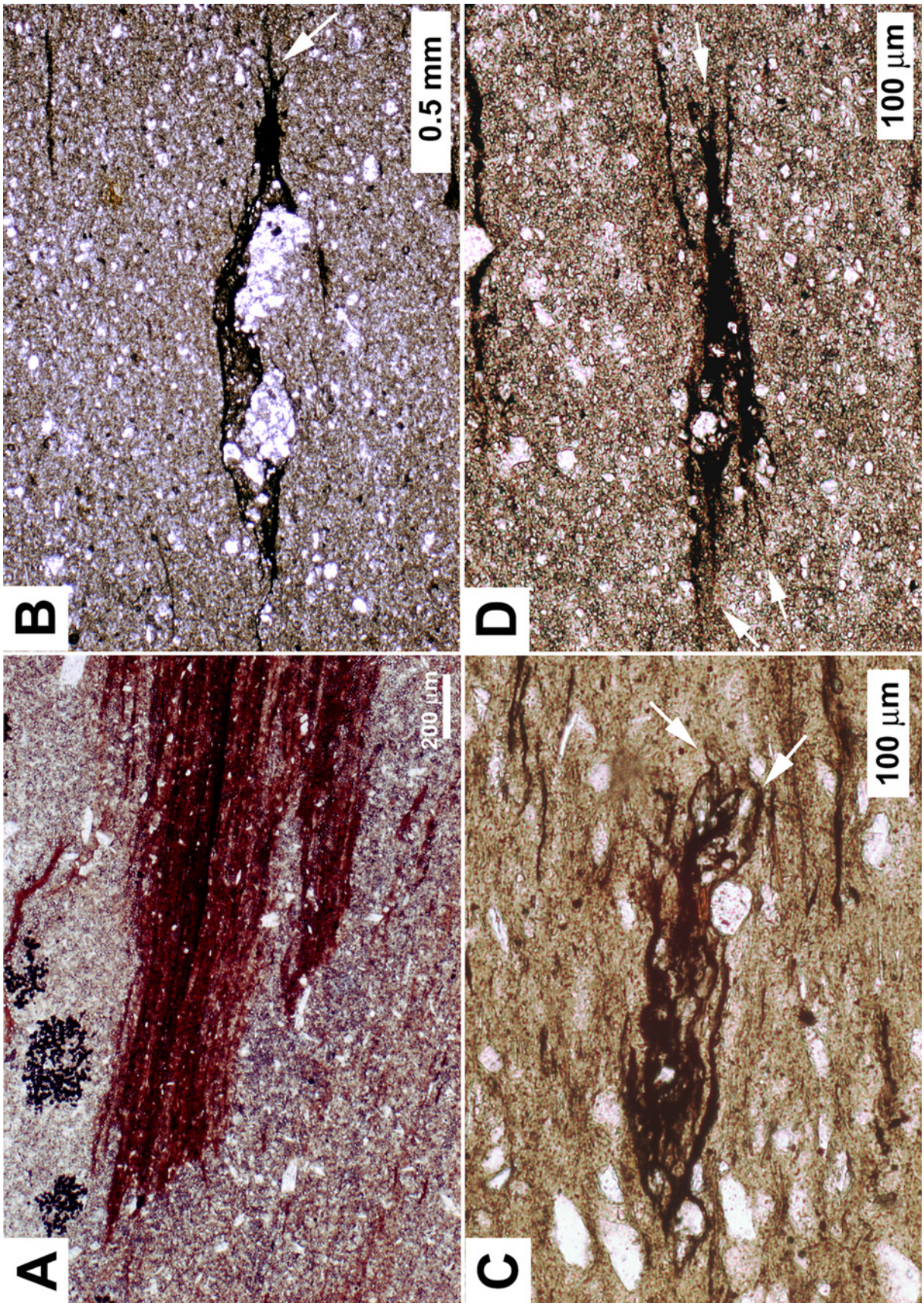

A
200 µm
B
0.5 mm
C
100 µm
D
100 µm

Figure 5-5: Torn and frayed edges of microbial mat fragments.
(A) Edge of carbonaceous fragment in oil shale of Green River Formation (Eocene of Wyoming). (B) Carbonaceous fragment with internal laminae and attached silt grains from Middle Proterozoic Somanpalli Group, India (see Chapter 7(c)). Frayed edge pointed out by arrow. (C) Carbonaceous fragment with internal laminae and frayed edge (arrows). Newland Formation of Belt Supergroup (Middle Proterozoic). (D) Carbonaceous fragment with attached silt grains and frayed edge (arrows). Rampur Shale of Middle Proterozoic Vindhyan Supergroup, India.

laminae due to mechanical deposition and those that owe their origin to *in situ* carbonate production in a microbial mat.

Given the right water chemistry, syngenetic carbonate precipitation in microbial mat laminae is a well known phenomenon (e.g., Thompson and Ferris, 1990; Pratt, 2001) and can occur in terrigenous clastic environments just as well as in carbonate dominated settings. In mudstones, one feature that might set apart microbially produced carbonate laminae from those related to allochthonous carbonate deposition could, for example, be diffuse lower and upper boundaries of carbonate-rich laminae (Figures 5-7A and -7B), suggesting *in situ* growth of carbonate grains rather than transport into a predominantly terrigenous clastic setting. The random orientation of mica flakes in such laminae (Figures 5-3D and -7B) is consistent with a scenario where currents transported micas across the mat surface and that these micas then were trapped in random orientation on a surface covered by a tangle of microbial filaments and EPS. Very early (pre-burial) cementation of these laminae probably preserved original orientation of the mica flakes. Cementation later in diagenetic history would have allowed for prior compaction and partial rotation of mica flakes into the horizontal (Figure 5-7C). Another textural feature that is consistent with an *in situ* cemented mat lamina and is hard to explain with deposition by lateral flow (gravity driven, storm and tidal currents, etc.) or vertical settling, is the presence of terrigenous grains 'floating' in a carbonate matrix, such as the already illustrated mica flakes and floating quartz grains (Figure 5-6D). Lateral transport is unlikely because carbonate mud, mica flakes, and quartz grains differ significantly in their hydrodynamic properties and would be segregated early on in any conceivable transport process. Deposition by settling through the water column would also have produced segregation of these three components into discrete laminae. Based on the sum of these considerations, interpreting the carbonate laminae in Mt. Shields mudstones as the *in situ* product of metabolic processes within a microbial mat is considered the most suitable interpretation because it is consistent with all the observed features.

FEATURES RELATED TO MAT DECAY AND DIAGENESIS

Gas development during decay of submerged mats may produce enough buoyancy to allow portions of a decaying mat to float to the surface and become an agent of grain rafting, in the same way as described above for desiccated mat fragments and photosynthesis-buoyed fragments. The result would be analogous clusters of coarser grains in a much finer matrix (Figure 5-6B). The caveats pointed out for desiccated and photosynthesis-buoyed fragments apply here as well.

Because mudstones tend to preserve organic matter, microbial mats may be preserved as beds of carbonaceous shale (see Chapter 7(b)). Formation of these beds through continued growth of microbial mats implies that earlier mat laminae become buried and undergo decay. Typically this decay occurs in an anaerobic environment and provides favourable conditions for the precipitation of 'anoxic' minerals, such as pyrite, siderite, and other ferroan carbonates. In marine settings sulphate reducing bacteria thrive in the sub-mat environment, produce hydrogen sulphide, and induce pyrite formation if soluble iron is available (Berner, 1984). In the Newland Formation of the Belt Supergroup, striped shales that consist of alternating carbonaceous layers (interpreted as benthic microbial mats) and silt/clay couplets (event deposits) can in places grade into a pyritic facies variant (Schieber, 1989a) where the carbonaceous microbial mat layers become increasingly pyritic (see Chapter 7(b)). Pyrite content ranges from carbonaceous laminae dusted with tiny pyrite grains (Schieber, 1989a) over moderately pyritic laminae with discontinuous wavy texture (Figures 5-6C and -6D) to strongly pyritic laminae that follow the original carbonaceous laminae and mimic their wavy anastomosing texture (Figures 5-8A and -8B). Thus, wavy anastomosing laminae that contain abundant fine crystalline pyrite (Figures 5-6 and -8) can also indicate former microbial mats in generally carbonaceous shales. They have been observed in the Newland Formation of the Belt Supergroup, in various pyritic striped shales in the Proterozoic of Australia (Schieber, 1989a; see Chapter 7(b)), and also in the Middle Proterozoic Bijaygarh Shale of the Vindhyan Supergroup in India (Figure 5-6D).

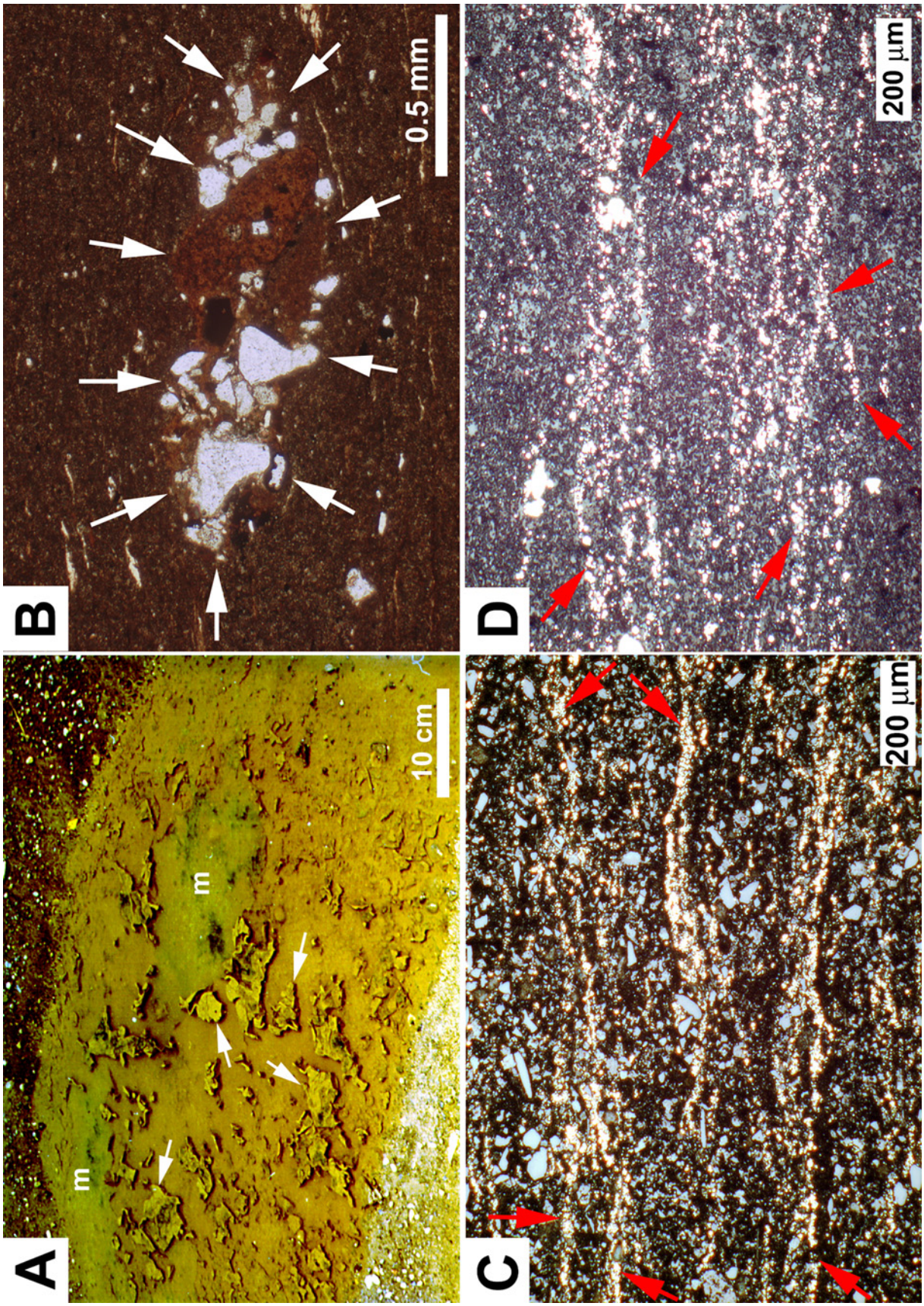

A
m
m
10 cm
B
0.5 mm
C
200 µm
D
200 µm

Figure 5-6:
(A) Modern puddle with benthic cyanobacterial mat on mud substrate (marked m). Portions of the mat have floated up (arrows) because of attached oxygen bubbles. These fragments can float and transport attached detrital grains. (B) Isolated cluster (marked by arrows) of sand- to silt-sized grains in a much finer mudstone matrix. Green River Formation, Eocene of Wyoming. (C) Wavy laminae of fine crystalline pyrite (red arrows) in carbonaceous beds of striped shale facies in the Newland Formation (Belt Supergroup, Middle Proterozoic of Montana). The pyrite enrichment coincides with carbonaceous laminae in wavy-crinkly laminated carbonaceous shale beds (Schieber, 1989). (D) Comparable pyritic laminae (red arrows) in carbonaceous shales from the Middle Proterozoic of India (Sur et al., 2006; Bijaygarh Shale, Vindhyan Supergroup).

The above illustrated pyritic laminae show on the one hand deformation by load casts (Figures 5-8B and -8C), but also evidence of early hardening through cementation by pyrite (see Chapter 7(b); Figure 5-5C). These observations suggest that the pyritic laminae were not pyritic from the start, and that pyrite formed at very shallow depth within the sediment. Because iron is very immobile in sediments with sulphidic pore waters (Berner, 1984), there is little chance that it could have been redistributed in the decay zone beneath the active mat. The fact that the pyrite distribution mimics the carbonaceous laminae indicates therefore that the iron distribution is a primary sedimentary feature and that an iron precursor, possibly floccules of iron hydroxide (Schieber, 1987, 1989a, 1995), was initially deposited on the growing mat surface. Later diagenetic effects may include further pyrite cementation between the original fine crystalline pyrite (Figure 5-8C), grain enlargement by overgrowth on original pyrite grains (Figure 5-8D), and formation of coarse crystalline pyrite nodules centred on earlier beds of fine crystalline pyrite (Strauss and Schieber, 1990).

CONCLUSION

The mudstone-hosted microbial mat features illustrated in this section do most likely not represent the full range of microbial mat features in mudstones. Mudstones comprise approximately two thirds of the sedimentary rock record, and only a small portion of them has been studied in any detail for their sedimentary features (Schieber, 1998a). Even fewer have been investigated for the potential presence of microbial mats. To make matters worse, there are few studies of modern muds where the effects of microbial mat colonisation have been adequately documented. Thus, as time goes by we can expect to witness the assembly of a substantially larger array of mat-related sedimentary features in mudstones than depicted here.

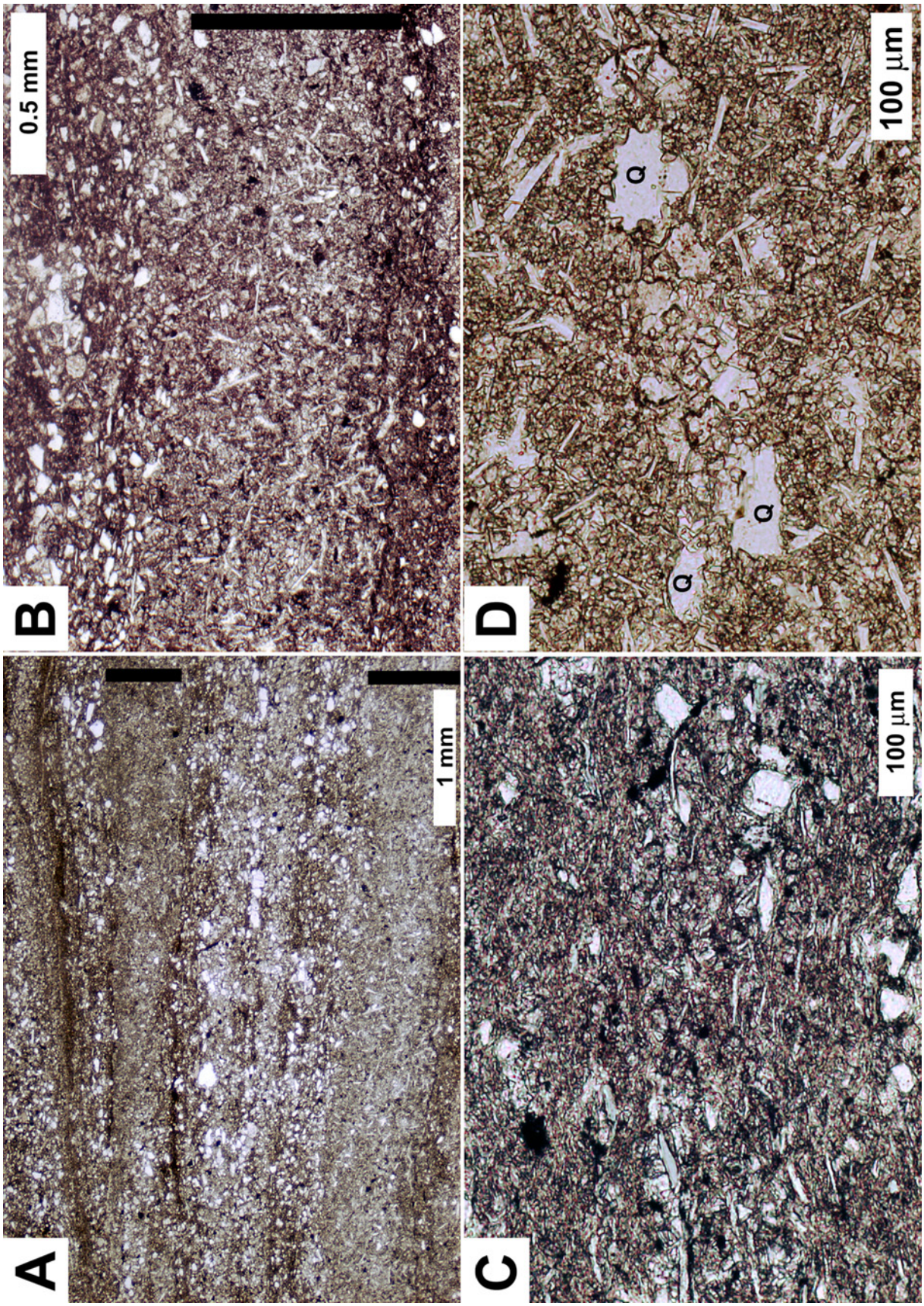

A
1 mm
B
0.5 mm
C
100 µm
D
100 µm
Q
Q
Q

Figure 5-7: Dolomitic laminae of probable microbial mat origin in mudstones and siltstones of the Mt. Shields Formation (Middle Proterozoic Belt Supergroup, Montana; see Chapter 7(b)).
(A) Laminae of fine crystalline dolomite with randomly oriented micas (marked with black bars) alternate with laminae that are dominated by clay and silt. (B) Close-up of dolomitic lamina (black bar) showing randomly oriented mica flakes. (C) Close-up of silt and clay dominated lamina. The mica flakes show preferred orientation parallel to bedding due to compaction of mud layer. (D) Floating grains of quartz (marked Q) and mica (flakes) in a fine crystalline matrix of dolomite.

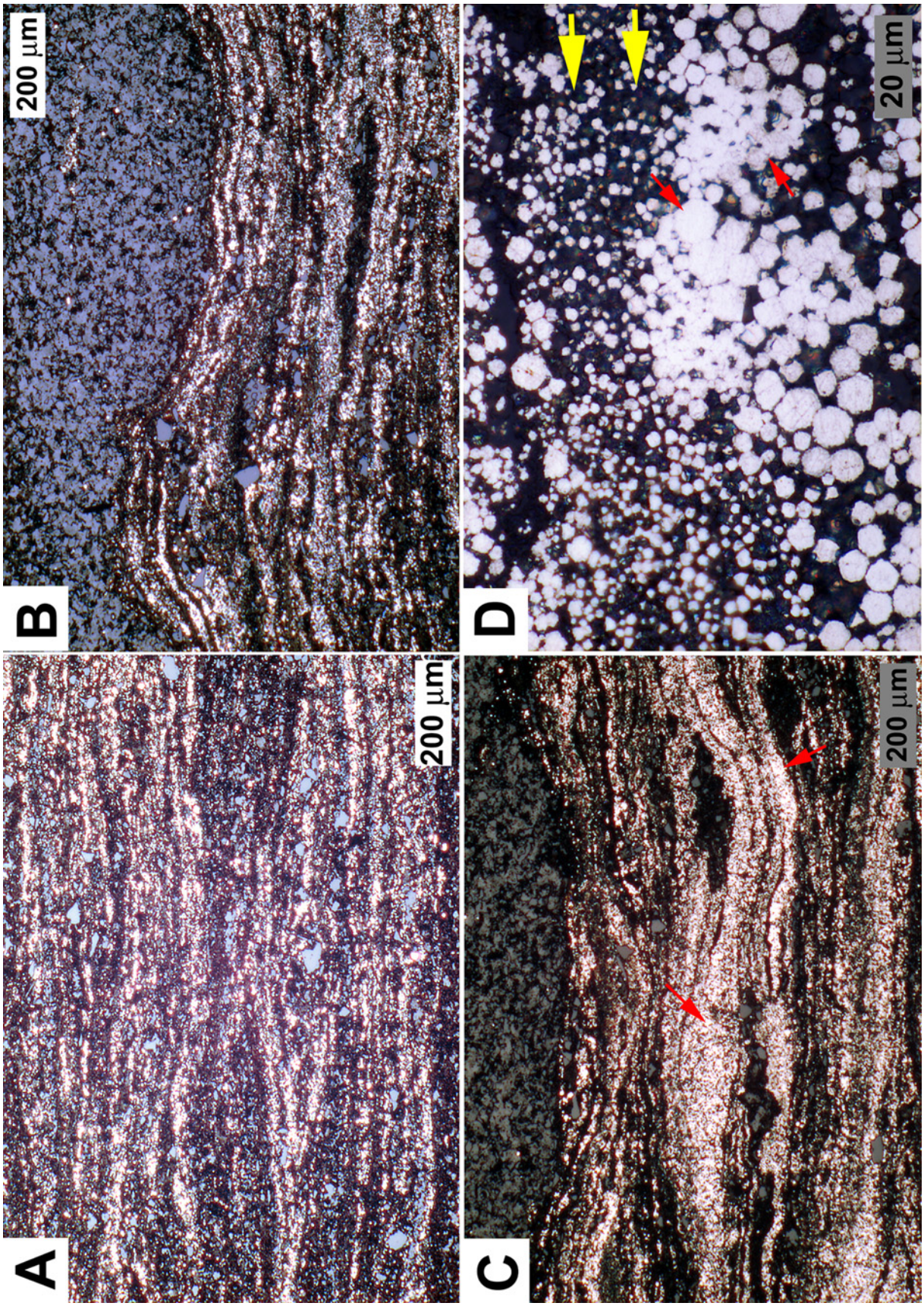

A
200 µm
B
200 µm
C
200 µm
D
20 µm

Figure 5-8: Images from pyritic striped shales in the Newland Formation, Belt Supergroup, Middle Proterozoic of Montana (see Chapter 7(b)).

(A) Wavy anastomosing laminae of fine crystalline pyrite in pyrite enriched bed. The pyritic laminae are also rich in organic matter. The texture is virtually identical to that observed in 'normal' carbonaceous shale beds of this facies that have been interpreted as benthic microbial mat deposits (Schieber, 1986). (B) An example of a wavy laminated pyritic bed that is overlain by a silt layer (event deposit). Note loading at the base of the silt layer. Deeper loading, such as pillow formation, was prevented by the cohesiveness of the mat-bound surface. (C) Another example of a wavy laminated pyritic bed with individual laminae that are more strongly pyritic. They contain a higher concentration of the same tiny pyrite grains that are found in laminae of A and B. Thickened portions of laminae (red arrows) show secondary pyrite cement between primary pyrite grains and thus resisted compaction. (D) Close-up of C. Shows typical lamina with tiny and probably primary micron-sized pyrite grains (yellow arrows) next to thickened lamina where impinging pyrite grains (red arrows) and grain enlargement by secondary overgrowth can be seen.

This page intentionally left blank

Atlas of Microbial Mat Features Preserved within the Siliciclastic Rock Record
Edited by J. Schieber et al.
© 2007 Elsevier B.V. All rights reserved
DOI: 10.1016/S1574-1966(07)02006-8

CHAPTER 6

Discussion of Some Problems: Unusual Features and the Importance of Terminology

INTRODUCTION

In all branches of science, terminology and the correct application thereof remains critical; the field of microbial mat features is no exception. In this chapter, two of the contributions (Sections 6(a) and 6(c)) examine terminology. In the former, the term 'wrinkle structure' is examined in great detail, as its usage over time has led to some confusion, and as it can easily be confused with several non-biogenic sedimentary structures. In the latter section, certain critical terms are defined and illustrated; although no attempt is made to provide a comprehensive glossary, these definitions should be useful to the non-specialist reader. In Section 6(b) some problematic features are illustrated, which have certain characteristics in common with known mat-related features, but whose genesis is often questionable, at the least.

6(a). 'WRINKLE STRUCTURES' – A CRITICAL REVIEW

H. Porada, E. Bouougri

Introduction

In this section, we critically review a variety of so-called 'wrinkle structures' in an attempt to help distinguish between crinkly decorations arising from physical processes that acted on siliciclastic bedding surfaces, and true microbially induced 'wrinkle structures'. The latter, however, are not easily differentiated from the numerous small-scale, crinkly irregularities on ancient bedding surfaces that originate from physical processes without participation of microbial communities, for instance: types of rill marks (e.g., Shrock, 1948; Reineck and Singh, 1980); swash marks (e.g., Reineck, 1956); foam and moving foam impressions (Häntzschel, 1935; Allen, 1966; Wunderlich, 1970; Reineck and Singh, 1980); adhesion warts and adhesion ripples ('antiripplets' after van Straaten, 1953; 'eolian microridges' after Hunter, 1969; see, e.g., Reineck, 1955; Kocurek and Fielder, 1982); rain impact ripples (e.g., Clifton, 1977; Reineck, 1984; Robb, 1992); and small-scale load structures (e.g., Allen, 1985). All these may occur, like microbially induced 'wrinkle structures', in the intertidal to lower supratidal zones. Furthermore, some current marks and fleur-de-lys patterns known from turbiditic successions (e.g., Dzulynski and Walton, 1965) as well as tectonically induced crenulations may develop similar appearances in response to physical processes.

Two types of small-scale, microbially induced sedimentary structures are prominent due to their distinct geometry and mode of occurrence: (1) 'elephant skin' (Runnegar and Fedonkin, 1992; Gehling, 1999) textures, characterised by reticulate patterns of sharp-crested ridges forming millimetre- to centimetre-scale polygons, occurring on argillite or argillaceous veneers above fine-grained sandstone and likely reflecting growth structures of microbial mats; (2) '*Kinneyia*' (Walcott, 1914) structures, characterised by millimetre-scale flat-topped, winding ridges and intervening troughs and pits, sometimes resembling small-scale interference ripples. '*Kinneyia*' structures usually occur on upper surfaces of siltstone/sandstone beds, themselves frequently event deposits, and are thought to have formed beneath microbial mats. Finally, some biogenic wrinkly structures resulting from tractional mat deformation or mat slumping are occasionally preserved. 'Wrinkle structures' occur more frequently in Proterozoic than in Phanerozoic siliciclastic rocks.

Historical review and discussion of terms

The term 'wrinkle marks' (Runzelmarken) was introduced by Häntzschel and Reineck (1968) to describe systems of straight or winding, flat-topped ridges, 0.5–1 mm wide and a few millimetres apart, which may run parallel or form honeycomb-like patterns with round or elongate pits between intervening ridges (see Figure 6(a)-1). Modern

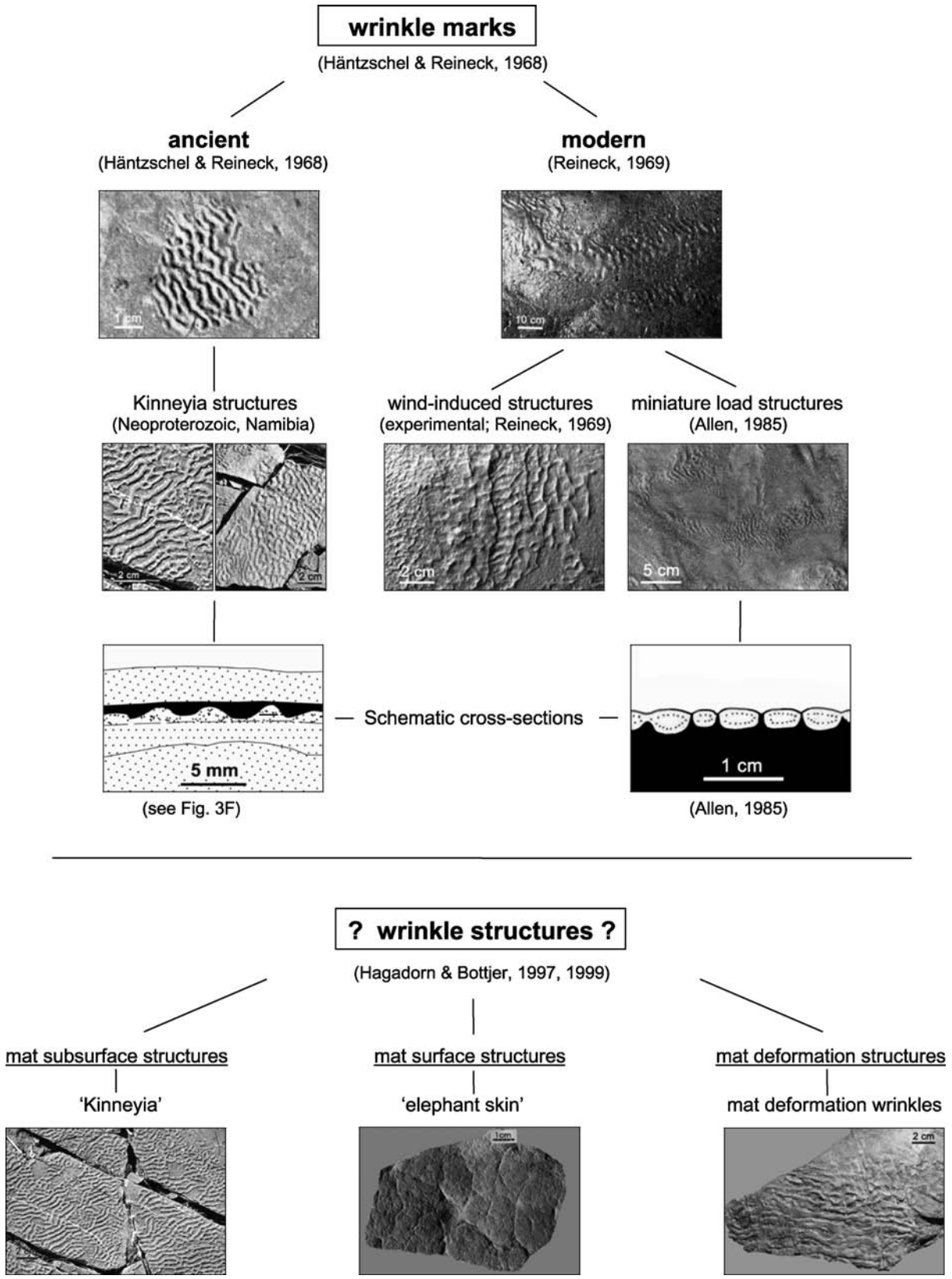


Figure 6(a)-1: Chart showing appearance and relationships of structures referred to as 'wrinkle marks' and 'wrinkle structures' in the historical context.

'Wrinkle structures' in the meaning of Hagadorn and Bottjer (1997, 1999) are suggested to represent mat surface structures, mat deformation structures, or mat subsurface structures, respectively.

structures identical to these have not been observed yet, but ancient examples are numerous. They have been described as '*Kinneyian* ripples' (Martinsson, 1965; Bloos, 1976), '*Kinneyia* structures' (e.g., Beukes, 1996) or briefly '*Kinneyia*' (Seilacher, 1982; Pflüger, 1999) and are grouped with 'wrinkle marks' since the publication of Reineck and Singh (1973). Based on the original structures presented by Häntzschel and Reineck (1968) and Reineck (1969), the term 'wrinkle marks' has a two-fold, divergent meaning. It refers to (1) *Kinneyia* structures likely resulting from microbial activities, and (2) structures of physical origin, likely miniature load structures (Allen, 1985). The two types of structures may show similar appearances on bedding surfaces, but differ distinctly in cross-section (see Figure 6(a)-1).

In 1997 (p. 1047) and 1999, Hagadorn and Bottjer distinguished between 'wrinkle marks' forming "elongate to honeycomb-shaped surface networks of sharp to round-crested ridges" (1999, p. 74) and '*Kinneyia* ripples' which "exhibit similar relief but have more parallel, typically flat-topped ridges" (1999, p. 74), and stated that both are "closely related sedimentary structures" which are "frequently confused for each other in the literature". Because both structures frequently "occur together and may represent preservational end-members of similar structures", they suggested to "refer to them collectively as wrinkle structures" resulting from microbial activities or representing mats (1997, p. 1047). However, the two types of 'wrinkle structures', as documented by Hagadorn and Bottjer (1997) in their Figure 1A–F, may all be described as variations of *Kinneyia*, when compared with examples presented by Pflüger (1999, his Figure 1A–C) and Bloos (1976, his Plate 9, Figures 1–4). Also, it is observed that on larger, *Kinneyia*-carrying bedding surfaces, the two types grade into each other (see Figure 6(a)-4E). On this basis, the term 'wrinkle structures' would be synonymous with the original term 'wrinkle marks', as introduced by Häntzschel and Reineck (1968), and with '*Kinneyian* ripples', as described by Martinsson (1965). In other words, Hagadorn and Bottjer's (1997, 1999) 'wrinkle structures' are indeed *Kinneyia*.

Subsequently, Hagadorn and Bottjer (1999, p. 74) stated that 'wrinkle structures' such as *Kinneyia* are "likely formed beneath buried microbial mats", whereas 'wrinkle structures discussed in their 1999 study "largely reflect original surface features". They described from modern mats, freshly formed in supratidal pools "immediately after they were flooded by a storm-induced high tide", small-scale linear growth patterns produced by vertically oriented cyanobacterial filaments on the mat surface, and suggested that these structures are the modern equivalents of ancient 'wrinkle structures'. Hagadorn and Bottjer (1999) thus grouped together *Kinneyia*-type 'wrinkle structures', formed beneath mats, and some other 'wrinkle structures' reflecting growth patterns on mat surfaces. But, as in their 1997 paper, examples shown in their Figure 1 may throughout be described as variations of *Kinneyia*.

Microbially induced wrinkle structures

From the historical review it becomes apparent that the term 'wrinkle structure' in its present use is not meaningful, if genetical aspects are addressed in detail. The term is historically cumbered due to its similarity with 'wrinkle marks' which has been applied to both biologically and physically induced structures. It is therefore suggested here, to use the term 'wrinkle structure' only if microbial participation is likely but a clear classification not possible. Otherwise, use of the well introduced terms '*Kinneyia*' and 'elephant skin' is recommended here (see Figure 6(a)-1).

Identification of microbially induced 'wrinkle structures' should be based on the following criteria: (a) the structures should occur in association with other mat-related structures, e.g., spindle-shaped cracks, 'sand chips'; (b) their origin on an upper bedding surface or on a sedimentary surface beneath a microbial mat should be possible; (c) their formation by localised growth of mat-forming microbes or mat expansion, or by physical deformation of epibenthic mats should be possible; (d) the structures should possess specific geometries and a size in the millimetre-range.

It is not intended here to explain ancient 'wrinkle structures' by a range of possible genetic processes acting on microbial mats. Instead, small-scale structures observed on modern mats will be described and possible ancient equivalents will be shown. This approach is not sustainable, however, for '*Kinneyia*' structures, which have not been observed in modern mats yet. With a view to the life and burial history of modern microbial mats, 'wrinkle structures' may reflect morphological surface and subsurface features, mat deformation patterns, or be structures arising from subsurface processes, e.g., gas trapping, dewatering, or liquefaction.

Structures reflecting mat surface morphologies

Reticulate growth pattern and 'elephant-skin' A specific type of modern mat surface structure that occurs rather frequently and in successive mat layers repeatedly, is related to mat growth and bacterial reaction to environmental stresses (Gerdes et al., 2000a). It is characterised by a reticulate pattern of bacterial bulges and tufts, in which the bulges tend to form polygonal networks with tufts or pinnacles in junctional positions (Figure 6(a)-2A). The bulges are 2–3 mm high and sharp-crested when fresh; the polygons are of varying size, ranging in diameter from less than 1 cm to more than 3 cm. Inside completed polygons, new tufts and radiating bulges may form, thus subdividing larger polygons into smaller units. At an advanced stage, diameters of the polygons may be less than 0.5 cm.

For the formation of the pattern, Gerdes et al. (2000a, p. 285) suggested that, "if the surface cover [mat] becomes too thick, or light conditions change because of increasing water cover after intermittent exposure", specific filamentous bacteria (*Microcoleus chthonoplastes, Lyngbya aestuarii*) phototactically respond by reorienting filaments upwards or by moving cell aggregates upwards and accumulating on the surface. According to Gerdes et al. (2000a), it is particularly *Lyngbya aestuarii* that forms elongated bulges, which are stabilised by EPS (extracellular polymer substances) produced by succeeding coccoidal cyanobacteria.

An ancient structure that shows striking similarity with the reticulate growth patterns in modern mats is named 'old-elephant-skin texture' (Runnegar and Fedonkin, 1992) or briefly 'elephant skin' (Gehling, 1999) (Figure 6(a)-2B). It has been described mainly from Vendian shallow-marine siliciclastic deposits (e.g., Runnegar and Fedonkin, 1992; Gehling, 1999, 2000; Steiner and Reitner, 2001) and rarely from older successions (Prave, 2002, his Figure 2A). The structure is characterised by 1–2 mm high, sharp-crested ridges on upper bedding surfaces, or respective impressions on lower bedding surfaces, forming irregular polygonal networks with a width of mesh of 0.5–1 cm. This faint, but geometrically distinct network clearly distinguishes 'elephant skin' from other 'wrinkle structures', which usually exhibit a certain linearity.

Linear patterns Mat growth structures consisting of subparallel, linear ridges with exposed bacterial filaments at ridge crests, have been described by Hagadorn and Bottjer (1997, 1999) from a freshly flooded supratidal pool at Redfish Bay (Texas). In this example, intercrest distances are between 0.5 and 1 cm and individual ridges may extend for tens of centimetres. Similar structures, though on a slightly larger scale, have been observed by the authors along the margin of an evaporating supratidal pool at Bhar Alouane tidal flats in southern Tunisia (Figure 6(a)-2C). The structures, dominated by linear ridges of bacterial filaments but partly also showing the typical reticulate growth pattern, are oriented about perpendicular to the water limit and appear more and more desiccated with increasing distance from the water, likely corresponding to the duration of subaerial exposure. At some distance from the pool, a pattern of sub-parallel, shallow and narrow, occasionally bifurcating, sharp-crested ridges remains (Figure 6(a)-2D). The straight to irregular ridges are developed at distances of 1–2 cm and are locally interrupted or reduced to faint lines on the flat mat surface. It appears that, with persisting subaerial exposure, the filamentous ridges develop distinctly sharp-crested shapes and a smooth and rigid surface, and are incorporated in stepwise fashion into the mat, the structure thus being a transient feature reflecting transitional conditions. It has to be mentioned that similar structures have been considered to result from deformation of a mobilised microbial slime-sediment sludge on slightly inclined slopes, or from microbial overgrowth of faint surface ridges (G. Gerdes, Chapter 2; personal comm., 2006). Strong arguments in favour of a microbial growth origin, however, would be provided by transitions between typical reticulate and linear patterns, and by a similar geometry of the ridges in all the transitional stages.

Some ancient structures observed on flat bedding surfaces of siltstone layers within Neoproterozoic intertidal successions of Zambia and Namibia (Figure 6(a)-2E) strongly resemble the linear pattern described above. Similar structures previously interpreted as wind-induced 'wrinkle marks' by Robb (1992), and exhibiting sharp-crested ridges with transitions from linear to reticulate patterns, may be of similar origin. As with 'elephant skin', linear ancient mat growth structures have in common that they consist of narrow, sharp-crested ridges on upper bedding surfaces. Due to the transient nature of the original structure, a wide range from continuous ridges to relict short ridges may be preserved.

Another mat surface structure characterised by parallel, discontinuous, sharp-crested ridges at a few millimetres distance from each other has been observed on the steep slope of a tidal channel at Sabkhat El Grine, southern Tunisia (Figure 6(a)-2F). The ridges run along the irregular sloping surface like contour lines and are not developed on less inclined parts. This indicates that slow downslope creeping of the mat may have been involved in their formation, whereas the sharp-crested geometry of the ridges would agree with microbial growth structures as

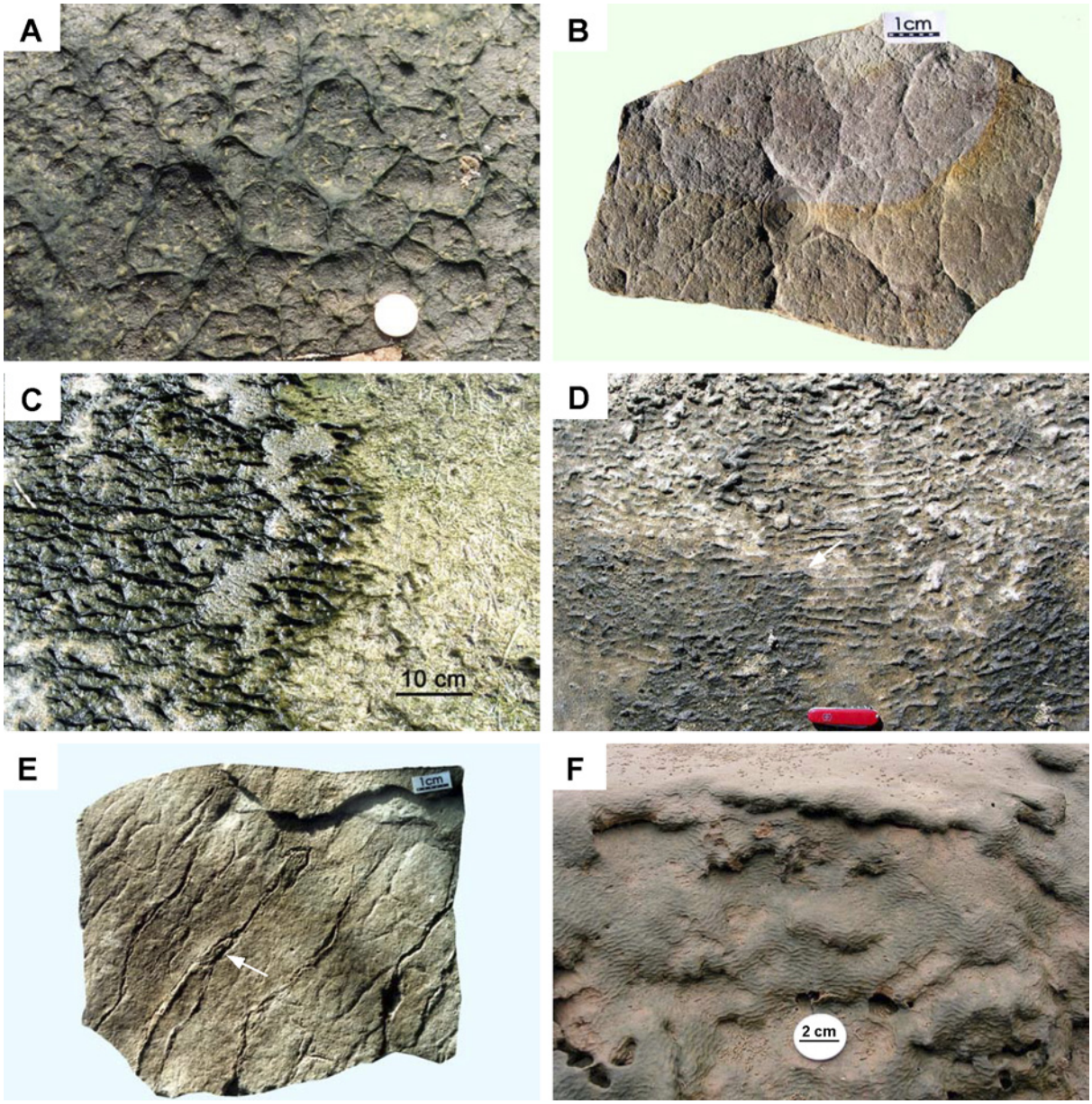


Figure 6(a)-2: Mat surface structures.

(A) Modern mat surface exhibiting reticulate growth pattern produced by sharp-crested bulges and pinnacles in junctional positions. Pinnacles result from "induced polarity changes of filamentous cyanobacteria", whereas "bulges are produced by *Lyngbya aestuarii*" (Gerdes et al., 2000a, p. 284). Coin is 20 mm in diameter. Supratidal pond, Bhar Alouane tidal flats, southern Tunisia. (B) 'Elephant skin' texture on lower bedding surface of fine-grained sandstone bed. Note Ediacara-type fossil of *Irridinites multiradiatus* near centre of sample. Upper Neoproterozoic Penaga Formation, East Archangelsk, Russia. (C) Modern mat developing more linear growth patterns along margin of evaporating supratidal pool (right part of photo). Note individual bulges may be more than 20 cm in length. Bhar Alouane tidal flats, southern Tunisia. (D) Linear growth pattern on modern mat after subaerial exposure and drying up of the mat surface. Arrow indicates structural detail to compare with similar structure observed in Figure 6(a)-2E. Bhar Alouane tidal flats, southern Tunisia. (E) System of linear to slightly curved shallow ridges (partly destroyed by weathering), developed on upper surface of thinly bedded, fine-grained quartzite. The structure is considered to represent linear growth features of a previous microbial mat. Note sub-circular to elliptic structures (upper left and right side) partly resembling 'elephant skin'. Arrow indicates structural detail as observed on modern example shown in Figure 6(a)-2D. 'Ore formation', Roan Group, Katanga Supergroup; Mindola open pit mine, copperbelt of Zambia. (F) Linear surface pattern developed on thin microbial mat covering the steeply inclined slope of a tidal channel. The pattern consists of small, discontinuous, sub-parallel, sharp-crested ridges, arranged like contour-lines at distances of a few millimetres from each other. Note that the pattern is not developed on flat portions of the slope. Sabkhat El Grine, southern Tunisia.

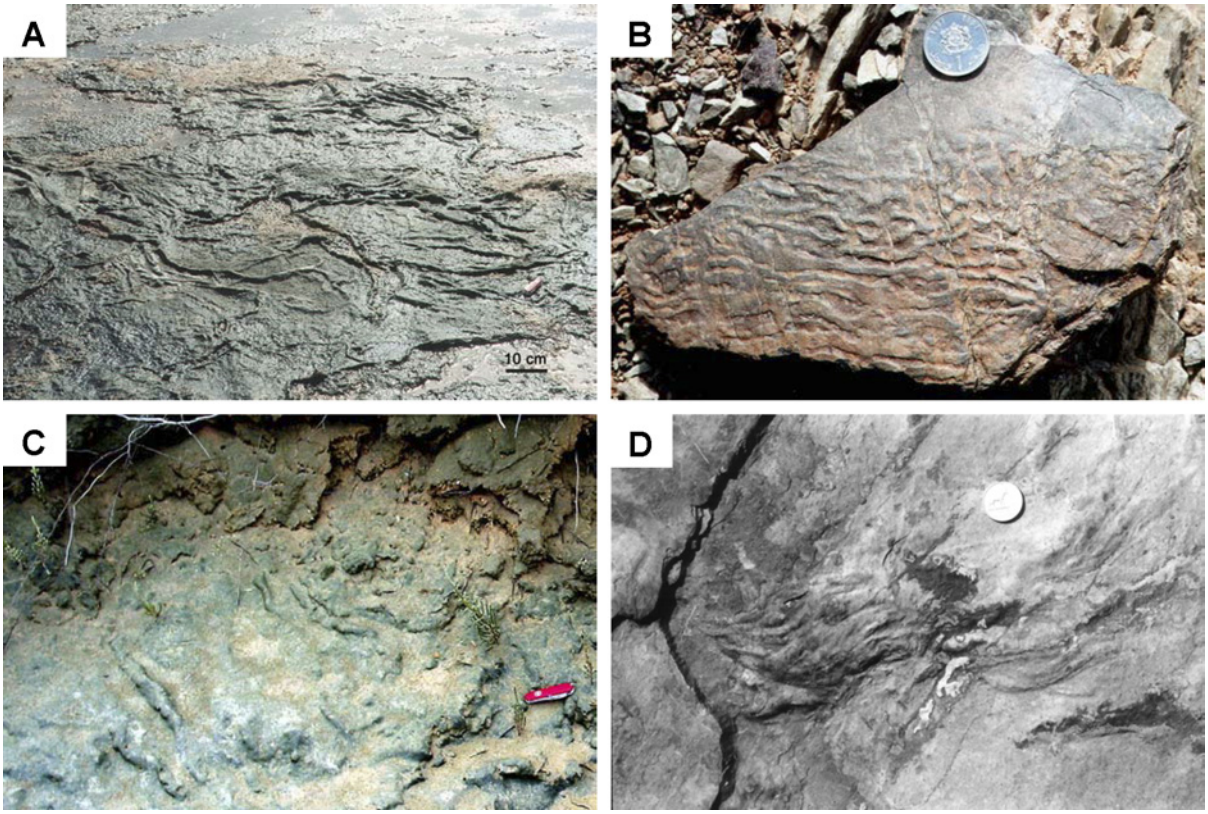


Figure 6(a)-3: Structures related to mat deformation in general.
(A) Detached and floating mat, torn and strongly folded by tractional wind or wind-induced waves. Coastal sabkha, ca. 10 km south of Skhira, southern Tunisia. (B) Wrinkle structure resulting from mat deformation. Belts of continuous, broad and flat-topped crests (lower part of photo) grade into shorter, more irregular and round-topped crests (centre) and eventually disappear (upper part). The structure is considered to result from crumpling of a disrupted and marginally detached mat. Direction of movement is towards upper part of photo. Wanimzi Formation, Neoproterozoic Tizi n-Taghatine Group, Anti-Atlas, Morocco. Coin is 24 mm in diameter. (C) Mat slump structures developed on the steep slope of a tidal channel. Sabkha El Gourine, southern Tunisia. Scale (knife) is 8 cm. (D) Mat slump structure in laminated siltstone/argillite of the Neoproterozoic 'Ore formation', Roan Group, Katanga Supergroup; Mindola open pit mine, copperbelt of Zambia. Coin is 21 mm in diameter.

described above. The structures may thus be considered as transitional between mat growth and mat deformation features.

Structures related to mat deformation in general Active microbial mats forming cohesive to leathery surface layers on fine-grained siliciclastic sediments, usually resist low-energy wave action in the upper intertidal to lower supratidal zones. At higher wave energy during spring tides or storms, however, they may undergo deformation, become locally detached and crumpled or may be torn into pieces and eventually eroded. Thin mats, desiccated to some extent, may undergo partial floatation after renewed flooding (Cameron et al., 1985) and also be intensely deformed, if still cohesive and plastic (Figure 6(a)-2E). In shallow pools, thin microbial mats may "behave like the 'skin' on top of a pudding" (Hagadorn and Bottjer, 1999, p. 76) and become deformed by strong winds driving the water (Singh and Wunderlich, 1978). Finally, down-slope gliding may lead to local slumping and folding. In all these cases, a cohesive surface layer (mat or biofilm) is deformed by tractional or gravitational forces. Usually, resulting folding and crumpling of the mat is on a decimetre-scale with fold amplitudes up to several centimetres (see Figure 6(a)-3A). Such structures do not meet the definition of 'wrinkle structures' which are on a millimetre-scale, but may rather be referred to as 'petees' in the original definition of Gavish et al. (1985). Very thin mats, however, may develop small-scale deformation features in the range of typical 'wrinkle structures', and there may be transitions between the various scales. It is thus not possible to draw a clear-cut borderline between 'deformation wrinkles' and larger linear structures related to mat deformation. Nevertheless, some 'wrinkle'-sized structures thought to have resulted from mat deformation will be discussed briefly.

Wrinkle structures resulting from mat deformation Small-scale, wrinkle-like mat deformation structures are scarcely documented from modern mats (e.g., Hagadorn and Bottjer, 1999) and only a few examples have been reported from the geological record (Singh and Wunderlich, 1978; Clemmey, 1978; Kopaska-Merkel and Grannis, 1990; Seilacher, 1999; Bouougri and Porada, 2002). Commonly, the structures are developed on fine-grained sandstone or siltstone and exhibit subparallel, slightly curved, continuous crests and troughs (Figure 6(a)-3B). Height of individual crests usually ranges from 1 to 2 mm, spacing from 5 to 10 mm, and length from 1 to 10 cm. The crests typically are asymmetric, the steeper sides facing in a common direction considered to be the direction of unidirectional stress (e.g., tractional current or wind). As a further common feature, the crests tend to fade out sideways and in the direction of shear stress. Altogether, the structures resemble miniature, arcuate fold-thrust belts.

Mat slump structures 'Mat slump structures' may be highly variable in shape and size but are basically characterised by irregularly folded bulges on otherwise smooth bedding surfaces (Figures 6(a)-3C, -3D). Impressive examples of 'mat slump structures' have been documented by Bernier et al. (1971) who described 'crescentic wavy structures' with crest heights of a few millimetres and spacings from 2–3 cm to more than 10 cm, developed on a bedding surface of Jurassic micritic limestone. They attributed the structures, which partly resemble 'wrinkle structures', to downslope gliding of a detached microbial mat.

'Mat slump structures' are not necessarily restricted to the uppermost cohesive layer of a mat, but may involve stacks of intercalated sand and microbial mat layers ('biolaminites' after Gerdes and Krumbein, 1987) which together undergo deformation. Within a biolaminite succession they may be bound to specific horizons. Millimetre- to centimetre-scale recumbent and overfold structures of thin carbonaceous laminae, reported by Simonson and Carney (1999) from Late Archaean lutites and by Schieber (1986, 1998a, 1999) from Mesoproterozoic interlaminated silt and mud deposits, may be examples of 'mat slump structures' within biolaminites. In both these cases, the structures have been related to penecontemporaneous deformation of cohesive, epibenthic microbial mats.

Structures suspected to have formed beneath microbial mats Two groups of structures developed in the sediment beneath or in the less cohesive underpart of microbial mats are distinguished: (1) 'subsurface structures' likely reflecting morphological details of the microbial mat, imprinted on the underlying sediment or sediment-rich lower part of the mat; (2) '*Kinneyia*' structures possibly produced by gas trapping below a sealing mat.

Subsurface structures During periods of subaerial exposure and increasing shortage of ground and surface water, microbial mats may desiccate and shrink, due to loss of water mainly bound in EPS (Decho, 1990; Dade et al., 1990; Krumbein et al., 1994; Neu, 1994). At a certain stage, the mat may crack and lose contact with its substratum, and may partially be removed by wind action. The exposed subsurface may then exhibit an irregular morphology dominated by rounded to elongate bulges, 3–10 mm in size, and intervening depressions (Figure 6(a)-4A). The preservation potential of exposed subsurface structures is considered low, but increases if the exposed surface is soon stabilised by microbes and overgrown by new cyanobacterial layers.

Figure 6(a)-4B shows patches of suspect subsurface structures consisting of small-scale, subrounded to elongate bulges, preserved on an upper bedding surface of fine-grained quartzite. The structures occur in a Neoproterozoic intertidal succession of quartzite/siltstone and argillite that hosts a range of microbially induced sedimentary structures, like 'elephant skin', circular cracks, and *Kinneyia* (see Bouougri and Porada, 2002). Similar structures with irregular, elongate, millimetre-size bulges have been documented from Cambro-Ordovician quartz arenites by Hilowle et al. (2000, their Figure 2) who suggested that they "record the subsurface morphology of a subsequently degraded microbial mat". Also, a structure characterised by millimetre-scale round bulges and referred to as 'transparent wrinkles' (Noffke et al., 2002, their Figure 7B) may be of a similar origin.

Kinneyia structures '*Kinneyia*' is the most typical, most frequent and genetically most problematic 'wrinkle structure'. It is characterised by sinuously curved, frequently bifurcating, flat-topped crests, usually 1 mm high and 1–2 mm wide, which are separated by parallel, round-bottomed depressions (Figures 6(a)-4C, -4E). The usually steep-sided crests may run parallel or form honeycomb-like patterns, sometimes with lateral transitions between the two shapes on the same surface (Figure 6(a)-4E). The depressions frequently show winding trends with 'neckings' (localised pinch-outs), but may be reduced to isolated, round or elongate pits. Intercrest distances vary between 2 mm and almost 10 mm in different occurrences, but are rather constant on the same bedding plane. The varying proportions of winding troughs vs. isolated pits, together with interference features of crests bring about a wide range of shapes with distinctly linear and distinctly pitted end-members. Further variations may result from weathering, by which crests gradually lose their steep-sided and flat-topped geometry and attain more rounded shapes.

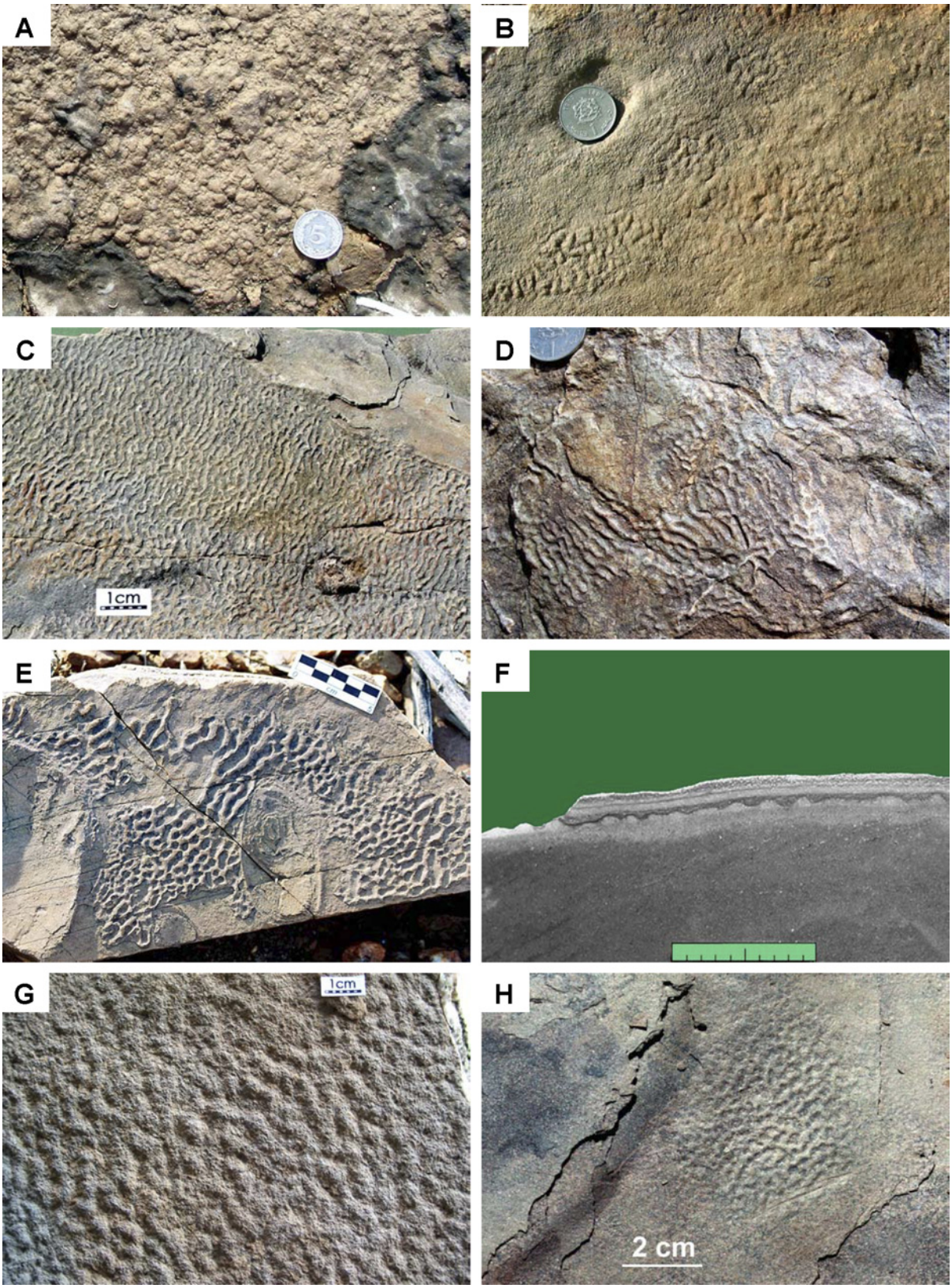


Figure 6(a)-4: Mat subsurface structures, load structures, adhesion structures.
(A) Morphological features of mat subsurface, subaerially exposed after removal of desiccated mat by wind action. Note round to elongate bulges, 3–10 mm in size. Tidal flats of Bahar Alouane, southern Tunisia. Coin is 24 mm in diameter. (B) Patches of elongate to irregular bulges on upper surface of fine-grained sandstone. The structures are considered to reflect subsurface morphological features developed beneath a microbial mat and biostabilised at subaerial exposure after removal of the mat. Wanimzi Formation, Neoproterozoic Tizi n-Taghatine

Group, Anti-Atlas, Morocco. Coin is 24 mm in diameter. (C) '*Kinneyia*' structure with long, flat-topped, winding crests developed on the flat upper surface of a siltstone layer (event deposit). Intercrest distances: 1.5–2 mm. Middle Cambrian *Paradoxissimus* Siltstone; Äleklinta, Oeland, Sweden (type locality of '*Kinneyian* ripples' of Martinsson, 1965). (D) Patchy development of '*Kinneyia*' with long winding crests on upper surface of fine-grained sandstone. Intercrest distances: 2–3 mm. Note that crests partly are round-crested, due to weathering. Wanimzi Formation, Neoproterozoic Tizi n-Taghatine Group, Anti-Atlas, Morocco. Coin is 24 mm in diameter. (E) '*Kinneyia*' structure showing transition from more linear to honeycomb-like arrangement of flat-topped crests and intervening elongate to round pits, developed on the flat upper surface of a fine-grained sandstone layer (storm deposit). Neoproterozoic Vingerbreek Member, Nudaus Formation, Nama Group; Farm Haruchas, Namibia. Scale is 5 cm. (F) Section across '*Kinneyia*' crests and troughs developed on top of an event deposit and overlain by silty argillite (dark) and layers of siltstone (lighter colours). '*Kinneyia*' has developed in a thin flat layer that discordantly overlies the event deposit characterised by oblique foreset lamination. The silty argillite which fills and covers '*Kinneyia*n' troughs and crests is considered to represent previous microbial mats. Note flat lower surface of siltstone layer above silty argillite, excluding loading as a process of '*Kinneyia*' formation. Middle Cambrian *Paradoxissimus* Siltstone; Äleklinta, Oeland, Sweden. Scale is 10 mm. (G) Lower bedding surface with small-scale load structures forming miniature, subcircular to elongate bulges. Lower Jurassic (Hettangian); Helmstedt, Lower Saxony, Germany. (H) Upper surface of wave-rippled fine-grained sandstone with a patch of crinkly structures. The structures are considered to have formed by adhesion of wind-blown sand grains to the still wet surface in a shallow depression. Note that structures fade out towards the margins. Upper Neoproterozoic (Vendian) Cerro Negro Formation; Cerro Negro Quarry, Tandilia System, Argentina.

According to reports in the literature (e.g., Martinsson, 1965; Häntzschel and Reineck, 1968; Bouougri and Porada, 2002; Noffke et al., 2002) and observations by the authors in Morocco and Namibia, *Kinneyia* structures preferentially (or exclusively?) occur on flat upper surfaces of fine-grained event layers, deposited in the intertidal to shallow subtidal zones. A section across *Kinneyia* (Figure 6(a)-4F; see also Bloos, 1976) reveals that the structure is developed in a millimetre-thick layer, which discordantly overlies the truncated foreset lamination of an event deposit. *Kinneyian* troughs and ripples are overlain by dark, fine-grained sediment, usually silty argillite which typically includes carbonaceous laminae and isolated silt-sized grains and which has been considered to represent former microbial mats (e.g., Noffke et al., 2002, 2003b; Bouougri and Porada, 2002). The occurrence of filamentous microstructures resembling trichomes of modern cyanobacteria, as reported by Noffke et al. (2003a) from similar layers above *Kinneyia*, corroborate this interpretation. These observations suggest that *Kinneyia* structures form beneath cohesive microbial mats and likely do not represent the microbial mat itself.

Kinneyia structures have frequently been documented in the literature and almost just as often been interpreted in different ways (e.g., Quenstedt, 1858; Geinitz, 1863; Shrock, 1948; McKee, 1954; Allen, 1966; Hunter, 1969; Kummel and Teichert, 1970; Wunderlich, 1970; Goldring, 1971; Bloos, 1976; Reineck and Singh, 1980; Seilacher, 1982; Seilacher and Aigner, 1991). They have been considered as small-scale interference ripples, rain impact ripples, or adhesion ripples and other wind-induced surface patterns. None of these interpretations is sustainable, as the steep to sometimes vertical slopes of '*Kinneyia*' ripples are unlikely to have formed at the sediment/water or sediment/air interface. Consequently, Seilacher and Aigner (1991) considered '*Kinneyia*' to be a post-burial, intrasedimentary structure, whereas Pflüger (1999) proposed that it results from gas trapping beneath sealing microbial mats. The interpretation of '*Kinneyia*' as a load structure (Noffke et al., 2002, 2003a) appears unlikely, as siltstone layers overlying '*Kinneyia*'–microbial mat doublets (see Figure 6(a)-4F) do not exhibit the typical downward protrusions but instead exhibit flat lower surfaces.

Non-biogenic structures that may be mistaken for '*Kinneyia*' are mainly small-scale load structures, partly formed in the presence of soft microbial mat layers which are deformed under load pressure, but also adhesion ripples and other wind-induced structures may develop similar shapes and patterns.

Small-scale load structures (Figure 6(a)-4G) may develop on lower bedding surfaces of thin sand/silt layers overlying mudstone/argillite. A range of patterns resulting from loading has been documented by Allen (1985) from modern intertidal sediments in which they formed without participation of microbial mats. Some of them bear amazing resemblance to *Kinneyia* structures. In section, load structures are distinguished from *Kinneyia* in that they overlie mudstone/argillite, whereas *Kinneyia* invariably is developed at the top of sandstone/siltstone beds and is overlain by argillite. Ancient small-scale load structures are characterised by circular to elongate, round-crested bulges, separated by comparatively narrow depressions, on lower bedding surfaces. They have rarely been

addressed as load structures in ancient sedimentary rocks, but rather as unexplained 'runzelmarken' or 'wrinkle marks'.

Adhesion ripples form when dry, wind-blown sand grains adhere to a wet or moist surface. The resulting structure consists of a series of winding, asymmetric ridges, ca. 2 mm high and 5 mm wide, at distances of ca. 1 cm (see also Reineck, 1955; Hunter, 1969; Kocurek and Fielder, 1982 and further references therein). Though a general linear trend is recognised, the ridges usually are oriented in various directions and partly overlap thus inducing rather irregular patterns, in detail (Figure 6(a)-4H). The preservation potential of adhesion ripples is considered low and ancient examples have only rarely been described (e.g., Kocurek and Fielder, 1982). Examples documented by Hunter (1969, his Figure 4) and Goldring (1971, his Plate 3c) are here interpreted as *Kinneyia* structures.

Discussion and conclusions

In a wide range of small-scale crinkly structures occurring on ancient bedding surfaces, 'wrinkle structures', following Hagadorn and Bottjer (1997, 1999), are defined as forming a specific group developed in close relationship to microbial mats. Consequently, other structures of similar size and appearance but suspected to be non-biogenic in origin do not fall into this group, and it is suggested here that these are named according to their specific origins (e.g., small-scale load structures, adhesion ripples, etc.).

The identification of 'wrinkle structures' in ancient siliciclastic successions may give valuable information about the depositional environment and facies. Thus, if compared with the distribution of modern microbial mats, 'wrinkle structures' may indicate deposition in intertidal to lower supratidal zones, e.g., on low-gradient tidal flats with occasional deposition of event layers. Assuming such environments, 'wrinkle structures' may occur in heterolithic successions of laminated siltstone/argillite and intercalated siltstone/sandstone beds. Indeed, many wrinkle structures have been described from just such successions (e.g., Martinsson, 1965; Häntzschel and Reineck, 1968; Bouougri and Porada, 2002; Noffke et al., 2002; 2003a).

In analogy to modern mats, it may furthermore be expected that 'wrinkle structures' occur in association with a set of other microbially induced structures, all together being components of a 'microbial mat facies'. As documented and discussed in the literature (e.g., Pflüger and Gresse, 1996; Pflüger, 1999; Porada and Löffler, 2000; Bouougri and Porada, 2002), fillings of short spindle-shaped cracks, longer curved cracks, and sinuous to circular cracks, frequently combined in unusual networks, as well as 'sand chips' may form part of the association. The significance of wrinkle structures clearly increases if some of these associated structures are additionally observed.

Within the group of 'wrinkle structures', two types are well defined and easily identified, due to their specific geometry and mode of occurrence, respectively. The one is known as 'elephant skin', reflects mat growth patterns, and occurs frequently on argillaceous siltstone or silty argillite bedding surfaces, sometimes together with numerous small flakes of detrital muscovite, which adhered to the sticky surface of the previous mat. The structure is characterised by sharp-crested ridges, up to 1 mm high, which typically are combined in a reticulate pattern forming networks with polygons, 0.5–1 cm wide (Figure 6(a)-2B). However, there may be transitions to incomplete networks and to more linear ridges running parallel to each other and at about 1 cm distance.

The other well defined type is '*Kinneyia*' which likely formed underneath microbial mats and usually is preserved on flat upper surfaces of siltstone or sandstone beds, mostly being event deposits. It is the classical and likely most frequent 'wrinkle structure' and has been documented from the Archaean to the Jurassic (e.g., Häntzschel and Reineck, 1968; Bloos, 1976; Noffke et al., 2003a). The structure resembles millimetre-scale interference ripples with all transitions from crest-dominated linear shapes to pit-dominated honeycomb-like patterns (see Figures 6(a)-4C, -4E). Characteristic features are the flat tops and steep sides of the ripple crests. Although quite distinctive when observed closely, some small-scale load structures, adhesion ripples and other wind-induced structures may be mistaken for '*Kinneyia*' (see Figures 6(a)-4G, -4H).

Besides these two types which by themselves indicate the former presence of mats, there remain other suspect microbial 'wrinkle structures' that are more variable in shape and size and are thus not clearly defined and unequivocal. Some of them may reflect mat deformation and mat slump structures. They usually appear as localised, more or less irregular, small-scale 'fold belts' on bedding surfaces (see Figure 6(a)-3B). Such structures have to be evaluated critically, and additional observations of sand cracks, 'sand chips' and other mat-indicative structures are required to support them as possibly microbially-induced.

6(b). SOME UNUSUAL AND/OR PROBLEMATIC INFERRED MAT-RELATED FEATURES

S. Sarkar, S. Banerjee

One may encounter from time to time structures that are more difficult than others to interpret in genetic terms, structures that may have some characteristics in common with identified or inferred mat structures, but not all. Some of these problematic structures which are preserved in Meso- to Neoproterozoic sandstones of the Vindhyan Supergroup in India are illustrated in Figure 6(b)-1. Discussion of their possible genesis is briefly outlined in the relevant captions.

6(c). INHERENT PROBLEMS OF TERMINOLOGY: DEFINITION OF TERMS FREQUENTLY USED IN CONNECTION WITH MICROBIAL MATS

E. Bouougri, G. Gerdes, H. Porada

Introduction

Like all branches of the earth sciences, the study of microbial mats and the features they leave behind preserved within clastic sediments of various calibres, is rife with terminology. As terms are used over several decades, the original meanings often become more imprecise as shades of meaning are added to an initial definition. One example examined briefly here is the term 'wrinkle mark', discussed in greater detail in Section 6(a) of this chapter.

Another example of changing uses of a single term over time is provided by 'petee'/'petee ridge' (Figures 6(c)-1B, -1C, -1D, -1G). Gavish et al. (1985) introduced the term in relation to modern mats, defining it as undulation and wrinkling of microbial mats due to either wind or gravity. Reineck et al. (1990) classified these forms into alpha-, beta- and gamma-petees, and considered the term in general to refer to biologically modified overthrust structures such as single domes, multitudes of buckles and transitions of the latter into domes. In both of these original definitions the petee forms were rounded, resulting from cohesiveness of the observed modern microbial mats. Reineck et al. (1990) interpreted the deformation of the mat inherent in petee formation as being due to sub-mat concentration of gas, to wind or water friction, or resulting from gravity. Neither of these earlier works really considered sediment filling in the positive deformation features of the mats growing above sandy substrates (see also Chapter 4(c)). An association of petees with cracks in the mats (e.g., Gehling, 1999, 2000) expanded the original definition, with Gehling (1999) defining petees *sensu stricto* as related to genesis through mat growth expansion and underlying gas pressure. Schieber (2004; see also Chapter 3) embraced this broader concept of the meaning of the term, and linked 'petee ridges' to positive features related to rupturing of mat surfaces; a relationship between the geometry of desiccation patterns and concomitant petee ridges (e.g., Figure 6(c)-1G) thus became implicit in this further expansion of the meaning of the term. Noffke et al. (2001a) espoused this broader, looser usage of petee/petee ridge to denote positive epirelief on a mat surface. This loose definition was also applied in this book in Chapter 4(c), and can perhaps be viewed as denoting petees *sensu lato*.

Although evolution in the meaning and usage of scientific terminology is almost inevitable, it is important to try and minimise the resulting confusion, particularly in an atlas-type publication such as this book. For this reason, this section attempts to clearly define certain critical terminology related to microbial mats and their preserved features in the clastic sedimentary record; in general, recourse is had to original definitions and usages rather than to those developed later, which often led to confusion. This endemic difficulty with scientific nomenclature is thus highlighted in this chapter as amongst the problems inherent in research on microbial mat-related features, and this section should thus not be viewed as a comprehensive glossary of relevant terminology, which would more logically appear either at the beginning or end of a book. Obviously, many mat-related structures are complex features, reflecting a multiple-structure genesis, as is illustrated in Figure 6(c)-1.

Some critical terms defined

Blister A descriptive term; in relation to microbial mats, blisters are photosynthetic gas bubbles, stabilised and overgrown by microbes; according to Stolz (2000), they are "pockets of trapped gas bubbles". Genetic relation to 'photosynthetic (PS) dome'. Blisters should not be confused with 'pustular' or 'nodular' patterns which evolve from localised growth and cell division of coccoids, e.g., *Entophysalis* sp.

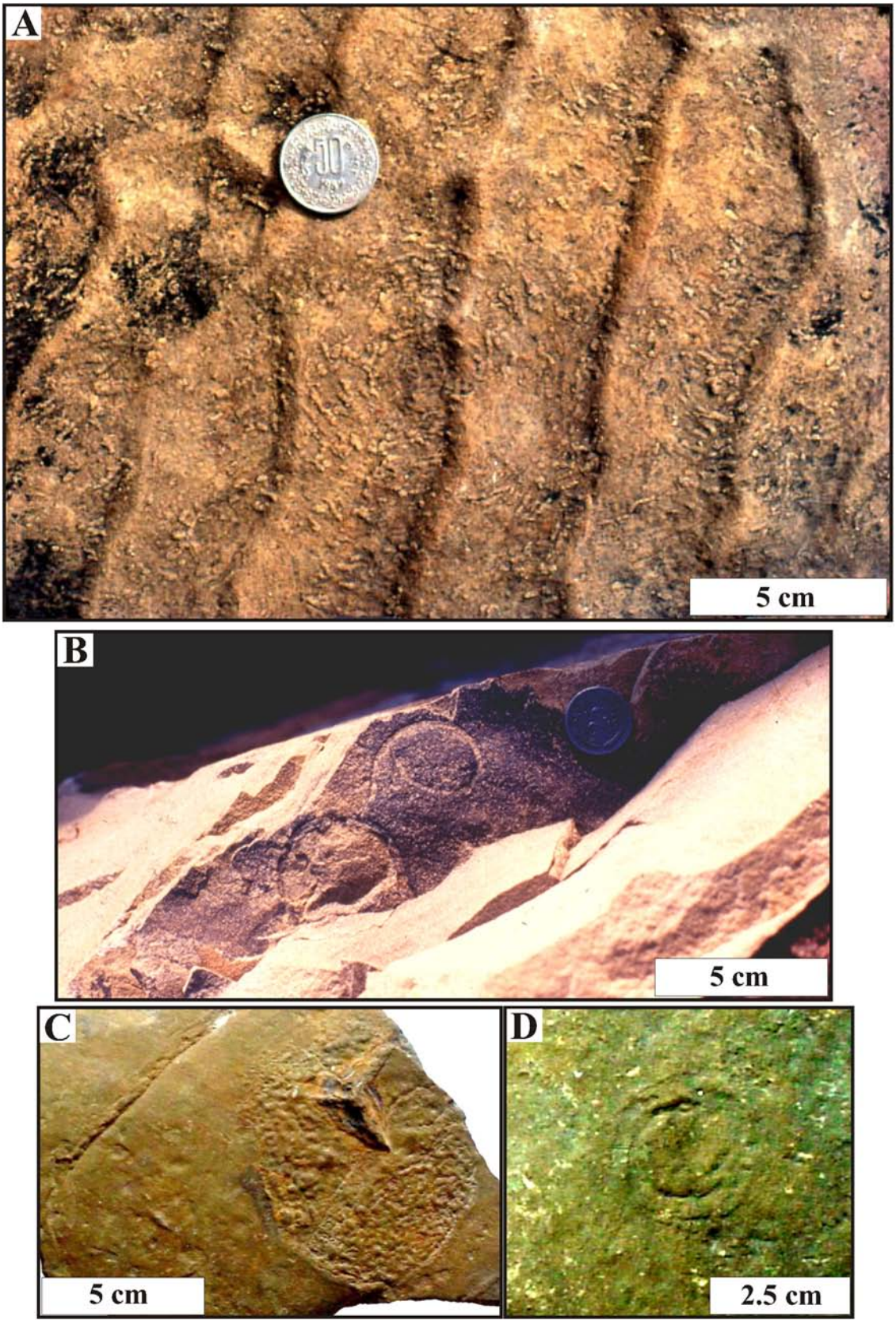


Figure 6(b)-1: Unusual and/or problematic features preserved in Meso- to Neoproterozoic Vindhyan Supergroup sandstones, India.

(A) Concentrically/spirally arranged elongated beads. *Description*: The structure is made up of small elongated beads of sand arranged in close concentric rims or spires, the exact pattern being indeterminable because of local obliterations. Some of the beads, however, defy this profound arrangement. Individual beads are spindle-shaped

and of average length 3.2 mm, width 1.3 mm and height 1 mm. End-to-end coalescence between adjacent beads gives rise to wrinkled thread-like shapes of maximum measured length 5.2 mm. Otherwise the beads maintain a fair degree of uniformity in length, width and height. In the example illustrated these concentrically or spirally arranged bead-like structures are present in the form of a crowded colony on a wave-rippled sandstone. The best-preserved overall disc-shaped colonial structure has a diameter of ca. 9 cm (coin diameter 2.5 cm). *Interpretation*: An origin without influence of biota, no matter whether unicellular or multicellular, cannot possibly be conceived for this structure. Though the structure shown here is from the Chorhat Sandstone, India (see Figure 7(d)-1) and may thus be as old as 1.6 Ga (Rusmussen et al., 2002) the influence of a multicellular organism on its origin cannot be ruled out in the light of the discovery of possible undermat burrows of a triploblastic organism, within the same formation (Seilacher et al., 1998). If the structure is, indeed, planispiral, one can interpret the minute elongated beads of roughly the same width and height as faecal pellets of a sediment- or mat-ingesting worm that scanned the rippled surface closely for food. A serious snag in this interpretation is the absolutely intact preservation of the ripples immediately underlying them. The putative animal track should have left some trace on the ripple crests, but then the organism could have restricted its movement on the mat protecting the ripples. On the other hand, concentric arrangements of minute pinnacles are generated on modern microbial mats possibly because of ring-like propagation of growth fronts of chemotactic bacteria releasing recurrent pulses of chemical compounds in response to their concentration gradients. However, till we know what indeed controlled the distribution and the profound circular arrangement of the spindle-shaped beads (or short wrinkles), genesis of the structure remains ambiguous. *Location*: The example shown comes from the upper part of the 1.6 Ga Chorhat Sandstone of the Vindhyan Supergroup, 2 km west–southwest of the town of Chorhat, India (see Chapter 7(d)). Palaeogeography: upper shoreface. (B) Spire-shaped tubular structure. *Description*: A spiral tube of diameter about 1.7 mm, partially exhumed on a sandstone bed surface (centre of photo). *Interpretation*: The structure appears as a horizontal burrow resembling *Planispiralichnus* of Fedonkin (1990), but this particular structure is more likely to be a synaeresis crack whose opposite tips closed upon the crack's fill of younger sand. *Location*: Documentation was made from the base of the 1.6 Ga Chorhat Sandstone exposed 1.5 km southwest of the town of Chorhat (see Chapter 7(d)). Palaeoenvironment: top of a fluvial mid-channel bar. (C) Roughly circular object bearing wrinkles and triradiate furrows (now seen in reverse as ridges) at the centre. *Description*: Reverse impression of a roughly circular wrinkled structure having three furrows radiating from the centre, but not reaching the periphery, at the sole of a sandstone bed. *Interpretation*: The wrinkled mass is similar to the frills of the objects described as mat structures in Figure 7(d)-4A, having the wrinkle ridges broadly in two sets at a high angle to each other. The wrinkles suggest a soft gelatinous sheet-like nature, as would be likely for a microbial mat. However, the central triangular symmetry expressed in the furrows suggests this is an impression of an animal-like cniderin or precursor of echinodermata. *Location*: Documentation comes from the Neoproterozoic Sirbu Shale (Figure 7(d)-1), Vindhyan Supergroup at Uchaihra, India. Palaeogeography: mid-shelf area, but the object, imprinted at the base of a storm sandstone bed, might have been transported from a shallower part of the Sirbu shelf. (D) Circular impression. *Description*: Circular impression of an object with diameter 2.6 cm and with concentric bands of average width 4.5 mm separated by thin ridges, now represented in reverse (sole marking) as furrows. The bands are presumably biogenic growth bands and ring-like structures do form in modern mats, involving growth dynamics with frequent polarity changes. Yet it is difficult to say whether these persistent bands around a circular central zone belong to unicellular or multicellular organisms. *Location*: Documentation was made from the base of a sandstone bed in the Sirbu Shale (Figure 7(d)-1), Vindhyan Supergroup at Uchaihra, India. Palaeoenvironment: mid-shelf, but the object might have been derived from a shallower part of the Sirbu shelf. All photos: Subir Sarkar, Santanu Banerjee, Snehasis Chakraborty, Pradip Samanta.

Bulge An elongated round-crested positive form on microbial mat surfaces, initiated by growth and confined biomass accretion; may be filled by sediment uprising from below; frequently related to mat polygons. 'Upturned' or 'curled' margins of cracks often are overgrown by new mat layers and become preserved as bulges (see Chapter 8(d), Figure 8(d)-2F). Bulges are members of a group of microbial mat-induced positive structures (see also 'petees', 'growth domes').

Complex structure (e.g., Figures 6(c)-1E, -1F, -1G, -1H) A structure in which physical and ecophysiological processes are intimately interrelated, e.g., an overgrown crack margin (bulge) is the product of induced polarity change and growth response of mat-forming microorganisms to physical deformation or destruction of a mat, which in turn means change of the habitat (e.g., polygonal cracking provides not only fissures and margins but aids also the emergence of groundwater as a trigger for growth). Most terms discussed here denote complex structures due to 'parahistological' behaviour of mat-forming biota (like living tissues).

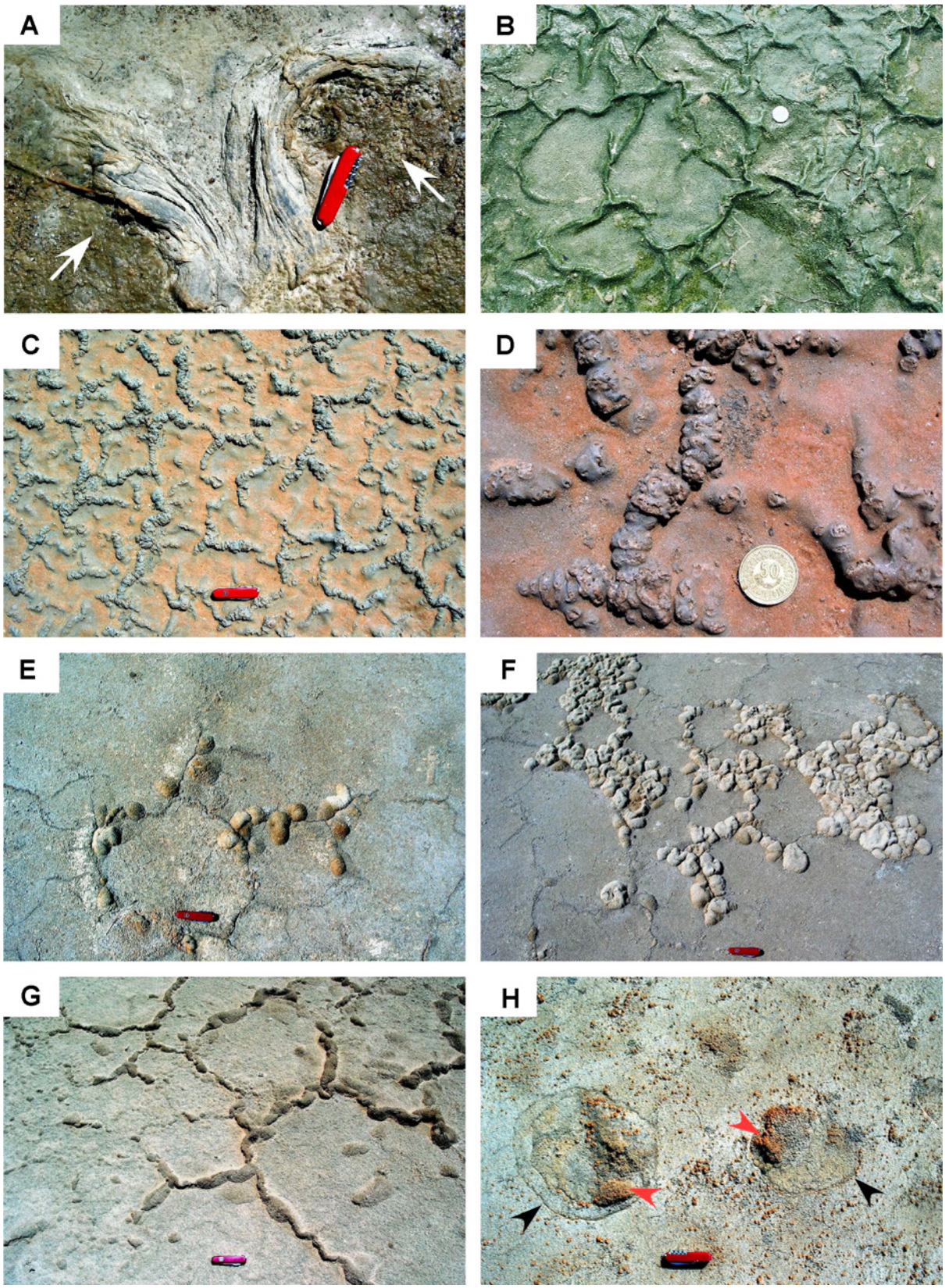


Figure 6(c)-1: Structures illustrating mat deformation, petees resulting from mat growth and expansion, gas domes and induced growth structures (domes and petees).

(A) Deformation along the margin of a leathery microbial mat. The deformation is due to water oscillation and friction along the mat margin, inducing formation of belts of irregular to curved ridges. The whole structure appears biostabilised by growth of new mat. White arrows indicate the direction of water movement. Preconcentration basin

of 'Salins du Midi' saltern, Réserve Nationale Camargue, Southern France. Scale (knife) is 8 cm. (B) Petees with round crests arranged into polygonal network. The petees start commonly as triradiate or isolated lenticular ridges evolving to a polygonal network during progressive and continuous mat growth and expansion. Supratidal pond, Djerba island, southern Tunisia. Scale (coin) is 25 mm. (C–D) Petees arranged into polygonal network and with pustular crest, these may due to other dominant taxa (coccoid possibly) increasing at the elevated part of the mat surface (crests), as well as photosynthetic activity that has produced blisters on/in slime which finally desiccated on the crests (pustular petees). The close-up view (D) shows that petee ridges may exhibit a nodular pattern and are filled from below by uprising of underlying sediment. Desiccation at peaks of petees frequently leads to circular/subcircular curled margin which subsequently may be overgrown. Lower supratidal zone, Bhar Alouane, southern Tunisia. Scales (knife) is 8 cm and (coin) is 25 mm. (E–F) Complex structures associating shrinkage cracks and growth domes aligned along the cracks. Crack formation starts with faint fissures in the mat which may create an immediate decrease of tension of the surface mat and ascent of water or moisture to which organisms respond in a very localised way. The biotic response encompasses active mat growth and expansion along the cracks with a development of incipient growth domes along one side or both sides (E). The resulting incipient growth domes exhibit round to slightly elongate shapes with diameters up to ∼5 cm. The continuous growth of domes may encompass the whole polygon surface and form coalesced structures (F). Supratidal zone, Sabkhat Boujmel, southern Tunisia. Scale (knife) is 8 cm. (G) Petees resulting from selective induced growth along faint polygonal shrinkage cracks. The process invoked is similar to that in photos (E–F). The petees ridges have rounded-crests and exhibit a polygonal network. Supratidal zone, Sabkhat Boujmel, Tunisia. Scale (knife) is 8 cm. (H) Complex structures associating collapsed gas domes and induced growth domes. The collapsed gas domes with diameter up to 20 cm are indicated by concentric flat pattern and remaining margins (black arrows). In between the collapsed domes, there are smaller growth domes more or less stippled by beetle pocks (red arrows). The growth of domes starts from the margins of collapsed gas domes which were not completely sealed. This as well as vertical to diagonal burrows induced by beetles below, may enhance localised seepage of groundwater which gives the microbes the growth impulse. Supratidal zone, Sabkhat Boujmel, Tunisia. Scale (knife) is 8 cm. All photos: El Hafid Bouougri and Hubertus Porada.

Curled margin Crack margin that has developed an involute structure, due to shrinkage-related contraction being strongest in the still flexible surface layer of a subaerially exposed mat. May be overgrown and remain as a bulge-like feature (cf. 'overgrown curled margin', see also complex structure, bulge).

Deformation (Figure 6(c)-1A) Contortion or distortion of surface mats due to external physical impacts, e.g., 'folding', 'flip-over', 'roll-up' due to tractional forces acting upon the mat. The term should not be confused with "destruction".

Destruction Deterioration of a mat, e.g., shrinkage cracking due to desiccation; also including erosion by strong currents and formation of mat fragments ('mat chips', 'sand chips').

Dome A descriptive term; several causes: see photosynthetic (PS) dome, gas dome, mat expansion structure, petee.

Gas dome (Figure 6(c)-1H) Domal feature on mat surface resulting from gas accumulation below mat; gas production due to decay of buried mats.

Growth dome (Figures 6(c)-1E, -1F, -1H) Domal mat expansion structure resulting from localised microbial growth; in the supratidal zone accompanied by crystallisation of evaporite minerals similar to tepees.

Induced growth Locally restricted microbial growth may be induced by ascending groundwater in shrinkage cracks, even in dry seasons; induced growth also applies to microtopographically-controlled, selective growth on ripple crests or in shallow depressions after rainfall or minor inundation (see also polarity).

Mat expansion structure Collective term including several positive structures resulting from 'microbial growth' and localised biomass accretion; see petees, growth domes, overgrown crack margins. Genetic relation to growth and to polarity.

Microbial growth Increase in the number of cells in a population due to binary fission, usually measured as an increase in microbial mass (see also polarity).

Nodular pattern Localised growth and cell division of coccoid cyanobacteria, e.g., *Entophysalis* sp., may lead to 'pustular' or 'cauliflower-like' surface structures.

Petee (Figures 6(c)-1B, -1G) Arched-up, sometimes undulated and wrinkled surface form. Petees owe their form primarily to the growth and expansion of coherent microbial surface mats. Original definition (Gavish et al., 1985) stresses the interactive role between mat growth/expansion (see mat expansion structures) and physical processes. The latter can include (i) wetting and drying ("wetting enables microbial mat to form new surface layers, drying desiccates and cracks the new crusts"; Gavish et al., 1985); (ii) rise in water level (see as well the important role of upwards-directed groundwater in the tepee definition); (iii) wind and slope gravity (may lead to undulated, wrinkled petee forms according to Gavish et al., 1985). In analogy to tepees (see below) in salt crusts resulting from surface crust expansion due to crystallisation of evaporite minerals, petees originate from mat expansion due to localised microbial growth and biomass accretion.

Petee ridge (Figures 6(c)-1C, -1D) According to Gehling (1999): "rounded and ruptured ridges in sinuous and polygonal patterns"... "Growth expansion and the gas pressure from buried decaying mats produces buckling..."; ... "desiccation, wind and wave action causes disruption and overturning of the mats...". While physical factors involved may be ambiguous, the unifying factor seems to be mat expansion due to growth which may allow one to subsume the term 'petee'/'petee ridge' under the collective term 'mat expansion structure'.

Photosynthetic (PS) dome Domal feature on mat surface, 0.5 to rarely 10 cm in diameter, resulting from photosynthetic gas production; domes may merge into each other and form also oval bodies. The structures form in highly elastic surficial EPS film and are stabilised by overgrowing microbes.

Pinnacle, tuft Growth structures, products of polarity changes of filamentous cyanobacteria originally contributing to condensed fibrillar meshworks. Tufts represent erected filament bundles rising some millimetres above mat base. Pinnacles are more rigid, stabilised forms due to amounts of EPS produced by associated community types, e.g., coccoids and diatoms that follow the slight microtopographic elevations.

Polarity The spatial orientation of mat-forming benthic cyanobacteria is of importance for the type of mat produced. Basically, the preferential spatial orientation of filamentous cyanobacteria (and others) is due to their polar attributes. Two possible pathways exist: a growth direction that is causal to the cell (cytoplasma) organisation and taxon-specific division planes, which is termed 'structural polarity'; growth directions induced by ecological factors (e.g., light, gravitation) are termed 'induced polarity'.

Reticulate growth pattern Surface ornamentation on microbial mats in which pinnacles/tufts and ridges (small-scale bulges) are the main constructive elements. The ridges in many modern examples are growth patterns of *Lyngbya* sp. Pinnacles often represent the focus of radially arranged ridges. Intersecting ridges and pinnacles form reticulate growth patterns that macroscopically resemble 'elephant skin'.

Subcircular crack Starting from a circular, subcircular or irregularly sinuous opening, and resulting from accelerated shrinkage and initial cracking at the top of a domal feature in a thin mat, the usually curled margin of the opening (see 'curled margin') may be preserved as a subcircular positive feature on the mat surface, particularly if subsequently overgrown by new mat layers.

Tepee (peritidal) "Arched-up antiform margins of expansion megapolygons...; ... when the surface area... increases; ... when repeated incremental fracturing and fracture fill by sediment and/or cement... causes the area of the hardgrounds to expand; ... where the marine phreatic lens is close to the sediment surface and the climate is tropical... where crusts experience alternating phreatic and vadose conditions, in time intervals of days to years..." (Kendall and Warren, 1987).

Upturned margin (see Figure 4(f)-1) A structure resulting from successive upturning of a crack margin due to desiccation and shrinkage advancing from the crack edge into the mat polygon; usually involving a stack of alternating sedimentary and organic-rich layers below the mat surface; typically occurring in mats overlying biolaminite successions. Antiformal, inverted 'V' structures (similar in shape to 'tepees') may result and be preserved in the ancient record, when opposite crack margins are upturned (see, for comparison, Gehling, 1999, his Figure 4B).

Wrinkle structure Member in a group of small-scale structures genetically related to microbial mats; characterised by alternating mm-scale crests and troughs of various length and more or less irregular trend (see Hagadorn and Bottjer, 1997, 1999). Various origins are discussed: (a) mat surface structure reflecting (exceptional) linear growth patterns; (b) mat deformation structure due to tractional or gravitational forces acting upon a thin mat; (c) mat subsurface structure formed beneath a cohesive microbial mat, e.g., '*Kinneyia*' structure (known from the ancient record only). Typical reticulate growth patterns and their ancient analogue 'elephant skin' texture (Runnegar and Fedonkin, 1992) should not be subsumed under the term 'wrinkle structures' (see Section 6(a)).

This page intentionally left blank

Atlas of Microbial Mat Features Preserved within the Siliciclastic Rock Record
Edited by J. Schieber et al.
© 2007 Elsevier B.V. All rights reserved
DOI: 10.1016/S1574-1966(07)02007-X

CHAPTER 7

Examples of Stratigraphic Units Bearing Outstanding Mat Features

INTRODUCTION

In this chapter ten examples of stratigraphic units, varying in age from Archaean to Eocene and from all parts of the world, which exhibit outstanding microbial mat-related features in clastic sedimentary rocks are described briefly. In each case, a locality map, stratigraphic setting and general geological framework are presented in abbreviated form, and remarkable mat features illustrated, and their genesis, where relevant, briefly discussed.

7(a). MICROBIALLY-INDUCED SEDIMENTARY STRUCTURES (MISS) OF EARLY AND MIDDLE ARCHAEAN AGES – MOODIES GROUP, PONGOLA SUPERGROUP, WITWATERSRAND SUPERGROUP (SOUTH AFRICA)

N. Noffke

The ca. 3.2 Ga Moodies Group

Introduction The oldest examples of microbially-induced sedimentary structures (MISS; see Chapter 3) have been detected in the 3.2 Ga Moodies Group (Swaziland Supergroup), Barberton Greenstone Belt, South Africa (Figure 7(a)-1). The outcrops are located in the Dycedale and Saddleback Synclines close to the town of Barberton. The Moodies Group records periodic transgressive drowning of wide, siliciclastic tidal flats, which were characterised by twice-daily tides, and spring-neap tidal rhythms (Eriksson and Simpson, 2000). The rock succession includes mud- and siltstone, as well as quartz-rich fine sandstone beds of 2–20 cm thicknesses. Because the rock successions have experienced only lower greenschist metamorphism, sedimentary structures are well preserved. The sandy tidal flats have been reworked only moderately, and storm-deposited layers are lacking. Studies in modern analogue environments, such as the tidal flats of Mellum Island (see also Chapter 2), suggest that such depositional environments and sediment successions are the preferred sites of occurrences of microbial mats (Noffke et al., 2002, 2006a; see also Chapter 9(a)).

Description of MISS Two occurrences of wrinkle structures (see also Chapter 6(a)), and one of a roll-up structure (Figure 7(a)-2; after Noffke et al., 2006b) were found in the field. The wrinkle structures are of 'non-transparent' type, where the wrinkles cover any preceding surface morphology to form an overall planar bed surface (Noffke et al., 2002). The structures occur in fine-grained sandstone beds that range between 2 and 20 cm in thickness. Associated physically-formed sedimentary structures include ripple marks that record only moderate reworking of the tidal flat deposits. Desiccation cracks record temporary subaerial exposure of the microbial mat-covered tidal areas.

Non-transparent wrinkle structures record thick and EPS-rich microbial mats, that can be found today, for example, in the lower supratidal zone of Mellum Island, North Sea (Noffke and Krumbein, 1999). The association of oriented grains within wrinkle structures supports this interpretation, as such textures occur in modern EPS-rich microbial mats as well. Oriented grains are textures that can be seen in thin sections through a living microbial mat (G. Gerdes, Chapter 2; Noffke et al., 1997a). In the organic matrix of an EPS-rich microbial mat, single grains 'float' without being in contact with each other. The long axes of those grains often are oriented parallel to the microbial mat surface. Laboratory experiments show that the grains originally stem from a substrate underneath a developing microbial mat. Individual sedimentary grains of the substrate initially became enveloped by a growing biofilm. Over time, those biofilms became thicker, and they lifted the grains up. Finally, the grains rotate, probably due to gravitational forces and become lined up like a string of pearls (Noffke et al., 1997a).

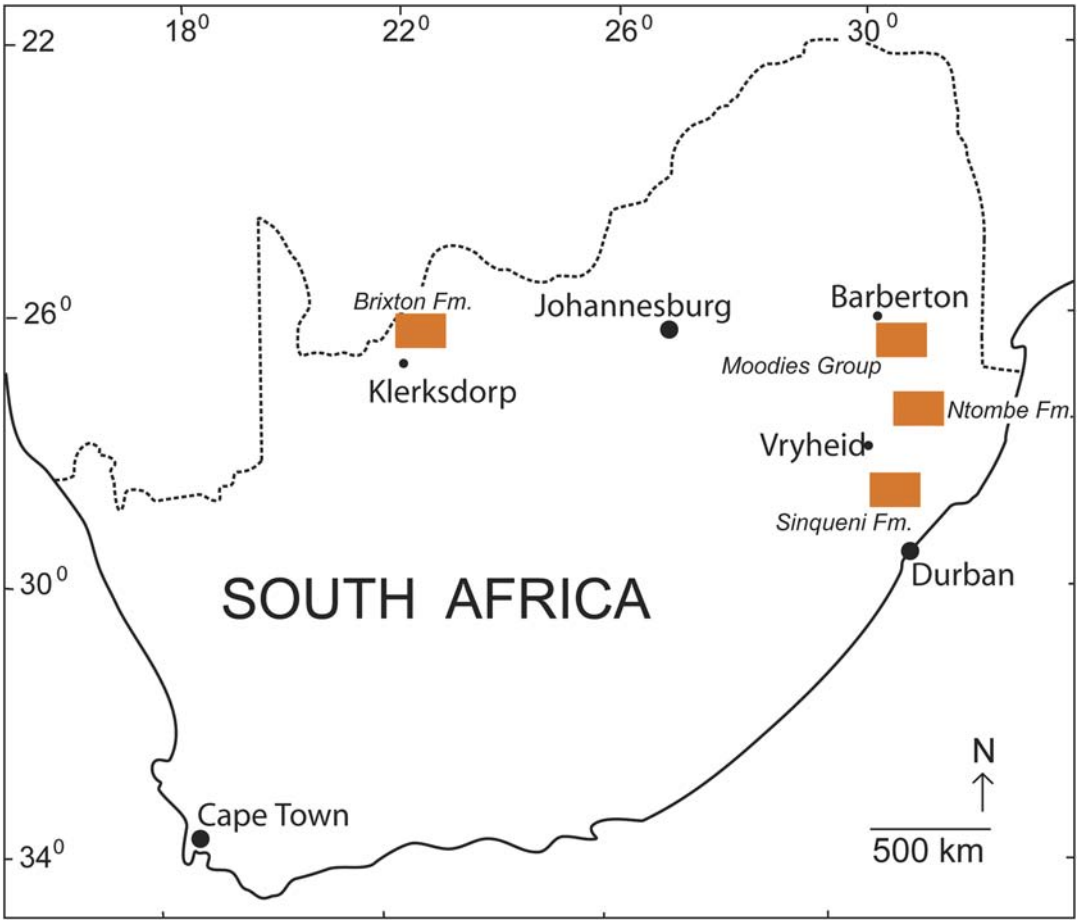


Figure 7(a)-1: Field localities of MISS from the Archaean of South Africa.
The Moodies Group (3.2 Ga) crops out close to the town of Barberton. The Sinqueni and Ntombe Formations (Pongola Supergroup, 2.9 Ga) occur west of Vryheid. The Brixton Formation (2.9 Ga Witwatersrand Supergroup) is exposed near Klerksdorp.

In the investigation of Archaean rocks, the question whether any sedimentary feature is of biogenic origin or not, must be addressed carefully. The macroscopic morphology of a structure alone does not prove its biogenicity, and the morphology of wrinkle and roll-up structures can be mimicked by a great variety of physical, syndepositional, or even tectonic processes (Noffke et al., 2006b; see also Chapter 6(a)). Additional optical and geochemical analyses must be conducted, and the palaeoenvironmental and stratigraphic position of a structure must be considered. All three features identified in the Moodies Group, wrinkle structures, roll-ups and oriented grains, are found associated directly with fossil filaments forming a characteristic mat fabric in thin sections (e.g., Figure 7(a)-2C). The inferred biogenicity of the filaments is supported by microprobe, RAMAN, and isotope analyses, which reveal organic C, as well as an array of typically associated minerals such as iron oxides (methods in Noffke, 2000; Noffke et al., 2003a, 2006a, 2006b). In addition, the stratigraphic position of the MISS at the tops of transgressive cycles, and the restriction of the structures to quiet and shallow water facies supports the interpretation as of biogenic origin.

The ca. 2.9 Ga Pongola and Witwatersrand Supergroups: Sinqueni and Ntombe Formations, Brixton Formation

Introduction MISS of Middle Archaean age are exposed at two locations in the Pongola Supergroup (Ntombe and Sinqueni Formations), and one location in the Witwatersrand Supergroup (Brixton Formation), South Africa (Figure 7(a)-1). The Ntombe Formation is well exposed at the Bibane River Dam, close to the village of Pongola. Siliciclastic successions of the Sinqueni Formation crop out along the White Mfolozi River, about 70 km west of the town of Vryheid. The Brixton outcrops detailed here are found close to the town of Klerksdorp. The relevant

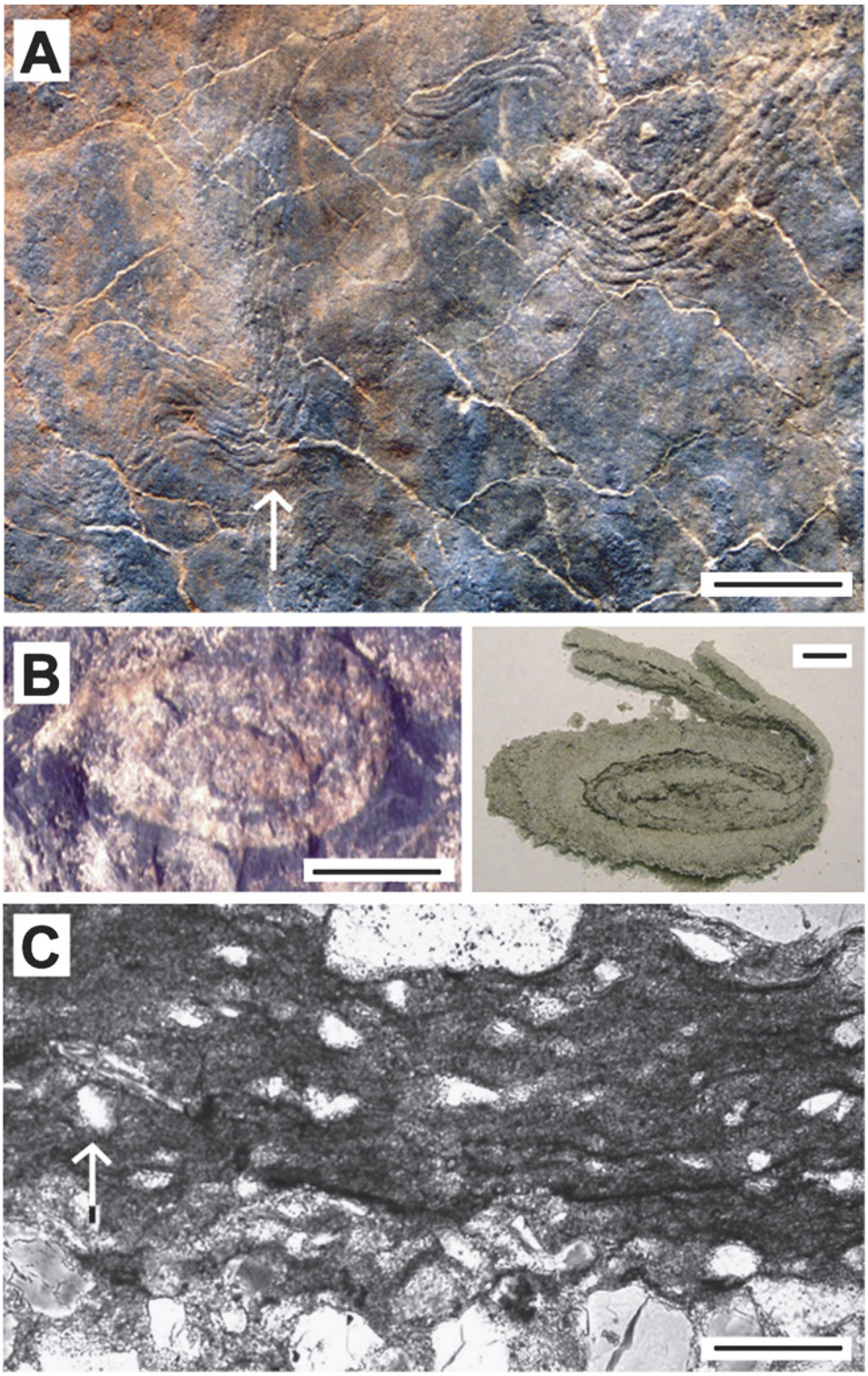


Figure 7(a)-2: Microbial mat structures from the Moodies Group.
(A) A wrinkle structure from the Saddleback Syncline. This structure is composed of wrinkles of 5 mm wavelength, and maximum height of 3 mm. The structure covers an area of 70 cm^2, and is composed of two sinus-shaped loops (scale = 10 cm, loop indicated by arrow). (B) Roll-up (or overfold) structures. The left figure shows the specimen from the Moodies Group, the right figure is a modern equivalent roll-up structure. The structures are 2.5 × 3 cm in dimension (scales = 1 cm). (C) Thin sections reveal 'oriented grains' (indicated by an arrow). The grains float independently from each other in the inferred preserved mat fabric of filamentous micro-organisms.

rock successions are composed of mud-, silt- and sandstones, as well as preserved quartzite bar bedforms. As with the Moodies Group, the deposits have experienced only greenschist grade metamorphism. The MISS occur in the same lithofacies as described for the Moodies Group.

The Brixton and the Ntombe Formations record a shelf palaeoenvironment (Eriksson et al., 1981; Beukes, 1996). The restriction of the MISS to interpreted shallow-water areas in the stratigraphic section shows that the microbial mats must have been photoautotrophic. Several transgression–regression cycles can be distinguished. The MISS occur explicitly at the turning points of these cycles. A similar relationship between the occurrence of MISS and transgression–regression cycles can be observed in equivalent shelf successions throughout Earth history (e.g., Noffke, 2000 (Ordovician); Noffke et al., 2002 (Proterozoic)). The Sinqueni Formation records sandy tidal flats, which were characterised by twice-daily tidal currents, and a spring-neap tidal rhythm (Beukes et al., 2002).

Description of MISS In the Ntombe Formation, eight examples of wrinkle structures have been detected; five have preserved extensions over ca. $5 \times 10\ cm^2$ and three have sizes of $20 \times 40\ cm^2$. The wrinkle structures are preserved in well sorted, fine-grained quartzitic sandstones. The wrinkle crests are 0.5–1 mm high, and the crest-to-crest distance ranges between 3 and 5 mm. Seven of the eight examples represent the non-transparent type, and one specimen is a transparent wrinkle structure (Noffke and Krumbein, 1999). Two types of wrinkle structures are thus distinguished: 'transparent' ones, where the original, physically shaped surface relief (e.g., ripple marks) are well visible underneath the wrinkles; 'non-transparent', where the wrinkles cover any preceding surface morphology to form an overall planar bed surface (Noffke et al., 2002).

MISS in the Sinqueni Formation are abundant, and include: wrinkle structures, erosional remnants and pockets (cf. ripple patches, Chapter 3), mat chips, multidirected ripple marks, gas domes, polygonal oscillation cracks (cf. mat cracks, Chapter 4(c); Figure 7(a)-3), roll-up structures, tufts, and oriented grains. Reticulate patterns of tufted mats that can become fossilised are not included under the term wrinkle structure, but are referred to as 'old elephant-skin structures' (Runnegar and Fedonkin, 1992; Gehling, 1999; see also Chapters 3 and 6(a)). The MISS of the Sinqueni Formation record a lateral succession of different microbial mat types such as planar microbial mats, tufted microbial mats, and others. Such a lateral succession of microbial mat types results from the response of the microbiota to the average hydraulic pattern in a tidal flat (Noffke et al., 2001b). Modern examples of this MISS lateral association occur in the Bahar Alouane, southern Tunisia. The term 'biofilm-catena' was introduced for this phenomenon (Noffke, 2003). The Brixton Formation hosts erosional remnants and pockets (on two bed surfaces), and a single example of oscillation cracks. Wrinkle structures are abundant (28 examples found), and reflect contacts at the transitions of the transgression–regression cycles (Noffke et al., 2006a).

Modern equivalents of erosional remnants and pockets on Mellum Island are typical for the lower supratidal zone, although less significant examples may occur temporarily in the upper intertidal zone as well (quantification in Noffke and Krumbein, 1999). Mat chips are frequently associated with erosional remnants and pockets. Gas domes (Chapter 6(c)) are often associated with oscillation cracks. The latter are cracks that form a polygonal pattern across a microbial mat-overgrown tidal surface. The name oscillation crack results from their modes of formation (Noffke et al., 2001b; their Figure 4): in vertical section through such a crack, several organic layers each representing a microbial mat generation are visible. The sections show how the microbial mats expand during periods of moist climatic conditions and that they overgrow and close the oscillation cracks. But during dry weather, the mats desiccate and crack to form the polygons.

Associated physically-formed sedimentary structures in the Ntombe and the Brixton Formations are oscillation ripple marks, recording a shelf environment above the fair-weather wave base, and hummocky cross-stratification resulting from episodic heavy storms. The Sinqueni Formation exposes typical tidal flat sedimentary structures including desiccation cracks, small-scale mini-ripples, and flaser bedding.

For all these study sites, the biogenicity of the observed structures is supported by the correlation of the MISS with the typical depositional facies of microbial mats, the correlation with transgression–regression cyclicity, and the optical and geochemical analyses on filamentous textures as described above for the samples of the Moodies Group. Filamentous textures of the Brixton Formation might show cell compartments, although the poor preservation does not permit certain conclusions on the ancient mat-building organisms (Figure 7(a)-3F; after Noffke et al., 2006a).

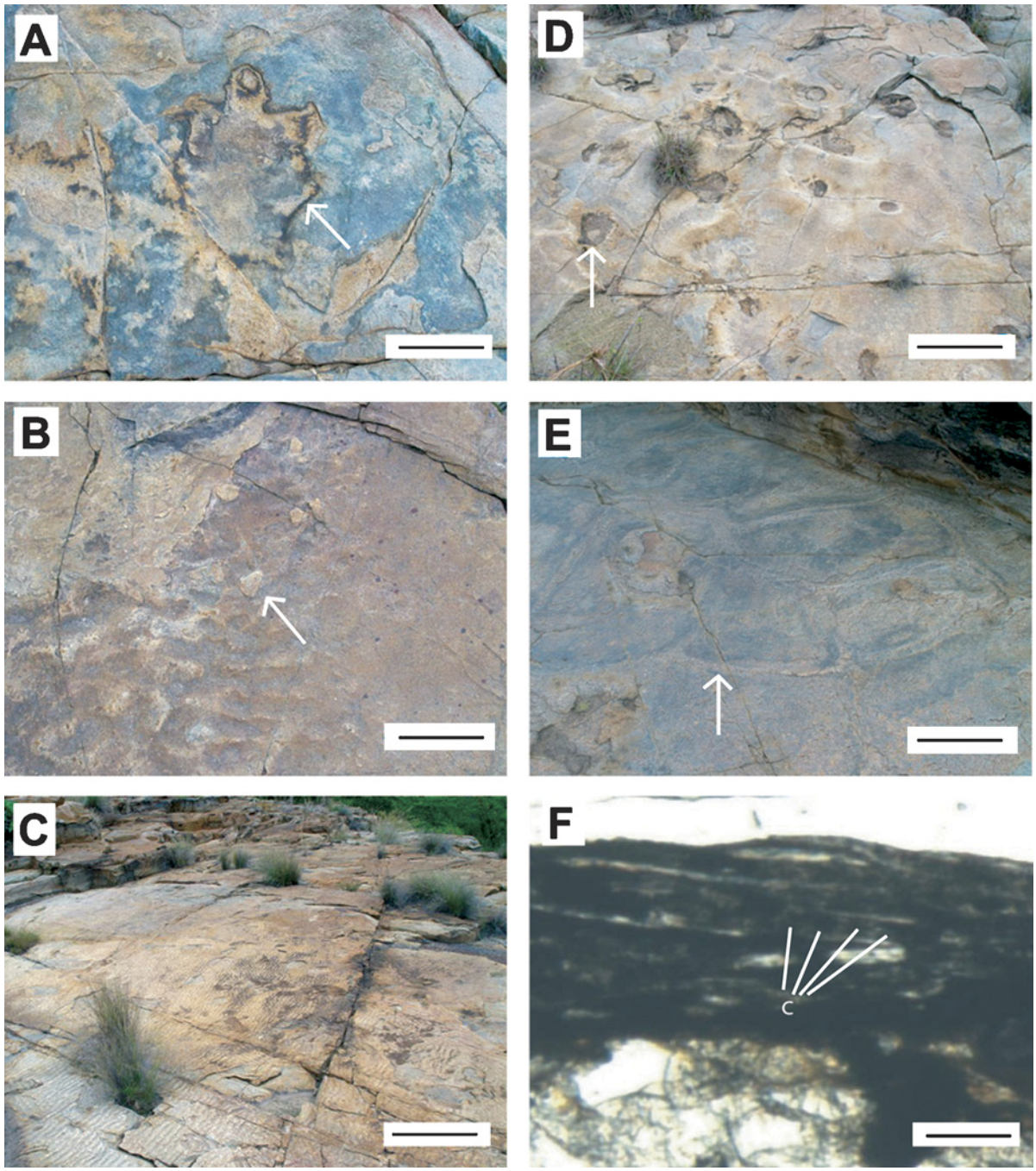


Figure 7(a)-3: Microbial mat structures from the Pongola and Witwatersrand Supergroups.
(A) Erosional remnants and pockets cover large areas of bedding planes. The erosional pocket shown here (arrow) is about 50 cm in diameter; scale = 20 cm. (B) Mat chips are scattered all across the preserved tidal flats, but they accumulated especially in erosional pockets, where the current velocities dropped (scale = 10 cm; arrow indicates a mat chip). (C) Several bedding planes display beautifully exposed multi-directed ripple marks (scale = 1.50 m). (D) Gas domes are frequent, and their sizes range from 0.5 to 15 cm in height, and 2–40 cm in diameter. Here, a bedding plane is shown, where the gas domes had collapsed, maybe during the burial of the ancient sedimentary surface (scale = 20 cm; arrow indicates one of the collapsed gas domes). Now only holes of 3–15 cm diameter are preserved. (E) Sometimes, oscillation cracks are visible, defining polygons of 40–50 cm dimensions (scale = 20 cm; arrow indicates an oscillation crack). (F) Filamentous textures of the Brixton Formation might show cell compartments, although the poor preservation does not permit certain conclusions on the ancient mat-building organisms; c indicates the potential cell compartments visible in the filament-like textures; scale = 50 μm.

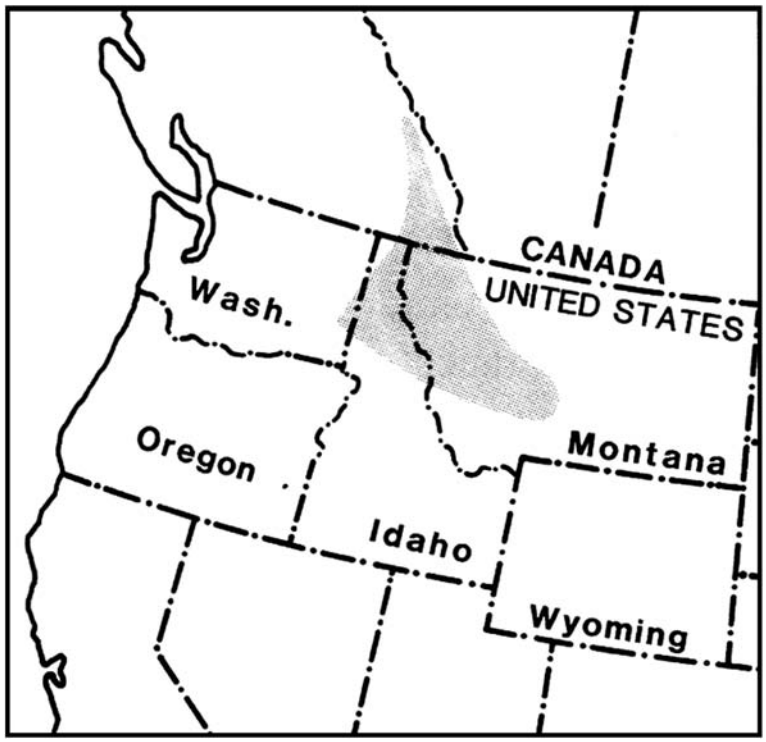


Figure 7(b)-1: Location of Belt Basin (stippled) and Belt Supergroup.
Equivalent strata in Canada are known as the Purcell Supergroup.

7(b). MICROBIAL MAT FEATURES IN TERRIGENOUS CLASTICS OF THE BELT SUPERGROUP, MID-PROTEROZOIC OF MONTANA, USA

J. Schieber

Introduction

Deposited between 1450 and 850 Ma (Harrison, 1972), the Belt Supergroup of Montana (Figure 7(b)-1) forms a thick and primarily terrigenous clastic succession (Figure 7(b)-2). Although today located on continental crust, initially the Belt basin probably formed a narrow gulf that was connected to the Proterozoic ocean (Cressman, 1989). The oldest sedimentary unit, the Prichard Formation (Figure 7(b)-2), has been interpreted as a turbidite succession and was probably deposited in comparatively deep water (Cressman, 1989). The basin shallowed towards the end of Prichard deposition, and then was filled with shallow water to subaerial deposits for the remainder of Belt sedimentation (Winston, 1986). A lacustrine depositional model has been proposed by Winston (1986) on the basis of facies comparisons with the lacustrine Green River Formation (Eocene; see also Section 7(j) below) of Wyoming. However, the lacustrine hypothesis conflicts with Cressman's (1989) work that suggests a gulf connected to the Proterozoic ocean. Geochemical considerations, such as chemical mass balances for the various formations and the problem of sourcing the large quantities of calcium and magnesium in the Middle Belt Carbonate, indicate that even though deposition was epicratonic, the basin was nonetheless in communication with the Proterozoic ocean (Schieber, 1998d). In this chapter microbial mat-related features observed in shales and sandstones of most of the Belt succession will be examined. Illustrated examples are from the Newland Formation, the Revett Formation, the Mt. Shields Formation, and the McNamara Formation (Figure 7(b)-2). They have been described in significantly more detail in prior publications (Schieber, 1986, 1998a, 1999).

Newland Formation: striped shales

Offshore shales in the Newland Formation of the eastern Belt basin (Schieber, 1985) have a characteristic striped appearance that has been interpreted as indicative of microbial mat colonisation of a muddy substrate (Schieber, 1986). In outcrop, dark grey to reddish-brown shale beds, a few millimetres to some centimetres in thickness,

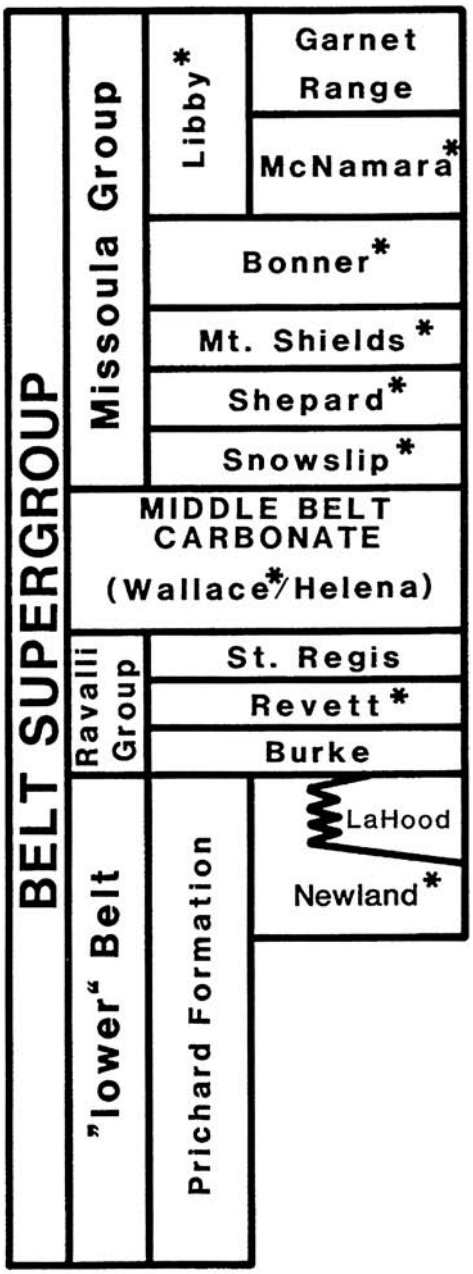


Figure 7(b)-2: Summary stratigraphic section of the Belt Supergroup.
Star symbol indicates formations with microbial mat features in terrigenous clastics (Schieber, 1998a).

alternate with beds of grey shale (Figures 7(b)-3, -4A) also some millimetres to centimetres in thickness and which may have silt or shale intraclasts at the base. Comparison of outcrop and drill core specimens (Figures 7(b)-4B, -4C) shows that the dark grey to reddish-brown beds are the weathered equivalent of carbonaceous silty shale beds with abundant (several percent) scattered pyrite grains, and that the grey beds are clay-dominated with minor amounts of pyrite and organic matter (Schieber, 1989a).

Although the wavy-crinkly internal laminae (Figure 7(b)-4D) of the carbonaceous beds hint at a possible microbial mat origin, the most convincing evidence for the microbial mat character of these beds is their behaviour during soft sediment deformation and erosion. During soft sediment deformation and erosion, carbonaceous beds and laminae behaved like tough leathery membranes (Figure 7(b)-5D), a mechanical behaviour that is consistent with microbial mats and not with a simple organic muck (Schieber, 1986). The grey interbeds, in contrast, behave mechanically like a fluid with the consistency of well stirred yoghurt, much more in keeping with a simple surficial mud deposit (these features are illustrated in Chapter 5).

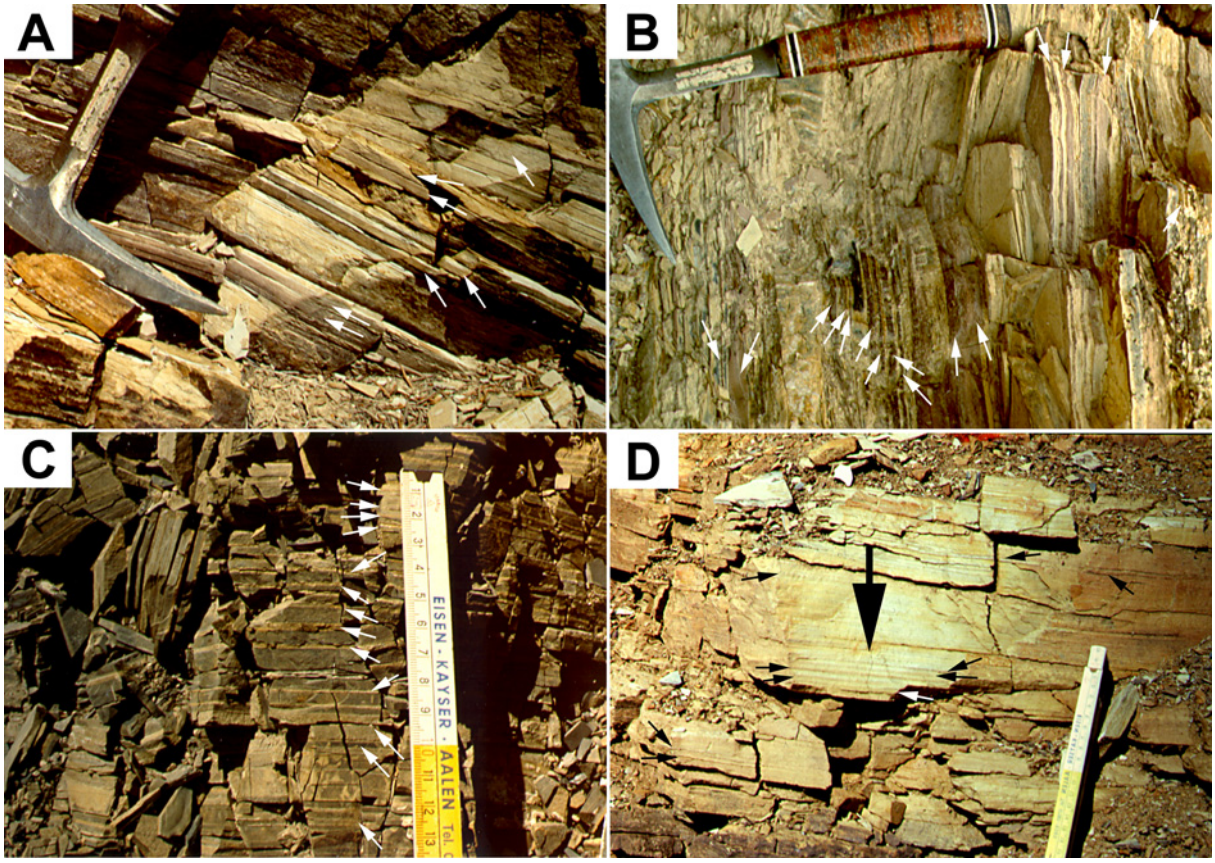


Figure 7(b)-3: Newland Formation.
(A) Outcrop photo of striped shale from the Newland Formation, Big Belt Mountains, Montana. Shows reddish–brownish shale beds (marked with arrows) that alternate with grey shale beds. The reddish–brownish colours are due to oxidation of disseminated pyrite in these originally carbonaceous shale beds (see Figure 7(b)-4). Hammer for scale. (B) Outcrop photo of striped shale from the Newland Formation, Big Belt Mountains, Montana. Same locality as A. Shows reddish–brownish shale beds (marked with arrows) that alternate with grey shale beds. The reddish–brownish colours are due to oxidation of disseminated pyrite in these originally carbonaceous shale beds (see Figure 7(b)-4). Hammer for scale. The weathered appearance of striped shales in A and B is very similar to the striped shales from the Tarur Nala Formation (Mid-Proterozoic of India, Figure 7(c)-4). (C) Outcrop photo of striped shale from the Newland Formation, Little Belt Mountains, Montana. The originally carbonaceous beds (marked with arrows) are light grey in this example, and interbedded with darker grey shales. The weathered carbonaceous–pyritic beds are also light grey in this example because iron was leached from these shales during weathering and thus did not produce the reddish stain observed in A and B. Ruler has centimetre divisions. (D) Outcrop photo of striped shale from the Newland Formation, Little Belt Mountains, Montana. Arrows point out weathered carbonaceous beds that alternate with grey shale beds. The carbonaceous–pyritic beds become reddish stained during weathering, whereas the grey shales do not show much discolouration. The area below the large black arrow yielded specimens with pronounced wavy-crinkly lamination, such as seen in Figure 7(b)-5. Ruler colour divisions (white–yellow) are 10 cm long.

The striped shales of the Newland Formation were deposited in a subtidal setting, basinwards of carbonates characterised by cryptalgal laminites, mudcracks, and flat pebble conglomerates (Schieber, 1986, 1998a). The microbial mats that gave rise to the carbonaceous silty shale beds colonised the shallow seafloor during periods of low sediment input. Comparison with modern muddy tempestites suggests that graded silt–clay couplets of the grey shale interbeds beds are storm deposits that intermittently interrupted the growth of subtidal benthic microbial mats (Schieber, 1986).

Whereas striped shales as described above are a common shale facies in the Newland Formation of the eastern Belt basin, locally a pyrite-enriched variant is also found. Pyritic striped shales are texturally analogous to ‘standard’ striped shales (Figure 7(b)-5A). They consist of layers of strongly pyritic shale that alternate with grey shale beds. The latter are identical in composition and sedimentary features to the grey shale interbeds in standard striped shales

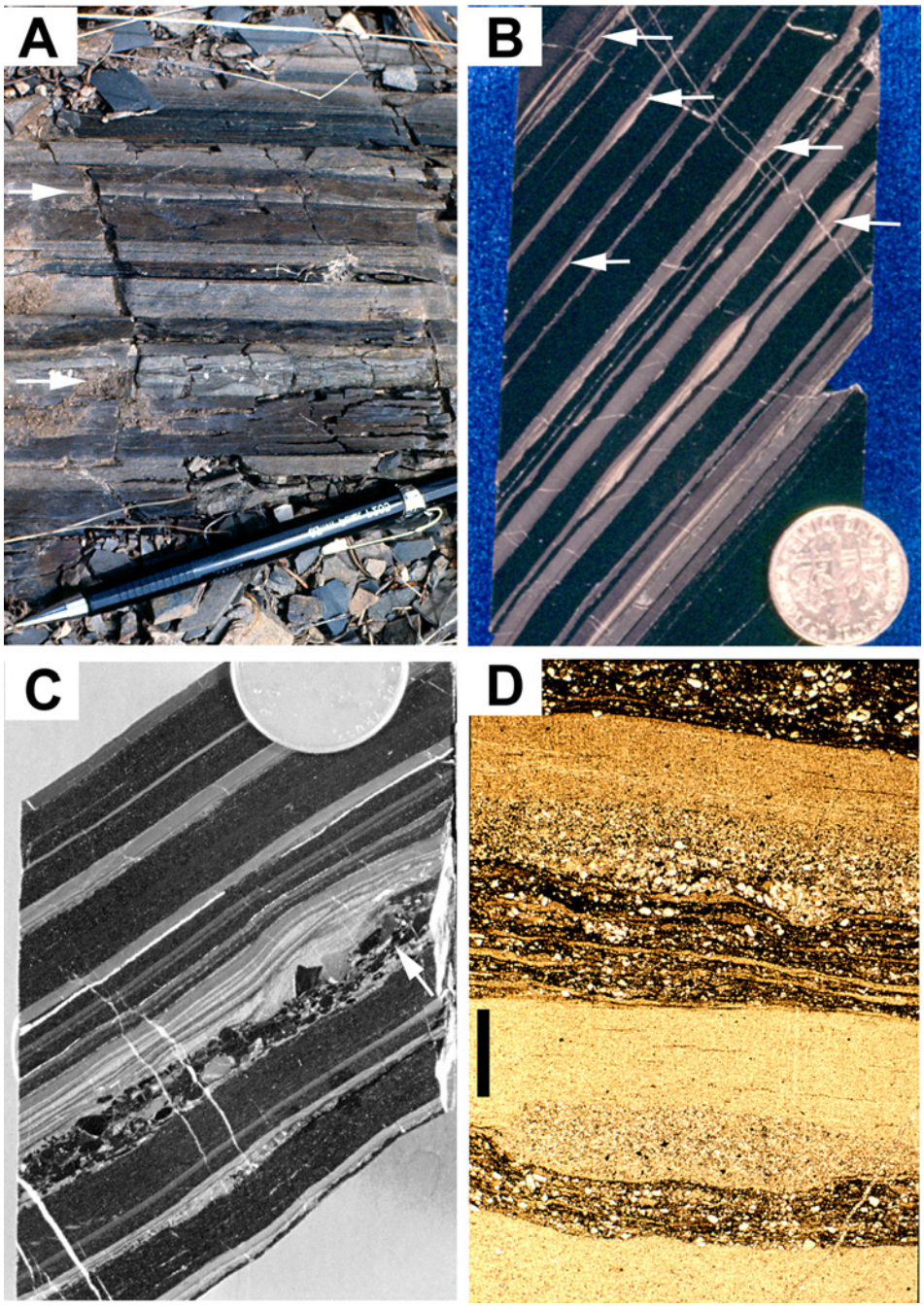


Figure 7(b)-4: Newland Formation.

(A) Outcrop photo of striped shales in the Newland Formation of the eastern Belt Basin (Schieber, 1986). The dark layers are carbonaceous and internally laminated shales, whereas the grey layers consist of clay and silt and typically show normal grading. Arrows point to grey layers that exhibit normal grading with silt at the bottom of the layer. These shales are interpreted as reflecting growth of benthic microbial mats (dark layers) that was on occasion interrupted by high energy events (storms or floods) that deposited the grey layers. The pencil is 130 mm long. (B) Photo of a cut and smoothed piece of drill core of striped shale. Shows the same layering as in A. Graded silt/mud couplets are clearly visible (arrows), as well as ripples in the silty portion of the grey layers. The coin is 18 mm in diameter. (C) Photo of a cut and smoothed piece of drill core of striped shale. Arrow points to thick graded layer that contains shale clasts at its base, is overlain by laminated silt, and finally grades into grey clay. Probably a more proximal storm deposit. Coin is 18 mm in diameter. (D) Photomicrograph of striped shale specimen. Shows very clearly the wavy-crinkly internal laminae of the dark carbonaceous layers (interpreted as benthic microbial mats). The non-carbonaceous inter-layers (clay/silt) show normal grading. Scale bar is 0.5 mm long. Because of the limited field of view of the typical petrographic microscope, a sample with very thin carbonaceous layers was chosen to illustrate the contrast between layer types.

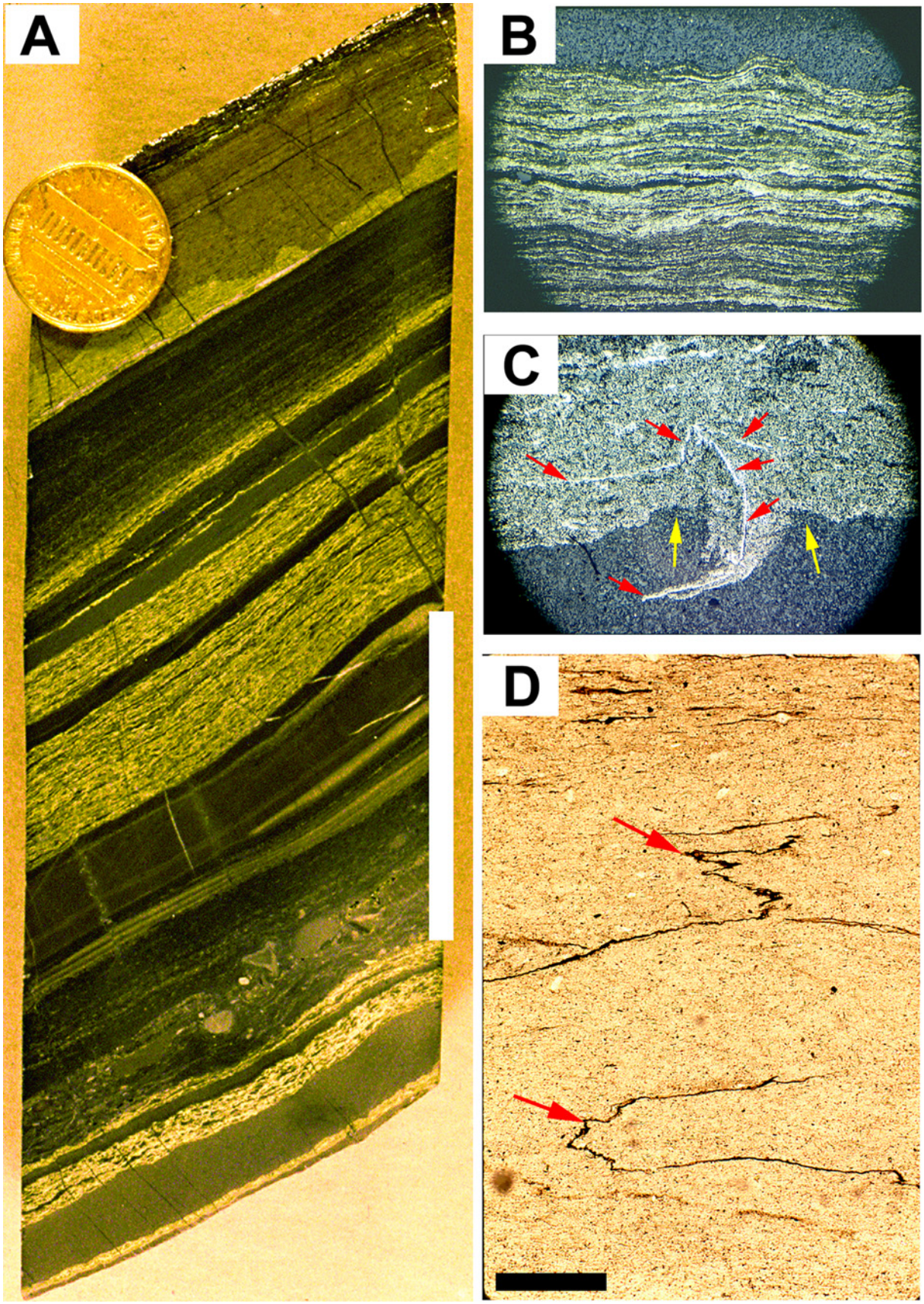

A
B
C
D

Figure 7(b)-5: Newland Formation.
(A) Photo of drill core specimen of pyrite-mineralised striped shale (Schieber, 1989a). Wavy-crinkly pyritic beds appear yellow and alternate with beds of dolomitic grey shale and a thick graded storm layer (white bar at right). The wavy-crinkly laminated pyritic beds are the direct facies equivalent of carbonaceous silty shale beds elsewhere in the striped shale facies, and are likewise interpreted as benthic microbial mat deposits. Coin is 19 mm in diameter. (B) Photomicrograph of pyritic bed from A. Shows wavy-crinkly lamination that texturally matches laminae observed in carbonaceous layers (interpreted as benthic microbial mats) from non-mineralised striped shales. Note load casts of overlying silt into underlying pyritic bed. Field of view is 7 mm in diameter. (C) Pyritic bed of the type seen in A and B that has undergone soft sediment deformation. Soft sediment deformation has disrupted and homogenised the original laminated fabric, but already-cemented and 'hardened' laminae (red arrows) were broken into plate-like bodies during soft sediment deformation, telescoped, and pushed into an underlying and still soft shale bed. Upwelling of shale at locations marked with yellow arrows indicates that both the pyritic bed and the underlying shale were still unconsolidated when break-up of already hardened pyrite laminae occurred. These observations attest to a syndepositional origin of the laminated pyrite beds, not simply a diagenetic overprint of previously deposited carbonaceous shale beds. Field of view is 7 mm in diameter. (D) Folded carbonaceous flakes (red arrows) in clayey shale. This suggests transport of thin, yet flexible pieces of carbonaceous material that measured as much as several centimetres across. In the Proterozoic, erosion of microbial mat surfaces would have produced fragments with those characteristics. Scale bar is 0.5 mm long.

---

described above. When examined in detail, the pyritic beds have internal pyritic laminae whose wavy-crinkly texture is very similar in appearance to the wavy-crinkly laminae of standard striped shales (compare Figure 7(b)-4D and Figure 7(b)-5B), suggesting that they have a comparable microbial mat origin. The iron enrichment in the pyritic striped shale facies is thought to reflect alluvial iron input along the basin margins (Schieber, 1985). Terrestrial runoff supplied iron in colloidal form as iron hydroxides to basin marginal lagoons. Iron hydroxide flocculates were incorporated into microbial mats and subsequently transformed into pyrite upon mat burial (Schieber, 1989a). Excess iron input by terrestrial runoff can be documented for most of the Newland Formation (Schieber, 1995), but only in protected nearshore lagoons did it give rise to distinctive pyritic striped shales. More detailed information concerning pyrite formation during microbial mat diagenesis is provided in Chapter 5, in the section dealing with features related to mat decay and diagenesis.

The striped shales of the Newland Formation are probably the first well-studied example of microbial mats in ancient mudstones, and since their original study (Schieber, 1986) comparable examples have been identified in other Proterozoic shale successions (e.g., Fairchild and Herrington, 1989; Logan et al., 1999a; Banerjee et al., 2006; Sur et al., 2006; Patranabis-Deb et al., this volume, Section 7(c)). In addition, the Native Bee Siltstone of the Mid-Proterozoic Mount Isa Supergroup of Queensland, Australia, appears texturally quite similar to the striped shales of the Newland Formation (personal observations) and may have a comparable origin. The host rocks of several large Australian stratiform base metal deposits of Proterozoic age, such as Mt. Isa (Bennet, 1965; Mathias and Clark, 1975), Lady Loretta (Loudon et al., 1975), Hilton (Mathias et al., 1973), and McArthur River (Cotton, 1965; Murray, 1975; Lambert, 1976; Williams, 1978a, 1978b) are extensive pyritic shale deposits that have the same striped character as those pictured from the Newland Formation, and show the same wavy-crinkly pyritic laminae within the pyritic beds. Although their microbial mat origin still needs to be established in each individual case through detailed study, the coincidence between pyritic striped shales and major base metal deposits is tantalising (Schieber, 1990). The figures for striped shales presented in this section mainly describe their overall appearance at the outcrop and hand specimen scale, whereas the features critical for microbial mat identification are covered in detail in Chapter 5.

Revett Formation: iron stains and domes in sandstones

In various outcrops, sandstones of the Revett Formation (Figure 7(b)-2) show conspicuous iron stains that are caused by the weathering of ferroan carbonate cements (siderite, ankerite, ferroan dolomite) and pyrite. These sandstones formed in a fluviodeltaic setting with local development of sandy tidal flats, channel-mouth bar deposits, and barrier bars (Boyce, 1973; Bowden, 1977; Mumma et al., 1982; White et al., 1984). Most of the microbial mat features illustrated here were initially reported by Garlick (1988) who realised that the ferroan minerals in Revett sandstones were probably the diagenetic imprint of former microbial mats.

These ferroan minerals formed early in diagenesis (Hayes and Einaudi, 1986) as a result of reducing pore waters. In most sediments, reducing pore waters are due to contained organic matter. Initial organic matter degradation

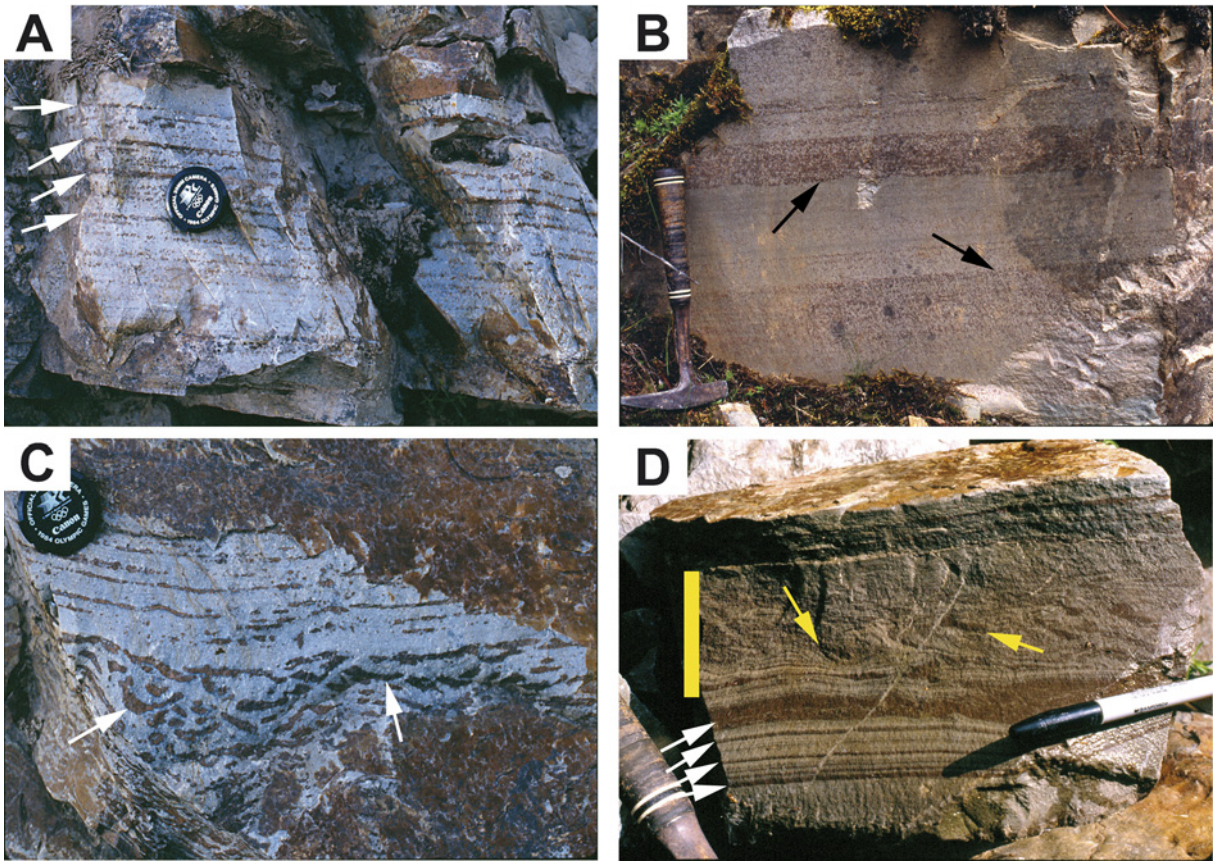


Figure 7(b)-6: Revett Formation.
(A) Photo of medium-grained quartz arenite in the Revett Formation. Arrows point to thin, bedding-parallel, iron stained (limonite) horizons that result from oxidation of ferroan carbonates (e.g., ankerite, siderite) and pyrite that are concentrated in pore spaces at these horizons. The very selective occurrence of these minerals at certain horizons is suggestive of mat decay mineralisation (Schieber, 1999), formed beneath a surface-sealing mat cover. Anoxic conditions are due to decay of organic matter beneath the active surface mat. Lens cap is 45 mm in diameter. (B) Photo of medium- to fine-grained quartz arenite in the Revett Formation. Two thicker horizons with abundant iron staining (limonite) are pointed out by arrows. The sharp contrast between these horizons and the intervening sandstone interval suggests that there was originally abundant organic matter in the marked, iron-stained horizons. As in A, the staining is due to oxidation of ferroan carbonates and pyrite. The more spotty nature of the iron stain suggests that the organic matter was in discrete particles that were mixed in with the sand during transport. The organic particles may have been derived from eroded and reworked mats. Hammer is 32 cm long. (C) Scour depression in Revett Formation medium-grained quartz arenite. The depression is filled with curved elements (arrows) that have limonitic stain, overlain by sandstone with horizontal to wavy-undulose limonite stained layers, like those shown in A. The latter are interpreted as diagenetic (mat decay mineralisation) remnants of thin microbial mats. The curved elements show sandstone with limonite and residual ferroan carbonate and pyrite cement, just like the limonite stained layers in A and B. They are interpreted as remnants of desiccated and transported fragments of microbial mat that decayed after burial and led to the observed mineralisation with ferroan carbonates and pyrite. Lens cap is 45 mm in diameter. (D) Fine-grained quartz arenite in the Revett Formation. Shows an interval with soft sediment deformation (marked by yellow bar) that is sandwiched by sandstone with horizontal limonitic laminae (white arrows). Note fragments of contorted limonitic laminae (yellow arrows). Hammer is 32 cm long.

by aerobic bacteria consumes the available oxygen, and then anaerobic bacteria continue the process and foster precipitation of minerals such as ferroan carbonates and pyrite (e.g., Brett and Allison, 1998).

At the time the Revett Formation was deposited, microbial mats were the most likely producers of organic matter in shallow water sedimentary environments. Thus, early diagenetic reducing pore waters could have been generated in two ways: (1) through decay processes within a layer of sand that contained organic (microbial mat) debris (Berner, 1984), or (2) through decay processes in the lower portions of a microbial mat (e.g., Bauld, 1981; Gerdes et al., 1985b).

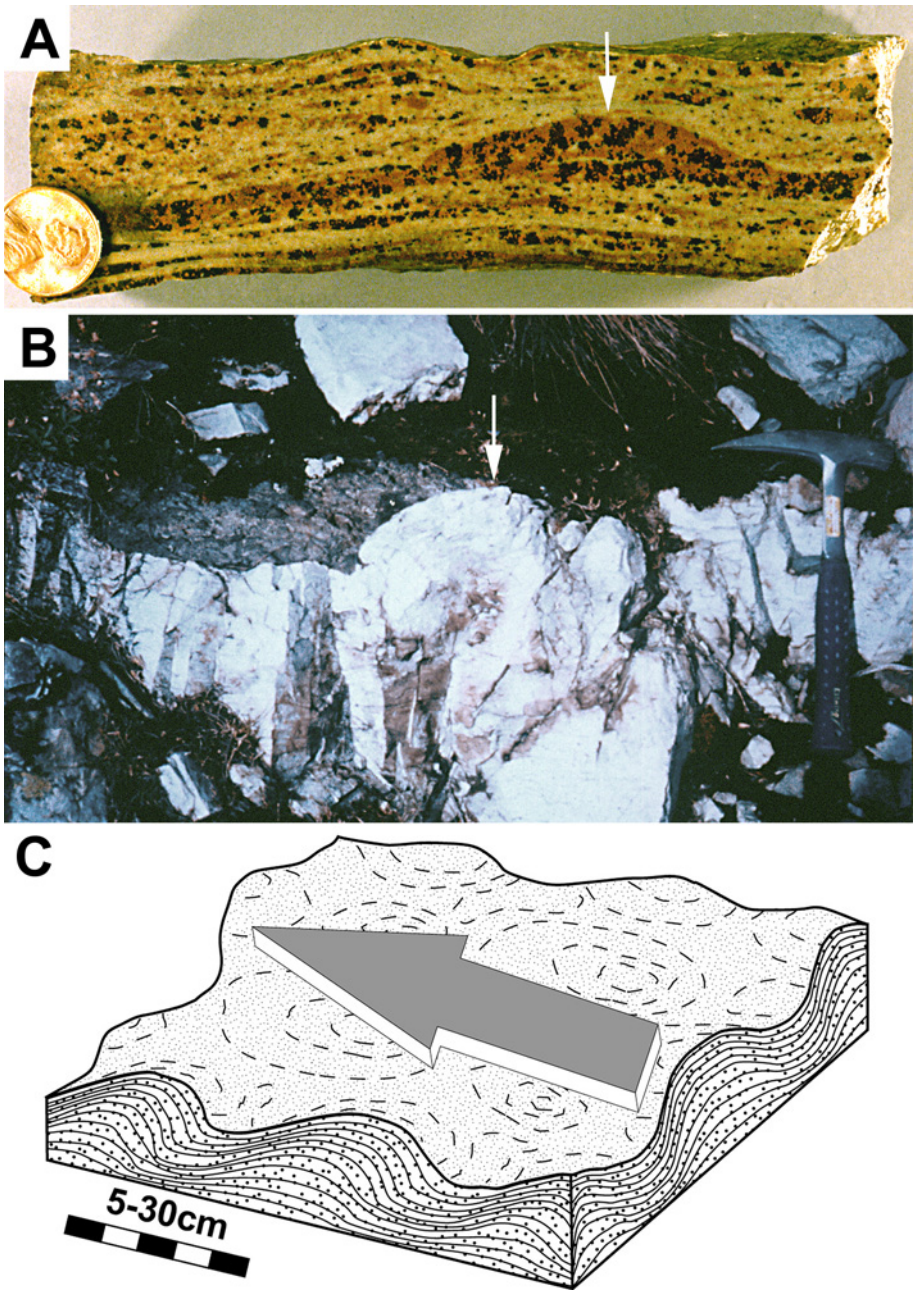


Figure 7(b)-7: Revett Formation.
(A) Hand specimen of Revett Formation sandstone with iron stained (limonitic) laminae. The arrow points to a layer with asymmetric domal thickening, possibly an incipient stromatolite of the type shown in B. The very dark patches are oxidised patches of siderite cement. The brownish-orange colour of the laminae is due to more finely distributed iron oxides. The coin is 19 mm in diameter. (B) Domal stromatolites in the upper portion of the Revett Formation near Troy, Montana. The hammer is 32 cm long. Photo courtesy of John Balla, ASARCO Inc. (C) A sketch of a bed with domal features as seen in B. Upward growth of mats is driven by competition for light, and as sediment is transported across the mat surface by currents it is trapped by the sticky mucilaginous mat surface. The latter results in preferred up-current growth of stromatolite laminae. From Schieber (1999); reproduced with permission of SEPM (Society for Sedimentary Geology).

Microbial mats produce stratiform chemical boundaries that may be recognised in the rock record. Formation of 'anoxic' minerals in the reducing pore waters beneath mats may thus produce thin, well defined, and laterally extensive horizons of minerals such as ferroan carbonates or pyrite. Observing such minerals in shallow water sandstones can therefore be a 'tip-off' for the former presence of microbial mats (Gerdes et al., 1985b; Garlick, 1988; Schieber, 1999).

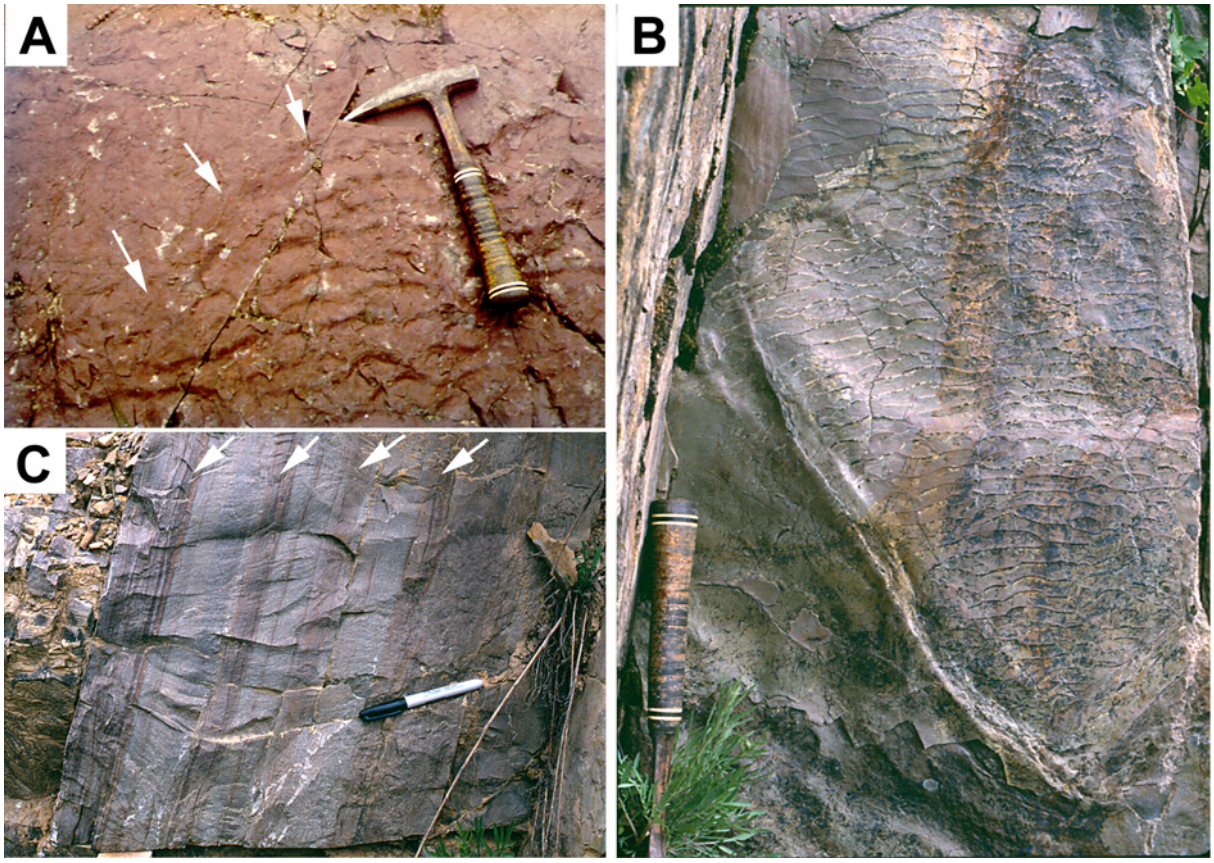


Figure 7(b)-8: Mt. Shields Formation.
(A) Photo of the edge of a ripple patch in the Mt. Shields Formation. The photo shows the smooth transition between the rippled area and the non-rippled part of the bed surface. This type of margin is typical for other ancient and modern examples of ripple patches in microbially stabilised sand surfaces (e.g., Schieber, 1999). It indicates a contemporaneous origin of the two surface types and provides an argument for microbial mat stabilisation of the non-rippled part of the bedding plane (Wunderlich, 1979). See also Section 7(i). Hammer is 32 cm long. (B) Photo of a patch of small ripples in an otherwise smooth bedding plane of the Mt. Shields Formation. The rippled surface passes without physical break into the surrounding smooth area (lower right corner of image). The small wave length of the ripples suggests that these may be what Singh and Wunderlich (1978) described as mini-ripples, produced by slow moving waves in water only a few centimetres deep. Hammer handle is 180 mm long. (C) Photo of a steeply dipping sandstone bed in the Mt. Shields Formation that has iron-stained intervals (marked with white arrows). The iron stain is due to oxidation of ferroan carbonate cement (ferroan dolomite, siderite) and/or dispersed diagenetic pyrite in these intervals. The strict stratiform distribution of these minerals indicates particularly reducing conditions in these horizons, possibly due to decay of organic matter beneath microbial mats that colonised these horizons. The marker pen is 135 mm long.

The outcrop photos in Figure 7(b)-6 illustrate several features that can be associated with this type of mat record. The thin stratiform iron stains in Figure 7(b)-6A may be horizons produced by comparatively thin mats that colonised a sandy surface in between sedimentation events. The thicker layers in Figure 7(b)-6B, in contrast, have a more spotted (speckled) appearance, which may reflect the decay of discrete organic particles (mat fragments) that were buried in an accumulating sand layer and led to localised reducing conditions as they decayed. This interpretation is supported by experiments that show (Chapter 8(c)) that physical diminution of eroded microbial mats during transport produces abundant millimetre-sized particles that are buried in associated sands.

Figure 7(b)-6C is from an exposure originally described by Garlick (1988), and shows what appears to be a scour depression that is filled with sand that has curved areas of iron stain. These are interpreted as the remains of curved microbial sand chips. These were presumably produced when microbial mats on sandy substrate desiccated, cracked, and formed abundant concave fragments. These fragments were entrained by the waters of a subsequent flood and redeposited and buried in a scour depression before they had a chance to soften again. Experimental work on transport of eroded microbial mats (Chapter 8(c)) suggests that they probably were transported for only

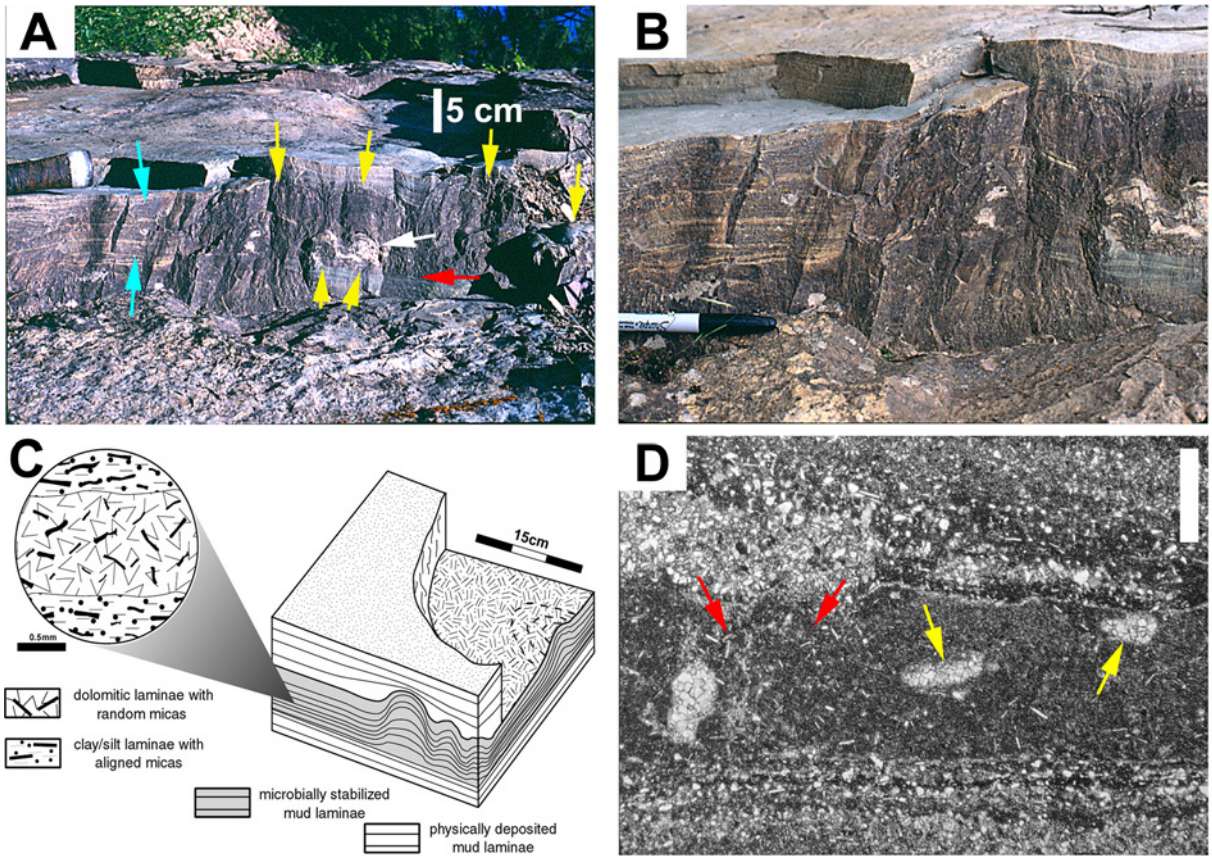


Figure 7(b)-9: Mt. Shields Formation.
(A) Photo of greenish shale (argillite) of the Mt. Shields Formation with small stromatolite-like domal buildups (yellow arrows). These buildups developed on an originally flat surface (red arrow), show over-steepened laminae (white arrow), and laminae pass into surrounding horizontally laminated shale. The turquoise arrows bracket a package of horizontal laminae that is the lateral equivalent to the buildup laminae. (B) Close-up photo of central portion of A. Felt pen cap is 5 cm long (scale). (C) Sketch of small domal buildups as seen in A and B. It highlights over-steepened laminae at the edges of buildups. Those intervals that contain domal buildups are characterised by alternating dolomitic and clay/silt laminae (see detail drawing). The dolomitic laminae are interpreted (Schieber, 1998b) as fossil microbial laminae on the basis of randomly oriented mica flakes and fenestral fabric (see D). The shale (argillite) draping over these small domes consists only of clay and silt laminae; dolomitic laminae are absent. From Schieber (1999); reproduced with permission of SEPM (Society for Sedimentary Geology). (D) Photomicrograph of dolomitic lamina. Shows fenestrae filled with clear dolomite spar (yellow arrows). Red arrows point out area with abundant randomly oriented mica flakes. Scale bar is 0.5 mm long. These laminae are thought to record microbial colonisation of the mud surface (Schieber, 1998a).

a short distance (1–2 km at most) and buried within an hour of being eroded. Burial in water-saturated sediments enabled microbial degradation of the organic matter in these sand chips, led to localised reducing pore waters, and to precipitation of ferroan minerals.

Limonite stains with a contorted appearance (Figure 7(b)-6D) are suggestive of sandstone intervals that experienced soft sediment deformation. Microbially bound sandstone surfaces behave like cohesive sheets under these conditions, rather than a simple mixture of sand and organic debris.

In places, Revett sandstones also formed dome-shaped buildups (Figure 7(b)-7B) that are reminiscent of domal stromatolites reported from carbonates (e.g., Water et al., 1992). More commonly, however, iron stained mat layers are largely planar (Figure 7(b)-6A) with minor local thickening (Figure 7(b)-7A) that may be considered as incipient stromatolites of the type shown in Figures 7(b)-7B and -7C.

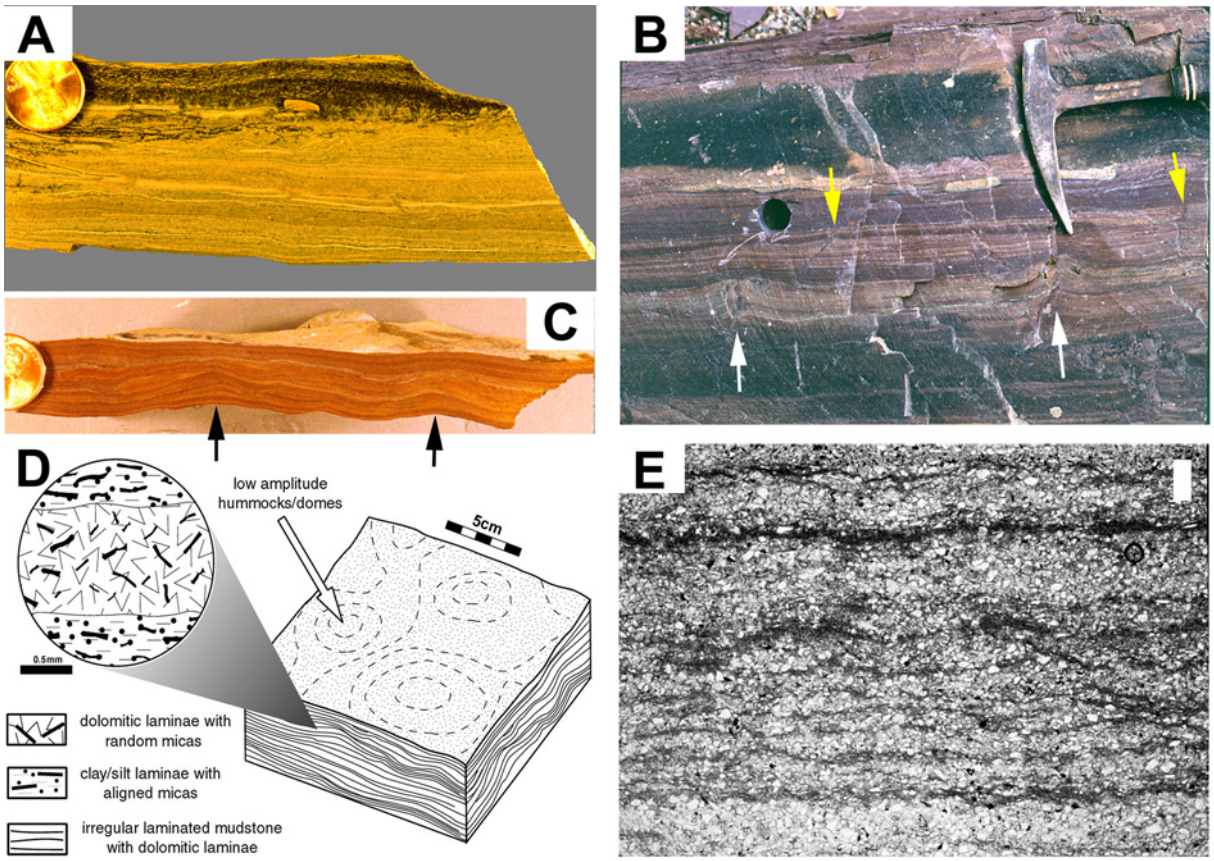


Figure 7(b)-10: Mt. Shields Formation.
(A) Photo of sawed and smoothed sample of greenish Mt. Shields shale (argillite) with lighter coloured dolomitic laminae. The latter show randomly oriented mica flakes and in places fenestral fabric, and are interpreted as laminae that record microbial colonisation of mud surfaces (Schieber, 1998a; see also Figure 7(b)-9). Note that in the upper third of the sample weathering-related oxidation is obscuring the depositional fabric. Coin is 19 mm in diameter. (B) Outcrop photo of Mt. Shields Formation that shows interbedded sandstone beds (dark, massive appearance) and intervals of red shale (argillite). For one shale horizon, this photo shows uparched shale (argillite) laminae adjacent to mudcracks (white arrows). These are interpreted as microbially induced growth ridges (Gerdes et al., 1993). The area between the arrows resembles the cross-section of a polygonal stromatolite. Note for contrast the much smaller relief next to mudcracks in the overlying shale interval (yellow arrows). The lighter coloured laminae are dolomitic, show randomly oriented mica flakes, and are interpreted as microbial. Hammer head is 18 cm long. (C) Photo of cut and ground specimen of red Mt. Shields shale (argillite). Note irregular lamina structure and small domal buildups (black arrows). Coin is 19 mm in diameter. (D) Sketch that shows the low amplitude dome/hummocks seen in C in a three-dimensional context. The irregular laminae of these reddish shales (argillites) are characterised by alternating dolomitic and clay/silt laminae (see detailed drawing). Micas are aligned in terrigenous laminae, and random in dolomite laminae. The latter are interpreted as microbial in origin (Schieber, 1998b). From Schieber (1999); reproduced with permission of SEPM (Society for Sedimentary Geology). (E) Photomicrograph of fine sandy to silty laminae in Mt. Shields shale (argillite). Note wavy-crinkly laminae that contrast with the more planar laminae typical for physically deposited laminae. This style of lamination may indicate surface binding by microbial mats. Scale bar is 0.2 mm long.

Mt. Shields Formation: ripple patches, iron stains, and domes

Wallace (1998) described the Mt. Shields Formation as a delta complex that prograded north into a shallow marine environment. Coarse sandstones were interpreted as deposited in delta-channel, delta-plain, delta-front, and strand-plain environments, fine sandstones were modelled as shallow marine deposits, and argillaceous and silty deposits ascribed to extensive shallow marine mudflats. In contrast, Winston (1986) has proposed a lacustrine interpretation. Yet, as summarised in the introduction to this chapter, the cumulative evidence suggests that the Belt Supergroup was deposited in an epicontinental basin that was connected to the Proterozoic ocean.

Although the Mt. Shields Formation is well known for bedding plane exposures with superbly preserved wave ripples, many sandstone bedding planes are nonetheless comparatively smooth and featureless. In a number of places these bedding planes show ripple patches (Figures 7(b)-8A and -8B) that compare well to those described from mat stabilised tidal sand flats of Mellum Island in the North Sea (Reineck, 1979), and to those described from the Cretaceous Dakota Sandstone (see this chapter, Section 7(i)). This suggests that the smooth sandstone surfaces were mat stabilised as well, and that the ripple patches mark places where storms partially eroded the mat and enabled ripple formation in the underlying sand stratum.

In various locations, nearshore and coastal plain sandstones of the Mt. Shields Formation also show stratiform iron stained intervals that look very similar to those observed in sandstones of the Revett Formation (Figure 7(b)-8C). They are likewise interpreted as the diagenetic testament of microbial mats that intermittently colonised and stabilised sandy surfaces.

Whereas microbial laminated layers in mudstones are in many instances planar due to the considerable post-depositional compaction that these rocks typically undergo, reddish and greenish mudstone-dominated intervals in the Mt. Shields Formation locally show domal features of considerable relief (Figures 7(b)-9 and -10). These domal features are associated with mudstones that in addition to clay- and silt-rich laminae contain dolomite-rich laminae (Figure 7(b)-9D). The latter contain variable amounts of finely crystalline dolomite, quartz silt, micas and clays, and occur in domal buildups as well as in adjacent evenly laminated mudstones (Figures 7(b)-9A and -9B). Where these laminae are dolomite-dominated they show fenestral fabric (Figure 7(b)-9D) and are indistinguishable from dolomite laminae in carbonate stromatolite horizons of the Mt. Shields Formation (Schieber, 1998a). The combination of randomly distributed and oriented micas, fenestrae, wavy-undulose laminae, and association with domal buildups suggest that these laminae mark microbial mat stabilised sediment surfaces (Schieber, 1998a). Early cementation of dolomite-enriched laminae may have helped to preserve relief in clay-rich facies (Figures 7(b)-9A and -9B). In silt-rich facies (Figures 7(b)-10C and -10E), a smaller degree of post-depositional compaction probably contributed to preservation of low amplitude domes (Figure 7(b)-9C).

The unusual raised rims of mudcrack polygons in some mudcracked intervals of the Mt. Shields Formation (Figure 7(b)-10B) may also be a reflection of surficial microbial mats. They are unusual because there is relief on the order of 1–2 cm between cracks and adjacent areas, whereas 'normal' mudcracked intervals show negligible relief in comparison (Figure 7(b)-10B). The raised polygon rims closely resemble cross-sections of polygonal mats from modern environments (Till, 1978). Upturned and uparched laminae adjacent to cracks look similar to what has been described as growth ridges from modern polygonal mats (Black, 1933; Ginsburg, 1960; Horodyski et al., 1977; Gerdes et al., 1993; see also Chapter 4, Figures 4(c)-5 and -6). Standing water in the cracks promoted preferential microbial growth adjacent to cracks, and continued growth accentuated the ridges and led to formation of concave-upwards saucers. This scenario is also supported by the observation of dolomitic laminae of presumed microbial mat origin (see above). These dolomitic laminae are discussed further in the section on metabolic effects on mat structure in sands and sandstones (Chapter 4(b)).

McNamara Formation: ripple patches and pustular surfaces

The overall depositional setting of the McNamara Formation was probably similar to that proposed for the Mt. Shields Formation above, with an abundance of sea-marginal sandflats and deltaic environments. Sandstone surfaces with ripple patches (Figure 7(b)-11A) have been observed in several places. Analogous to interpretation of these features in the Mt. Shields Formation (see above) and the Dakota Sandstone (Section 7(i)), they are considered to have resulted from partial erosion of a microbially bound sand surface.

Figure 7(b)-11B shows a sandstone bed with a variably 'bumpy' surface. The 'bumpy' areas may represent interference ripples, but there are also comparatively smooth areas that carry millimetre-scale wrinkles and pustules. In thin section, the uppermost centimetre of the sandstone bed consists of wavy-crinkly clay and silt laminae (Figure 7(b)-11C). They resemble laminae seen in cross-sections of microcolumnar buildups or microbial tufts from modern mats (Gerdes and Krumbein, 1987). The interlaminated clay and silt (Figure 7(b)-11D) indicates that this surficial layer had formed under conditions of lower and fluctuating energy, after the surface of the sandstone bed had been partially rippled.

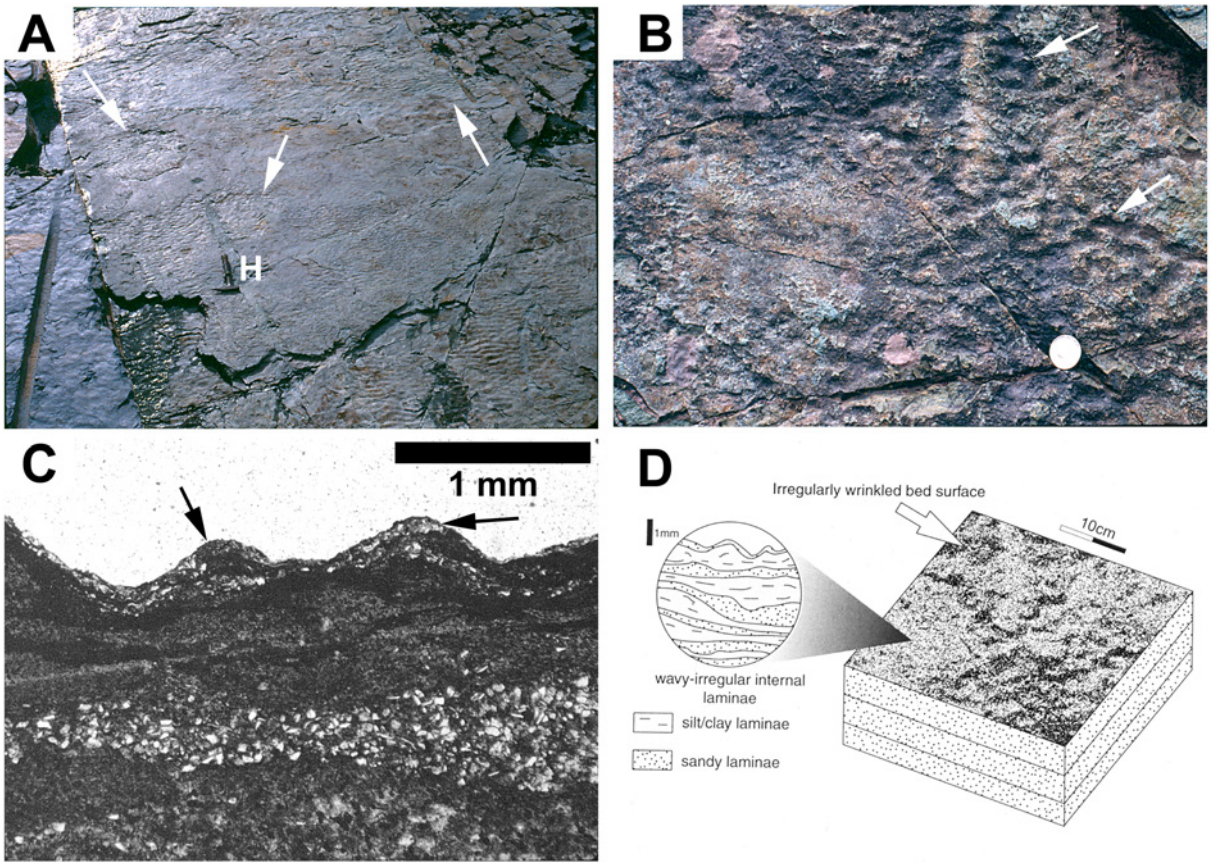


Figure 7(b)-11: McNamara Formation.

(A) Ripple patches (arrows) on sandstone bedding plane in McNamara Formation. This bedding plane shows considerable resemblance to partially eroded microbially stabilised surfaces as illustrated by Reineck (1979) and Gerdes et al. (1985b). The rippled surface above the hammer (marked H) passes without a break into the surrounding smooth surface (see D), an indication that the rippled surface and the smooth surface are contemporaneous. Hammer is 31.5 cm long. (B) Pustular-crinkled bedding plane surface in fine sandstone of the McNamara Formation. Surface features pointed out by arrows probably represent rippled (interference ripples?) surfaces. In detail there is a pustular-crinkled surface morphology superimposed on these ripples (see C and D). Coin is 24 mm in diameter. (C) Photomicrograph of thin section cut perpendicular to surface in B. Note the mm-scale surface wrinkles (arrows) that contrast with laminae below surface. This surface morphology is superimposed on the larger scale ripple morphology, and is potentially of microbial origin. (D) A sketch that contrasts the irregularly wrinkled/rippled bed surface seen in B (due to interference ripples) with the finely wrinkled surface morphology of presumed microbial origin as seen in C. From Schieber (1999); reproduced with permission of SEPM (Society for Sedimentary Geology).

7(c). MICROBIAL MAT FEATURES IN MUDSTONES OF THE MESOPROTEROZOIC SOMANPALLI GROUP, PRANHITA-GODAVARI BASIN, INDIA

S.P. Deb, J. Schieber, A.K. Chaudhuri

The Pranhita-Godavari Basin is located in the northeastern portion of peninsular India (Figure 7(c)-1) and contains several kilometres of Proterozoic sediments (Chaudhuri et al., 1999, 2002). A mudstone-shale dominated succession of Mesoproterozoic age developed around Somanpalli along the northeastern margin of the Pranhita-Godavari valley adjoining the Bastar craton (Figure 7(c)-1), is known as the Somanpalli Group (Saha and Gosh, 1998).

Recent stratigraphic analysis of the Somanpalli Group indicates that the lowest formation of the group, the Somnur Formation, comprises a thick shelf sequence of cross-stratified and planar-stratified sandstone, sandstone–mudstone heterolithic intervals, and shale, approximately 1000 m thick. The Somnur Formation grades upwards into the Tarur Nala Formation, an approximately 1000 m thick succession dominated by mudstones and shales, minor carbonates, and very minor amounts of fine-grained dark sandstone. The lower part of the Tarur Nala Formation is dominated by black to steel grey mudstone and shale (Sample No. S-3-3A), whereas its upper part comprises a very persistent striped-shale with red and light buff banding (Rest House Shale; samples SGH 1 and 2). A few lenses of coarse-grained to gritty sandstone occur at the top of the Rest House Shale, probably the fill of erosive submarine channels (Sample BJ 07/03). The sandstone lenses represent the coarsest grade of siliciclastics, constitute a minor fraction of the succession, and may be an indicator of falling sea level towards the end of Tarur Nala deposition.

The Tarur Nala Formation is overlain by the Bodela Vagu limestone, interpreted as a slope-basin deposit (Figure 7(c)-2). The Bodela grades upwards into the Kopela Shale, a turbidite–pelagite deposit with very minor amounts of sandstone. The Kopela Shale is dominated by massive and thinly laminated black shale (Sample Nos. 8E/95 and 4/5). The Somanpalli Group is unconformably overlain by the Po Gutta Sandstone. This unconformity most likely denotes a major hiatus. The Po Gutta Sandstone is a formation of the Neoproterozoic Albaka Group.

Figure 7(c)-3 (images A–D) illustrates carbonaceous shales from the lower portion of the Tarur Nala Formation. A characteristic feature of these shales is that they contain carbonaceous fragments (1 mm or less in size) that look variably degraded when compared with likely microbial mat fragments from other units in the Somanpalli Group (Figures 7(c)-4 and -6). Whether these fragments are indeed degraded and redeposited microbial mat fragments is difficult to ascertain, but they do appear to be fragments that were deposited in a soft and pliable state and contained carbonaceous laminae (Figure 7(c)-3B). These shales resemble grey shales with carbonaceous streaks and lumps that were described from distal shale facies in the eastern Belt Basin (Schieber, 1989b). In the latter example carbonaceous streaks and lumps were interpreted as redeposited microbial mat fragments because of lateral association with shale facies that contained benthic microbial mats (Schieber, 1986).

Figure 7(c)-4 illustrates shales from the middle portion of the Tarur Nala Formation. The most striking feature of these shales is their banded or striped nature (Figure 7(c)-4A). The shales consist of grey clay-dominated layers that alternate with reddish layers that show a faint wavy internal lamination. When viewed in detail, it is obvious that the reddish colour is due to secondary formation of iron oxides (Figures 7(c)-4B to -4E), probably derived from oxidation of finely disseminated pyrite during weathering. The reddish layers also show more abundant and larger silt grains and wavy-crinkly internal laminae (Figures 7(c)-4D to -4F). Texturally, these shales are a very close match to striped shales from the Mid-Proterozoic Belt Supergroup (Schieber, 1986; compare with Figure 5-3 of this book). The latter were interpreted as the deposits of benthic microbial mats (carbonaceous pyritic layers) whose accumulation was intermittently interrupted by rapid deposition of storm-derived mud drapes (grey clay layers). By direct comparison with its Belt Basin counterpart (Schieber, 1986), the reddish layers in the striped shales from the Tarur Nala Formation are interpreted as the weathered equivalents of wavy laminated carbonaceous–pyritic layers in Belt Basin striped shales. Although in the Tarur Nala samples all of the original pyrite and carbonaceous matter have been oxidised, the textural details, such as wavy-crinkly internal lamination, silt enrichment, and sharp contacts between grey and red layers (Figure 7(c)-4E) are the same as in the Belt Basin striped shales. Vertically and obliquely oriented embedded mica flakes in grey interbeds of the Tarur Nala striped shales (Figures 7(c)-4G and -4H) suggest 'hindered' settling in a rapidly accumulating clay deposit. This supports the notion that, as in the Belt Basin example, these interlayers were event deposits, possibly due to storms or flood-related river plumes. Also, weathered and fully oxidised samples collected from Belt Basin outcrops look identical to the pictured samples of the Tarur Nala Formation (Schieber, 1985).

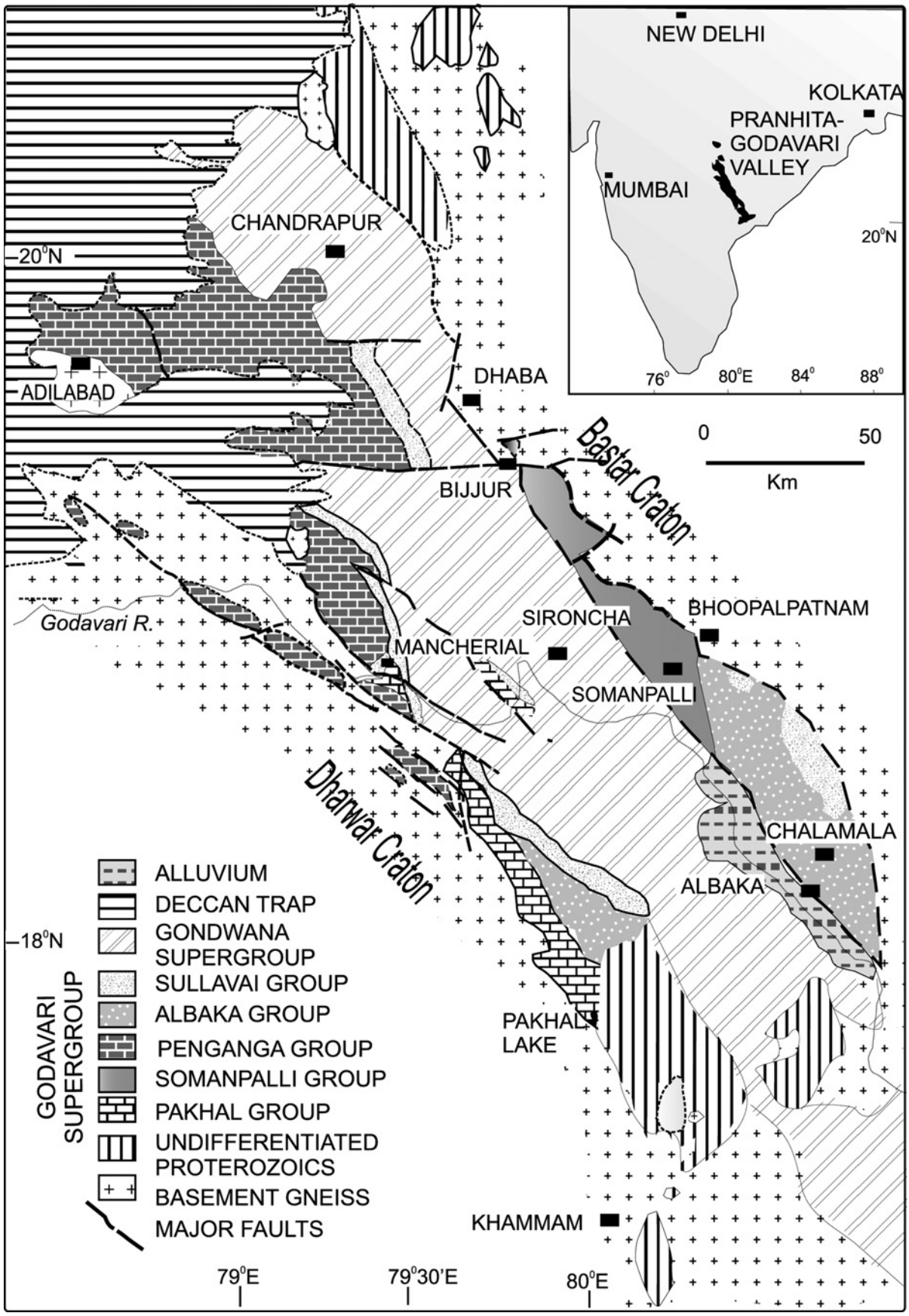


Figure 7(c)-1: Schematic geological map of the Pranhita-Godavari valley region. Outcrops of the Somanpalli Group occur to the right of the centre of the map.

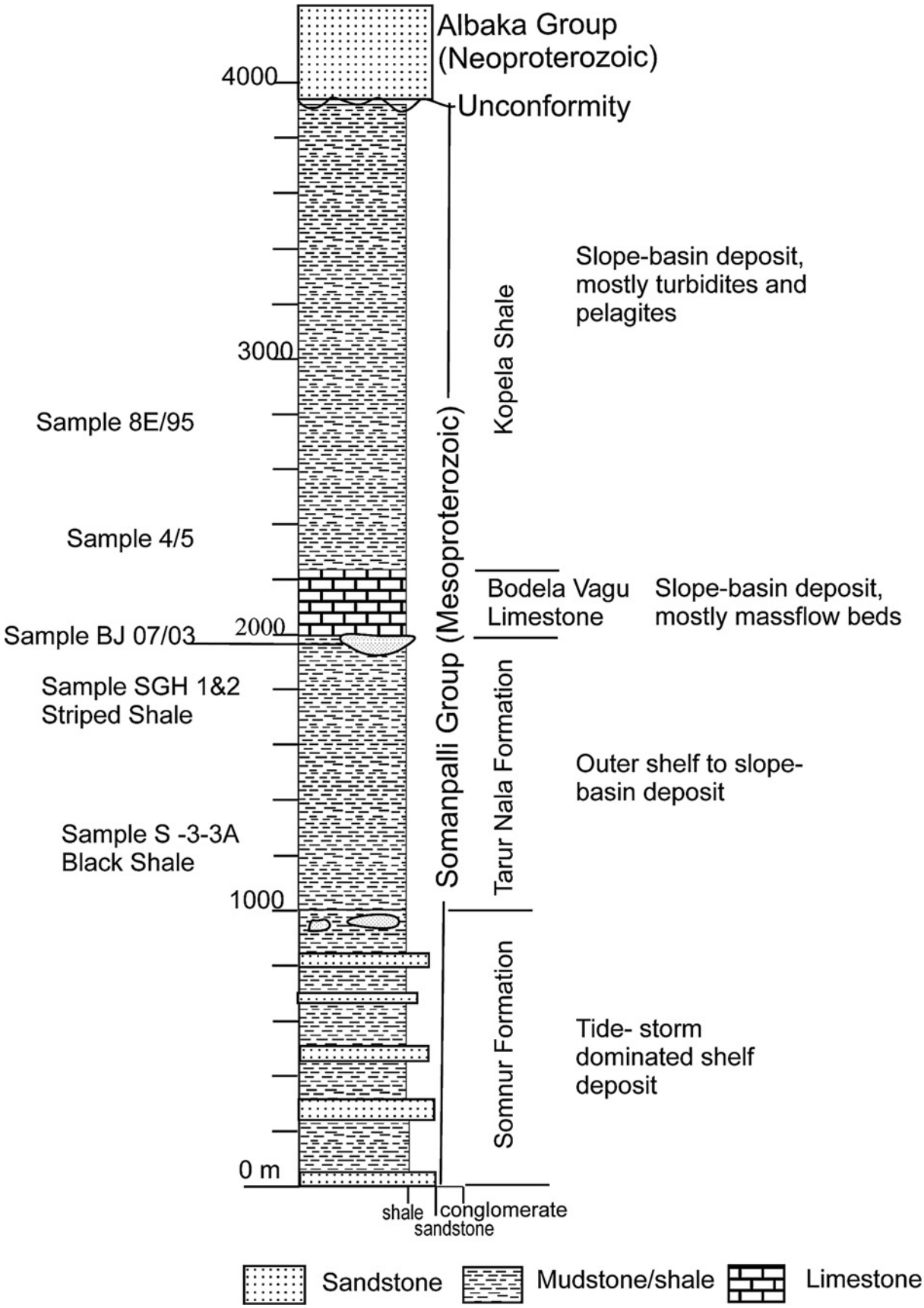


Figure 7(c)-2: Simplified stratigraphic column of the Somanpalli Group with locations of described samples, and inferred depositional setting.

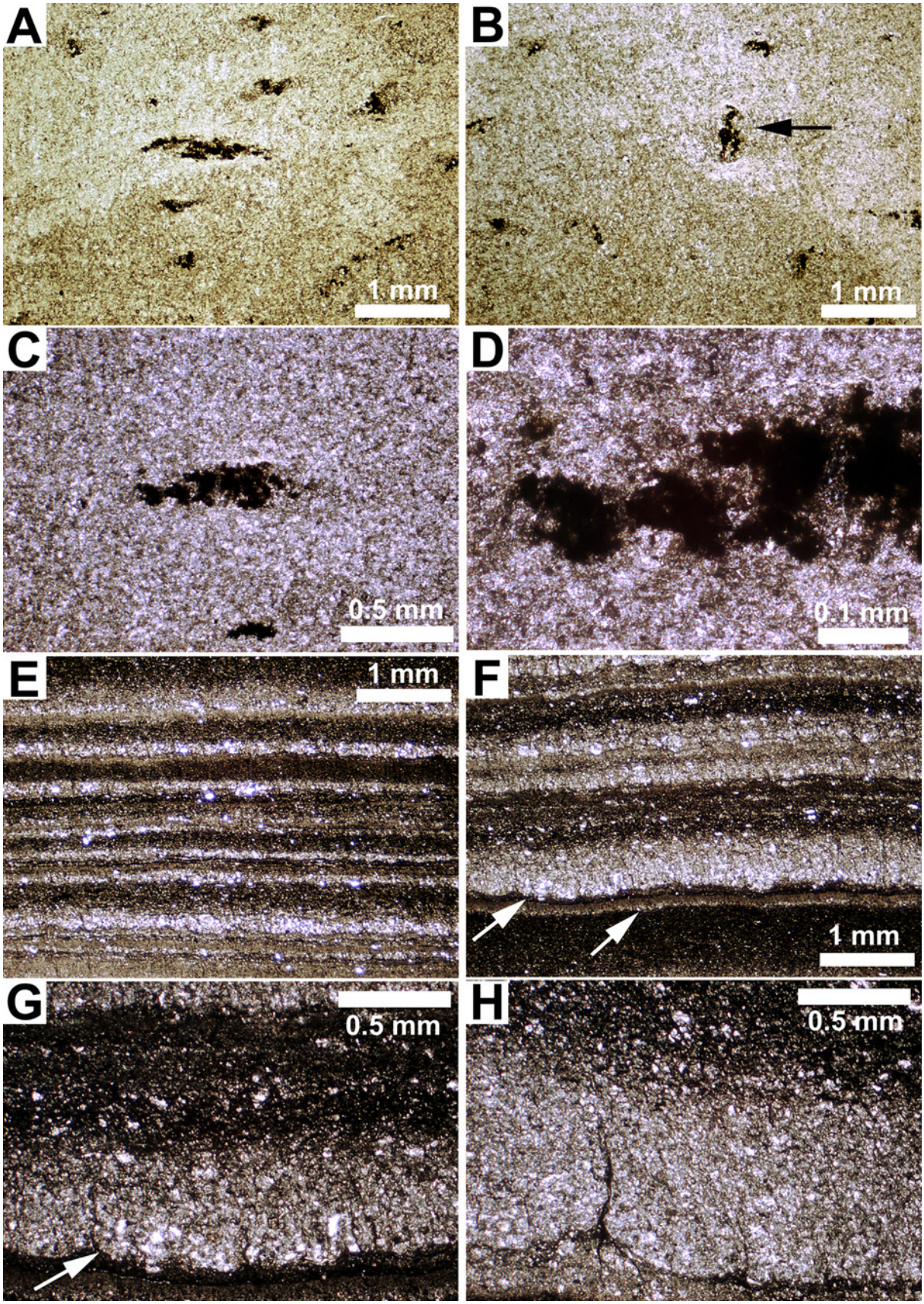

A
1 mm
B
1 mm
C
0.5 mm
D
0.1 mm
E
1 mm
F
1 mm
G
0.5 mm
H
0.5 mm

Figure 7(c)-3: (A–D) Lower portion of Tarur Nala Formation, photomicrographs of carbonaceous shales. (E–H) Lower portion of Kopela Shale, photomicrographs of laminated silty shales.
(A) Gray shale with carbonaceous lumps. These may be the degraded remains of microbial mat fragments that were transported into a deeper water setting. (B) In places these lumps show contortions (black arrow) that suggest shortening due to compaction of vertically embedded fragments of carbonaceous laminated shales. (C, D) Close-up views of carbonaceous lump in grey shale. Textural features of microbial mat laminae, such as seen in eroded mat fragments in Figures 8(c)-2 and -4, are not visible. (E) Photomicrograph of finely silt-laminated grey shale from the lower portion of the Kopela Shale. (F) Photomicrograph of finely silt-laminated grey shale from the lower portion of the Kopela Shale. Shows graded silt–mud couplets (lower white arrow), and graded silt layer with sharp base (upper white arrow). The irregular base of the latter layer is suggestive of scouring. (G) Close-up of graded silt layer with sharp, possibly micro-scoured base. (H) Close-up of graded silt layer with darker clay-rich tongues that extend upwards from the base. This may suggest that the irregular base may in part be due to formation of small load casts and the formation of complementary flame structures. However, caution needs to be exercised here because these rocks show in places a weakly developed slaty cleavage. Where this cleavage cuts across the base of graded layers it may produce features very similar to micro-scouring or tiny load and flame structures.

Figure 7(c)-5 illustrates shale fragments that occur in small lenses towards the top of the Tarur Nala Formation. Many of these fragments show wavy-crinkly carbonaceous laminae (Figures 7(c)-5A, -5B, -5D, -5E, -5F), soft sediment deformation, and overfolding (Figure 7(c)-5C) that in the context of other observations (Figures 7(c)-4 and -6) strongly suggest that these fragments were eroded from shales that were stabilised by benthic microbial mats. Non-carbonaceous shale fragments (Figures 7(c)-5G and -5H) probably represent eroded grey interbeds and/or clay- dominated shale facies from nearshore areas (e.g., Schieber, 1989b).

In context, the samples from the Tarur Nala Formation suggest an overall shallowing-upwards trend. Distally deposited carbonaceous-streak-shales occur at the base of the succession (sample S-3-3A), pass upwards into striped shales deposited in an offshore shelf setting (samples SGH 1 and 2), and erosive sand-filled channels with reworked mat fragments occur at the very top (sample BJ 07/03).

Shales from the Kopela Shale (Figure 7(c)-2) are illustrated in Figures 7(c)-3 (images E–H) and 7(c)-6. Photomicrographs from the lower portion of the Kopela Shale show it to be a largely grey shale with abundant fine silt laminae (Figures 7(c)-3E and -3F). In many instances the silt laminae show grading and may also form discernible silt–clay couplets (Figure 7(c)-3F). Graded silt layers have sharp bases that may be erosional, and may also show evidence of loading of an unconsolidated surface (Figures 7(c)-3G and -3H). In the context of observed sandy turbidites within this unit (Saha and Ghosh, 1998), these graded laminae and couplets are interpreted as fine-grained turbidites (Stow and Shanmugam, 1980). Figure 7(c)-6 shows photomicrographs from a massively bedded carbonaceous shale somewhat higher in the Kopela Shale succession (Figure 7(c)-2). A characteristic feature of these shales is that they contain carbonaceous fragments (less than 1 mm to 10 mm in size) in a fine crystalline clay–silt matrix. The carbonaceous fragments can be very thin carbonaceous films that show overfolding and deformation (Figures 7(c)-6A and -6B), or they are fragments of a shale with abundant wavy carbonaceous laminae (Figures 7(c)-6C and -6D). These fragments have a high degree of textural similarity to redeposited microbial mat fragments in shales of the Mid-Proterozoic Belt Supergroup of Montana (Schieber, 1986, 1989b). Overfolding of thin fragments during transport (Figures 7(c)-6A and -6B) indicates that the material that constituted the thin carbonaceous films possessed considerable cohesive strength during transport and deposition. Frayed edges of these fragments (Figures 7(c)-6E and -6F) also attest to internal cohesion, and adherence of silt lenses during fragment transport (Figure 7(c)-6E) suggests some binding material. All of these features are consistent with a microbial mat origin for the carbonaceous fragments. Larger fragments also show wavy-crinkly carbonaceous laminae of the same style as observed in benthic microbial mats from the Belt Supergroup (Schieber, 1986).

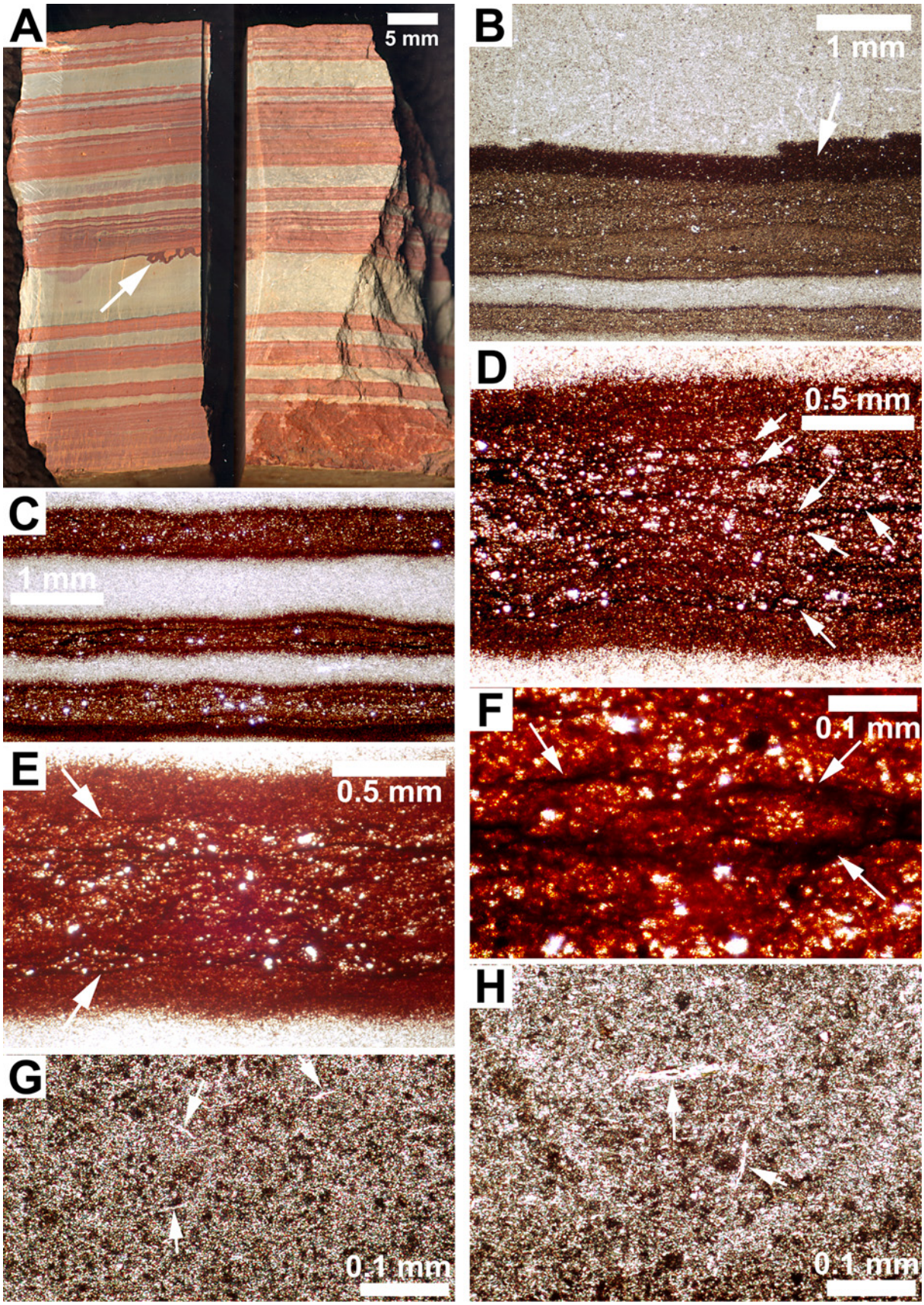

A
5 mm
B
1 mm
C
1 mm
D
0.5 mm
E
0.5 mm
F
0.1 mm
G
0.1 mm
H
0.1 mm

Figure 7(c)-4: Upper portion of Tarur Nala Formation, photos and photomicrographs of striped carbonaceous shales.

(A) Photo of hand specimen of shale with alternating reddish and light buff layers. The red colour is due to oxidation. These specimens are texturally and compositionally very similar to strongly weathered striped shales from the Belt Basin (Section 7(b)). It is presumed that beneath the zone of weathering, these shales will show alternating carbonaceous (wavy laminated and pyritic) and grey layers (mostly clay and silt), just like their textural counterparts in the Belt Basin (Schieber, 1986). During oxidation and pyrite destruction, dissolved iron migrated into the clay-dominated grey layers and locally caused cross-cutting impregnations with iron oxides (white arrow). (B) Photomicrograph (transmitted light) of thin section from same specimen as in A. Shows that the darker (reddish-brown) layers are enriched in silt, and have wavy internal laminae. Also shows heavy iron oxide impregnation (white arrow) just above the silty and wavy laminated layer. (C) Photomicrograph of alternating dark (iron oxide-enriched) and light layers (clay-enriched). The darker iron-enriched layers have higher silt content, show wavy laminae, are iron oxide-enriched, and have diffuse iron oxide-enriched margins that fade into over- and underlying grey layers. (D) Close-up of dark (reddish) layer (photomicrograph, transmitted light). Shows wavy anastomosing laminae (arrows) and silt content. In striped shales of the Belt Basin (Schieber, 1986), the carbonaceous layers that are interpreted as microbial mat deposits are likewise enriched in silt and show wavy anastomosing internal laminae. In unweathered shale of this type (Belt Basin) the latter contain abundant organic matter and finely crystalline pyrite. (E) Another close-up (photomicrograph, transmitted light) of dark (reddish) layer with more abundant silt and wavy anastomosing laminae. White arrows point to upper and lower boundaries of the original carbonaceous and pyritic layer. The iron stained zones above and below the original layer represent weathering-related iron migration and impregnation. (F) Detail of anastomosing laminae (white arrows) seen in D and E (photomicrograph, transmitted light). (G, H) Detailed view of grey-buff interbeds as seen in A (photomicrograph, transmitted light). In comparison with F (taken at the same magnification), the grey-buff layers are clearly lower in silt content. Large mica flakes are pointed out by white arrows. Note that the mica flakes are not aligned with bedding and may also be almost vertical (see H). This suggests rapid deposition from a turbulent suspension. In the Belt Basin, analogous layers were interpreted as distal muddy tempestites.

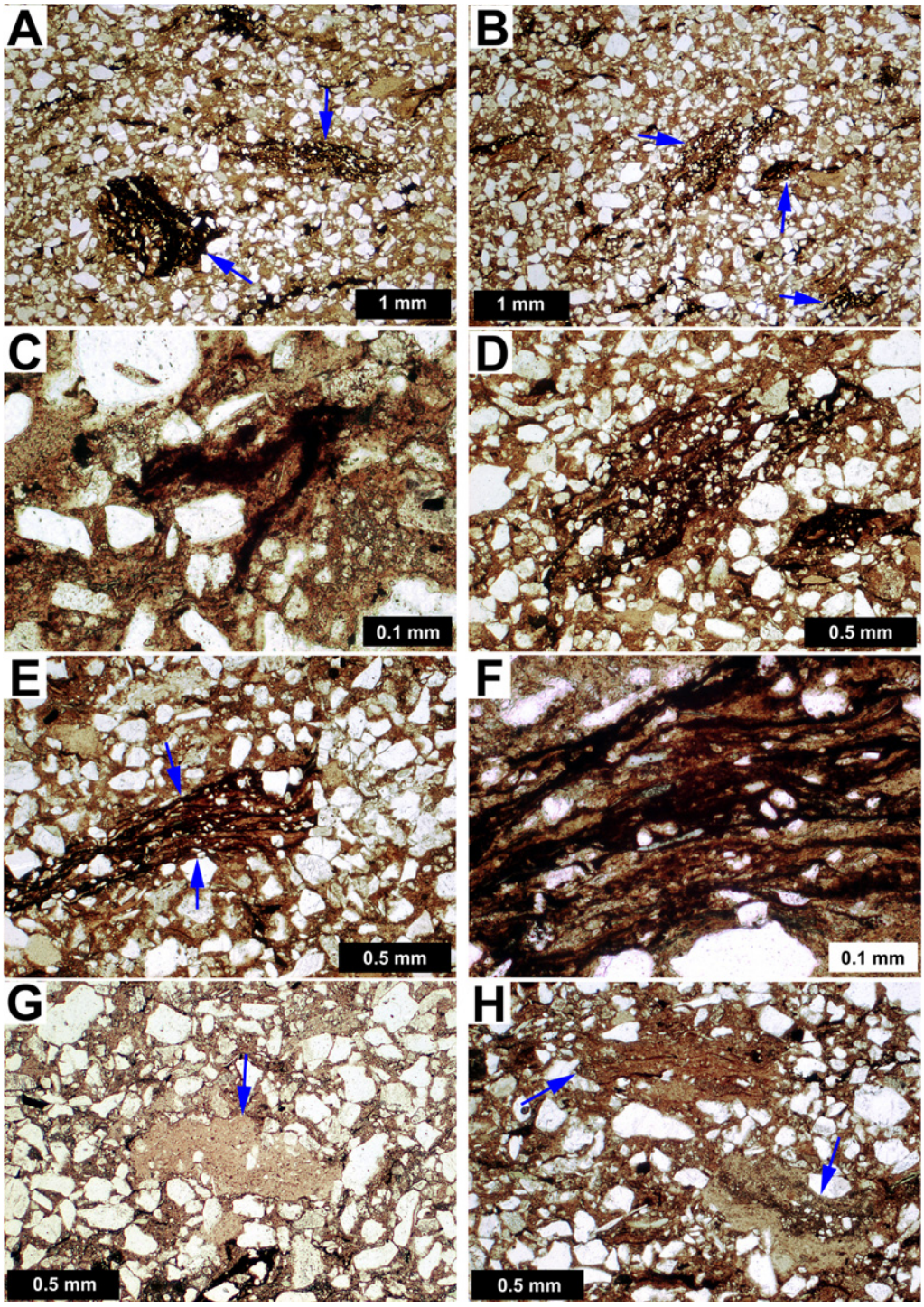


Figure 7(c)-5: Upper Portion of Tarur Nala Formation, photomicrographs from sandstone channel-fills within striped carbonaceous shales.

(A, B) Photomicrographs (transmitted light) of channel sandstone. These sandstones contain abundant shale clasts. Shale clasts are typically carbonaceous and have wavy-anastomosing internal laminae, and show soft sediment deformation (arrows). (C) Close-up photomicrograph (transmitted light) of strongly deformed small shale clast with a single carbonaceous lamina. (D) Close-up photomicrograph (transmitted light) of deformed shale clast seen in centre portion of B. Note deformation and the much finer grain size (silt) that contrasts with the sand grains in the rock matrix. (E, F) Photomicrographs (transmitted light) of shale clast (arrows) with well developed wavy-anastomosing carbonaceous laminae (close-up in F). Note again the grain size contrast with the surrounding sand matrix, and the soft sediment deformation of the clast (see image E). (G, H) Close-up photomicrograph (transmitted light) of deformed shale clasts that lack carbonaceous laminae (arrows). These are clasts derived from other shale facies types that were laterally associated with the carbonaceous shales.

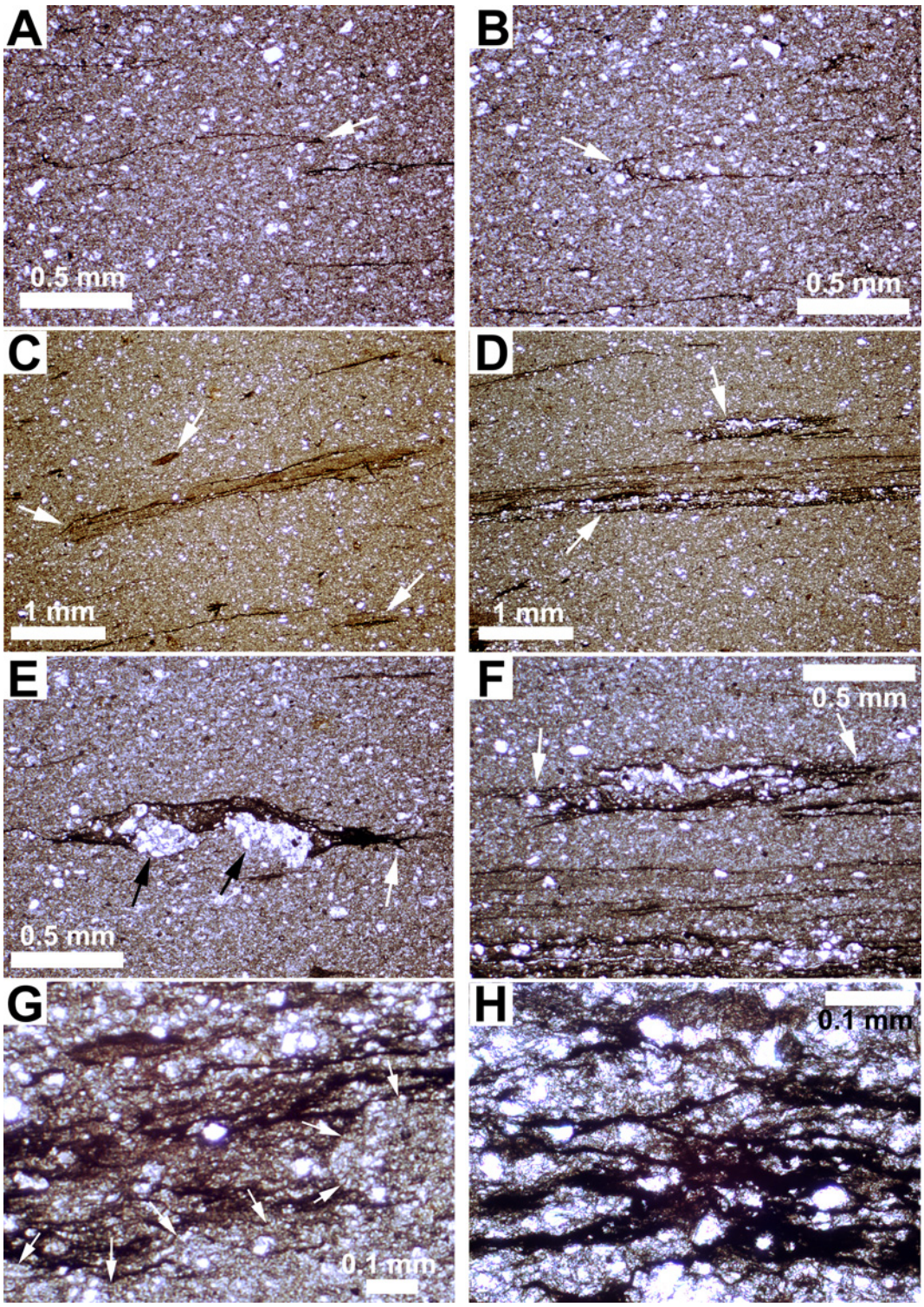


Figure 7(c)-6: Kopela Shale, photomicrographs of carbonaceous shales with microbial mat fragments. (A, B) Gray shale with thin carbonaceous wisps. These very thin carbonaceous features show frequent occurrence of 'fold-overs' (white arrows), an indication that they were thin, cohesive, sheet-like features at the time of deposition. (C) Carbonaceous wisps and larger shale clasts with internal carbonaceous laminae of the same appearance as carbonaceous wisps in A and B. (D) More large shale clasts with internal carbonaceous laminae as in C. These clasts also contain silt-rich carbonaceous laminae (white arrows). (E) Close-up of silty carbonaceous shale clast. Note deformation of shale clast around compaction-resistant 'silt pockets' (black arrows) and wavy-anastomosing carbonaceous laminae. Also note the frayed character of carbonaceous laminae at right side of clast (white arrow). The more or less pure 'silt pockets' associated with this fragment suggest that they adhered to the shale fragment during transport. Such adherence can be attributed to the binding properties of microbial slime (EPS) and/or

microbial filaments, and the frayed edges attest to the tearing of a sheet-like material of comparatively high internal coherence. (F) Close-up of another silty carbonaceous shale clast. Note silt-rich lamina and frayed edges at either end of the clast (white arrows). The frayed character is accentuated by carbonaceous laminae and suggests that the cohesiveness of these clasts derives from the substance that formed the (now) carbonaceous laminae. These observations are consistent with a microbial mat origin for the carbonaceous laminae. (G) Frayed edge of carbonaceous silty shale clast in close-up. Note textural and compositional contrast between the clast and the surrounding matrix (lower right corner of image). Clast is higher in organic matter and silt-enriched, whereas surrounding shale matrix has more clay and less silt and organic matter. Contact between clast and shale matrix marked with white arrows. (H) Close-up of texture of silty carbonaceous shale clast. Note anastomosing carbonaceous laminae and silt-rich lenses of clast.

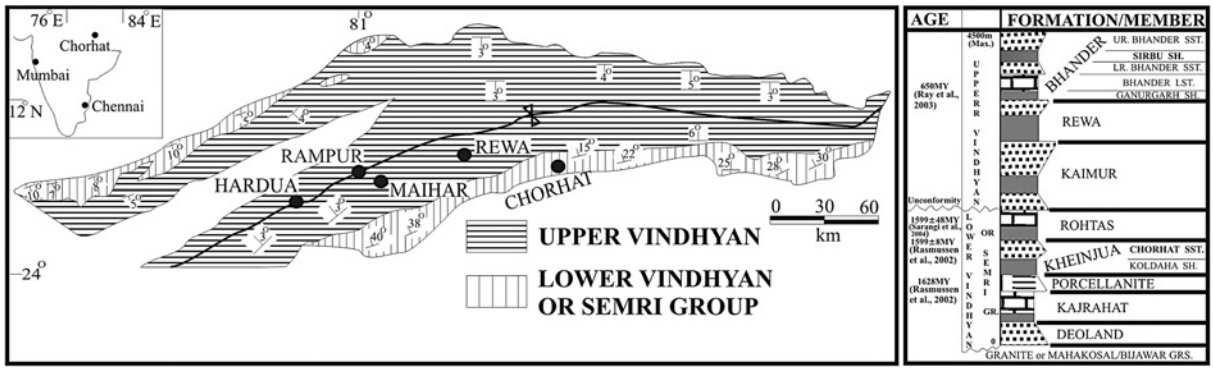


Figure 7(d)-1: Geological map and stratigraphy of the Vindhyan Supergroup.
Geological map of the Vindhyan syncline, showing its lower and upper (in black) divisions, with detailed stratigraphic subdivision of the Vindhyan Supergroup shown on the right.

7(d). MAT-RELATED FEATURES FROM SANDSTONES OF THE VINDHYAN SUPERGROUP IN CENTRAL INDIA

P.K. Bose, S. Sarkar, S. Banerjee, S. Chakraborty

This section addresses mat-related features in sandstone in the Palaeoproterozoic–Neoproterozoic Vindhyan Supergroup in central India (Figures 7(d)-1A, -1B) focusing upon the extraordinarily rich assemblages located within the 1.6 Ga Chorhat Sandstone (Rasmussen et al., 2002; Ray et al., 2002) and the 0.6 Ga Sirbu Shale (Ray et al., 2002). Both formations largely originated on prograding wave-dominated open shelves (Banerjee, 1997; Seilacher et al., 1998; Sarkar et al., 2002, 2005), that emerged eventually in the case of the Chorhat Sandstone and which remained permanently submerged for the Sirbu Shale. Since the relevant features in the Chorhat Sandstone are on the tops of sandstone beds or at interfaces between amalgamated ones and many of them have already been cited in Chapter 4, the present discussion dwells exclusively on those features not presented before or which have some new characteristic or appendage (Figure 7(d)-2). Greater attention is paid to the features in the Sirbu Shale that are impressions of mat fragments preserved on the soles of storm-laid sandstone beds, and found only towards the base of the thickest shelf section where the strata are muddiest (Bose et al., 2001; Sarkar et al., 2002; Figures 7(d)-3, -4, -5). The mud interbeds are generally thick, planar laminated but locally massive, while the sandstone beds are thin and massive or laminated, but more often wave-rippled at their tops. Presumably the mat fragments were swept down from the shallower shelf and redeposited in the deeper shelf where wave action was very limited (Bose et al., 2001; Sarkar et al., 2002). It is apparent that microbial mats have a better chance of preserving their primary biogenic features if they get buried rapidly. In the case of the Sirbu Shale microbial sole structures are concentrated locally.

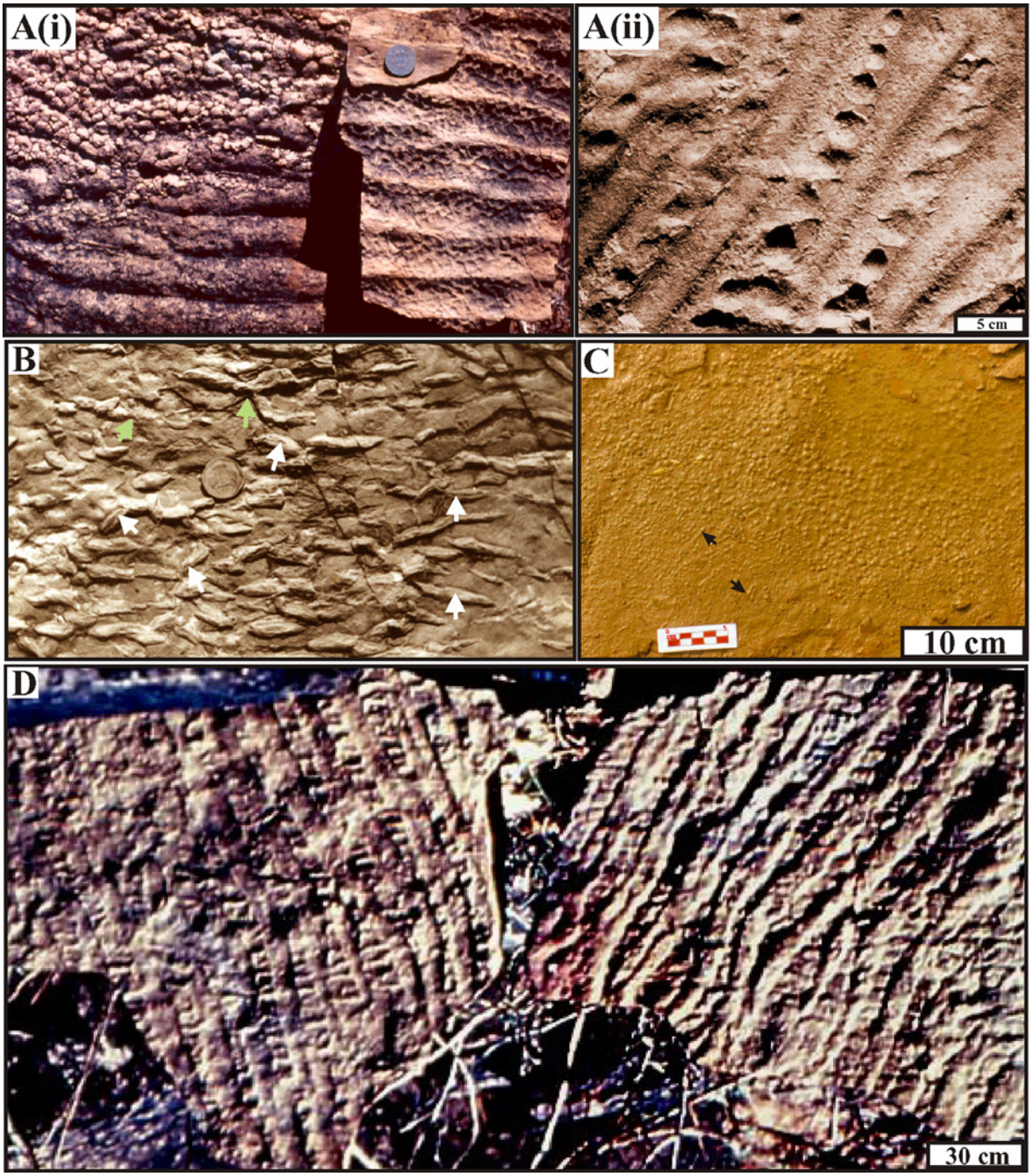

A(i)
A(ii)
5 cm
B
C
10 cm
D
30 cm

Figure 7(d)-2: Features in the Chorhat Sandstone (coin for scale is 2.6 cm in diameter).
(A) Load balls and their casts. (i) Steep-flanked load balls at the sole of a rippled sandstone bed, clustered so closely together that they almost touch each other (left block, upper part) and casts of similar load balls separated by very thin boundaries, on top of another rippled sandstone bed (right block). A thin sandstone bed still adhering to the top of the latter bears at its sole the load balls that would correspond to these load casts. The load casts are distributed nearly uniformly over the ripple crests and troughs. However, as noted in the left block, loading in a bed may be localised, with the size of load balls decreasing downward from a cluster above. No mud is present at the bed interface, not even within the depressions. Liquefaction of sand in response to rapid settling of another mass of similar sand is inferred. Growth of a gelatinous microbial mat presumably made the sand that had already settled thixotropic. Lateral size variation of the load balls depended possibly on thickness variation in the mat. A palimpsest ripple (just above the coin on the right-hand block) replicated from the underlying bed is further evidence of mat growth at the bed interface. Light in this photo is from the top. (ii) Load casts (bowl-like depressions) here occur only along ripple troughs (light in photo is from top left). Such a preferred occurrence is expected because of preferred growth of mats within ripple troughs. The structures in this figure are documented from the immediate outskirts of the town of Chorhat, central India. Associated Structures: thin, often less than a centimetre thick sandstone beds, internally massive, but wave rippled at their tops and frequently amalgamated. Palaeoenvironment: outer shelf near the storm wave base. (B) Spindle-shaped ridges with a median furrow. Numerous spindle-shaped ridges with local cross-cutting relationships (black arrows) that support their synaeresis origin: note median furrows within many of the spindles (white arrows). Although it is likely that cracks were modified into these ridges, their characteristic median furrows relate them preferably to synaeresis rather than desiccation; their cross-cutting relationships corroborate this. The following sequence of events can perhaps explain the genesis of these features best: (i) a surface layer of a buried sand bed, made cohesive with mat growth, cracked and sand derived from the overlying bed filled the cracks; (ii) sediment flowage from the sides under ever increasing confining pressure tended to close the cracks on top of the crack-fill; (iii) in the process, the two sides of the latter curled up and approached each other creating a median furrow between them; (iv) partial exhumation later presented the now-modified crack-fills as spindles raised above the bed surface. The structure is documented at the western outskirts of the town of Chorhat. Associated structures: thick (often more than 10 cm) sandstone beds with massive bases, followed upwards by planar and quasi-parallel stratification and wave ripples at the top; with carved tool marks at bed soles, frequently amalgamated. Palaeoenvironment: inner shelf. (C) Sand bulges with setulfs attached. Small sand bulges in a cluster decrease gradually in diameter from 0.1 to $<$0.3 cm towards the left bottom of the figure. While the larger bulges are circular in plan, the smaller ones have minute setulfs (Friedman and Sanders, 1974) elongated both ways along a preferred alignment (steeper ends arrowed). The 'tail'-like setulfs are likely to have formed through limited reworking of sand bulges by waves propagating to-and-fro, and not because of accretion of wind (unidirectional)-deflated sand on the lee of the bulges, otherwise the larger bulges would have served better as current obstacles. Larger bulges were apparently not reworked. This fact suggests that the latter formed where the mat grew thicker, while thinner mat covers on smaller bulges were subsequently easily modified by waves. Location: on the roadside 4 km west of the town of Chorhat. Associated structures: thicker sandstone beds with occasional partings of thin, centimetre-thick laterally impersistent reddish silty mudstone. The bases of the beds are often enriched in oxidised mudclasts and are massive. Planar laminae, centimetres-thick cross-laminae and wave ripples follow upwards from the massive base. Wave ripples are often interfering or superimposed. Parting lineations and rill marks are preserved locally. Palaeoenvironment: intertidal zone. (D) Preservation of delicate ripples. Multiple sets of delicate wave ripples (right block) and their casts (left block) are found preserved upon prising open an interface between two essentially similar amalgamated storm sandstone beds, which are generally massive internally. Ripples in one of the sets have an amplitude of only about a millimetre, yet they too are spectacularly preserved and perfectly mirrored at the sole of the bed overlying them. Abundant sand fall-out on the ripples from a subsequent storm-induced highly turbulent flow is implied. In the total absence of mud even within the ripple troughs, it is difficult to infer any means other than the influence of a microbial mat, to conserve delicate structures like these, including the minute ripples, despite storm onslaught. Associated structures: thin amalgamated sandstone beds (centimetre-scale), internally massive at the base followed upwards by planar laminae at places, but almost always wave-rippled at the top. Soles of the beds often bear tool marks. Palaeoenvironment: between fair-weather and storm wave-base; location: three kilometres southwest of Chorhat. All photographs by Subir Sarkar, Santanu Banerjee and Pradip K. Bose.

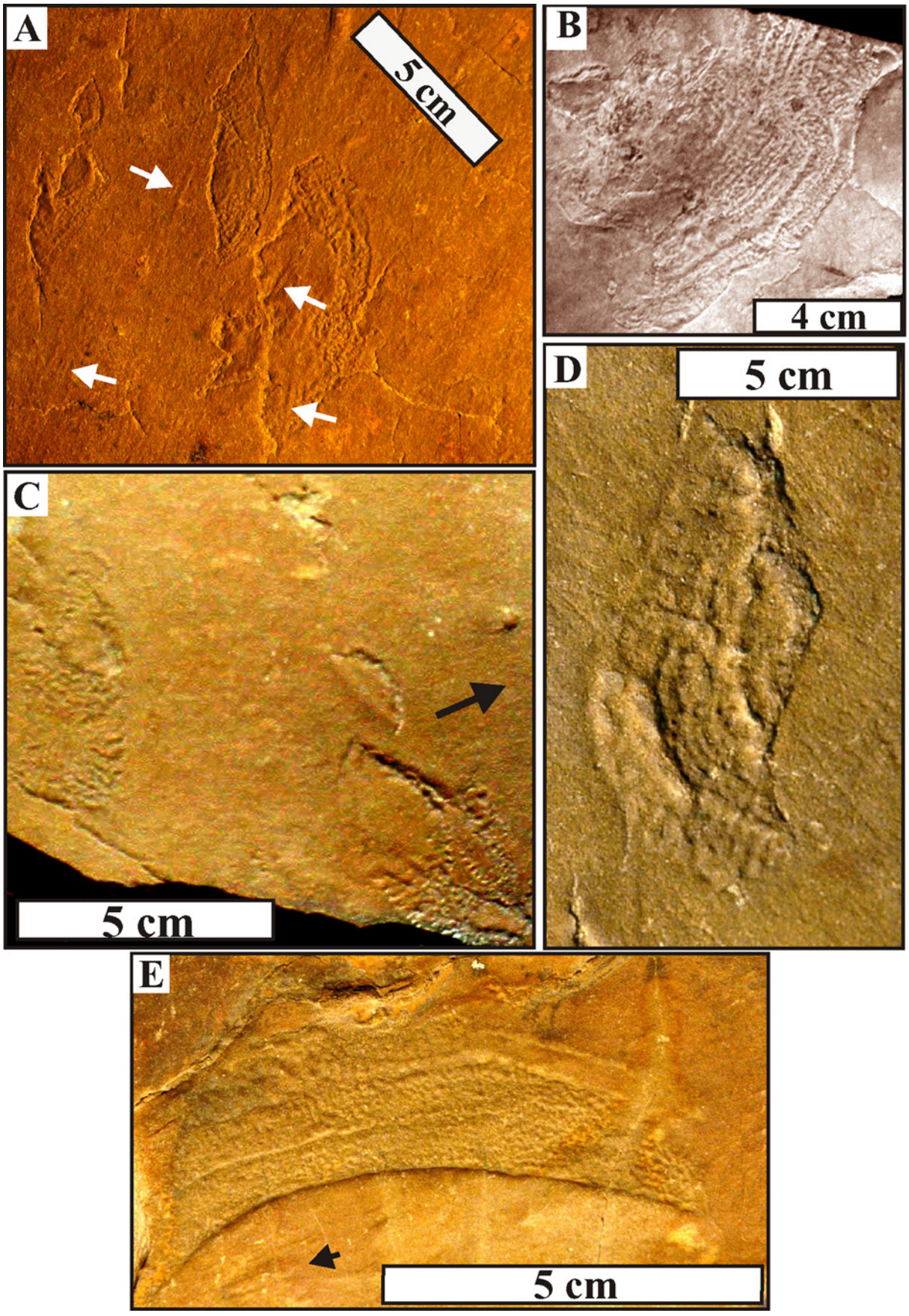

A
5 cm
B
4 cm
C
5 cm
D
5 cm
E
5 cm

Figure 7(d)-3: Impressions of mat fragments (possibly originally circular or elliptical in form) with smooth curved margins, at sandstone bed-soles in the Sirbu Shale (arrows point to prod marks, or their directions). (A) Impressions of four discrete, elongated, lenticular objects of broadly similar nature, but of different sizes, all aligned roughly parallel to the prod marks, and thus explicitly swept by currents during their genesis. One of their boundaries is invariably smooth and curved, and the other definitely jagged. Within them, two sets of fine ridges are in orthogonal relation (better preserved in the larger two examples at the centre). One of the sets runs parallel to the curved boundary that seems intact, but gradually becomes fainter away from this. Ridges of the other set are straight and seem to radiate from an unseen centre to meet the curved ridges almost at right angles. From their curved geometry in one set and radiating arrangement in the other, the ridges cannot be current-generated and none of them are parallel to the prod marks either. The internal structure of the objects thus appears biogenic. Prod marks clearly visible on the surrounding sediment as well as on the larger impression (white arrows) indicate that the objects whose impressions are preserved were thin, sheet-like and soft enough, possibly gelatinous, to yield under impact of particles impinging upon them. The objects thus appear to be pieces torn from the fringes of microbial mats, probably of disc-like shape. Associated structures: sandstone beds, around a centimetre-thick, and with sheet-like geometry, alternate with thicker shale beds. The sandstone beds are either massive or partly ripple cross-laminated, but bear tool marks on their bases and wave ripples on their tops. Shale beds are generally planar laminated. Palaeoenvironment: mid–outer shelf transition; locality: ca. 10 km south of Uchaihra, and from the basal segment of the Sirbu Shale shelf succession. (B) Impression of a discrete lenticular fragment that has one margin (right) which is smooth, curved and also a bit undulating, apparently deformed, and with the other margin being highly irregular and jagged. Thin and close-spaced ridges run roughly parallel to its seemingly uninterrupted, but slightly folded right margin and the other set of fainter ridges runs across them at a high angle. Because they grow increasingly small and less distinct away from the right margin and replicate folding of the same margin, the first set of ridges may not be intrinsic to the parent object, but may be folds (wrinkles) created by gentle wave action. It is imperative then that the parent object had been thin, sheath-like and soft. However, this argument does not eliminate the possibility that these ridges are biogenic. In that case inward blurring of the ridges can perhaps best be attributed to an increasing amount of newer mat overgrowth towards the inner or, in other words, older part of the microbial colony, of possible discoid shape. The other set of minute ridges at high angle to the presumed primary margin on the right, is also equivocal in its current-derived or possible biotic origin. Associated structures: as for A, but shale beds are often partly massive. Palaeoenvironment: outer shelf; locality: as for A. (C) Two elongated leaf-shaped impressions (at the left- and right-bottom; the latter is better preserved); within them close-spaced ridges in two sets cut across each other. One of the sets comprises straight parallel ridges running perpendicular to the median axes of the 'leaves'. Ridges of the other set are comparatively wider and not so precisely mutually parallel, although they are roughly parallel to the median 'leaf'-axis. They are at a high angle to the prod mark orientation (arrow), and thus are either primary, or in other words biogenic, or were created by contraction of a thin sheet-like object because of flow shear across its margin. Ridges of the first set, on the other hand, being more or less parallel to the prod marks, may indeed be current markings. If they are current markings, their distinct prominence confined within the impressions would suggest that the parent material had been very thin and soft, like gelatinous microbial mats, readily amenable to marking. Associated structures: as for B. Palaeoenvironment: outer shelf; locality: as for A. (D) Impression of a discrete lenticular fragment with a smooth left margin, which is curved without any marked undulation; in contrast, the right margin is bevelled, angular and a bit irregular. It bears prominent ridges (positive on the bed-sole) that conform to the seemingly intact left margin, and another set of finer straight and radiating ridges cuts across them. The intact margin of the object and also the ridges parallel to it, unlike their counterparts in Figure 7(d)-3C, are so regular in form that they seem to be primary, presumably biogenic, and not generated by secondary wave action. The ridges radiating from an unseen centre and maintaining an orthogonal relationship with the left margin are, on the other hand, almost certainly biogenic. Their possible origin through current action can be readily discarded, firstly on the basis of their radiating arrangement and then for the high angle they generally make with the mutually parallel current-generated ridges present outside the object. Associated structures: as in B. Palaeoenvironment: outer shelf; locality: as for A. (E) A discrete, elongated, parallel-sided and smoothly curved impression of an object that looks like the swerving track of a tyre. Two prominent, but partially preserved ridges (positive on the bed-sole), running parallel to the curved margins, divide the band-like form into three longitudinal segments. Numerous finer ridges, mutually parallel, run at a high angle to these ridges. None of the ridge-sets is parallel to the prod mark orientation (arrow) and they cannot therefore be current marks, and are very likely biogenic in origin. Associated structures: as for A. Palaeoenvironment: mid–outer shelf transition; locality: as for A. All photographs were taken by Subir Sarkar, Snehasis Chakraborty, Santanu Banerjee and Pradip Bose.

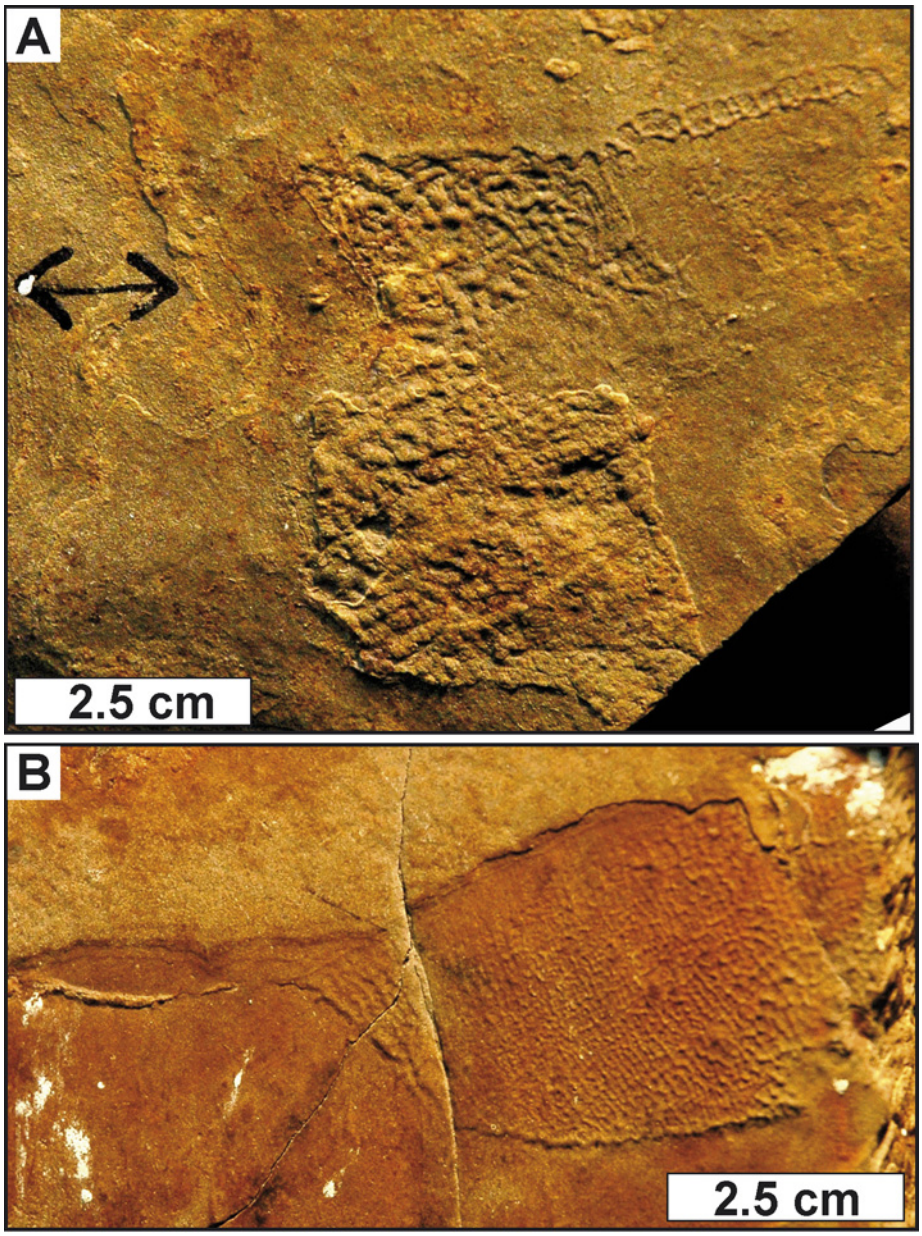


Figure 7(d)-4: Impressions of mat fragments bearing two sets of straight ridges at a high angle to each other, at sandstone bed-soles, in the Sirbu Shale.

(A) Impression of a roughly rectangular object with a narrow, long extension attached at one end, bears two sets of ridges at high angles to each other, continuing into the extension. The ridges of the comparatively more prominent set are roughly parallel to the general prod mark orientation as indicated by the bidirectional arrow and thus may be current-generated grooves now seen in reverse. The first set almost certainly does not have any relation to current or wave action and is inferred to be biogenic. The feature, being present on the sole of a bed, is illustrated on a fragment of a rock slab pulled out from under a pile of beds. Associated structures: as for Figure 7(d)-3A. Palaeoenvironment: mid-shelf; locality: ca. 10 km south of Uchaihra, and from the basal segment of the Sirbu Shale shelf succession. (B) A roughly circular impression, with discrete, sharp boundary, bears two sets of fine, well-defined closely spaced ridges subtending an acute angle between themselves, unlike the ridge-pairs in the previous case, A. Sand grains impinging upon the object might have created one of the sets, but then the other set is almost certainly biogenic. Preservation of grain impingement structures would mean that the object had been thin, sheet-like and soft, non-elastic. Associated structures: as for Figure 7(d)-3A. Palaeoenvironment: mid-shelf; locality: as for A. All photographs were taken by Subir Sarkar, Snehasis Chakraborty, Santanu Banerjee and Pradip Bose.

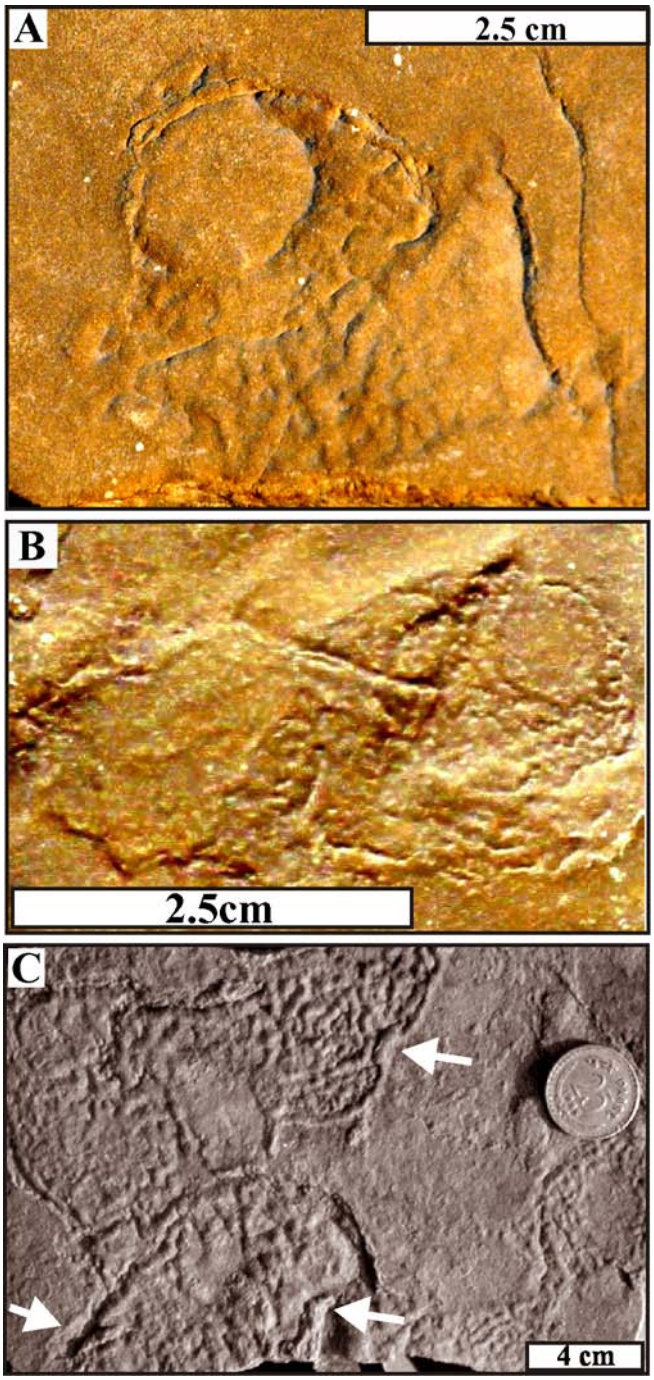


Figure 7(d)-5: Impression of wrinkled (microbial) mass.
(A) Impression of an object that included a nearly circular structureless part, of diameter about 2.0 cm, delimited by a thin raised rim, now seen in reverse as a hair-thin furrow. Immediately outside this object, a textured area suggests the presence of a frill of maximum width about 1.2 cm attached to the central disc. The frill bears two sets of irregular wrinkles cutting across each other at an acute angle, and is preserved on one side of the rim. Lateral continuity of the wrinkles suggests wave action (cf. Hagadorn and Bottjer, 1997; Bougouri and Porada, 2002) rather than gas expulsion (Pflüger, 1999) or burial diagenesis (Noffke et al., 2003a) for their origin. The rimmed, circular, structureless part suggests the presence of some kind of substrate attachment mechanism. Associated structures: as for Figure 7(d)-3B. Palaeoenvironment: mid-shelf–outer shelf transition; locality: as for C. (B) Impression of a wrinkled mass with a circular structureless part with a diameter of ca. 2.0 cm (top right). The rim defining the circular part is wider and segmented, unlike that in the immediately preceding figure. The wrinkled frill around the rim reveals, on close examination, two sets of crinkled ridges at high angles to each other. As suggested in the previous case the circular part likely represents some kind of attachment mechanism, but a wider knobby collar apparently strengthened this. Associated structures: as for Figure 7(d)-3B. Palaeoenvironment: mid-shelf–

outer shelf transition; locality: as for C. (C) The impression is in highly irregular patches interconnected by narrow 'bridges', while the patch boundaries are well defined. Thickening of the margin of these patches at places (arrows) suggests a tendency for 'flipping-over' of a sheet-like mat. The patches bear wrinkles in two nearly orthogonal sets, not as regular as in the preceding figures. These irregular wrinkles may be a mirror-image of a myriad of mutually overlapping gas expulsion pits, or of pits created by impinging particles or, more likely, minor folding generated by gentle wave action (Banerjee and Jeevankumar, 2005). The appearance of the interconnected patches suggests a gelatinous nature for the mat, portions of which were torn away by currents or waves. Associated structures: shale interspersed with laterally impersistent siltstone beds which are either massive or faintly normally graded, bearing minute tool marks at their bases and minute ripples at their tops. Shale beds are planar laminated or massive. Palaeoenvironment: outer shelf, near the storm wave base. The inferred mat fragments were found in deeper shelf facies where fair-weather waves either could not reach or touched the sea-bottom only marginally. However, the inferred mats must have colonised the upper reaches of the shelf. Locality: ca. 10 km south of Uchaihra, and from the basal segment of the Sirbu Shale shelf succession. All photographs taken by Subir Sarkar, Snehasis Chakraborty, Santanu Banerjee and Pradip Bose.

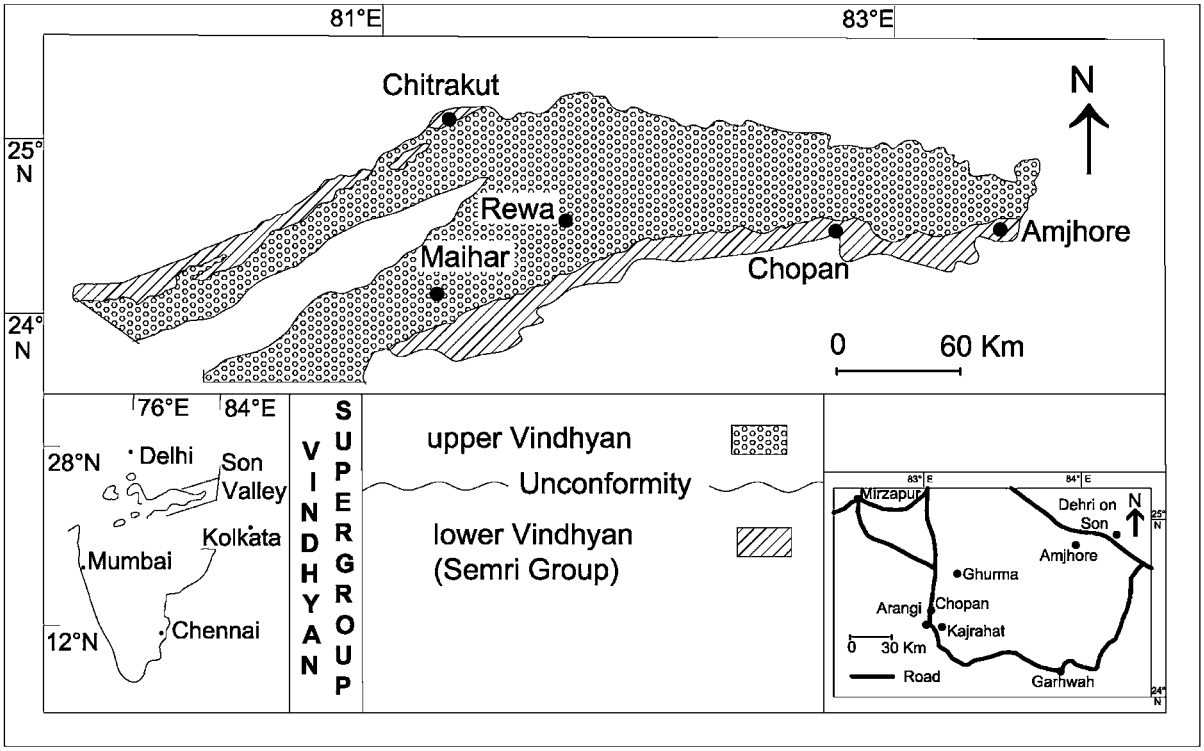


Figure 7(e)-1: Geological map showing outcrop distribution of the Vindhyan Supergroup in central India (map of India within inset). Detailed road map is at bottom right.

7(e). BENTHIC MICROBIAL MATS IN BLACK SHALE UNITS FROM THE VINDHYAN SUPERGROUP, MIDDLE PROTEROZOIC OF INDIA: THE CHALLENGES OF RECOGNISING THE GENUINE ARTICLE

J. Schieber, S. Sur, S. Banerjee

Introduction

The Palaeoproterozoic to Neoproterozoic sediments of the Vindhyan Supergroup (Figure 7(e)-1) were deposited in a westward-opening shallow epeiric sea (Bose et al., 2001). Its shallow marine siliciclastics and carbonates measure up to 4500 m in thickness, and are interpreted to have been deposited in an intracratonic rift basin that in later stages transformed into an intracratonic sag (Bose et al., 1997, 2001). A basin-wide unconformity subdivides the Vindhyan Supergroup into the carbonate-dominated lower Vindhyan (also known as the Semri Group) and the siliciclastic- dominated upper Vindhyan (Figure 7(e)-1). Recent radiometric age determinations indicate that the Vindhyan Supergroup spans an age range from 1.75 to 0.6 Ga (Ray et al., 2002; Rasmussen et al., 2002; Ray, 2006).

Minor deformation and only slight metamorphism of the Vindhyan have resulted in superb preservation of delicate sedimentary features, and microbially produced sedimentary features have been reported from both siliciclastics and carbonates (Sarkar et al., 1996; Banerjee, 1997; Chakraborty, 2004; Banerjee and Jeevankumar, 2005; Sur et al., 2006). Organic-rich shales (TOC $>$ 1%) occur at three stratigraphic horizons, in the Kajrahat Formation, the Rampur Shale, and the Bijaigarh Shale (Figure 7(e)-2). The oldest black shale, in the lower part of the Kajrahat Formation, is up to 12.5 m thick, and the Rampur Shale at the mid-level of the Vindhyan Supergroup occurs at the base of the Rohtas Limestone and is up to 55 m thick. In both of these black shales, carbonate beds alternate with shale intervals. The youngest black shale unit, the Bijaigarh Shale, is up to 70 m thick and occurs sandwiched between the Lower and Upper Kaimur sandstones (Figure 7(e)-2). Prior petrographic studies found microbial mat-related features within these black shales (Sur et al., 2006). Shales examined for this study occur in the area between Amjhore and Chopan in the eastern part of the Son valley (Figure 7(e)-1).

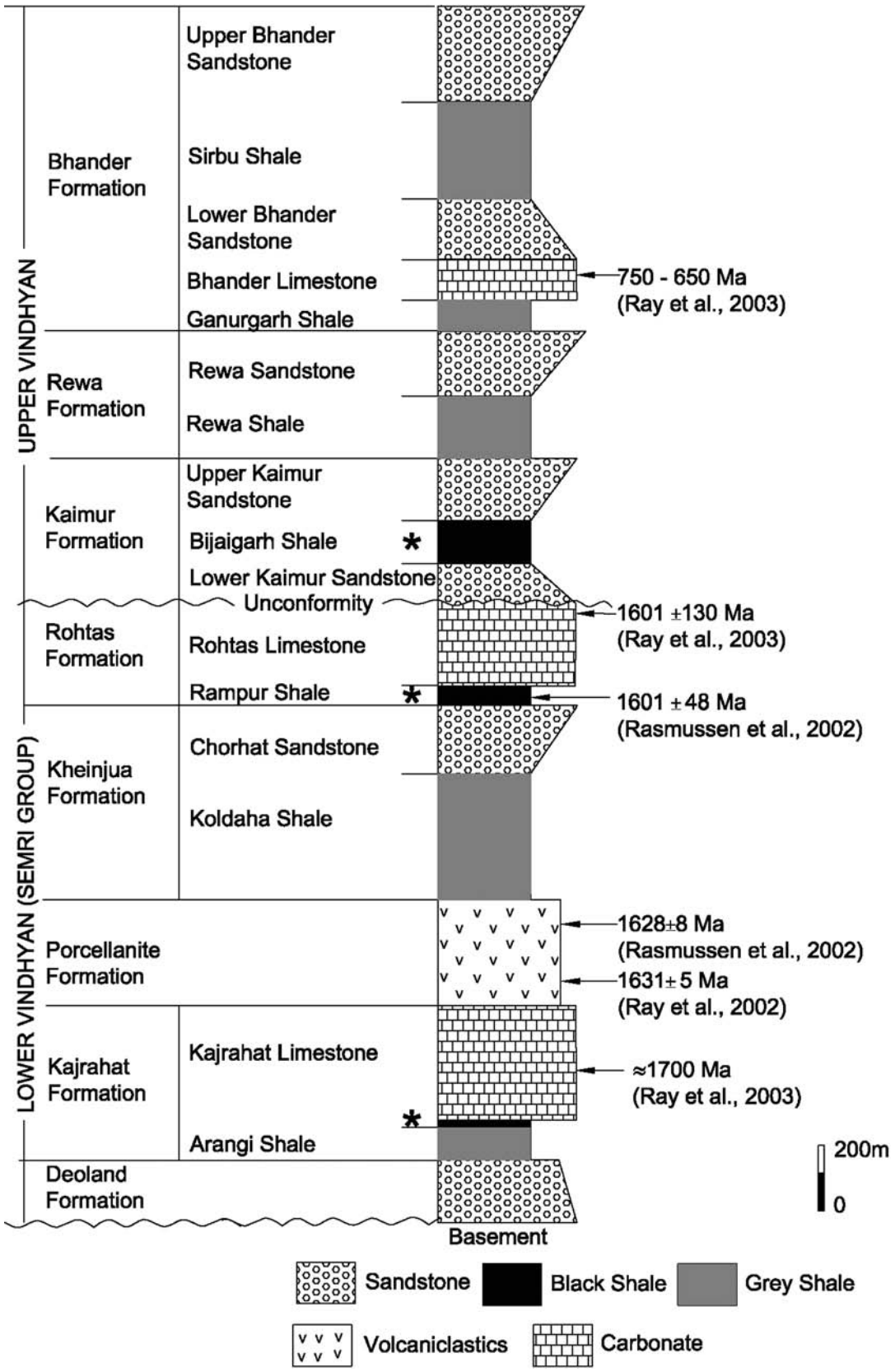


Figure 7(e)-2: General lithology, age and stratigraphy of the Vindhyan Supergroup up to member level (after Bose et al., 2001). The black shale units are marked by asterisks.

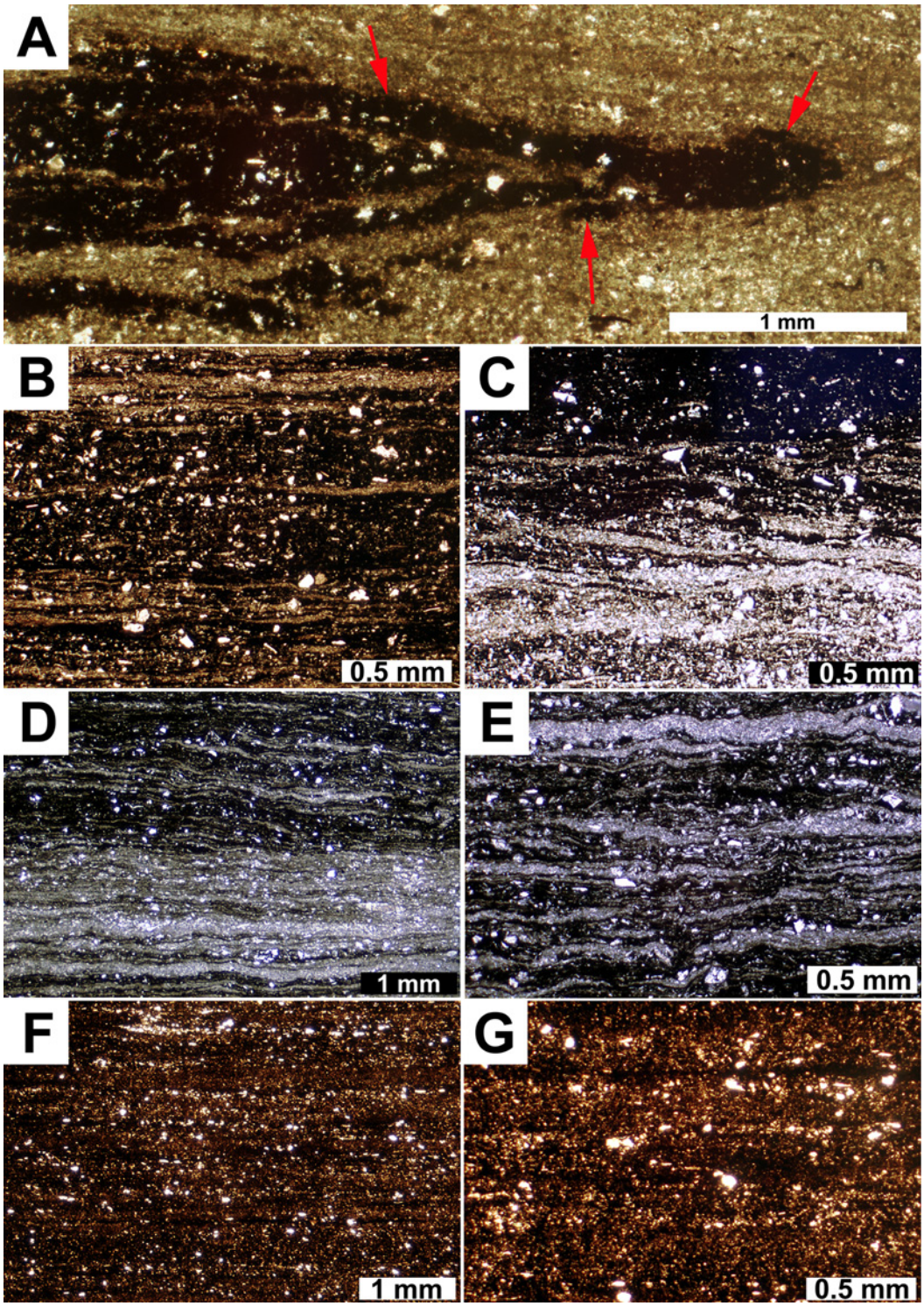


Figure 7(e)-3: Photomicrographs of the Kajrahat black shale.
(A) A folded-over and rolled-up thin carbonaceous fragment (arrows) in a grey shale matrix. (B) Wavy carbonaceous laminae in black shale. Continuous clay films accentuate the lamination. (C) Base of black shale bed overlying grey shale. At the base carbonaceous and clay laminae are inclined to the right, resembling false cross-lamination shown in Figure 5-3A of Chapter 5 in this book. (D) Wavy carbonaceous laminae with variable thickness and intercalated clay drapes. (E) Close-up view of same thin section as in D. Shows strong resemblance to lamina style in microbial mat deposits from the Newland Formation of the Belt Basin (Schieber, 1986; and Figure 5-1A of Chapter 5 in this book). (F) Even parallel laminae in a bed of carbonaceous shale from the Kajrahat Formation. (G) Close-up view of laminae in F. Wavy crinkly texture that is so obvious in D and E is absent. Lamination is caused by slight compositional variations from lamina to lamina.

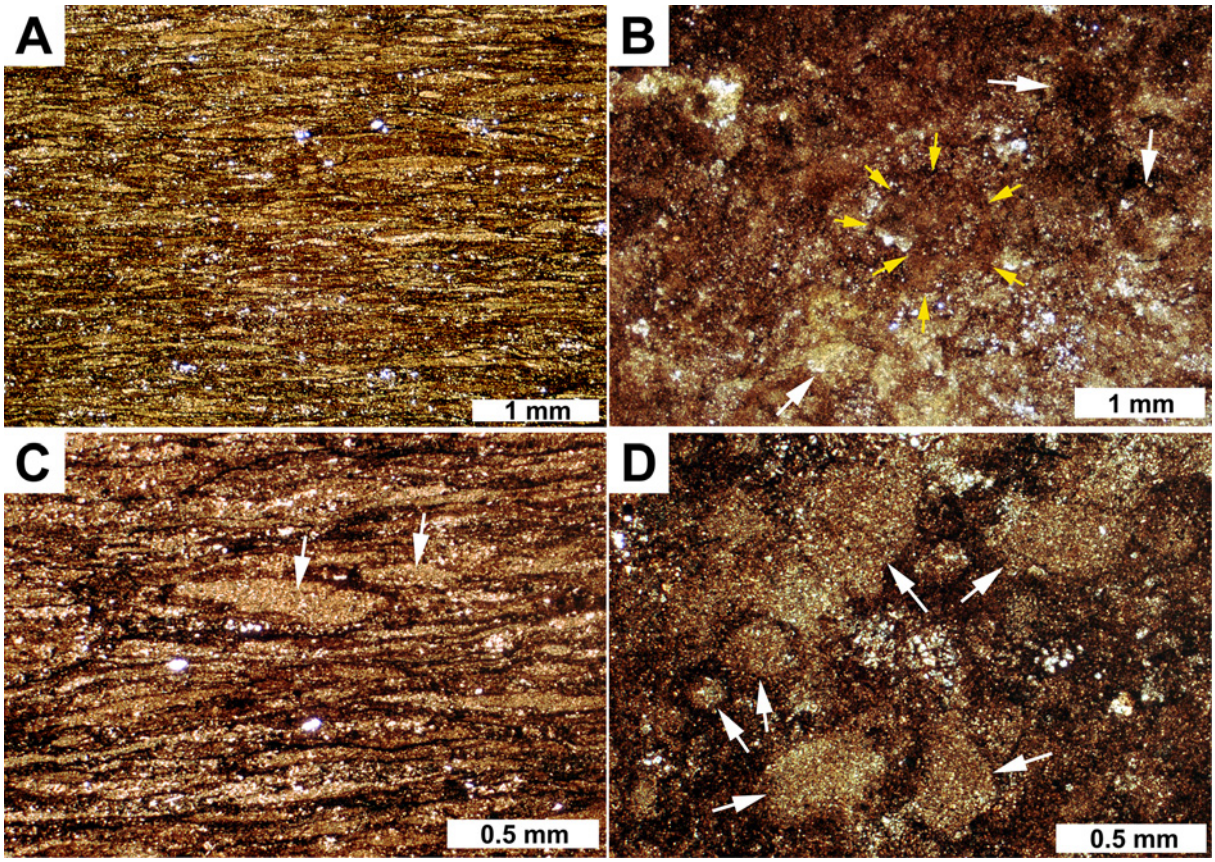


Figure 7(e)-4: Photomicrographs of the Rampur Shale.
(A) Wavy lenticular lamination that appears to be the result of piled-up and compressed fragments of clay-rich mudstone. (B) A thin section of the same sample cut parallel to bedding. It shows that lamina surfaces are covered by discrete particles. Large particle in centre is marked by yellow arrows, other particles pointed out by white arrows. (C) Close-up view of wavy-lenticular laminated shale as in A. Arrows point out particles with distinct boundaries that are most likely shale fragments. (D) A thin section of the same sample cut parallel to bedding. As in B, lamina surfaces are covered by discrete particles that are pointed out by arrows.

Kajrahat Formation black shale

Of the three shale units, the black shale interval in the Kajrahat Formation (Figure 7(e)-2) probably has the most compelling indications of microbial mat formation at the sediment surface. Features like thin carbonaceous fragments that apparently have been contorted, folded, and rolled up during transport (Figure 7(e)-3A) point to the presence of cohesive carbonaceous films. This cohesive nature is not the likely behaviour of a simple settled mixture of clays and small organic particles, but is consistent with microbial surface binding. The lamina style itself (Figures 7(e)-3B, -3D, and -3E) bears strong resemblance to wavy-crinkly laminae observed in other occurrences of Proterozoic carbonaceous shales that have been studied in some depth for microbial mat features (e.g., Schieber, 1986). The basal contacts of some of the black shale beds with underlying grey shales show inclined carbonaceous laminae and clay drapes suggestive of false cross-lamination (Figure 7(e)-3C), produced when the lateral expansion of a mat through time is intermittently interrupted by pulses of sediment (see Chapter 5). In addition, some samples of the Kajrahat Formation black shale show even parallel laminae that reflect physical sedimentation, such as settling and current reworking. Thus, microbial mat colonisation appears to have been intermittent and/or spatially limited and prone to interruption when sedimentation rates were too high or sedimentation pulses persisted for longer time periods.

Rampur Shale

The Rampur Shale contains abundant evidence of intermittent erosion of unconsolidated muds. Many thin sections show a wavy lenticular fabric that on first glance closely resembles microbial mat laminated carbonaceous

shales from the Belt Basin (e.g., Schieber, 1986). However, what initially appears as wavy clay drapes that separate carbonaceous silty laminae (Figure 7(e)-4A) looks upon closer inspection like stacked up clay-rich fragments that were soft when deposited and were squeezed together when compacted. This impression is reinforced when a cut parallel to lamination is made. If a laminated shale is cut parallel to bedding, multiple laminae are intercepted because of slight irregularities and, when ground, this surface shows a pattern that resembles the isolines of a topographic map. In contrast, when wavy lenticular laminated Rampur Shale specimens are ground parallel to lamination we see a surface that is strewn with shale particles (Figure 7(e)-4B). At higher magnification one sees that the shale does indeed consist of discrete shale particles and that these fragments are compacted and deformed (Figure 7(e)-4C). In plan view the irregular shaped shale particles are clearly visible at higher magnification (Figure 7(e)-4D).

Other samples show layers of grey shale with irregular carbonaceous fragments that are up to 10 mm in size (Figure 7(e)-5B). In thin section these fragments are quite thin (0.1–0.2 mm; Figure 7(e)-5A) and may show deformation and folded-over portions. This mechanical behaviour suggests a within-fragment cohesiveness that one should not expect if this material originated as a simple mixture of clays, silt, and organic matter. Such behaviour is, however, consistent with binding by microbial surface films. Intervals of the Rampur Shale that contain these fragments also show wavy anastomosing carbonaceous laminae interspersed with clay drapes (Figures 7(e)-5C to -5F). In close-up view these bear striking resemblance (Figure 7(e)-5D) to the lamina pattern in other examples of Proterozoic carbonaceous shales of microbial mat origin (Schieber, 1999).

In the Rampur Shale indications of surface binding by microbial mats appear to be less abundant than in the Kajrahat Formation black shale interval. The abundance of Rampur shales that consist of compacted shale fragments suggests an overall more energetic environment when compared to black shales in the Kajrahat Formation.

Bijaigarh Shale

Features that suggest microbial mat colonisation in the Bijaigarh Shale are typically found in its upper third (Sur, 2004). One shale type (or facies) shows the same lenticular lamination as described from the Rampur Shale above. It shows discrete flattened shale particles (Figure 7(e)-6A) in cuts perpendicular to bedding, and fragment-strewn surfaces in cuts parallel to bedding (Figure 7(e)-6B). Just like in the Rampur Shale, these features are interpreted to indicate erosion of a mud substrate by strong currents. The majority of thin sections from the upper third of the Bijaigarh Shale, however, show features that closely resemble those observed in microbial mat laminated Proterozoic black shales from elsewhere (Schieber, 1999). Many thin sections are either entirely characterised by wavy-crinkly anastomosing carbonaceous laminae that alternate with clay drapes of variable thickness and continuity (Figure 7(e)-6D), or show carbonaceous layers of this type interspersed with beds of non-laminated shale (Figure 7(e)-6C). These shale beds are texturally comparable to microbial mat-produced Proterozoic black shales described by Schieber (1986, 1999). Petrographic observations by Sur (2004) and Sur et al. (2006) indicate the former presence of cohesive carbonaceous surface films, suggesting microbial mat binding of the mud surface.

Reflected light and SEM studies of polished sections of Bijaigarh Shale from the upper third of the unit also show that fine crystalline early diagenetic pyrite is largely confined to carbonaceous laminae and displays a wavy anastomosing texture as well (Figures 7(e)-6E, -6F). This has also been observed in the pyritic facies of microbial mat shales from the Middle Proterozoic Belt Basin (Schieber, 1989a; and Section 7(b)). This facies of the Bijaigarh Shale also contains abundant clusters of phosphatic spheres (Figure 7(e)-6G) that seem to fill in and accrete around original spherical structures of a few microns diameter. In places multiple spheres are encased in a single phosphatic overgrowth (Figure 7(e)-6H). These phosphatic spheres resemble phosphate precipitation on bacterial cell walls from the Neoproterozoic of China (Xiao and Knoll, 1999), and may be the remains of coccoid bacterial clumps. Whether they were part of a mat-forming community is an unresolved question.

In the lower two thirds of the Bijaigarh Shale, wavy anastomosing laminated carbonaceous shales (Figures 7(e)-6C, -6D) seem absent. This portion of the succession is instead dominated by massive to evenly laminated carbonaceous shales (Figure 7(e)-6I) that closely resemble their physically deposited Phanerozoic counterparts (see Chapter 5, Figure 5-1).

Conclusion

That microbial mats can have an important impact on the preservation and modification of siliciclastic sediment surfaces is increasingly being recognised (e.g., Schwarz et al., 1975; Seilacher and Pflüger, 1994; Schieber, 2004).

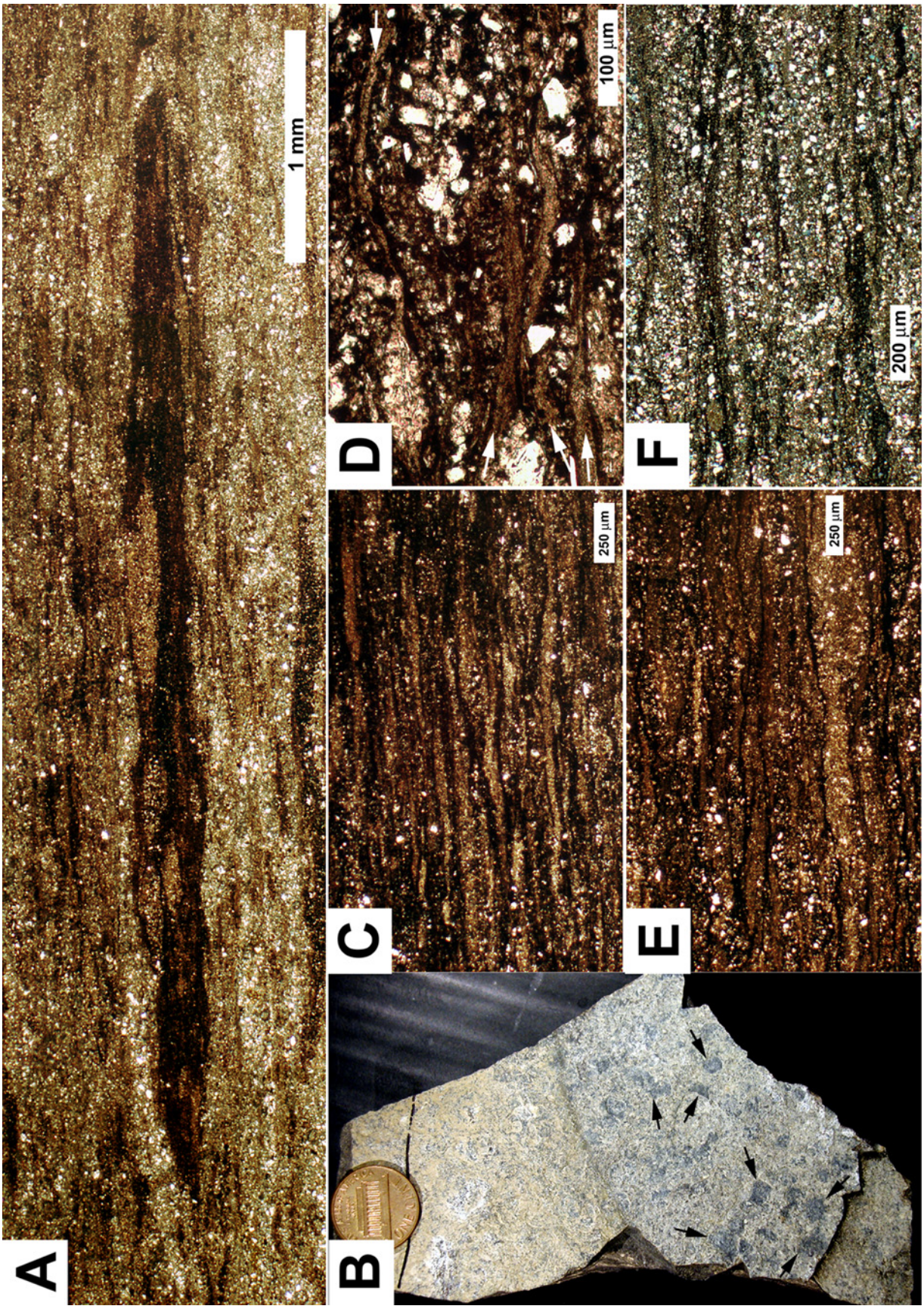

A
1 mm
B
C
250 µm
D
100 µm
E
250 µm
F
200 µm

Figure 7(e)-5: Photographs of the Rampur Shale.
(A) Photomicrograph of large elongate and possibly folded over carbonaceous fragment, as well as numerous smaller fragments, in a matrix of clays, quartz silt, and fine crystalline calcite. (B) Hand specimen with irregular carbonaceous flakes (arrows) on bedding planes. The photomicrograph in A was made from a thin section cut from this sample. (C) Wavy anastomosing carbonaceous laminae (dark-black) interspersed with clay drapes. (D) Close-up view of laminae in C. Shows 'lumpy'-looking carbonaceous silty laminae that alternate with thin clay drapes (arrows). (E) Carbonaceous shale with wavy carbonaceous laminae. Clastic layers (clay drapes) form a larger proportion of the overall rock. (F) Similar to E, but with large proportion of calcite grains in clastic layers (crossed polarisers).

In the absence of grazing metazoans many Precambrian sediment surfaces, including muddy substrates, were probably covered with microbial mats and biofilms when a favourable balance existed between sedimentation rate, availability of moisture, and an energy source (Schieber, 1999). Yet, whereas microbial mats were a major producer of biomass in the Precambrian, not all carbonaceous shales of that age necessarily represent *in situ* microbial mats. Although there are indications for microbial mat colonisation of mud surfaces in all of the three carbonaceous shales pictured here, there is also evidence in all instances of shale facies that either mimic microbial mat style lamination (Figure 7(e)-4 and Figures 7(e)-6A, -6B) or are evenly laminated and quite comparable to Phanerozoic non-mat carbonaceous shales (Figure 7(e)-6I).

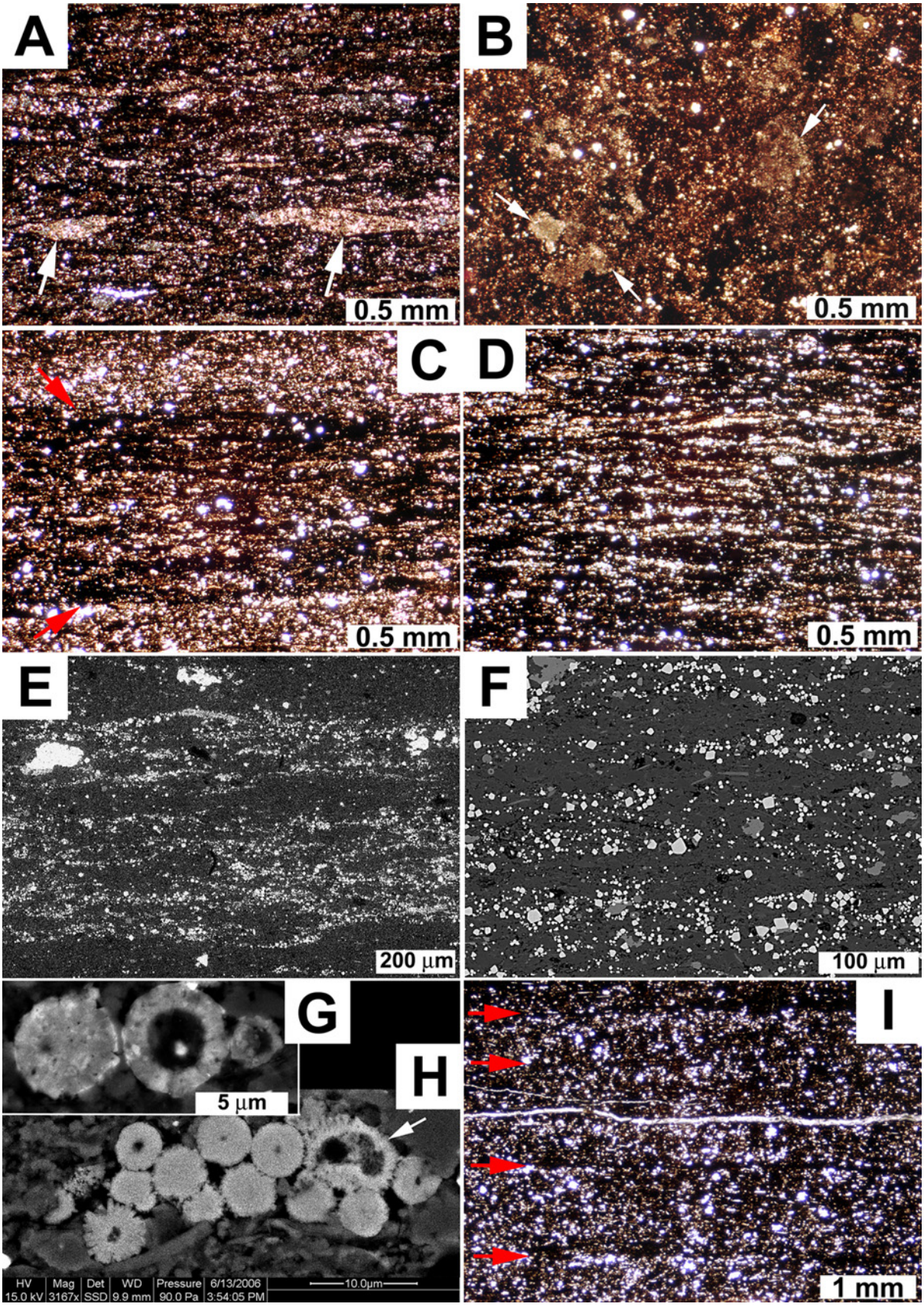

A
0.5 mm
B
0.5 mm
C
0.5 mm
D
0.5 mm
E
200 µm
F
100 µm
G
5 µm
H
HV 15.0 kV | Mag 3167x | Det SSD | WD 9.9 mm | Pressure 90.0 Pa | 6/13/2006 3:54:05 PM
10.0µm
I
1 mm

Figure 7(e)-6: Photomicrographs of carbonaceous shales from the Bijaigarh Shale.
A through H are from the upper portion of the Bijaigarh Shale, image I is representative of carbonaceous shales in the lower portion. (A) Wavy lenticular laminae in carbonaceous shale that appear to be the result of piled-up and compressed fragments of clay-rich mudstone, just like in Figure 7(e)-5 from the Rampur Shale. (B) A thin section of the sample in A, cut parallel to bedding. Just like in the Rampur Shale (Figure 7(e)-5), lamina surfaces are covered by discrete particles that are pointed out by arrows. (C) Thin layer of shale with wavy anastomosing carbonaceous laminae (lower and upper boundary pointed out by arrows). The layer is under- and overlain by non-laminated shale, analogous to striped shales from other studies (e.g., Schieber, 1986). (D) A thicker bed of silty carbonaceous shale with wavy anastomosing laminae. (E) Backscatter electron image of thin shale layer with wavy anastomosing pyritic laminae. (F) Close-up view from E. Shows the confinement of scattered pyrite grains to discrete (carbonaceous) laminae. (G) Hollow and fully mineralised phosphatic spheroids. (H) Clump of phosphatic spheroids. Note joined spheres pointed out by arrow. (I) Evenly laminated silty carbonaceous shale from the lower portion of the Bijaigarh Shale. Lamina boundaries pointed out by arrows.

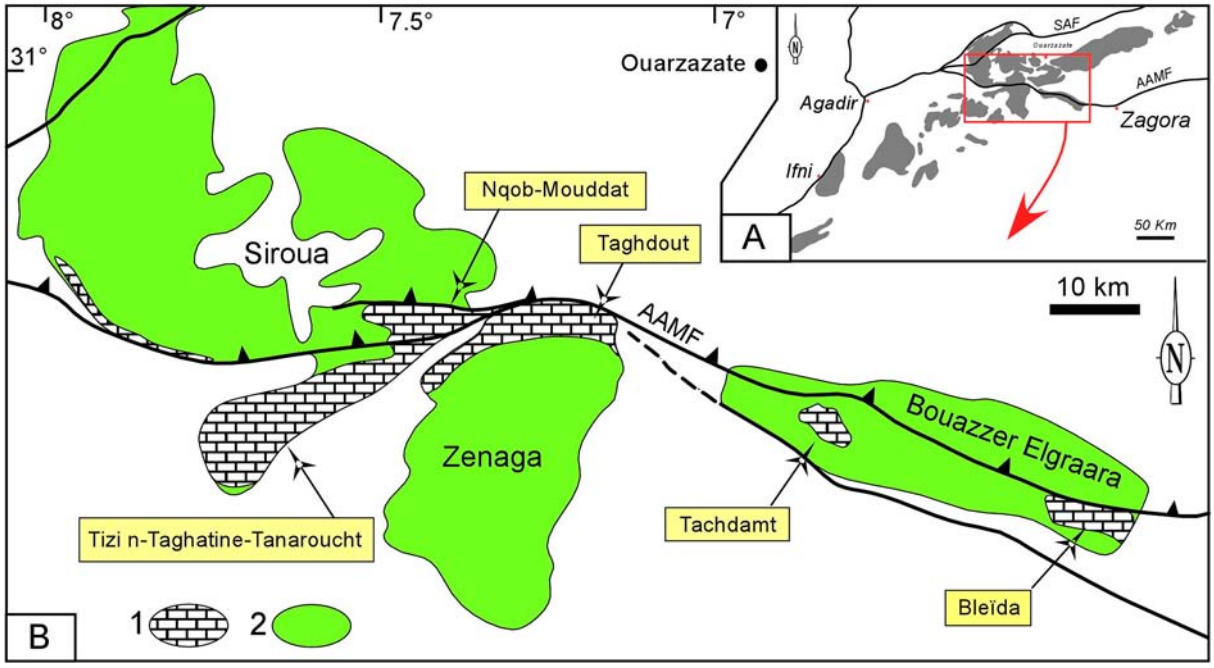


Figure 7(f)-1: Simplified map showing distribution of the Precambrian inliers in the Anti-Atlas mountains (A) and outcrop distribution of the Neoproterozoic Tizi n-Taghatine Group (1) in Proterozoic inliers (2) of the central Anti-Atlas. SAF: South Atlas Fault; AAMF: Anti-Atlas Major Fault.

7(f). MAT-RELATED FEATURES FROM THE NEOPROTEROZOIC TIZI N-TAGHATINE GROUP, ANTI-ATLAS BELT, MOROCCO

E. Bouougri, H. Porada

In the Anti-Atlas mountains, a variety of mat-related structures is extensively preserved in silicilastic deposits of the Tizi n-Taghatine Group, mainly in peritidal facies associations. This Neoproterozoic Group (~0.8 Ga) is a volcano-sedimentary cover, about 2 km thick, deposited on the northern continental margin of the West African craton (WAC). The group crops out discontinuously in all the Proterozoic inliers along the southern side of the central Anti-Atlas Pan-African suture and has been studied in three separate areas, viz. from west to east: (i) the southern edge of the Siroua massif, (ii) the northern edge of the Zenaga inlier, and (iii) the southern side of the Bouazzer Elgraara inlier (Figure 7(f)-1). The lithostratigraphic organisation of the Tizi n-Taghatine Group reflects a stratigraphic record of large cyclic changes in the depositional system due to relative sea-level variations, the palaeogeographic setting and the tectono-sedimentary evolution of the northern Neoproterozoic WAC passive margin (Bouougri and Saquaque, 2004; Figure 7(f)-2). The lower sedimentary package records the first basin-fill stage and reflects the establishment, on a relatively stable margin, of a shallow-water and gently dipping mixed siliciclastic–carbonate ramp facing northwards and attached to a braided alluvial plain in the south. The middle volcanic Tachdamt Formation consists of tholeiitic, alkaline and transitional flood basalts interpreted to represent a widespread extensional event at 788 ± 10 Ma (Rb/Sr; Clauer, 1976). Cessation of major volcanism was followed by deposition of the upper sedimentary package (Bleïda Formation), which records the late basin-fill stage and reflects a shelf-basin environment filled with thinly bedded and fine-grained turbidite deposits. The Lower sedimentary ensemble (Figure 7(f)-2) of the Tizi n-Taghatine Group consists of interfingering siliciclastic and carbonate facies associations, ranging from fluvial to siliciclastic and carbonate shallow platform domains. Within this package, occurrences of mat-related structures are found in siliciclastic facies of the Taghdout, Wanimzi, Tamgarda, Imi n-Tizi and Ifarkhs-n-Tirsal Formations.

Mat-related features presented here are documented from three areas: Agoummy (Figures 7(f)-3B to -3E and Figures 7(f)-4B, -4C, -4F, -4G), Tirsal (Figure 7(f)-3A and Figures 7(f)-4A, -4D, -4E) and Nqob (Figure 7(f)-3H). The structures are generally related to decimetre- to metre-thick biolaminate horizons and to millimetre- and centimetre-thick organo-sedimentary, laminated layers draping centimetre-thick sandstone beds. The latter reflect distinct stages within microbial mat life cycles (e.g., growth, destruction, overgrowth, biostabilisation, etc.). Most of the structures are found in a heterolithic facies association deposited in the intertidal to supratidal zones of a

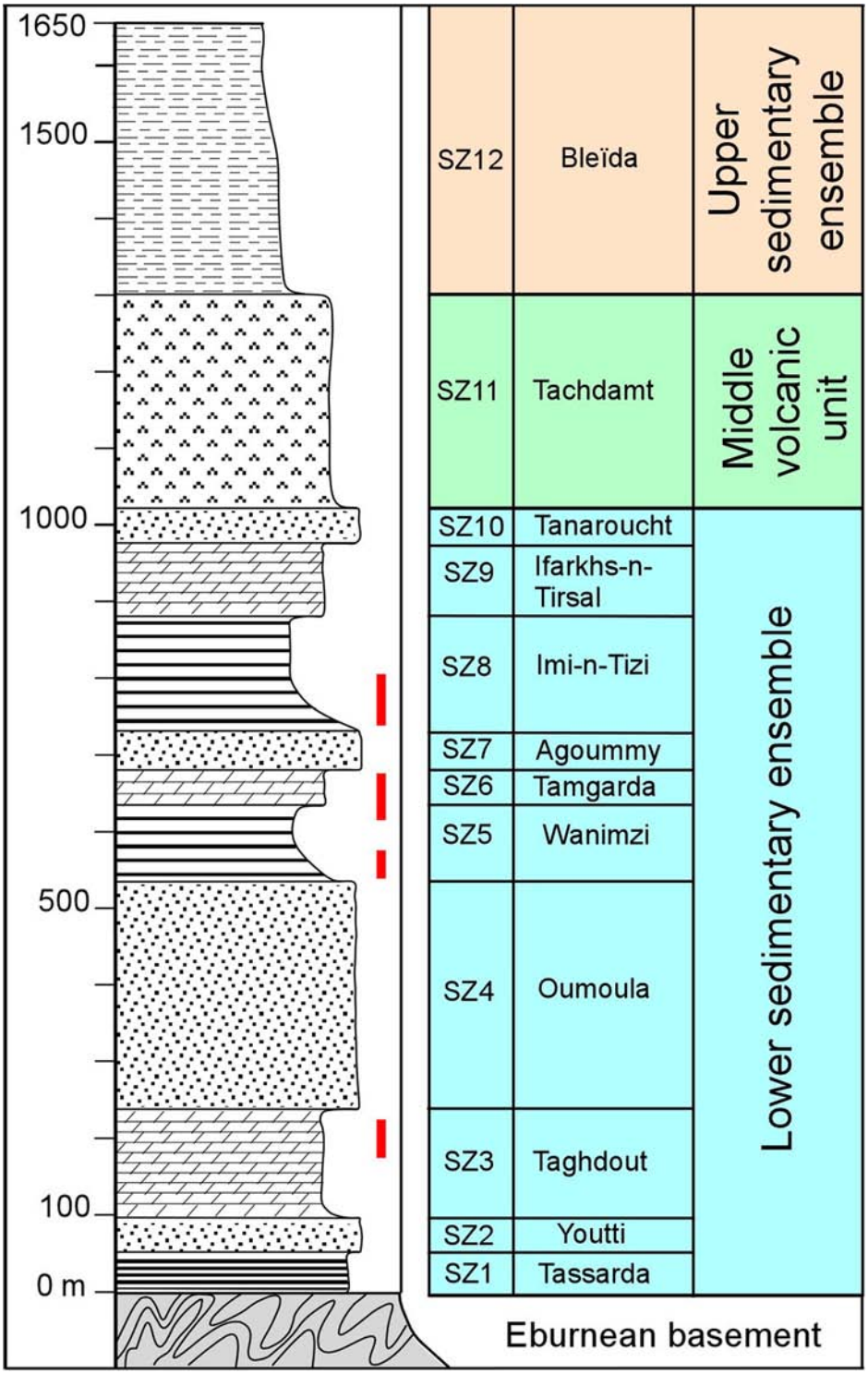


Figure 7(f)-2: Simplified lithostratigraphic column of the Tizi n-Taghatine Group showing (in red) stratigraphic distribution of mat-related features.

broadly peritidal coastal environment that experienced episodic emergence, intermittent fluvial sheet-floods and high-energy storm-tide events. The heterolithic deposits occur in decimetre- to metre-thick units and consist of interlaminated and thinly interbedded sandstone, laminated siltstone, and sericitic mudstone. They form rhythmic alternations of 0.5–15 cm thickness, comprising medium- to fine-grained quartzite layers with 0.5–5 cm thick interbeds of laminated siltstone or sericitic argillite. The intervals dominated by siltstone and sericitic argillite display flat internal bedding or wavy and lenticular bedding. They include layers of fine-grained sandstone with single sets of cross-lamination and a few centimetre-thick lenticular quartzite beds with symmetrical wave rippled tops. The

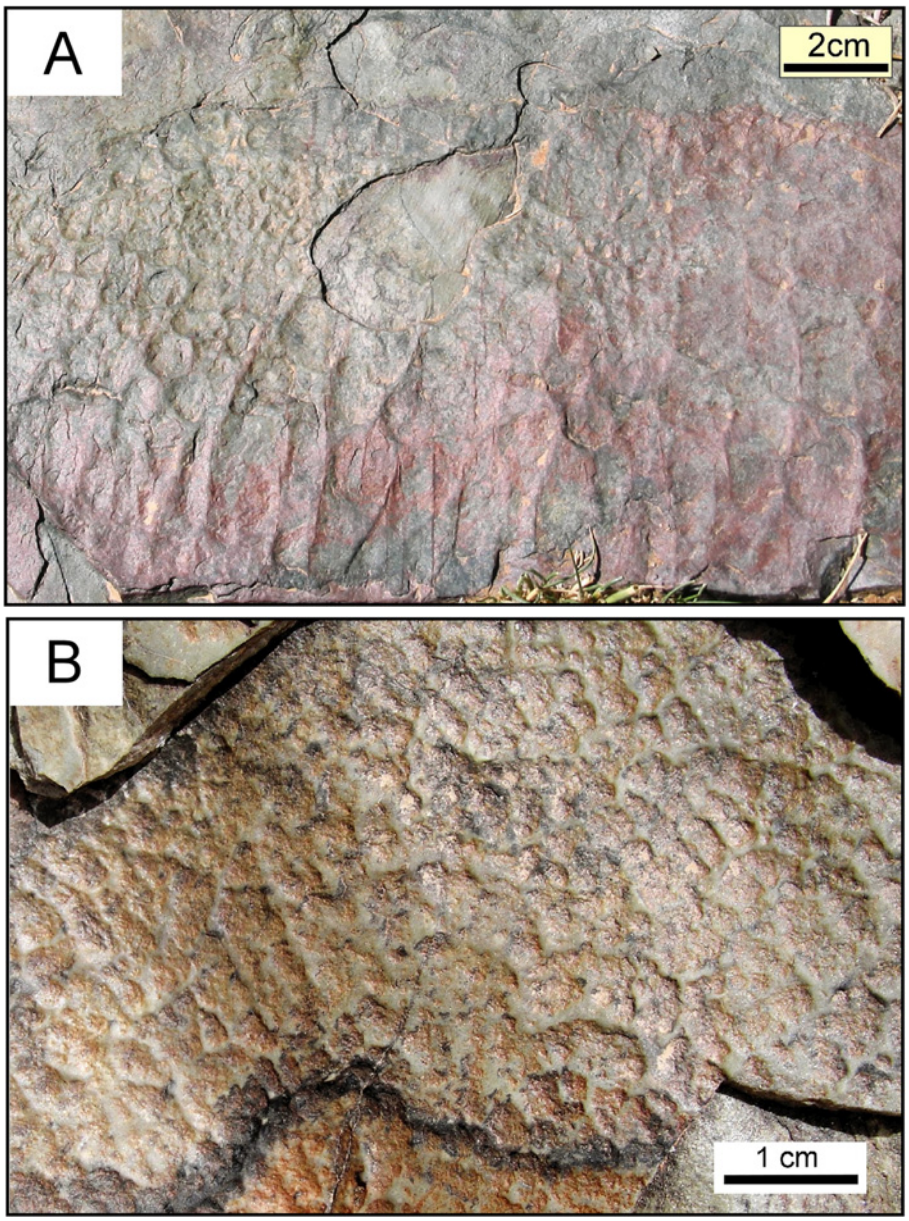


Figure 7(f)-3: Mat-growth features (A, B), subsurface *Kinneyia* structures (C–E) and subsurface sand protrusions (F).

(A) Reticulate 'elephant skin' pattern on upper bedding surface of siltstone. The surface shows a polygonal to hexagonal arrangement of sharp-crested ridges of variable size, partly evolving into a more linear pattern. In the centre of the photo, the underlying layer is flat indicating that the structure is restricted to the upper millimetre-thick siltstone lamina. (B) Close-up view of small-scale reticulate 'elephant skin' pattern on upper bedding surface of thinly laminated siltstone layer. The smooth-crested ridges are arranged in a subcircular to hexagonal pattern with hollows of 2–5 mm in diameter. According to the size and shape of this growth pattern, the term 'net structures' or 'honeycomb growth structures' may be more appropriate. For both A and B: *Locality*: Agoummy area, Anti-Atlas; Wanimzi Formation; *Genesis*: the two examples show the diversity in size and shape of reticulate growth patterns developed on thin microbial mats. Similar structures have been described from a modern tidal flat environment in Tunisia (e.g., Gerdes et al., 2000a) and attributed to vertical growth of cyanobacterial filaments (e.g., of *Microcoleus chthonoplastes*, *Lyngbya aestuarii*) forming tufts, pinnacles and ridges; *Associated structures*: desiccation cracks, current and wave ripple cross-laminations, oscillation and interference ripples, small-scale load structures, millimetre- to centimetre-scale alternation of sedimentary sandstone event layers of storm or fluvial origin, and organosedimentary laminated layers of siltstone and sericitic argillite; *Palaeoenvironment*: intertidal to lower supratidal zones of a peritidal coastal plain. (C) Upper flat surface of 5 cm thick fine-grained sandstone layer showing typical *Kinneyia* structures. The structures consist of flat-topped crests arranged in a honeycomb-like pattern. Depressions and pits vary from subcircular to hexagonal or elongate and gently curved. Coin for scale is 24 mm in

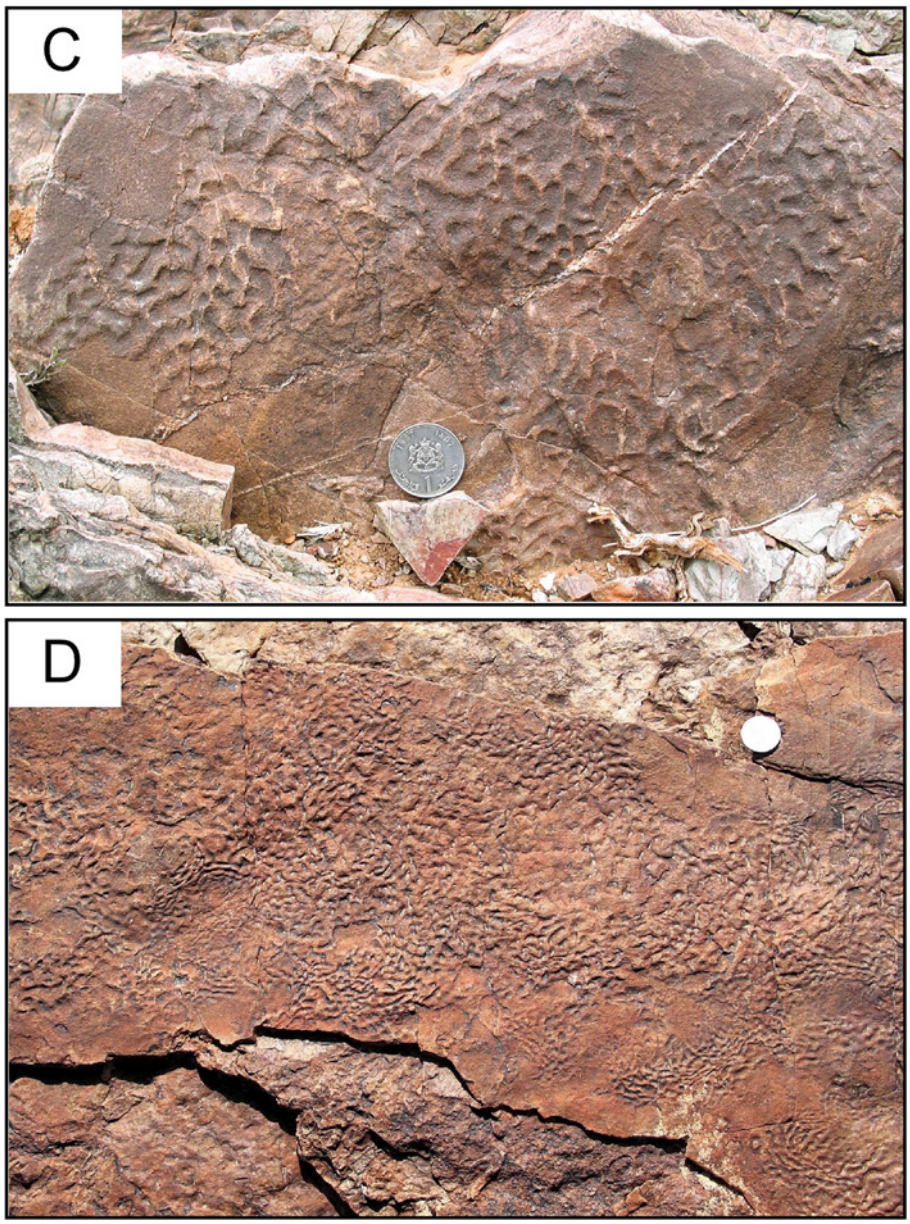


Figure 7(f)-3: ***Continued.***

diameter. Locality: Agoummy area, Anti-Atlas; Wanimzi Formation. Associated sedimentary structures: interference and oscillation ripples, wave ripple cross-laminations, shrinkage cracks, few hummocky cross-stratification (HCS) structures, heteroliths, and thickening-up parasequences. Palaeoenvironment: wave and storm influenced shoreface to intertidal coastal plain of a braid-delta environment. (D) Upper surface of 2 cm thick quartzite layer with *Kinneyia* structures. *Kinneyia* crests are irregularly distributed and partly curved, forming large elongate and subcircular structures with diameters ranging from 10 to 15 cm. The central flat parts of these structures exhibit sparse and short crests and depressions. Depressions between crests form isolated, subrounded to elongate pits, 8 to 15 mm long. Coin for scale is 24 mm in diameter. Locality: Agoummy area, Anti-Atlas, Imi n-Tizi Formation. Associated sedimentary structures: shrinkage cracks, interference and oscillation ripples, heteroliths with wavy bedding, biolaminites, wave induced structures, mud chips, sand clasts, and fluvial/tidal channels. Palaeoenvironment: peritidal coastal plain. (E) Upper surface of 4.5 cm thick quartzite layer (storm deposit) showing well developed *Kinneyia* structure. The structure consists of meandering and partly interfering, flat-topped to rounded crests and intervening troughs or pits. Inter-crest distance is 4–5 mm. Locality: Agoummy area, Anti-Atlas, Wanimzi Formation. Genesis: *Kinneyia*-type wrinkle structures are considered here as a category of 'subsurface structures' developed on a flat sandy surface underneath a mat (see Chapter 6(a)). Similar modern examples have not been described yet. Some modern growth structures with honeycomb-like patterns, developed on the upper sides of 2 mm thick microbial mats, induce nodular structures with intervening pits and grooves, resembling *Kinneyia* in size and shape, on the lower side of the mat (e.g., from Tunisia). Associated sedimentary structures: heterolithic deposits

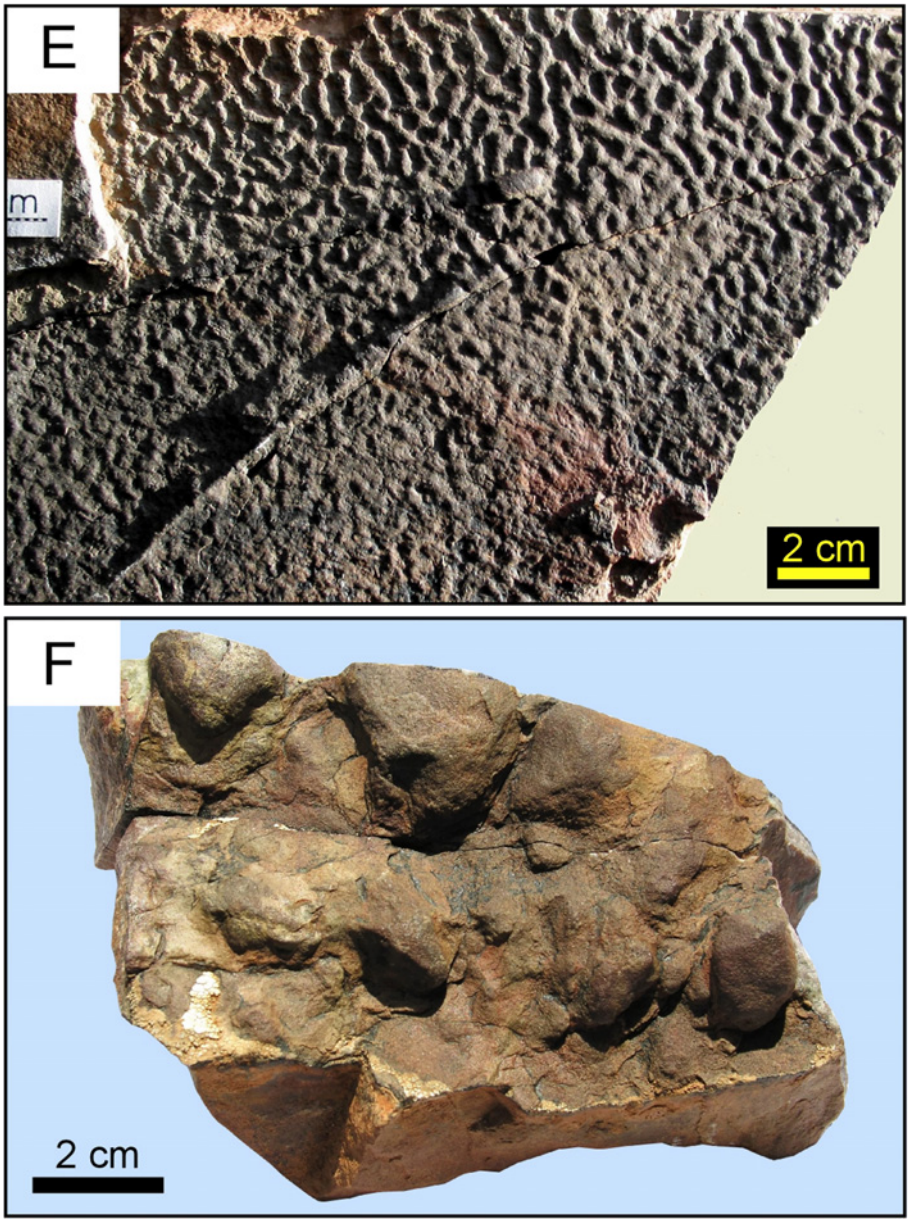


Figure 7(f)-3: ***Continued.***

with alternation of sericitic mudstone and centimetre- to decimetre-thick quartzite beds, HCS, wave ripple cross-laminations, interference and oscillation ripples, gutter and groove casts, and thickening-upward parasequences. Palaeoenvironment: inner shelf environment influenced by storms. (F) Upper surface of 4 cm thick quartzite bed with rounded to elongate upward protrusions of sand. The blister- or dome-shaped sand protrusions are separated from each other by relics of thinly laminated sericitic mudstone with lenses of siltstone and sparse isolated grains of quartz. The sand protrusions cross-cut the lower laminae of the overlying drapes, indicating that their formation postdates deposition of the layer above, which itself preserves lenticular shrinkage cracks. Locality: Agoummy area, Anti-Atlas, Imi n-Tizi Formation. Genesis: the structure is developed on a sediment surface beneath a mat and reflects mat surface morphological details, like blisters and domes. Preservation of mat morphological details is due to upward protrusion of sediment, partly or completely filling bulges and domes developed in the mat. Modern examples (e.g., Tunisia) show that bulges or domes developed in the mat are partially or completely filled with sediment rising up from below (see Chapter 8(d)). Upward protrusion of sediment may be induced by hydraulic upward pressure in confined groundwater below mat or by 'evaporative pumping' (Hsü and Siegenthaler, 1969). Associated sedimentary structures: oscillation, interference and current ripples, desiccation cracks, mud clasts, few small fluvial/tidal channels, heterolithic deposits with centimetre-scale interbedded sandstone and organo-sedimentary sericitic layers, and a few event deposits related to fluvial sheet floods or storms. Palaeoenvironment: intertidal to lower supratidal zones of a coastal plain. All photographs (A to F): E. Bouougri and H. Porada.

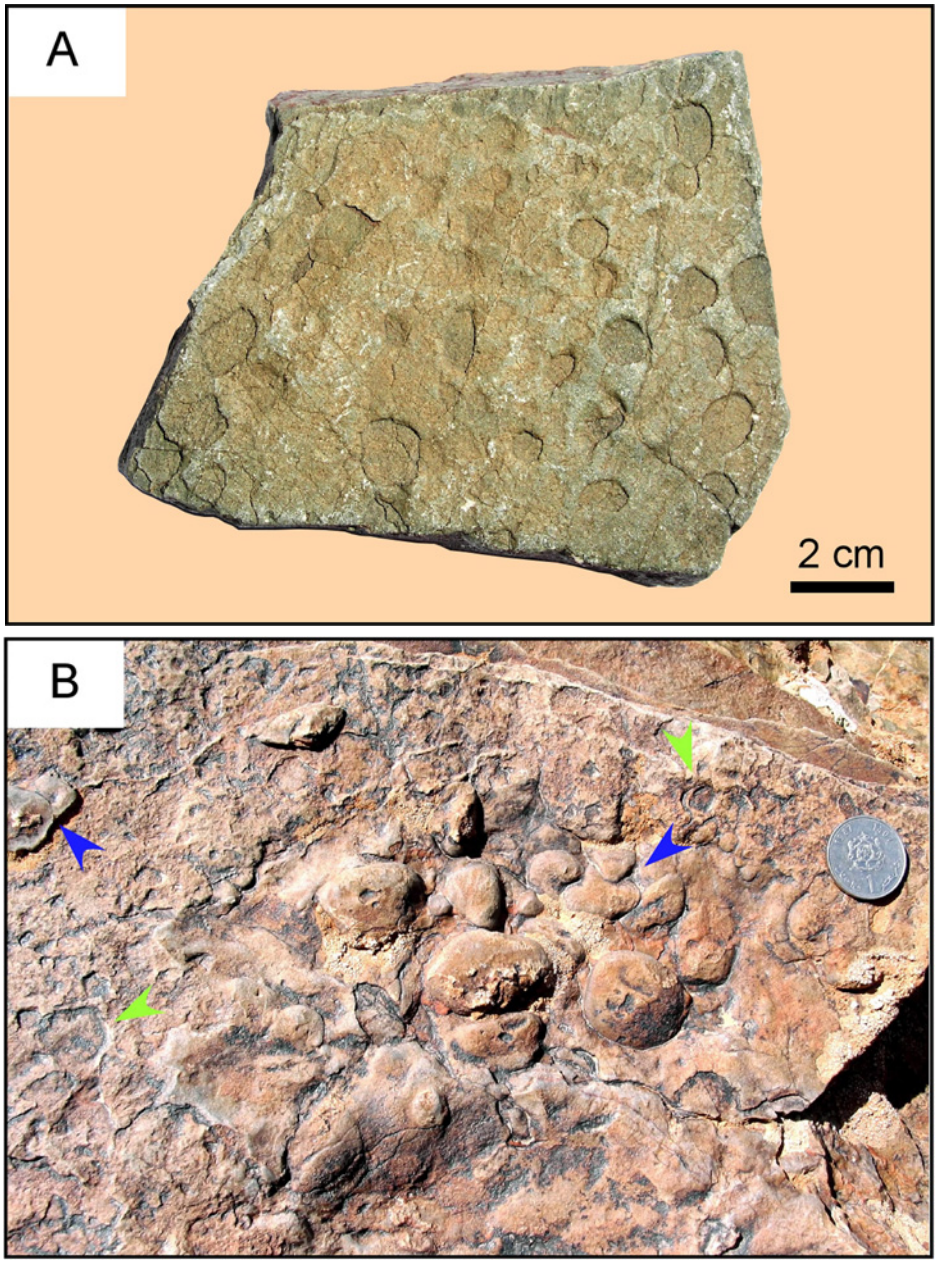


Figure 7(f)-4: Mat destruction-growth features: erosion marks (A), microbial sand/silt clasts (B), microbial shrinkage/sand cracks (C–E), large desiccation polygons in biolaminites (F, G) and shrinkage and overgrown upturned crack margin in biolaminite (H).

(A) Upper surface of 3 cm thick fine-grained quartzite layer with flat-bottomed, round to elliptical depressions in the upper millimetre-thick lamina. The structures are 0.5–1.2 cm in diameter, with long axes between 0.8 and 1.3 cm and short axes between 0.4 and 0.8 cm, and are usually aligned. The margins of the depressions are remarkably regular and sharp, the bottoms are flat and expose the underlying lamina. Locality: Tirsal section, Anti-Atlas, Wanimzi Formation. Genesis: the flat bottoms and sharp margins of the structures suggest that pieces of an upper fine-grained cohesive veneer have been removed by tractional currents and reworked as platy rounded 'microbial chips'. The structures are considered to represent erosion marks of a fine-grained and millimetre-thick biostabilised veneer. In modern environments, e.g., the tidal-flats of the North Sea coast, erosion marks have been recognised in the middle to upper intertidal zones (Gerdes et al., 1993, 2000a). These and some ancient examples (see Reineck, 1979) usually have greater dimensions than those presented here, which are rather of the size of raindrop impacts. An interpretation as raindrop impacts or mud-chip imprints is, however, excluded mainly due to the flat bottoms and sharp and regular margins and, less stringently, due to the varying sizes, elliptical forms and preferred orientation of the structures. Associated sedimentary structures: oscillation, interference and current ripples, desiccation cracks, mud clasts, few small fluvial/tidal channels, heterolithic deposits with centimetre-scale interbedded sandstone and

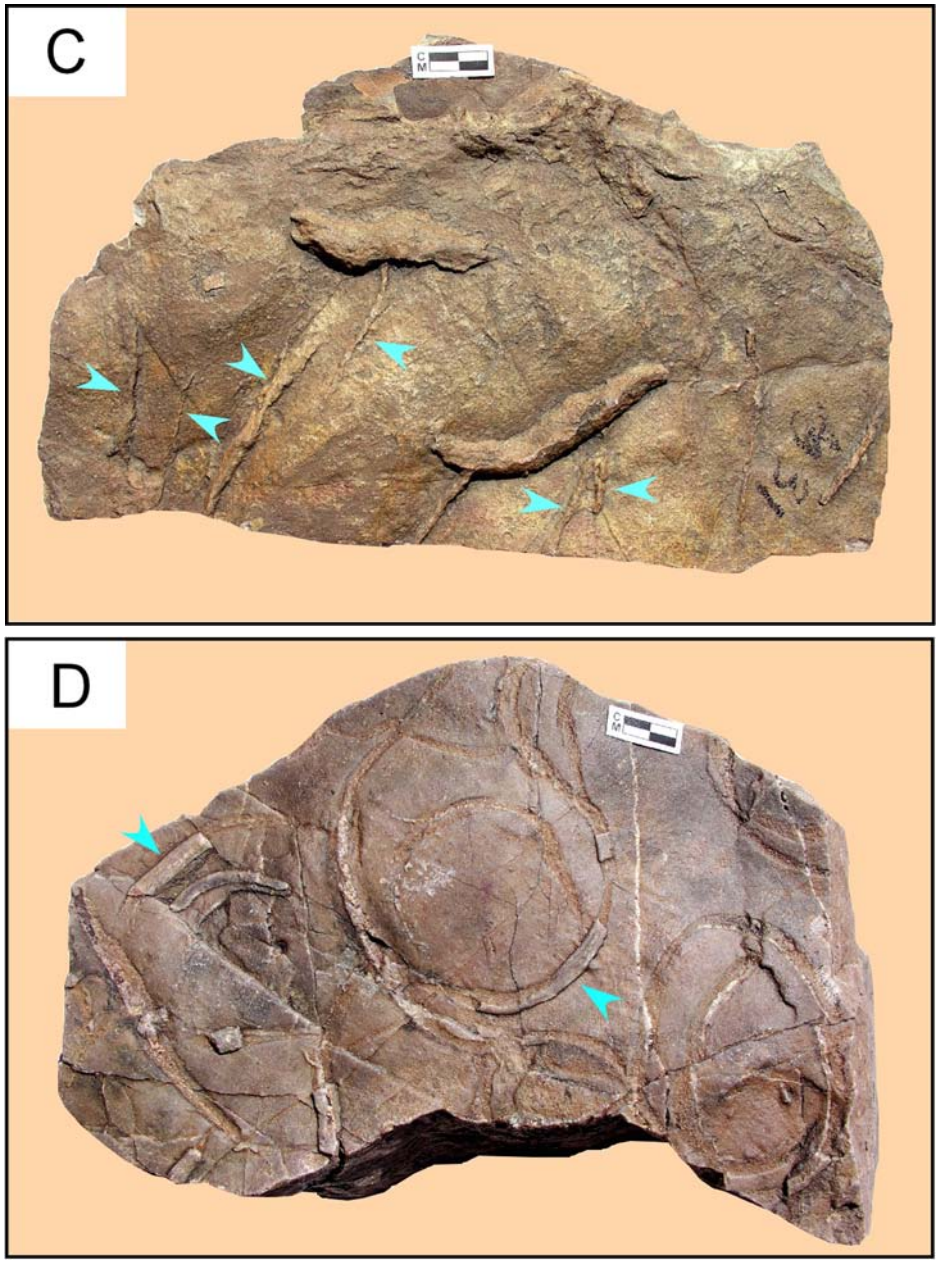


Figure 7(f)-4: ***Continued.***

organo-sedimentary sericitic layers, and a few event deposits related to fluvial sheet floods or storms. Palaeoenvironment: intertidal to lower supratidal zones of a coastal plain. (B) Upper surface of 5 cm thick fine-grained sandstone layer with subrounded and elongate, platy sand clasts. Size of the clasts varies between 1 and 3.5 cm (long axis), whereas thickness varies from 2 to 5 mm. Clasts are slightly oriented and some of them are clustered closely together, partly with overlapping relationships (blue arrows). The sand chips are preserved either as compacted intraclasts or weathered-out moulds (green arrows). The contact between sand chips and adjoining sediment is sharp and usually enhanced by limonitic staining. The clasts are finer-grained and more sericitic than the underlying sediment layer. The texture of the sand chips is matrix-supported with 'coated grains'; a sericitic component fills the pore spaces and coats individual sediment grains. Coin for scale is 24 mm in diameter. Locality: Agoummy area, Anti-Atlas, Imi n-Tizi Formation. Genesis: the clasts of sand- to silt-sized sediment are considered to result from physical erosion of a thin microbially-bound layer and subsequent reworking of the chips by wave and current action. Imbrication of clasts may indicate transport by currents. In modern environments, microbial mat chips preferably occur in the intertidal to lower supratidal range (e.g., Gerdes et al., 2000a). Ancient examples are reported from the upper intertidal zone (Gehling, 2000) and nearshore environment (Gehling, 2000) where a mat could grow unimpeded to form a resistant cohesive layer, and nevertheless be destroyed by wave action and strong currents during a storm. Associated sedimentary structures: oscillation, interference and current ripples, desiccation

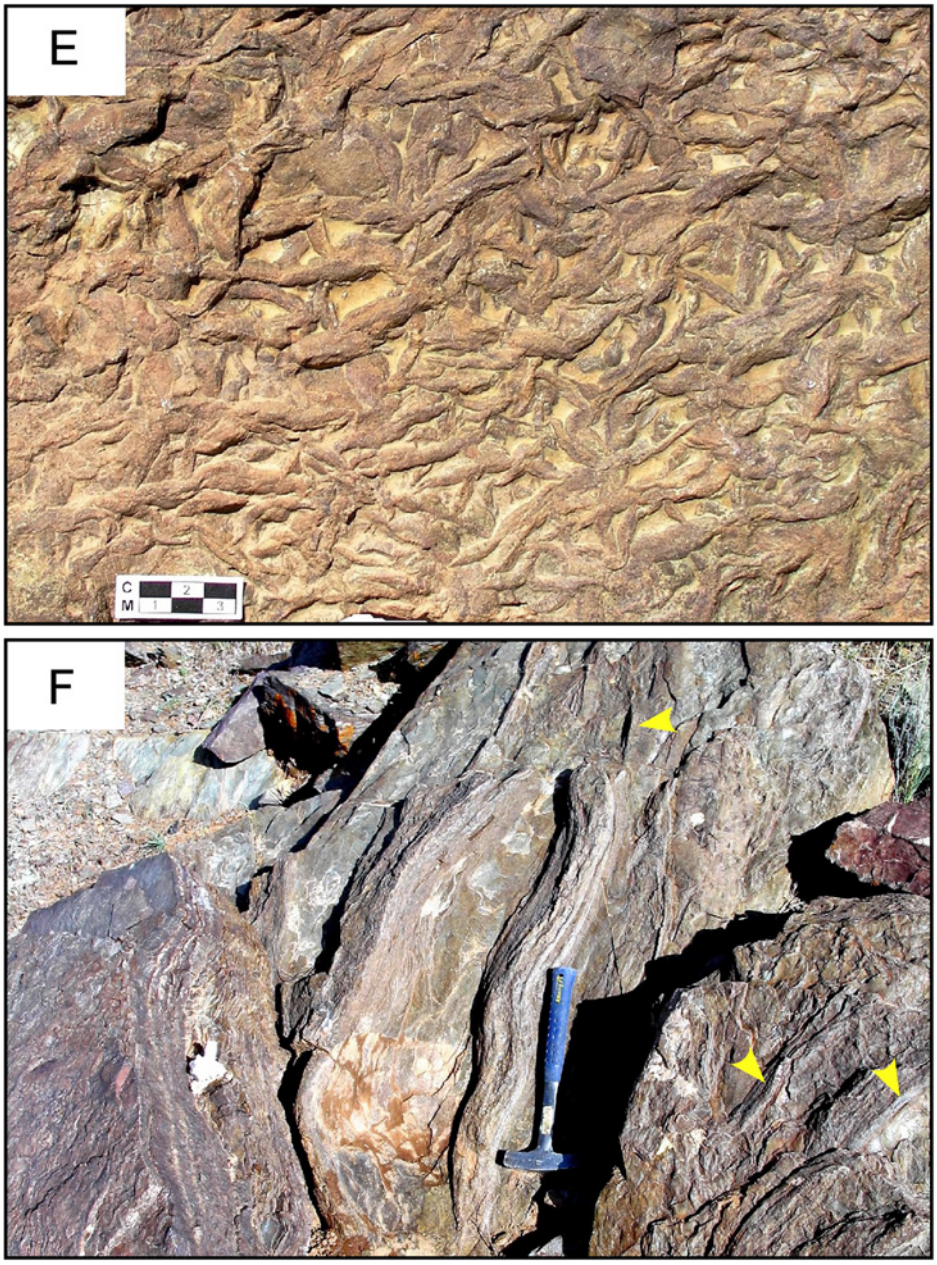


Figure 7(f)-4: ***Continued.***

cracks, mud clasts, few small fluvial/tidal channels, heterolithic deposits with centimetre-scale interbedded sandstone and organo-sedimentary sericitic layers, and a few event deposits related to fluvial sheet floods or storms. Palaeoenvironment: intertidal zone of a peritidal coastal plain. (C) Upper surface of 2.5 cm thick quartzite bed with isolated, lenticular and spindle-shaped sand-filled cracks. The surface shows two types of cracks forming two superimposed generations. The first one consists of narrow cracks (0.5 cm maximum width) preserved as isolated or subparallel and slightly curved ridges which frequently meet at the ends (blue arrows), thus surrounding lenticular structures up to 2 cm wide. The second generation consists of isolated platy sand ridges, 1.5 cm high and a few millimetres thick, with a length of up to 10 cm. Scale is 2 cm. Locality: Agoummy area, Anti-Atlas; Imi n-Tizi Formation. Associated sedimentary structures: heterolithic deposits with centimetre-scale interbedded sandstone and organo-sedimentary sericitic layers, event deposits related to fluvial sheet floods or storms, few small fluvial/tidal channels, mud clasts, oscillation ripples, interference and current ripples, desiccation cracks, and adhesion warts. Palaeoenvironment: intertidal to lower supratidal zones of a peritidal coastal plain. (D) Upper surface of 10 cm thick quartzite bed with spindle-shaped, curved, sinuously curved, circular and 'wriggly' microbial sand cracks. The surface shows impressions of removed sandy crack-fills with tapering ends and crack-fillings preserved as flat sand ridges (indicated by arrows). The length of the cracks varies from 2 to 17 cm and the average width is 0.8 cm. The cracks may merge together but do not show any cross-cutting relationship. Scale is 2 cm. (E) Upper

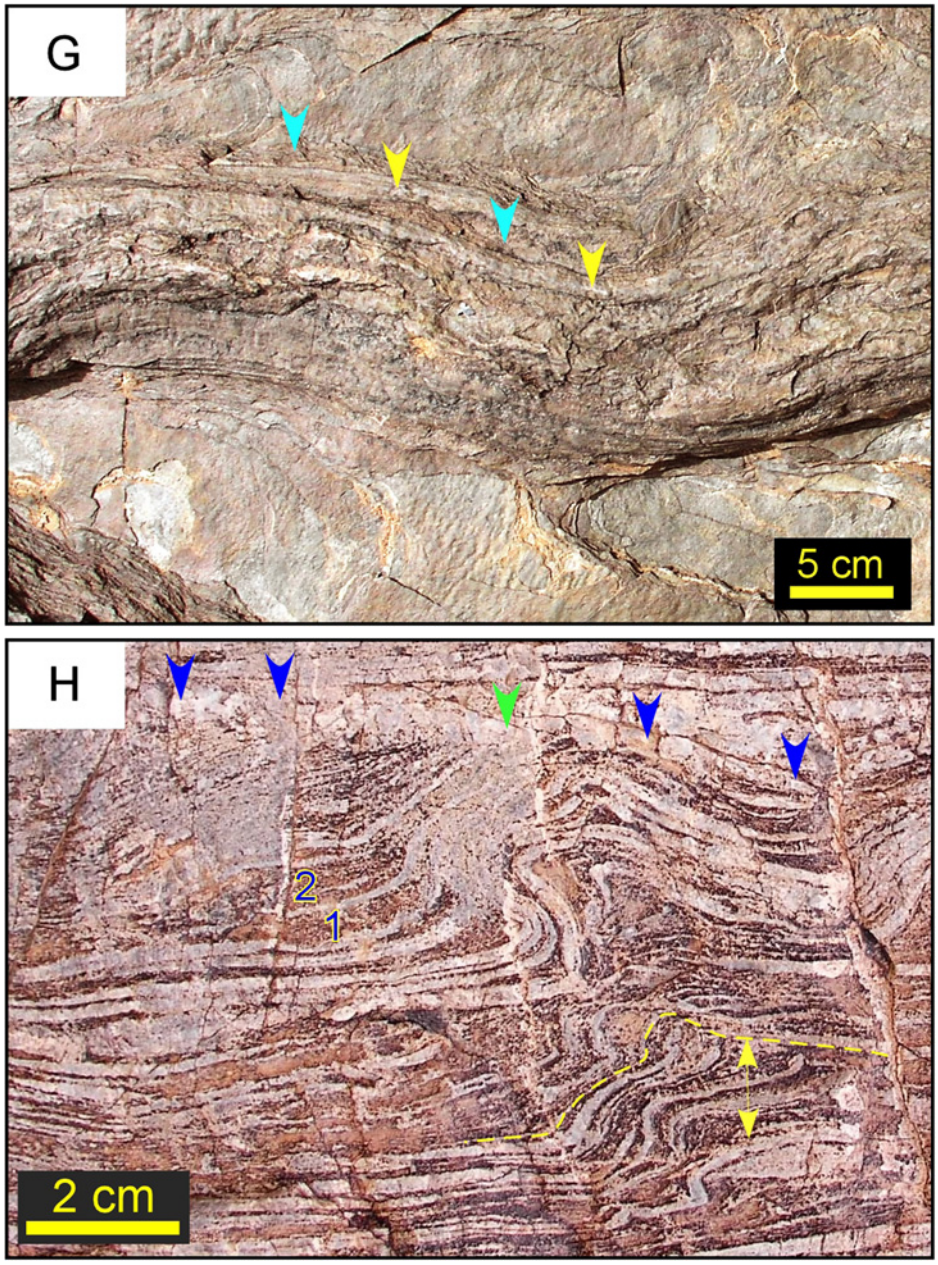


Figure 7(f)-4: ***Continued.***

surface of 3 cm thick quartzite bed exhibiting high density of filled sand cracks. The fills are lenticular, straight, spindle-shaped to sinuously curved and form a network of differently oriented bodies, which usually meet at high angles. Some of the fills are juxtaposed or arranged in two opposite ridges. Length of individual bodies varies from 2 to 8 cm, average width is between 0.5 and 1 cm. The crack-fills form superimposed bodies with tapering ends and overlapping relationships. They occur in distinct thin, laminated sericitic layers preserved between the cracks (yellow layers). Distinction of generations is based on the criterion that in a shrinking layer cracks do not develop cross-cutting relationships. Rather propagating cracks merge if meeting at low angles, or form high angle junctions if laterally arriving at existing ones. Due to high rate of compaction, the crack-fills appear as a single generation on the bedding surface. The sericitic layers hosting the cracks display a laminated fabric with matrix-supported grains, lenticular lenses of isolated and aligned grains, and black carbonaceous laminae. Scale is 3 cm. For both D and E: *Locality*: Tirsal area, Anti-Atlas; Wanimzi Formation; *Genesis*: the sand cracks illustrated here are examples of a variety of shrinkage cracks developed in organo-sedimentary microbial layers that underwent subaerial desiccation in the intertidal to lower supratidal range of peritidal environments (e.g., Porada and Löffler, 2000; Bouougri and Porada, 2002). Similar cracks have previously been documented as synaeresis cracks, *Manchuriophycus*, *Rhysonetron*, etc. The term 'microbial shrinkage cracks' proposed by Porada and Löffler (2000) is genetic and refers to an association of cracks related to shrinkage of microbial mats or, more generally, organo-sedimentary

material. Such cracks may develop in millimetre- to centimetre-thick organo-sedimentary argillaceous layers draping sand surfaces (photos C, E). The observation that cracks may be isolated from sand layers above and below, and may be preserved as casts and moulds on bedding surfaces indicates that filling occurs mainly during tidal floods and before deposition of the event sand layer above (photo D). The development of subparallel opposing cracks which seem to surround openings (photo C), is one of the typical shrinkage features associated with thin and still living microbial mats, as observed in modern examples in Tunisia (personal observation). In the example of photo D, the thin microbial mat that underwent shrinkage was not preserved during burial. The superimposed crack generations (photo E) formed in a stack of organo-sedimentary layers which underwent repeated events of subaerial exposure and flooding during buildup; *Associated sedimentary structures*: millimetre- to centimetre-scale alternation of sedimentary sandstone event layers of storm or fluvial origin and organo-sedimentary laminated layers of siltstone and sericitic argillite, wave and current ripple cross-lamination, oscillation and interference ripples, small-scale load structures, and polygonal desiccation cracks; *Palaeoenvironment*: intertidal to lower supratidal zones of a peritidal coastal plain. (F) Large desiccation polygon, seen in plan view, preserved in planar laminated siliciclastic biolaminite. The large cracks extending 4 cm upwards, cut across several layers in which small isolated lenticular and spindle-shaped cracks are preserved (indicated by arrows). In detail, each large crack cuts through a multilayered structure of millimetre-thick alternating siltstone and laminated sericitic layers. The isolated spindle-shaped cracks are V-shaped, tapering downward, and are filled with fine-grained sandstone material. (G) Close-up view of a large, sinuously curved crack showing laminated structure. Blue arrows indicate sericitic–organic layers; yellow arrows indicate siltstone layers. Locality: Agoummy area, Anti-Atlas; Imi n-Tizi Formation. Genesis: the large cracks forming polygonal networks are interpreted as the upturned margins of major polygonal cracks formed during shrinkage of biolaminite. Such upturned crack edges are typical of biolaminite deposits in the intertidal zone and have been observed in the modern tidal flats at Bhar Aloune, Tunisia (see Figure 4(c)-6). The small spindle-shaped cracks filled by sandy material constitute another aspect of desiccation, with limited opening of cracks and rapid subsequent filling by sediment during tidal flood events. Associated sedimentary structures: oscillation, interference and current ripples, desiccation cracks, mud clasts, few small fluvial/tidal channels, heterolithic deposits with centimetre-scale interbedded sandstone and organo-sedimentary sericitic layers, and a few event deposits related to fluvial sheet floods or storms. Palaeoenvironment: upper intertidal to lower supratidal zones, periodically submerged and regularly flooded by tides or during storm events. (H) Simple structure developed by overgrowth of an upturned crack margin in biolaminites that underwent subaerial shrinkage. The laminae of the upturned margin are very thin and are mainly of microbial origin, whereas behind the overgrown edge, lamination consists of a millimetre-scale alternation of continuous white laminae and discontinuous brown sedimentary laminae (1 and 2 as examples). The white laminae consist mainly of laminated sericitic layers including floating sand- to silt-sized quartz grains and lenses of silt-sized quartz. The brown layers consist of alternations of sericitic laminae and fine-grained siltstone laminae with a few flakes of mica. The whole structure is sealed by a horizontal and continuous white quartzitic layer (indicated by blue arrows). Behind the edge (on the left side of the green arrow), laminae of the polygon are discontinuous and slightly upturned. To the right side of the green arrow, laminae continuously overgrow the upturned edge. Yellow arrows indicate initial upturned margin laminae, whereas the yellow dashed line indicates the first overgrowing laminae. Locality: Nqob area, Anti-Atlas; Tamgarda Formation. Associated sedimentary structures: centimetre-thick quartzite beds with wave and current ripple cross-lamination, few centimetre-thick sandstone layers of storm or sheet flood events, desiccation cracks, interference and oscillation ripples, and planar biolaminites with shrinkage cracks. Palaeoenvironment: intertidal zone regularly flooded during high tides. All photographs (A to H): E. Bouougri and H. Porada.

---

sandstone intervals preserve a variety of internal structures including wavy to planar lamination, wave and current generated lamination, occasionally with foreset dip directions in bipolar orientation. Additionally, bedding surfaces are flat or wave rippled with interference and oscillation ripples and rare current ripples. A common feature of the heterolithic deposits is the frequent occurrence of shrinkage cracks with various shapes, sizes and densities. Microbial mat structures and additional features, like adhesion warts, normal polygonal desiccation cracks, evaporite pseudomorphs, mud- and sand-chips, together indicate deposition in low-energy coastal shallow marine environments, likely on intertidal to supratidal flats with periodic subaerial exposure.

The Anti-Atlas example shows that peritidal conditions are particularly suitable for the formation and preservation of microbial mat structures. Seaward, in zones above or below storm wave base, establishment of continuous, cohesive microbial mats appears less likely, and only one single horizon (a sandstone storm bed) with *Kinneyia* structures was found in heterolithic deposits of a storm influenced inner shelf environment (Figure 7(f)-3E).

7(g). MICROBIAL MAT SEDIMENTARY STRUCTURES AND THEIR RELATION TO ORGANIC-CARBON BURIAL IN THE MIDDLE NEOPROTEROZOIC CHUAR GROUP, GRAND CANYON, ARIZONA, USA

K.M. Bohacs, C.K. Junium

The mudstones of the Kwagunt Formation of the Chuar Group display a wide range of sedimentary and geochemical attributes that indicate burial of organic carbon was mediated, if not controlled, by benthic microbial mats. We also observed that the sedimentary structures were not randomly distributed, but occurred in two commonly recurring associations that correspond with two modes in the relation between organic-carbon and silt content: a positive relation with silt content proportional to weight % total organic carbon (TOC), and an inverse relation with silt content proportional to 1/weight % TOC. These facies associations support the previously reported interpretation of a higher energy, 'shallower-water' setting (based on coarse-grained lithofacies; e.g., Vidal and Ford, 1985; Reynolds and Elston, 1986; Reynolds et al., 1988; Cook, 1991; Dehler et al., 2001) as well as an additional lower energy, more distal, 'deeper-water' environment.

The Kwagunt Formation (~500 m thick, Figure 7(g)-2A) accumulated in a relatively shallow rift embayment near the northwestern margin of the equatorial region of Laurentia during the Middle Neoproterozoic (~800–740 Ma). Previous work suggests that deposition occurred in relatively shallow marine waters, not deeper than 100 m, based upon the common occurrence of desiccation features, rippled thin sand beds, dolomite and sandstone bedsets and the interpretation of 'ripples' in mudstones (Dehler et al., 2001). Variations in base level and climatic wetness are thought to have been rapid and possibly glacio-eustatic based on observations of commonly occurring sharp, conformable transitions from black shale to dolomite. Deposition is interpreted to have occurred in an intra-cratonic rift embayment, possibly silled like the Black Sea (Cook, 1991), or in a half-graben (Seeley and Keller, 2003).

We observed previously unreported sedimentary structures that reveal abundant evidence of microbial mat features during the course of our detailed analysis of the mudstone facies and stratigraphy, as part of an integrated study of the biogeochemical system of the Chuar Group (Junium and Bohacs, 2005). Previous work concentrated on the coarser grained lithologies, with 75% of facies description concentrated on 20% of the outcrop interval (Dehler et al., 2001). Our samples were collected from the Awatubi and Walcott Members of the Kwagunt Formation in the Nankoweap Butte area, Arizona in 1986, by researchers from Exxon Production Research Company (Figure 7(g)-1). In all, the fine-grained strata can be divided into five facies based on lithology, bedding, physical and biogenic sedimentary structures, and bulk, molecular, and isotopic organic geochemical attributes (Junium and Bohacs, 2005). Sedimentary structures observed that indicate microbial-mat influence include: (1) wavy, crinkly, anastomose or discontinuous laminae; (2) desiccation features and roll-up structures; (3) fenestral laminae; (4) 'pustular' or wavy surfaces; (5) pseudo-cross-laminae; (6) mica flecks adhered to inferred mat surface; (7) graded beds with carbonaceous caps; (8) pyrite associated with carbonaceous laminae (Figures 7(g)-2, -3). These all accord with features deemed diagnostic of microbial mats by Schieber (1999, 2004). Fragments of microbial filaments have been observed in pulverised, acid-digested samples from the area (Vidal and Ford, 1985), but the microbial mat features that are common in hand specimen have not been reported.

Molecular geochemical analyses reveal even-over-odd preferences in *n*-alkane distributions and possible monomethyl-alkane series. These results support previous findings of quaternary-branched-diethylalkanes and monomethyl-alkane series (Hieshima and Pratt, 1991; Logan et al., 1999b; Kenig, 2000) – geochemical features interpreted by those workers as indications of sulphide-oxidising bacteria and benthic microbial mats. Figure 7(g)-3F shows the well-developed even/odd predominance in the C20–C26 *n*-alkanes with C20 being the most abundant compound. This geochemical character is seen in modern and ancient examples with microbial mat structures (Logan et al., 1999b; Kenig, 2000). Similar characteristics have been reported from other proven Precambrian organic-rich rocks: Centralian Superbasin, Australia (Logan et al., 1999b), Nonesuch Formation, USA (Hieshima and Pratt, 1991), and from Late Precambrian oils from eastern Siberia (Fowler and Douglas, 1987). Other molecular characteristics indicate significant, but variable amounts of planktonic algal input: dominance of C27 steranes, hopane/sterane ratios of 1 to 2, pristane/phytane ratios between 0.7 and 1.4, and extended isoprenoids (Peters et al., 2005).

Pseudo-cross laminated structures, carbonaceous lenses, crinkly, silty, anastomosing and discontinuous laminae are found in facies interpreted to have accumulated in more distal, quieter, 'deeper' water (Figures 7(g)-2B to -2D). This facies also tends to have TOC contents greater than 4% and an inverse relation between silt content and TOC. These intervals have the even/odd *n*-alkane carbon number predominance of the rest of the Kwagunt Formation,

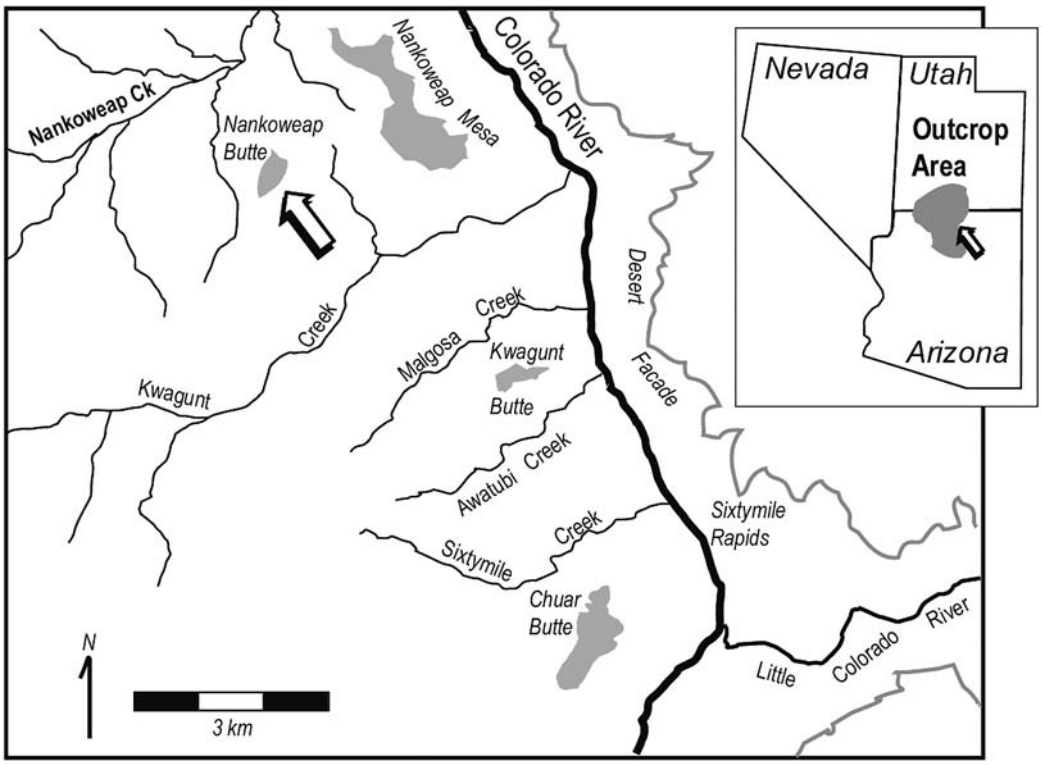


Figure 7(g)-1: Location of outcrop pictured in Figure 7(g)-2.
The outcrop is located around Nankoweap Butte, west of the Colorado River between Nankoweap and Kwagunt Creeks, approximately 9.8 km upstream of the confluence with the Little Colorado River, Grand Canyon National Park, Arizona (arrow: 36.26316° N, 111.88376° W, WGS84).

but they show a much stronger planktonic-algal (normal-marine microbial) signature with high concentration of shorter chain *n*-alkanes (Figure 7(g)-2E).

Fenestral laminae, roll-up features and pustular surfaces, indicative of mat desiccation, are more common in regions interpreted to have been deposited in higher-energy, more proximal, 'shallower-water' settings (Figures 7(g)-3A to -3E). TOC content in this facies tends to be less than 3% and is positively correlated with silt content. Its geochemical character is the most common throughout the Chuar Group (Figure 7(g)-3F) and shows significant input of organic matter associated with microbial mats (e.g., as seen in other formations by Logan et al., 1999b and Kenig, 2000).

These observations of microbial-mat features and distributions integrated with the full range of physical and geochemical data, indicate that the depositional setting of the Kwagunt Formation varied systematically along a depositional gradient. It ranged from more distal, quieter, relatively clear but 'deeper-water' areas with intermittent sediment transport and significant planktonic algal input along with patchy benthic microbial mats, to more proximal reaches. These higher energy, 'shallower-water' areas also had relatively clear water but were intermittently exposed subaerially and benthic microbial mats were widespread.

These findings demonstrate the power of a fully integrated approach that includes careful consideration of the finer-grained strata to provide detailed insight into depositional conditions at this critical time in Earth history.

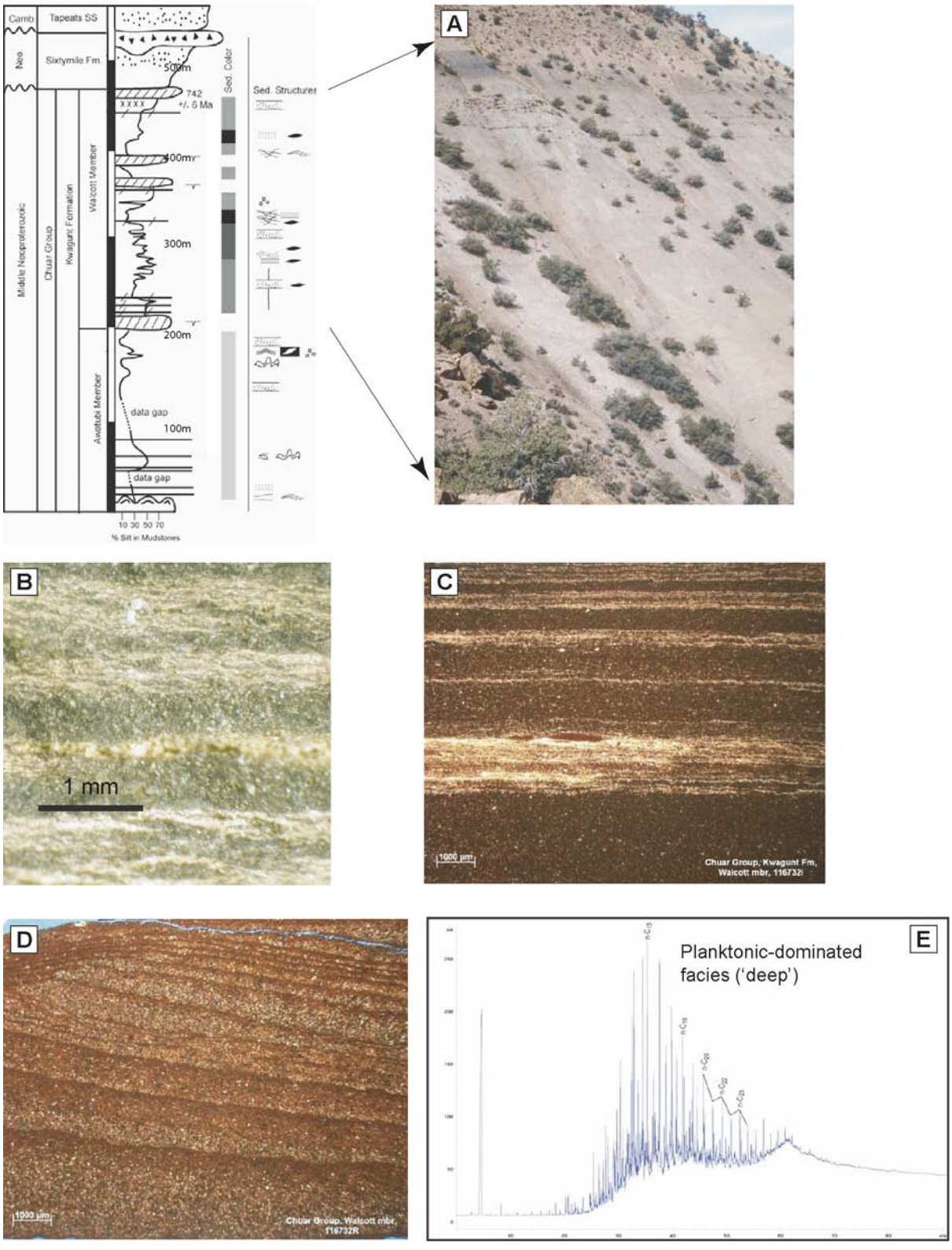

Camb
Neo
Middle Neoproterozoic
Tapeats SS
Sixtymile Fm.
Chuar Group
Kwagunt Formation
Walcott Member
Awatubi Member
500m
742
+/- 6 Ma
400m
300m
200m
data gap
100m
data gap
10 30 50 70
% Silt in Mudstones
Sed. Color
Sed. Structures
A
B
1 mm
C
1000 µm
Chuar Group, Kwagunt Fm,
Walcott mbr, 116732i
D
1000 µm
Chuar Group, Walcott mbr,
116732R
Planktonic-dominated
facies ('deep')
E

Figure 7(g)-2:
(A) Vertical profile of Kwagunt Formation at the Nankoweap Butte measured section showing vertical stacking of lithology, rock colour, silt content, and sedimentary structures. Fenestral laminae, roll-up structures, and pustular surfaces (facies association B) are more common in the basal third. Pseudo cross-bedding, carbonaceous lenses, crinkly, silty, anastomosing and discontinuous laminae (facies association A) occur most commonly in the darker, more silt-lean portions of the upper two-thirds of the section. (B) Hand sample showing anastomose and discontinuous laminae in very dark grey, silt-bearing, clay-rich mudstone of the Walcott Member, Kwagunt Formation (from approximately 323 m on the measured section in Figure 7(g)-2A). These structures are interpreted to record potentially chemosynthetic microbial mats and relatively distal and quiet-water conditions. (C) Thin section detail of anastomose and discontinuous laminae in black, organic-matter-rich, clay-dominated mudstone of the Walcott Member (∼418 m on measured section). Organic-carbon content is 9.8%, comprising both benthic microbial and planktonic algal input. These structures are interpreted to record possibly chemosynthetic microbial mats in relatively distal and quiet bottom conditions. This bedding style is probably analogous to the 'striped shales' described by Schieber (1986) and shown in other examples in this volume (see Chapter 5 and Sections 7(b), 7(c)). (D) Thin section image of pseudo-cross-bedding in dark grey, clay-bearing, silt-rich mudstone with black carbonaceous laminae atop inclined graded beds (from ∼398 m on measured section). These structures indicate intermittent transport of sediment over a microbial mat-covered substrate (see Schieber, 2004). (E) Gas-chromatograph trace of solvent-extracted organic matter from sample shown in Figure 7(g)-2C. The high concentration of shorter chain *n*-alkanes indicates a dominance of organic matter derived from planktonic algae/photosynthetic protests, whereas the even/odd distribution in the higher carbon-number *n*-alkanes portrays significant content of microbial-mat organic matter, both consistent with a more distal depositional setting.

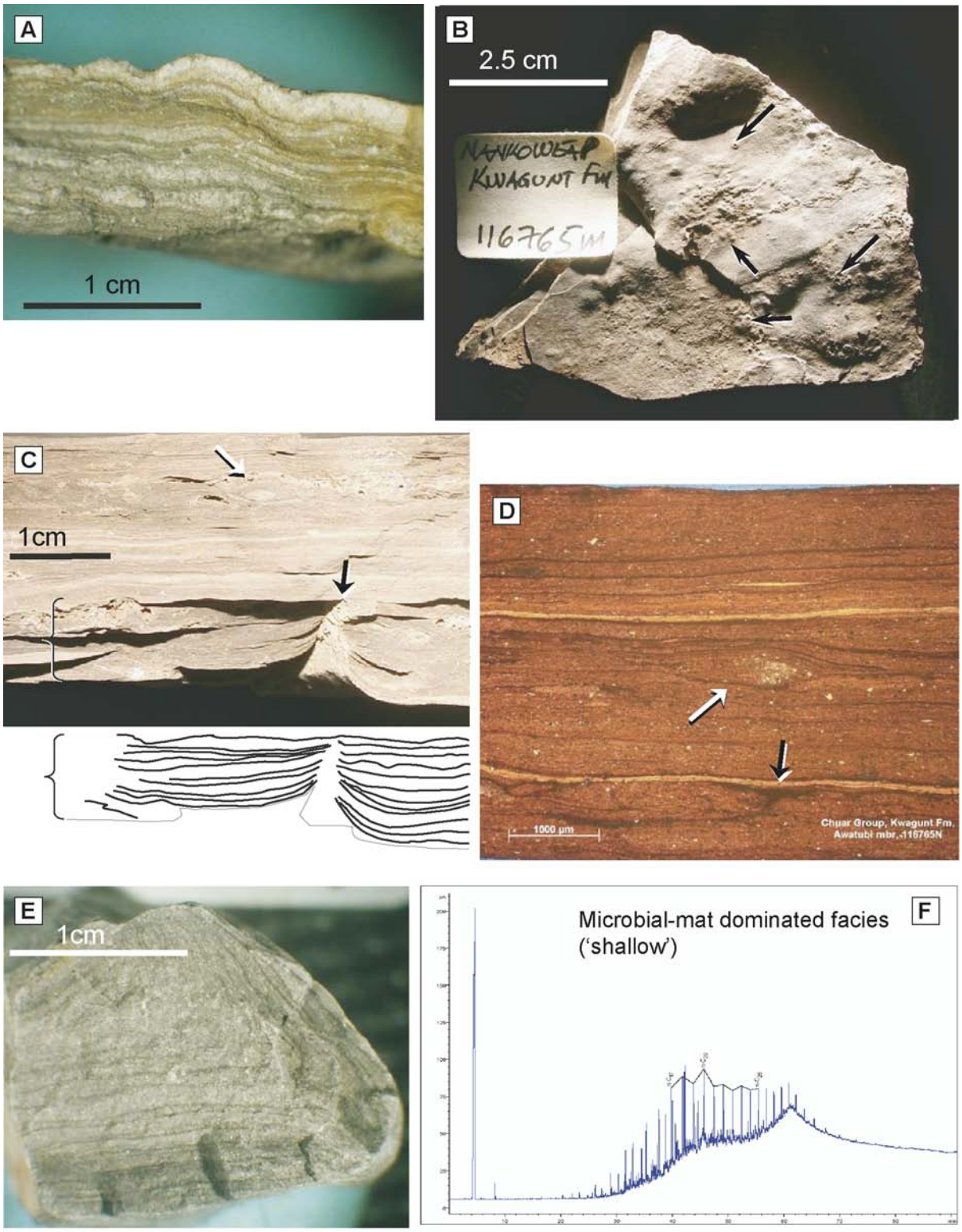

A
1 cm
B
2.5 cm
NANKOWEAP
KWAGUNT FM
116765M
C
1cm
D
1000 µm
Chuar Group, Kwagunt Fm,
Awatubi mbr.,116765N
E
1cm
Microbial-mat dominated facies
('shallow')
F

Figure 7(g)-3:
(A) Hand specimen of wavy and crinkly carbonaceous and silty laminae in a grey silt-bearing, clay-rich mudstone from the Awatubi Member, Kwagunt Formation (from approximately 62 m on the measured section in Figure 7(g)-2A). These laminae are interpreted to record microbial-mat (probably photosynthetic) accumulation under intermittent clastic sedimentation in relatively shallow water. (B) Bedding-plane view of hand specimen with well-developed pustular surface structures at several stratigraphic levels in dark grey, clay-bearing, silt-rich mudstone with black carbonaceous laminae, from the Walcott Member (∼173 m on measured section). Arrows indicate pustules, including several 'popped' pustules. Pustular surfaces arise from gas bubbles trapped below cohesive microbial mats and can form in emergent and submergent conditions (see discussion in Schieber, 2004). (C) View of fenestral laminations on surface perpendicular to bedding (white arrow) and upturned laminae terminating at a vertical surface interpreted as a desiccation crack (black arrow). Line drawing below shows convergent geometry of laminae at several levels, indicating intermittent development of upturned laminae (contrast with consistently parallel pattern of laminae observed in simple desiccation cracks). Specimen is a grey-brown, silt-bearing, clay-rich mudstone with common carbonaceous laminae from the Awatubi Member (∼161 m on measured section). Both structures are interpreted to represent sedimentation among microbial mats under intermittent subaerial exposure. (D) Thin section detailed image of fenestral lamination (white arrow) and abruptly discontinuous laminae probably related to desiccation (black arrow) in hand specimen described in Figure 7(g)-3C. The very thin and dark laminae are interpreted to be remains of microbial mats. (E) View of vertical face of roll-up structure in a medium grey, clay-bearing siltstone with common to abundant carbonaceous laminae, from near the base of the Awatubi Member (∼60 m on measured section). Roll-up structures probably represent microbial mat mediated sediment accumulation under more prolonged subaerial exposure and subsequent high-energy bottom conditions (see discussion in Schieber, 2004). (F) Gas-chromatograph trace of solvent-extracted organic matter from dark grey, clay-bearing mudstone with abundant carbonaceous laminae from the upper portion of the Awatubi Member (∼175 m on measured section). Total organic-carbon content is 1.8%. The well-developed even/odd distribution in the C20–C26 *n*-alkanes and peak abundance of C20 *n*-alkane indicate organic matter is dominantly from microbial mats.

7(h). MAT-RELATED FEATURES FROM THE TERMINAL EDIACARAN NUDAUS FORMATION, NAMA GROUP, NAMIBIA

E. Bouougri, H. Porada

The Nama Group in central to southern Namibia (Figure 7(h)-1A) represents the filling of a foreland basin related to the Neoproterozoic–Early Palaeozoic collision and uplift of the Damara and Gariep belts. The group is subdivided (from base to top) into the Kuibis, Schwarzrand and Fish River Subgroups (e.g., Germs, 1983; Gresse and Germs, 1993). During deposition of much of the earlier subgroups, the basin was divided by a flexural high (Osis ridge) into the southern Witputs and the northern Zaris sub-basins (Germs, 1983). Deformation of the Nama Group generally is weak but increases in the peripheries of the belts where open folds, slaty cleavage and minor thrusts occur. Based on palaeontological and radiometric data (Germs et al., 1986; Grotzinger et al., 1995, 2000), deposition of the Kuibis and most of the Schwarzrand Subgroups occurred in the Ediacaran. The studied outcrops belong to the Niederhagen and Vingerbreek members (Nudaus Formation) of the lower Schwarzrand Subgroup (Figure 7(h)-1B). The age of the Nudaus Formation is between ca. 548 and 545 Ma, according to U–Pb zircon dates from ash layers in the underlying Kuibis Subgroup and overlying Urusis Formation, respectively (Grotzinger et al., 1995). The members consist of shale, siltstone and sandstone, all deposited in tidal and low-energy shoreline depositional environments (Germs, 1983). The study area (Figure 7(h)-1C), located in the northwestern part of the Zaris sub-basin, straddles the facies boundary of "mainly sandy tidal" and "muddy tidal without carbonate, some distal fluvial sediments" (Germs, 1983, p. 102). Sequence stratigraphic studies further south in the basin showed the Vingerbreek member to include shallowing-upward cycles of nearshore to mid-shelf shale, siltstone and intercalated sandstone beds, deposited in a transgressive systems tract (Saylor et al., 1995).

Occurrences of mat-related structures described here from the Nudaus Formation, come mainly from the lowermost part of the Vingerbreek Member, exposed near Haruchas homestead (Figures 7(h)-2A, -2E, -2H, -3 and -4). At this locality, a section of about 46 m thickness contains various microbial mat-related structures (Porada and Bouougri, 2006) which complement 'wrinkle structures' described by Noffke et al. (2002) from the upper part of the member, further to the SW near the Sattelberg mountain. The section consists mainly of thinly bedded, fine-grained siliciclastic deposits bounded by major sandstone bodies below and above. The section starts with a sheet-like sandstone bed, 0.8 m thick, with large-scale hummocky cross-stratification (HCS) reflecting a depositional environment influenced by storms. Overlying this is a heterolithic succession, about 43 m thick, of laminated siltstone/argillite with few interbedded sandstone layers. Within this interval, the biolaminite lithofacies constitutes the main component and alternates with minor laminated siltstone–mudstone lithofacies. Intercalated sandstone beds and bodies originated from intermittent storm-induced oscillatory currents or represent small-scale tidal channel-fills cutting into the heterolithic deposits.The section is capped by a 3 m sandstone body that is interpreted as fluvial channel deposits, consisting of coarse- to medium-grained cross-bedded and lenticular sandstone with lenses of conglomerate, which also exhibits erosional scouring as indicated by gutter casts, flute casts and the erosional base.

The biolaminite lithofacies is developed in metre-scale intervals, separated by centimetre-scale fine-grained sandstone beds, and consists of thinly interlaminated layers of siltstone and dark to black material of variable thickness and proportions. The silty laminae frequently exhibit wave ripple cross-lamination and small interference and oscillation ripples with sharp crests. The rippled surfaces are commonly draped by a dark and continuous film of mudstone.

The biolaminite lithofacies encompasses structures which record cyclic mat growth and destruction processes during biosedimentary accretion. Evidence of the participation of microbial mats that once colonised the sedimentary surfaces and contributed to the accretion of thick stacked layers of biolaminite include microscopic and macroscopic features like 'wavy-crinkly' lamination, isolated silt-sized grains enclosed in sericitic carbonaceous layers, 'elephant skin' textures, spindle-shaped and lenticular shrinkage cracks, lenticular cracks with upturned margins and subcircular cracks with upturned and curled margins (Figures 7(h)-2, -3). The structures are developed on single and thin microbial mat layers or encompass stacks of biolaminites. Most diagnostic are networks of upturned to overturned crack margins (Figure 7(h)-3H; see also Figures 4(c)-6D, -6E) which are overlain by continuous, planar biolaminated deposits preserving the original sedimentation plane.

The sedimentary features of the heterolithic and biolaminated deposits collectively indicate sedimentation in a shallow, intertidal to lower supratidal environment characterised by periodic emergence and occasional high energy events such as storms or tidal floods. The vertical facies organisation records an upward evolution from storm-dominated subtidal sand bar to fluvial deposits, and indicates progradational and shallowing-upward trends. In

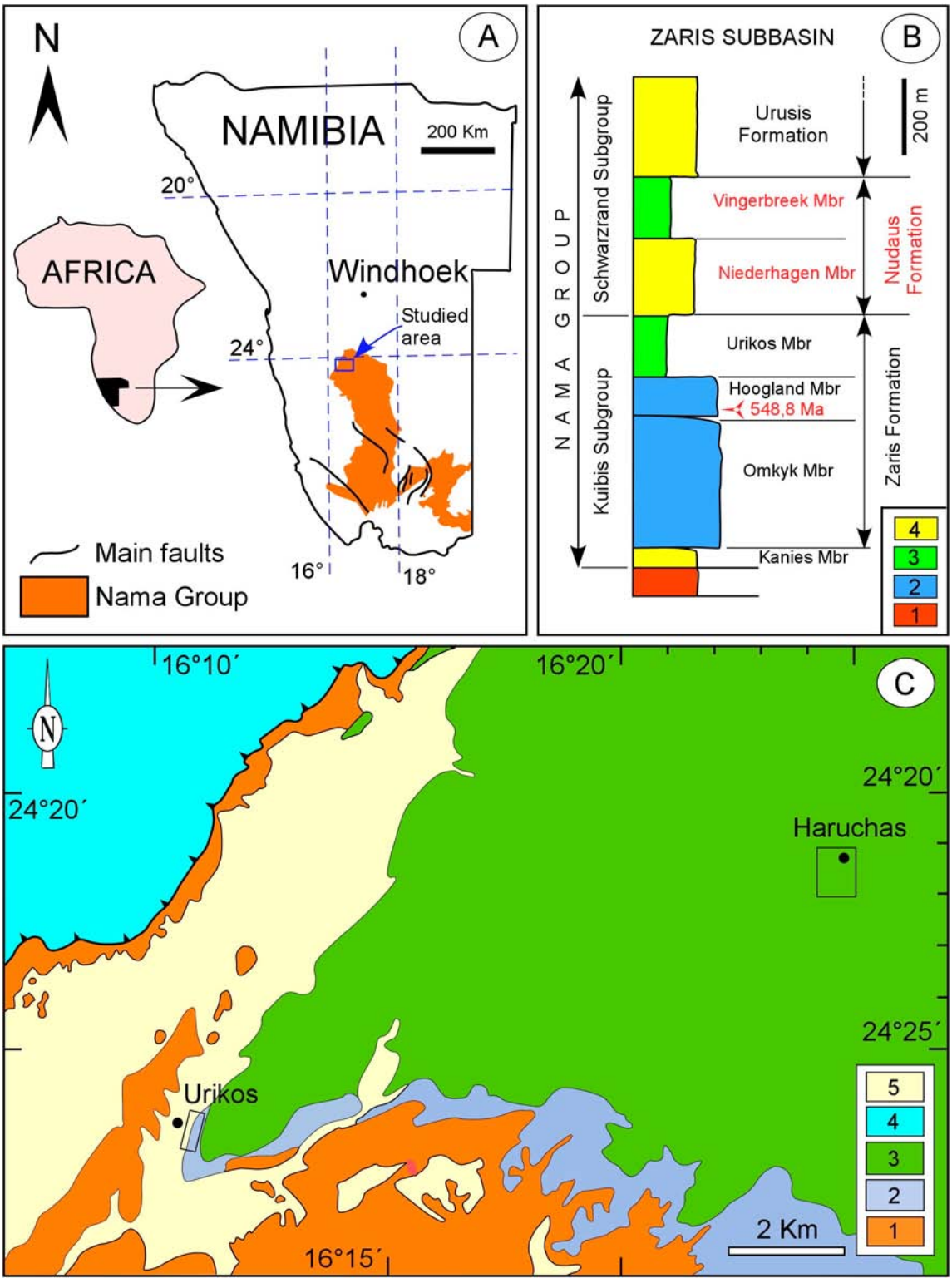


Figure 7(h)-1: Location and stratigraphy of the Nama Group study area.

(A) Distribution of Nama Group deposits in central and southern Namibia and location of study area (simplified from Geological Map of Namibia). (B) Generalised lithostratigraphic column of part of the Nama Group in the study area of the Zaris Sub-basin (age data from Grotzinger et al., 1995). 1 – Basement, 2–4 – Dominant lithologies in Kuibis and Schwarzrand Subgroup: 2 – limestone, 3 – mudstone, 4 – sandstone. (C) Simplified geological map of the study area showing the localities of Haruchas and Urikos (from Geological Survey of Namibia, 1980, 1/250000 Geological series, Sheet 2416 Mariental). 1 – Kuibis Subgroup; 2, 3 – Schwarzrand Subgroup: 2 – Niederhagen Member, 3 – Vingerbreek Member; 4 – Naukluft nappe complex; 5 – Quaternary deposits.

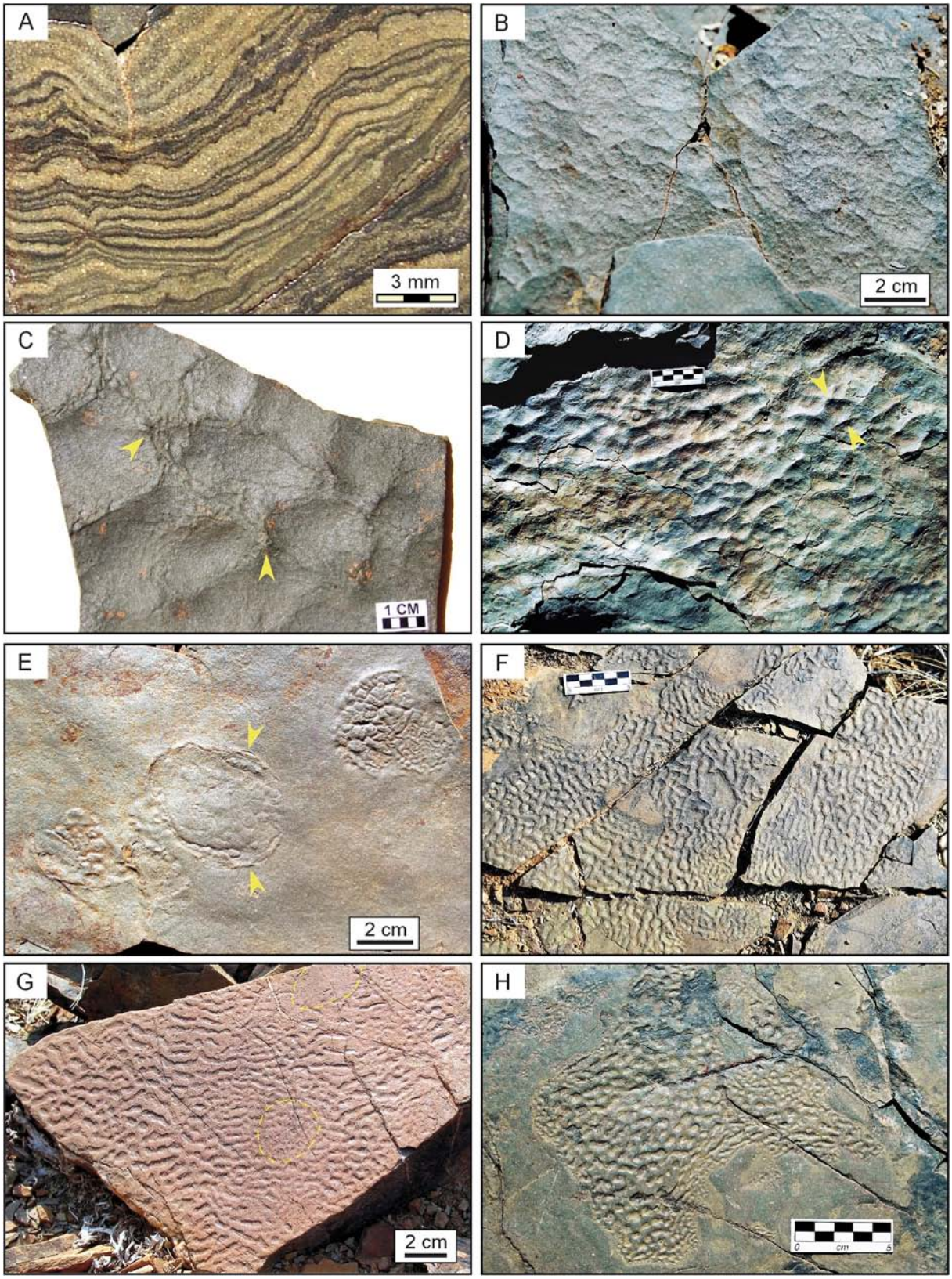


Figure 7(h)-2: Growth, surface and subsurface structures: biolaminites (A), mat-growth and mat surface structures (B–E), subsurface *Kinneyia* structures (F–H).

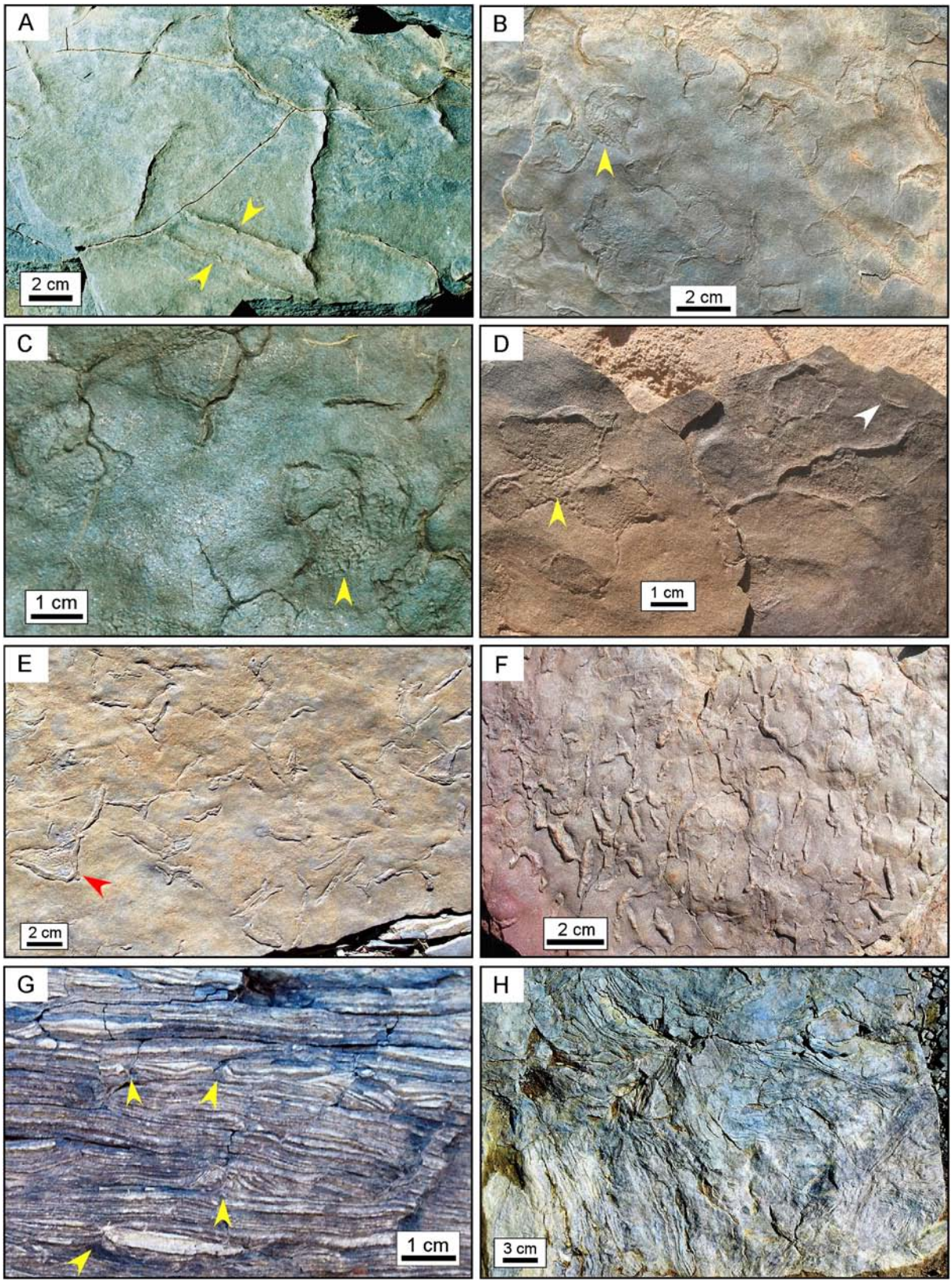
(A) Polished section of biolaminite showing millimetre-scale alternation of dark microbial mat layers and light silt/sand-sized quartz layers. Thickness and proportions of the layers are variable. The dark microbial mat layers consist of sericite and relics of carbonaceous material and include isolated silt-sized grains and abundant muscovite

flakes 'floating' in the sericitic groundmass. Such organic layers draping siltstone laminae may be reduced to a very thin veneer of a few μm in thickness. In the light layers, sediment grains frequently are surrounded by sericite, developing a 'coated grain fabric'. Locality: Vingerbreek Member, Farm Haruchas. Genesis: The millimetre-scale multilayered biolaminites result from the interplay of microbial mat growth and sediment deposition. The resulting bio-sedimentary lamination developed in a low-energy intertidal zone as indicated by associated sedimentary and other mat-related structures. Variations in thickness of microbial mat–siltstone doublets may have been controlled by tidal cycles, rate of sediment supply and frequency of high energy events. The process leading to biolaminites includes periods of non-deposition in which cyanobacteria produce and establish mat layers on a sediment surface, and periods of sedimentation in which the mat is covered by a thin layer of fine-grained sediment through which motile bacteria can move upwards to establish a new mat on top of this sediment (Gerdes et al., 2000a). Establishment of a new mat layer was usually achieved within several weeks of almost zero deposition, by motile bacterial taxa (e.g., *Microcoleus chthonoplasates, Lynbya aestuarii, Oscillatoria limosa*) or cell aggregates of them, which phototactically moved upwards from the buried mat and accumulated on the new surface (see Gerdes et al., 2000a; Gerdes and Klenke, 2003; also this volume: Chapter 2). (B) Upper bedding surface showing 'elephant skin' pattern consisting of narrow and sharp-crested ridges arranged in polygons with preferred orientation. In between the centimetre-scale sinuous ridges, a millimetre-scale reticulate pattern with polygonal network is developed. Locality: Vingerbreek Member, Farm Haruchas. (C) Close-up view of upper bedding surface showing 'reticulate pattern' of sharp-crested ridges in a centimetre-scale polygonal to almost hexagonal arrangement. A millimetre-scale reticulate structure is superposed on the large one, developed mainly along the higher parts of the troughs. Relics of tufts, up to 3 mm high (arrows), are preserved at junctional positions of the crests. The polygons are symmetric or elongate and are of varying diameter. Locality: Vingerbreek Member, Farm Haruchas. (D) Upper bedding surface exhibiting a network of discontinuous and sinuous sharp-crested ridges in a linear arrangement partly evolving into a polygonal pattern. The ridges follow continuously along the tops of the ripple crests but in a few cases may extend to the inter-crest zones. Length of crests may be up to 12 cm, whereas inter-crest distances are less than 4 cm. The crests may be symmetric or asymmetric in section (arrows). The sharp-crested 'rippled' surface is restricted to a 2 mm thick siltstone lens. Locality: Vingerbreek Member, Farm Haruchas. Scale is in cm. (E) Upper bedding surface with centimetre-scale subcircular structures. The structure in the centre preserves relics of a flattened sand margin (arrows) which corresponds to a curled crack margin related to desiccation of a thin microbial mat (see Figures 7(h)-3B to -3D). The structure in the upper right part of the photo displays a crinkly surface consisting of millimetre-scale round-crested to partly sharp-crested ridges separated by narrow troughs. Locality: Vingerbreek Member, Farm Haruchas. *Genesis of structures in Figures 7(h)-2B to -2E*: The structures in Figures 7(h)-2B, -2C are typical 'mat surface structures' resulting from reticulate growth patterns, called 'elephant-skin texture' in ancient deposits (Gehling, 1999). The structures associated with bedding surfaces of biolaminites illustrate the diversity in development and preservation of growth structures. Similar growth patterns have been described from modern tidal flats in southern Tunisia (e.g., Gerdes et al., 2000a) and attributed to vertical growth of cyanobacterial filaments (e.g., of *Microcoleus chthonoplastes*, *Lyngbya aestuarii*) forming tufts, pinnacles and ridges. The bedding surface characterised by sharp-crested linear to partly polygonal ridges (Figure 7(h)-3D) suggests a dominating linear growth pattern, which occasionally is also observed on the modern tidal flats of Southern Tunisia (see Figure 3(c)-3A). Linear growth patterns may be induced by a rippled sedimentary surface on which growth ridges preferably follow a ripple crest. Some linear growth patterns may present similarities with ridges resulting from slow downslope creeping of mat layers (G. Gerdes, personal comm., 2006). The structures seen in Figure 7(h)-2E are developed in subcircular openings of a mat with relics of a curled margin (see Figure 7(h)-3); they reflect surface or subsurface structures of a very thin mat which newly grew within the opening (see also Figure 7(h)-3B). (F) Upper bedding surface of 10 cm thick quartzite bed with well developed typical *Kinneyia* structure. The structure, occurring on a flat bedding surface, consists of irregular and sinuously curved crests, gently oversteepened and partly bifurcating. Crests are separated by subcircular to elongate curved inter-crest depressions and pits with an average diameter/width of 4–6 mm. Locality: Vingerbreek Member, Farm Haruchas (S 24°22′37.5″, E 016°22′42.4″). Scale in cm. (G) Upper bedding surface of 8 cm thick quartzite bed with typical *Kinneyia* structure. The structure consists of long winding and flat-topped crests with a preferred orientation, and intervening pits and troughs. The regularly distributed pits and depressions are elongate (1 to 3 cm in length) and sinuously to gently curved; a few are subrounded with a diameter of 3 mm. Note subcircular flat area (surrounded by yellow dashed line) without *Kinneyia*; around the flat area, crests and pits are fine-scaled and narrow, increasing in length and width outwards. Locality: Niederhagen Member, Farm Urikos (S 24°.26′.56″, E 016°.10′.56.6″). (H) Flat upper bedding surface of 15 cm thick quartzite bed with *Kinneyia* structure developed in an irregular patch with sharp margin. The margin of the patch is smooth and curved on the left side, but more irregular on the right side. The *Kinneyia* structure consists of crests and pits arranged mainly in a honeycomb-like pattern in the central part of the patch. Along the margin, pits and crests are much reduced in size. This is visible particularly along the left side of the patch; the crests and pits are fine-scaled and very narrow and seem aligned parallel to the margin. Locality: Vingerbreek

Member, Farm Haruchas (S 24°.21′.46.5″, E 016°.24′.21.5″). Scale in cm. *Genesis of structures in Figures 7(h)-2F to -2H*: These examples illustrating '*Kinneyia* structures' show a diversity in shape and size, varying from simple, long, flat-topped crests covering large areas of a bedding surface to honeycomb-like arrangements of flat-topped crests and intervening elongate to round pits partly occurring as patches. Common features include the occurrence on flat bedding surfaces of sandstone layers and the occasional preservation of fine-grained sericitic material in the depressions. '*Kinneyia* structures' commonly occur on upper surfaces of sandy event beds, below fine-grained sericitic layers which may represent former microbial mat layers previously growing on the new sediment surface. *Kinneyia* structures are considered here as a category of 'subsurface structures' developed on flat sandy surfaces underneath mats (see Chapter 6(a)).

Figure 7(h)-3: Mat destruction features: tepee-like shrinkage cracks in thin mat layers (A), curled shrinkage crack margins in thin mat layers (B–D), microbial shrinkage/sand cracks (E, F), upturned crack margins in biolaminites (G), polygonal pattern of upturned crack margins in biolaminites (H).

(A) Upper bedding surface of a biolaminite showing tepee-like structures. The structures are developed in a 2 mm thick layer and consist of isolated to bifurcating, straight to sinuous, upturned crack margins with inverted V-shaped cross-section, 2–3 mm high, and with tapering ends. In a few cases, the margins are gently overthrust and are organised as opposite/symmetric cracks (arrows). (B) Upper bedding surface of biolaminite showing narrow shrinkage cracks. The cracks are preserved either as imprints or narrow ridges on adjoining upper and lower surfaces of thin siltstone laminae within the biolaminites. The surface preserves isolated lenticular and curved cracks, subcircular cracks (upper right part of photo) and subrounded cracks with sinuous and irregular margins. Within one of the crack openings, millimetre-scale round-crested bulges forming a nodular structure (arrow) are preserved. (C) Close-up view of upper bedding surface in biolaminites showing imprints of simple isolated microbial shrinkage cracks and crack openings with subcircular to elongate irregular margins. Some of the crack openings preserve a millimetre-scale honeycomb-like reticulate pattern (arrow). (D) Upper bedding surface with incomplete network of microbial shrinkage cracks, partly arranged in a subcircular to elongate pattern. Green arrow indicates millimetre-scale round-crested bulges forming nodular structures in subcircular crack openings, similar to that of Figure 7(h)-3B. Note local development of isolated lenticular cracks (blue arrow). (E) Upper bedding surface of 3 cm thick fine-grained sandstone bed with microbial shrinkage cracks occurring as a single generation. The cracks form flattened ridges, randomly oriented and with lenticular, spindle or tri-radiate shape. They occur as isolated, straight to gently curved ridges, tapering at the ends. Locally the ridges are located along three opposite margins surrounding an opening in which a millimetre-scale reticulate pattern is preserved (arrow). (F) Upper bedding surface of 3 cm thick fine-grained quartzite layer with microbial shrinkage cracks preserved mainly as lenticular and partly as tri-radiate sandstone ridges. The cracks, tapering at the ends, merge together at high angles without cross-cutting relationships, and with a preferred orientation. (G) Section across a package of biolaminites showing 'upturned margin' structures (indicated by arrows). The cracks cut through multilayered biolaminite sections of variable thickness and their upturned margins form a symmetric inverted V-shaped structure. The structures are limited to thin packages of layers, usually less than 1 cm, which are upturned at an angle of 60–90°. (H) Upper bedding surface of biolaminite preserving a polygonal network of subvertically upturned shrinkage crack margins. The upturned margins, 1–2 cm thick, form polygons of variable size and appear as sharp-crested folds or isolated belts of upturned lamination. *Genesis of structures in Figure 7(h)-3*: The shrinkage features presented in A to F illustrate the diversity in geometry and shape of structures related to subaerial desiccation of thin microbial mat layers. Similar structures occur in modern microbial mats that undergo shrinkage and cracking during subaerial exposure in the intertidal/lower supratidal zones of the southern Tunisian tidal flats (see Figure 4(c)-5D). The examples illustrate different stages of crack margin evolution and crack preservation. Tepee-like structures (Figure 7(h)-3A) develop in single and thin mat layers when crack margins are upturned without being completely detached from the sediment below, and without being involuted ('curled'). Such structures may be considered as the incipient stage within the evolution of shrinkage cracks in thin mat layers. When the crack margins evolve during progressive shrinkage, they may develop irregular to subcircular involute ridges surrounding the crack openings (Figures 7(h)-3B to -3D). Similarly, lenticular cracks may reflect an early stage of shrinkage without yet evolving to curled structures (Figures 7(h)-3C, -3D). The millimetre-scale bulges and reticulate patterns developed partly in the crack openings may reflect growth features of a new mat that grew on the exposed sediment surfaces. Preservation of such structures was favoured either by subsequent deposition of thin siltstone laminae or overgrowth of new mat layers. Cracks developed in thin microbial mat layers may be preserved as sand ridges by simple infillings of cracks by sand/silt sediment during subsequent tidal floods (Figures 7(h)-3E, -3F; see also Section 7(f)). Abundance of short lenticular and tri-radiate cracks indicates an incipient stage of shrinkage. Figure 7(h)-3F preserves also structures indicating



curled margins (arrow) with millimetre-scale reticulate growth structure developed in the opening, similar to that of Figure 7(h)-3C. In contrast, subaerial desiccation of biolaminites and development of large and deep cracks involving thick 'multilayered' organo-sedimentary layers (biolaminites) produce structures of sub-vertically thin to thick upturned margins, which can form a wide polygonal network on bedding surfaces (Figures 7(h)-3G, -3H; see also Figure 4(c)-6). All shrinkage features illustrated here are developed during growth and accretion of biolaminite facies and record subaerial desiccation restricted to single microbial mat layers or encompassing thick biolaminite layers.

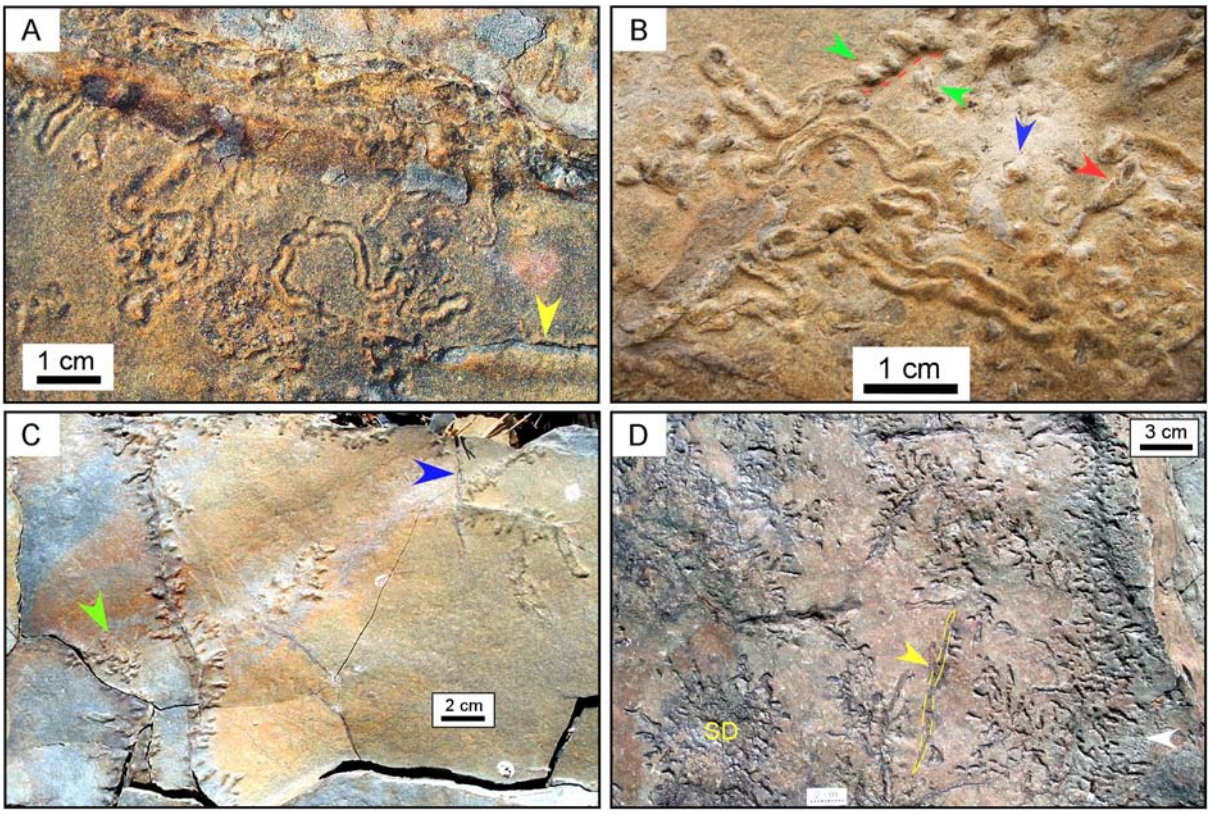


Figure 7(h)-4: Trace fossils/mat miners.

(A) Upper flat bedding surface of a 3 mm thick siltstone layer with straight to slightly irregular short tunnels, a few millimetres to less than 2 cm long, and simple meandering tunnels, ca. 6 cm long. Each trace fossil structure consists of an unbranched horizontal trail with a median groove flanked on both sides by ridges which usually have a curved termination at one end of the trace. Width of traces is uniform and ca. 2 mm. Arrow indicates associated spindle-shaped shrinkage crack. (B) Close-up view of upper bedding surface of a 4 mm thick siltstone layer with unbranched, sinuous to irregularly meandering and curved traces with a median furrow. The traces are 3 mm wide, 1–6 cm long, and flanked on both sides by round-crested ridges which usually join at one end of the trace. Some grooves preserve concentric curved lines (red arrow). Rarely, a median furrow (dashed line) is perpendicularly flanked on both sides by straight and elongate ridges (green arrows), 1–3 mm in length and about 1 mm wide. The ridges occur in positive relief and form spaced lateral bodies along the margin of a furrow or form isolated subrounded elements (blue arrow). (C) Upper bedding surface of millimetre-thick siltstone layer exhibiting straight to sinuous lines, from which straight to slightly curved irregular segments extend perpendicularly on both sides. The segments are 0.5 to 2 cm long and 1–2 mm wide, and are preserved in positive epirelief. Occasionally the segments form small isolated and irregular patches (green arrow). Blue arrow indicates associated lenticular shrinkage crack. (D) Upper bedding surface of a millimetre-thick siltstone layer with a high density of trace fossils in negative epirelief, consisting of up to 20 cm long, slightly curved furrows, from which straight to irregular troughs, 0.5–2 cm long, extend perpendicularly on both sides. In some cases, the central furrows contain imprints or relics of sand-fillings of lenticular shrinkage cracks (yellow arrow). Occasionally, short troughs radiate from subcircular depressions (SD) or occur in irregular patches or as isolated features (white arrow). *Locality*: All photos from Vingerbreek member, Haruchas area. *Interpretation*: The trace fossils illustrated here form two distinct types (A–B and C–D) of bedding-parallel, horizontally oriented forms which may occur together on the same surfaces. The first type (A–B) is similar to traces which have been described from another section of the Vingerbreek member and referred to as *nereites and chondrites* by Crimes and Germs (1982). These trace fossils, also assigned to *Archaeonassa sp.* (Jensen, 2003; Jensen and Runnegar, 2005), are believed to reflect movement over a sandy surface at the sediment–water or sediment–air interface. The trace is also similar to that made by gastropods or mollusk-like bilateral producers, left on wet sediment surfaces, by displacing sediment along the sides from the front into a terminal backfill (Jensen et al., 2005; Seilacher et al., 2005). The second type of trace fossils (C–D) are virtually identical to tunnel patterns of 'undermat miners', as documented by Seilacher (1999) from the Upper Cambrian of Oman. Seilacher (1999) noted the similarity of the traces to tunnel systems produced by bark beetles below modern mats which have become updomed. The position of the tunnels along shrinkage cracks seems to indicate that the miners use small crack openings in the mat surface to move underneath the mat. The cracks, moreover are sites of

increased moisture and microbial activity. The trace fossils illustrated here have common features with the majority of trace fossils reported from Ediacaran strata (Hagadorn and Bottjer, 1999; Jensen et al., 2000, 2005; Seilacher et al., 2005): (i) they generally form simple and unbranched grazing trails; (ii) are essentially 'bed-parallel forms' indicating horizontally oriented behavioural activities, and (iii) are constructed close to the sediment surface or at the sediment–water interface. The two types of trace fossils are consistently bed-parallel forms, suggesting that the burrowing organisms were restricted to the uppermost, well oxygenated and microbially colonised sediment surface. This is also consistent with their association with microbial shrinkage cracks, developed in thin veneers of microbial mats. Also, preservation of such subtle structures would have been favoured by biostabilising microbes or covering microbial mats.

---

this scenario, the basal, HCS-bearing sandstone bed is considered to reflect a storm barrier or sand-shoal in a nearshore setting. Landwards, behind the barrier, low hydrodynamic energy combined with a low rate of sediment supply would have been expected, thus creating favourable conditions for microbial mat growth and biosedimentary accretion of biolaminites. Indeed, development of microbial mats is indicated by strong bioturbation by undermat miners (Figure 7(h)-4) just a few decimetres above the storm bar (cf. Aigner and Reineck, 1982). Microbial growth was occasionally interrupted by storms or high-energy tidal events resulting in the deposition of thicker sandy layers. One of them is extensively covered by *Kinneyia*-type wrinkle structures (Figure 7(h)-2H). Still further landwards, the peritidal deposits graded into fluvial sandy deposits, due to seaward progradation of a fluvial system onto the peritidal area.

Further structures of *Kinneyia*-type wrinkles are reported from the Niederhagen Member near Urikos homestead (Figure 7(h)-2G) and from the middle part of the Vingerbreek Member at Haruchas (Figure 7(h)-2F). In both cases, the structures occur at the tops of thickening- and shallowing-upward cycles, reflecting fluvial/storm influenced delta front-peritidal coastal/delta plain evolutions. As indicated by the thickness of the corresponding deposits, the coastal/delta plain settings formed only short time intervals within prograding cycles. The *Kinneyia* structures are developed on centimetre- to decimetre-thick sandstone layers of an intertidal 'coastal/delta plain' setting, in which high-energy event sand layers are capped by low-energy laminated siltstone/mudstone. Only a few, centimetre-thick sandstone layers of the coastal/delta plain deposits preserve lenticular and tri-radiate shrinkage cracks similar to those of Figure 7(h)-3E. The rarity of mat-related structures in such settings seems to be controlled by sedimentary dynamics. Within the cycles, short-time developments of peritidal coastal/delta plain environments appear to be related to rapid drowning and resulting increase in accommodation space, which inhibited widespread growth of microbial mats and accretion of thick biolaminites.



Figure 7(i)-1: Location of Dakota Sandstone outcrop pictured in Figure 7(i)-2.
The outcrop is located on the east side of the Dakota hogback along West Alameda Parkway (yellow arrow). It is easily reached by heading south from interstate I-70. The outcrop coordinates are 39°40′48″ N and 105°11′32″ W. Airphoto courtesy of the USGS.

7(i). RIPPLE PATCHES IN THE CRETACEOUS DAKOTA SANDSTONE NEAR DENVER, COLORADO, A CLASSICAL LOCALITY FOR MICROBIALLY BOUND TIDAL SAND FLATS

J. Schieber

The Dakota Sandstone marks the Early Cretaceous transgression onto the North American craton in Colorado, and forms prominent N–S trending hogback ridges just west of Denver, Colorado. Deposition in a tidal setting is inferred from the presence of dinosaur tracks, root casts and branches of mangroves, channels filled with muddy sediments and mud clasts, and ripples modified by flowing water during emergence (McKenzie, 1972).

McKenzie (1972) noticed unusual rippled patches on otherwise non-rippled bedding planes of the Dakota Sandstone (Figure 7(i)-1), and tentatively interpreted them as due to microbial mat stabilisation of the surface. He felt, however, that the energy regime in a tidal flat setting would not allow partial erosion of mat-bound surfaces. H.-E. Reineck was able to match the morphology of these ripple patches closely to modern examples from intertidal sandflats of the island of Mellum in the North Sea, firmly establishing the microbial mat-related origin of these rippled patches in the Dakota Sandstone (Reineck, 1979). Since then the microbial mats of Mellum have figured prominently in many other studies of microbial mats on sandy substrates (e.g., Gerdes and Krumbein, 1987; Noffke and Krumbein, 1999; Draganits and Noffke, 2004).

Colonisation by microbial mats renders sandy surfaces substantially more resistant to erosion (Neumann et al., 1970; Yallop et al., 1994; Paterson, 1997), but erosion and reworking will commence once currents are sufficiently

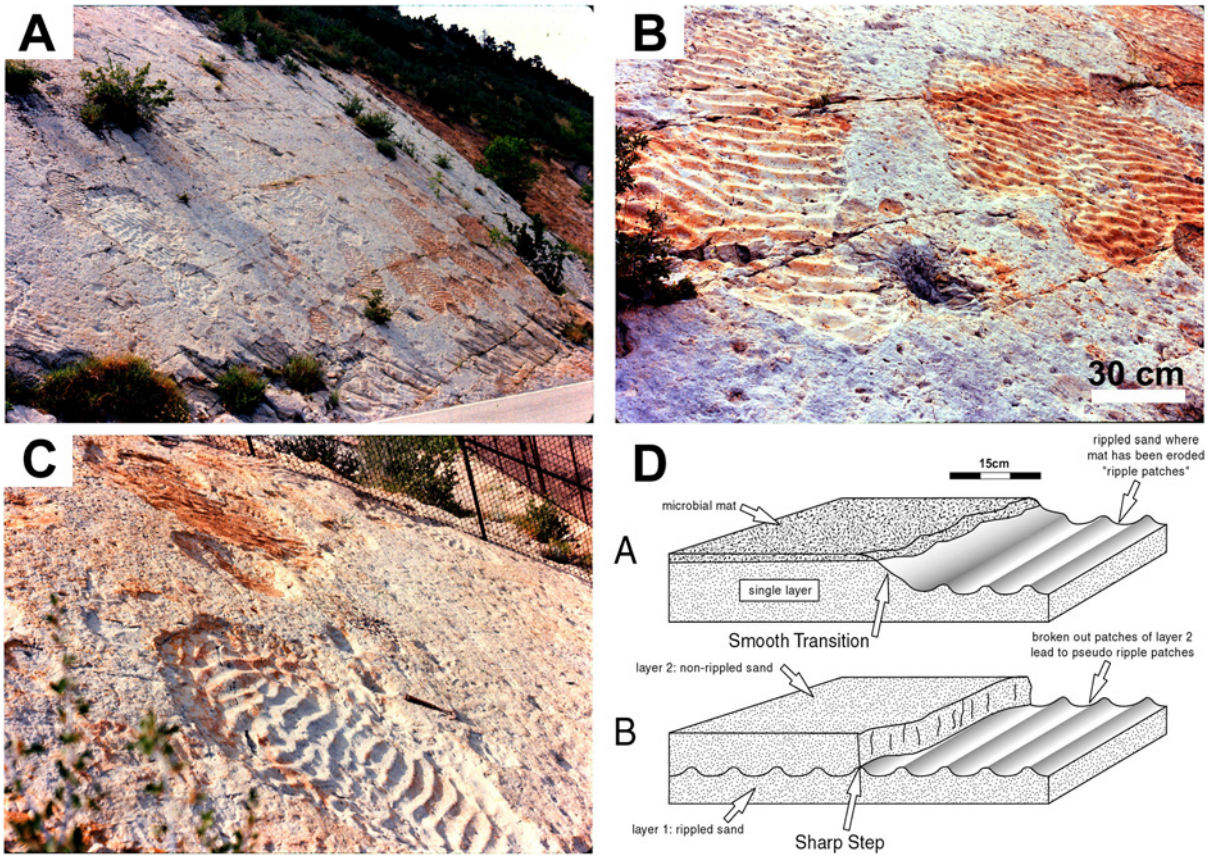


Figure 7(i)-2: Upper third of the Dakota Sandstone west of Denver, showing ripple patches.
(A) Road cut in the Dakota Sandstone along West Alameda Parkway, Denver, Colorado, USA. Sandstone beds dip steeply to the right and ripple patches are clearly visible. On the right side of the image ripple patches are accentuated by reddish brown colouration (probably a result of pre-roadcut outcrop weathering). Ripple patches measure from some decimetres to as much as two metres across. (B) Close-up of ripple patches from A. Note symmetrical nature of ripples, straight ripple crests, and tuning-fork splits of ripple crests. Collectively these features indicate a wave action origin (Reineck and Singh, 1980). Spacing of ripple crests is approximately ten centimetres. (C) Oblique close-up of another ripple patch from A. Shows smooth transition between ripples in the erosive 'pocket' and the surrounding non-rippled surface. This smooth transition has also been documented from modern counterparts (Reineck, 1979). Hammer (32 cm long) for scale. (D) Sketch that illustrates the morphological difference between erosive ripple patches and rippled layers that are seen because pieces of an overlying layer broke out during weathering and erosion. The smooth transition between the purported mat surface and the rippled sand surface in the erosive patch indicates that the rippled surface formed later than the presumably mat-bound flat surface. A sharp break between non-rippled surface and ripple patch strongly suggests that the lower rippled layer is older than the non-rippled surface. From Schieber (1999); reproduced with permission of SEPM (Society for Sedimentary Geology).

strong. In Phanerozoic mats, like those of the Dakota Sandstone, erosion will typically start at those places where the mat has previously been weakened, for example by grazing or by burrow perforations. The bound nature of the sand surface leads upon erosion to sedimentary features that are distinctively different from what would be expected from erosion of a non-cohesive substrate. On modern tidal sand flats, local erosion of the mat-bound surface exposes underlying sand to wave and current action and leads to rippled patches in an otherwise smooth surface (Reineck, 1979; Gerdes et al., 1985b). More extensive erosion can also lead to erosional remnants (equivalent to a mesa or inselberg) of a mat-bound surface that are surrounded by rippled sand (Gerdes and Krumbein, 1987).

Figure 7(i)-2 shows examples of ripple patches from the Dakota Sandstone that are probably among the closest match to mat-erosive ripple patches in modern settings, such as at Mellum. Figures 7(i)-2A, -2B and -2C show variously magnified views of what is interpreted as erosive ripple patches on a microbially bound sand surface. The way in which the rippled surfaces and their ripple crests blend into the edges of the smooth surface surrounding the ripple patches (Figures 7(i)-2B, -2C) is a good indication that the rippled erosive 'pockets' formed after the

flat non-rippled surface (Reineck, 1979). From a distance (Figure 7(i)-2A) the outcrop first gives the appearance that the rippled surfaces may belong to a lower-lying bedding plane and have been revealed because pieces of the upper layer weathered out. Such a mode of origin, however, would give rise to sharp steps between upper and lower layers (Figure 7(i)-2D). Thus, the smooth transition between ripple patches and the surrounding surface is a key observation that indicates that the ripple patches were eroded into an originally mat-bound surface.

7(j). BENTHIC MICROBIAL MATS AS AN OIL SHALE COMPONENT: GREEN RIVER FORMATION (EOCENE) OF WYOMING AND UTAH

J. Schieber

The lacustrine Green River Formation (Eocene) of Wyoming, Utah, and Colorado (Figure 7(j)-1) is best known for its fish fossils and its oil shales (Bradley, 1964; Surdam and Stanley, 1979; Roehler, 1990; Russel, 1990; Ferber and Wells, 1995). It contains extensive horizons of carbonaceous shale (Figure 7(j)-2) with high contents of organic matter and kerogen, and is considered one of the largest oil shale deposits of the world (Tuttle, 1991). In most publications the organic matter is presumed to have originated from planktonic organisms (Bradley, 1964), yet the possibility of benthic microbial mats has been considered (Smoot, 1983; Schieber, 1999). The lakes in which the Green River Formation accumulated were, at times quite shallow (Surdam and Wolfbauer, 1975; Bohacs et al., 2000) and it is therefore conceivable that at certain periods portions of the lake bottoms were colonised by photosynthetic or non-photosynthetic microbial mats.

Smoot (1983) considered the possibility of a microbial mat origin for the Green River oil shales, based on the observation of eroded and transported oil shale intraclasts and the lack of soft sediment deformation (loading) beneath silt ripples overlying oil shale beds. The latter observation suggested that the organic-rich layers that were to become future oil shale beds were cohesive at the time of deposition. This is a behaviour one would more readily associate with a microbial mat than with a simple organic bottom 'muck'. Though these observations are most intriguing, Smoot (1983) mentioned this issue only in passing and did not provide any illustration of the observed features.

The following considerations are based on personal observations from field work and thin section study of Green River Formation shales from the various sub-basins in which it accumulated (Figure 7(j)-1). Surveying these oil shales on the hand specimen scale it is clear that not all organic-rich beds were created equal (Figure 7(j)-3). Some oil shale beds are finely laminated with wavy, continuous laminae (Figures 7(j)-3A and -3D), whereas others show a more discontinuous lamina style (Figure 7(j)-3C), and yet others are homogeneous and lack lamination altogether (Figure 7(j)-3E). Whereas the finely laminated type (Figures 7(j)-3A and -3D) can persuade one to consider a microbial mat origin, such a case is more difficult to make for the discontinuous lamina style (Figure 7(j)-3C), and quite implausible for the homogeneous type (Figure 7(j)-3E). The wavy lamina style of laminated oil shale beds (Figures 7(j)-3A and -3D), however, is a weak argument for a microbial mat origin because it could be an artifact of compaction around lenses of detrital or diagenetic dolomite (Schieber, 1999).

Further insights into the origin of the laminated oil shale beds come from shale beds with abundant streaks of carbonaceous material that measure from a few millimetres to several centimetres in size (Figure 7(j)-3B) and appear to be fragments of laminated oil shale as seen in Figures 7(j)-3A and -3D. These fragments were transported as discrete particles and show soft deformation and even over-folding. Such features suggest that these fragments had internal cohesiveness, an unlikely behaviour for settled organic-rich bottom muds, but one that is consistent with a mat-bound surface sediment. In keeping with interpretations of cohesive organic-rich fragments in other mudstone units (Chapter 5), it is therefore assumed that the carbonaceous streaks in Figure 7(j)-3B represent eroded and transported mat fragments. By extension, this also implies a microbial mat interpretation for laminated oil shales as seen in Figures 7(j)-3A and -3D.

Examining oil shale samples under the petrographic microscope also indicates multiple modes of origin. At this magnification level, samples from laminated oil shales show continuous wavy laminae of organic material (Figures 7(j)-4A to -4C) that are a few microns to tens of microns in thickness. This is a feature that is consistent with microbial mats, a conclusion that receives further support from the observation of transported fragments that indicate internal cohesiveness (Figure 7(j)-4E).

In contrast, the oil shale samples pictured in Figures 7(j)-4D, -4F, and -4G lack continuous laminae and contain discrete organic particles that are dispersed in a clay and dolomite matrix. These are from oil shale beds with homogeneous appearance (Figure 7(j)-3E) and the organic particles are most readily interpreted as phytoplankton remains that settled to the bottom. In the case of Figures 7(j)-4F and -4G there is considerable resemblance to shales elsewhere in the rock record that contain abundant compressed remains of spores, pollen, and algal cysts (cf. Taylor et al., 1998).

The laminated organic intervals in Figures 7(j)-4A, -4B, and -4C are at first glance very similar to what has been described as 'lamalginites' from other lacustrine oil shales (Taylor et al., 1998), yet the organic laminae in the Green

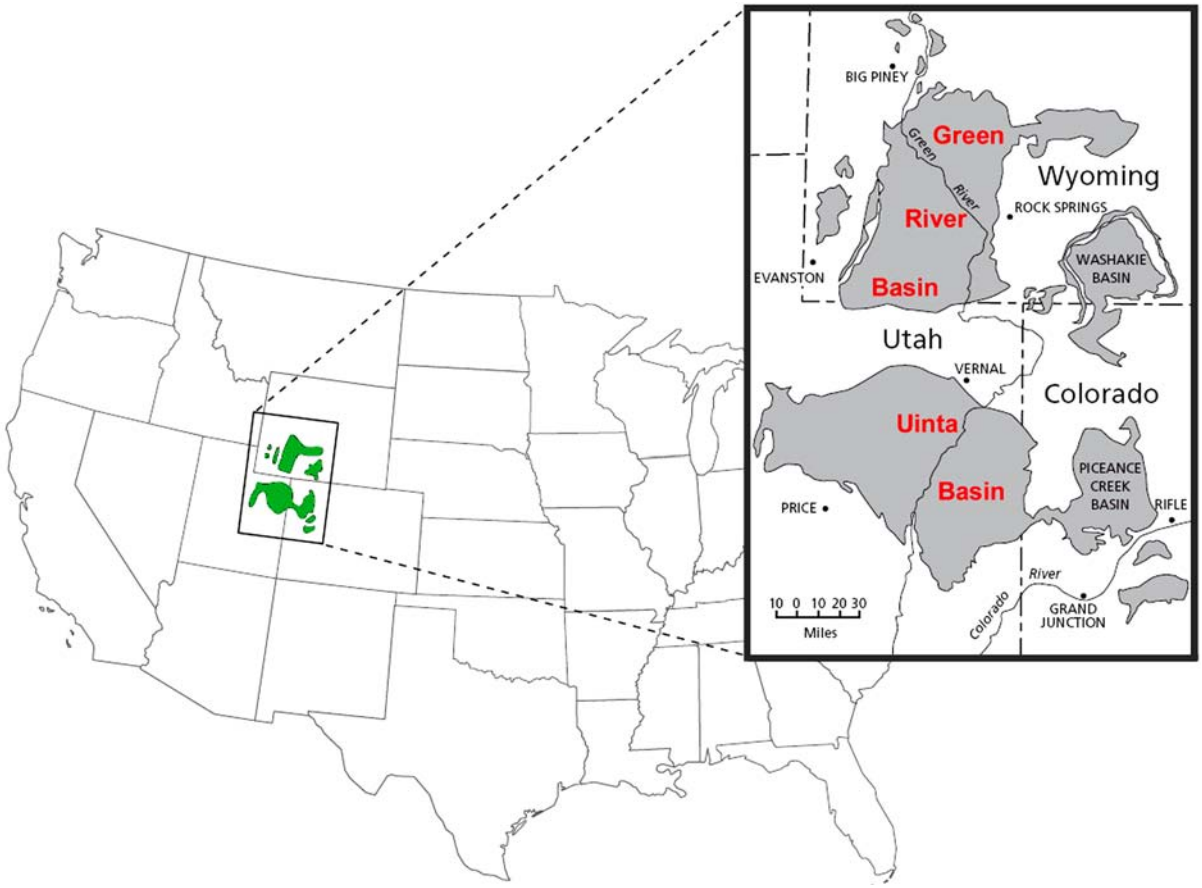


Figure 7(j)-1: Location map, Green River Formation.
Location of the Green River Formation in North America. Inset shows location of individual depocentres. Wilkins Peak oil shales shown in this contribution come from the Green River Basin of Wyoming, and samples of Parachute Creek oil shale come from the Uinta Basin of Utah. Figure adapted from Smith (1980).

River examples show considerably more lateral persistence than the laminae of 'normal' lamalginites, a property that one would expect in case of a continuous microbial cover of the sediment surface. It is hard to imagine how accumulation of land- or plankton-derived organic particles could have produced such a structure. The presence of detrital lenses and particles within these laminated organic intervals furthermore indicates a benthic origin, rather than deposition from mid-water mats (Dickman and Artuz, 1978; Dickman, 1985). In conjunction with the cohesive behaviour demonstrated by eroded and transported fragments of this laminated material, and bearing in mind the frayed edges of these fragments that imply strength in the lamina plane (Chapter 5), it is plausible to interpret finely laminated oil shale intervals as the deposits of benthic microbial mats.

Comparable organic-rich beds with wavy laminae have been reported from other lacustrine successions and were likewise interpreted as the result of benthic microbial mats (Hutton et al., 1980; Gibling et al., 1985a, 1985b; Goth, 1990; Wuttke and Radtke, 1993; Goth and Schiller, 1994). Oschmann (2000) described texturally very similar layers from the Kimmeridge Clay, a marine black shale of Jurassic age. Yet, although microbial mats are clearly capable of producing organic-rich shale beds in lacustrine and marine successions, the above observations show that the assessment can not be made uncritically. In the Green River Formation at least, there seem to be fundamentally two pathways that lead to formation of oil shale beds: (1) accumulation of abundant planktonic organic matter in the bottom sediments, or (2) buildup of organic matter through the growth of benthic microbial mats. The former process led to formation of homogeneous oil shale beds, and the latter resulted in finely laminated oil shales. In both cases very low net sedimentation rates were an additional prerequisite. The photos in Figure 7(j)-4 also show that laminated oil shales generally have higher concentrations of organic matter than the homogeneous type, possibly a suggestion that autotrophic rather then heterotrophic bacteria were involved in mat formation (heterotrophic bacteria would have reduced the amount of organic carbon).

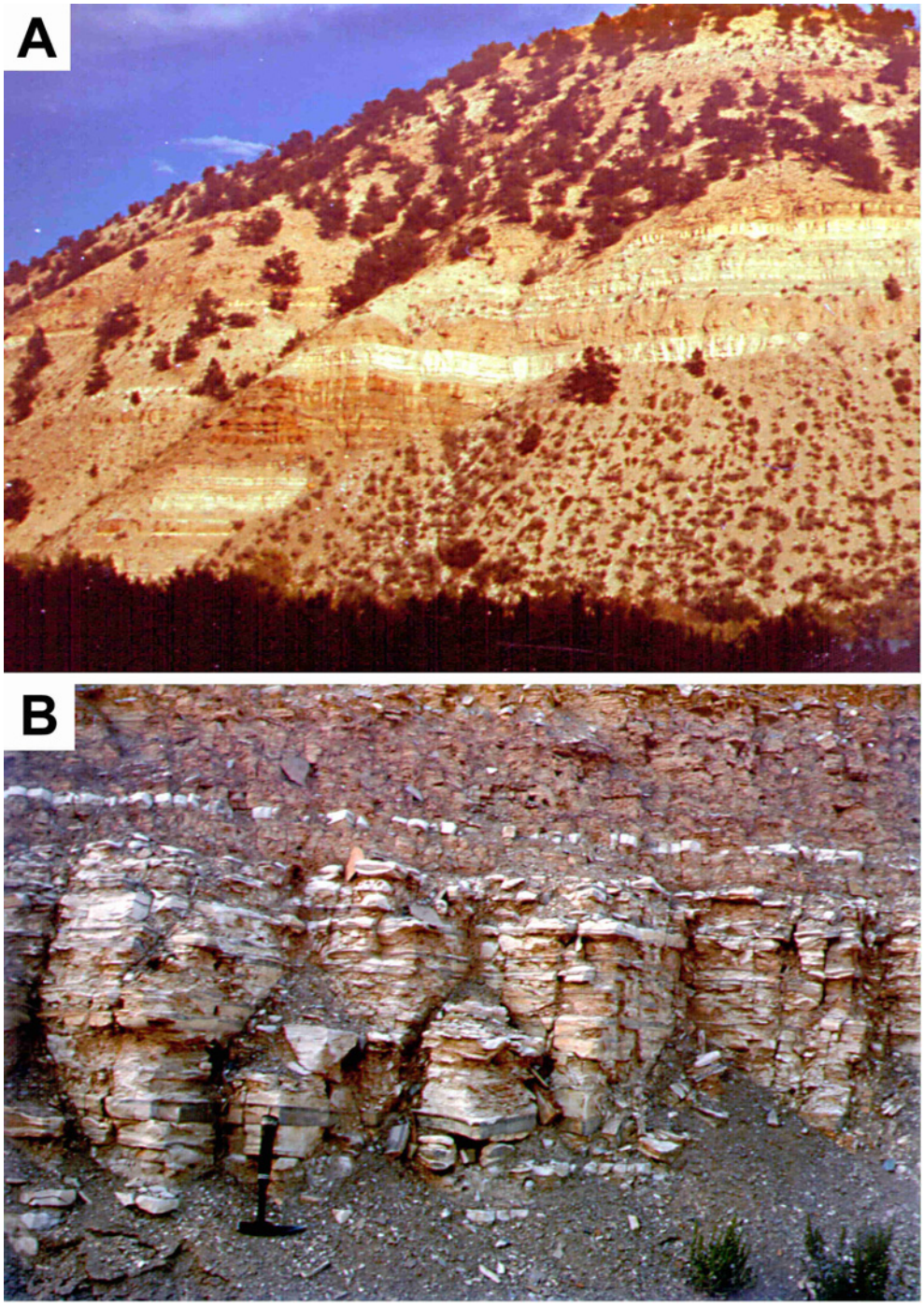


Figure 7(j)-2: Outcrop views of Green River Formation oil shales.
(A) A slope exposure of the Parachute Creek Member of the Green River Formation, south of Duchesne, Utah, along US Highway 191. It shows cyclic deposition of strata. Whitish-pale coloured intervals are rich in oil shale beds. Although fresh oil shale samples look dark brown to black because of an abundance of organic matter and kerogen, outcrop oxidation of organic matter leaves behind the light coloured mineral matrix and gives the rocks a very different appearance. (B) Outcrop photo of one of the whitish-pale oil shale intervals from A. The lightest, almost white, ledge-forming beds are most strongly enriched in organic matter. These beds show wavy internal laminae that may have formed as benthic microbial mats. If a sample is cracked with a hammer, it is seen that the rock turns dark brown to black just a few millimetres below the weathering surface. Its resistance to weathering (ledge-former) is due to its 'water-proofed' (by kerogen) nature. Hammer for scale is 32 cm long.

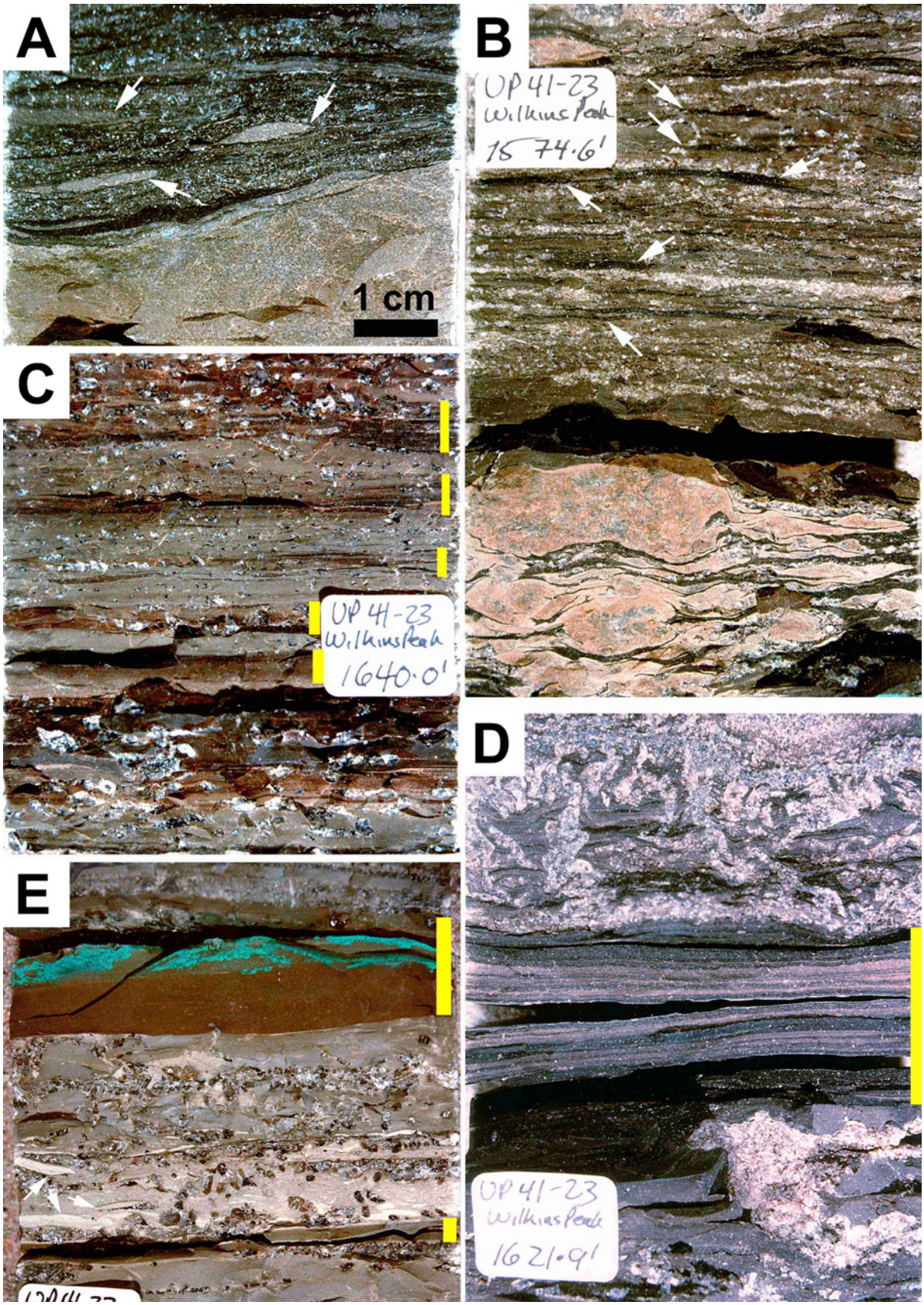

A
1 cm
B
UP 41-23
Wilkins Peak
1574.6'
C
UP 41-23
Wilkins Peak
1640.0'
D
UP 41-23
Wilkins Peak
1621.9'
E

Figure 7(j)-3: Views of diamond drill core from the Wilkins Peak Member of the Green River Formation (core diameter 55 mm) (scale bar in A applies to all other core pictures in this figure).
(A) Wavy laminated carbonaceous oil shale (dark laminae) in upper half of image, above a dolomite bed below. Small crystals of dolomite and other diagenetic minerals are sprinkled through the carbonaceous laminae. Small lenses of dolomite between carbonaceous laminae (arrows) accentuate wavy appearance, but carbonaceous laminae are also wavy-crinkly at a much smaller wave length. These are potential microbial mat layers. (B) The upper two thirds of the photo show grey mudstone with dark streaks (arrows) that are aligned parallel to bedding. The latter are of the same material that forms the dark laminae in A. The whitish grains are lacustrine evaporite minerals, such as trona, shortite, northrupite, etc. Because 'normal' organic-rich bottom muds do not have much internal cohesion, they would be dispersed by erosion and mixed with detrital components before re-deposition. In contrast, the streaks suggest that they were transported as individual particles. Thus, the interpretation here is that these streaks represent eroded and transported mat fragments. The lower third of the photo shows an oil shale layer with abundant growth of early diagenetic trona (light coloured) that destroyed the original fabric. (C) This photo shows an oil shale interval with abundant grey mud interbeds, particularly in the upper half. The alternation of grey shale beds with intervals that contain brownish (kerogen-rich) laminae (marked with yellow bars), bears some resemblance to Proterozoic striped shales. The whitish and clear (dark) grains are lacustrine evaporite minerals. (D) Oil shale interval with abundant intergrowth of lacustrine evaporites (trona, light-pinkish colour). The early diagenetic growth of these minerals completely disrupts the original oil shale fabric. The layer in the middle was not affected and shows wavy carbonaceous laminae (dark) that alternate with wavy-lenticular dolomite laminae. This is potentially a microbially laminated interval. (E) An oil shale with two kerogen-rich intervals (marked with yellow bars) interbedded with grey shale. As in previous images, the latter contain scattered lacustrine evaporite minerals that grew during early diagenesis. The oil shale beds are rather homogeneous and do not show a wavy-crinkly internal lamination. The sediment interval between the two marked oil shale beds appears graded. It has dolomite rip-up clasts (white arrows) and dolomitic sand (lighter colour) in the base, and the clay content increases upwards (as it gets darker). This could be interpreted as an event deposit related to flash floods that entered the lake basin. All photos: Dr. Kevin Bohacs (Exxon Research Laboratory).

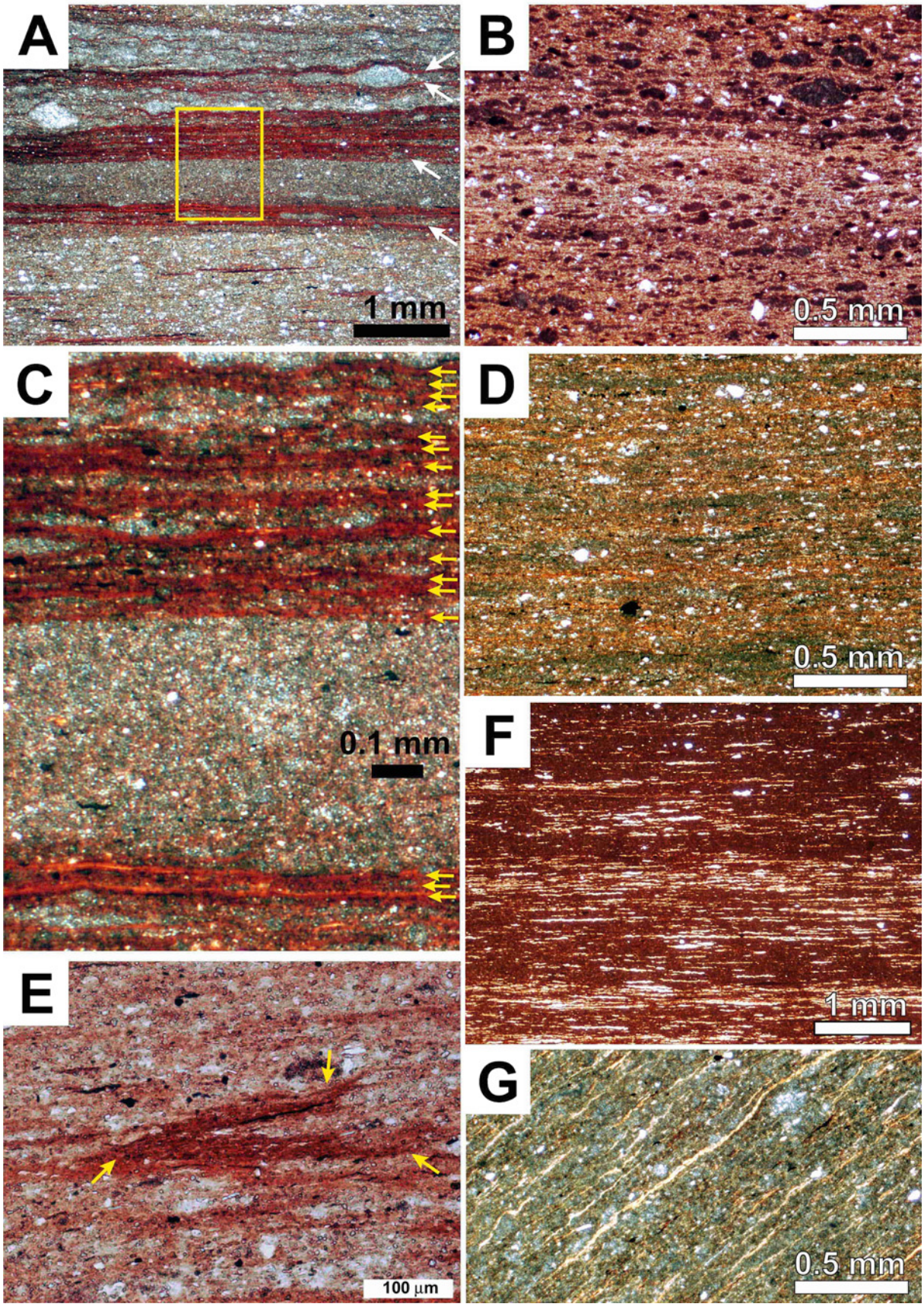

A
1 mm
B
0.5 mm
C
0.1 mm
D
0.5 mm
F
1 mm
E
100 µm
G
0.5 mm

Figure 7(j)-4: Photomicrographs of various Green River oil shale samples.
(A) Dolomitic oil shale (Wilkins Peak Member) with well defined kerogen-rich (brownish) intervals (arrows). Kerogen-rich intervals consist of brownish laminae that are continuous on the thin section scale. The kerogen-rich intervals in turn are continuous at the hand specimen scale, and may be traced in outcrop for several metres in fresh exposures. These are the layers that were interpreted as microbial mat deposits in Figure 7(j)-2. (B) Another Wilkins Peak oil shale with well defined continuous laminae. Tiny dolomitic lenses produce wavy laminated appearance. (C) Enlarged portion of Figure 7(j)-4A (marked with yellow box on A). It shows that individual laminae (marked with yellow arrows) are from ten to tens of microns thick and continue at approximately constant thickness. The wavy nature of these laminae is due to small lenses of dolomite. (D) Lean dolomitic oil shale (Parachute Creek Member) with discontinuous brownish kerogen streaks. The latter do not appear to be concentrated in certain intervals, but are rather randomly distributed. In hand specimen this type of oil shale is homogeneous rather than laminated, as for example in Figure 7(j)-3E. (E) Eroded piece of organic material that was deformed and folded over during transport. It appears to have been derived from erosion of organic-rich layers like those shown in Figures 7(j)-4A to -4C. Deformation and folding implies internal cohesive strength and is suggestive of a microbial mat origin. Parachute Creek Member, Piceance Basin, Colorado. (F) Green River oil shale from the Uinta Basin in Utah. It shows discontinuous yellow organic streaks of variable length. Some horizons contain a larger concentration of these streaks. (G) Low grade dolomitic oil shale from the Wilkins Peak Member. Image rotated forty degrees for better contrast. This shale also contains discontinuous yellow organic streaks of variable length.

This page intentionally left blank

Atlas of Microbial Mat Features Preserved within the Siliciclastic Rock Record
Edited by J. Schieber et al.
© 2007 Elsevier B.V. All rights reserved
DOI: 10.1016/S1574-1966(07)02008-1

CHAPTER 8

New Developments in Research on Microbial Mats

INTRODUCTION

Although by no means meant to be an exhaustive overview of current experimental work and new developments in microbial mat research, this chapter illustrates several innovative and informative research avenues wherein investigations are ongoing. In the first section, 8(a), the role of iron bacteria in building mats and even stromatolite-like morphologies under dynamic environmental conditions is investigated, and these processes may also have important connotations for the genesis of Precambrian BIF's. Regrowth of such mats which have been partially or even completely eroded by high energy sedimentary events is found to be remarkably rapid. Partly analogous stromatolite-like forms may also develop when mat-bound sands are subjected to seismic deformation, as outlined in Section 8(b). In the following section, 8(c), ongoing flume experiments with both live and desiccated mat fragments are discussed in some detail. The comparison of the behaviour of these two contrasting mat fragment types enables an estimation of the significance of microbial surface binding on the durability of mat fragments within sandy depositional systems. Mat fragments also tend to lose most of their attached clastic grains during early transportational history. Hydraulic modelling within the tidal to supratidal zones of coastal sabkhas as discussed in the last section, 8(d), suggests that significant upward directed hydraulic pressure can be built up in the mat substratum, and that potential for liquefaction within the sub-mat sediments can occur. The pressure head may supply groundwater to overlying mats to enable their survival over long dry seasons. Where the mats crack, however, the pressure will result in groundwater discharge, as a result of which stimulated microbial growth will re-seal and "heal" the cracks, often also with development of mat expansion structures such as petees. These features may also be filled from below due to the hydraulic pressure.

8(a). MICROBIAL MATS BUILT BY IRON BACTERIA: A MODERN EXAMPLE FROM SOUTHERN INDIANA

J. Schieber, M. Glamoclija

Iron biominerals comprise approximately 40% of all minerals formed by organisms (Lowenstam, 1986; Bazylinski and Frankel, 2003, p. 6), and play an important role in biogeochemical redox reactions of marine and fresh water environments. Biogenic iron oxides have been the focus of a number of studies in recent years (e.g., Straub et al., 2001; Emerson and Weiss, 2004; Kappler and Newman, 2004; Fortin and Langley, 2005), and their most common forms include oxides (magnetite, hematite), oxyhydroxides (e.g., goethite, akagenite, lepidocrocite) and poorly ordered phases (Cornell and Schwertmann, 2003). Amorphous iron, ferrihydrite and lepidocrocite have been identified in association with bacterial cell walls and extracellular polymers in fresh water environments (e.g., Tipping et al., 1989; Fortin et al., 1993), wetlands (e.g., Emerson et al., 1999), iron rich seepage areas (James and Ferris, 2004), as well as in deep aquifers (Hallberg and Ferris, 2004). Studies of vent systems around the world show that amorphous iron-oxides and ferrihydrite are commonly associated with bacteria (see review article by Little et al., 2004).

Biotic reactions that form iron oxides include microbial oxidation of Fe(II) to Fe(III), and depend on pH and O_2 concentrations. In pH neutral environments *Gallionella* spp. and *Leptothrix* spp. are common microaerophilic bacterial species involved in biogenic iron oxidation (Emerson and Weiss, 2004). Whether and how these bacteria derive energy from the oxidation of Fe(II) while in competition with rapid abiotic oxidation of Fe(II) at neutral pH is still a matter of debate (Sobolev and Roden, 2004), but the intimate association of iron precipitation and microbial extracellular polymer material (EPS) suggests that they most likely do derive some benefit. Chemolithotrophy of Fe-oxidising bacteria in pH neutral environments provides at least a partial rationale (Hallbeck and Pedersen, 1991). For example, iron oxidation by *Gallionella* shows close spatial correlation with stalk production because the organism continuously produces fresh stalk material in order to nucleate iron oxides and thus to gain energy for survival (Anderson and Pedersen, 2003). *Leptothrix* has the ability of passive sorption of iron and iron oxides

onto the sheath (Emerson and Weiss, 2004), yet it remains difficult to clearly differentiate between true biogenic Fe oxides and those formed as a result of abiotic reactions.

A better appreciation of iron oxidising bacteria may be vital for understanding the processes that formed Archaean and Proterozoic banded iron formations (BIF), deposits that are critical for reconstructing the early evolution of Earth's atmosphere. While there are multiple hypotheses to explain these deposits (e.g., Holland, 1973; Morris and Horwitz, 1983; Isley, 1995; Rasmussen and Buick, 1999), the potential role of iron oxidising bacteria has yet to be evaluated seriously in these scenarios.

The current understanding is that oxygenic photoautotrophs forced the oxidation of ferrous iron in ancient depositional basins via the production of molecular oxygen (Pierson et al., 1999; Kamber et al., 2004). Because the biochemical pathways necessary to deal with molecular oxygen had not yet evolved, oxygenic photoautotrophs of the time would have depended on the ready availability of ferrous iron to "neutralize" the toxic oxygen they produced (Cloud, 1973). Alternatively, ferrous iron might have been oxidised via early anaerobic photosynthesis (Pierson et al., 1999). Iron-oxidising bacteria gain energy from the oxidation of ferrous iron and offer an alternative or additional pathway (in addition to photosynthetic production of O_2) of iron oxidation and deposition. For example, bacterial stalks of *Gallionella* spp. and *Gallionella*-like organisms almost completely compose iron-rich layers near the exhalative zone of a shallow hydrothermal vent near the island of Santorini and near the hydrothermal outflows in Iceland (Holm, 1987). Iron oxidation by microaerophilic species (*Gallionella* and *Chromatium*) that can occupy ecological niches with limited O_2 availability has been proposed as a mechanism for widespread deposition of ferric iron in BIF's (Holm, 1989; Konhauser et al., 2002). Iron-reducing bacteria were suggested as a third group of organisms involved in the formation of BIF's. The hypothesis derives from the observation that within BIF's, iron-poor layers with carbonates contain isotopically light carbon. The source of that light carbon may have been remains of phototrophic organisms that accumulated on the surface of oxidised iron layers (Baur et al., 1985; Nealson and Myers, 1990).

For all these reasons it is essential to better understand the textural and isotopic biosignatures of iron oxidising bacteria, and we are therefore currently studying a modern system where *Gallionella* and *Leptothrix* produce copious quantities of iron oxides under constantly fluctuating environmental conditions. Studying the processes and dynamics of this system may eventually provide critical new insights into mechanisms that may have produced the banded iron formations of the past.

Our study site, a groundwater-fed small creek near Bloomington/Indiana, USA, is characterised by prominent reddish–brownish deposits of iron hydroxides. The water seeps into the creek from a sandstone horizon within the Mississippian Borden Formation, a succession of marine marls, carbonates, and sandstones. These sediments contain variable amounts of diagenetic pyrite that is oxidised as surface waters percolate through the sediments. In the process, iron goes into solution as ferrous iron (the Fe^{2+} ion). Discharge of these iron-rich waters is intimately linked to an occurrence of masses of iron bacteria. Under the given environmental conditions, iron bacteria oxidise Fe(II) and gain energy according to the following reaction:

$$Fe^{2+} + 0.25O_2(aq) + 2.5H_2O \rightarrow Fe(OH)_3(s) + 2H^+$$
$$\Delta G^{\circ\prime} = -111.3\ \text{kJ/e}^-$$

where $\Delta G^{\circ\prime}$ is the overall amount of energy available for cellular metabolism at neutral pH.

This reaction occurs at redox interfaces where diffusion-limited O_2 transport leads to low dissolved O_2 partial pressure (microaerobic conditions) within the zone of Fe(II)–O_2 overlap (Roden et al., 2004). With continued reaction the iron bacteria at our study site form loaf-shaped and bulbous buildups, as well as flat to undulose mats that cover the creek bed (Figure 8(a)-1A). The sheath-forming bacterium *Leptothrix* dominates, but spiral stalks of *Gallionella* are common and can be abundant during certain growth stages (Figure 8(a)-4). Microbial growth forms are fragile and of the consistency of custard. During rainstorms, when surface runoff dominates creek flow, they can be partially or completely eroded depending on the intensity of rainfall (Figure 8(a)-1B).

Mat erosion produces partially eroded mat remnants (Figure 8(a)-2A), upturned and flipped-over edges of mats (Figures 8(a)-1B, 8(a)-2C), mat roll-ups (Figure 8(a)-2B) as known from other microbial mat occurrences (e.g., Schieber, 1999; Simonson and Carney, 1999), large quantities of irregularly shaped and sized mat fragments (Figure 8(a)-2A), and surface wrinkles due to current drag on the mat surface (Figures 8(a)-2C and -2D). The latter effect actually produces a morphology that resembles the "elephant skin" texture described from microbial mats on

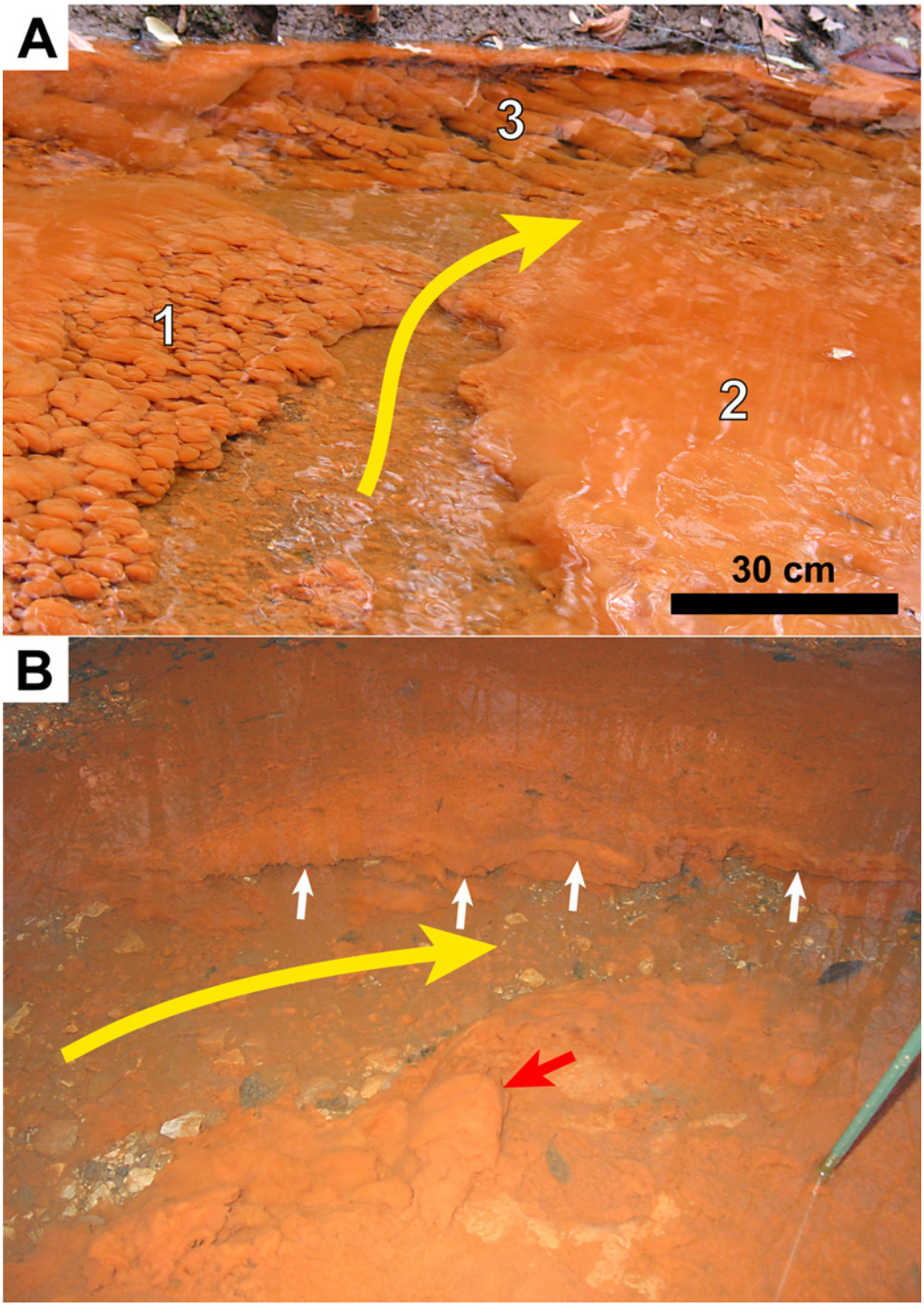


Figure 8(a)-1: Two views of creek bed with iron bacterial mat. Scale approximate, scale bar applies to both images.

(A) Shows active growth stage of mat. At left, in the area of stronger current, development of a field of bulbous mat buildups (marked 1) can be seen. At right, in an area of weaker current, development of an essentially planar mat (marked 2) is seen. The creek channel curves to the right (yellow arrow). At the far side of the image, the cut bank of the channel which suffers erosion during maximum flow, microbial buildups are inclined (marked 3) at approximately 30 degrees to the right. This inclination probably reflects the downwelling of the current that is typical for flow in stream channels (Reineck and Singh, 1980). (B) Appearance of mat after erosive event (rainstorm). The central channel where the swiftest flow is concentrated (yellow arrow) has been swept clean and is in the process of mat resurfacing. The edge of the mat has been eroded, undercut, and partly turned up (white arrows). In the foreground a large mat fragment can be seen that has been rolled up (red arrow) while being transported across the mat surface.

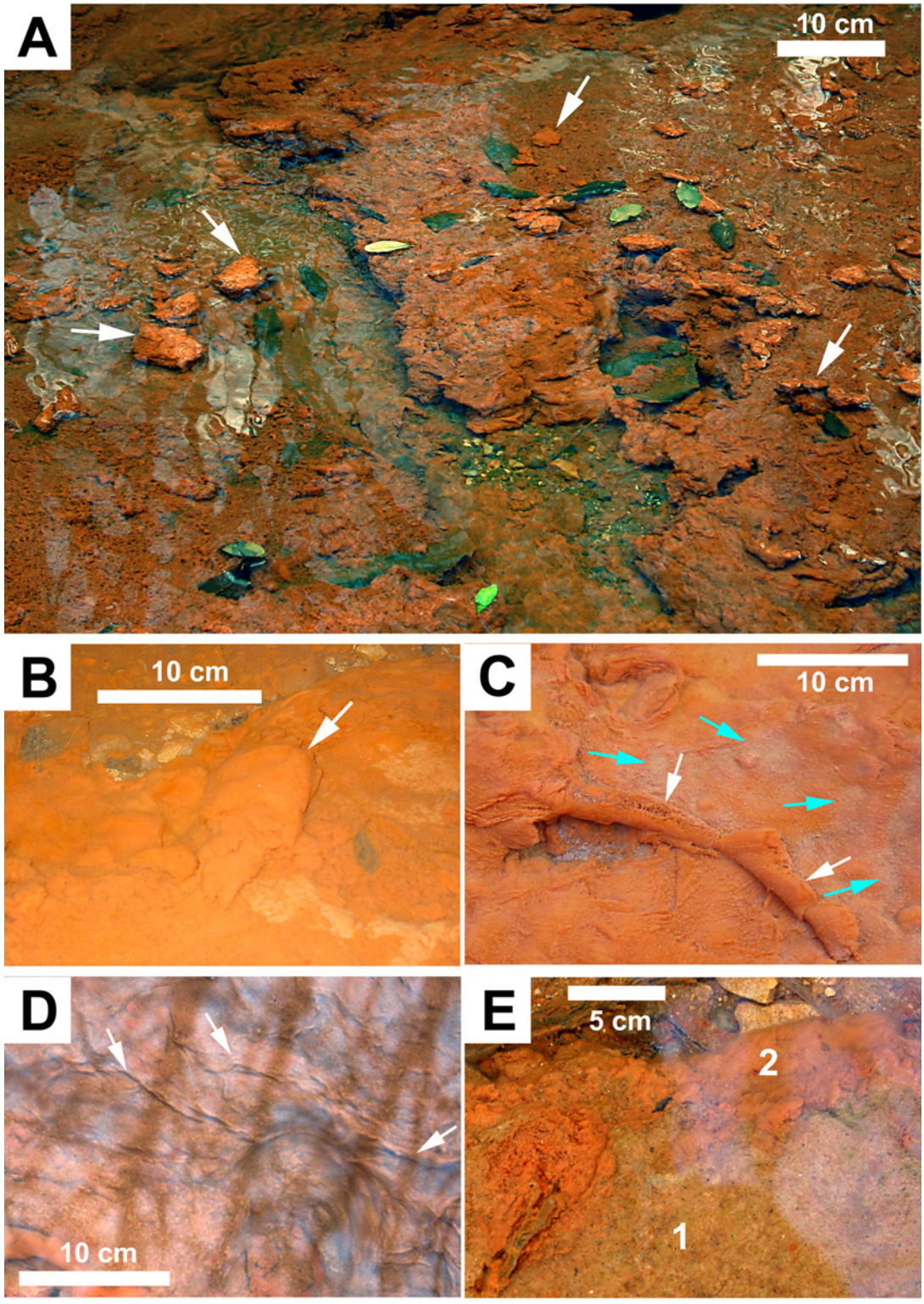


Figure 8(a)-2: Erosion related features.
(A) Partially eroded mat and ripped-up mat fragments. (B) Mat roll-up from Figure 8(a)-1B (white arrow). (C) Multi-layered mat with the uppermost layer partially eroded and flipped over at the edge (white arrows). The mat surface has accumulated thin patches of sand (turquoise arrows) that was carried with flood waters (current from lower left to upper right). Note the wrinkled nature of the mat surface. (D) Current-wrinkled mat surface with a thin veneer of sand. The surface wrinkles on the mat (white arrows) are oriented approximately perpendicular to the current (from lower left to upper right). This may reflect creeping of the uppermost mat layer in response to bottom shear stress. (E) Eroded edge of a thick planar mat (marked 2) that is covered with a layer of sand (marked 1).

sandy substrates (e.g., Gehling, 1999; see also Chapter 6(a)). Sediment transport during high-flow interludes can deposit sand and clay on mat surfaces that are strong enough to resist erosion (Figures 8(a)-2C, -2D, and -2E). Sediment accumulation on these mats can produce macroscopically recognisable internal laminae (Figure 8(a)-5E) and opens up the potential for the generation of stromatolite-like structures that have long term preservation potential (Figure 8(a)-5).

Re-growth of iron microbial mats is vigorous and full mat coverage after storm washout is typically achieved within a week (Figure 8(a)-3A). A large portion of the mat structure consists of iron hydroxide encrusted sheaths of *Leptothrix*, shed constantly by this organism as it multiplies. The sheaths themselves are composed of polysaccharide based materials, and as growth continues there is a rapid buildup of organic matter that provides food for other microorganisms. Thus, mats that form early in a post-washout growth cycle may show signs of decay and disintegration within a few days of their formation (Figures 8(a)-3A and -3C). It is at this point in mat development that a different growth form, light coloured streamlined clumps, appears superimposed on the earlier mat (Figures 8(a)-3A, -3B, and -3C). The observation that the best growth of these secondary growth forms occurs where flow is swiftest (Figure 8(a)-3B), suggests a response of the microbial community to the flux density of essential water borne nutrients such as dissolved organic compounds and dissolved iron. Better mixing with surface oxygen in the more turbulent fast flowing sections of the creek is likely a contributing factor. Somewhat deeper portions of the creek with a water depth of a few centimetres to 20 cm are the preferred site of growth for thicker mat developments (Figure 8(a)-1). In steeper portions of the creek the flow is very fast and consequently the water cover is only a few millimetres to perhaps a centimetre in thickness. Under those conditions the mat cover is only a few millimetres thick at best (Figure 8(a)-3D) and may peel off as thin crumbled sheets (Figure 8(a)-3E) when eroded.

As summarised above, the iron microbial community in this creek shows morphologic response to changes in flow velocity, recycling of organic matter in the environment, flow depth influences and other factors. Whereas the above-described responses are clearly visible at the macroscopic level, they are most likely also reflected in the microscopic structure of these mats. The work on that aspect of the system is still in progress, but a few observations are presented here (Figure 8(a)-4) to illustrate the finer details of mat construction.

Mat surfaces show three basic ingredients (Figure 8(a)-4), *Leptothrix* sheaths, twisted *Gallionella* stalks, and extracellular polymer substance (EPS). In places either one of these may be found to dominate the mat surface (Figures 8(a)-4A, -4B, and -4F). Iron microbe layers show a considerable degree of internal organisation at the microscopic level. Freeze dried samples, freeze-fractured perpendicular to macroscopic lamination, show a fine scale layering consisting of "storeys" of matted *Leptothrix* sheaths that exhibit regular spacing of some ten microns (Figures 8(a)-4C and -4D). The "storeys" seem to be held apart by other *Leptothrix* sheaths that are oriented at steep angles to the planes defined by the "storeys". These structural elements are held together by a carbon-rich and iron hydroxide encrusted matrix, presumably EPS. This structural style actually shows an uncanny resemblance to bamboo scaffolding that is seen in many Asian cities, delicate appearing structures of surprising strength that consist of bamboo poles tied together by ropes. On breaks parallel to lamination it becomes clear that what holds the "storeys" apart is a honeycomb structure of entwined *Leptothrix* sheaths, *Gallionella* stalks, unidentified filaments, and more EPS (Figure 8(a)-4E). The outermost microlamina, the actual growth surface of the mat at the time of collection, shows in addition to *Leptothrix* sheaths and *Gallionella* stalks a surface texture that has the appearance of thin sheets of a stretchable substance criss-crossing and covering "holes" not occupied by sheaths and stalks (Figure 8(a)-4E). The stretched sheets consist of an organic matrix (probably EPS) that is encrusted with nanoscale balls of iron hydroxides (Figure 8(a)-4F).

It appears thus that the observed mats consist of a framework in which stiff, mineralised *Leptothrix* sheaths are probably the dominant load-carrying elements. This framework compartmentalises the occupied volume into numerous hollow spaces that are filled with water. The EPS matrix that holds the structural elements together also prevents, or at least severely limits, water exchange between compartments. Production of EPS requires energy and nutrients, and by following the observed building strategy the microbes conserve resources while still increasing their structural surface to support a growing population.

In order to examine how iron microbial mats as described above may appear in the rock record, selected spots on the creek bed were marked with PVC tubing (Figure 8(a)-5A) and the area repeatedly sprinkled with fine sand (Figure 8(a)-5B) to produce easily recognisable laminae within the growing mat. After collecting the mat sample contained in the PVC tubing, a portion of the mat was shock frozen in liquid nitrogen and freeze dried

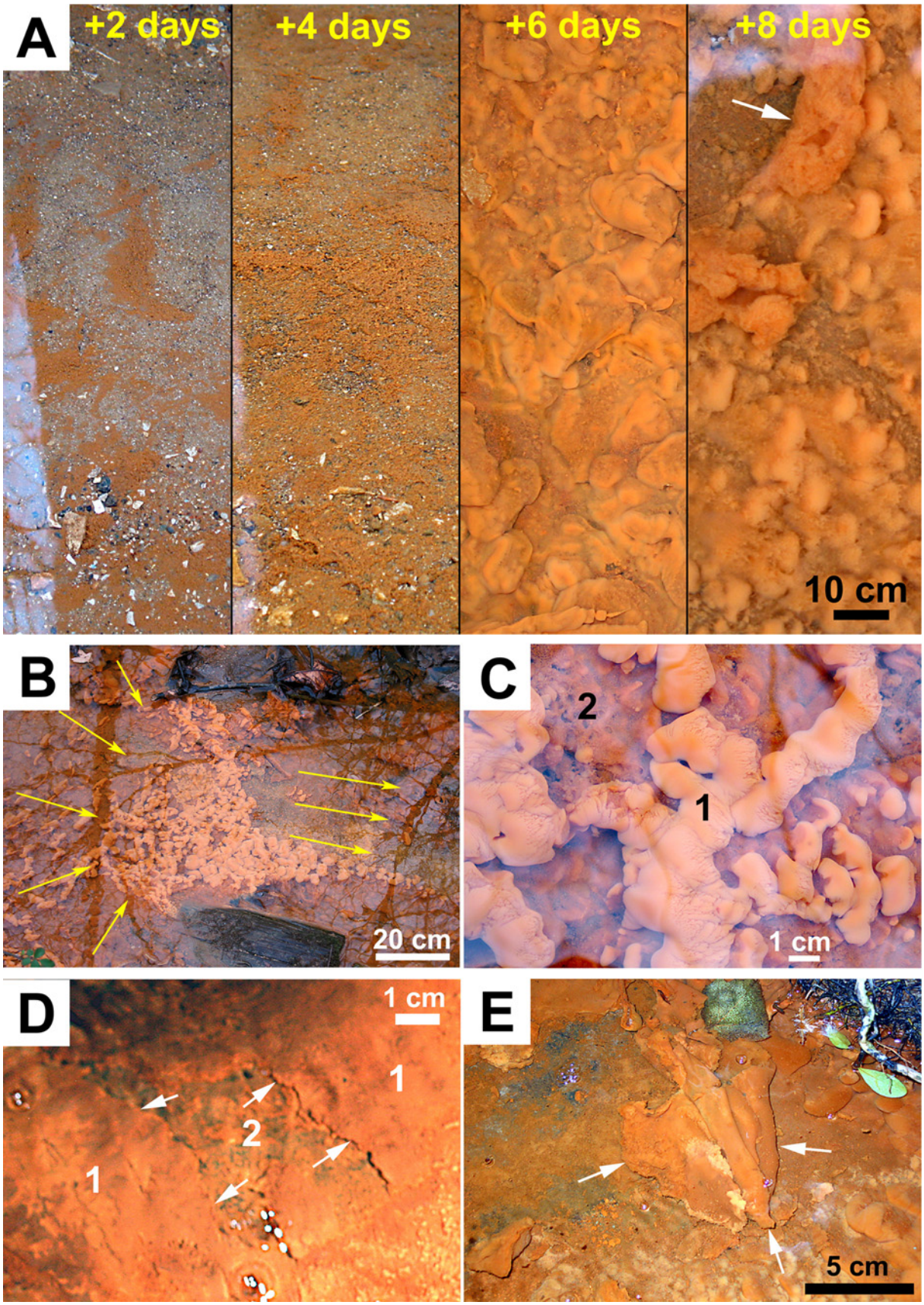

A
+2 days
+4 days
+6 days
+8 days
10 cm
B
20 cm
C
2
1
1 cm
D
1 cm
1
2
1
E
5 cm

Figure 8(a)-3: Mat growth, flow velocity, and flow depth.
(A) Photos that illustrate the speed of mat recovery. The four images were taken 2 days apart; starting two days after a rainstorm had completely "washed out" the previously existing mat. Once surface runoff ends and flow is spring-fed only, small tufts of iron microbes (mostly *Leptothrix*), a few millimetres in size, start to form loose accumulations on the creek bed (+2 days). Four days after "washout" these loose accumulations start to fuse into contiguous microbially bound patches. After six days a microbial "fluff", a few millimetres thick, covers most surfaces on the creek bed. After eight days the earlier grown mat has peaked, starts to decay, and may in places peel off (arrow 1) even under weak currents. Bulbous secondary growth forms (light coloured streamlined clumps) are established on top. (B) The effect of flow constriction on mat growth. The flow in the creek is from left to right (yellow arrows), and the channel narrows to about half its width due to obstacles. Whereas upstream (far left) the initial mat (Figure 8(a)-2A) shows a cover of scattered bulbous (light coloured streamlined clumps) growth forms, the latter grow much more densely in the area where the flow narrows (centre of image) and flow velocity is increased. (C) Detail of secondary growth forms (also referred to as light coloured streamlined clumps). Shows older decaying mat of darker reddish-brown colour (marked 2) overgrown by secondary forms (beige colour, marked 1) that are streamlined and flow oriented (flow from left to right). (D) Photo from a steeper sloping (10 to 15 degrees) portion of the creek. Under normal conditions, the water flow is only a few millimetres to 1 cm deep, and as a result the iron microbial mat only grows to a thickness of a few millimetres. Photo shows where a layer of mat (marked 1) has been scraped off the bedrock for sampling (area marked 2), and illustrates the thinness of the mat (arrows). (E) Another photo from steeper sloping (10 degrees) portion of the creek. It shows a thin mat layer (white arrows) that has just become detached from the bedrock surface and is being crumbled up by currents.

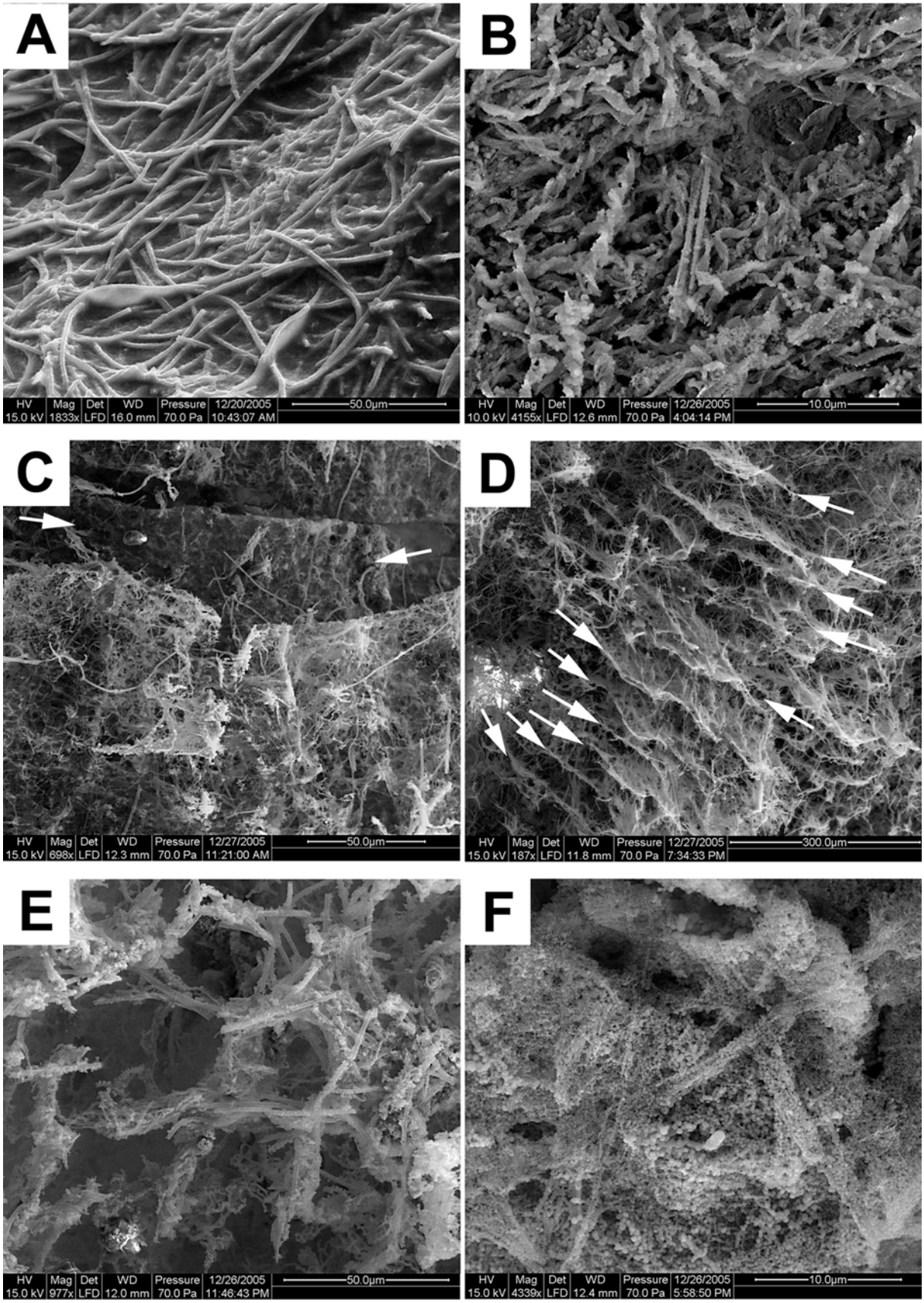

A
HV 15.0 kV | Mag 1833x | Det LFD | WD 16.0 mm | Pressure 70.0 Pa | 12/20/2005 10:43:07 AM | 50.0µm
B
HV 10.0 kV | Mag 4155x | Det LFD | WD 12.6 mm | Pressure 70.0 Pa | 12/26/2005 4:04:14 PM | 10.0µm
C
HV 15.0 kV | Mag 698x | Det LFD | WD 12.3 mm | Pressure 70.0 Pa | 12/27/2005 11:21:00 AM | 50.0µm
D
HV 15.0 kV | Mag 187x | Det LFD | WD 11.8 mm | Pressure 70.0 Pa | 12/27/2005 7:34:33 PM | 300.0µm
E
HV 15.0 kV | Mag 977x | Det LFD | WD 12.0 mm | Pressure 70.0 Pa | 12/26/2005 11:46:43 PM | 50.0µm
F
HV 15.0 kV | Mag 4339x | Det LFD | WD 12.4 mm | Pressure 70.0 Pa | 12/26/2005 5:58:50 PM | 10.0µm

Figure 8(a)-4: Mat textures.

(A) ESEM image of *Leptothrix* dominated mat surface. Note films of EPS between filaments. (B) SEM image of another mat surface sample. This sample was shock frozen in liquid nitrogen and freeze dried. This particular sample shows an abundance of *Gallionella* stalks on the surface. (C) Lower magnification SEM top-view of a mat surface that consists of intertwined *Leptothrix* sheaths and *Gallionella* stalks in a matrix of EPS. Freeze drying reduces the EPS matrix to very thin films between filaments and stalks. The sample was fractured and shows an older mat surface beneath (arrows). Shock frozen and freeze dried sample. (D) SEM view of a fracture surface perpendicular to the mat surface. Arrows point to multiple storeys of matted *Leptothrix* sheaths that represent former mat surfaces and now give rise to an internal laminar structure. Storeys are interconnected by variably inclined (relative to storey plane) *Leptothrix* sheaths. Shock frozen and freeze dried sample. (E) SEM view of a honeycomb-like structure that consists of intertwined *Leptothrix* sheaths and *Gallionella* stalks that are held together by EPS. This is a common structural element that holds apart (separates) successive storeys. Shock frozen and freeze dried sample. (F) Detail of EPS covered surface. Strands of EPS are criss-crossing the surface and are encrusted by small round spheres that consist of precipitated iron hydroxides. These spheres are on the order of some tens to several hundred nanometres in size. Shock frozen and freeze dried sample.

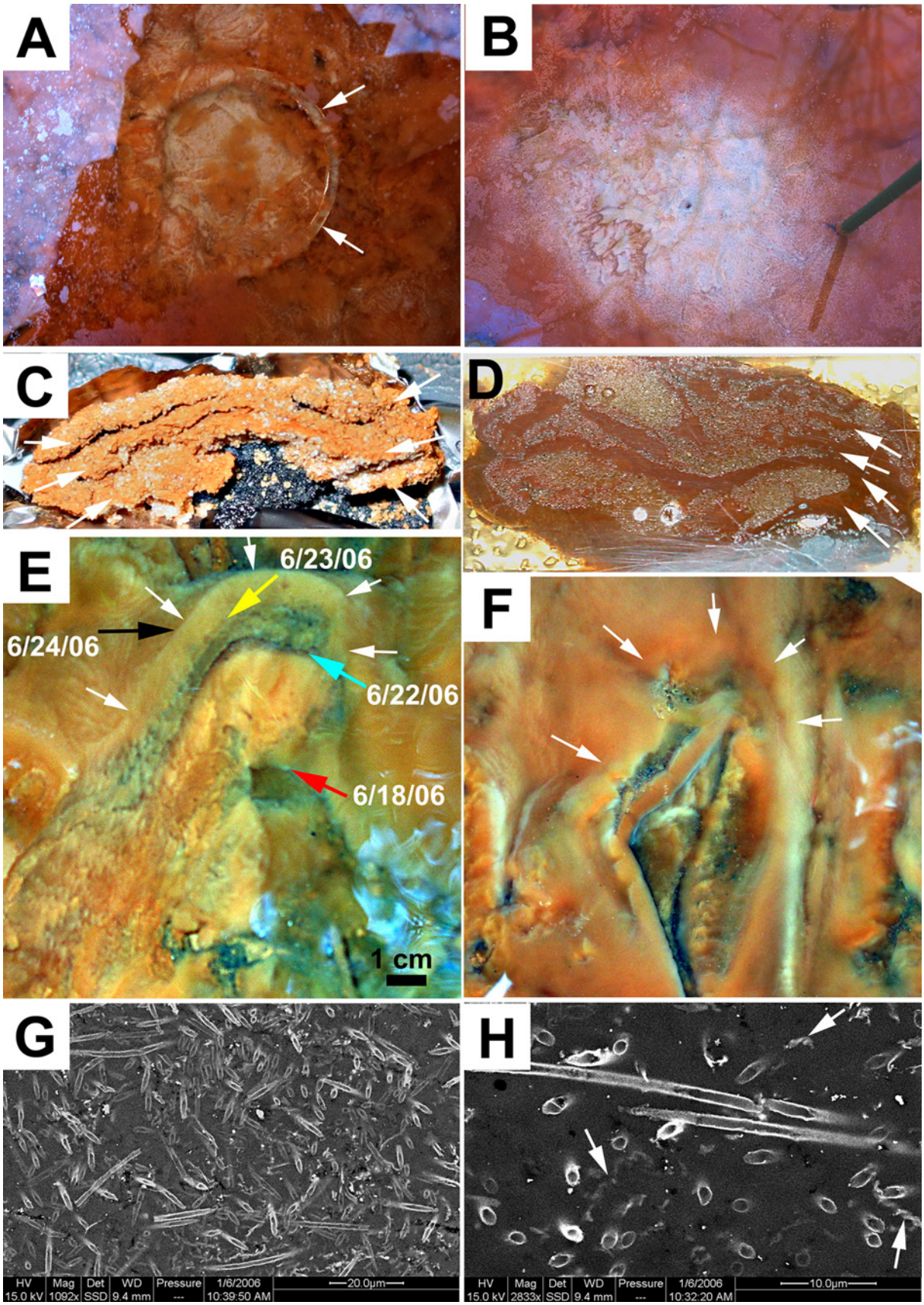

A
B
C
D
E
6/23/06
6/24/06
6/22/06
6/18/06
1 cm
F
G
HV 15.0 kV | Mag 1092x | Det SSD | WD 9.4 mm | Pressure --- | 1/6/2006 10:39:50 AM | 20.0µm
H
HV 15.0 kV | Mag 2833x | Det SSD | WD 9.4 mm | Pressure --- | 1/6/2006 10:32:20 AM | 10.0µm

Figure 8(a)-5: Potential preservational textures.
(A) Sampling site for iron bacteria stromatolite growth test. A plastic pipe (arrows) of 10 cm diameter was buried in the creek bed and gradually raised as the mat grew in thickness. (B) Same place as in A, but with mat covering the pipe rim. In order to preserve and mark lamination, fine sand was sprinkled on the mat every few days. The mat would re-cover the sedimented area within a matter of several days. (C) Shock frozen and freeze dried sample (vertical section) of the mat in A and B. Three successive layers (arrows) are clearly visible. Scale bar is 10 mm long. (D) Another vertical section through the same mat as shown in A. This sample was soaked with Spurr resin after sectioning, cured and hardened. The resulting slab was then ground flat and polished to show internal laminae. It shows alternating reddish mat layers and sand layers (granular), as well as ball-and-pillow structures because the much denser sand was sinking down into the watery mat layers. Scale bar is 10 mm long. (E) Photo of *in situ* bulbous iron microbial mat buildup (similar to those seen in Figure 8(a)-1A, area 1). This "bulb" has been cut open to expose interior layering (photo taken at noon on June 24, 2006). The entire mat cover in the creek channel was eroded during a rainstorm on June 18, 2006, and new growth starts at that surface (red arrow). From June 22 (turquoise arrow) to June 23 (yellow arrow), 2006 a series of rain showers moved across the area over a 24 hour period. Because individual rainfall events were not as severe, multiple pulses of surface runoff moved sand and clay through the creek channel, but caused little or no erosion of prior mat growth. The corresponding mat layer (between turquoise and yellow arrow) is darkened by sediment grains. The mat layer bracketed by the yellow and black arrows formed over a time period of approximately 24 hours following the end of overland flow on June 23. (F) The same area as shown in E, but 18 hours later. Mat growth has already obscured and softened the sharp rim seen in E. For easier location, the white arrows point to the same spots as marked with white arrows in E. (G) A closer view of the arrangement of *Leptothrix* sheaths in the Spurr resin matrix of the sample shown in D. Elongate and round features are iron hydroxide encrusted sheaths of *Leptothrix*. Their iron encrustation makes for the bright response in backscatter mode. (H) High magnification SEM image (backscatter mode) of same mat lamina as shown in G. Arrows point to *Gallionella* stalks.

(Figure 8(a)-5C), and another portion was infused with Spurr resin, cured, and then ground and polished (Figure 8(a)-5D). Both preparation methods show preserved layering (Figures 8(a)-5C and -5D). Even though the mat is constructed very lightly (Figure 8(a)-4), it is able to support the weight of sand layers that are several mm thick (Figure 8(a)-5D). That this type of lamination can indeed occur naturally is illustrated by Figure 8(a)-5E. Thus, iron microbial mats can form potentially preservable stromatolites. Preservation potential is probably greatly enhanced by rapid burial with other sediments. Alternatively, if eroded mat material is for example washed into a lake basin, it could form deposits of microbially precipitated iron that have unique textural attributes and could as well become part of the geological record.

Our observations demonstrate that under sufficiently dynamic environmental conditions, iron oxidising bacteria can produce layered, stromatolite-like morphologies. The formation of stromatolite laminae may mimic processes that were present during the formation of BIF's. Ongoing *in situ* experiments are designed to help us understand microbial morphological and geochemical responses to different environmental conditions. Microbial mat deposits in multiple periods of Earth history were iron-mineralised to various degrees and may also contain remains of the organisms that formed them (LaBerge, 1973; Gerdes and Krumbein, 1987; Schieber, 1989a, 2002; Konhauser et al., 2002). The common association of microbes and iron accumulations on Earth holds out the prospect that a similar association may exist on Mars as well. Thus, Martian hematite accumulations, such as those of Meridiani Planum (Christensen et al., 2000), are currently favoured targets in the search for ancient microbial life on that planet.

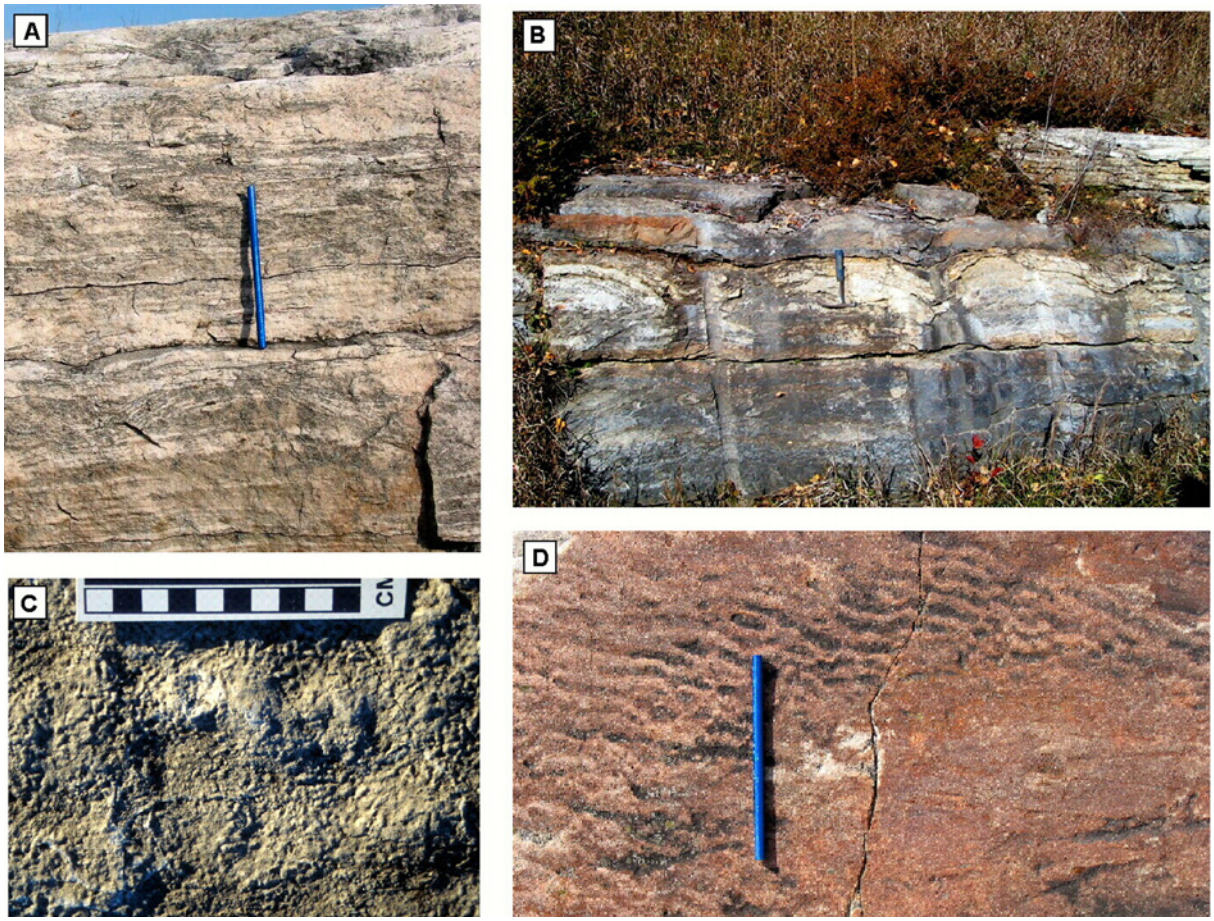


Figure 8(b)-1: Primary structures.
(A) Biofilm structures, Nepean Formation, Canada. The crinkly and discontinuous laminations above and below the truncated gently domed stromatolite (immediately below the blue bar – 15 cm) are interpreted as biomat layers, some of which were folded or torn up during storm events. (B) Low-amplitude, laterally-linked stromatolites from the Potsdam Sandstone, along Highway 12 just east of Chippewa Bay, New York, approximately >85 km due south of Ottawa. The host rock is a medium-grained, quartz cemented, quartz arenite. Geological pick for scale. (C) Top view of stromatolite outcrop in A displaying low amplitude, domal stromatolites ornamented with a knobby surface. This bedding plane morphology is inferred to mimic an original biomat developed in a shallow subtidal environment. (D) Iron oxide stained wrinkle structures capping a bed of medium-grained quartz arenite. Such "microripple"-like patterns are inferred to have been formed under the influence of a continuous biofilm that coated the original unindurated sand in a shallow marine setting. The smooth surface to the right of the scale bar (15 cm) has been modified by glacial polishing.

8(b). DISRUPTION OF MATS BY SEISMIC EVENTS

J.A. Donaldson, J.R. Chiarenzelli

This series of photographs documents structures in quartz arenites of the Nepean Formation (Cambro-Ordovician) in Ottawa, Canada, attributed to the influence of biofilms during sedimentation and subsequent seismically related deformation (Donaldson and Hilowle, 2002; Donaldson et al., 2002b, 2005a, 2005b; Donaldson and Chiarenzelli, 2004). Similar structures have been seen in the stratigraphically equivalent Potsdam Sandstone in northern New York State (USA), so these structures are likely widespread throughout the region. The rocks depicted are texturally and compositionally mature quartz arenites (95% to 98.2% SiO_2, total whole rock analyses). They are virtually devoid of fine detrital material other than illite; framework grains consist of well-rounded quartz grains, traces of chert and feldspar, and <2% heavy minerals. The detrital grains are cemented primarily with epitaxial overgrowths of quartz, and up to 5% carbonate in recessively weathered layers. Laminations and primary structures are accentuated by darker colouration of the beds containing carbonate cement, which has facilitated the accumulation of modern organic matter. No original cyanobacterial matter has been detected; in fact, the beds inferred to represent

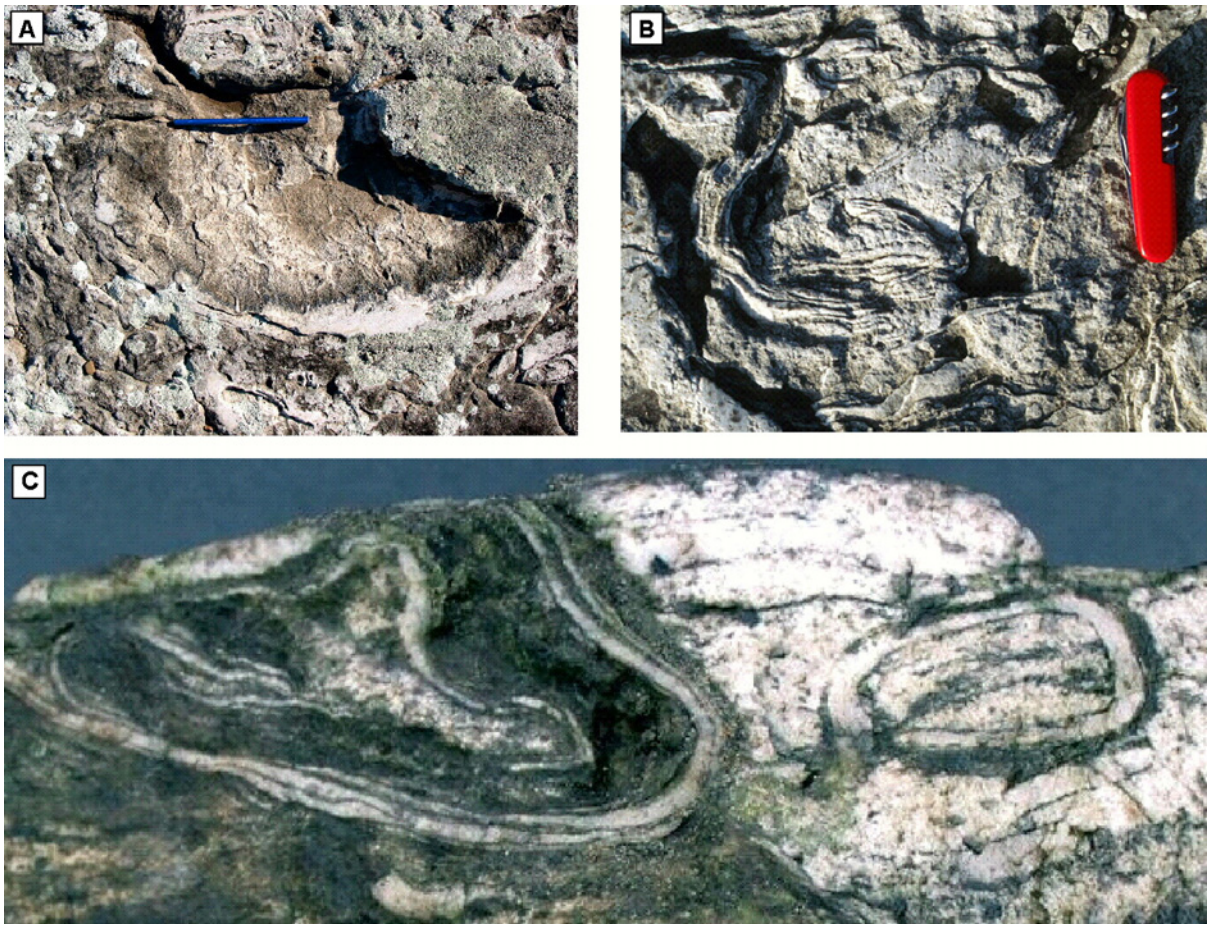


Figure 8(b)-2: Reworking of biofilms.
(A) Sand ridges lining the concave underside of a lamination within an overturned domal stromatolite, as seen on the upper bedding surface of the chaotic zone described in Figures 8(b)-3A to -3D. The reticulate ridges are inferred to represent infills in desiccation cracks within a subsequently degraded biomat layer. (B) Quartz arenite showing folding in biofilm-bound sand sheets intricately folded by storm events in a shallow marine setting. The length of the pocket knife is 9 cm. (C) Roll-up structures in quartz arenites of the Nepean Formation, inferred to have developed in a supratidal environment. The long axis of the large roll-up at left is 10 cm.

sand layers originally bound by microbial mats are almost universally free of carbonate cement, appear white on both fresh and weathered surfaces, and have been essentially unaffected by weathering.

These quartz arenites often display both the original biofilm growth forms, as well as subsequent modifications of primary mat morphologies. Most of the photographs represent features whose mechanical behaviour is inconsistent with consolidated and/or unconsolidated sand, thus requiring the influence of biofilms in their formation. Primary growth forms include low-relief stromatolitic domes and wrinkled, crinkly, or knobby textured bedding surfaces, often superimposed on non-biogenic sedimentological features (Figure 8(b)-1). Modified biofilm morphologies include desiccation cracks (i.e., sand cracks), roll-ups, rip-ups, flip-over folds, erosional truncations, and the foundering and reorientation of stromatolitic heads (Figure 8(b)-2). Evidence of evaporitic conditions during deposition is provided by the close association with pseudomorphs after gypsum.

Among the most intriguing findings is the disruption of a distinct half-metre-thick stratigraphic interval, presumably by palaeoseismic events. In this zone low-amplitude, decimetre-scale, domal stromatolites, composed of rounded quartz grains have sunk or foundered into underlying unconsolidated layers (Figure 8(b)-3). This implies that the stromatolites were at least semi-consolidated to behave as coherent blocks during disruption. The glacially polished outcrop displays numerous, random cross-sections through the stromatolites which show a variety of internal features emphasised by slight variation in the ratio of quartz to carbonate cement. These striking outcrops convincingly document the influence of organic mats on sedimentation, and during their subsequent seismically activated deformation, in a shallow marine depositional environment.

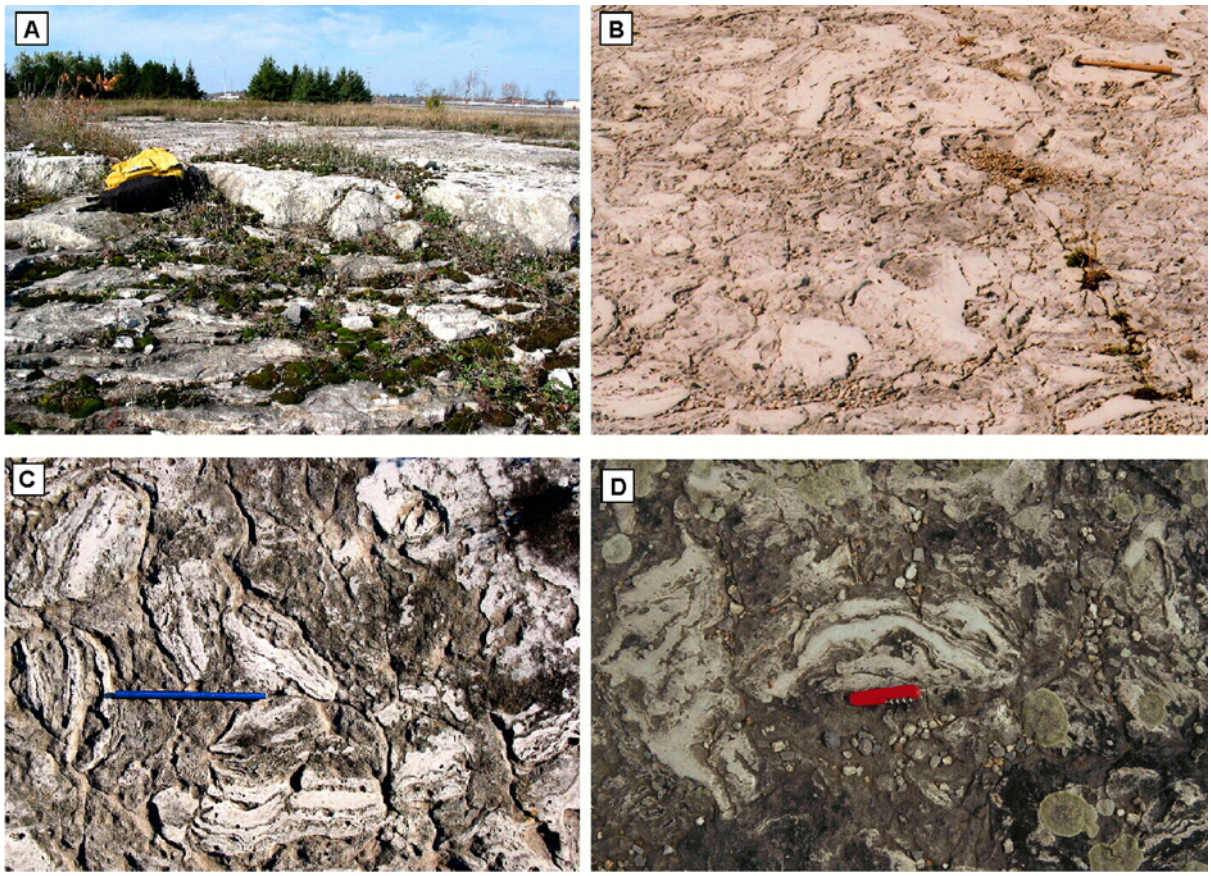


Figure 8(b)-3: Palaeoseismic mat disruption features.
(A) Outcrop photograph of glacially polished Nepean quartz arenites along Highway 417, near Kanata, western Ottawa. Note the thin centimetre-scale horizontal bedding in the foreground. An approximately half-metre thick "chaotic" zone, which begins at the base of the backpack, is shown in detail in photographs C to D. (B) Bedding-parallel surface showing extent of disruption in the chaotic zone. Note size of the disrupted blocks. Hammer for scale. (C and D) Close-up views of glacially polished surface of the chaotic zone in which silicified biomats and stromatolites have foundered, during a palaeoseismic event. The chaotic zone has been traced for several kilometres to another location and in both places is composed of rotated, decimetre-scale blocks that must have been coherent (penecontemporaneously cemented) at the time of disruption above the still-unconsolidated sand. Layering is accentuated by zones of calcite cementation. In some blocks, pointed terminations of pseudomorphs after gypsum are apparent (D, in domal stromatolite above right end of the knife). The blue scale-bar is 15 cm long and the pocket-knife is 9 cm.

8(c). FLUME EXPERIMENTS ON THE DURABILITY OF SANDY MICROBIAL MAT FRAGMENTS DURING TRANSPORT

J. Schieber

It is widely understood that benthic microbes impart a considerable increase in erosion resistance to the substrate by acting as a binding matrix between sediment grains (Neumann et al., 1970). The interplay of sedimentation processes, environmental parameters, and microbial responses produces a wide array of sedimentary features that are increasingly recognised in the rock record and aid in putting the microbial contribution to sediment surface dynamics into proper perspective (e.g., Schieber, 2004). When eroded, either wholly or partially, microbial mat fragments also form sedimentary particles with unique properties (physical and chemical) and responses (biological) to external stimuli.

Whereas the parameters that are associated with microbial mat erosion, such as cohesiveness, current strength, and prior history, are at least known in their magnitude from several case studies (e.g., Neumann et al., 1970; Yallop et al., 1994; Paterson et al., 1994; Paterson, 1997), little direct observational data exist that document what happens to microbial mat fragments during transport. Basic questions of interest to the sedimentologist are for example the survivability of mat fragments over the course of transport, as well as their transport modifications and eventual destruction or burial.

Study materials

In the study presented here, microbial mat fragments from a natural occurrence of a cyanobacterial mat (Figure 8(c)-1A) were studied in a sand-filled racetrack flume (Figures 8(c)-1B, -1C, -1D) in order to arrive at estimates of likely transport distance prior to complete mat destruction. Desiccated fragments of the mat shown in Figure 8(c)-1A were collected for the experiment. Half of the fragments were kept moistened for one week prior to the flume run to allow the mat to revitalise.

Examination of the desiccated starting material under the SEM shows a top to bottom decline in visible microbial filaments and a corresponding increase in mineral matter (Figure 8(c)-2A). Identifiable microbial filaments only occur in the top portion of the mat (Figures 8(c)-2B and -2C), whereas further down (Figures 8(c)-2D, -2E, -2F) filaments become less conspicuous and the connective matter between mineral grains is largely extracellular polymer substance (EPS). The mat surface consists mainly of tangled microbial filaments set in a matrix of EPS (Figures 8(c)-2G through -2K). The EPS matrix gives the surface a "smoothed" appearance (Figures 8(c)-2I, -2J).

Macroscopically, the dried mat fragments consist of a mixture of organic debris and mineral grains in a microbial matrix and have curved up edges (Figures 8(c)-3A, -3B). They are of grey-brownish appearance after several days of desiccation (Figure 8(c)-3A) due to bleaching of cyanobacterial pigments in sunlight. The mat may still appear green if freshly desiccated or if dried away from sunlight (Figure 8(c)-3B). Closer inspection shows that most fragments contain narrow desiccation-related cracks (Figures 8(c)-3A, -3B) that predetermine future fragmentation.

Observations from flume runs with desiccated mat fragments

Initial flume runs were conducted at various flow velocities (40 to 70 cm/s, measured mid-channel at half depth) and at a flow depth of 8 cm. The sand surface was rippled (lower flow regime) across the entire velocity range. At low velocities (40 to 50 cm/s), after being added to the flow, desiccated curved fragments (5 to 8 cm in size) tumbled a metre or two across the flume bottom before locking into the sand with their curved edges (convex up orientation, Figure 8(c)-3C). Hydration and softening of the fragment, in combination with continued flow, then induced "shedding" of particles from the exposed "back side" of the mat fragment (Figure 8(c)-3C). For sustained transport, higher flow velocities (60–70 cm/s) were needed. At such velocities fragments crept over the surface and were picked up by the current intermittently before settling to the surface again. Within 15 minutes the larger fragments (5 to 10 cm across) broke up into smaller pieces because of pre-existing fractures (Figures 8(c)-3A, -3B). These smaller fragments (2–4 cm in size) readily "fit" into ripple troughs and were buried rapidly by migrating ripples (Figures 8(c)-3E, -3F). Because net sedimentation was zero in these experiments, fragments could move again once the ripple had migrated down-current. In a situation of net sedimentation, on the other hand, they would not

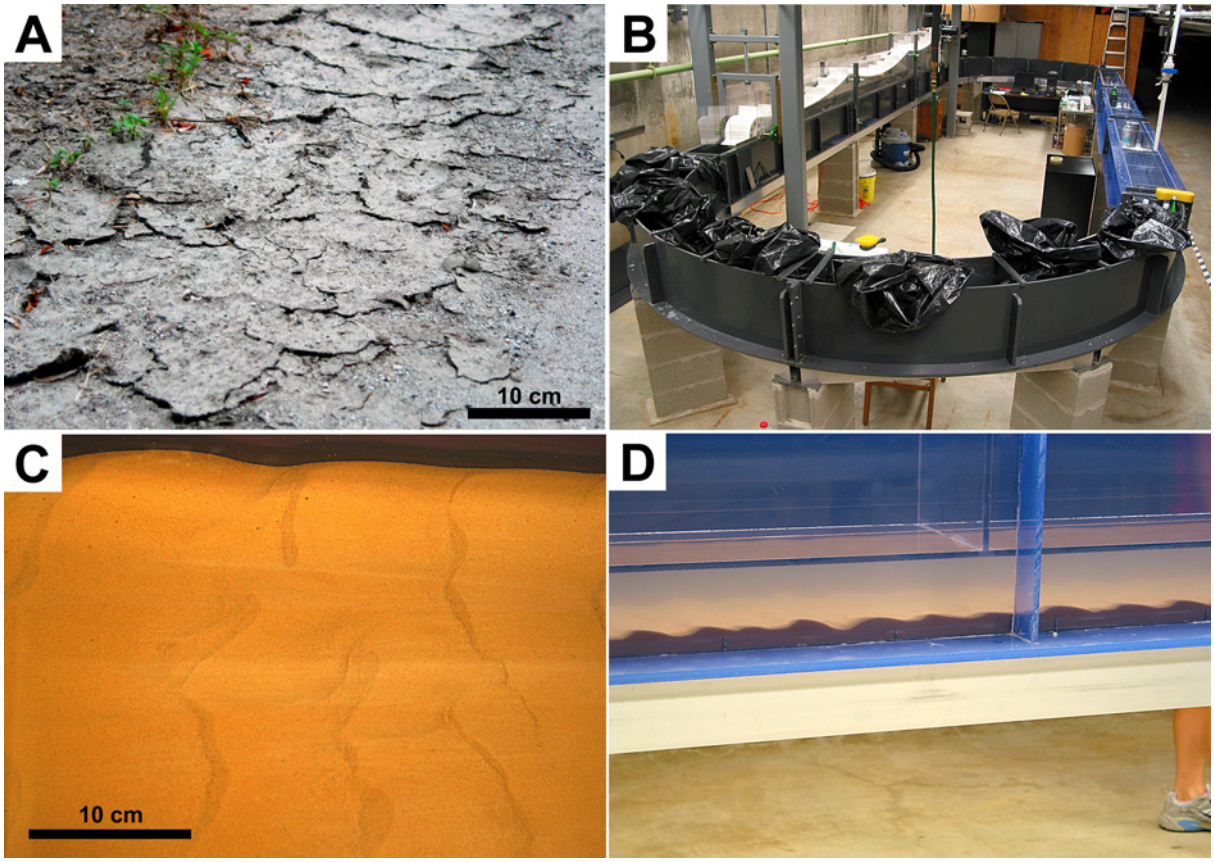


Figure 8(c)-1: The flume experimental setup.
(A) The raw material, desiccation-cracked cyanobacterial (*Oscillatoria* spp.) mats on a sandy substrate from a roadside ditch. (B) The racetrack flume at the Shale Research Laboratory of Indiana University. The flume has an 11.5 × 3.25 m footprint and the water is moved with a paddle belt (left side of flume). This method of propulsion minimises the shredding and disintegration of cohesive particles, such as clay flocs and microbially bound materials. (C and D) The sand bed on which the experiments were conducted: (C) plan view of migrating current ripples (10–15 cm wavelength); (D) side view of rippled sand bed.

be remobilised. As fragments continued to travel, they continuously lost adherent sediment grains (Figure 8(c)-3C) and the lower, poorly bound part of the mat (Figure 8(c)-2) was largely lost within an hour of immersion. The original mat chips slimmed down to thin leathery "skins" of 1–2 mm thickness (Figure 8(c)-3D) that now travelled much easier and were quite durable. This shedding of adherent sediment grains occurs for both desiccated ("dry") and revitalised moist ("live") mat fragments. Whereas large fragments (5 cm's or more) were dragged and rolled over the bed surface, small centimetre-size fragments tended to travel in bounces and hops and were in suspension for considerable portions of the transport path.

In an extended flume run, starting with eight fragments measuring 5–10 cm across (Figure 8(c)-3A, -3B), fragments were collected with a 2 mm mesh screen several times during the run, for examination of size reduction (Figure 8(c)-3). After approximately one hour, the largest remaining fragments measured less than 5 cm across (Figure 8(c)-3G), and a significant portion (∼75%) of the mat material had disintegrated into particles of a few millimetres in size that tended to become buried in the sand substrate (Figures 8(c)-4F, -4G) or travelled in suspension and passed through the screen. Approximately twelve hours later the largest remaining fragments typically were less than 3 cm in size (Figure 8(c)-3H), and between 80–85% of the original material had disaggregated into mm-size or smaller particles. After another twelve hours the largest recoverable fragments measured a mere 1 and 2 cm across, and approximately 95% of the original material had disaggregated (Figure 8(c)-3I). At a flow velocity between 60–70 cm/s, mat fragments as pictured in Figures 8(c)-3G, -3H, -3I take, on average, 1 minute or less to cover the 25 m roundtrip through the flume. Thus, at the 25 hour mark the average fragment had travelled a distance equivalent to 35 to 50 km of transport.

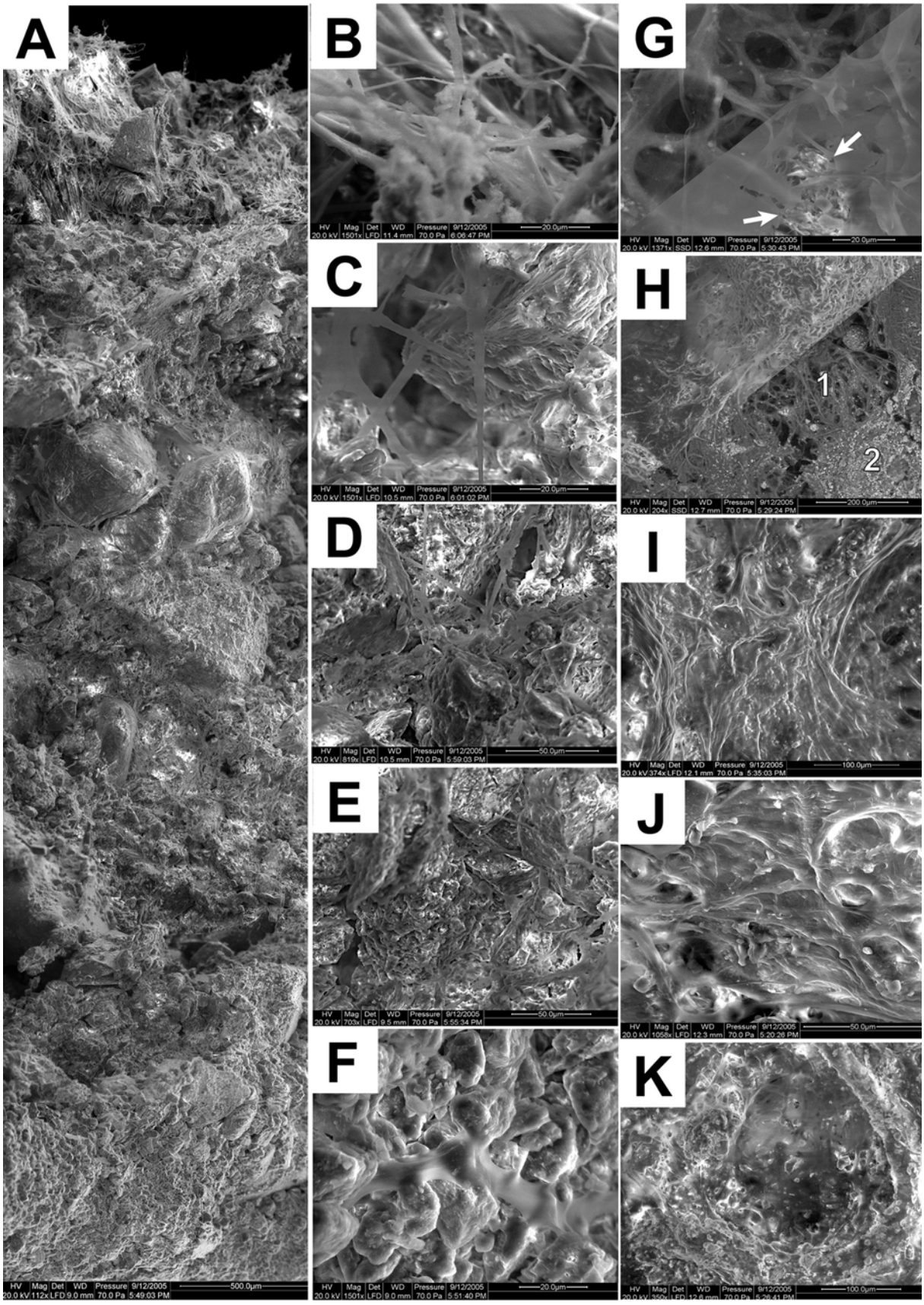

A
B
G
C
H
1
2
D
I
E
J
F
K

Figure 8(c)-2: A collection of SEM images of a dried piece of microbial mat (see Figure 8(c)-1A). (A) Mosaic of low magnification SEM images across the entire thickness of a dried mat sample (total thickness ~5 mm). The image shows a general downward decline in visible microbial filaments and a corresponding increase in mineral matter (quartz, carbonate particles, clay). The images in the middle row (B through F) are higher magnification images from the cross-section shown in (A) and are arranged top to bottom. (B) At the very top of the mat abundant dried filaments of *Oscillatoria* spp. and little mineral matter can be seen. (C) Somewhat below, a meshwork of dried filaments can be seen, that surround and hold together mineral grains, but there is still abundant pore space. (D and E) Further down into the mat the filaments are less conspicuous, porosity has decreased, and there is connecting matter between and on grains that is of variable morphology and which represents a mixture of dried filaments and extracellular polymer substance (EPS). (F) A close-up of a dried out strand of EPS that connects detrital grains. The images in the right row (G through K) are SEM photos of the mat surface. (G) Split backscatter (upper left) and secondary electron image of mat surface. The secondary electron image shows mainly surface topography which is smoothed by a film of dried out EPS. Where the EPS film is disrupted (arrows) we can see into lower layers of the mat. Backscatter electrons image density (lower right) and therefore "see" through the low density EPS surface and show the denser filaments embedded in it. (H) Another split image, but this time the upper left corner is the secondary electron (SE) image, and the lower right corner is the backscatter (BSE) image. The image demonstrates that although the surface may look more or less uniform in SE, this is mainly due to masking by the surficial EPS film. Beneath the surface (BSE) the mat may be heterogeneous, with some areas dominated by microbial filaments (area 1), and others by mineral matter (area 2). (I and J) Variable magnification SE images of mat surface with *Oscillatoria* spp. filaments and small mineral grains enclosed by dried out EPS matrix. (K) SE image of mat surface with mineral grains adhering to surficial EPS.

Observations from flume runs with "live" mat fragments

Moistened and revitalised mat fragments felt soft and pliable and the originally dried out mat surface had returned to a vibrant dark green colour. Mat disintegration over the first 24 hours of transport is visibly reduced (Figure 8(c)-4) in comparison with "dry" mat fragments. While there was a general increase in the number of fragments, most of the fragmentation occurred in the first 12 hours of the run (Figure 8(c)-4D). Even after 12 hours several fragments still measured more than 5 cm across, and fragment #1 still measured 5 cm after 24 hours of transport (see Figure 8(c)-4E). Between 12 and 24 hours, neither fragment size nor fragment numbers changed substantially (Figures 8(c)-4D, -4E). There was an initial loss of about 25% of mat material due to disintegration into mm-size or smaller particles over the first 6 hours of the experiment. Loss was minor or negligible over the following 18 hours of the experiment. The edges of fragments were ragged initially (Figure 8(c)-4A), but became quite smooth within the first 6 hours of the experiment (Figure 8(c)-4C).

Differences between "dry" (desiccated) and "live" (moistened) mat fragments

Comparing the results from the two flume runs (Figures 8(c)-3 and -4), it is quite clear that "live" mat fragments survive transport much better than "dry" fragments from the same mat. Considering the excellent survival of "live" mat fragments that were still several centimetres in size after 24 hours (Figure 8(c)-4) of transport, it is likely that these fragments would have been transported for another day or two without significant further degradation.

In both experiments, fragment size-decrease is most notable in the first 12 hours of transport. This probably reflects the fact that small fragments are more likely to travel in suspension, especially if they have lost most of their original mineral ballast. The density of the fragments is then only slightly larger than that of water, and even if they interact intermittently with the sand surface the impact forces are minor. However, whereas there was not much further reduction of fragment size after 12 hours in the case of "live" mat material, fragment size continued to decrease in the case of "dry" mat material, albeit more slowly than in the first 12 hours of the run.

Microscopic examination of mat fragments that were collected after the termination of the respective flume runs shows clearly that a biologically active mat surface is the reason for the observed differences in mat fragment behaviour. Both "live" and "dry" mat fragments were only approximately 1 mm thick (Figures 8(c)-5A and -6A) because most of the mineral grains of the lower portions of the mat (Figure 8(c)-2A) had been lost due to transport. The major difference between the two types of mat material was the presence of a tangled felt of active *Oscillatoria* spp.

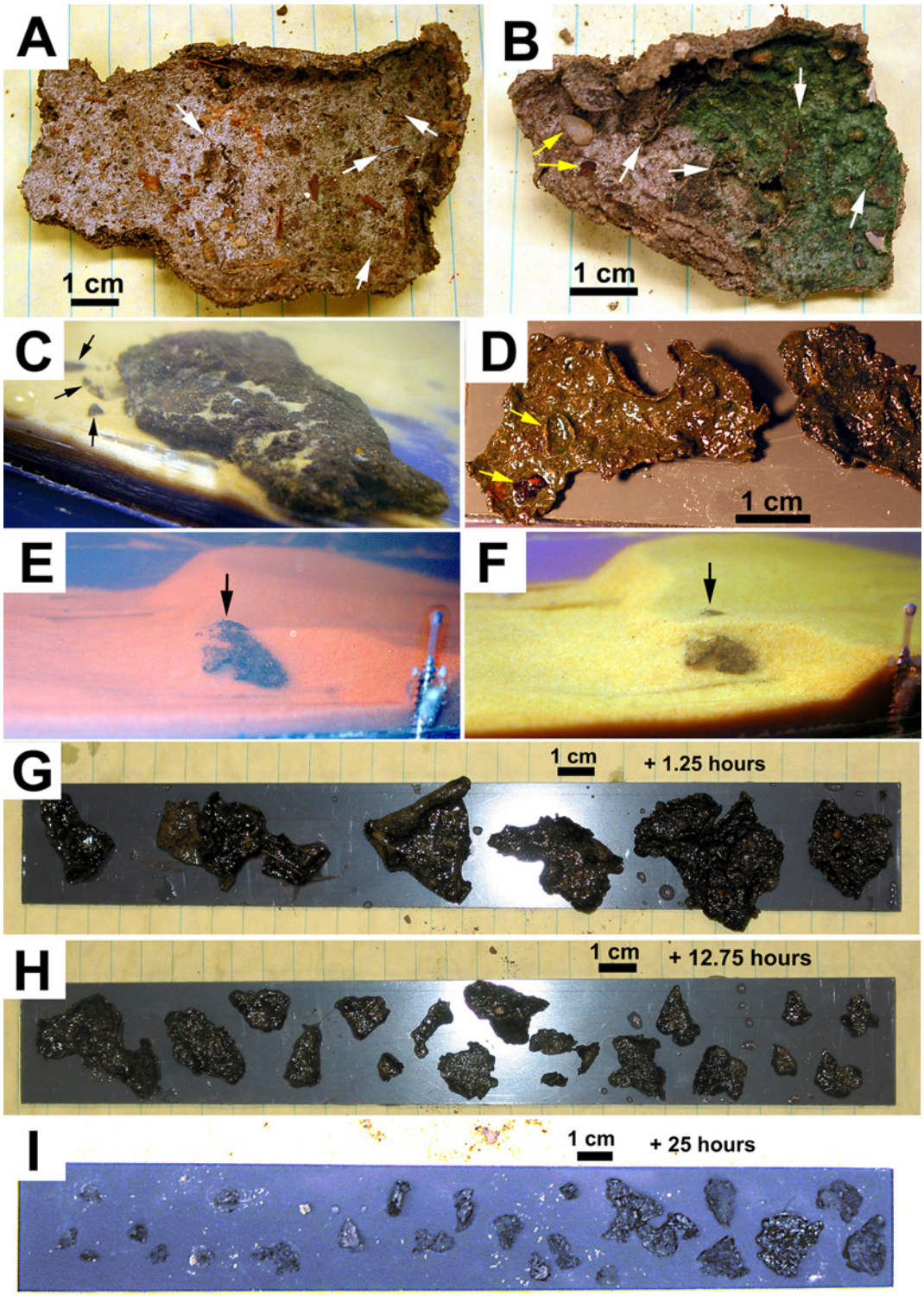


Figure 8(c)-3: Observations from flume run with dried mat fragments.
(A and B) Examples of mat fragments. Fragments have curled-up edges and embedded plant particles (brownish) and small pebbles and granules. White arrows point to existing fractures along which initial disintegration will begin. (C) The fragment from A has turned convex-up and stopped moving. Note scouring at upstream edge of fragment and breaking off of small pieces due to current drag (black arrows). (D) After one hour the initially 5 mm thick fragments have been reduced to thin (1–2 mm) leathery "skins". The fragment shown broke off the larger piece in B and can be identified because of the mould of a small pebble and a piece of plant matter (yellow arrows in B and D). (E and F) A mat fragment (black arrow) being buried by a migrating ripple. The pictures were taken 1 min apart. (G) Remaining large fragments after 1.25 hours. (H) Remaining large fragments after 12.75 hours. (I) Remaining recoverable fragments after 25 hours.

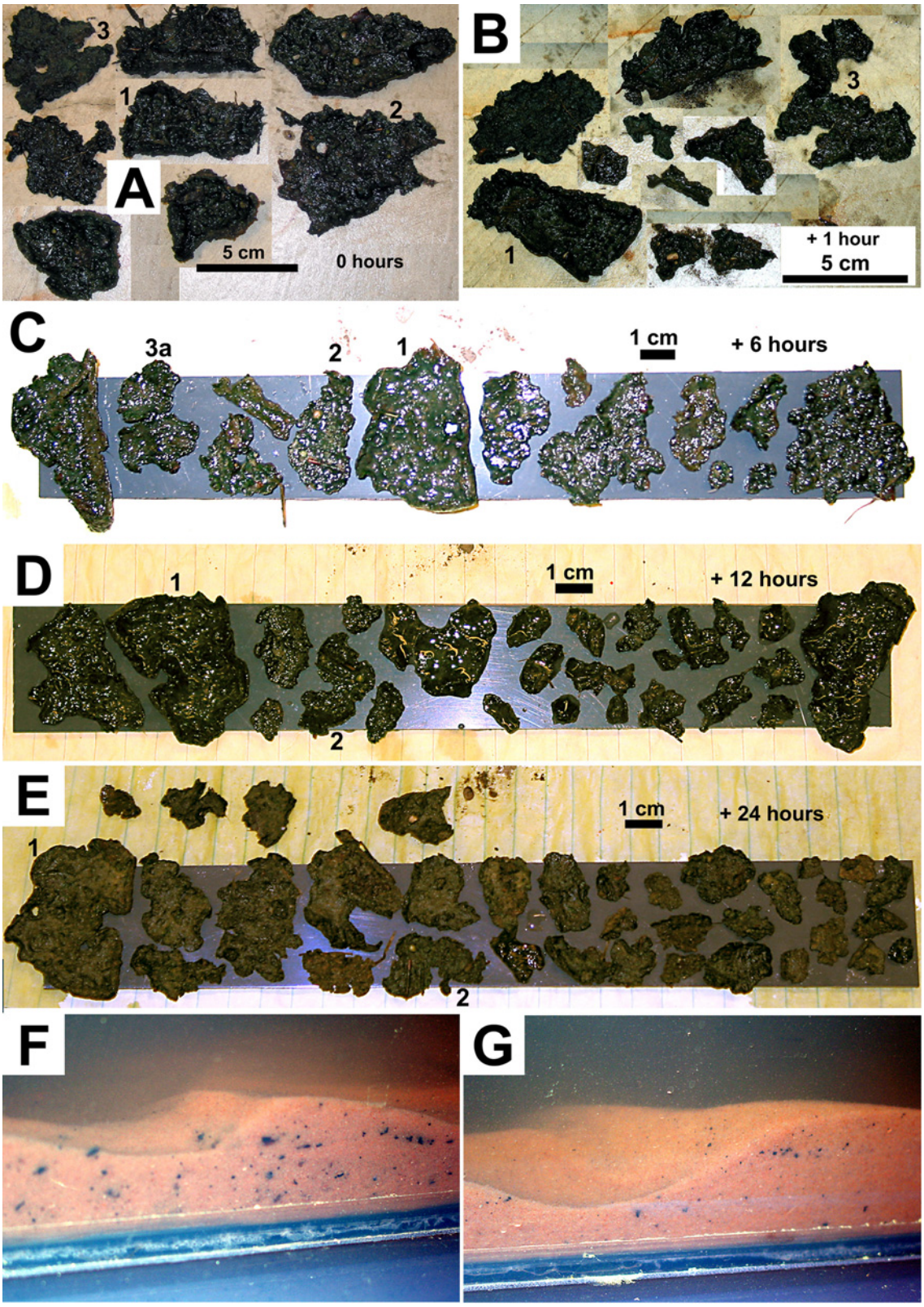


Figure 8(c)-4: Observations from flume run with wet "live" mat fragments.
(A) The eight mat fragments that were placed into the flume at the start of the experiment. The fragments are soft and flexible. (B) After one hour several samples are still largely unchanged, whereas others have broken into several pieces of a few cm across. (C) Recovered mat fragments after 6 hours. (D) Recovered mat fragments after 12 hours. (E) Recovered mat fragments after 24 hours. Some fragments with unique shape or components (marked 1 and 2) can be tracked through the course of the experiment. (F and G) Sand bed with ripples and incorporated dark particles that resulted from mat disintegration.

filaments at the surface of "live" mat material (Figure 8(c)-6), and the absence thereof in the case of "dry" mat material (Figure 8(c)-5). The surface of the latter was instead covered with a rehydrated film of EPS that contained old microbial filaments (Figure 8(c)-5B). The only viable *Oscillatoria* spp. filaments were found in the interior, protected by a thick cover of EPS (Figure 8(c)-5A). The surfaces of "live" and "dry" mats also differ in two other aspects. First, there is clear evidence of adhesion of new detrital material to the surface of "live" mat fragments (Figures 8(c)-6A, -6B). The sand in the flume was fine, well sorted quartz sand, whereas the detrital material attached to the original mat fragments was coarse, poorly sorted, and polymineralic (quartz and carbonate grains). Figure 8(c)-6A shows the addition of a layer of fine quartz grains at the surface of transported "live" mat that is not observed on the surface of transported "dry" mat (Figure 8(c)-5A). This difference can readily be attributed to the stickiness of freshly produced EPS and the upward growth of *Oscillatoria* spp. filaments (Figures 8(c)-6C, -6D, -6E) in "live" mat. Secondly, by comparison with untransported "dry" mat (Figures 8(c)-2I, -2J), SEM images of the surface of transported "dry" mat show that the surface has been roughened and that variably eroded old microbial filaments are now present at the surface. These features are best explained by abrasion of the EPS surface layer while the fragment travelled over the sandy flume bottom.

Implications for the rock record

There are several implications from these experiments for the interpretation of the sedimentary rock record. For example, physical diminution of eroded microbial mats during transport will produce abundant millimetre-sized particles that are buried in associated sands (Figures 8(c)-4F, -4G). However, erosion and transport of desiccated "dry" mat fragments is likely to produce a much larger proportion of small (millimetre-sized) mat debris than erosion and transport of fresh "live" mat fragments.

Finding large curved fragments (5 cm or larger) of "dry" mat buried in sandy sediments probably indicates burial shortly after onset of transport (probably within an hour) and close to their point of origin (a few kilometres at best). These time and distance constraints should be considered maximum estimates because in actual sedimentary systems erosion and transport is episodic, and typically related to short-lived erosive events (floods, storms, etc.) followed by deposition due to decreasing wave action and/or current flow (e.g., Reineck and Singh, 1980). Thus, unlike in our flume experiments, net deposition is likely to prevail after initial erosion, and burial of a mat fragment will occur earlier in transport history and closer to its point of origin.

Finding significant amounts of centimetre-size "dry" mat debris in an ancient sandstone should probably be taken as an indication that the source of this material was at best no further than a day's travel or 30–50 km away, and quite probably originated closer. In contrast, the "self-repair" potential of "live" mats can potentially allow centimetre-size fragments to travel for multiple days and distances of the order of hundreds of kilometres. This effect could be significant in a setting with very small net sedimentation rates, and would be negligible in cases of high net sedimentation. In the latter case, because of rapid burial of mat fragments (Figures 8(c)-3E and -3F) there should not be much difference from the travel time and distance estimated for "dry" mat material.

The thickness of microbial mats that grow on sandy substrates can be in excess of a centimetre when a fresh mat is examined (e.g., Gerdes and Krumbein, 1987), but in the illustrated experiments only the topmost layer with abundant EPS and microbial filaments (Figure 8(c)-2A) showed a high degree of cohesiveness during transport experiments. Whereas one can sample a centimetre-thick mat because bacterial mucilage holds together the lower portions of the mat, during transport this portion disintegrates rapidly and leaves mainly a leathery membrane of 1–2 mm thickness (Figure 8(c)-3E). Thus, mat fragments that have been transported for more than a short distance (less than 1 km) are likely reduced to thin sheets. Conversely, if we find thick (5 to 10 mm) microbial sand chips in the rock record (cf. Pflüger and Gresse, 1996) it can probably be taken as an indication that they were transported for a short distance only.

One should point out in this context that the types of cyanobacteria that dominate a given mat can exert an influence on the transport behaviour. For example, in mats dominated by *Lyngbya* spp. or *Microcoleus chtonoplastes*, the highly cohesive surface layer with felted filaments may be as much as 10 mm deep (G. Gerdes, personal comm., 2006). Consequently, such mats may be able to retain their initial thickness for greater transport distances than the observed *Oscillatoria* spp. mats. No experimental work with such strongly felted mat fragments has been conducted to date.

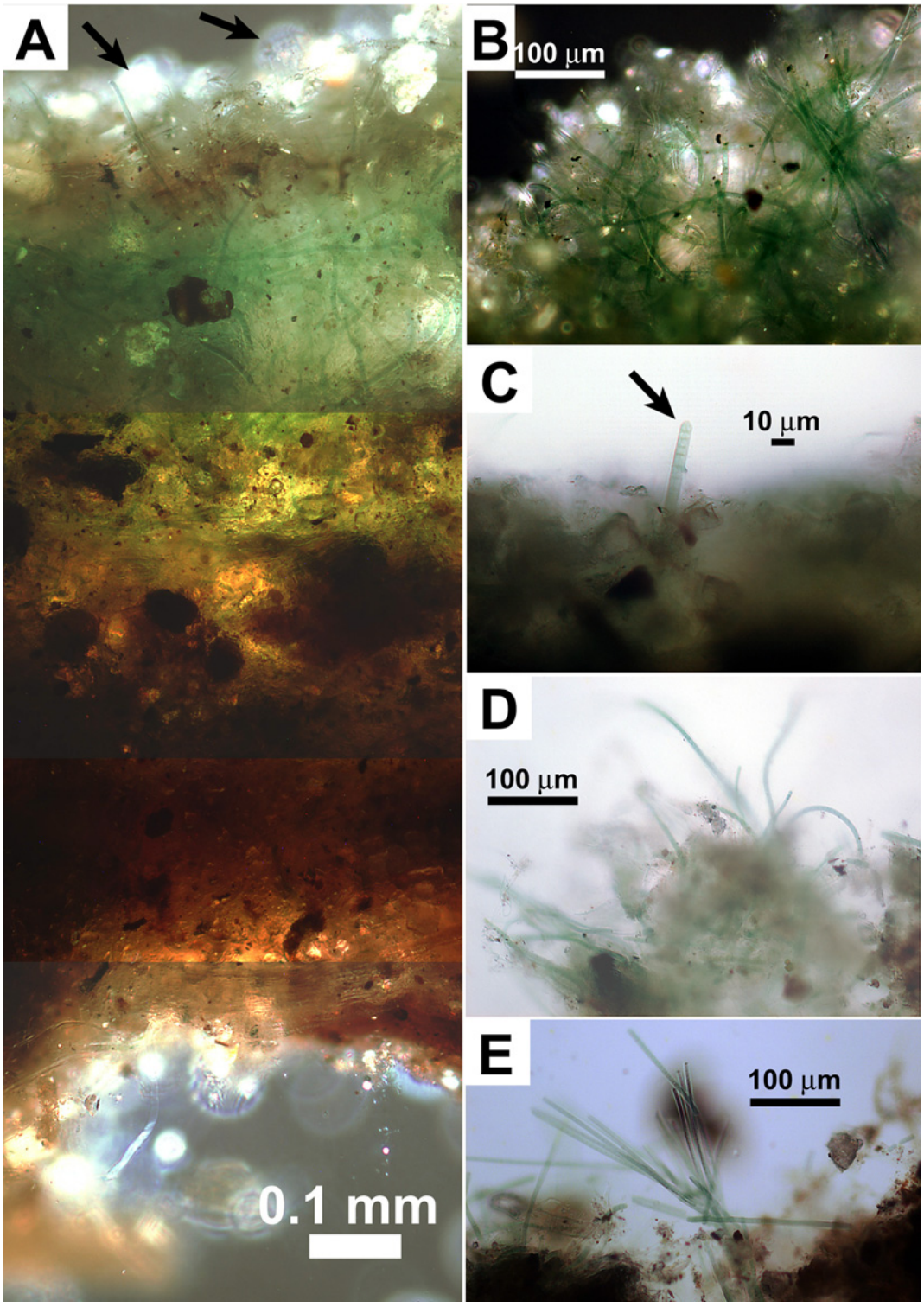


Figure 8(c)-5: A collection of photomicrographs through a "live" mat sample that was retrieved after flume run.

(A) Cross-section through mat that shows a green top portion because of actively growing *Oscillatoria* spp. filaments. The lower, darker, portion of the sample consists of detrital mineral grains held together by dead filaments and EPS. A surficial layer of quartz grains (whitish; black arrows) is attached to the underlying microbial layer (green). This mat sample is much thinner (1.2 mm) than the mat prior to transport (5 mm, Figure 8(c)-2) because most of the more loosely attached lower sediment (Figure 8(c)-2) has been lost during transport. (B) Close-up of the actively growing top portion of the mat. *Oscillatoria* spp. filaments are weaving around newly trapped surficial sand grains. (C) Close-up of *Oscillatoria* spp. filament (arrow) that is poking through the quartz grain encrusted surface. (D and E) Bundles of *Oscillatoria* spp. filaments growing at the mat surface.

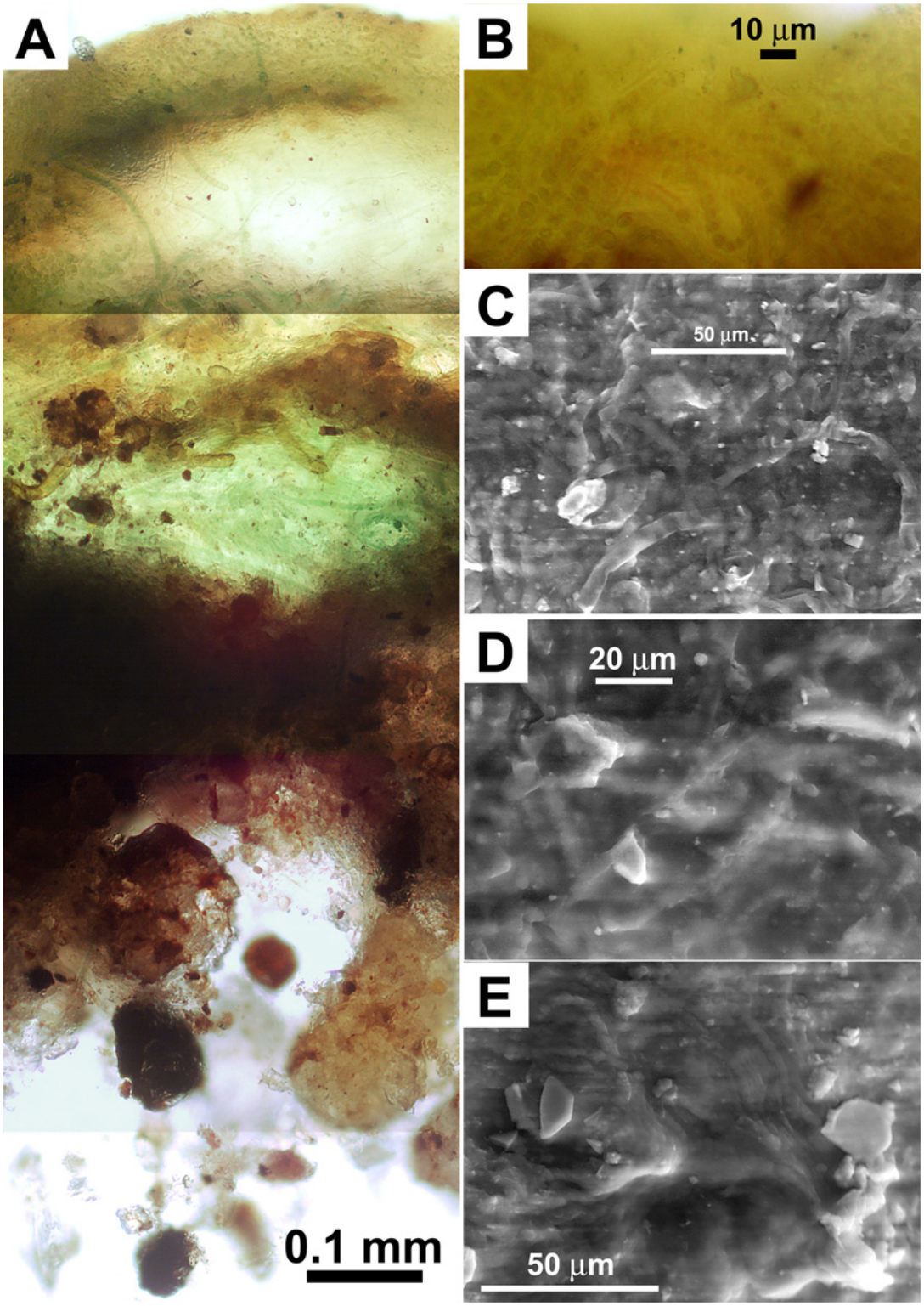


Figure 8(c)-6: A collection of photomicrographs through a "dry" mat sample that was retrieved after flume run.

(A) Cross-section through mat that shows a yellowish top with some filaments inside. This appears to be mainly rehydrated EPS with embedded dead cyanobacterial filaments. (B) Enlargement of this top zone that shows entombed cyanobacterial filaments. Beneath this top layer of EPS, still green filaments (probably *Oscillatoria* spp.) are hidden in the core zone of the fragment. (C through E) SEM images of the mat surface. By comparison with images taken before the flume run (Figure 8(c)-2), these surfaces are rougher and show exposure and erosion of textural features such as cyanobacterial filaments. These features are due to abrasion of the mat while it travelled over the sandy flume bottom.

Summary

The above discussion indicates that it can make a difference to our conclusions whether a mat fragment was eroded from a dried out mat, or from a biologically active ("live") mat. It is therefore desirable to distinguish between the two mat fragment types when analysing the rock record. Presence of curved fragments can probably be taken as a good indication of a desiccated mat source, whereas signs of soft deformation, such as large (5 to 10 cm across) mat fragments that show roll-ups or fold-overs (Simonson and Carney, 1999; Schieber, 1999) would suggest that the fragments were more likely eroded from a "live" mat.

By contrasting "live", photosynthetically active mat fragments with desiccated fragments from the same occurrence, flume experiments allowed a determination of the geological significance of active microbial surface binding on the durability of microbial mat fragments in a sandy depositional system. Both types of mat material undergo an initial rapid reduction of size. Size degradation slows down once the population of mat fragments largely consists of centimetre-size fragments and transport is mainly in suspension instead of as bedload. However, whereas the size of "live" fragments stabilises at that point, "dry" mat fragments suffer continued size reduction due to abrasion. Desiccated mat fragments behave in a brittle fashion during initial transport, break down into smaller fragments than the flexible "live" fragments, and show evidence of surface abrasion of the dried organic matrix. Under conditions of significant net sedimentation and lower flow regime (ripples) many mat fragments are likely to be buried by migrating ripples early in transport history, close to their point of origin.

Unless strongly felted, microbial mat fragments will tend to lose most of their attached ballast of sediment grains early in transport history and turn into thin leathery films of one to two millimetre thickness within an hour. Thus, under upper flow regime conditions all but the largest of these fragments will travel in suspension due to the small density contrast between mat fragments and water, and may therefore travel considerable distances.

8(d). HYDRAULIC CONDITIONS AND MAT-RELATED STRUCTURES IN TIDAL FLATS AND COASTAL SABKHAS

H. Porada, E. Bouougri, J. Ghergut

Introduction

Under specific conditions, cohesive microbial mats may spread out over large areas in the intertidal to lower supratidal zones of tidal flats and coastal sabkhas. In such environments where abundant energy is available from solar irradiation, and CO_2 from the atmosphere, supply of water is the main factor controlling biological activities. Beneficial for initial microbial colonisation and establishment of extensive mats are: (i) low hydrodynamic energy; (ii) a fine-grained sandy to silty substrate; (iii) low rate of sediment supply and deposition; (iv) suppressed activities of marine mat consumers and burrowers; (v) a steady groundwater flow from the hinterland (see Noffke, 1998b; Gerdes et al., 2000a). Examples of extensive microbial mats in such environments have been described from numerous localities in the arid and humid zones, e.g., from the Persian Gulf coast (e.g., Kendall and Skipwith, 1969; Kinsman and Park, 1976), the Mediterranean coast of southern Tunisia (Gerdes et al., 2000a; Noffke et al., 2001b), the northeastern coast of Massachusetts (Cameron et al., 1985, with extensive bibliography), and the southern North Sea coast of Germany (e.g., Reineck, 1979; Gerdes et al., 1985c, 2000b; Noffke et al., 1996).

In all these cases, the laminated microbial mat is composed of photoautotrophic, filamentous cyanobacteria (e.g., *Microcoleus chthonoplastes*, *Lyngbya aestuarii*) and coccoid cyanobacteria (e.g., *Entophysalis* sp. or *Synechococcus* sp.), which together form the cohesive upper part of the mat, usually between 1–3 mm thick. Underlying are zones with sulphate-reducing bacteria and, in many cases, various anoxygenic phototrophic bacteria (e.g., purple and green sulphur bacteria).

Microbial mats that repeatedly are subaerially exposed, as in the intertidal/lower supratidal zones, tend to develop strongly cohesive, 'felty' layers in the upper photic zone, and a 'leathery' surface. The internal structure of the 'felty' layers is best described as a "condensed fibrillar meshwork" consisting of more or less parallel, "horizontally stretched ensheathed filament bundles" (Gerdes et al., 2000b, p. 285) which in neighbouring laminae develop perpendicular orientations, leading to a kind of 'plywood texture' (Fenchel and Kühl, 2000). A further component in microbial mats is various extracellular polymeric substances (EPS). They are secreted by coccoid cyanobacteria in considerable volume, surround the bacterial cells and sediment grains, and some types may exist in an aggregated gel state of high cohesiveness (Decho, 1994; Stal, 2000). In many modern mats, EPS form a 'leathery' surface film which combines high mechanical resistance with very low permeability, inhibiting even the escape of gas rising up from below.

Altogether, the upper part of epibenthic cyanobacterial mats forms a continuous, strongly cohesive zone of low permeability, separating the substratum from the atmosphere and protecting it against water loss. *Vice versa*, the layer of water-saturated sediment below the sealing mat may be described as a 'confined aquifer'. Therefore, numerical simulations as applied to respective situations in porous media hydraulics, may be used to compute the hydraulic conditions prevailing in the confined mat substratum.

This paper is focused on some implications, both biological and physical, arising from upward directed force of hydraulic pressure, locally providing a potential for liquefaction in the mat substratum. It will be argued that hydraulic 'upward pressure' strongly contributes to the survival of mats during dry seasons, that it may trigger localised microbial growth at cracks, and that it may cause local ascent of sediment in the mat substratum. The tidal flats of Bhar Alouane in southern Tunisia (see Figure 8(d)-1) will serve as an example, but similar conditions are also expected at Sabkhas El Grine, Jellabia, El Mdeina, and Bou Jemel, all in the same region. Modelling of the hydraulic conditions, considering also tidal influences, is presented in Appendix A.

Some basic considerations about hydraulics

Water completely filling the pore space and flowing downslope through a confined aquifer is under pressure. This 'hydraulic pressure' is a function of the difference in elevation between points where the flow of water enters the confined layer and where it leaves it ('hydraulic heads'). It has the same value along 'equipotential lines'

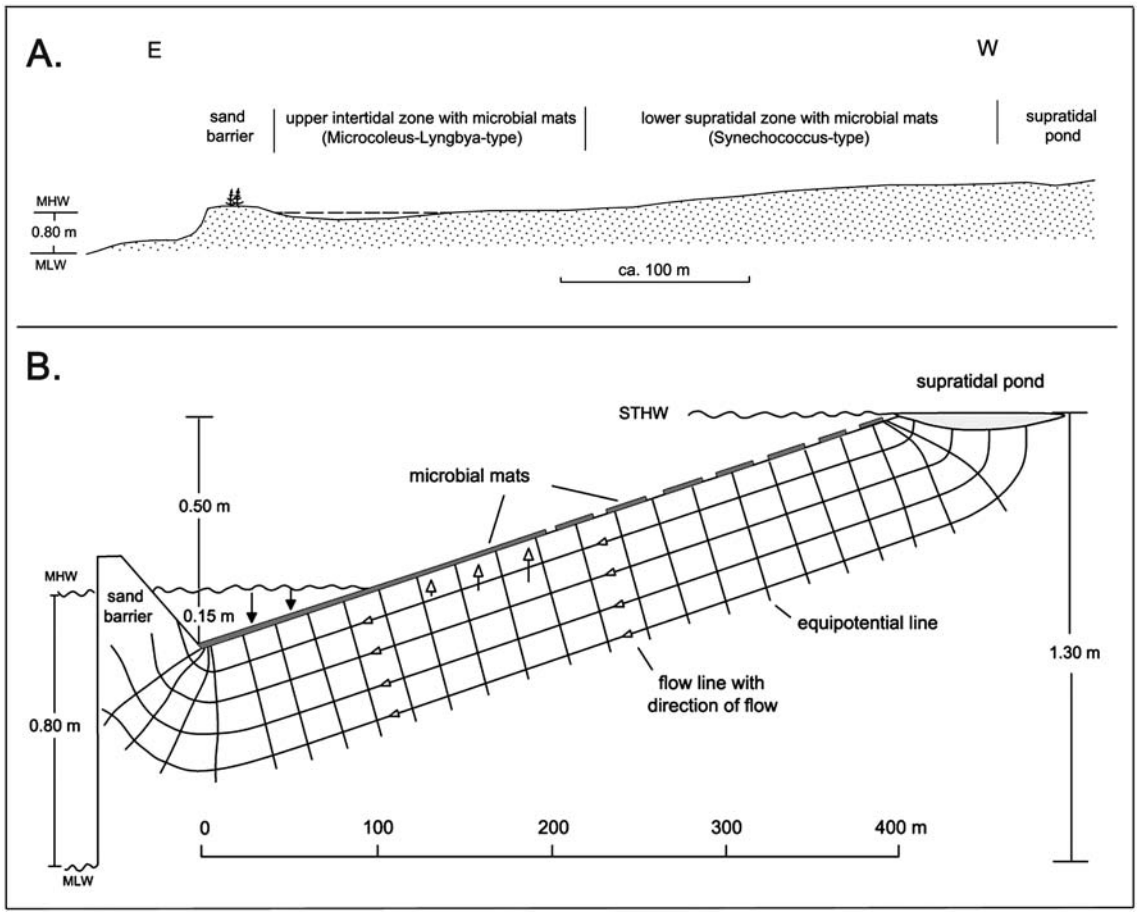


Figure 8(d)-1: Siliciclastic tidal flat hydraulics.
(A) Schematic section across Bhar Alouane tidal flat, Mediterranean coast of southern Tunisia. Tidal range is ca. 0.80 m. Dashed line indicates level and distance up to which the tidal flat is regularly inundated at high tide. MLW = mean low water; MHW = mean high water. Modified after Noffke et al. (2001b). (B) Scenario of a siliciclastic tidal flat protected behind a sand barrier and regularly flooded through tidal channels at high tide. A supratidal pond is assumed to have been filled with water at spring tide or during a storm. Solid arrows indicate hydrostatic pressure; open arrows indicate hydraulic 'upward pressure'. STHW = spring tide high water.

(see Figure 8(d)-1B), but continuously decreases downslope, in the direction of flow. Hydraulic pressure is thus greatest in the upper part of the slope, where the confining mat begins. It acts against the mat as an 'uplift force' or 'seepage pressure' (e.g., Watson and Burnett, 1995) and may lead to detachment of the mat ('floating failure') and subsequent seepage of groundwater (Figure 8(d)-2A). Downslope, where the sea temporarily encroaches upon the mat, hydraulic pressure is superimposed by hydrostatic pressure resulting from the load of sea water, increasing in total the 'pore water pressure' in the sediment. From the hydraulic perspective, liquefaction of the sediment may occur when the 'pore water pressure' becomes equal to or exceeds the 'effective stress' induced by the weight of the sediment grains ('excess pressure head'). This may be achieved either if the hydraulic head is raised (e.g., after heavy rains in the hinterland) or if the hydrostatic pressure is increased. The latter is usually the case in the intertidal zone where alternately increasing and decreasing hydrostatic pressures are exerted on the mat surface, according to tidal frequencies.

If evaporation occurs, hydraulic pressure resulting from elevation differences of heads may be complemented by a vertical hydraulic gradient resulting from replacement of the evaporative water-loss near the surface. This 'evaporative pumping' (Hsü and Siegenthaler, 1969) creates an additional uplift force depending on the rate of loss of pore fluids. It will be most effective where microbial mats are not or only scarcely developed and the sediment surface is subaerially exposed, but may also take place beneath mats during low tides to replace water that is lost by evaporation or consumed by the mat organisms.

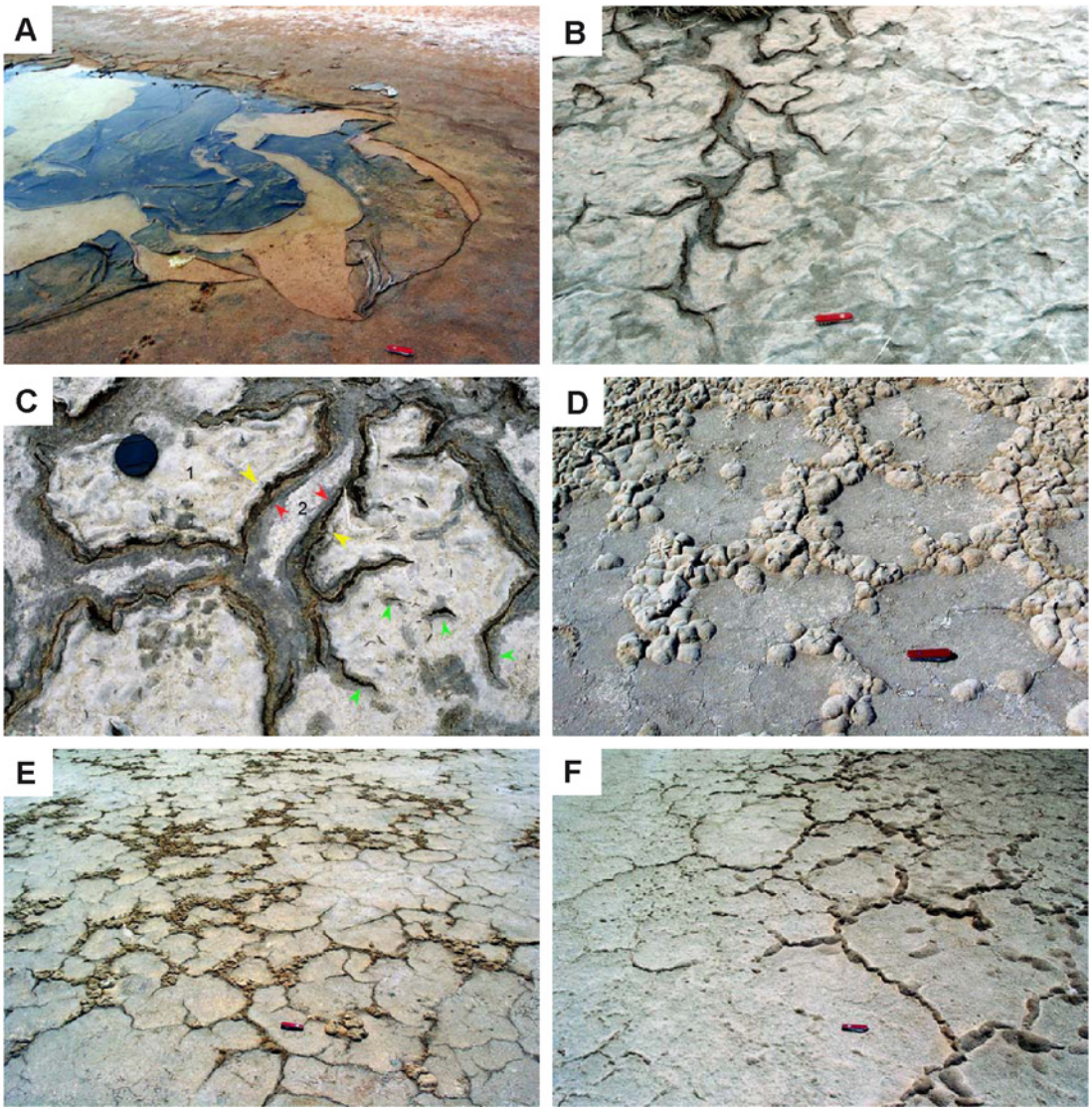


Figure 8(d)-2: Possible implications of elevated seepage pressure in confined sediment underneath microbial mat.

(A) Detached and floating mat in supratidal pond. Mat detachment and outflow of groundwater is interpreted here as 'floating failure' due to groundwater recharge after heavy rainfall in the hinterland. Mat detachment and flotation may, however, also have resulted from excessive photosynthetic gas production or may have occurred after flooding of a desiccated mat. Sabkha El Grine, southern Tunisia. Scale (knife) is 8 cm. (B) Strongly cohesive microbial mat with 'leaking' shrinkage cracks. Cracks and crack margins are overgrown by new microbial layers due to availability of water rising up from below. Sabkha Jellabia, southern Tunisia. Scale (knife) is 8 cm. (C) Details of shrinkage, 'leaking cracks' and microbial overgrowth in subaerially exposed mat. Old mat (1) with first generation cracks (yellow arrows) overgrown by younger mat (2) undergoing renewed cracking (red arrows). Dark zones along new cracks indicate elevated humidity and microbial activity. Green arrows show new cracks accompanied by increased microbial activity in old mat. Sabkha Jellabia, southern Tunisia. Scale (lens hood) is 6 cm. (D) Structures resulting from localised microbial growth along narrow shrinkage cracks in flat mat. Doming supported by a *Microcoleus* mat, irregular shape of these growth-induced 'mat expansion structures' ('petees') suggests preferential activity of coccoid bacteria. Upper intertidal to lower supratidal zone, Sabkha Bou Jemel, southern Tunisia. Scale (knife) is 8 cm. (E) Domal 'mat expansion structures' resulting from localised microbial growth along polygonally arranged shrinkage cracks. Groundwater discharge at crack openings is considered responsible for local growth activity. Upper intertidal to lower supratidal zone, Sabkha Bou Jemel, southern Tunisia. Scale (knife) is 8 cm. (F) Round-crested bulges following trends of polygonal shrinkage cracks. The bulges are interpreted as 'mat expansion structures' resulting from localised microbial growth along 'leaking cracks'. Desiccated, shallow, supratidal pond, Sabkha Bou Jemel, southern Tunisia. Scale (knife) is 8 cm.

A naturally occurring example

As a natural example for hydraulic modelling, the tidal flats of Bhar Alouane in southern Tunisia have been selected (Figure 8(d)-1A). The low-gradient tidal flats extend over several hundred metres inland and are separated from the open sea by a sand barrier which is stabilised by scattered vegetation. The upper intertidal zone behind the barrier is regularly inundated through narrow tidal channels at high tides. The flats are extensively covered, up to the supratidal zone, by microbial mats which have been described in some detail by Noffke et al. (2001b). Two main mat types have been distinguished by these authors. Firstly, a dark, thick, multi-layered mat dominated by filamentous cyanobacteria, mainly *Microcoleus chthonoplastes* and *Lyngbya aestuarii*. This type is developed in the regularly inundated intertidal zone, locally overlying biolaminites, and in some supratidal ponds. It tends to develop large, polygonally arranged shrinkage cracks which, however, are soon overgrown by new mat layers. Secondly, a brownish, thin, mono-layered mat is found, formed mainly by coccoid cyanobacterial taxa, predominantly *Synechococcus* sp. This mat develops a tough, leathery and very irregular surface, and overlies much of the uppermost interdidal and supratidal zones. Shrinkage cracks are quite rare and usually small in this type of mat. Average annual precipitation in this part of Tunisia is about 175 mm with a large variability, however, between 530 and 40 mm/a, and with a generally high occurrence of excess rainfall and surface runoff events.

Modelling results and implications

Main results of the hydraulic modelling (see Appendix A) include: (i) that in coastal sabkhas like Bhar Alouane, considerable upward directed hydraulic pressure (seepage pressure) is built up in the mat substratum; (ii) that over much of the intertidal and supratidal zones, hydraulic pressure attains sufficiently high values to create a potential for liquefaction down to a few centimetres in the sedimentary mat substratum; and (iii) that seepage pressure increases upslope under steady groundwater flow conditions, but decreases in the same direction as the flow of groundwater ceases and tidal hydrodynamics gain in importance. Based on these results the following implications are envisaged:

(1) The results, in general, suggest that groundwater supply to the overlying mat may be sustained even after months of subaerial exposure, as long as traces of groundwater exist in the confined sediment below. This is due to hydraulic 'upward pressure', implying upward movement of groundwater. Indeed, it is observed that in the supratidal zone, mats may still contain moisture even after long periods of subaerial exposure. Thus, hydraulic 'upward pressure' may be a major factor in maintaining microbial mats over dry seasons.
(2) If the sealing mat is interrupted by cracks, however, hydraulic pressure will lead to groundwater discharge at the surface. At such 'leaking cracks', availability of water will trigger microbial growth processes in the near-surface population, resulting in overgrowth of the crack opening and the crack margins (Figures 8(d)-2B, -2C). This 'self-healing effect' keeps the mat intact and resistant against tractional forces acting on the surface (e.g., wind, water currents) and prevents the mat substratum from further groundwater loss.
(3) At narrow 'leaking cracks', rapidly initiated microbial growth may spatially not be accommodated in the crack and adjoining mat, leading to bulges and domes along the cracks (Figures 8(d)-2D to -2F). Such localised 'mat expansion structures' ('petees' in the original sense of Reineck et al., 1990; see Chapter 6(c)) may be arranged in a polygonal distribution tracing the original shrinkage crack pattern. The shape of the individual structures appears to depend on the microbial species which reacts fastest or most effectively on the sudden availability of water. Thus, bulges (Figure 8(d)-2F) may indicate that mainly filamentous cyanobacteria were involved, whereas the domes in Figures 8(d)-2D, -2E may have resulted from the association between filamentous (*Microcoleus chthonoplastes*) and coccoid cyanobacteria, whereby the filamentous organisms have contributed to the coherent arches, and the coccoids according to their specific way of cell division to irregularities at micro-scales.
(4) Isolated domes, occasionally observed on subaerially exposed mats in supratidal zones (Figure 8(d)-3A), may also originate from localised water availability. In the supratidal zone of Bou Jemel where gypsum encrusted surface mats of mainly coccoidal bacteria are developed, isolated domes show a close relationship to vertical burrows of rove beetles (*Bledius* sp.; G. Gerdes, personal comm., 2006). It is envisaged that traces of water were seeping out of the burrows thus triggering localised microbial growth and concomitant precipitation of gypsum.
(5) The potential for liquefaction computed for parts of the intertidal/supratidal zones implies that in the mat substratum, grains may momentarily float under effective stress conditions tending to zero, thus loosening the packing in the uppermost millimetres to centimetres of the confined layer. Due to the upward directed force of the hydraulic pressure (possibly complemented by 'evaporative pumping'), an upward movement of grains

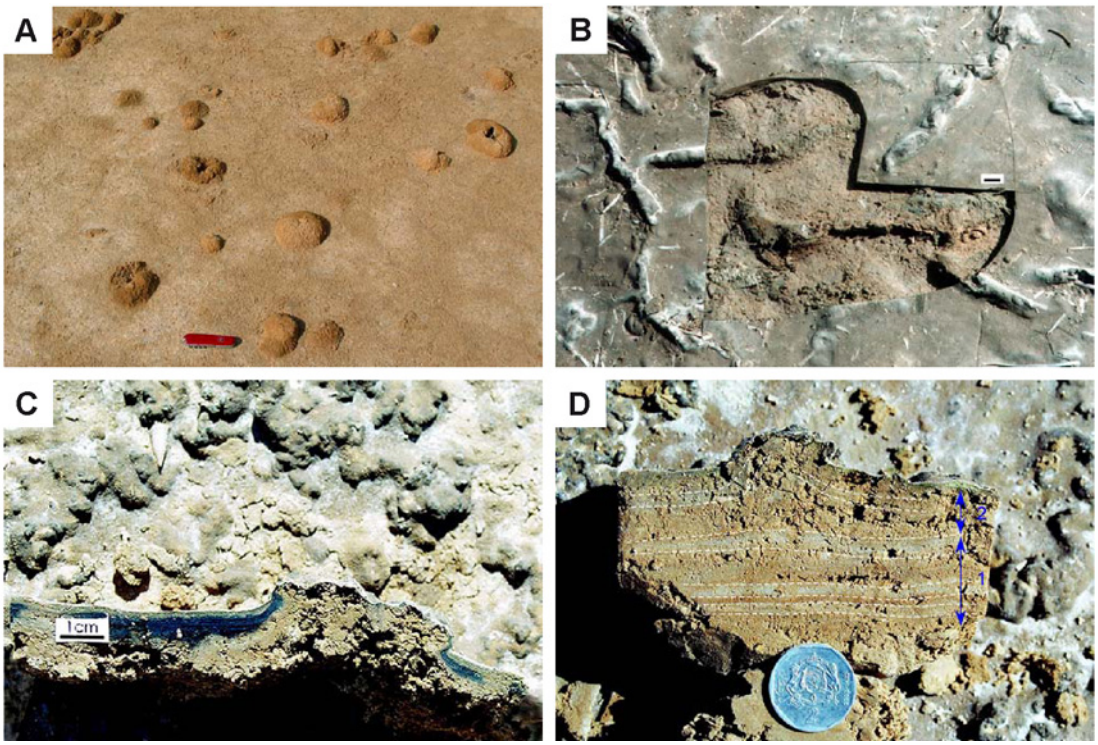


Figure 8(d)-3: Possible implications of seepage pressure and a potential for liquefaction in confined sediment underneath microbial mat.

(A) Isolated domal structures developed on thin, gypsum-encrusted microbial mat of mainly coccoid cyanobacteria. The domes have formed above vertical burrows of rove beetles (*Bledius* sp.). The burrows provided pathways for seepage of groundwater triggering local microbial growth and precipitation of gypsum. Supratidal zone, Sabkha Bou Jemel, southern Tunisia. Scale (knife) is 8 cm. (B) Microbial mat with linear and irregular bulges, filled from below by ascending sediment of the mat substratum. Scale is 2 cm. Bhar Alouane tidal flat, southern Tunisia. (C) Section across 'pustular', *Synechococcus*-type mat showing surface irregularities filled from below by rising sediment. Surface features of the mat are seen in background (upper part of photograph). Sabkha El Mdeina, southern Tunisia. (D) Section across microbial mat with bulge filled by sediment rising up from the mat substratum. Dashed lines indicate layers of undisturbed bedding (1) overlain by disturbed layers in the top 15–20 mm (2). Supratidal zone, Sabkha El Grine, southern Tunisia. Scale (coin) is 24 mm.

and water may then be anticipated. This effect may lead to a gradual 'filling from below' of bulges and folds developed in the mat. Even small irregularities of the overlying cohesive mat may be traced in the substratum and become preserved after burial (Figures 8(d)-3B to -3D. Also shrinkage cracks, if not instantaneously overgrown by new microbial layers, may become filled from below in this way. The process of contemporaneous, hydraulic 'upward pressure'-induced sediment ascent may thus be one of the fundamental mechanisms leading to the preservation of a range of mat-related structures. These may be considered as 'subsurface structures' according to their mode of formation. Sediment ascent and 'filling from below' will be effective mainly in the upper intertidal zone under 'normal' conditions, but may also take place in the supratidal zone after groundwater recharge due to storm-induced flooding or heavy rainfall in the hinterland.

Finally, it has to be stressed that hydraulic conditions and resulting mat-related structures as described in this paper, only apply to the intertidal to supratidal zones of tidal flats/coastal sabkhas, particularly of the arid to subarid climate zone. In other environments, similar structures may evolve from different processes.

APPENDIX A

Modelling hydraulic conditions in a sediment layer confined beneath a microbial mat

As previously described in the text, upwardly directed 'hydraulic pressure' (seepage pressure) is implicit when water completely filling the pore space is flowing downslope through a confined aquifer. In the following modelling,

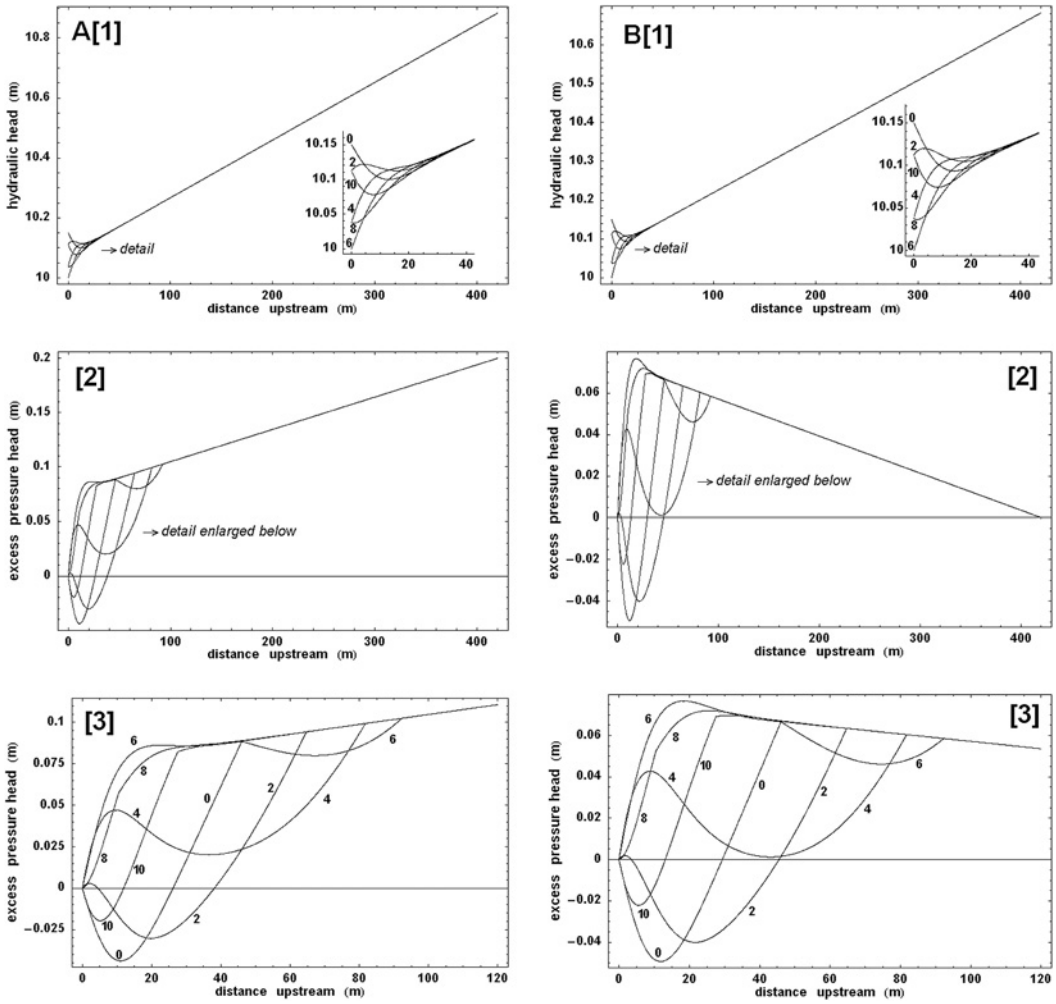


Figure 8(d)-4: Hydraulic head profiles.
Spatial distribution of hydraulic head and of excess pressure head: case A (plots on the left, A) and case B (plots on the right, B). The head profiles ($A_{[1]}$, $B_{[1]}$) are almost identical but the excess pressure head, i.e., the energy available for liquefaction ($A_{[2]}$, $B_{[2]}$) is lower in case B, and generally decreases with the distance from the sand barrier, vanishing in the vicinity of the pond. Within some 90 m from the sand barrier, the thickness of the liquefied layer oscillates in both cases, experiencing periodic 'freezing'; beyond about 90 m distance from the sand barrier, the liquefied thickness no longer varies with time (tide influence is no longer felt). Labels "0", "2", ..., "10" on the zoom-in plots ($A_{[3]}$, $B_{[3]}$) indicate hours elapsed from high-tide. Simulation parameters: aquifer length: 420 m, geodetic slope: 1/615, hydraulic conductivity: 10^{-5} m/s, aquifer thickness: 10 m, storativity: 2×10^{-2} (or 2×10^{-3} m^{-1}), maximum tide height: 15 cm, water level in pond: 20 cm (case A), 0 (case B).

the tide-modulated distribution of this pressure will be calculated. Additionally, the question is posed whether, and under which conditions, 'hydraulic pressure' may attain values sufficient for liquefaction. This is of particular interest as potential for liquefaction would allow grain displacement and structural changes in the sediment underneath microbial mats.

Boundary conditions

Boundary conditions for hydraulic modelling (Figure 8(d)-4) are based on data derived from the natural example described above in the text. Conditions embrace a low-gradient, seaward sloping flat sediment surface that is continuously covered by a quasi-impermeable surface layer. The sediment confined beneath the sealing surface layer is water-saturated and, following the 'flood water recharge model' of Butler (1969), a steady or periodic downslope groundwater flow from the hinterland or from supratidal ponds that were filled with water during spring tides, storms or rainfalls is assumed. The grain size of the sediment is in the range of fine-grained sand. Tidal waters encroach upon the surface, up to a distance of 100 m from the sea, at high tides.

Modelling hydraulic conditions in the confined layer

In the following, it will be shown how tide-modulated seepage pressure distribution is computed for a gently-sloping confined aquifer, and how conditions for liquefaction of an unconsolidated sand layer at the aquifer-top can be derived. Two cases will be considered: Case A is a time when the groundwater flow is still strong, visualised by a completely filled supratidal pond. Case B is a later point of time when the groundwater flow is waning to almost ceasing, but traces of water are still present (the pond is close to drying out).

For a loosely-granular aquifer layer, a criterion for liquefaction onset can be formulated in terms of the weight of an individual grain to be displaced locally by virtue of seepage pressure, whereas for liquefaction across a finite layer thickness a condition can be formulated in terms of the weight of the corresponding grain-filled column to be displaced by the action of seepage pressure over a finite height. Denoted by $h = h(x, z)$, the hydraulic head driving water flow ($v = K \cdot \nabla h$) in the aquifer (treated as two-dimensional, with geodetic height z and longitudinal coordinate x), the seepage pressure at point (x, z) is $P(x, z) = \rho_w g(h(x, z) - z)$ and it will exceed the weight pressure of a single grain if $h(x, z) - z > \rho_g d_g/(n_0\rho_w)$, in which n_0 denotes the undisturbed (initial) porosity, d_g a characteristic grain size, ρ_g the bulk grain density and ρ_w water density. By this criterion, very little seepage pressure (just a few millimetres) would be sufficient to lift a single grain against its own gravity, were there no further cohesion or confining (downward) forces, including the weight of the material column on top of the grain. For seepage pressure to displace against gravity a whole grain-filled column of undisturbed porosity n_0 and thickness δ_{liq} (neglecting any cementation, cohesion and contact forces), the seepage pressure head $h(x, z) - z$ must exceed $\delta_{\text{liq}}\rho_g/\rho_w$, the result being in the range of 3–4 times the thickness δ_{liq}. For instance, to achieve liquefaction across the topmost centimetre of unconsolidated granular aquifer material, the seepage pressure head at the aquifer-top must exceed 3–4 cm.

As mentioned before, this criterion relies on the idealised assumption that there are no further confining (downward) forces acting on the grain layer at the aquifer-top. In reality, the aquifer will either be confined, which means additional downward forces acting on the material at the aquifer-top, or it will have a phreatic surface at which $h(x, z) - z \to 0$. So, the liquefaction criterion formulated in terms of 'material column weights' will only find its application in certain exceptional situations in which, for instance, the aquifer may be treated as confined, as regards the hydraulic flow field, but the confining force on the aquifer-top may be considered as negligible, as regards force balances. One such exceptional situation is that of a shallow aquifer under direct tidal influence and 'confined' by a thin microbial mat as described before.

The time-periodical distribution of seepage pressure head $p(x, z, t) \to p(x, t)$ at the aquifer-top is computed for peritidal conditions in the sandy aquifer under the following simplifying assumptions:

(1) The aquifer-base is horizontal ($z = 0$), the aquifer-top $z(x) = B + \gamma x$ is gently sloping with constant geodetic slope $\gamma \ll 1$, thus the aquifer extends from $x = 0$ to $x = L$ with approximately constant thickness (B) and transmissivity ($k_f B$). At $x = 0$ the aquifer is in direct contact with the sea water surface; at $x = L$ there is a supratidal pond, in which the water level may vary between 0 and $H_{\max}$, but may be treated as approximately constant over a short succession of tidal events (say, a couple of days).
(2) The Dupuits assumption applies: $\partial_z h \ll \partial_x h$, the head distribution can be approximated as 1D: $h(x, z, t) \to h(x, t)$.
(3) Apart from liquefaction within a very thin layer at the aquifer-top, material aquifer properties do not vary in space and time; hydraulic diffusivity (transmissivity/storativity) $k_f B/S$ maintains the same value throughout.
(4) The sand material under the mat is fully water-saturated at all times, and mat elasticity (deformation) has negligible impact upon storage in the aquifer, thus the aquifer may be treated as fully confined.
(5) Direct recharge/infiltration through the microbial mat is negligible; driving forces for flow in the aquifer (which may change direction) are provided by tidal height as well as by the water level in the supratidal pond at the other end and, of course, gravity itself throughout the aquifer. Consistently with the Dupuits assumption, the aquifer boundaries at $x = 0$ and $x = L$ enjoy full hydraulic contact over the whole aquifer depth.

At the aquifer-top, the excess pressure $p^*(x, t)$ (i.e., the part of seepage pressure actually available for liquefaction), is what remains from seepage pressure $p(x, t)$ after subtracting the confining (downward) force acting on the grains at aquifer-top, assumed to consist only of the weight of the water column above the mat (mat thickness being negligible, and mat substance not being essentially heavier than water). The height of the water column varies in time, but is assumed to be determined only by the advancing or regressing tidal water-front. Solving the boundary-

value problem for $p(x,t)$ with a time-periodic boundary condition at $x = 0$, yields the following closed form for $p^*(x,t)$:

$$
\begin{aligned}
& H_{\mathrm{T}} + \left(\frac{H_{\mathrm{P}} - H_{\mathrm{T}}}{L} + \frac{q_{\mathrm{R}} L}{2a}\right)x - \frac{q_{\mathrm{R}}}{2a}x^2 \\
& \quad + \frac{H_{\mathrm{T}}}{2}\frac{e^{k\tilde{x}}\cos(\omega t - kx) + e^{-k\tilde{x}}\cos(\omega t + kx) - e^{kx}\cos[\omega t - k\tilde{x}] - e^{-kx}\cos[\omega t + k\tilde{x}]}{\cosh(2kL) - \cos(2kL)} \\
& \quad \underbrace{- \frac{1}{2}\left\{\left|\gamma x - H_{\mathrm{T}}\left[1 + \cos\left(\omega t - \pi\frac{\gamma x}{2H_{\mathrm{T}}}\right)\right]\right| + \gamma x - H_{\mathrm{T}}\left[1 + \cos\left(\omega t - \pi\frac{\gamma x}{2H_{\mathrm{T}}}\right)\right]\right\}} \\
& \quad = \begin{cases} 0 & \text{if } x \leqslant \frac{H_{\mathrm{T}}}{\gamma}\left[1 + \cos\left(\omega t - \pi\frac{\gamma x}{2H_{\mathrm{T}}}\right)\right], \\ \gamma x - H_{\mathrm{T}}\left[1 + \cos\left(\omega t - \pi\frac{\gamma x}{2H_{\mathrm{T}}}\right)\right] & \text{if } x > \frac{H_{\mathrm{T}}}{\gamma}\left[1 + \cos\left(\omega t - \pi\frac{\gamma x}{2H_{\mathrm{T}}}\right)\right], \end{cases}
\end{aligned}
$$

incorporating the effect of following factors:

Notation	Meaning	Dimension	Value used to produce the plots (Figure 8(d)-2)
H_{T}	Tide amplitude (half of max. tide level)	Length	7.5 cm
H_{P}	Thickness of water layer in pond (pond water level, relative to pond-bottom)	Length	20 cm (case A), 0 (case B)
L	Aquifer length	Length	420 m
γ	Geodetic slope (assumed as uniform)	1	1/615
a	Hydraulic diffusivity (aquifer transmissivity/storativity)	Length^2/time	432 m^2/day
ω	Tide (angular) frequency	Time^{-1}	$2\pi \times (12\text{ hours})^{-1} = 12.6\text{ day}^{-1}$
k	Coupling parameter (tides–hydraulics), defined as $k = \omega^{1/2}(2a)^{-1/2}$	Length^{-1}	0.121 m^{-1}
q_{R}	Surface recharge through mat	Length/time	Neglected as it has no influence upon time-varying terms
T	Time variable	Time	(Variable)
x	Space variable (distance from barrier; $x = 0$ at barrier; $x = L$ at upslope pond)	Length	(Variable)
$\tilde{x}$	Reflected space variable, defined as $2L - x$	Length	(Variable)

Interpretation

Depending on the aquifer parameters and the relative tide vs. pond heights, there will exist a region between $x = 0$ and $x = L$ in which sand liquefaction underneath the mat appears possible at all times. For the examples shown in Figures 8(d)-4A, -4B this will be the case at distances exceeding ca. 40 m and ca. 50 m from the sand barrier, respectively. Below these distances are complementary regions in which sand liquefaction underneath the mat appears possible only for a certain number of hours every day. Also, the depth of the (potentially) liquefied layer δ_{liq} varies with the distance from the barrier and, additionally, with the tides (variations remaining strictly periodic as long as no macroscopic change of the system or material hysterese effects become noticeable). Thus, within ca. 90 m from the barrier, the liquefied layer oscillates in thickness between +0 cm and about 3 cm and will experience periodic 'freezing', i.e. compression around high tides, due to the load of overlying tidal water. Close to the barrier, the direction of flow within the sand layer will periodically revert from prevailing downslope to an upslope direction, for about 6 hours every tide period (±3 hours from high tide).

As may be inferred from Figures 8(d)-4A$_{[1]}$ and -4B$_{[1]}$, the direction of flow within the sand layer periodically reverts from prevailing downslope to upslope direction, close to the barrier. Thus, at about 40 m distance from the sand barrier a local, minor 'groundwater divide' will exist for about 6 hours every tide period (±3 hours from high tide).

This page intentionally left blank

Atlas of Microbial Mat Features Preserved within the Siliciclastic Rock Record
Edited by J. Schieber et al.
© 2007 Elsevier B.V. All rights reserved
DOI: 10.1016/S1574-1966(07)02009-3

CHAPTER 9

Palaeoenvironmental and Chronological Relationships of Mat-Related Features, and Sequence Stratigraphic Implications of Microbial Mats

INTRODUCTION

Accepting that microbial mat-related structures are complimentary to the well-known physically formed sedimentary structures, they will naturally aid in definition and interpretation of depositional (palaeo)environments and sequence stratigraphy within modern settings and the ancient rock record. These relationships, however, are likely to be as complicated and multi-faceted as those of their more widely known and physically formed counterparts, and are discussed in further detail in the following two sections.

9(a). PALAEOGEOGRAPHY OF MICROBIAL MATS IN TERRIGENOUS CLASTICS – ENVIRONMENTAL DISTRIBUTION OF ASSOCIATED SEDIMENTARY FEATURES AND THE ROLE OF GEOLOGIC TIME

J. Schieber, P.K. Bose, P.G. Eriksson, S. Sarkar

Introduction

In classical studies of the relationships between organisms and environments, the environment or palaeoenvironment is defined by a range of physical and chemical parameters (water depth, energy regime, temperature, salinity, etc.). Whether or not an organism can live in a given environment depends on its ability to tolerate or adapt to the given conditions, and whether suitable food sources are available. For elephants for example, the environment needs to be situated in tropical latitudes and must support sufficient plant growth, and as a consequence elephants only occur in tropical Africa and Asia. Other organisms, such as rats, are known for their ability to extract sustenance from a great range of environments and are found across the globe. Thus, in general terms one should expect that environmental parameters do have an impact on what types of organisms will thrive in a given locale.

Yet, biofilms and microbial mats have been reported from such a wide range of environments that one might think that environmental parameters exert little influence. Once a moist substrate and an energy source are provided, microbial mats will enter the scene quickly as long as grazers are kept at bay. Most of us can probably recall multiple examples of 'opportunistic' mats (Figure 9(a)-1) from visits to construction sites and other areas affected by human impact. Microbial mats are found in the deep oceans surrounding hot spring vents (Figure 9(a)-2A), and even deeper, coating fracture surfaces within ocean floor basalts (Cregg et al., 1992; Reysenbach and Cady, 2001). They occur near methane seeps at various depths, on the ocean floor, the continental slope, and even the continental shelf (Joye et al., 2004; Reitner et al., 2005). We also find them in areas where oxygen concentrations are below the threshold of metazoan grazers (Schulz et al., 1996; Bernhard et al., 2000), regardless of actual water depth (Figure 9(a)-2B). Because of comparatively easy access, the study of tidally influenced sedimentary environments has generated the largest number of published records on modern microbial mats (e.g., Gerdes et al., 2000a; see Chapter 2 for images). Yet, modern microbial mats do not stop at the ocean's edge. We find them in fluvial settings, such as in rivers and streams with a low sediment load (Figures 9(a)-2C, -2D), in lakes (Figure 9(a)-3A) and hot spring pools (Figure 9(a)-3B) (Ward et al., 1998; Last and Ginn, 2005), in deserts as cryptobiotic soil crusts (Figure 9(a)-3C) (Belnap and Gardner, 1993; Eldridge and Green, 1994), and in the frozen expanses of Antarctica beneath the permanent ice cover of lakes (Figure 9(a)-3D) (Hawes and Schwarz, 1999; Sabbe et al., 2004).

Once the above examples (Figures 9(a)-2 and -3) are examined in detail it becomes clear, however, that each given environment presents unique challenges, and that in each case different consortia of bacteria are involved in mat formation. Biofilms and microbial mats are ubiquitous in a multitude of environments not because they are some

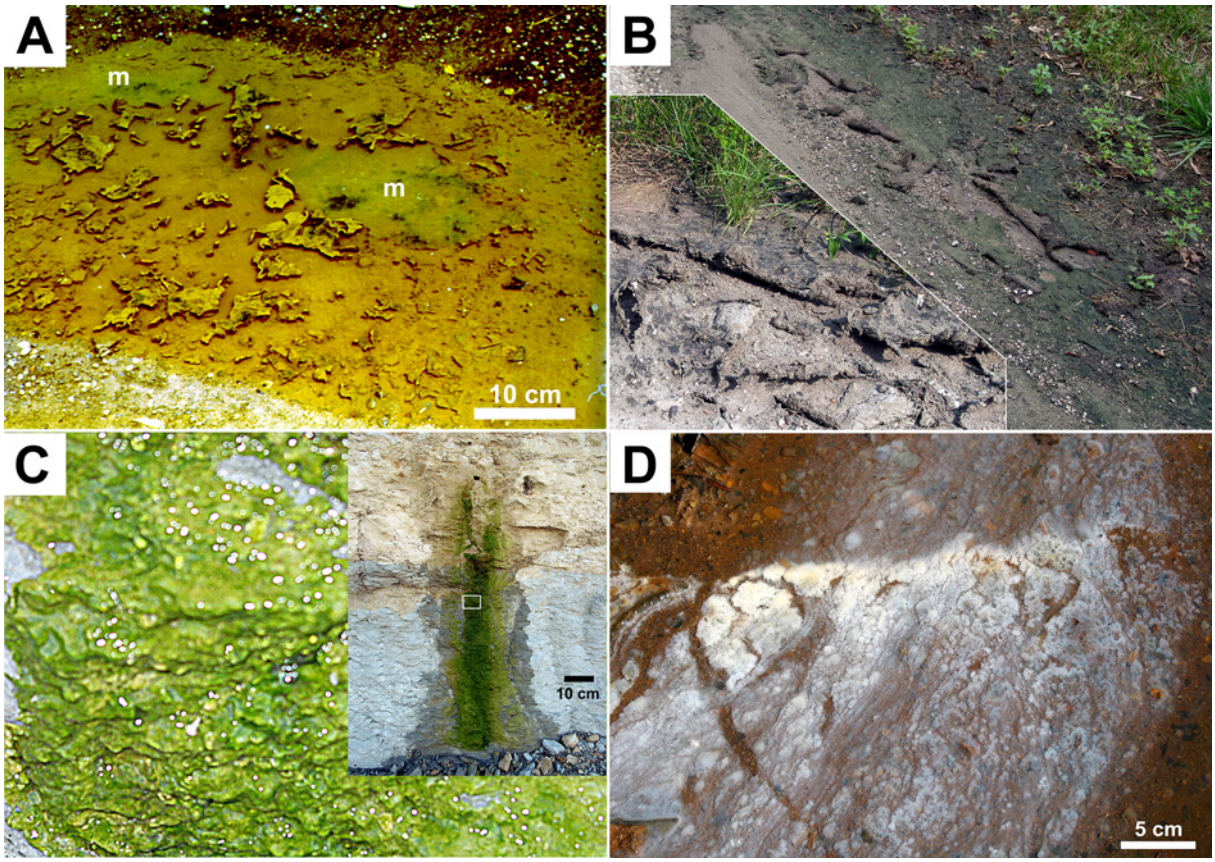


Figure 9(a)-1: 'Opportunistic' mats in modern settings.
(A) A modern puddle with benthic cyanobacterial mat on mud substrate (marked 'm'). Portions of the mat have floated up because of attached oxygen bubbles. Photo by J. Schieber. (B) Modern cyanobacterial mat in a roadside ditch on a sandy substrate. Fast currents during rainstorms have caused the mat to be partially eroded and/or 'flipped over' at the edges. Inset shows dried-out, cracked and curled mat from same locality. Vegetation for scale. Photo by J. Schieber. (C) 'Vertical' microbial mat on the wall of a construction pit (inset). Water flow from a spring provides continuous moisture. Photo by J. Schieber. (D) Whitish mat of acidophile bacteria that thrive in low pH runoff from a weathering exposure of pyrite-bearing black shale. Pyrite oxidation is the cause for low pH values. Photo by J. Schieber.

highly adaptable organism, but rather because mat formation appears to represent a very effective strategy for optimising microbial survival in a wide range of environments. It is a strategy that apparently is employed with great success by a large variety of microbial communities (Figures 9(a)-2 and -3).

Common to many mats is that they enhance sediment cohesion and resistance to erosion, as well as stabilising vertical chemical gradients within the sediment. Thus, their mechanical interactions with the sediment, such as for example the formation of fold-overs, rip-ups, roll-ups, ripple patches, domal buildups, etc. (see Chapter 3), may be qualitatively similar for mats that were produced by distinctively different microbial consortia. In the rock record, therefore, we may find that sedimentary features left behind by photosynthetic cyanobacterial mats that thrived in the photic zone (Figure 9(a)-1B and Chapter 2), may be quite similar to those found in much more distal and deeper water settings that may actually testify to the former presence of chemosynthetic microbial mats (Figure 9(a)-2B and Chapter 7(e)). Yet, although features due to mechanical interactions can not help us to make that distinction, the associated diagenetic minerals, as well as geochemical fingerprints, may point us in the right direction (Logan et al., 1999a).

Chronology of microbial mats

At the very beginning of the history of life on Earth, primitive life forms may well have tested multiple approaches to optimise microbial survival. By the time of the Apex Chert microbiota (Schopf, 1993), however, at ~3.5 Ga,

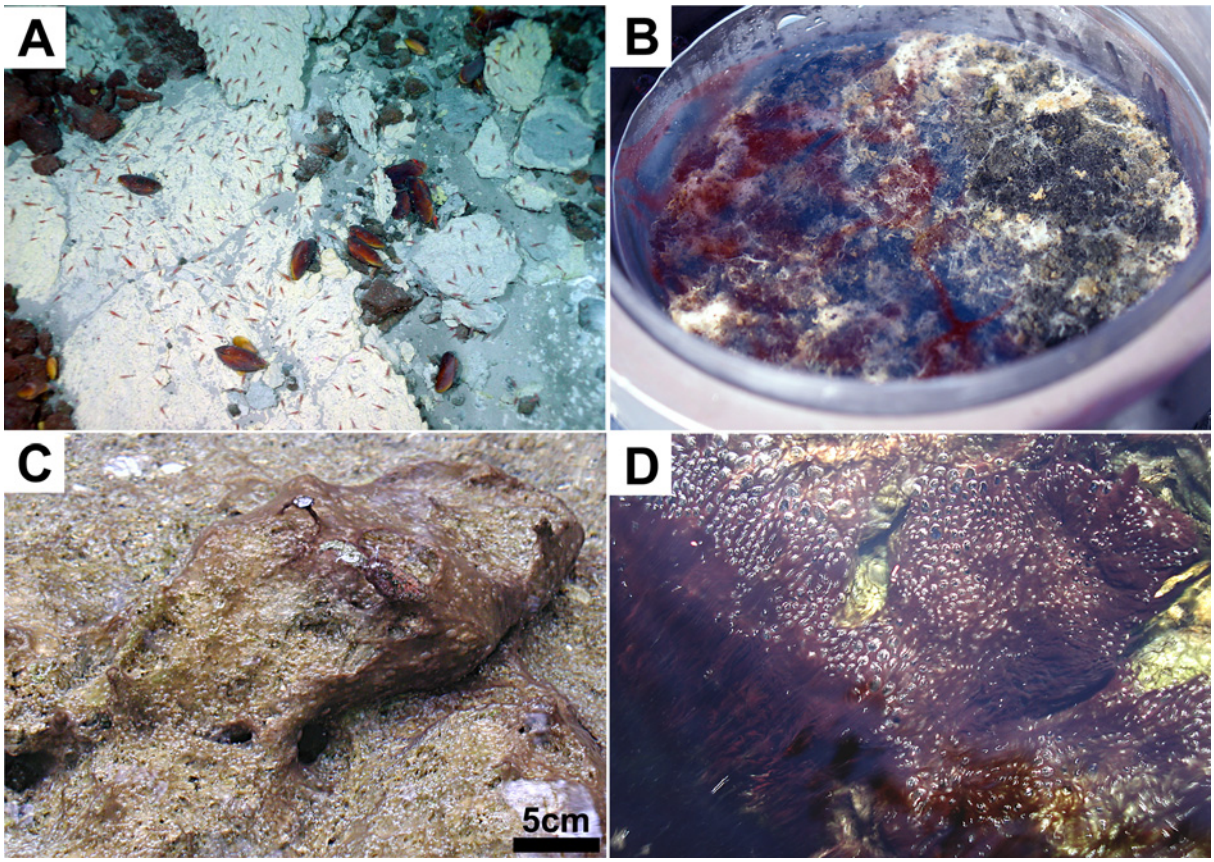


Figure 9(a)-2:
(A) Thick, fragile mat of whitish sulphide oxidising bacteria near a white smoker vent. The mat biomass constitutes the base of the food chain in this area and is utilised by small vent shrimp and larger mussels. Photo from NOAA Explorer web site, http://www.oceanexplorer.noaa.gov/explorations/04fire/logs/april12/. (B) Top of sediment core from Santa Barbara Basin, offshore California. The whitish clumps and filaments are formed by the sulphide oxidising bacterium *Beggiatoa*. This is a *Beggiatoa* mat in its early stages and will eventually cover the sediment surface with a solid layer of entangled filaments. Diameter of core barrel is 10 cm. Photo by J. Schieber. (C) Mat consisting of cyanobacteria and diatoms coating the bottom of a shallow creek near Sulfur, Oklahoma. The Creek normally has a very low sediment load because it is spring-fed. Photo by J. Schieber. (D) Same Creek as before, mat with abundant trapped oxygen bubbles (2–5 mm in size). Flow is from the upper right to the lower left. Photo by J. Schieber.

microbial fossils are already so similar to modern counterparts that they must represent considerable evolution from the earliest microorganisms. At this point in time as well, microbial mats and stromatolites already show the structural and textural features that they maintain for the remainder of Earth history (Hofmann et al., 1999). We must conclude then that at least as far back in time as 3.5 Ga, microbial mats comparable to modern counterparts were already a common presence in marine and marginal marine environments. Evidence for microbial mats in terrestrial environments, such as rivers and lakes, goes back as far as 2.7 Ga (Buck, 1980; Buick, 1992), and geochemical considerations suggest that as early as 2.6 Ga microbial mats had become a factor in soil formation (Watanabe et al., 2000). It is therefore reasonable to assume that by Late Archaean times at the latest, microbial mats most likely flourished in all environmental settings that we find them in today. In essence, from that point forward we can expect to find them in any conceivable environment that meets their moisture, nutritional, and energy needs.

Microbial mats and (palaeo-)environmental settings

As indicated above, because of the ubiquity of microbial mats across a broad range of environments, the mere presence of mats in a given rock unit has limited value for the assessment of palaeoenvironment. In Precambrian sediments, however, this shortcoming is partially mitigated by the lack of bioturbation that allows much better

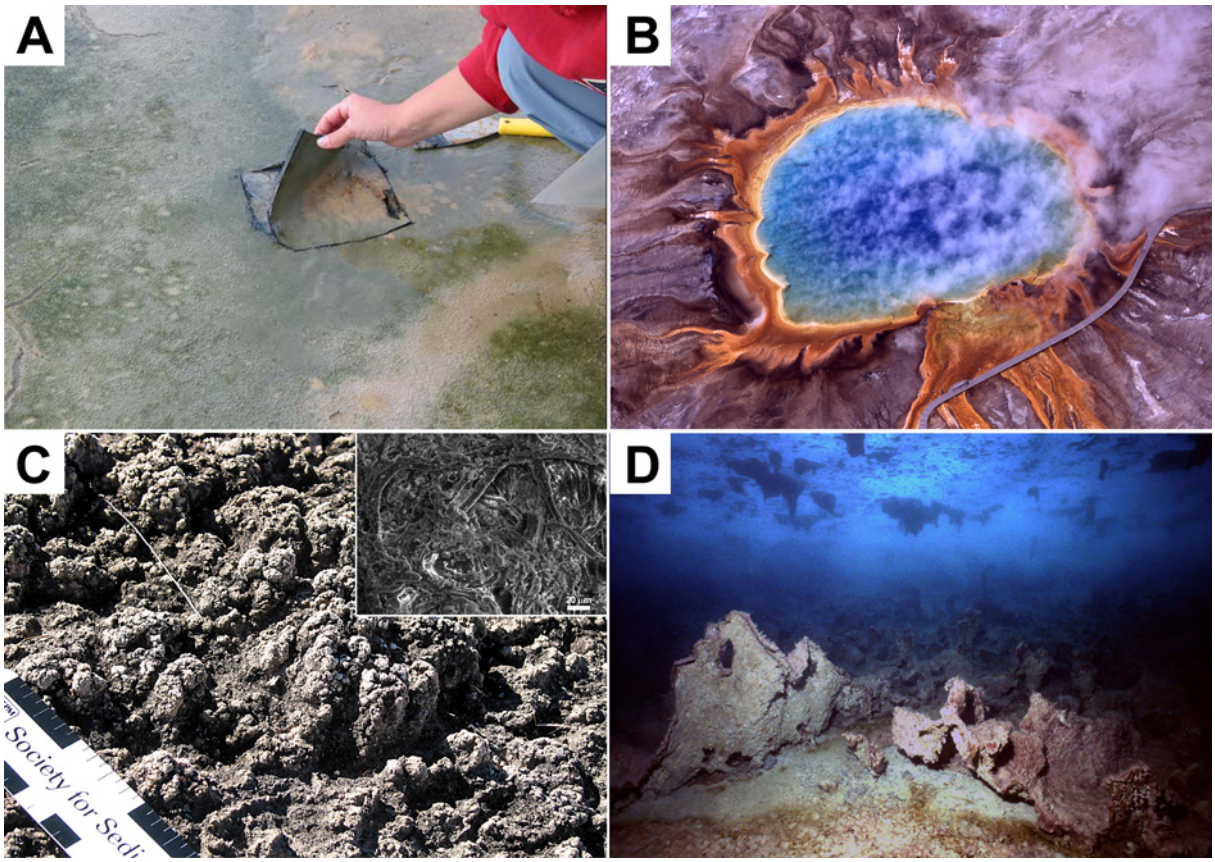


Figure 9(a)-3:
(A) Example of living microbial mat near a saline spring, Lake Winnipegosis region, Manitoba, Canada. These mats can reach several centimetres in thickness and are often laminated (image courtesy of Last and Ginn, 2005). (B) Aerial view of the Grand Prismatic hot spring in the Midway Geyser Basin, Yellowstone National Park, USA. Steam is rising from the hot and sterile central portion (deep blue water). The orange coloured periphery constitutes the much shallower overflow areas where the water cools rapidly as it moves away from the spring. The orange colour is due to microbial mats, and the concentric zonation marks microbial consortia with different temperature preferences. The spring is approximately 115 m in diameter, and over 40 m deep. Image courtesy of US National Park Service. (C) Rugged surface expression of cryptobiotic crust on desert soil from White Sands National Monument, New Mexico. Scale has long black bars of 1 inch length, and short black bars of 1 cm length. Inset shows scanning electron micrograph of crust surface with entangled microbial filaments and mineral grains. Both photos by J. Schieber. (D) Microbial mats at the bottom of permanently ice covered Lake Bonney in Antarctica (depth ~5–6 m). These mats are photosynthetic in spite of low light intensities and can float up because of attached oxygen bubbles. Photo courtesy of Dale T. Andersen (© All Rights Reserved).

preservation of all types of sedimentary features, including those that are related to mat-sediment interaction. In addition, specific features of microbial mat deposits, such as for example elongated domal buildups, 'soft' microbial sand chips, and rigid curved sand chips (Garlick, 1981, 1988; Schieber, 1998a; Pflüger and Gresse, 1996; Bouougri and Porada, 2002; Sarkar et al., 2006), can give information about environmental energy levels, episodes of desiccation and reworking, etc., and thus allow narrowing of the number of feasible environments.

The published literature gives the impression that microbial mat features are most common, in the rock record, from deposits formed within high energy shallow marine settings. This, however, is most likely a perception skewed by fortuitous availability of exposures (sandstones make better exposures than mudstone-dominated successions) and because their identification is easier due to an abundance of modern analogues (see Chapter 2). Scattered reports of, for example, subtidal, distal deep basin, fluvial, and lacustrine environments (e.g., Schieber, 1986; Eriksson et al., 2000; Yeo et al., 2002; Prave, 2002; Sur et al., 2006) indicate that future systematic study of all terrigenous clastic rock types is likely to erase this bias.

Having indications of terrestrial and potentially pedogenic microbial mats as early as the Late Archaean (Watanabe et al., 2000) also speaks to another conundrum, the common occurrence of extremely pure quartz arenites in Proterozoic and lower Palaeozoic strata. While long thought of as a result of multicycling and aeolian abrasion, we do have evidence for first-cycle quartz arenites in the Proterozoic that formed in the absence of the efficient chemical weathering that we associate with vascular land vegetation (Dott, 2003). This suggests that microbial crusts like the one illustrated in Figure 9(a)-3 already occupied Precambrian land surfaces, promoted intense weathering and destruction of chemically labile components, and left behind a quartzose residue that was then reworked into quartz arenites (Dott, 2003).

Many of the classic occurrences of microbial mat features in terrigenous clastics are found within epeiric marine coastal settings, such as for example the Mid-Proterozoic Belt basin of North America and the Palaeo- to Neoproterozoic Vindhyan basin of India. The sandy nearshore facies of these basins has much in common with the famous tidal flats of Mellum Island in the North Sea, where much of the research on sandy microbial mats has been undertaken (see Chapter 2). Because most large basins preserved on cratons tend to be marine and are affected by relative sea level movements of both global and local origin throughout their history, widespread coastal marine facies will tend to dominate their rock record. Apart from anything else, the arenitic rocks formed within most coastline settings will resist weathering and erosion more easily, and be topographically more prominent in forming accessible outcrops than central-basinal argillaceous rocks. Disputed ophiolites apart, very little of the Precambrian seafloor has been preserved in the record, once again enhancing the apparent importance of coastal arenitic settings. However, in the succeeding section of this chapter, Catuneanu discusses the fact that certain mat-related features may have been preferentially preserved in Precambrian subtidal shelf settings rather than the higher energy coastal palaeoenvironments. He attributes this feature to enhanced wind regimes (and thus concomitantly, enhanced wave energy) that affect the preservation potential of mat related structures within coastal facies.

Phanerozoic microbial mats

While today we still find microbial mats in all the ecological niches and environments that they presumably occupied in the Precambrian (Figures 9(a)-2 and -3), the advent of metazoans in the Cambrian effectively ended 3 billion years of mat-dominated surface environments (Garrett, 1970). Yet, while metazoans might have laid waste to surficial mats, they did not eliminate their constituent microbes. The latter point is easily demonstrated by stratified and mat-forming microbial assemblages in Winogradsky columns (microbiological enrichment columns; Sagan and Margulis, 1988) prepared from random soil and sediment samples (Figure 9(a)-4). In essence, the microbes that potentially form mats are ever-present in the environment, they just need a chance to thrive (Figure 9(a)-4). Thus, just like in areas disturbed by human activity (Figure 9(a)-1) where microbial mats are early colonisers, they probably did the same in Phanerozoic environments when the prior ecosystem had been disrupted by ‘catastrophes’, such as storms, volcanic eruptions, impacts, etc. If these disruptions were short-lived, the mats probably were soon after eaten and/or destroyed by returning metazoans, making for negligible preservation potential. If, on the other hand, disruptions resulted in environmental change that adversely affected metazoans, such as high salinity, lack of oxygen, etc., thick mats with a potential to be preserved in the rock record could form. Thus, although the evolution of metazoans in the Cambrian caused a major shift in mat preservation, mats could still develop given an opportunity.

The Proterozoic–Phanerozoic transition not only witnessed a major reduction of three-dimensional mat proliferation, but also a shift to abundant development of thin biofilms around discrete particles (Seilacher and Pflüger, 1994). Fragmentation of sandy or muddy mat surfaces by metazoans, in tandem with current and wave reworking, probably was a major factor in the formation of features like ‘algal biscuits’, oncoids, and generally coated grains. These mobile ‘granular mats’, such as microbially formed oncoidal pyrite grains in the Ordovician Winnipeg Formation of Saskatchewan, Canada (Schieber and Riciputi, 2005), might have been of less interest to metazoans because they did not offer a contiguous food supply, and as loose grains were more difficult to graze on. Regardless of these changes, however, we still find evidence of mat colonisation in Phanerozoic terrigenous clastics (see Chapter 7), and a growing awareness on how they might be identified will probably lead to recognition in many additional places, even when partially obscured by grazing and bioturbation.

Conclusions

As pointed out above, although in times past microbial mats may have been as widespread environmentally and geographically as today, not all locales may have offered the same preservation potential. While processes of

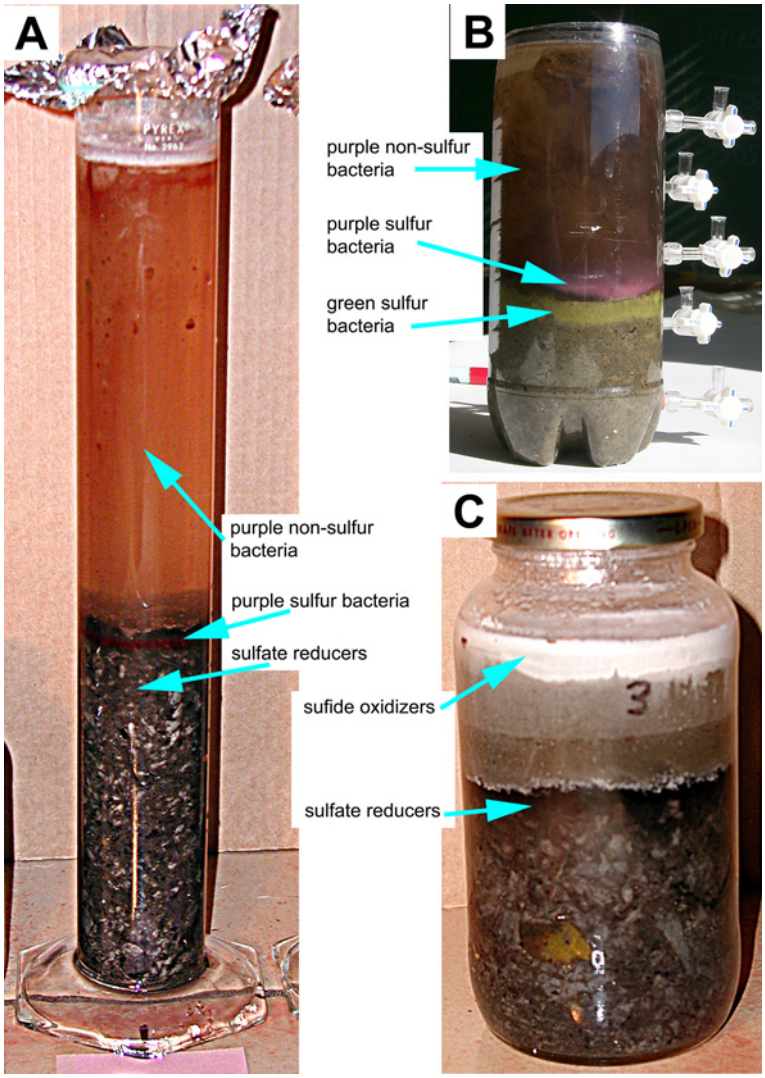


Figure 9(a)-4: Microbial stratification of Winogradsky columns prepared from lake mud. (A) Shows darkening by sulphate reducing bacteria in the bottom portion, a horizon with purple sulphur bacteria (anaerobic photosynthetic) just below the sediment/water interface, and purple non-sulphur bacteria (photoheterotroph, low H_2S tolerance) in most of the rest of the water column. Photo by J. Schieber. (B) Column has well developed zones of green and purple sulphur bacteria (just like in microbial mats from sandy tidal flats), overlain by water with purple non-sulphur bacteria. Image courtesy of Dr. Joe Vallino, Semester in Environmental Science, Marine Biological Laboratory, Woods Hole, MA 02543. (C) A column with restricted oxygen access. Shows well-developed darkened lower layer with sulphate reducing bacteria, and an upper layer (microbial mat) that consists of sulphide oxidising bacteria. Photo by J. Schieber.

mat erosion and deformation may well be similar between environments occupied by photosynthetic mats versus those covered by chemosynthetic mats, the mats might have offered different levels of 'resistance' under otherwise identical conditions of flow. Because photosynthetic cyanobacteria are very adept at mat generation (Chapter 2), lighting conditions are most likely an important factor for the growth of many structured mats in the rock record. Our current knowledge base about modern mats constructed by chemoautotrophs is much smaller than that for photosynthetic microbes. More work needs to be done on modern chemosynthetic mats if we, for example, want to evaluate whether coccoidal bacteria-rich mats from the Triassic deep sea (Mastandrea et al., 2006) could indeed form a sustainable mat.

If one sees microbial mat-related structures as part of the larger continuum of physically-formed sedimentary structures, such as suggested by Noffke et al. (2001a) in an adaptation of the well-known Pettijohn and Potter (1964) classification, then mat-induced features may not be any more facies-specific than their physically-formed counterparts. Noffke and co-workers (e.g., Noffke et al., 2001a, 2006a, 2006b) instead suggest that microbially-induced

sedimentary structures (MISS) are very facies-specific. They also relate them to regression–transgression turning points, and thus imbue them with very specific sequence stratigraphic meaning as well. As can be seen in Section 9(b) of this chapter, this is to be disputed. Those who work in modern mat-bound clastic sedimentary settings, such as the famous Mellum Island in the North Sea, or the tidal flats and sabkhas of the Tunisian coast, will obviously find it easy to establish direct relationships between mat-related structures and well-defined depositional environments (e.g., Gerdes et al., 1985b, 1985c; Noffke et al., 2001b). The same applies, however, to most investigations of modern sedimentary settings and their component physically-formed sedimentary structures. Elucidation of palaeoenvironments from the rock record is almost always a much greater challenge with a less certain result.

The relatively limited reports on the occurrence of ancient mat-related structures and the observed distribution of their modern counterparts can be integrated to predict the palaeoenvironmental distribution of the various mat-related features. Because the palaeoenvironmental relationships of mat features are seldom very specific, they are presented here within a broad framework: coastal, shallow sea/lake, deep sea/lake, fluvial and aeolian settings. The first includes beach, intertidal–supratidal, delta plain, coastal swamp, etc. above mean sea level, while the second includes the generally agitated shallow water environments like the shoreface and the shelf beneath mean sea level. The third covers the quiet deep-water environments, which may only occasionally be agitated. Table 9(a)-1 shows features in sandstone, and Table 9(a)-2 their equivalents in shale, in their respective palaeoenvironmental context (bar thickness stands for relative abundance, as reported or projected).

In summary we can say that probably since the Late Archaean, microbial mats and the microbial communities that form them have occupied every conceivable ecological niche on the planet, much as they do today (Figures 9(a)-1, -2 and -3). Many published examples of microbial mats in terrigenous clastics are from marginal marine sandy deposits, both in the Precambrian and the Phanerozoic. This bias, however, will probably gradually disappear as we learn how to more reliably identify microbial mat deposits in other facies and lithologies. A major shift in mat preservation occurred with the evolution of metazoan grazers in the Cambrian. Mats still grew whenever given a chance, but typically were ‘eaten’ or destroyed almost as fast as they formed. Thus, extensive sediment colonisation with a potential for preservation in the rock record was severely curtailed. Nonetheless, we do find evidence of mat colonisation in Phanerozoic terrigenous clastics (see Chapter 7), and a growing awareness on how they might be identified will probably lead to recognition in many other places, even when partially obscured by grazing and bioturbation. Integration of textural studies that focus on sediment rheology as influenced by microbial binding, with mineralogical/geochemical studies should help our ability to identify which microbial ‘lifestyle’ (e.g., photosynthesis versus chemosynthesis) dominated a given mat community.

Table 9(a)-1
Features in sandstones (see Chapter 3)

		Palaeoenvironment					
		Coastal	Shallow Sea/lake	Deep Sea/lake	Fluvial	Aeolian	Remarks
Mat-related features	Multi-directed, Palimpsest Ripples	▬	▬				Very shallow water to fair weather wave base. Most likely preserved in coastal to shallow sea/lake settings.
	Surface Ornamentation, Wrinkle Structures, "Elephant Skin" etc.	▬	▬	- - - - -	▬	- - - - - - -	Judging from modern analogues these should be most common in coastal to shallow sea/lake settings. Potentially also associated with shallow water bodies on floodplains and coastal plains.
	Domal, Convex-Up Features	▬	▬		▬		Current energy required for accretion, thus more likely in shallow water settings. In high energy coastal settings, poorer development due to erosion? May occur locally in fluvial channels with strongly episodic sediment transport.
	Petees & Ridges	▬			▬	- - - - -	Modern analogues suggest need for at least one of the following: strong shear forces, desiccation, or gas expansion. Thus, coastal and other very shallow water environments most likely.
	Cements & Floating Grains	▬	▬	▬			It helps if surface sediment maintains similar pore space chemistry for extended time periods (small sedimentation rates). Coastal to shallow/deep sea/lake should be most common environments.
	Sand Cracks, Manchuriophycus etc.	▬			▬	▬	Requires desiccation, thus mainly expected in coastal and fluvial environments. Also possible in intermittently moist interdune depressions.
	Ripple Patches	▬	- - - - -				Within fair weather wave base, need for powerful erosive events. Coastal setting most likely. Minor occurrences in shallow offshore?
	Flip-Overs, Roll-Ups, Sand Chips	▬	▬	▬	- - - - -	- - - - - - -	Strong currents/wave action needed. Most likely to form in coastal environments. Petering out into deeper water. Potentially also in moist terrestrial settings.
	Curved Sand Chips	▬			▬	- - - - - - -	Desiccation and strong currents required. Most likely in terrestrial and coastal environments.
	Gas Domes & Kinneyia	▬	- - - - -		- - - - - - -		Shallow water favours formation of larger gas buildups. Likely environments are coastal and possibly shallow ponds on floodplains.
	Mat Decay Mineralization	▬	▬	▬	- - - - - - -		Permanently water-logged pores enhance preservation potential. Thus, preservation more likely in shallow-deep sea/lake settings. In terrestrial environments, only if sediment is continuously water-logged for long periods of time.

Table 9(a)-2
Features in shales (see Chapter 3)

Mat-related Features	Palaeoenvironment						
		Coastal	Shallow Sea/lake	Deep Sea/lake	Fluvial	Aeolian	Remarks
	Wavy-Crinkly Carbonaceous Laminae	▬	▬	▬	———	———	Probably best preserved below storm wave-base. Preservation unlikely in environments with ready oxygen access (oxidation of organic matter), such as terrestrial and supratidal. Exception for areas with permanent water cover (lakes, swamps, lagoons). Potential for preservation also in wet interdune depressions with clay-rich sediment.
	Bed-Smoothing	▬	▬				Because the surface of coarser layers (granule to pebble size particles) is to be smoothed, more likely observed in coastal and shallow sea/lake settings.
	Domal Build-up	▬	▬		———		Current energy probably required for accretion, thus more likely in shallow water settings. In high energy coastal settings, poorer development due to erosion?
	Striped Shale	—	▬	▬			Requires episodic sedimentation to cover mats, thus not too distal is better. Coastal setting unlikely because of reworking. Shelf below storm wave base most likely. In deeper water only when influx of storm- and flood-reworked sediment possible.
	False X-laminae	—	▬	▬			Best developed where there are abundant small sediment pulses during mat growth. Should be best developed in shallow sea/lake environments below storm wave-base.
	Lamina-specific Grain selection	▬	▬	▬	▬	———	Requires across-mat sediment transport by currents, thus effect more likely seen in higher energy settings.
	Random Mica Flakes	▬	▬		- - - -		Requires across-mat sediment transport by strong currents, thus effect more likely seen in higher energy settings. Also, a need for early cement formation. Thus not as likely in terrestrial environments.
	Rafted Grain Cluster	▬	▬	▬	- - - -		Could occur everywhere, but best recognized in the most fine-grained facies.
	Irregular Impressions	———			▬	———	Requires surfaces of still somewhat moist, stiff mud. Microbial flakes derived from dried-out mats on mud surfaces. Impossible in permanently water-covered areas. Most likely to occur in coastal supratidal settings, alluvial floodplains, and interdune depressions.
	Roll-Ups, & Flip-Overs,	———	▬	▬	- - - -	- - - -	Related to erosion/transport, thus should be more typical for higher energy settings. Offshore transport has to be considered. Roll-ups of thin organic 'skins' may also be found in current-affected deeper water environments. Not as likely in environments affected by desiccation (rigidity factor), but desiccated-curled mat fragments may look very similar.
	Mat Decay Mineralization	▬	▬	▬	- - - -	------	Permanently water-logged pores enhance preservation potential. Thus, preservation more likely in shallow-deep sea/lake settings.

9(b). SEQUENCE STRATIGRAPHIC CONTEXT OF MICROBIAL MAT FEATURES

O. Catuneanu

Introduction: microbial mats in the rock record

Microbial mats may form in a wide range of depositional environments, from fully marine to continental (Section 9(a)), and their presence in the rock record is established for most of geological time (e.g., Seilacher, 1999; Eriksson et al., 2000; Watanabe et al., 2000; Noffke et al., 2003a, 2006a, 2006b; Banerjee and Jeevankumar, 2005). The earliest evidence of microbial mat formation has been reported from the 3.2 Ga siliciclastic marine strata of the Moodies Group of the Barberton greenstone belt in South Africa (Noffke et al., 2006b), while the earliest inferred fully continental example comes from the 1.8 Ga palaeodesert deposits of the Waterberg Group, also in South Africa (Eriksson et al., 2000).

The abundance of microbial mats within depositional environments has changed through geological time (Section 9(a)), with the highest proliferation during the Mesoproterozoic (Pflüger and Sarkar, 1996; Eriksson et al., 2000; Schopf, 2004; Altermann, 2004; Sarkar et al., 2005). The Proterozoic dominance of these micro-organisms was followed by a sharp decline at the onset of the Phanerozoic with the rapid growth of grazing metazoan communities (Grotzinger, 1990). The effect of microbial mats on stratigraphic architecture is thus more evident for Proterozoic successions than for strata accumulated during the Phanerozoic.

Numerous types of microbial structures have been described in siliciclastic and carbonate rocks, as summarised in recent publications (e.g., Gerdes et al., 2000a; Noffke et al., 2001a; Schieber, 2004; Sarkar et al., 2004; Banerjee and Jeevankumar, 2005; and this volume). Depositional and post-depositional processes associated with most sedimentary environments, particularly those of marine affinity, favour the preservation of microbial mat structures in carbonate systems, while the evidence for microbial activity in siliciclastic environments is often indirect and circumstantial. Laboratory experiments (see Chapter 2) have contributed significantly to improving understanding of mats forming in clastic settings. The low preservation potential of microbial mats in siliciclastic rocks is explained by processes such as syndepositional wave and current reworking of unconsolidated sediment, the degradation of microbial textures soon after burial in the absence of early cements, or by a variety of deeper-burial diagenetic processes (Banerjee and Jeevankumar, 2005). However, indirect signatures of microbial growth and decay are often recognisable in the field, and materialise in sedimentary features such as wrinkle structures, sand cracks, roll-up structures, gas domes, petee structures, palimpsest ripples, and others (e.g., Noffke, 1998a; Schieber, 1999, 2004; Eriksson et al., 2000; Gerdes et al., 2000a; Noffke et al., 2001a; Banerjee and Jeevankumar, 2005).

The influence of microbial mats on sedimentation has been investigated in numerous publications, particularly from the point of view of process-sedimentology and the mechanisms of formation of microbial activity-related sedimentary structures. At larger scales of observation, however, the stratigraphic context of microbial mats is less understood, and the relationship between the occurrence of microbial mats and the architecture of the stratigraphic record has only begun to be documented (e.g., Sarkar et al., 2005). This paper examines the current understanding of the position and role of microbial mats within a sequence stratigraphic framework.

The standard sequence stratigraphic model

Definition and basic concepts Sequence stratigraphy studies the sedimentary response to changes in base level, and the depositional trends that emerge from the interplay of accommodation (i.e., space available for sediments to fill) and sedimentation. These depositional trends refer to aggradation, erosion, progradation and retrogradation. The applications of sequence stratigraphy are tremendous, from deciphering the Earth's geological record of local to global changes, to improving the success of economic exploration and production. Multiple data sets are integrated for this purpose, and insights from several disciplines are required (Figure 9(b)-1).

The predictive aspect of sequence stratigraphy is the key to its appeal and success, as models of facies relationships and development can be constructed from local to regional scales. The predictable association of depositional systems into sequences and component systems tracts is made possible by the fact that processes in all depositional environments respond to a common control: base-level changes. In turn, changes in base level depend on the interplay of allogenic controls such as eustasy, tectonism, and climate. Base level is therefore the link that 'synchronises' depositional processes in all environments across a sedimentary basin, bringing coherence to the sequence

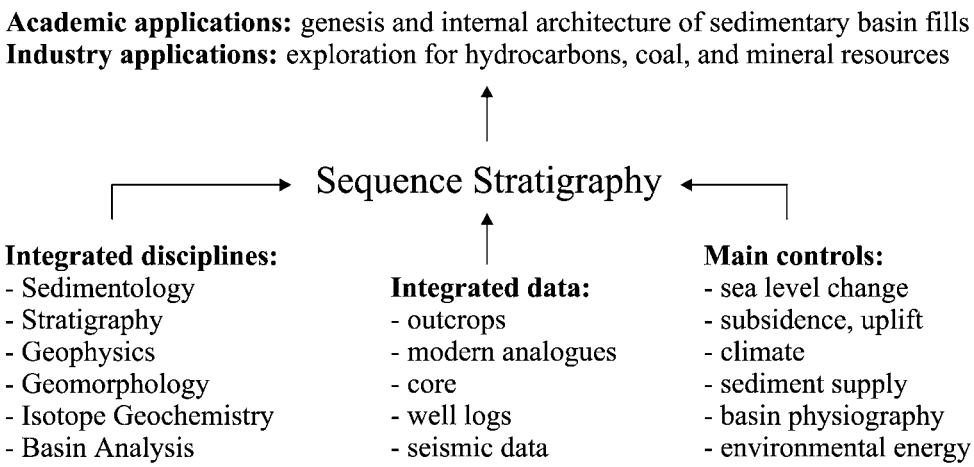


Figure 9(b)-1: Sequence stratigraphy in the context of interdisciplinary research: main controls, integrated data sets and subject areas, and applications (from Catuneanu, 2006).

stratigraphic model. The complex interplay of allogenic controls, and the variability added to the sequence stratigraphic model by the contribution of independent factors such as autogenic processes, rock types in the source areas, sediment supply and basin physiography, have been discussed in a number of syntheses including Payton (1977), Wilgus et al. (1988), Emery and Myers (1996), Galloway and Hobday (1996), Miall (1997), Gradstein et al. (1998), Shanley and McCabe (1998), Posamentier and Allen (1999), Coe (2003), Schlager (2005) and Catuneanu (2006).

The concept of 'base level' defines a dynamic and imaginary surface of balance between erosion and deposition, i.e. the highest level up to which a sedimentary succession can be built (Twenhofel, 1939; Sloss, 1962). A rise in base level creates accommodation, whereas a fall in base level destroys accommodation. The base level is commonly approximated with the sea level (e.g., Jervey, 1988; Schumm, 1993; Posamentier and Allen, 1999), and it is generally used in the context of marine environments. The equivalent concept in the alluvial realm is the fluvial graded profile. Even though the marine base level and the fluvial graded profile are often in a process–response relationship (see full discussion in Catuneanu, 2006), the two concepts may be amalgamated into one 'stratigraphic base level' that marks the surface of equilibrium between sedimentation and erosion in all depositional environments (Cross and Lessenger, 1998). A base level positioned below the topographic profile (seascape or landscape) is referred to as 'negative' accommodation, and triggers downcutting, whereas a base level above the topographic profile marks 'positive' accommodation, and it is accompanied by sediment accumulation.

Changes in accommodation, and their interplay with the rates of sedimentation, control the manifestation of all types of depositional trends in the stratigraphic record. Figure 9(b)-2 depicts the complex relationship between all main controls on stratigraphic architecture, and the definition of basic concepts such as sea-level changes (fluctuations in the position of the sea level relative to the centre of the Earth), relative sea-level changes (fluctuations in the position of the sea level relative to a datum that records the rates of subsidence or uplift), base-level changes (fluctuations in the position of the base level relative to the same datum that records the rates of subsidence or uplift), and the transgressive and regressive shifts of the shoreline. Furthermore, regressive shoreline shifts are classified into 'forced regressions' (progradation during base-level fall, driven by negative accommodation) and 'normal regressions' (progradation during base-level rise, driven by sediment supply).

Building blocks of the sequence stratigraphic framework The building blocks of the sequence stratigraphic framework include sequences, systems tracts, and parasequences. A 'sequence' is a relatively conformable succession of genetically related strata bounded by unconformities or their correlative conformities (Mitchum, 1977). A sequence corresponds to a full cycle of base-level changes. The definition of a sequence is independent of temporal and spatial scales. The relative importance of sequences is resolved via the concept of hierarchy, whereby higher-rank sequences may consist of two or more lower-rank sequences.

The addendum to the original definition of Mitchum (1977) that a sequence corresponds to a full cycle of base-level changes is required to separate a sequence from component systems tracts. As more than one sequence stratigraphic surface may have unconformable portions, the package of strata between two consecutive unconformities in the

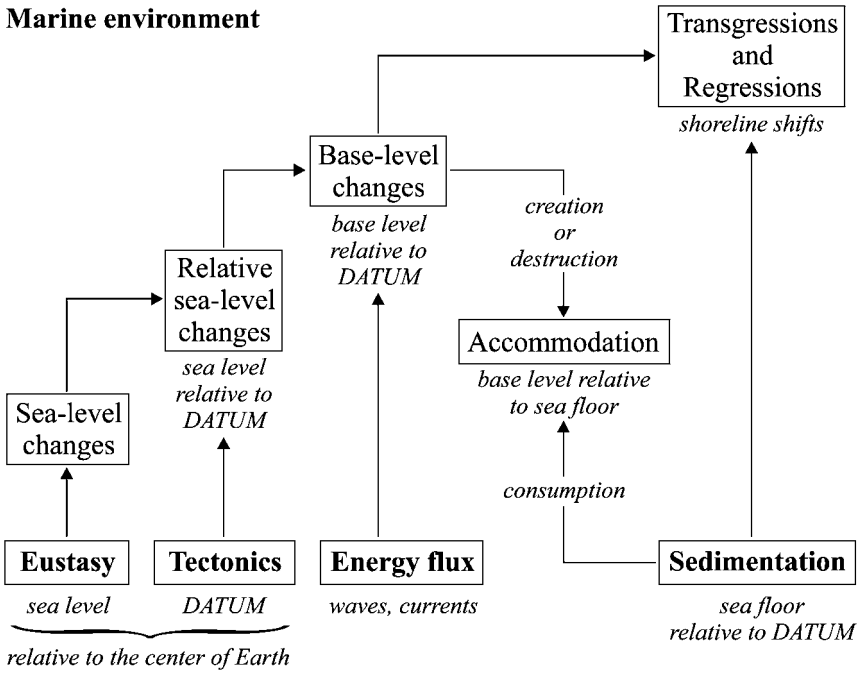


Figure 9(b)-2: Controls on accommodation and shoreline shifts in a marine environment (from Catuneanu, 2006). The 'DATUM' is a reference horizon, independent of sedimentation, which monitors tectonic motions (subsidence, uplift) relative to the centre of the Earth. See Catuneanu (2006) for additional definitions and explanations.

rock record is likely to correspond to only one stage of a full cycle of base-level changes, i.e. to a systems tract. The bounding unconformities and correlative conformities referred to in the definition of a sequence have to be consistently represented by the same type(s) of sequence stratigraphic surfaces, albeit not specified in the definition.

A sequence is subdivided into component systems tracts, which consist of a linkage of contemporaneous depositional systems that accumulate during a particular stage of shoreline shifts (Brown and Fisher, 1977). The timing of systems tract boundaries is set by the four main events of the base-level cycle, i.e. the onset of base-level fall at the shoreline, the end of base-level fall at the shoreline, the end of shoreline regression and the end of shoreline transgression (Catuneanu, 2006; Figure 9(b)-3). Systems tracts are interpreted based on stratal stacking patterns, position within the sequence, and types of bounding surfaces. Figure 9(b)-4 illustrates a generalised model for the types and distribution of depositional systems within the various systems tracts.

Parasequences are stratigraphic units bounded by 'flooding surfaces' (Van Wagoner et al., 1988, 1990), which, depending on circumstances, may be represented by transgressive ravinement surfaces, maximum flooding surfaces, maximum regressive surfaces, or facies contacts within the transgressive systems tract (see Catuneanu, 2006 for a recent discussion and examples). Consequently, parasequences are not just smaller-scale sequences, as parasequence boundaries may be represented by surfaces other than sequence boundaries.

Parasequences are commonly used to describe individual prograding lobes in coastal to shallow-water systems, where evidence of abrupt water deepening (i.e., documentation of flooding surfaces) is easiest to demonstrate. Confusion regarding the meaning of parasequences arose with the application of the term to all shoaling-upward stratal units, whether or not they were bounded by flooding surfaces, which is beyond the original intent of Van Wagoner et al. (1988, 1990). The applicability and the usefulness of the 'parasequence' concept in fully fluvial and deep-water systems have been questioned by Posamentier and Allen (1999). The restriction of parasequences to coastal and shallow-water systems marks another difference between the concepts of sequence and parasequence.

Variability of the sequence stratigraphic model Lessons learned from sequence stratigraphic work over the past two decades show that no single template can provide the optimum solution for the interpretation of every data set. The variability of the sequence stratigraphic model is caused by at least two different factors, one related to the fact that allogenic mechanisms are not the only controls on sedimentation, and another related to the change in subsidence patterns and basin physiography from one tectonic setting to another.

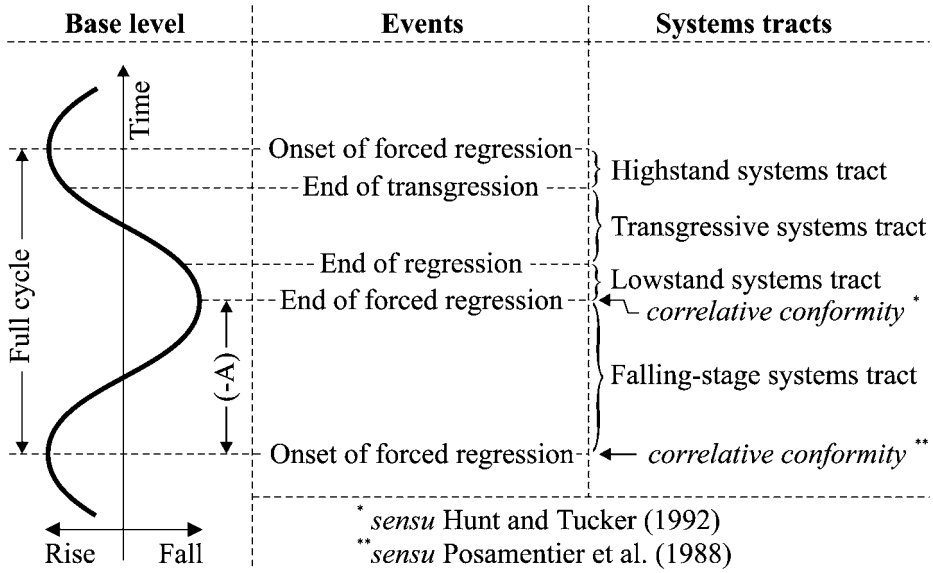


Figure 9(b)-3: The four main events of the base-level cycle, and the timing of the falling-stage, lowstand, transgressive and highstand systems tracts. See Catuneanu (2006) for a discussion on alternative definitions of systems tracts.

The role of fluctuating base level is central to sequence stratigraphy, and places emphasis on the allogenic controls on sedimentation. While allowing for the construction of a basic predictable stratigraphic framework, this approach generates a 'static sea' model whereby any other stratigraphic events (e.g., the effects of earthquakes or other short-term events on sediment supply and depositional processes) are ignored. However, one should keep in mind that autocyclic controls or short-term events may leave an equally important imprint on the architecture of the stratigraphic record. At the scale of individual depositional environments, the tendency to self organisation toward the most energy-efficient state of equilibrium may generate stratigraphic signatures similar to the ones produced by allogenic mechanisms. The inclusion of autocyclic controls and stratigraphic events in sequence analysis may explain the unpredictable distribution of some depositional elements within the basic sequence stratigraphic framework. This full-spectrum analysis of long- and short-term controls on sedimentation translates into a 'dynamic sea' approach, which requires a case-by-case study for the construction of any sequence stratigraphic model.

Changes in tectonic setting may also explain variability in the relative contribution of systems tracts to the make-up of a sequence. Each tectonic setting is unique in terms of tectonics, subsidence rates, sediment flux, physiography and topographic gradients within the basin and along the basin margins, and as a result differences in stratal architecture and the development and preservation of particular depositional systems are expected. As pointed out by Diessel et al. (2000) and Davies and Gibling (2003), the subsidence history of any sedimentary basin controls the distribution of accommodation in time and space, and as a result, the stratal architecture of each basin-fill reflects the unique regional and temporal variations in subsidence rates that characterise different types of tectonic settings. The basic contrasts between low- and high-gradient settings in terms of the resulting stratigraphic architecture of the basin-fill have been discussed by Catuneanu (2006) (Figure 9(b)-5).

Influence of microbial mats on sequence architecture

The implications of microbial mats for sequence architecture are most evident for Proterozoic successions, as the proliferation of microbial activity was probably highest during that time (Pflüger and Sarkar, 1996; Eriksson et al., 2000; Schopf, 2004; Altermann, 2004; Sarkar et al., 2005). Recently, strong evidence for microbial mats influencing clastic sedimentation during the Meso- to Neoarchaean period has also been found (e.g., Noffke et al., 2003a, 2006a, 2006b); however, the broad siliciclastic shelf environments that accompanied Proterozoic continental and supercontinental environments (e.g., Eriksson et al., 2004) vastly expanded suitable marine settings conducive to flourishing microbial mat communities. The strong evolution of grazing metazoan communities at the onset of the Phanerozoic marked a corresponding decline in the relative role of microbial mats on sedimentation (Grotzinger, 1990). As sequence stratigraphy developed as a new method of stratigraphic analysis based primarily on Phanerozoic case studies, the influence of microbial mats on sequence architecture remained largely overlooked and poorly

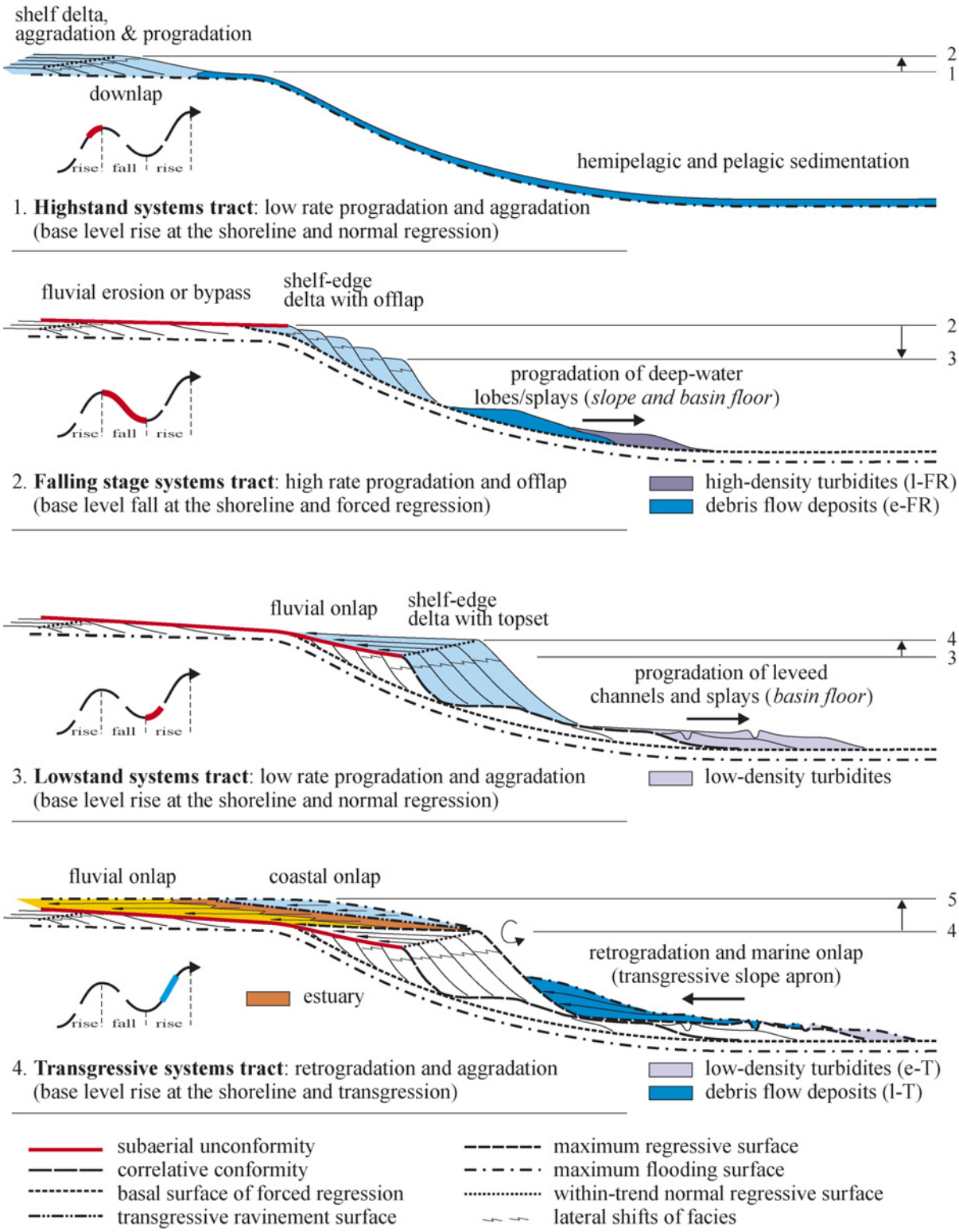


Figure 9(b)-4: Regional architecture of depositional systems, systems tracts and sequence stratigraphic surfaces (from Catuneanu, 2006). The systems tract nomenclature follows the scheme of Hunt and Tucker (1992). Systems tracts are defined by stratal stacking patterns and bounding surfaces, with an inferred timing relative to the reference curve of base-level changes at the shoreline.

Basin types / Shoreline shifts	**Low-gradient ('shelf') settings** (continental shelves, filled foreland basins, intracratonic basins)	**High-gradient ('ramp') settings** (continental slopes, underfilled forelands, rift and strike-slip basins)
Transgressions	Estuaries are likely to form. The preservation of estuarine facies is a function of the rates of base-level rise and wind/wave energy.	Estuaries are unlikely to form, due to the steep topography, higher fluvial energy, wave erosion, and slope instability.
Normal regressions	Deltas have diagnostic topsets, as a result of aggradation in the delta plains.	
	Fluvial aggradation extends over a relatively large distance upstream (inconspicuous onlap onto the subaerial unconformity at lowstand).	Fluvial aggradation is restricted to a relatively small area adjacent to the shoreline (pronounced onlap). Fluvial strata have low preservation potential.
Forced regressions	Deltas have diagnostic offlapping geometries (delta plain erosion or bypass).	
	The regressive surface of marine erosion forms in the lower shoreface in wave-dominated settings.	No erosion in the lower shoreface, as the sea floor is already steeper than the shoreface equilibrium profile.

Figure 9(b)-5: Contrasts between low- and high-gradient tectonic settings, in terms of processes and products of transgressions, normal regressions and forced regressions (from Catuneanu, 2006).

understood until recently. The exceptional preservation of some Precambrian sedimentary basin-fills, such as in South Africa and India (e.g., work by Eriksson et al., 2000; Noffke et al., 2003a, 2006b; Banerjee and Jeevankumar, 2005; Sarkar et al., 2005) has allowed for more insights into the role of microbial mats on sedimentation within a sequence stratigraphic framework, which are summarised below.

The influence of microbial mats on the sedimentary record may be analysed from both sedimentological and stratigraphic perspectives. From a process-sedimentology standpoint, the organic binding of sediments afforded by microbial mats increases the cohesiveness of the depositional surface and results in the formation of particular sedimentary structures that provide direct or indirect evidence of syn-depositional microbial activity (Chapters 2, 3, 4 and 5). Examples of such microbial activity-related features include the wrinkle structures described by Banerjee and Jeevankumar (2005) from the Palaeoproterozoic strata of the Vindhyan Basin in central India. The formation of these structures requires an interaction of physical processes (e.g., traction currents or gas escape) with a cohesive substrate 'cemented' by microbial mats. The distribution of microbial structures within the sedimentary basin may be used to infer the change in the nature and relative energy of physical processes that operated in different depositional environments during geological time. For example, microbial-related wrinkle structures that formed in the Proterozoic are best preserved within the shelf system (below the fairweather wave-base), which is contrary to modern trends that show a better preservation potential within the intertidal to subtidal zones (Banerjee and Jeevankumar, 2005; see, however, Chapter 7(a) where Noffke argues for a close association of mat-related features and tidal settings in the Archaean). This fact suggests that wind energy and associated wave erosion may have been stronger in the Precambrian, affecting preferentially the coastal to shoreface environments, and leading to the observed inversion in the locus of preservation of wrinkle structures across the Precambrian–Phanerozoic boundary. A greater polarisation of Earth's thermal zones (Rautenbach, 2001) combined with enhanced global rotation in the Precambrian (Williams, 2004) help to explain this inferred greater wind (and concomitant wave) energy. This conclusion is also supported by the fact that the proliferation of grazing organisms in the shallow subtidal environment only took place following the onset of the Phanerozoic, thus contributing toward trends that are opposite relative to those preserved in the rock record. This means that the importance of wave energy to the preservation of microbial features in the shallow-water areas outpaces the effects of grazing organisms, as the latter would tend to decrease, rather than increase, the preservation potential of microbial features in the subtidal environment.

From a stratigraphic perspective, the inferred changes in wave energy with geological time, based on the distribution of preserved microbial structures, are important to understand the differences between the architecture of Proterozoic and Phanerozoic sequences, and in particular, the relative contribution of systems tracts to the make-up of a sequence. Notably, the Precambrian sequences lack well-developed transgressive systems tracts, and are

dominated by stacked highstand systems tracts that may be separated by thin veneers of transgressive deposits, often reduced to transgressive lags only (e.g., Sarkar et al., 2005). In contrast, many Phanerozoic sequences include fully developed transgressive systems tracts, which consist of all depositional systems from fluvial, to coastal (particularly estuarine) and fully marine. Whether this trend can be generalised or not, still requires further research. It is possible that insufficient Precambrian successions have been studied so far to draw meaningful conclusions. Even for the Phanerozoic, changes in the tectonic setting may generate significant departures from the 'standard' sequence stratigraphic template, and the relative development of systems tracts may vary significantly between low- and high-gradient settings (Figure 9(b)-5; Catuneanu, 2006). This may also be the case with the Precambrian. However, evidence so far suggests that physical processes, particularly stronger wave energy, combined with a greater proliferation of microbial mats may explain the lesser development of transgressive systems tracts during the Precambrian.

Work on the Palaeoproterozoic and Neoproterozoic successions of central and western India (Banerjee and Jeevankumar, 2005; Sarkar et al., 2005) has documented the poor representation of transgressive systems tracts in comparison with the well-developed underlying and overlying normal regressive deposits. A transgressive systems tract consists, in a most general scenario, of transgressive fluvial to coastal facies scoured at the top by the transgressive wave-ravinement surface, which in turn is onlapped by transgressive shallow-marine strata. The absence (or poor development) of the fluvial to coastal section of the Precambrian transgressive systems tracts may be attributed to the inferred strong wave scouring in the upper shoreface during transgression, which may have removed much of the underlying section in the processes of shoreline backstepping. This also explains why microbial mats are not documented commonly from coastal to shoreface systems of Precambrian age, even though grazing organisms (common in the shoreface environment during the Phanerozoic) were not present during that time. The amount of erosion associated with the transgressive wave ravinement surfaces is generally within a range of 20 m for the Phanerozoic (Demarest and Kraft, 1987), with exceptional values of 40 m recorded along the coastline of the present-day Canterbury Plains (Leckie, 1994). The latter magnitude of erosion may have been the norm in the pre-Phanerozoic time, thus explaining the poor preservation of the fluvial to coastal portion of the Precambrian transgressive systems tracts. The transgressive wave-ravinement processes may, however, not be used to explain the poor development of the marine shale portion of the Precambrian transgressive systems tracts (e.g., Catuneanu and Eriksson, 1999; Sarkar et al., 2005), as the transgressive shales accumulate on top of wave-ravinement surfaces. The issue of the thin or absent transgressive shales of Precambrian sequences has been tackled by Sarkar et al. (2005), who interpreted that low sea-floor gradients, promoting rapid transgressions, coupled with a low sediment supply, may explain the observed lack of significant development of transgressive shales in the studied Proterozoic sections. In these case studies, the transgressive systems tract is typically reduced to a transgressive lag, which is preserved between stacked normal regressive systems tracts (interpreted as 'highstand' by Sarkar et al., 2005) of prograding and aggrading deposits. Aggradation under normal regressive conditions, in spite of the low sediment supply, was attributed to the prolific growth of microbial mats below the fairweather wave-base (within the shelf environment) which prevented deeper-water current reworking of sediments by the organic binding of particles (Sarkar et al., 2005). The preferential preservation of microbial mat-related structures within the deeper (shelf) portions of parasequences has also been documented by Banerjee and Jeevankumar (2005).

Conclusions

1. Microbial mats influenced sedimentary processes and the architecture of the stratigraphic record for at least the past 3.2 Ga of geological time. The relative importance of microbial activity impacting on sedimentation changed through time as a function of changing environmental-energy conditions and the evolution of competing groups of organisms.
2. The influence of microbial mats on sequence architecture is most evident for Proterozoic successions, as the proliferation of microbial mat activity was highest during that time. The strong evolution of grazing metazoan communities following the onset of the Phanerozoic marked a corresponding decline in the relative role of microbial mats on sedimentation.
3. From a sedimentological viewpoint, the organic binding of sediments afforded by microbial mats increases the cohesiveness of the substrate and results in the formation of particular sedimentary structures that provide direct or indirect evidence of syndepositional microbial activity.
4. The distribution of microbial structures within a sedimentary basin may be used to infer the change in the nature and relative energy of physical processes that operated in different depositional environments during geological time. It is inferred that coastal to shoreface wave erosion may have been stronger in the Precambrian, leading to the preferential preservation of microbial structures within shelf systems. This is contrary to modern trends, where most evidence of microbial activity is preserved in coastal to shoreface environments.

5. Research so far indicates that Precambrian sequences lack well-developed transgressive systems tracts, and are dominated by stacked systems tracts of normal regressive deposits that may be separated by thin veneers of transgressive deposits, often reduced to transgressive lags. This is in contrast to many Phanerozoic sequences, which include fully developed transgressive systems tracts consisting of all depositional systems from fluvial, to coastal and fully marine.
6. The absence (or poor development) of the fluvial to coastal section of the Precambrian transgressive systems tracts may be attributed to the inferred strong wave scouring in the upper shoreface during shoreline transgression. The lack of significant development of transgressive shales above wave ravinement surfaces may be attributed to low sea-floor gradients, promoting rapid transgressions, coupled with a low sediment supply.
7. Within Precambrian sequences, the aggradation of normal regressive deposits in spite of the low sediment supply may be explained by the prolific growth of microbial mats below the fairweather wave-base (within the shelf environment) which prevented deep-water current reworking of sediments, by the organic binding of clastic particles. As such, microbial structures are preferentially preserved within the deeper-water portions of parasequences.

This page intentionally left blank

Atlas of Microbial Mat Features Preserved within the Siliciclastic Rock Record
Edited by J. Schieber et al.
© 2007 Elsevier B.V. All rights reserved
DOI: 10.1016/S1574-1966(07)02010-X

CHAPTER 10

Conclusions

J. Schieber, G. Gerdes, P.G. Eriksson, S. Sarkar, P.K. Bose, S. Banerjee, O. Catuneanu, W. Altermann

Life on Earth is largely microbial, both in terms of biomass and the length of its existence. Approximately eighty percent of the entire history of life on Earth is exclusively microbial, and the biosphere acts as a 'geobiological agent' that has adapted to as well as modified a constantly changing environment (Altermann, 2002). When it comes to sustaining life on a geologically active planet, we can learn a great deal from the history of microbial life on Earth.

In the Precambrian, when mat-consuming metazoans were absent, microbial mats probably thrived in all environments where energy and sufficient moisture were available and where mat growth could outpace sedimentation (Schieber, 1999). Even today the global biomass is strongly influenced by the contribution from microbial life, and microbial cycling of elements significantly influences the composition of the atmosphere and hydrosphere (e.g., Fenchel and Finlay, 1995; Banfield and Nealson, 1997; Ehrlich, 1998).

As pointed out already in the introduction to this book, the first description of microbial mats and biofilms in the literature is attributed to Paracelsus (approx. 1519; Krumbein, 1994), long before the term microbial mat came into common usage. Since then various authors have written on the topic, usually from a biologic or geologic perspective (see Krumbein, 1983, 1994 for further references). The term algal mat gained considerable popularity when growth forms of blue-green algae in tropical seas were viewed as equivalent to those of Precambrian stromatolites (Darwin, 1839; Kalkowsky, 1908; Black, 1933; Cloud, 1942). When blue-green algae turned out to be cyanobacteria (Krumbein, 1979; Krumbein et al., 1979a; Rippka et al., 1979) and the mats were found to be a consortium of varied kinds of symbiotic/syntrophic organisms (Brock et al., 1994), the term microbial mat was widely adopted.

Microbial communities organise themselves in response to environmental gradients (e.g., light, moisture, nutrients) and form sheet-like structures known as microbial mats at the sediment–water interface. Within these thin (millimetre-scale) zoned communities of micro-organisms photosynthetic cyanobacteria typically (but not always) predominate over bacteria, algae, and fungi. An upper layer of aerobic phototrophs (cyanobacteria) typically passes successively downwards into anoxygenic phototrophs, and chemo-organotrophs (sulphur bacteria, sulphate-reducing bacteria and sulphide-oxidising bacteria) requiring neither oxygen (which is toxic to some species) nor light (Revsbech et al., 1983; Jørgensen et al., 1983; Pierson et al., 1987; Stolz, 1990, 1991, 2000; Brock et al., 1994). Mats of sulphide-oxidising bacteria, such as *Beggiatoa*, that cover the seafloor in low oxygen settings, for example in the Santa Barbara Basin off the coast of California, are an example of non-photosynthetic mat communities (Bernhard et al., 2000). Within these multi-layered mats, the nature of the community changes rapidly downwards, and light, oxygen, and other chemical gradients are very steep. Multi-layered mats are known already from the Archean (Altermann et al., 2006).

Just like a complex food web, microbial mats are communities of micro-organisms in which each member depends and is depended on by others in the community. Within microbial mats we see an amazing array of energy harvesting strategies, and virtually every way in which energy can be extracted from the environment can be found in microbial mats, often over vertical distances of only a few millimetres. Yet, while the active mat community may extend just a few millimetres deep into the sediment, its chemical impact, via buried and decaying biomass, may influence the sediment for decimetres and even metres beneath the surface. Identification of the actual participants in a mat-forming microbial community is hardly ever possible in the terrigenous clastic rock record. As has been illustrated in the preceding chapters of this book, however, indirect evidence is potentially plentiful.

With the advent of metazoan grazers in the Cambrian, mats became restricted to settings where extreme conditions, such as high salinity (Shark Bay), elevated temperatures (Yellowstone), or strong currents (Bahamas) exclude or severely restrict access by metazoans. In areas where metazoans destroyed mats and reworked the sediment, microbial life did not disappear but simply went underground, and formed microbial coatings on grains rather than contiguous biofilms (Monty, 1972). The vanishing of the Precambrian matground (Seilacher and Pflüger, 1994) may have been responsible for the demise of many Ediacaran organisms which were no longer able to anchor themselves easily to their shallow marine substrates (Gehling, 1999). The abundance of mat-related structures in preserved Precambrian shelf sequences suggests that *in-situ* production and preservation of organic carbon was important, a factor which needs to be considered in conceptual models for sedimentary carbon burial, global carbon cycling, and source rock formation in this era.

To date, the oldest known microbial mats in siliciclastic settings have been reported from ca. 3.2 Ga old rocks in South Africa (Noffke et al., 2006b). There are numerous occurrences in Proterozoic siliciclastics, probably reflective of the many epeiric seas of that era (e.g., Eriksson et al., 2005), where generally low sedimentation rates allowed microbial mats to thrive in many places. Interestingly, however, reduced erosion due to microbial mat binding of surface sediments may in fact result in increased rates of *net local* sedimentation (Sarkar et al., 2005). Surface stabilisation by mats may also have caused bedforms to be generally smaller in the Precambrian, when compared to what physical flow modelling would predict. The implications of bedform size and sedimentation rates at the large scale, particularly in a sequence stratigraphic context, are discussed in more detail in Chapter 9(b) of this book. Terrestrial (i.e., non-marine) mat systems have been documented as far back as 1.8 Ga (Eriksson et al., 2000).

Microbial mats within siliciclastic sediments lose their characteristic forms readily in the general absence of early cements. Compaction, decomposition and consumption by other organisms generally obliterate mat-produced organic matter within siliciclastic (and other) deposits. Anoxia and low sediment permeability underneath a mat cover may make offshore shales a relatively better host of organic carbon-rich mat laminae (Schieber, 1986, 1998; Banerjee and Jeevankumar, 2005), but a high degree of sediment compaction renders biotic and textural elements hardly recognisable within them. Factors like frequent sediment reworking, rapid sedimentation and oxidation, generally hinder mat growth and make maintaining a mat cover on shallow-water sands more difficult. Notwithstanding these disadvantages, excellent preservation of microbial mats and their associated features is possible within sandstones, including beach arenites. Fragments torn away from active surface mats may also be found locally, on or beneath sandstone beds. Microbial growth in mud-depositing offshore environments may be disturbed periodically and the microbial mat cover may be destroyed partially by distal tempestites and turbidites. Pieces of torn mat fragments produced by such erosional action can be recognised and be distinguished from *in-situ* mats in shales.

After some burial, it is rarely possible to actually identify mat-building organisms in terrigenous clastics. Fortunately, the associated sediment binding, grain agglutination, and chemical effects produce proxy structures that have much better preservation potential. Microbial filaments and EPS (extracellular polymeric substances) transform the stress response of originally loose (sand) or barely cohesive (watery mud) sediment, and make it behave in ways that are atypical for such a sediment in the absence of microbial binding. For example, upon colonisation by a microbial mat, an originally granular and non-cohesive sand will respond differently to physical stress. Added cohesion and EPS infusion will actually make it behave more like a layer of mud. It will form desiccation cracks upon drying, curl up due to differential shrinkage between top and bottom, and form pebble-sized flat and rolled-up fragments upon erosion. Microbially colonised mud surfaces as well show a range of features that are incompatible with the expected behaviour of a watery mixture of clay minerals and silt grains. In addition to unexpected cohesiveness and sedimentary features resulting from it, microbially stabilised mud surfaces are also characterised by lamina textures that suggest microbial growth, and are associated with authigenic minerals that reflect sub-mat decay of organic matter. Many microbially bound mud layers show wavy and crinkly lamination, are dark due to decaying organic matter, and may show lamina-specific pyrite enrichment (Schieber, 2004). It is these atypical and unexpected behaviours that most commonly guide us towards identification of microbial mats in terrigenous clastics.

Carbonate stromatolites and microbial laminites extend far below the Proterozoic–Archaean boundary (up to 3.5 Ga; Golubic and Seong-Joo, 1999; Altermann and Kazmierczak, 2003), and one might expect that microbial mat features in siliciclastic rocks should show a comparable temporal extent. Yet, at present their known record extends only to about 3.2 Ga (Noffke et al., 2006b). Is this circumstance merely a sampling artifact, or does it signify something of importance for the evolution of life?

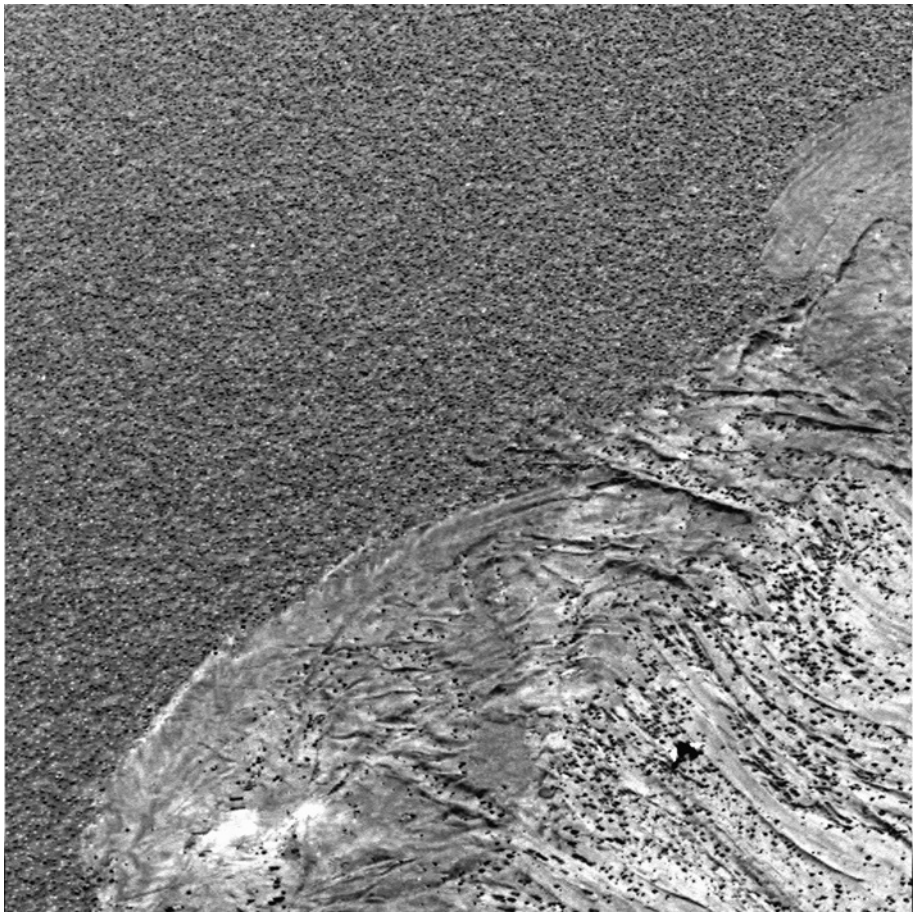


Figure 10-1: Wrinkle structures from the landing site of the Mars rover *Opportunity* (January 2004, image courtesy of NASA).
These wrinkles were produced when the deflated airbags were pulled in towards the lander, prior to egress of *Opportunity*. They attest to a cohesive nature of the surface sediment and temporarily did get some people excited about the possibility for microbial life at the surface. Closer inspection, however, showed that the soil matrix is fine grained in nature (detection of clays is not possible with the rover instruments) and that the cohesiveness is a physical phenomenon, comparable to the way in which fine powders can readily be molded into a wide variety of three dimensional shapes.

Mats possibly also played an important role in biological evolution. For example, one of the plausible explanations for the demise of many Ediacaran organisms is that their ability to anchor themselves to the substrate with holdfasts was degraded concurrent with the rapid decline in microbial mat coverage at the Proterozoic–Phanerozoic transition (Seilacher and Pflüger, 1994). With the advent of burrowers, microbial influence extended deeper beneath the sediment surface, but contiguous biofilms were more difficult to sustain. This may have shifted the balance of sedimentary biofilms towards those that form as microbial coatings around individual grains, such as oncoids and 'algal biscuits' (Monty, 1972). Abundance of mat-related structures in shelf sequences also implies *in-situ* production and preservation of organic carbon. Conceptual models for sedimentary carbon burial and source rock formation in the Precambrian have to take this significant difference to the Phanerozoic into account. There is also a growing interest in terrestrial microbial mat systems and in the freshwater microbes that produce stromatolites (Freytet and Verrecchia, 1998).

Due to the large contribution of microbial life to the global biomass, atmosphere-hydrosphere chemical cycles are strongly influenced by microbes (e.g., Fenchel and Finlay, 1995; Banfield and Nealson, 1997; Ehrlich, 1998). For example, close to the depositional site, ammonification, denitrification and sulphate reduction of microbial sediment leads to a rise in alkalinity of ambient water (Krumbein, 1979; Visscher et al., 1992; Castanier et al., 2000; Knorre and Krumbein, 2000; Riding, 2000). Microbial mats also play an important chemical role in the reductive fixing of metals like iron, manganese, gold and uranium (Milodowski et al., 1990; Watterson, 1992;

Nealson and Saffarini, 1994; Ferris, 2000). Thus, the trace element geochemical signatures of sedimentary rocks may be misinterpreted if the former presence of microbial mats goes undetected.

Aside of their utility for palaeoenvironmental reconstructions, mat-induced structures can also serve as important palaeogeographic indicators and have potential for refining techniques of basin analysis in Precambrian strata. The impediment to erosion caused by prolific mat growth may be a key factor that encouraged vertical stacking of highstand systems tracts in the Precambrian. At a smaller scale, mat growth reflects a low rate and the discontinuous nature of sedimentation, and partly controls bedform evolution. Establishing an interest in microbial mat structures in siliciclastic sediment is, therefore, laden with the possibility of elucidating a wide range of geological phenomena.

Fossil microbial mats, or stromatolites, attest to the existence of water or moisture in which microbial life thrived, and constitute the oldest and most pervasive evidence of life on Earth. Therefore they also figure prominently in our attempts to identify life on other planets. NASA's Mars rovers *Spirit* and *Opportunity*, for example, have sufficient optical resolution to readily image all of the mat-related morphological features illustrated from sandstones in this book, and the Microscopic Imager on these rovers has enough resolution to image at least a portion of the features we might expect to find in fine-grained rocks. In NASA's upcoming Mars Science Lab mission (launch planned for 2009), more sophisticated imaging devices are bundled with an instrument suite (mass spectrometer, gas chromatograph, tunable laser spectrometer) for detection and analysis of carbon compounds. Any rocks with features that would suggest the former presence of microbial mats would also be a logical target for additional geochemical analysis. Due to surface waters that were apparently of quite low pH (Squires et al., 2004) our chances of finding nicely preserved carbonate stromatolites might be negligible. However, that still leaves us with plenty of clastic rocks that can be examined for microbial mat indications. Thus, learning as much as we can about microbial mats in terrigenous clastics on Earth will benefit our efforts to detect life elsewhere in the solar system. In absence of the preserved mat-building organisms, detecting the former presence of microbial mats in terrigenous clastics necessarily depends on judicious assembly of indirect evidence. Thus, careful evaluation of non-mat processes is a must (Figure 10-1).

Building broader awareness of what microbial mats and their proxies might look like in terrigenous clastic sediments and sedimentary rocks is the main objective of this book. Nonetheless, the sampling of microbially produced sedimentary features in terrigenous clastics provided in this atlas is far from exhaustive. The illustrations of modern and ancient mat features in sandstones and mudstones are intended as a starting point for identification of potential occurrences by others. They should not be viewed as a definitive listing of all things microbial in sandstones and mudstones. A good deal of valuable geological information will remain out of our reach unless the mat-related structures within siliciclastic sedimentary rocks receive the attention they deserve, and we are confident that increased awareness will bring forth many additional features that simply have not yet been described. If this richly illustrated compendium spurs new research into microbial mats in terrigenous clastic sediments, their temporal and spatial distribution, and their role and significance for past and present siliciclastic depositional systems, we will have accomplished our goal.

Reference List

Aigner, T., 1985. Storm Depositional Systems: Dynamic Stratigraphy in Modern and Ancient Shallow Marine Sequences. Lecture Notes in Earth Sciences, vol. 3. Springer-Verlag, Berlin, 174 pp.

Aigner, T., Reineck, H.-E., 1982. Proximality trends in modern storm sands from the Helgoland Bight (North Sea) and their implications for basin analysis. Senckenbergiana Maritima 14, 183–215.

Aitken, J.D., 1967. Classification and environmental significance of cryptalgal limestones and dolomites with illustrations from the Cambrian and Ordovician of southwestern Alberta. J. Sediment. Petrol. 37, 1163–1178.

Allen, J.R.L., 1966. A beach structure due to wind-driven foam. J. Sediment. Petrol. 37, 691–692.

Allen, J.R.L., 1985. Wrinkle marks: an intertidal sedimentary structure due to aseismic soft-sediment loading. Sediment. Geol. 41, 75–95.

Alsharhan, A.S., Kendall, C.G.St.C., 2003. Holocene coastal carbonates and evaporites of the southern Arabian Gulf and their ancient analogues. Earth-Sci. Rev. 61, 191–243.

Altermann, W., 2002. The evolution of life and its impact on sedimentation. In: Altermann, W., Corcoran, P.L. (Eds.), Precambrian Sedimentary Environments: A Modern Approach to Ancient Depositional Systems. Int. Assoc. Sediment. Spec. Publ. 33. Blackwell Science, Oxford, pp. 15–32.

Altermann, W., 2004. Evolution of life and Precambrian bio-geology. In: Eriksson, P.G., Altermann, W., Nelson, D.R., Mueller, W.U., Catuneanu, O. (Eds.), The Precambrian Earth: Tempos and Events. Developments in Precambrian Geology, vol. 12. Elsevier, Amsterdam, pp. 587–591.

Altermann, W., Kazmierczak, J., 2003. Archean microfossils: A reappraisal of early life on Earth. Res. Microbiol. 154, 611–617.

Altermann, W., Kazmierczak, J., Oren, A., Wright, D., 2006. Microbial calcification and its impact on the sedimentary rock record during 3.5 billion years of Earth history. Geobiology 4, 147–166.

Anderson, C.R., Pedersen, K., 2003. In situ growth of Gallionella biofilms and partitioning of lanthanides and actinides between biological material and ferric oxyhydroxides. Geobiology 1, 169–178.

Arp, G., Reimer, A., Reitner, J., 2001. Photosynthesis-induced biofilm calcification and calcium concentrations in Phanerozoic oceans. Science 292, 1701–1704.

Assereto, R.L.A.M., Kendall, C.G.St., 1977. Nature, origin and classification of peritidal tepee structures and related breccias. Sedimentology 24, 153–210.

Astin, T.R., Rogers, D.A., 1991. "Subaqueous shrinkage cracks" in the Devonian of Scotland reinterpreted. J. Sediment. Petrol. 61, 850–859.

Astin, T.R., Rogers, D.A., 1993. "Subaqueous shrinkage cracks" in the Devonian of Scotland reinterpreted – reply. J. Sediment. Petrol. 63, 566–567.

Awramik, S.M., 1984. Ancient stromatolites and microbial mats. In: Cohen, Y., Castenholz, R.W., Halvorson, H.O. (Eds.), Microbial Mats: Stromatolites. Alan R. Liss, New York, pp. 1–22.

Baker, P.A., Kastner, M., 1981. Constraints on the formation of sedimentary dolomite. Science 213, 214–216.

Banerjee, S., 1997. Facets of Mesoproterozoic Semri sedimentation, Son valley, M.P. Ph.D. thesis (unpubl.), Jadavpur University, Kolkata, 137 pp.

Banerjee, S., Jeevankumar, S., 2005. Microbially originated wrinkle structures on sandstones and their stratigraphic context: Paleoproterozoic Koldaha Shale, central India. Sediment. Geol. 176, 211–224.

Banerjee, S., Dutta, S., Paikaray, S., Mann, U., 2006. Stratigraphy, sedimentology and bulk organic geochemistry of black shales from the Proterozoic Vindhyan Supergroup (central India). J. Earth Syst. Sci. 115, 37–48.

Banfield, J.F., Nealson, K.H. (Eds.), 1997. Interactions Between Microbes and Minerals. Rev. Mineral., vol. 35. Mineral. Soc. Amer., Washington, DC, 448 pp.

Barclay, W.J., Glover, B.W., Mendum, J.R., 1993. "Subaqueous shrinkage cracks" in the Devonian of Scotland reinterpreted – discussion. J. Sediment. Petrol. 63, 564–565.

Bauld, J., 1981. Geobiological role of cyanobacterial mats in sedimentary environments: production and preservation of organic matter. BMR J. Austral. Geol. Geophys. 6, 307–317.

Bauld, J., D'Amelio, E., Farmer, J.D., 1992. Modern microbial mats. In: Schopf, J.W., Klein, C. (Eds.), The Proterozoic Biosphere: A Multidisciplinary Study. Cambridge University Press, New York, pp. 261–269.

Baur, M., Hayes, J., Studley, S., Walter, M., 1985. Millimeter-scale variations of stable isotope abundances in carbonates from banded iron formations in the Hamersley Group of western Australia. Econ. Geol. 80, 270–282.

Bazylinski, D.A., Frankel, R.B., 2003. Biologically controlled mineralization in prokaryotes. Rev. Mineral. Geochem. 54, 217–247.

Belnap, J., Gardner, J.S., 1993. Soils microstructure in soils of the Colorado Plateau: the role of the cyanobacterium Microcoleus vaginatus. Great Basin Naturalist 53, 40–47.

Bennet, E.M., 1965. Lead-zinc-silver and copper deposits of Mount Isa. In: McAndrew, J. (Ed.), Geology of Australian Ore Deposits. Proc. 8th Commonwealth Min. Metall. Congr., vol. 1, Melbourne, pp. 233–246.

Berner, R.A., 1984. Sedimentary pyrite formation: an update. Geochim. Cosmochim. Acta 48, 605–615.

Bernhard, J.M., Buck, K.R., Farmer, M.A., Bowser, S.S., 2000. The Santa Barbara basin is a symbiosis oasis. Nature 403, 77–80.

Bernier, P., Gaillard, C., Gall, J.C., Barale, G., Bourseau, J.P., Buffetaut, E., Wenz, S., 1991. Morphogenetic impact of microbial mats on surface structures of Kimmeridgian micritic limestones (Cerin, France). Sedimentology 38, 127–136.

Bertrand-Sarfati, J., 1994. Siliciclastic-carbonate domes in the Early Carboniferous of the Ajjers Basin (eastern Sahara, Algeria). In: Bertrand-Sarfati, J., Monty, C.L.V. (Eds.), Phanerozoic Stromatolites II. Kluwer Academic Publishers, Dordrecht, pp. 395–419.

Bertrand-Sarfati, J., Freytet, P., Plaziat, J.C., 1994. Microstructures in Tertiary nonmarine stromatolites (France). Comparison with Proterozoic. In: Bertrand-Sarfati, J., Monty, C.L.V. (Eds.), Phanerozoic Stromatolites II. Kluwer Academic Publishers, Dordrecht, pp. 155–191.

Beukes, N.J., 1996. Sole marks and combined-flow storm event beds in the Brixton Formation of the siliciclastic Archean Witwatersrand Supergroup, South Africa. J. Sediment. Res. 66, 567–576.

Beukes, N., Eriksson, E., Sumner, D., 2002. Archean to Proterozoic sedimentological superlatives along the eastern Kaapvaal Craton. Excursion Guide, 16th International Sedimentologists Congress, Rand Afrikaans University, South Africa, 79 pp.

Black, M., 1933. The algal sediments of Andros Islands, Bahamas. Phil. Trans. Roy. Soc. London Ser. B, 165–192.

Blatt, H., 1992. Sedimentary Petrology, second ed. W.H. Freeman, New York, 514 pp.

Bloos, G., 1976. Untersuchungen über Bau und Entstehung der feinkörnigen Sandsteine des Schwarzen Jura α (Hettangium u. tiefstes Sinemurium) im schwäbischen Sedimentationsbereich. Arb. Inst. Geol. Paläont. Univ. Stuttgart 71, 1–270.

Boggs, S., 1995. Principles of Sedimentology and Stratigraphy, second ed. Prentice Hall, Upper Saddle River, NJ, 774 pp.

Bohacs, K.M., Caroll, A.R., Neal, J.E., Mankiewicz, P.J., 2000. Lake-basin type, source potential and hydrocarbon character: an integrated sequence stratigraphic-geochemical framework. In: Gierlowski-Kordesch, E.H., Kelts, K.R. (Eds.), Lake Basins Through Space and Time. Studies in Geology, vol. 46. Amer. Assoc. Petrol. Geol., Tulsa, OK, pp. 3–34.

Bose, P.K., Banerjee, S., Sarkar, S., 1997. Slope-controlled seismic deformation and tectonic framework of deposition of Koldaha Shale, India. Tectonophysics 269, 151–169.

Bose, P.K., Sarkar, S., Chakraborty, S., Banerjee, S., 2001. Overview of the Meso- to Neoproterozoic evolution of the Vindhyan basin, central India (1.4–0.55 Ga). Sediment. Geol. 141/142, 395–419.

Bouougri, E., Porada, H., 2002. Mat-related sedimentary structures in Neoproterozoic peritidal passive margin deposits of the West African Craton (Anti-Atlas, Morocco). Sediment. Geol. 153, 85–106.

Bouougri, E.H., Saquaque, A., 2004. Lithostratigraphic framework and correlation of the Neoproterozoic northern western African craton passive margin sequence (Siroua-Zenaga-Bou Azzer El Graara Inliers, central Anti-Atlas, Morocco): an integrated approach. J. African Earth Sci. 39, 227–238.

Bowden, T.D., 1977. Depositional processes and environments within the Revett Formation, Precambrian Belt Supergroup, northwestern Montana and northern Idaho. M.S. thesis (unpubl.), University of California, Riverside, 161 pp.

Boyce, R.L., 1973. Depositional systems in the Ravalli Group: a conceptual model and possible modern analogue. In: Belt Symposium 1973, vol. I. Idaho Bureau of Mines Geol. Spec. Publ. 2, pp. 139–158.

Bradley, W.H., 1964. Geology of the Green River Formation and associated Eocene rocks in southwestern Wyoming and adjacent parts of Colorado and Utah. U.S. Geol. Surv. Prof. Paper 496A, 86 pp.

Braga, J.C., Martin, J.M., 2000. Subaqueous siliciclastic stromatolites: a case history from Late Miocene beach deposits in the Sorbas Basin of SE Spain. In: Riding, R.E., Awramik, S.M. (Eds.), Microbial Sediments. Springer-Verlag, Berlin, pp. 226–232.

Brassell, S.C., 1992. Biomarkers in sediments, sedimentary rocks and petroleums: biological origins, geological fate and applications. In: Pratt, L.M., Comer, J.B., Brassell, S.C. (Eds.), Geochemistry of Organic Matters in Sediments and Sedimentary Rocks. Soc. Econ. Paleontol. Mineral. Short Course 27, Tulsa, OK, pp. 29–72.

Brett, C.E., Allison, P.A., 1998. Paleontological approaches to the environmental interpretation of marine mudrocks. In: Schieber, J., Zimmerle, W., Sethi, P. (Eds.), Shales and Mudstones, vol. 1, Basin Studies, Sedimentology and Paleontology. Schweizerbart'sche Verlagsbuchhandlung, Stuttgart, pp. 301–349.

Brock, T.D., Madigan, M.T., Martinko, J.M., Parker, J., 1994. Biology of Microorganisms, seventh ed. Prentice Hall, Englewood Cliffs, NJ, 909 pp.

Bromley, R.G., 1990. Trace Fossils: Biology and Taphonomy. Unwin Hyman Ltd., London, 280 pp.

Brown, L.F., Jr., Fisher, W.L., 1977. Seismic stratigraphic interpretation of depositional systems: examples from Brazilian rift and pull apart basins. In: Payton, C.E. (Ed.), Seismic Stratigraphy – Applications to Hydrocarbon Exploration. Amer. Assoc. Petrol. Geol. Mem. 26, Tulsa, OK, pp. 213–248.

Browne, K.M., Golubic, S., Seong-Joo, L., 2000. Shallow marine microbial carbonate deposits. In: Riding, R.E., Awramik, S.M. (Eds.), Microbial Sediments. Springer-Verlag, Berlin, pp. 233–249.

Buck, S.G., 1980. Stromatolite and ooid deposits within the fluvial and lacustrine sediments of the Precambrian Ventersdorp Supergroup of South Africa. Precambrian Res. 12, 311–330.

Buick R., 1992. The antiquity of oxygenic photosynthesis: evidence from stromatolites in sulphate-deficient Archaean lakes. Science 255, 74–77.

Burne, R.V., Moore, L.S., 1987. Benthic microbial communities and microbialites. In: Annual Report 1985, Baas Becking Geobiological Laboratory, pp. 10–12.

Butler, G., 1969. Modern evaporite deposition and geochemistry of coexisting brines, the sabkha, Trucial Coast, Arabian Gulf. J. Sediment. Petrol. 39, 70–89.

Cameron, B., Cameron, D., Richard J., 1985. Modern algal mats in intertidal and supratidal quartz sands, northeastern Massachusetts, U.S.A. In: Curran, H.A. (Ed.), Biogenic Structures: Their Use in Interpreting Depositional Environments. Soc. Econ. Paleontol. Mineral. Spec. Publ. 35, Tulsa, OK, pp. 211–223.

Castanier, S., Le Métayer-Levrel, G., Perthuisot, J.-P., 2000. Bacterial roles in the precipitation of carbonate minerals. In: Riding, R., Awramik, S.M. (Eds.), Microbial Sediments. Springer-Verlag, Berlin, pp. 32–39.

Catuneanu, O., 2006. Principles of Sequence Stratigraphy, first ed. Elsevier, Amsterdam, 375 pp.

Catuneanu, O., Eriksson, P.G., 1999. The sequence stratigraphic concept and the Precambrian rock record: an example from the 2.7–2.1 Ga Transvaal Supergroup, Kaapvaal craton. Precambrian Res. 97, 215–251.

Chafetz, H.S., 1994. Bacterially induced precipitates of calcium carbonate and lithification in microbial mats. In: Krumbein, W.E., Paterson, D.M., Stal, L.J. (Eds.), Biostabilization of Sediments. Bibliotheks- und Informationsystem der Carl von Ossietzky Universität Oldenberg, (BIS)-Verlag, Oldenburg, pp. 149–164.

Chafetz, H.S., Buczynski, C., 1992. Bacterially induced lithification of microbial mats. Palaios 7, 277–293.

Chakraborty, P.P., 2004. Facies architecture and sequence development in a Neoproterozoic carbonate ramp: Lakheri Limestone Member, Vindhyan Supergroup, central India. Precambrian Res. 132, 29–53.

Chakraborty, S., 2002. Sedimentation sequence of the three youngest members of the Vindhyan Supergroup, central India. Ph.D. thesis (unpubl.), Jadavpur University, Kolkata, 150 pp.

Chaudhuri, A.K., Mukhopadhyay, J., Patranabis Deb, S., Chanda, S.K., 1999. The Neoproterozoic cratonic successions of Peninsular India. Gondwana Res. 2, 213–225.

Chaudhuri, A.K., Saha, D., Deb, G.K., Patranabis Deb, S., Mukherjee, M.K., Ghosh, G., 2002. The Purana basins of southern cratonic province of India – A case for Mesoproterozoic fossil rifts. Gondwana Res. 5, 23–33.

Christensen, P.R., Clark, R.N., Kieffer, H.H., Malin, M.C., Pearl, J.C., Bandfield, J.L., Edgett, K.S., Hamilton, V.E., Hoefen, T., Lane, M.D., Morris, R.V., Pearson, R., Roush, T., Ruff, S.W., Smith, M.D., 2000. Detection of crystalline hematite mineralization on Mars by the Thermal Emission Spectrometer: evidence for near-surface water. J. Geophys. Res. 105, 9623–9642.

Clauer, N., 1976. Géochimie isotopique du strontium des milieux sédimentaires. Application à la géochronologie du craton Ouest Africain. Sciences Géologiques, Thèse Université de Strasbourg, Strasbourg, 256 pp.

Clemmey, H.A., 1978. Proterozoic lacustrine interlude from the Zambian copperbelt. In: Matter, A., Tucker, M.E. (Eds.), Modern and Ancient Lake Sediments. Int. Assoc. Sediment. Spec. Publ. 2. Blackwell Science, London, pp. 259–278.

Clifton, H.E., 1977. Rain-impact ripples. J. Sediment. Petrol. 47, 678–679.

Cloud, P., 1973. Paleoecological significance of the banded iron-formation. Econ. Geol. 68, 1135–1143.

Cloud, P.E., 1942. Notes on stromatolites. Amer. J. Sci. 240, 363–379.

Coe, A.L. (Ed.), 2003. The Sedimentary Record of Sea-Level Change. Cambridge University Press, New York, 287 pp.

Cohen, Y., Krumbein, W.E., Shilo, M., 1977. Solar Lake (Sinai). 3. Bacterial distribution and production. Limnol. Oceanogr. 22, 621–634.

Cook, D.A., 1991. Sedimentology and shale petrology of the upper Proterozoic Walcott Member, Kwagunt Formation, Chuar Group, Grand Canyon, Arizona. M.S. thesis (unpubl.), Northern Arizona University, Arizona, 158 pp.

Cornell, R.M., Schwertmann, U., 2003. The Iron Oxides: Structure, Properties, Reactions, Occurrences and Uses, second ed. Wiley–VCH Verlag, Weinheim, 703 pp.

Correns, C.W., 1934. Grundsätzliches zur Darstellung der Korngrößenverteilung. Zbl. Min. Geol. Palaeont. Abtl. A 11, 321–331.

Costerton, J., Stoodley, P., 2003. Microbial biofilms: protective niches in ancient and modern geomicrobiology. In: Krumbein, W.E., Paterson, D.M., Zavarzin, G.A. (Eds.), Fossil and Recent Biofilms (Preface). Kluwer Academic Publishers, Dordrecht, pp. xv–xxi.

Cotton, R.E., 1965. H.Y.C. lead-zinc-silver deposit, McArthur River. In: McAndrew, J. (Ed.), Geology of Australian Ore Deposits. Proc. 8th Commonwealth Min. Metall. Congr., vol. 1, Melbourne, pp. 197–200.

Cregg, B.A., Harvey, S.M., Fry, J.C., Herbert, R.A., Parks, R.J., 1992. Bacterial biomass and activity in deep sediment layers of the Japan Sea, Hole 798 B. Proc. Scientific Results, ODP, Legs 127/128, Japan Sea, pp. 761–776.

Cressman, E.R., 1989. Reconnaissance stratigraphy of the Prichard Formation (Middle Proterozoic) and the early development of the Belt Basin, Washington, Idaho and Montana. U.S. Geol. Surv. Prof. Paper 1490, 80 pp.

Crimes, T.P., Germs, G.J.B., 1982. Trace fossils from the Nama Group (Precambrian–Cambrian) of southwest Africa (Namibia). J. Paleontol. 56, 890–907.

Cross, T.A., Lessenger, M.A., 1998. Sediment volume partitioning: rationale for stratigraphic model evaluation and high-resolution stratigraphic correlation. In: Gradstein, F.M., Sandvik, K.O., Milton, N.J. (Eds.), Sequence Stratigraphy – Concepts and Applications. Norwegian Petroleum Society (NPF) Spec. Publ. 8. Elsevier, Amsterdam, pp. 171–195.

Dade, W.B., Davis, J.D., Nichols, P.D., Nowell, A.R.M., Thistle, D., Trexler, M., White, D.C., 1990. Effects of bacterial exopolymer adhesion on the entrainment of sand. Geomicrob. J. 8, 1–16.

Dahanayake, K., Gerdes, G., Krumbein, W.E., 1985. Stromatolites, oncolites and oolites biogenically formed in situ. Naturwissenschaften 72, 513–518.

Darwin, C., 1839. Journal of the researches into the geology and natural history of the various countries visited by HMS Beagle, vol. 1. Appleton and Company, New York (reprint 1958).

Davies, S.J., Gibling, M.R., 2003. Architecture of coastal and alluvial deposits in an extensional basin: the Carboniferous Joggins Formation of eastern Canada. Sedimentology 50, 415–439.

Davis, R.A., 1968. Algal stromatolites composed of quartz sandstone. J. Sediment. Petrol. 38, 953–955.

Dawson, J.W., 1878. Supplement to the second ed. of Acadian Geology. Acadian Geology, the Geological Structure, Organic Remains and Mineral Resources of Nova Scotia, News Brunswick, and Prince Edward Island, third ed. Macmillan & Co., London, 102 pp.

Decho, A.W., 1990. Microbial exopolymer secretions in ocean environments: their roles in food webs and marine processes. Oceanogr. Mar. Biol. Ann. Rev. 28, 73–153.

Decho, A.W., 1994. Molecular-scale events influencing the macroscale cohesiveness of exopolymers. In: Krumbein, W.E., Paterson, D.M., Stal, L.J. (Eds.), Biostabilization of Sediments. Bibliotheks- und Informationsystem der Carl von Ossietzky Universität Oldenberg, (BIS)-Verlag, Oldenburg, pp. 134–148.

Decho, A.W., 2000. Exopolymer microdomains as a structuring agent for heterogeneity within microbial biofilms. In: Riding, R., Awramik, S.M. (Eds.), Microbial Sediments. Springer-Verlag, Berlin, pp. 9–15.

Dehler, C.M., Elrick, M., Karlstrom, K.E., Smith, G.A., Crossey, L.J., Timmons, J.M., 2001. Neoproterozoic Chuar Group (∼800–742 Ma), Grand Canyon: a record of cyclic marine deposition during global cooling and supercontinent rifting. Sediment. Geol. 141/142, 465–499.

Demarest, J.M., Kraft, J.C., 1987. Stratigraphic record of Quaternary sea levels: implications for more ancient strata. In: Nummedal, D., Pilkey, O.H., Howard, J.D. (Eds.), Sea Level Fluctuation and Coastal Evolution. Soc. Econ. Paleontol. Mineral. Spec. Publ. 41, Tulsa, OK, pp. 223–239.

Demicco, R.V., Hardie, L.A., 1994. Sedimentary Structures and Early Diagenetic Features of Shallow Marine Carbonate Deposits. Soc. Econ. Paleontol. Mineral. Atlas Series 1, Tulsa, OK, 265 pp.

Dickinson, W.R., 1970. Interpreting detrital modes of grey-wackes and arkose. J. Sediment. Petrol. 40, 695–707.

Dickman, M., 1985. Seasonal succession and microlamina formation in a meromictic lake displaying varved sediments. Sedimentology 32, 109–118.

Dickman, M., Artuz, I., 1978. Mass mortality of photosynthetic bacteria as a mechanism of dark lamina formation in sediments of the Black Sea. Nature 275, 191–195.

Diessel, C., Boyd, R., Wadsworth, J., 2000. On balanced and unbalanced accommodation/peat accumulation ratios in the Cretaceous coals from the Gates Formation, Western Canada, and their sequence-stratigraphic significance. Int. J. Coal Geol. 43, 143–186.

Donaldson, J.A., Hilowle, M.A., 2002. Organic mats, evaporite pseudomorphs and soft-sediment deformation in quartz arenites of the Cambro-Ordovician Nepean Formation. Abstract, Geol. Assoc. Canada/Mineral. Assoc. Canada Joint Annual Meeting, 27–29 May 2002, Saskatoon. Program with Abstracts 27, p. 29.

Donaldson, J.A., Eriksson, P.G., Altermann, W., 2002a. Actualistic versus non-actualistic conditions in the Precambrian: a reappraisal of an enduring discussion. In: Altermann, W., Corcoran, P.L. (Eds.), Precambrian Sedimentary Environments: A Modern Approach to Ancient Depositional Systems. Int. Assoc. Sediment. Spec. Publ. 33. Blackwell Science, Oxford, pp. 3–13.

Donaldson, J.A., Munro, I., Hilowle, M.A., 2002b. Biofilm structures, trace fossils and stromatolites in Early Paleozoic quartz arenites and carbonates of the Ottawa region, Ontario. Abstract, 12th Canadian Paleontology Conference (CPC-2002), 29–30 September. Program and Abstracts, p. 12.

Donaldson, J.A., Chiarenzelli, J.R., 2004. Stromatolites and associated biogenic structures in Cambrian and Ordovician strata in and near Ottawa, Ontario. Trip F-1, New York Geological Assoc., 76th Annual Meeting, Suny Potsdam. Field Trip Guidebook, pp. 1–20.

Donaldson, J.A., Chiarenzelli, J.R., Aspler, L., 2005a. Siliciclastic biofilm structures and stromatolites: conditions for preservation. Abstract, Geol. Assoc. Canada/Mineral. Assoc. Canada Meeting/Canadian Soc. Petrol. Geol./Canadian Soc. Soil Sci. Joint Meeting, 15–18 May 2005, Halifax, Nova Scotia. Program with Abstracts 30, pp. 45–46.

Donaldson, J.A., Chiarenzelli, J.R., Aspler, L.B., 2005b. Cambro-Ordovician stromatolite occurrences in the Ottawa region. Abstract, Geological Society of America, Northeastern Section 40th Annual Meeting, 14–16 March 2005, Saratoga Springs, NY, p. 3.

Donovan, R.N., Foster, R.J., 1972. Subaqueous shrinkage cracks from the Caithness Flagstone Series (Middle Devonian) of north east Scotland. J. Sediment. Petrol. 42, 309–317.

Dott, R.H., 2003. The importance of eolian abrasion in supermature quartz sandstones and the paradox of weathering on vegetation free landscapes. J. Geol. 111, 387–405.

Draganits, E., Noffke, N., 2004. Siliciclastic, domed stromatolites from the Lower Devonian Muth Formation, NW Himalaya. J. Sediment. Res. 74, 191–202.

Dzulynski, S., Walton, E.K., 1965. Sedimentary Features of Flysch and Greywackes. Developments in Sedimentology, vol. 7. Elsevier, Amsterdam, 274 pp.

Ehrenberg, C.G., 1839. Uber das im Jahre 1686 in Curland vom Himmel gefallene Meteorpapier und uber dessen Zusammensetzung aus Conferven und Infusorien. Ann. Phys. Chem. 16, 187–188.

Ehrlich, H.L., 1998. Geomicrobiology: its significance for geology. Earth-Sci. Rev. 45, 45–60.

Eldridge, D.J., Green, R.S.B., 1994. Microbiotic soil crusts – a review of their roles in soil and ecological processes in the rangelands of Australia. Austral. J. Soil Res. 32, 389–415.

Emerson, D., Weiss, J.V., 2004. Bacterial iron oxidation in circumneutral freshwater habitats: findings from the field and the laboratory. Geomicrobiol. J. 21, 405–414.

Emerson, D., Weiss, J.V., Megonigal, J.P., 1999. Iron-oxidizing bacteria are associated with ferric hydroxide precipitates (Fe-plaque) on the roots of the wetland plants. Appl. Environ. Microbiol. 65, 2758–2761.

Emery, D., Myers, K.J., 1996. Sequence Stratigraphy. Blackwell Science, Oxford, 297 pp.

Eriksson, K.A., Simpson, E.L., 2000. Quantifying the oldest tidal record: The 3.2 Ga Moodies Group, Barberton Greenstone Belt, South Africa. Geology 28, 831–834.

Eriksson, K.A., Turner, B.R., Vos, R.G., 1981. Evidence of tidal processes from the lower part of the Witwatersrand Supergroup, South Africa. Sediment. Geol. 29, 309–325.

Eriksson, P.G., Simpson, E.L., Eriksson, K.A., Bumby, A.J., Steyn, G.L., Sarkar, S., 2000. Muddy roll-up structures in siliciclastic interdune beds of the ca. 1.8 Ga Waterberg Group, South Africa. Palaios 15, 177–183.

Eriksson, P.G., Altermann, W., Nelson, D.R., Mueller, W.U., Catuneanu, O. (Eds.), 2004. The Precambrian Earth: Tempos and Events. Developments in Precambrian Geology, vol. 12. Elsevier, Amsterdam, 941 pp.

Eriksson, P.G., Catuneanu, O., Sarkar, S., Tirsgaard, H., 2005. Patterns of sedimentation in the Precambrian. Sediment. Geol. 176, 17–42.

Fagerstrom, J.A., 1967. Development, flotation and transportation of mud crusts-neglected factors in sedimentology. J. Sediment. Petrol. 37, 73–79.

Fairbridge, R.W., Bourgeois, J. (Eds.), 1978. The Encyclopedia of Sedimentology. Hutchinson and Ross, Dowden, Strasbourg, 901 pp.

Fairchild, I.J., Herrington, P.M., 1989. A tempestite-stromatolite-evaporite association (late Vendian, East Greenland): a shoreface-lagoon model. Precambrian Res. 43, 101–127.

Fedonkin, M.A., 1990. Systematic description of Vendian Metazoa. In: Sokolov, B.S., Iwanowski, A.B. (Eds.), The Vendian System, vol. 1, Paleontology. Springer-Verlag, Berlin, pp. 71–120.

Fenchel, T., Finlay, B.J., 1995. Ecology and Evolution in Anoxic Worlds. Oxford University Press, Oxford, 276 pp.

Fenchel, T., Kühl, M., 2000. Artificial cyanobacterial mats: growth, structure, and vertical zonation patterns. Microbial Ecol. 40, 85–93.

Ferber, C.T., Wells, N.A., 1995. Paleolimnology and taphonomy of some fish deposits in 'Fossil' and 'Uinta' lakes of the Eocene river formation, Utah and Wyoming. Palaeo. Palaeo. Palaeo. 117, 185–210.

Ferris, F.G., 2000. Microbe–metal interactions in sediments. In: Riding, R., Awramik, S.M. (Eds.), Microbial Sediments. Springer-Verlag, Berlin, pp. 121–126.

Fischer, A.G., 1964. The Lofer cyclothems of the Alpine Triassic. Kansas Geol. Surv. Bull. 169, 107–149.

Flügel, E., 2004. Microfacies of Carbonate Rocks. Springer-Verlag, Berlin, 976 pp.

Fortin, D., Langley, S., 2005. Formation and occurrence of biogenic iron-rich minerals. Earth-Sci. Rev. 72, 1–19.

Fortin, D., Tessier, A., Leppard, G.G., 1993. Characteristics of lacustrine iron oxyhydroxides. Geochim. Cosmochim. Acta 57, 4391–4404.

Fowler, M.G., Douglas, A.G., 1987. Saturated hydrocarbon biomarkers in oils of late Precambrian age from eastern Siberia. Org. Geochem. 11, 201–213.

Freytet, P., Verrecchia, E.P., 1998. Freshwater organisms that build stromatolites: a synopsis of biocrystallization by prokaryotic and eukaryotic algae. Sedimentology 45, 535–563.

Friedman, G.M., Krumbein, W.E. (Eds.), 1985. Hypersaline Ecosystems: the Gavish Sabkha. Springer-Verlag, Berlin, 484 pp.

Friedman, G.M., Sanders, J.E., Kopaska-Merkel, D., 1992. Principles of Sedimentary Deposits. MacMillan, New York, 717 pp.

Füchtbauer, H. (Ed.),1988. Sedimente und Sedimentgesteine. Schweizerbart, Stuttgart, 1141 pp.

Gallardo, V.A., 1977. Large benthic microbial communities in sulfide biota under Peru–Chile subsurface counter current. Nature 268, 331–332.

Galloway, W.E., Hobday, D.K., 1996. Terrigenous Clastic Depositional Systems, second ed. Springer-Verlag, Berlin, 489 pp.

Garcia-Pichel, F., Castenholz, R.W., 1994. On the significance of solar ultraviolet radiation for the ecology of microbial mats. In: Stal, L.J., Caumette, P. (Eds.), Microbial Mats: Structure, Development and Environmental Significance. Springer-Verlag, Berlin, pp. 77–84.

Garlick, W.G., 1981. Sabkhas, slumping, and compaction at Mufulira, Zambia. Econ. Geol. 76, 1817–1847.

Garlick, W.G., 1988. Algal mats, load structures, and synsedimentary sulfides in Revett Quartzites of Montana and Idaho. Econ. Geol. 83, 1259–1278.

Garrett, P., 1970. Phanerozoic stromatolites: noncompetitive ecologic restriction by grazing and burrowing animals. Science 169, 171–173.

Gavish, E., Krumbein, W.E., Halevy, J., 1985. Geomorphology, mineralogy and groundwater chemistry as factors of the hydrodynamic system of the Gavish Sabkha. In: Friedman, G.M., Krumbein, W.E. (Eds.), Hypersaline Ecosystems: the Gavish Sabkha. Springer-Verlag, Berlin, pp. 186–217.

Gebelein, C.D., Hoffman, P., 1973. Algal origin of dolomite laminations in stromatolitic limestone. J. Sediment. Petrol. 43, 603–613.

Gehling, J.G., 1991. The case for Ediacaran fossil roots to the metazoan tree. Geol. Soc. India Mem. 20, 181–224.

Gehling, J.G., 1999. Microbial mats in terminal Proterozoic siliciclastics: Ediacaran death masks. Palaios 14, 40–57.

Gehling, J.G., 2000. Environmental interpretation and a sequence stratigraphic framework for the terminal Proterozoic Ediacara Member within the Rawnsley Quartzite, south Australia. Precambrian Res. 100, 65–95.

Geinitz, H.B., 1863. Beiträge zur Kenntnis der organischen Überreste in der Dyas (oder permischen Formation zum Theil) und über den Namen Dyas. Neues Jb. Min. Geol. Paläontol., 385–398.

Gerdes, G., Krumbein, W.E., 1987. Biolaminated Deposits. Lecture Notes in Earth Sciences, vol. 9. Springer-Verlag, Berlin, 183 pp.

Gerdes, G., Klenke, T., 2003. Geologische Bedeutung ökologischer Zeiträume in biogener Schichtung (Mikrobenmatten, potentielle Stromatolithe). Mitt. Ges. Geol. Bergbaustud. Österr 46, 35–49.

Gerdes, G., Krumbein, W.E., Holtkamp, E.M., 1985a. Salinity and water activity related zonation of microbial communities and potential stromatolites of the Gavish Sabkha. In: Friedman, G.M., Krumbein, W.E. (Eds.), Hypersaline Ecosystems: the Gavish Sabkha. Springer-Verlag, Berlin, pp. 238–266.

Gerdes, G., Krumbein, W.E., Reineck, H.-E., 1985b. The depositional record of sandy, versicolored tidal flats (Mellum Island, southern North Sea). J. Sediment. Petrol. 55, 265–278.

Gerdes, G., Krumbein, W.E., Reineck, H.-E., 1985c. Verbreitung und aktuogeologische Bedeutung mariner mikrobieller matten im Gezeitenbereich der Nordsee. Facies 12, 75–96.

Gerdes, G., Krumbein, W.E., Reineck, H.-E., 1991. Biolaminations – ecological versus depositional dynamics. In: Einsele, G., Ricken, W., Seilacher, A. (Eds.), Cycles and Events in Stratigraphy. Springer-Verlag, Berlin, pp. 592–607.

Gerdes, G., Claes, M., Dunajtschik-Piewak, K., Riege, H., Krumbein, W.E., Reineck, H.-E., 1993. Contribution of microbial mats to sedimentary surface structures. Facies 29, 61–74.

Gerdes, G., Krumbein, W.E., Reineck, H.-E., 1994a. Microbial mats as architects of sedimentary surface structures. In: Krumbein, W.E., Paterson, D.M., Stal, L.J. (Eds.), Biostabilization of Sediments. Bibliotheks- und Informationsystem der Carl von Ossietzky Universität Oldenberg, (BIS)-Verlag, Oldenburg, pp. 165–182.

Gerdes, G., Dunajtschik-Piewak, K., Riege, H., Taher, A.G., Krumbein, W.E., Reineck, H.-E., 1994b. Structural diversity of biogenic carbonate particles in microbial mats. Sedimentology 41, 1273–1294.

Gerdes, G., Klenke, T., Noffke, N., 2000a. Microbial signatures in peritidal siliciclastic sediments: a catalogue. Sedimentology 47, 279–308.

Gerdes, G., Krumbein, W.E., Noffke, N., 2000b. Evaporite microbial sediments. In: Riding, R.E., Awramik, S.M. (Eds.), Microbial Sediments. Springer-Verlag, Berlin, pp. 196–208.

Germs, G.J.B., 1983. Implications of a sedimentary facies and depositional environmental analysis of the Nama Group in south west Africa/Namibia. Geol. Soc. South Africa Spec. Publ. 11, 89–114.

Germs, G.J.B., Knoll, A.H., Vidal, G., 1986. Latest Proterozoic microfossils from the Nama Group, Namibia (south west Africa). Precambrian Res. 32, 45–62.

Gibling, M.R., Tantisukrit, C., Uttamo, W., Thanasuthipitak, T., Haraluck, M., 1985a. Oil shale sedimentology and geochemistry in Cenozoic Mae Sot basin, Thailand. Amer. Assoc. Petrol. Geol. Bull. 69, 767–780.

Gibling, M.R., Ukakimaphan, Y., Srisuk, S., 1985b. Oil shale and coal in intermontane basins of Thailand. Amer. Assoc. Petrol. Geol. Bull. 69, 760–766.

Ginsburg, R.N., 1960. Ancient analogs of recent stromatolites. In: Proceedings 21st Int. Geol. Congr., Copenhagen, Pt. 22, pp. 26–35.

Goldring, R., 1971. Shallow-water sedimentation as illustrated in the Upper Devonian baggy beds. Geol. Soc. London Mem. 5, 80 pp.

Golubic, S., 1973. The relationship between blue-green algae and carbonate deposits. In: Carr, N.G., Whitton, B.A. (Eds.), The Biology of Blue-Green Algae. Blackwell Science, Oxford, pp. 434–472.

Golubic, S., 1976. Organisms that build stromatolites. In: Walter, M.R. (Ed.), Stromatolites. Developments in Sedimentology, vol. 20. Elsevier, Amsterdam, pp. 113–126.

Golubic, S., 1992. Microbial mats of Abu Dhabi. In: Margulis, L., Olendzenski, L. (Eds.), Environmental Evolution, Effects of the Origin and Evolution of Life on Planet Earth. MIT Press, Cambridge, pp. 131–147.

Golubic, S., Seong-Joo, L., 1999. Early cyanobacterial fossil record: preservation, palaeoenvironments and identification. Eur. J. Phycol. 34, 339–348.

Goth, K., 1990. Der Messeler Ölschiefer – ein Algenlaminit. Courier Forschungsinst. Senckenberg. 131, 1–143.

Goth, K., Schiller, W., 1994. Miozäene Algenlaminite von Hausen in der Rhön. Palaeontolog. Z. 68, 287–297.

Gradstein, F.M., Sandvik, K.O., Milton, N.J. (Eds.), 1998. Sequence Stratigraphy – Concepts and Applications. Norwegian Petroleum Society (NPF) Special Publication 8. Elsevier, Amsterdam, pp. 171–195.

Gresse, P.G., Germs, G.J.B., 1993. The Nama foreland basin: sedimentation, major unconformity bounded sequences and multisided active margin advance. Precambrian Res. 63, 247–272.

Grotzinger, J.P., 1990. Geochemical model for Proterozoic stromatolite decline. Amer. J. Sci. 290A, 80–103.

Grotzinger, J.P., Bowring, S.A., Saylor, B.Z., Kaufman, A.J., 1995. New biostratigraphic and geochronologic constraints on early animal evolution. Science 270, 598–604.

Grotzinger, J.P., Watters, W.A., Knoll, A.H., 2000. Calcified metazoans in thrombolite–stromatolite reefs of the terminal Proterozoic Nama Group, Namibia. Paleobiology 26, 334–359.

Gunatilaka, A., 1975. Some aspects of the biology and sedimentology of laminated algal mats from Mannar Lagoon, northwest Ceylon. Sediment. Geol. 14, 275–300.

Hagadorn, J.W., Bottjer, D.J., 1997. Wrinkle structures: microbially mediated sedimentary structures common in subtidal siliciclastic settings at the Proterozoic–Phanerozoic transition. Geology 25, 1047–1050.

Hagadorn, J.W., Bottjer, D.J., 1999. Restriction of a Late Neoproterozoic biotope: suspect-microbial structures and trace fossils at the Vendian–Cambrian transition. Palaios 14, 73–85.

Hagadorn, J.W., Pfluger, F., Bottjer, D.J., 1999. Unexplored microbial worlds. Palaios 14, 1–2.

Hallberg, R., Ferris, F.G., 2004. Biomineralization by *Gallionella*. Geomicrobiol. J. 21, 325–330.

Hallbeck, L., Pedersen, K., 1991. Autotrophic and mixotrophic growth of *Gallionella ferruginea*. J. Gen. Microbiol. 137, 2657–2661.

Häntzschel, W., 1935. Erhaltungsfähige Schleifspuren von Gischt am Nordseestrand. Natur und Volk 65, 461–465.

Häntzschel, W., 1975. Trace Fossils and Problematica, second ed. In: Teichert, C. (Ed.), Treatise on Invertebrate Paleontology, Part W. Miscellanea, Suppl. 1. Geol. Soc. Amer. and Univ. of Kansas Press, Boulder, CO, and Lawrence, pp. W1–W269.

Häntzschel, W., Reineck, H.-E., 1968. Fazies-Untersuchungen im Hettangium von Helmstedt (Niedersachsen). Mitt. Geol. Staatsinst. Hamburg 37, 5–39.

Harrison, J.E., 1972. Precambrian Belt basin of northwestern United States: its geometry, sedimentation and copper occurrences. Geol. Soc. Amer. Bull. 83, 1215–1240.

Harwood, G., 1990. "Sandstone stromatolites" – an example of algal trapping of sand grains from the Permian Yates Formation, New Mexico, USA. Abstracts of Posters, Sediments 1990, 13th International Sedimentological Congress, Nottingham, England, p. 97.

Hawes, I., Schwarz, A.-M., 1999. Photosynthesis in an extreme shade environment: benthic microbial mats from Lake Hoare: a permanently ice-covered Antarctic lake. J. Phycol. 35, 448–459.

Hayes, T.S., Einaudi, M.T., 1986. Genesis of the Spar Lakestrata-bound copper–silver deposit, Montana (Part 1): controls inherited from sedimentation and preore diagenesis. Econ. Geol. 81, 1899–1931.

Hieshima, G.B., Pratt, L.M., 1991. Sulfur/carbon ratios and extractable organic matter of the middle Proterozoic Nonesuch Formation, north American Mid-continent Rift. In: Walter, M.R. (Ed.), Special Issue: Proterozoic Petroleum. Precambrian Res. 54, 65–79.

Hilowle, M.A., Donaldson, J.A., Arnott, R.W.C., 2000. Biofilm-mediated structures in quartz arenites of the Cambro-Ordovician Nepean Formation. Abstract, Canadian Soc. Exp. Geophys. Conference, May 29–June 2, No. 868.

Hofmann, H.J., 1967. Precambrian fossils (?) near Elliot Lake, Ontario. Science 156, 500–504.

Hofmann, H.J., 1971. Precambrian fossils, pseudofossils and problematica in Canada. Geol. Surv. Canada Bull. 189, 1–146.

Hofmann, H.J., 1973. Stromatolites: characteristics and utility. Earth-Sci. Rev. 9, 339–373.

Hofmann, H.J., Grey, K., Hickman, A.H., Thorpe, R.I., 1999. Origin of 3.45 Ga-old stromatolites in Warrawoona Group, Western Australia. Geol. Soc. Amer. Bull. 111, 1256–1262.

Hofmann, H.J., 2000. Archean stromatolites as microbial archives. In: Riding, R.E., Awramik, S.M. (Eds.), Microbial Sediments. Springer-Verlag, Berlin, pp. 315–327.

Hoffman, P.F., 1976. Stromatolite morphogenesis in Shark Bay, western Australia. In: Walter, M.R. (Ed.), Stromatolite. Developments in Sedimentology, vol. 20, Elsevier, Amsterdam, pp. 261–271.

Holland, H.D., 1973. The oceans: a possible source of iron in iron-formations. Econ. Geol. 68, 1169–1172.

Holm, N.G., 1987. Biogenic influences on the geochemistry of certain ferruginous sediments of hydrothermal origin. Chem. Geol. 63, 45–57.

Holm, N.G., 1989. The 13C/12C ratios of siderite and organic matter of a modern metalliferous hydrothermal sediment and their implications for banded iron formations. Chem. Geol. 77, 41–45.

Horodyski, R.J., 1982. Impressions of algal mats from the Middle Proterozoic Belt Supergroup, northwestern Montana. Sedimentology 29, 285–289.

Horodyski, R.J., 1983. Sedimentary geology and stromatolites of the Middle Proterozoic Belt Supergroup, Glacier National Park, Montana. Precambrian Res. 20, 391–425.

Horodyski, R.J., 1993. Paleontology of Proterozoic shales and mudstones: examples from the Belt Supergroup, Chuar Group and Pahrump Group, western USA. Precambrian Res. 61, 241–278.

Horodyski, R.J., Bloeser, B., Vonder Haar, S., 1977. Laminated algal mats from a coastal lagoon, Laguna Mormona, Baja California, Mexico. J. Sediment. Petrol. 47, 680–696.

Hsü, K., Siegenthaler, C., 1969. Preliminary experiments on hydrodynamic movement induced by evaporation and their bearing on the dolomite problem. Sedimentology 12, 11–25.

Hunt, D., Tucker, M.E., 1992. Stranded parasequences and the forced regressive wedge systems tract: deposition during base-level fall. Sediment. Geol. 81, 1–9.

Hunter, R.E., 1969. Eolian microridges on modern beaches and a possible ancient example. J. Sediment. Petrol. 39, 1573–1578.

Hutton, A.C., Kantsler, A.J., Cook, A.C., McKirdy, D.M., 1980. Organic matter in oil shales. APEA J. 20, 44–67.

Isley, A.E., 1995. Hydrothermal plumes and the delivery of iron to banded iron formation. J. Geol. 103, 169–185.

James, R., Ferris, F.G., 2004. Evidence for microbial-mediated iron oxidation at a neutrophilic groundwater spring. Chem. Geol. 212, 301–311.

Javor, B., 1989. Hypersaline Environments – Microbiology and Biogeochemistry. Springer-Verlag, Berlin, 328 pp.

Jensen, S., 2003. The Proterozoic and earliest Cambrian trace fossil record; patterns, problems and perspectives. Integr. Compar. Biol. 43, 219–228.

Jensen, S., Runnegar, B.N., 2005. A complex trace fossil from the Spitskop Member (terminal Ediacaran-? Lower Cambrian) of southern Namibia. Geol. Mag. 142, 561–569.

Jensen, S., Saylor, B.Z., Gehling, J.G., Germs, G.J.B., 2000. Complex trace fossils from the terminal Proterozoic of Namibia. Geology 28, 143–146.

Jensen, S., Droser, M.L., Gehling, J.G., 2005. Trace fossil preservation and the early evolution of animals. Palaeo. Palaeo. Palaeo. 220, 19–29.

Jervey, M.T., 1988. Quantitative geological modeling of siliciclastic rock sequences and their seismic expression. In: Wilgus, C.K., Hastings, B.S., Kendall, C.G.St.C., Posamentier, H.W., Ross, C.A., Van Wagoner, J.C.

(Eds.), Sea Level Changes – An Integrated Approach. Soc. Econ. Paleontol. Mineral. Spec. Publ. 42, Tulsa, OK, pp. 47–69.

Johnston, D.T., Wing, B.A., Farquhar, J., Kaufman, A.J., Strauss, H., Lyons, T.W., Kah, L.C., Canfield, D.E., 2005. Active microbial sulfur disproportionation in the Mesoproterozoic. Science 310, 1477–1479.

Jørgensen, B.B., 1994. Diffusion processes and boundary layers in microbial mats. In: Stal, L.J., Caumette, P. (Eds.), Microbial Mats. Springer-Verlag, Berlin, pp. 243–253.

Jørgensen, B.B., Revsbech, N.P., Cohen, Y., 1983. Photosynthesis and structure of benthic microbial mats: microelectrode and SEM studies of four cyanobacterial communities. Limnol. Oceanogr. 28, 1075–1093.

Joye, S.B., Boetius, A., Orcutt, B.N., Montoya, J.P., Schulz, H.N., Erickson, M.J., Lugo, S.K., 2004. The anaerobic oxidation of methane and sulfate reduction in sediments from Gulf of Mexico cold seeps. Chem. Geol. 205, 219–238.

Junium, C., Bohacs, K.M., 2005. Sedimentary, petrographic, and geochemical evidence for benthic microbial mats and a refined mudstone stratigraphy for the Neoproterozoic Kwagunt Formation, Chuar Group, Grand Canyon. In: Geol. Soc. Amer. and Geol. Assoc. Canada Earth System Processes 2 Conference, Calgary, Canada, paper 8-1.

Kalkowsky, E., 1908. Oolith und stromatolith in norddeutschen Bundsandstein. Z. Deutsche Geol. Ges. 60, 68–125.

Kamber, B.S., Bolhar, R., Webb, G.E., 2004. Geochemistry of late Archean stromatolites from Zimbabwe: evidence for microbial life in restricted epicontinental seas. Precambrian Res. 132, 379–399.

Kappler, A., Newman, D.K., 2004. Formation of Fe(III)-minerals by Fe(II)-oxidizing photoautotrophic bacteria. Geochim. Cosmochim. Acta 68, 1217–1226.

Kendall, C.G.St.C., Skipwith, P.A.d'E., 1969. Geomorphology of a recent shallow-water carbonate province: Khor Al Bazam, Trucial coast, southwest Persian Gulf. Geol. Soc. Amer. Bull. 80, 865–891.

Kendall, C.G.St., Warren, J., 1987. A review of the origin and setting of tepees and their associated fabrics. Sedimentology 34, 1007.

Kenig, F.C., 2000. $^{16}C_{29}$ homologous series of monomethylalkanes in the pyrolysis products of a Holocene microbial mat. Org. Geochem. 31, 237–241.

Kinsman, D.J.J., Park, R.K., 1976. Algal belt and coastal sabkha evolution, Trucial Coast, Persian Gulf. In: Walter, R.M. (Ed.), Stromatolites. Developments in Sedimentology, vol. 20. Elsevier, Amsterdam, pp. 421–433.

Knorre, H.V., Krumbein, W.E., 2000. Bacterial calcification. In: Riding, R., Awramik, S.M. (Eds.), Microbial Sediments. Springer-Verlag, Berlin, pp. 25–31.

Kocurek, G., Fielder, G., 1982. Adhesion structures. J. Sediment. Petrol. 52, 1229–1241.

Konhauser, K.O., Hamade, T., Raiswell, R., Morris, R.C., Ferris, F.G., Southam, G., Canfield, D.E., 2002. Could bacteria have formed the Precambrian banded iron formations? Geology 30, 1079–1082.

Kopaska-Merkel, D.C., Grannis, J., 1990. Detailed structure of wrinkle marks. J. Alabama Acad. Sci. 61, 236–243.

Kropp, J., Block, A., Von Bloh, W., Klenke, T., Schellnhuber, H.J., 1997. Multifractal characterization of microbially induced magnesian calcite formation in recent tidal flat sediments. Sediment. Geol. 109, 37–51.

Krumbein, W.E., 1974. On precipitation of aragonite on the surface of marine bacteria. Naturwissenschaften 61, 167.

Krumbein, W.E. (Ed.), 1979. Cyanobakterien – Bakterien oder Algen? Oldenburger Symposium über Cyanobakterien. Littman-Druck, Oldenburg, 130 pp.

Krumbein, W.E., 1983. Stromatolites – the challenge of a term in space and time. Precambrian Res. 20, 493–531.

Krumbein, W.E., 1986. Biotransfer of minerals by microbes and microbial mats. In: Leadbeater, B.S.C., Riding, R. (Eds.), Biomineralization in Lower Plants and Animals. Proc. Systematics Assoc. Symposium, Univ. Birmingham, April 1985. Oxford University Press, Oxford, pp. 55–72.

Krumbein, W.E., 1994. The year of the slime. In: Krumbein, W.E., Paterson, D.M., Stal, L.J. (Eds.), Biostabilization of Sediments. Bibliotheks- und Informationsystem der Carl von Ossietzky Universität Oldenberg, (BIS)-Verlag, Oldenburg, pp. 1–7.

Krumbein, W.E., Cohen, Y., 1977. Primary production, mat formation and lithification: contribution of oxygenic and facultative anoxygenic cyanobacteria. In: Flügel, E. (Ed.), Fossil Algae. Springer-Verlag, Berlin, pp. 37–56.

Krumbein, W.E., Jens, K., 1981. Biogenic rock varnishes of the Negev Desert (Israel) an ecological study of iron and manganese transformation by cyanobacteria and fungi. Oecologia 50, 25–38.

Krumbein, W.E., Werner, D., 1983. The microbial silica cycle. In: Krumbein, W.E. (Ed.), Microbial Geochemistry. Blackwell Science, Oxford, pp. 125–157.

Krumbein, W.E., Schellnhuber, H.J., 1990. Geophysiology of carbonates as a function of bioplanets. In: Ittecot, V.S. (Ed.), Facets of Modern Biogeochemistry. Springer-Verlag, Berlin, pp. 5–22.

Krumbein, W.E., Schellnhuber, H.J., 1992. Geophysiology of mineral deposits – a model for a biological driving force of global changes through earth history. Terra Nova 4, 351–362.

Krumbein, W.E., Rippka, R., Waterbury, J.B., 1979a. Schematische bacteriologische Gliederung der Cyanophyten im Vergleich zur phykologischen. In: Krumbein, W.E. (Ed.), Cyanobakterien: Bakterien oder Algen. Littman-Druck, Oldenburg, pp. 85–87.

Krumbein, W.E., Buchholz, H., Franke, P., Giani, D., Giele, C., Wonneberger, C., 1979b. O_2 and H_2S coexistence in stromatolites. A model for the origin of mineralogical lamination in stromatolites and banded iron formations. Naturwissenschaften 66, 381–389.

Krumbein, W.E., Paterson, D.M., Stal, L. (Eds.), 1994. Biostabilization of Sediments. Bibliotheks- und Informationsystem der Carl von Ossietzky Universität Oldenberg, (BIS)-Verlag, Oldenburg, 526 pp.

Krumbein, W.E., Brehm, U., Gerdes, G., Gorbushina, A.A., Levit, G., Palinska, K.A., 2003. Biofilm, biodictyon, biomat microbialite, oolites, stromatolites – geophysiology, global mechanisms and parahistology. In: Krumbein, W.E., Paterson, D.M., Zavarzin, G.A. (Eds.), Fossil and Recent Biofilms. Kluwer Academic Publishers, Dordrecht, pp. 1–28.

Krynine, P.D., 1948. The megascopic study and field classification of sedimentary rocks. J. Geol. 56, 130–165.

Kühl, M., Fenchel, T., Kazmierczak, J., 2003. Growth, structure and calcification potential of an artificial cyanobacterial mat. In: Krumbein, W.E., Paterson, D.M., Zavarzin, G.A. (Eds.), Fossil and Recent Biofilms. Kluwer Academic Publishers, Dordrecht, pp. 77–102.

Kummel, B., Teichert, C., 1970. Stratigraphy and paleontology of the Permian–Triassic boundary beds, Salt Range and Trans Indus Ranges, west Pakistan. In: Kummel, B., Teichert, C. (Eds.), Stratigraphic Boundary Problems: Permian and Triassic of West Pakistan. Department of Geology, Univ. of Kansas Spec. Publ. 4, pp. 1–110.

LaBerge, G.L., 1973. Possible biological origin of Precambrian iron-formations. Econ. Geol. 68, 1098–1109.

Lambert, I.B., 1976. The McArthur zinc-lead-silver deposit: features, metallogenesis and comparisons with some other stratiform ores. In: Wolf, K.H. (Ed.), Handbook of Strata-Bound and Stratiform Ore Deposits, vol. 6. Elsevier, Amsterdam, pp. 535–585.

Last, W.M., Ginn, F.M., 2005. Saline systems of the Great Plains of western Canada: an overview of the limnogeology and paleolimnology. Saline Syst. 1, 1–38.

Leckie, D.A., 1994. Canterbury Plains, New Zealand – implications for sequence stratigraphic models. Amer. Assoc. Petrol. Geol. Bull. 78, 1240–1256.

Little, C.T.S., Glyn, S.E.J., Mills, R.A., 2004. Four-hundred and ninety-million-year record of bacteriogenic iron oxide precipitation at sea-floor hydrothermal vents. Geomicrobiol. J. 21, 415–429.

Logan, B.W., Rezak, R., Ginsburg, R.N., 1964. Classification and environmental significance of algal stromatolites. J. Geol. 72, 68–83.

Logan, B.W., Hoffman, P., Gebelein, C.D., 1974. Algal mats, cryptalgal fabrics, and structures, Hamelin Pool, Western Australia. In: Logan, B.W., Hoffman, P., Gebelein, C.D. (Eds.), Evolution and Diagenesis of Quaternary Carbonate Sequence, Shark Bay, West Australia. Amer. Assoc. Petrol. Geol. Mem. 22, Tulsa, OK, pp. 140–194.

Logan, G.A., Calver, C.R., Gorjan, P., Summons, R.E., Hayes, J.M., Walter, M.R., 1999a. Terminal Proterozoic mid-shelf benthic microbial mats in the Centralian Superbasin and their environmental significance. Geochim. Cosmochim. Acta 63, 1345–1358.

Logan, G.A., Calver, C.R., Gorjan, P., Summons, R.E., Hayes, J.M., Walter, M.R., 1999b. Terminal Proterozoic benthic microbial mats and their environmental significance. Ninth annual V.M. Goldschmidt conference, 22–27 August, Cambridge, MA, LPI-CONTRIB-971, p. 176.

Loudon, A.G., Lee, M.K., Dowling, J.F., Bourn, R., 1975. Lady Loretta silver-lead-zinc deposit. In: Knight, C.L. (Ed.), Economic Geology of Australia and Papua New Guinea, I Metals. Australas. Inst. Min. Metall. Mon. 5, pp. 66–74.

Lovelock, J.E., 1988. The Ages of Gaia. W.W. Norton, New York, 252 pp.

Lowenstam, H.A., 1986. Mineralization processes in monerans and potoctists. In: Leadbeater, B.S.C., Riding, R. (Eds.), Biomineralization in Lower Plants and Animals, vol. 30. Oxford Univ. Press, New York, pp. 1–17.

Madigan, M.T., Martinko, J.M., 2006. Brock Biology of Microorganisms, 11th ed. Prentice Hall, Upper Saddle River, NJ, 992 pp.

Maia, L.P., 1998. Processos costeiros y balance sedimentario a lo largo de Fortaleza (NE Brazil): implicationes para una gestión adecuada de la zona litoral. Ph.D. thesis (unpubl.), University of Barcelona, Barcelona–ES, 269 pp.

Margulis, L., Dolan, M.F., 2002. Early Life: Evolution on the Precambrian Earth, second ed. Jones and Bartlett, Sudbury, Boston, Toronto, London, Singapore, 168 pp.

Martin, J.M., Braga, J.C., Riding, R., 1993. Siliciclastic stromatolites and thrombolites, late Miocene, S.E. Spain. J. Sediment. Petrol. 63, 131–139.

Martinsson, A., 1965. Aspects of a Middle Cambrian thanatotope on Öland. Geol. Fören. Stockh. Förh. 87, 181–230.

Mastandrea, A., Perri, E., Russo, F. Spadafora, A., Tucker, M. 2006. Microbial primary dolomite from a Norian carbonate platform: northern Calabria, Southern Italy. Sedimentology 53, 465–480.

Mathias, B.V., Clark, G.J., 1975. Mount Isa copper and silver-lead-zinc orebodies – Isa and Hilton Mines. In: Knight, C.L. (Ed.), Economic Geology of Australia and Papua New Guinea, I Metals. Australas. Inst. Min. Metall. Mon. 5, pp. 351–372.

Mathias, B.V., Clark, G.J., Morris, D., Russel, R.E., 1973. The Hilton deposit – stratiform silver-lead-zinc mineralization of the Mt. Isa type. Geol. Geophys. Bull. 141, 33–58.

McKee, E.D., 1954. Stratigraphy and history of the Moenkopi Formation of Triassic age. Geol. Soc. Amer. Mem. 61, 133 pp.

McKenzie, D.B., 1968. Studies for students: sedimentary features of Alameda Avenue cut, Denver, Colorado. Mountain Geol. 5, 3–13.

McKenzie, D.B., 1972. Tidal sand flat deposits in Lower Cretaceous Dakota Group near Denver, Colorado. Mountain Geol. 9, 269–277.

Merz, M.U.E., 1992. The biology of carbonate precipitation by cyanobacteria. Facies 26, 81–102.

Miall, A.D., 1997. The Geology of Stratigraphic Sequences. Springer-Verlag, Berlin, 433 pp.

Milodowski, A.E., West, J.M., Pearce, J.M., Hyslop, E.K., Basham, I.R., Hooker, P.I., 1990. Uranium mineralized microorganisms associated with uraniferous hydrocarbons in southwest Scotland. Nature 347, 465–467.

Mitchum, R.M., Jr., 1977. Seismic stratigraphy and global changes of sea level, Part 11: glossary of terms used in seismic stratigraphy. In: Payton, C.E. (Ed.), Seismic Stratigraphy – Applications to Hydrocarbon Exploration. Amer. Assoc. Petrol. Geol. Mem. 26, Tulsa, OK, pp. 205–212.

Monty, C.L.V., 1972. Recent algal stromatolitic deposits, Andros Island, Bahamas. Geol. Rundschau 61, 742–783.

Morris, R.C., Horwitz, R.C., 1983. The origin of the iron-formation-rich Hamersley Group of Western Australia – deposition on a platform. Precambrian Res. 21, 273–297.

Mumma, M., Harbour, G., Jayne, D., 1982. Prichard–Ravalli (Belt–Precambrian) sediments through space and time. In: Reid, R.R., Williams, G.A. (Eds.), Society of Economic Geologists' Coeur d'Alene Field Conference – 1977. Idaho Bureau of Mines Geol. Bull. 24, 1.

Murray, W.C.J., 1975. McArthur River H.Y.C. lead-zinc and related deposits. In: Knight, C.L. (Ed.), Economic Geology of Australia and Papua New Guinea, I Metals. Australas. Inst. Min. Metall. Mon. 5, pp. 329–339.

Nealson, K.H., Myers, C.R., 1990. Iron reduction by bacteria: a potential role in the genesis of banded iron formations. Amer. J. Sci. 290A, 35–45.

Nealson, K.H., Saffarini, D., 1994. Iron and manganese in anaerobic respiration – environmental significance, physiology, and regulation. Ann. Rev. Microbiol. 48, 311–343.

Neu, T.R., 1994. Biofilms and microbial mats. In: Krumbein, W.E., Paterson, D.M., Stal, L.J. (Eds.), Biostabilization of Sediments. Bibliotheks- und Informationsystem der Carl von Ossietzky Universität Oldenberg, (BIS)-Verlag, Oldenburg, pp. 6–16.

Neumann, A.C., Gebelein, C.D., Scoffin, T.P., 1970. The composition, structure and erodability of subtidal mats, Abaco, Bahamas. J. Sediment. Petrol. 40, 274–297.

Noffke, N., 1997. Mikrobiell induzierte Sedimentstrukturen (M.I.S.S.) in siliziklastischen Wattablagerungen. Ph.D. thesis (unpubl.), University of Oldenburg, Oldenburg, 127 pp.

Noffke, N., 1998a. Multidirected ripple marks rising from biological and sedimentological processes in modern lower supratidal deposits (Mellum Island, southern North Sea). Geology 26, 879–882.

Noffke, N., 1998b. Environmental requirements for microbial mat formation in Recent tidal systems. In: 13th Meeting of Sedimentologists Sediment '98, 9–13 June 1998, Erlangen (Germany). Erlanger Geologische Abhandlungen, Sonderband 2.

Noffke, N., 1999. Erosional remnants and pockets evolving from biotic–physical interactions in a Recent lower supratidal environment. Sediment. Geol. 123, 175–181.

Noffke, N., 2000. Extensive microbial mats and their influences on the erosional and depositional dynamics of a siliciclastic cold water environment (Lower Arenigian, Montagne Noire, France). Sediment. Geol. 136, 207–215.

Noffke, N., 2003. Epibenthic cyanobacterial communities counteracting sedimentary processes within siliciclastic depositional systems (present and past). In: Paterson, D.M., Zavarzin, G., Krumbein, W.E. (Eds.), Biofilms Through Space and Time. Congress Proceedings. Kluwer Academic Publishers, Dordrecht, pp. 265–280.

Noffke, N., Krumbein, W.E., 1999. A quantitative approach to sedimentary surface structures contoured by the interplay of microbial colonization and physical dynamics. Sedimentology 46, 417–426.

Noffke, N., Gerdes, G., Klenke, T., Krumbein, W.E., 1996. Microbially induced sedimentary structures – examples from modern sediments of siliciclastic tidal flats. Zentralbl. Geol. Paläontol. Teil I, 1995, H. 1/2, 307–316.

Noffke, N., Gerdes, G., Klenke, T., Krumbein, W.E., 1997a. A microscopic sedimentary succession indicating the presence of microbial mats in siliciclastic tidal flats. Sediment. Geol. 110, 1–6.

Noffke, N., Gerdes, G., Klenke, T., Krumbein, W.E., 1997b. Biofilm impact on sedimentary structures in siliciclastic tidal flats. Courier Forschungsinst. Senckenberg 201, 297–305.

Noffke, N., Gerdes, G., Klenke, T., Krumbein, W.E., 2001a. Microbially induced sedimentary structures – a new category within the classification of primary sedimentary structures. J. Sediment. Res. A 71, 649–656.

Noffke, N., Gerdes, G., Klenke, T., Krumbein, W.E., 2001b. Microbially induced sedimentary structures indicating climatological, hydrological and depositional conditions within Recent and Pleistocene coastal facies zones (Southern Tunisia). Facies 44, 23–30.

Noffke, N., Knoll, A.H., Grotzinger, J.P., 2002. Sedimentary controls on the formation and preservation of microbial mats in siliciclastic deposits: a case study from the Upper Neoproterozoic Nama Group, Namibia. Palaios 17, 533–544.

Noffke, N., Hazen, R., Nhleko, N., 2003a. Earth's earliest microbial mats in a siliciclastic marine environment (2.9 Ga Mozaan Group, South Africa). Geology 31, 673–676.

Noffke, N., Gerdes, G., Klenke, T., 2003b. Benthic cyanobacteria and their influence on the sedimentary dynamics of peritidal depositional systems (siliciclastic, evaporitic salty, and evaporitic carbonatic). Earth-Sci. Rev. 62, 163–176.

Noffke, N., Beukes, N., Hazen, R., 2006a. Spatial and temporal distribution of microbially induced sedimentary structures: a case study from siliciclastic storm deposits of the 2.9 Ga old Witwatersrand Supergroup, South Africa. Precambrian Res. 146, 35–44.

Noffke, N., Eriksson, K.A., Hazen, R.M., Simpson, E.L., 2006b. A new window into Early Archean life: microbial mats in Earth's oldest siliciclastic deposits (3.2 Ga Moodies Group, South Africa). Geology 34, 253–256.

O'Brien, N.R., 1990. Significance of lamination in the Toarcian (Lower Jurassic) shales from Yorkshire, Great Britain. Sediment. Geol. 67, 25–34.

Olsen, P.E., Remington, C.L., Corliss, B., Thompson, K.S., 1978. Change in Late Triassic lacustrine communities. Science 201, 729–733.

Oschmann, W., 2000. Microbes and black shales. In: Riding, R.E., Awramik, S.M. (Eds.), Microbial Sediments. Springer-Verlag, Berlin, pp. 137–148.

Parizot, M., Eriksson, P.G., Aifa, T., Sarkar, S., Banerjee, S., Catuneanu, O., Altermann, W., Bumby, A.J., Bordy, E.M., Louis van Rooy, J., Boshoff, A.J., 2005. Suspected microbial mat-related crack-like sedimentary structures in the Palaeoproterozoic Magaliesberg Formation sandstones, South Africa. Precambrian Res. 138, 274–296.

Park, R.K., 1977. The preservation potential of some recent stromatolites. Sedimentology 24, 485–506.

Paterson, D.M., 1997. Biological mediation of sediment erodibility: ecology and physical dynamics. In: Burt, N., Parker, R., Watts, J. (Eds.), Cohesive Sediments. John Wiley and Sons, London, pp. 215–229.

Paterson, D.M., Yallop, M., George, C., 1994. Stabilization. In: Krumbein, W.E., Paterson, D.M., Stal, L.J. (Eds.), Biostabilization of Sediments. Bibliotheks- und Informationsystem der Carl von Ossietzky Universität Oldenberg, (BIS)-Verlag, Oldenburg, pp. 401–432.

Paterson, D.M., Wiltshire, K.H., Miles, A., Blackburn, J., Davidson, I., Yates, M.G., McGorty, S., Eastwood, J.A., 1998. Microbiological mediation of spectral reflectance from intertidal cohesive sediments. Limnol. Oceanogr. 43, 1207–1221.

Paterson, D.M., Perkins, R., Consalvey, M., Underwood, G.J.C., 2003. Ecosystem function, cell micro-cycling and the structure of transient biofilms. In: Krumbein, W.E., Paterson, D.M., Zavarzin, G.A. (Eds.), Fossil and Recent Biofilms. Kluwer Academic Publishers, Dordrecht, pp. 47–63.

Payton, C.E. (Ed.), 1977. Seismic Stratigraphy – Applications to Hydrocarbon Exploration. Amer. Assoc. Petrol. Geol. Mem. 26, Tulsa, OK, 516 pp.

Peters, K.E., Walters, C.C., Moldowan, J.M., 2005. The Biomarker Guide, vol. 2, Biomarkers and Isotopes in Petroleum Exploration and Earth History, second ed. Cambridge University Press, Cambridge, New York, 1132 pp.

Pettijohn, F.J., 1957. Sedimentary Rocks, second ed. Harper, New York, 718 pp.

Pettijohn, F.J., Potter, P.E., 1964. Atlas and Glossary of Primary Sedimentary Structures. Springer-Verlag, Berlin, 370 pp.

Pettijohn, F.J., Siever, R., Potter, P.E., 1987. Sand and Sandstone, second ed. Springer-Verlag, Berlin, 553 pp.

Pflüger, F., 1999. Matground structures and redox facies. Palaios 14, 25–39.

Pflüger, F., Gresse, P.G., 1996. Microbial sand chips – a non-actualistic sedimentary structure. Sediment. Geol. 102, 263–274.

Pfluger, F., Sarkar, S., 1996. Precambrian bedding planes – bound to remain. Geological Society of America Abstracts with Program 28, p. 491.

Pickerill, R.K., Harris, I.M., 1979. A reinterpretation of *Astropolithon hindii* Dawson 1878. J. Sediment. Petrol. 49, 1029–1036.

Pierson, B.K., Oesterle, A., Murphy, G.L., 1987. Pigments, light penetration and photosynthetic activity in the multilayered microbial mats of Great Sippewisset Salt Marsh, Massachusetts. FEMS Microbiol. Ecol. 45, 365–376.

Pierson, B.K., Parenteau, M.N., Griffin, D.B.M., 1999. Phototrophs in high-iron-concentration microbial mats: physiological ecology of phototrophs in an iron-depositing hot spring. Appl. Environ. Microbiol. 65, 5474–5483.

Porada, H., Löffler, T., 2000. Microbial shrinkage cracks in siliciclastic rocks of the Neoproterozoic Nosib Group (Damara Supergroup) of central Namibia. Commun. Geol. Surv. Namibia 12, 63–72.

Porada, H., Bouougri, E., 2006. Siliciclastic biolaminites and microbial mats structures in the terminal Proterozoic Vingerbreek Member, Nama Group, Namibia. Abstract, Sediment 2006, 6–11 June, Göttingen, p. 136.

Posamentier, H.W., Allen, G.P., 1999. Siliciclastic Sequence Stratigraphy: Concepts and applications. Concepts in Sedimentology and Paleontology, vol. 7. Soc. Econ. Paleontol. Mineral., Tulsa, OK, 210 pp.

Posamentier, H.W., Jervey, M.T., Vail, P.R., 1988. Eustatic controls on clastic deposition I – conceptual framework. In: Wilgus, C.K., Hastings, B.S., Kendall, C.G.St.C., Posamentier, H.W., Ross, C.A., Van Wagoner, J.C. (Eds.), Sea Level Changes – An Integrated Approach. Soc. Econ. Paleontol. Mineral. Spec. Publ. 42, Tulsa, OK, pp. 110–124.

Pratt, B.R., 2001. Calcification of cyanobacterial filaments: *Girvanella* and the origin of lower Paleozoic lime mud. Geology 29: 763–766.

Prave, A.R., 2002. Life on land in the Proterozoic: evidence from the Torrodonian rocks of northwest Scotland. Geology 30, 811–814.

Pruss, S., Fraiser, M., Bottjer, D.J., 2004. Proliferation of Early Triassic wrinkle structures: implications for environmental stress following the end-Permian mass extinction. Geology 32, 461–464.

Quenstedt, F.A., 1858. Der Jura. Verlag Laupp, Tübingen, 842 pp.

Rasmussen, B., Buick, R., 1999. Redox state of the Archean atmosphere: evidence from detrital heavy metals in ca. 3250–2750 Ma sandstone from the Pilbara Craton, Australia. Geology 27, 115–118.

Rasmussen, B., Bose, P.K., Sarkar, S., Banerjee, S., Fletcher, I.R., McNaughton, N.J., 2002. 1.6 Ga U–Pb zircon ages for the Chorhat Sandstone, Lower Vindhyan, India: possible implication for early evolution of animals. Geology 30, 103–106.

Rautenbach, C.J.deW., 2001. A hypothetical approach to determining the effect of palaeorotational rates on Earth's Neoproterozoic palaeoclimate. J. African Earth Sci. 33, 463–473.

Ray, J.S., Martin, M.W., Veizer, J., 2002. U–Pb zircon dating and Sr isotope systematics of the Vindhyan Supergroup, India. Geology 30, 131–134.

Ray, J.S., 2006. Age of the Vindhyan Supergroup: a review of recent findings. J. Earth Syst. Sci. 115, 149–160.

Reading, H.G. (Ed.), 1996. Sedimentary Environments: Processes, Facies and Stratigraphy. Blackwell Science, Oxford, 688 pp.

Reading, H.G., Levell, B.K., 1996. Controls on the sedimentary record. In: Reading, H.G. (Ed.), Sedimentary Environments: Processes, Facies and Stratigraphy. Blackwell Science, Oxford, pp. 5–36.

Reineck, H.-E., 1955. Haftrippeln und Haftwarzen, Ablagerungsformen von Flugsand. Senckenbergiana Lethaea 36, 347–357.

Reineck, H.-E., 1956. Die Oberflächenspannung als geologischer Faktor in Sedimenten. Senckenbergiana Lethaea 37, 265–287.

Reineck, H.-E., 1969. Die Entstehung von Runzelmarken. Natur und Museum 99, 386–388.

Reineck, H.-E., 1979. Rezente und fossile Algenmatten und Wurzelhorizonte. Natur und Museum 109, 290–296.

Reineck, H.-E., 1984. Aktuogeologie Klastischer Sedimente. Verlag Waldemar Kramer, Frankfurt, 328 pp.

Reineck, H.-E., Singh, I.B., 1973. Depositional Sedimentary Environments, first ed. Springer-Verlag, Berlin, 439 pp.

Reineck, H.-E., Singh, I.B., 1980. Depositional Sedimentary Environments, second ed. Springer-Verlag, Berlin, 549 pp.

Reineck, H.-E., Gerdes, G., 1997. Tempestites in Recent shelf and tidal environments of the southern North Sea. Courier Forschungsinst. Senckenberg 201, 361–370.

Reineck, H.-E., Gerdes, G., Claes, M., Dunajtschik, K., Riege, H., Krumbein, W.E., 1990. Microbial modification of sedimentary surface structures. In: Heling, D., Rothe, P., Förstner, U., Stoffers, P. (Eds.), Sediments and Environmental Geochemistry. Springer-Verlag, Berlin, pp. 254–276.

Reitner, J., Peckmann, J., Reimer, A., Schumann, G., Thiel, V., 2005. Methane-derived carbonate build-ups and associated microbial communities at cold seeps on the lower Crimean shelf (Black Sea). Facies 51, 66–79.

Revsbech, N.P., Jørgensen, B.B., Blackburn, T.H., Cohen, Y., 1983. Microelectrode studies of the photosynthesis and O_2, H_2S and pH profiles of a microbial mat. Limnol. Oceanogr. 28, 1062–1074.

Reynolds, M.W., Elston, D.P., 1986. Stratigraphy and sedimentation of part of the Proterozoic Chuar Group, Grand Canyon, Arizona. Geological Society of America Abstracts with Program 18, p. 405.

Reysenbach, A.L., Cady, S.L., 2001. Microbiology of ancient and modern hydrothermal systems. Trends Microbiol. 9, 79–86.

Reynolds, M.W., Palacas, J.G., Elston, D.P., 1988. Potential petroleum source rocks in the Late Proterozoic Chuar Group, Grand Canyon, Arizona. USGS Circular 1025, pp. 49–50.

Riding, R., 2000. Microbial carbonates: the geological record of calcified bacterial-algal mats and biofilms. Sedimentology 47, 179–214.

Riding, R.E., Awramik, S.M., 2000. Microbial Sediments. Springer-Verlag, Berlin, 331 pp.

Rippka, R., Deruelles, J., Waterbury, J.B., Herdman, M., Stanier, R.Y., 1979. Generic assignments, strain histories and properties of pure cultures of cyanobacteria. J. Gen. Microbiol. 111, 1–61.

Robb, A.J., III, 1992. Rain-impact microtopography (RIM): an experimental analogue for fossil examples from the Maroon Formation, Colorado. J. Sediment. Petrol. 62, 530–535.

Roden, E.E., Sobolev, D., Glazer, B., Luther, G.W., 2004. Potential for microscale bacterial Fe redox cycling at the aerobic–anaerobic interface. Geomicrob. J. 21, 379–391.

Roehler, H.W., 1990. Sedimentology of freshwater lacustrine shorelines in the Eocene Scheggs Bed of the Tipton Tongue of the Green River Formation, Sand Wash Basin, Northwest Colorado. U.S. Geol. Surv. Bull. 1911, 49 pp.

Runnegar, B., Fedonkin, M., 1992. Proterozoic metazoan body fossils. In: Schopf, J.W., Klein, C. (Eds.), The Proterozoic Biosphere: A Multidisciplinary Study. Cambridge University Press, New York, pp. 369–387.

Russell, P.L., 1990. Oil Shales of the World, Their Origin, Occurrence and Exploitation. Pergamon Press, New York, 753 pp.

Sabbe, K., Hodgson, D.A., Verleyen, E., Taton, A., Wilmotte, A., Vanhoutte, K., Vyverman, W., 2004. Salinity, depth and the structure and composition of microbial mats in continental Antarctic lakes. Freshwater Biol. 49, 296–319.

Sagan, D., Margulis, L., 1988. Garden of Microbial Delights. Harcourt Brace Jovanovich, Boston, 229 pp.

Saha, D., Ghosh, G., 1998. Lithostratigraphy of deformed Proterozoic rocks from around the confluence of Godavari and Indravati rivers, south India. Indian J. Geol. 70, 217–230.

Sami, T.T., James, N.P., 1993. Evolution of an early Paleozoic foreland basin carbonate platform, lower Pethei Group, Great Slave Lake, north-west Canada. Sedimentology 40, 403–430.

Sarangi, S., Gopalan, K., Kumar, S. 2004. Pb–Pb age of earliest megascopic eukaryotic alga bearing Rohtas Formation, Vindhyan Supergroup, India: implications for Precambrian atmospheric oxygen evolution. Precambrian Res. 132, 107–121.

Sarkar, S., Chakraborty, P.P., Bose, P.K., 1996. Proterozoic Lakheri Limestone, central India: facies, paleogeography and physiography of the Lakheri Limestone. In: Bhattacharyya, A. (Ed.), Recent Advances in Vindhyan Geology. Mem. Geol. Soc. India 36, 5–26.

Sarkar, S., Chakraborty, S., Banerjee, S., Bose, P.K., 2002. Facies sequence and occult imprint of sag tectonics in Sirbu Shale. In: Altermann, W., Corcoran, P.L. (Eds.), Precambrian Sedimentary Environments: A Modern Approach to Ancient Depositional Systems. Int. Assoc. Sediment. Spec. Publ. 33. Blackwell Science, Oxford, pp. 369–381.

Sarkar, S., Banerjee, S., Eriksson, P.G., 2004. Microbial mat features in sandstones illustrated. In: Eriksson, P.G., Altermann, W., Nelson, D.R., Mueller, W.U., Catuneanu, O. (Eds.), The Precambrian Earth: Tempos and Events. Developments in Precambrian Geology, vol. 12. Elsevier, Amsterdam, pp. 673–675.

Sarkar, S., Banerjee, S., Eriksson, P.G., Catuneanu, O., 2005. Microbial mat control on siliciclastic Precambrian sequence stratigraphic architecture: examples from India. Sediment. Geol. 176, 191–205.

Sarkar, S., Banerjee, S., Samanta, P., Jeevankumar, S., 2006. Microbial mat-induced sedimentary structures in siliciclastic sediments: examples from the 1.6 Ga Chorhat Sandstone, Vindhyan Supergroup, M.P., India. J. Earth Syst. Sci. 115, 49–60.

Saylor, B.Z., Grotzinger, J.P., Germs, G.J.B., 1995. Sequence stratigraphy and sedimentology of the Neoproterozoic Kuibis and Schwarzrand subgroups (Nama Group), southwestern Namibia. Precambrian Res. 73, 153–172.

Schieber, J., 1985. The relationship between basin evolution and genesis of stratiform sulfide horizons in Mid-Proterozoic sediments of central Montana (Belt Supergroup). Ph.D. dissertation (unpubl.), University of Oregon, Eugene, 811 pp.

Schieber, J., 1986. The possible role of benthic microbial mats during the formation of carbonaceous shales in shallow Mid-Proterozoic basins. Sedimentology 33, 521–536.

Schieber, J., 1987. Small scale sedimentary iron deposits in a Mid-Proterozoic basin: viability of iron supply by rivers. In: Appel, P.W.U. (Ed.), Precambrian Iron Formations. Theophrastus Publications, Athens, pp. 267–295.

Schieber, J., 1989a. Pyrite mineralization in microbial mats from the Mid-Proterozoic Newland Formation, Belt Supergroup, Montana, U.S.A. Sediment. Geol. 64, 79–90.

Schieber, J., 1989b. Facies and origin of shales from the Mid-Proterozoic Newland Formation, Belt basin, Montana, U.S.A. Sedimentology 36, 203–219.

Schieber, J., 1990. Pyritic shales and microbial mats: significant factors in the genesis of stratiform Pb–Zn deposits of the Proterozoic? Mineral. Deposit. 25, 7–14.

Schieber, J., 1995. Anomalous iron distribution in shales as a manifestation of non-clastic fluvial iron supply to sedimentary basins: relevance for pyritic shales, base metal mineralization, and oolitic ironstone deposits. Mineral. Deposit. 30, 294–302.

Schieber, J., 1998a. Possible indicators of microbial mat deposits in shales and sandstones: examples from the Mid-Proterozoic Belt Supergroup, Montana, USA. Sediment. Geol. 120, 105–124.

Schieber, J., 1998b. Deposition of mudstones and shales: overview, problems, and challenges. In: Schieber, J., Zimmerle, W., Sethi, P. (Eds.), Shales and Mudstones, vol. 1, Basin Studies, Sedimentology and Paleontology. Schweizerbart'sche Verlagsbuchhandlung, Stuttgart, pp. 131–146.

Schieber, J., 1998c. Sedimentary features indicating erosion, condensation, and hiatuses in the Chattanooga Shale of Central Tennessee: relevance for sedimentary and stratigraphic evolution. In: Schieber, J., Zimmerle, W., Sethi, P. (Eds.), Shales and Mudstones, vol. 1, Basin Studies, Sedimentology and Paleontology. Schweizerbart'sche Verlagsbuchhandlung, Stuttgart, pp. 187–215.

Schieber, J., 1998d. Sedimentologic, geochemical, and mineralogical features of the Belt Supergroup and their bearing on the lacustrine vs marine debate. In: Berg, R.B. (Ed.), Belt Symposium III. Montana Bureau of Mines Geol. Spec. Publ. 112, pp. 177–189.

Schieber, J., 1999. Microbial mats in terrigenous clastics: the challenge of identification in the rock record. Palaios 14, 3–12.

Schieber, J., 2002. Sedimentary pyrite: a window into the microbial past. Geology 30, 531–534.

Schieber, J., 2004. Microbial mats in the siliciclastic rock record: a summary of the diagnostic features. In: Eriksson, P.G., Altermann, W., Nelson, D.R., Mueller, W.U., Catuneanu, O. (Eds.), The Precambrian Earth: Tempos and Events. Developments in Precambrian Geology, vol. 12. Elsevier, Amsterdam, pp. 663–673.

Schieber, J., Riciputi, L., 2005. Pyrite and marcasite coated grains in the Ordovician Winnipeg Formation, Canada: An intertwined record of surface conditions, stratigraphic condensation, geochemical "reworking," and microbial activity. J. Sediment. Res. 75, 907–920.

Schlager, W., 2005. Carbonate Sedimentology and Sequence Stratigraphy. Concepts in Sedimentology and Paleontology, vol. 8. Soc. Econ. Paleontol. Mineral., Tulsa, OK, 200 pp.

Schneider, J., 1995. Eindunstung von Meerwasser und Salzbildung in Salinen. Kali Steinsalz 11, 325–330.

Schneider, J., Le Campion-Alsumard, T., 1999. Construction and destruction of carbonates by marine and freshwater cyanobacteria. Eur. J. Phycol. 34, 417–426.

Schneider, J., Herrmann, A.G., 1980. Saltworks – natural laboratories for microbiological and geochemical investigations during the evaporation of seawater. In: Coogan, A.H., Hauber, L. (Eds.), 5th Symposium on Salt, vol. 2. Northern Ohio Geol. Soc., Ohio, pp. 371–381.

Schopf, J.W., 1993. Microfossils of the Early Archean Apex Chert: new evidence of the antiquity of life. Science 260, 640–646.

Schopf, J.W., 2004. Earth's earliest biosphere: status of the hunt. In: Eriksson, P.G., Altermann, W., Nelson, D.R., Mueller, W.U., Catuneanu, O. (Eds.), The Precambrian Earth: Tempos and Events. Developments in Precambrian Geology, vol. 12. Elsevier, Amsterdam, pp. 516–539.

Schulz, E., 1936. Das Farbstreifen-Sandwatt und seine Fauna, eine ökologisch-biozönotische Untersuchung an der Nordsee. Kie. Meeresforsch. 1, 359–378.

Schulz, H.N., Jørgensen, B.B., Fossing, H.A., Ramsing, N.B., 1996. Community structure of filamentous, sheath-building sulfur bacteria, Thioploca spp., off the coast of Chile. Appl. Environ. Microbiol. 62, 1855–1862.

Schumm, S.A., 1993. River response to baselevel change: implications for sequence stratigraphy. J. Geol. 101, 279–294.

Schwarz, H.U., Einsele, G., Herm, D., 1975. Quartz sandy, grazing contoured stromatolites from coastal embayments of Mauritania, west Africa. Sedimentology 22, 539–561.

Seeley, J.M., Keller, G.R., 2003. Delineation of subsurface Proterozoic Unkar and Chuar Group sedimentary basins in northern Arizona using gravity and magnetics; implications for hydrocarbon source potential. Amer. Assoc. Petrol. Geol. Bull. 87, 1299–1321.

Seilacher, A., 1964. Sedimentological classification and nomenclature of trace fossils. Sedimentology 3, 253–256.

Seilacher, A., 1982. Distinctive features of sandy tempestites. In: Einsele, G., Seilacher, A. (Eds.), Cyclic and Event Stratification. Springer-Verlag, Berlin, pp. 333–349.

Seilacher, A., 1999. Biomat-related lifestyles in the Precambrian. Palaios 14, 86–93.

Seilacher, A., Aigner, T., 1991. Storm deposition at the bed, facies, and basin scale: the geologic perspective. In: Einsele, G., Ricken, W., Seilacher, A. (Eds.), Cycles and Events in Stratigraphy. Springer-Verlag, Berlin, pp. 249–267.

Seilacher, A., Pfluger, F., 1994. From biomats to benthic agriculture: a biohistoric evolution. In: Krumbein, W.E., Paterson, D.M., Stal, L.J. (Eds.), Biostabilization of Sediments. Bibliotheks- und Informationsystem der Carl von Ossietzky Universität Oldenberg, (BIS)-Verlag, Oldenburg, pp. 97–105.

Seilacher, A., Goldring, R., 1996. Class Psammocorallia (Coelenterata, Vendian–Ordovician): recognition, systematics, and distribution. Geol. Fören. Stockholm Förhandl. 118, 207–216.

Seilacher, A., Bose, P.K., Pfluger, F., 1998. Triploblastic animals more than 1 billion years ago: trace fossil evidence from India. Science 282, 80–83.

Seilacher, A., Buatois, L.A., Mángano, M.G., 2005. Trace fossils in the Ediacaran–Cambrian transition: behavioral diversification, ecological turnover and environmental shift. Palaeo. Palaeo. Palaeo. 227, 323–356.

Shanley, K.W., McCabe, P.J. (Eds.), 1998. Relative Role of Eustasy, Climate and Tectonism in Continental Rocks. Soc. Econ. Paleontol. Mineral. Spec. Publ. 59, Tulsa, OK, 234 pp.

Shrock, R.R., 1948. Sequence in Layered Rocks. McGraw-Hill, New York, 507 pp.

Simonson, B.M., Carney, K.E., 1999. Roll-up structures: evidence of *in situ* microbial mats in Late Archean deep shelf environments. Palaios 14, 13–24.

Singh, I.B., Wunderlich, F., 1978. On the terms wrinkle marks (Runzelmarken), millimetre ripples, and mini ripples. Senckenbergiana Maritima 10, 75–83.

Skyring, G.W., Lynch, R.M., Smith, G.D., 1989. Quantitative relationships between carbon, hydrogen, and sulphur metabolism in cyanobacterial mats. In: Cohen, Y., Rosenberg, E. (Eds.), Microbial Mats, Physiological Ecology of Benthic Microbial Communities. Amer. Soc. Microbiol., Washington, DC, pp. 170–179.

Sloss, L.L., 1962. Stratigraphic models in exploration. Amer. Assoc. Petrol. Geol. Bull. 46, 1050–1057.

Smith, J.W., 1980. Oil shale resources of the United States. Colorado School Mines Mineral Energy Res. 23, 1–30.

Smoot, J.P., 1983. Depositional subenvironments in an arid closed basin; the Wilkins Peak Member of the Green River Formation (Eocene), Wyoming, U.S.A. Sedimentology 30, 801–827.

Sobolev, D., Roden, E.E., 2004. Characterization of a neutrophilic, chemolithoautotrophic Fe(II)-β-proteobacterium from fresh-water wetland sediments. Geomicrobiol. J. 21, 1–10.

Soudry, D., Weissbrod, T., 1995. Morphogenesis and facies relationships of thrombolites and siliciclastic stromatolites in a Cambrian tidal sequence (Elat area, southern Israel). Palaeo. Palaeo. Palaeo. 114, 339–355.

Squyres, S.W., Grotzinger, J.P., Arvidson, R.E., Bell, J.F., III, Calvin, W., Christensen, P.R., Clark, B.C., Crisp, J.A., Farrand, W.H., Herkenhoff, K.E., Johnson, J.R., Klingelhofer, G., Knoll, A.H., McLennan, S.M., McSween, H.Y., Jr., Morris, R.V., Rice, J.W., Jr., Rieder, R., Soderblom, L.A., 2004. In situ evidence for an ancient aqueous environment at Meridiani Planum, Mars. Science 306, 1709–1714.

Stal, L.J., 1994. Microbial mats: ecophysiological interactions related to biogenic sediment stabilization. In: Krumbein, W.E., Paterson, D.M., Stal, L.J. (Eds.), Biostabilization of Sediments. Bibliotheks- und Informationsystem der Carl von Ossietzky Universität Oldenberg, (BIS)-Verlag, Oldenburg, pp. 41–53.

Stal, L.J., 2000. Cyanobacterial mats and stromatolites. In: Whitton, B.A., Potts, M. (Eds.), The Ecology of Cyanobacteria. Kluwer Academic Publishers, Dordrecht, pp. 61–120.

Steiner, M., Reitner, J., 2001. Evidence of organic structures in Ediacara-type fossils and associated microbial mats. Geology 29, 1119–1122.

Stolz, J.F., 1990. Distribution of phototrophic microbes in the stratified microbial community at Laguna Figueroa, Baja California, Mexico. Biosystems 23, 345–357.

Stolz, J.F., 1991. The ecology of phototrophic bacteria. In: Stolz, J.F. (Ed.), Structure of Phototrophic Prokaryotes. CRC Press, Boca Raton, pp. 105–123.

Stolz, J.F., 2000. The structure of microbial mats and biofilms. In: Riding, R., Awramik, S.M. (Eds.), Microbial Sediments. Springer-Verlag, Berlin, pp. 1–8.

Stow, D.A.V., Shanmugam, G., 1980. Sequence of structures in fine-grained turbidites: comparison of recent deep-sea and ancient flysch sediments. Sediment. Geol. 25, 23–42.

Straub, K.L., Benz, M., Schrink, B., 2001. Iron metabolism in anoxic environments at near neutral pH. FEMS Microbiol. Ecol. 34, 181–186.

Strauss, H., Schieber, J., 1990. A sulfur isotope study of pyrite genesis: the Mid-Proterozoic Newland Formation, Belt Supergroup, Montana. Geochim. Cosmochim. Acta 54, 197–204.

Sur, S., 2004. An integrated sedimentological, stratigraphical and geochemical study of two proterozoic black shales from Vindhyan Supergroup, India. M.S. thesis (unpubl.), Indiana University, Bloomington, Indiana, 176 pp.

Sur, S., Schieber, J., Banerjee, S., 2006. Petrographic observations suggestive of microbial mats from Rampur Shale and Bijaigarh Shale, Vindhyan basin, India. J. Earth Syst. Sci. 115, 61–66.

Surdam, R.C., Wolfbauer, C.A., 1975. Green River Formation, Wyoming; a playa-lake complex. Geol. Soc. Amer. Bull. 86, 335–345.

Surdam, R.C., Stanley, K.O., 1979. Lacustrine sedimentation during the culminating phase of Eocene Lake Gosiute, Wyoming (Green River Formation). Geol. Soc. Amer. Bull. 90, 93–160.

Taylor, G.H., Teichmuller, M., Davis, A., Diessel, C.F.K., Littke, R., Robert, P., 1998. Organic Petrology. Gebrüder Borntraeger, Berlin, Stuttgart, 704 pp.

Thompson, J.B., Ferris, F.G., 1990. Cyanobacterial precipitation of gypsum, calcite, and magnesite from natural alkaline lake water. Geology 18, 995–998.

Thompson, J.B., Schultz-Lam, S., Beveridge, T.J., Des Marais, D.J., 1997. Whiting events: biogenic origin due to the photosynthetic activity of cyanobacterial picoplankton. Limnol. Oceanogr. 42, 133–141.

Till, R., 1978. Arid shorelines and evaporites. In: Reading, H.G. (Ed.), Sedimentary Environments and Facies. Blackwell Science, Oxford, pp. 178–206.

Tipping, E., Thompson, D.W., Woof, C., 1989. Iron oxides particulates formed by the oxygenation of natural and model lakewaters containing Fe(II). Arch. Hydrobiol. 115, 59–70.

Trusheim, F., 1936. Wattenpapier. Natur und Volk 66, 103–106.

Tuttle, M.L., 1991. Introduction to geochemical, biogeochemical and sedimentologic studies of the Green River Formation, Wyoming, Utah Colorado. U.S. Geol. Surv. Bull. 1973 A–G, pp. A1–A11.

Twenhofel, W.H., 1939. Principles of Sedimentation. McGraw-Hill, New York, 610 pp.

Van Lith, Y., Warthmann, R., Vasconcelos, C., McKenzie, J.A., 2003. Microbial fossilization in carbonate sediments: a result of the bacterial surface involvement in dolomite precipitation. Sedimentology 50, 237–245.

Van Straaten, L.M.J.U., 1953. Rhythmic pattern on Dutch North Sea beaches. Geol. Mijnbouw 15, 31–43.

Van Wagoner, J.C., Posamentier, H.W., Mitchum, R.M., Vail, P.R., Sarg, J.F., Loutit, T.S., Hardenbol, J., 1988. An overview of sequence stratigraphy and key definitions. In: Wilgus, C.K., Hastings, B.S., Kendall, C.G.St.C., Posamentier, H.W., Ross, C.A., Van Wagoner, J.C. (Eds.), Sea Level Changes – An Integrated Approach. Soc. Econ. Paleontol. Mineral. Spec. Publ. 42, Tulsa, OK, pp. 39–45.

Van Wagoner, J.C., Mitchum, R.M., Jr., Campion, K.M., Rahmanian, V.D., 1990. Siliciclastic sequence stratigraphy in well logs, core, and outcrops: concepts for high-resolution correlation of time and facies. Methods in Exploration Series, vol. 7. Amer. Assoc. Petrol. Geol., Tulsa, OK, 55 pp.

Vidal, G., Ford, T.D., 1985. Microbiotas from the Late Proterozoic Chuar Group (northern Arizona) and Uinta Mountain Group (Utah) and their chronostratigraphic implications. Precambrian Res. 28, 349–389.

Visscher, P.T., Prins, R.A., van Gemerden, H., 1992. Rates of sulfate reduction and thiosulfate consumption in a marine microbial mat. FEMS Microbiol. Ecol. 86, 283–294.

Wachendörfer, V., Krumbein, W.E., Schellnhuber, H.J., 1994. Bacteriogenic porosity of marine sediments – a case of biomorphogenesis of sedimentary rocks. In: Krumbein, W.E., Paterson, D.M., Stal, L.J. (Eds.), Biostabilization of Sediments. Bibliotheks- und Informationsystem der Carl von Ossietzky Universität Oldenberg, (BIS)-Verlag, Oldenburg, pp. 203–220.

Walcott, C.D., 1914. Cambrian geology and palaeontology III, No. 2 – Precambrian, Algonkian algal flora. Smithsonian Misc. Collection 64, 77–156.

Wallace, C., 1998. Paleotransport directions and basin configuration, middle part of the Missoula Group (Belt Supergroup, Middle Proterozoic) western Montana. In: Berg, R.B. (Ed.), Belt Symposium III, Montana Bureau of Mines Geol. Spec. Publ. 112, pp. 88–103.

Walter, M.R. (Ed.), 1976. Stromatolites. Developments in Sedimentology, vol. 20. Elsevier, Amsterdam, 790 pp.

Walter, M.R., Bauld, J., Des Marais, D.J., Schopf, J.W., 1992. A general comparison of microbial mats and microbial stromatolites: bridging the gap between the modern and the fossil. In: Schopf, J.W., Klein C. (Eds.), The Proterozoic Biosphere: An Interdisciplinary Study. Cambridge University Press, New York, pp. 335–338.

Ward, D.M., Ferris, M.J., Nold, S.C., Bateson, M.M., 1998. A natural view of microbial biodiversity within hot spring Cyanobacterial mat communities. Microbiol. Mol. Biol. Rev. 62, 1353–1370.

Watanabe, Y., Martini, J.E.J., Ohmoto, H., 2000. Geochemical evidence for terrestrial ecosystems 2.6 billion years ago. Nature 408, 574–578.

Watson, I., Burnett, A.D., 1995. Hydrogeology: An Environmental Approach. CRC Press, Boca Raton, London, Tokyo, 702 pp.

Watterson, J.R., 1992. Preliminary evidence for the involvement of budding bacteria in the origin of Alaskan placer gold. Geology 20, 315–318.

White, B.G., Mauk, J., Winston, D., 1984. Stratigraphy of the Revett Formation. In: Hobbs, S.W. (Ed.), The Belt: Abstracts with Summaries, Belt Symposium II, 1983. Montana Bureau of Mines Geol. Spec. Publ. 90, pp. 16–17.

Wilgus, C.K., Hastings, B.S., Kendall, C.G.St.C., Posamentier, H.W., Ross, C.A., Van Wagoner, J.C. (Eds.), 1988. Sea Level Changes – An Integrated Approach. Soc. Econ. Paleontol. Mineral. Spec. Publ. 42, Tulsa, OK, 407 pp.

Williams, G.E., 2004. Earth's Precambrian rotation and the evolving lunar orbit: implications of tidal rhythmite data for palaeogeophysics. In: Eriksson, P.G., Altermann, W., Nelson, D.R., Mueller, W.U., Catuneanu, O. (Eds.), The Precambrian Earth: Tempos and Events. Developments in Precambrian Geology, vol. 12. Elsevier, Amsterdam, pp. 473–482.

Williams, L.A., Reimers, C., 1983. Role of bacterial mats in oxygen-deficient marine basins and coastal upwelling regimes: preliminary report. Geology 11, 267–269.

Williams, N., 1978a. Studies of the base metal sulfide deposits at McArthur River, Northern Territory, Australia: I. The Cooley and Ridge Deposits. Econ. Geol. 73, 1005–1035.

Williams, N., 1978b. Studies of the base metal sulfide deposits at McArthur River, Northern Territory, Australia: II. The sulfide-S and organic-C relationships of the concordant deposits and their significance. Econ. Geol. 73, 1036–1056.

Winston, D., 1986. Middle Proterozoic tectonics of the Belt basin, western Montana and northern Idaho. In: Roberts, S.M. (Ed.), Belt Supergroup: A Guide to Proterozoic Rocks of Western Montana and Adjacent Areas. Montana Bureau of Mines Geol. Spec. Publ. 94, pp. 245–257.

Witkowski, A., 1990. Fossilization processes of the microbial mat developing in clastic sediments of the Puck Bay (southern Baltic Sea, Poland). Acta Geol. Polon. 40, 1–27.

Wunderlich, F., 1970. Genesis and environment of the "Nellenköpfchenschichten" (Lower Emsian, Rheinian Devon) at locus typicus in comparison with modern coastal environment of the German Bay. J. Sediment. Petrol. 40, 102–130.

Wuttke, M., Radtke, G., 1993. Agglutinierende Mikrobenmatten im Profundal des mitteleozaenen Eckelfelder Maar – Sees bei Manderscheid/Eifel (Bundesrepublik Deutschland). Mainzer Naturwiss. Arch. 31, 115–126.

Xiao, S., Knoll, A.H., 1999. Fossil preservation in the Neoproterozoic Doushantuo phosphorite Lagerstatte, South China. Lethaia 32, 219–240.

Yallop, M.L., De Winder, B., Paterson, D.M., Stal, L.J., 1994. Comparative study on primary production and biogenic stabilization of cohesive and non-cohesive marine sediments inhabited by microphytobenthos. Estuar. Coast. Shelf Sci. 39, 565–582.

Yeo, G., Percival, J.B., Jefferson, C.W., Bernier, S., Hunt, P., 2002. Clay oncoids and crypto-microbial laminates from the late Paleoproterozoic Manitou Falls Formation, Athabasca Basin, Saskatchewan. Summary of Investigations 2002, vol. 2. Saskatchewan Geological Survey, Sask. Industry Resources, Misc. Rep. 2002-4.2, CD-ROM, Paper D-9, pp. 1–9.

Zavarzin, G.A., 2003. Diversity of cyano-bacterial mats. In: Krumbein, W.E., Paterson, D.M., Zavarzin, G.A. (Eds.), Fossil and Recent Biofilms. Kluwer Academic Publishers, Dordrecht, pp. 141–150.

Subject Index

accommodation 276, 277
adhesion ripples 144
adhesion warts 91, 101, 205, 207
aeolian settings 273
aggradation 276, 283
algal balls 54, 55, 103
algal biscuits 271, 287
alpha-petees 38, 145
anaerobic photosynthesis 234
anastomosing carbonaceous laminae 46, 193
animal carcasses 125
ankerite 73
anoxic 127
anoxic minerals 72, 73
Antarctica 267
Anti-Atlas 207
Apex Chert microbiota 268
Aphanocapsa 27
Archaean 153, 154, 281
Astropolithon 6, 31, 33, 43, 67, 69, 106, 107, 109, 110

ball-and-pillow structures 121, 243
banded iron formations (BIF) 233, 234, 244
Barberton Greenstone Belt 153, 276
base level 276, 277, 279
beach 273, 286
bed-smoothing 44
beds of carbonaceous shale 127
Beggiatoa 13, 269, 285
Belt Basin 125, 158, 271
Belt Supergroup 33, 73, 74, 117, 119, 121, 123, 125, 127, 129, 131, 133, 158, 159, 168, 171, 175
beta-petees 38, 145
Bijaigarh Shale 189, 193, 197
biodyctions 29
biofilm-catena 156
biofilms 40, 53, 56, 57, 59, 62, 63, 68, 72, 153, 195, 245, 267, 271
biogenic iron oxidation 233, 234
biolaminate horizons 198
biolaminites 6, 10, 40, 50, 111, 115, 141, 201, 203, 207, 214, 216–219
biomarkers 44
biomat 62
biominerals 7
biostabilisation 25, 31
bioturbation 269, 273
biovarvites 9, 11
biscuits 6, 13
Bledius 261, 262
blister 145
blister- or dome-shaped sand protrusions 202
blotting paper effect 46, 121
blue-green algae 285
Borden Formation 234
broached ripples 71
bulges 16, 42, 147, 202
buoyed mat fragments 125
burst bubbles 48

cabbage-head structure 35, 36
calcified filaments 72
calcite- and/or dolomite-rich laminae 73, 127
calcium carbonate 73
calcium carbonate precipitates 6
Cambrian 271, 286
carbon-rich mat laminae 286
carbonaceous flake 125
carbonaceous fragments 171, 175, 192, 193, 195
carbonaceous laminae dusted with tiny pyrite grains 46
carbonaceous lumps and streaks 171, 175, 225
carbonaceous shale layers 121
carbonaceous wisps 179
carbonaceous-streak-shales 175
carbonate cement 75
carbonate laminae 125, 127
carbonate precipitation 32, 33
catastrophes 271
cauliflower-like nodules 25
cements of reducing minerals 73
chemosynthetic microbial mats 268, 272
Chorhat Sandstone 181, 183
Chromatium 36, 234
Chuar Group 208
clay drapes 117
clusters of coarser grains 46, 125, 127
coastal 273
coastal marine facies 271
coastal sabkhas 258
coastal swamp 273
coated grain fabric 42
coated grains 271
coccoid bacterial clumps 193
coccoidal cyanobacteria 138, 258
cohesion 268
cohesive behaviour of microbial mats 125
cohesive sheets 121
complex structures 47, 111, 113, 115, 147
compression double bulges 7
concave eroded ripple crests 70, 71
concave-upwards saucers 169
concentric micro-faults 105
condensed fibrillar meshwork 258
consortia of bacteria 267
continental shelf 267
continental slope 267
contraction cracks 7
convoluted internal lamination 43
convoluted structures 17
correlative conformities 277
cracked ripple crests 69, 70, 97
crinkly, silty, anastomosing and discontinuous laminae 208, 211
curled crack margins 42, 50, 76, 81, 95, 147, 149, 218
curled margin structures 50
curved sand chips 43
cushion-like features 16
cushion-like or cauliflower-like patterns 14
cyanobacteria 5, 44, 258, 285
cyanobacterial filaments 256

Dakota Sandstone 33, 169, 222, 223
deep oceans 267
deep sea 272
deep sea/lake 273
delta plain 273
depositional (palaeo)environments 267, 273

desert 267, 270
desiccation cracks/polygons 200, 203, 207
destruction-related features 89
diagenetic features related to mat metabolism and decay 72
diagenetic mat features 53, 111
diagenetic pyrite 234
distal deep basin 270
dolomitic laminae 131
domal buildups 44, 73, 119, 125, 167–169, 268, 270
domal features/domes 42, 111, 119, 123, 149, 163, 165, 168, 169, 202
domal sand buildups 63–65, 67, 69
domal stromatolites 167
dried mat fragments 233, 248, 249, 251, 252
dried out mat 257

Earth's atmosphere 234
Ediacaran 214, 221, 287
Ediacaran Nudaus Formation 214
Ediacaran organisms 286
elephant skin (cf. old elephant skin, OES) 42, 101, 104, 135, 137, 138, 141, 144, 151, 200, 217, 234
elephant-skin texture 214, 217
Entophysalis 145, 150, 258
environmental associations 7
environmental settings 8
epeiric marine coastal settings 271
epeiric sea 189, 286
epibenthic microbial mats 141
epicontinental basin 168
eroded mat remnants 156, 234
erosion marks 203
erosional edges 6, 30
erosional remnants and pockets 157
escape structure 48
evaporative pumping 202, 259
evaporite pseudomorphs 207
exfoliating sand laminae 61, 62, 64
experimental work 233
extracellular polymeric substances (EPS) 5, 9, 12, 14, 38, 117, 119, 125, 127, 153, 179, 237, 248, 251, 254, 256, 258, 286

fairy rings 14
false cross-lamination 44, 119, 123, 191, 192
features derived from mat decay and post-burial effects 6
features derived from metabolic effects 6
features derived from physical mat destruction 6
fenestrae 33, 72
fenestral cavities 9
fenestral fabrics 6, 7, 33, 34
ferroan carbonates 73, 74, 127
ferroan dolomite 46, 73
filamentous 258
filled sand cracks 85, 97, 99, 206
first-cycle quartz arenites 271
flake 125
flame structures 121
flipped-over mat edges/fragments (cf. fold-overs and flip-overs) 6, 29, 43, 46, 76, 86, 87, 95, 101–103, 121, 125, 149, 188, 191, 236, 246, 257, 268
floating grains 42, 127, 131, 153
floating mat fragments 129
floating plant debris 125
floating quartz and mica 74
floating quartz grains 72, 127
floating terrigenous grains 42
flooding surfaces 278
flume experiments 233, 248, 249, 257
fluvial (settings) 267, 270, 273
forced regressions 277
fragments of microbial mat 164, 191

Gallionella 233, 234, 241
Gallionella stalks 237
gamma-petees 38, 145
gas bubbles 20, 48
gas domes 6, 9, 34–37, 43, 47, 48, 50, 106, 109, 148, 149, 156, 157, 276
gas or fluid escape structures 106, 108
ghost outline 44
ghosts of filaments 43
Gloeothece 27
graded silt/mud couplets 117
grain rafting 127
granular mats 271
grazing 273
grazing metazoans 195
Green River Formation 119, 121, 125, 127, 129, 158, 225–227, 229
groundwater 259–262
groundwater flow 258
growth bedding 6, 11
growth domes 147, 149
growth ridges 169
growth-related features and structures 6

heavy mineral 18
heterolithic facies association 198
high salinity 271
highstand systems tracts 282
horizontally oriented mineral grains 40
hot springs 267, 270
hydraulic conditions 258
hydraulic modelling 233, 261
hydraulic pressure 233, 258, 259, 261
hydrothermal vent 234

ice covered lake 270
impression of wrinkled (microbial) mass 187
impressions of mat fragments 185, 186
induced growth 48–50, 149
infillings of cracks 218
intertidal–supratidal 273
intertidal/lower supratidal zones 258
intra-cratonic rift embayment 208
inverted flutes 66, 68
involute structures 6
iron 25, 27, 233, 234
iron bacteria 233
iron bacteria stromatolite 243
iron bacterial mat 235
iron biominerals 233
iron carbonate cements 74
iron hydroxides 234
iron microbe 237
iron microbial community 237
iron microbial mat 239
iron oxidising bacteria 234, 244
iron precipitation 25, 233
iron reducing bacteria 234
iron stained laminae 164–166
iron stained mat layers 167
iron stains 75, 163, 164, 168
irregular impressions 46
Irridinites multiradiatus 139
isolated silt-sized grains 214

jelly rolls (cf. roll-ups) 6, 9, 13, 29, 31, 76, 87, 102, 103

Kajrahat Formation 189, 191–193
Kinneyia 6, 9, 24, 27, 43, 54, 58, 60, 62, 135, 137, 141, 143, 144, 151, 200, 201, 207, 216–218, 221
Kopela Shale 171, 175, 179

lacustrine 270
lakes 267, 269
lamalginites 225
lamina-conformable distribution of pyrite 42
lamina-specific grain selection 44
lamina-specific mineral enrichment 42
lamina-specific pyrite enrichment 286
laminated carbonaceous shale beds 117
larger biofilms 5
Late Archaean 269, 273
layered iron enrichment 6, 23
leaking cracks 261
Leptothrix 233, 234, 237, 239, 241
Leptothrix sheaths 237, 241
liquefaction 259, 261, 262
"live" mat 257
"live" mat fragments 233, 249, 251, 253
lizard-skin textures 48, 50
load balls and their casts 183
load casts 121
load resistance 121
loaded ripples 56, 57
low amplitude domes 121
Lyngbya (L.) 13, 14, 16, 150, 217, 254, 258, 261
Lyngbya aestuarii 138, 139

Manchuriophycus 43, 82, 89, 91–93, 97, 99, 101, 104, 206
Manchuriophycus/Rhysonetron 76
marginal marine environments 269
Mars 244
mat chips 6, 7, 9, 30, 31, 76, 97, 103–106, 149, 156, 157, 249
mat cracks 156
mat decay and diagenesis 127
mat decay features 53, 106, 109
mat decay mineralisation features 43, 73, 164
mat destruction 101
mat destruction features 53, 76, 89
mat destruction settings 89
mat expansion structure 149
mat fragments 46, 121, 125, 127, 171, 175, 181, 225, 229, 234, 235, 248, 249, 251, 254, 257, 286
mat growth features 53, 54, 101, 117
mat metabolism features 53, 125
mat slump structures 141
mat stabilised mud layers 121
mat-confined bubbles 6
maximum flooding surfaces 278
maximum regressive surfaces 278
McNamara Formation 158, 169, 170
Mellum Island 153, 156, 169, 222, 223, 271, 273
Meso- to Neoarchaean 279
Mesoproterozoic 276
metazoan grazing 117, 273, 286
metazoans 271, 276, 282, 285, 286
meteor paper 31
methane seeps 267
mica flecks 208
micas 169
micritic laminae 72
micro-faults 105
microbial binding structures 6, 18
microbial coatings 286
microbial crusts 271
microbial filaments 127, 248, 286
microbial laminites 286
microbial mat chips 30, 96, 103, 203
microbial mat fragments 125, 171, 179, 248, 257
microbial mat laminae 119
microbial oxidation 233
microbial sand chips/clasts 7, 30, 43, 99, 103, 166, 270
microbial sand/silt clasts 203
microbial shrinkage cracks 76, 77, 89, 91, 206, 218, 221
microbial shrinkage/sand cracks 203, 218
microbial sole structures 181
microbial tufts 169
microbially induced growth ridges 168
microbially induced sedimentary structures (MISS) 6, 39, 153, 273
microbially-bound ripples 54
Microcoleus (M.) 11, 14, 17–19, 23, 25, 27, 217, 254, 258, 260, 261
Microcoleus chthonoplastes 138
microcolumnar buildups 169
microstromatolites 6, 14
mineral precipitation effects 42
Moodies Group 153–155, 276
Mt. Shields Formation 121, 123, 125, 131, 158, 166–169
mud chips 201
mud- and sand-chips 207
mudstone diagenesis 117
multi-directed ripple marks 40, 156, 157

Nama Group 214, 215
narrow ridges 40
Neoproterozoic 198, 282
Newland Formation 117, 119, 121, 123, 125, 127, 129, 133, 158, 160, 161, 163, 191
nivellement of ripples 6
nodules 6, 13
non-penetrative micro-faults 43, 76, 105
non-photosynthetic mat 285
non-radial gas or fluid escape structures 109
non-transparent 156
non-transparent wrinkles 153
normal regressions 277, 282, 283
Nudaus Formation 214

ocean floor 267
ocean floor basalts 267
oil shales 225–227, 229, 231
old elephant skin (OES; cf. elephant skin) 54, 58–62, 64, 156
oncoids 271
oolitic coatings 72
'opportunistic' mats 267, 268
oriented grains 154–156
oscillation cracks 156, 157
Oscillatoria 17, 217, 249, 251, 254–256
overfolded mat layers 46, 121
overgrown, upturned crack margins 42, 76, 83, 96, 111, 115, 203
overgrowth, fixation and nivellement of ripples 19
oxygenic photoautotrophs 234

palaeoenvironmental reconstructions 288
Palaeoproterozoic 282
Palaeo- to Neoproterozoic 189
palaeoseismic mat disruption features 247
palimpsest ripples 7, 40, 56, 57, 104, 276
parahistological behaviour 147
parasequences 278
patchy reworking of ripples 76, 104
patchy ripples 67–69, 104
peloidal and clotted micrite 72
petee ridges 42, 76, 77, 82, 85–87, 89, 97, 99, 101, 145, 150

petees 6, 35, 37, 38, 42–44, 54, 64, 76, 77, 82, 86, 89, 93, 96, 97, 99, 104, 105, 140, 147, 148, 150, 233, 260, 261, 276
Phanerozoic 223, 271, 273, 276, 279, 281–283, 287
Phormidium sp. 10
phosphatic spheres/spheroids 193, 197
photic zone 258, 268
photosynthesis-buoyed fragments 127
photosynthetic bubbles 49
photosynthetic cyanobacteria 272, 285
photosynthetic mats 272
photosynthetic (PS) domes 47–49, 145, 149, 150
photosynthetic sulphur bacteria 44
physically-formed sedimentary structures 272
pinnacles 6, 7, 14, 16, 20, 42, 150, 200, 217
Pleurocapsa 13
Pleurocapsalean 14
pockets 156, 223
polygonal bulges 6, 17
polygonal oscillation cracks 156
polygonal shrinkage cracks 260
Pongola Supergroup 153, 154, 157
Precambrian 195, 198, 208, 269, 273, 281–283, 285–288
Precambrian–Phanerozoic 281
precipitation of 'anoxic' minerals 46
progradation 276
Proterozoic 127, 171, 193, 276, 279, 281, 282, 286
Proterozoic shale 119
Proterozoic–Archaean boundary 286
Proterozoic–Phanerozoic transition 271, 287
pseudo-cross-bedding/lamination 208, 211
pustular or wavy surfaces 169, 208, 209, 211, 213
pustular-crinkled bedding plane 170
pustules 42, 169
pyrite 46, 73, 127, 129
pyritic laminae 129
pyritic striped shales 133, 160, 163

quiet deep-water environments 273

radial gas or fluid escape structures 106, 107
rafts/raft deposition 46, 125
Rampur Shale 125, 127, 189, 192, 193, 195, 197
randomly oriented mica flakes 44, 119, 123, 127, 131, 167, 168
recrystallisation and enlargement of carbonate minerals 46
redox-discontinuity-layer (RDL) 23
reducing cement minerals 75
reducing minerals 73
regression–transgression 273
resistance to erosion 268
reticulate patterns/ornamentation 6, 16, 20, 42
retrogradation 276
Revett Formation 73, 74, 158, 163–165, 169
Rhysonetron (cf. Manchuriophycus) 82, 89, 91, 101, 206
ridges 200, 217
rigid curved sand chips 270
ripped-up mat fragments 236, 246, 268
ripple patches 6, 31, 43, 76, 89, 102, 104, 156, 166, 168–170, 222–224, 268
ripples with cracked crests 54, 70, 76, 80, 97
rivers 269
Rohtas Limestone 189
roll-up structures/roll-ups (cf. jelly rolls) 7, 9, 43, 46, 54, 76, 87, 94, 101–103, 121, 149, 153–156, 191, 208, 209, 211, 213, 234, 236, 246, 257, 268, 276
rolled-up mat fragments 43, 76, 86, 87, 94, 95, 102, 103, 106, 286
round-crested microbial wrinkle marks 43
Runzelmarken 7, 54, 58, 60, 62, 135
ruptured gas domes 43

sabkhas 233, 261, 262, 273
saline spring 270
sand balls 54, 55, 103
sand bulges 183
sand chips/clasts 40, 53, 57, 76, 103, 104, 137, 144, 149, 167, 201, 204
sand crack patterns 42
sand cracks 76–80, 86, 87, 91, 97, 99, 101, 104, 105, 144, 205, 246, 276
sand ooids 54, 55, 103
sand ridges 205
sand shadow structures 54, 66, 68
sand stromatolites 42, 54, 63–65, 67–70, 106, 110
sand volcanoes 6, 106
sandy crack-fills 205
sandy tidal flats 156
Schizothrix 14
scyphomedusae 55
sea level movements 271
sediment volcanoes 33
sedimentary augen structure 32, 33
seepage pressure 260, 262
seismic deformation 233
seismic events 245, 246
sequence stratigraphy 267, 273, 276
sequences 277
setulfs 183
shale particles 193
shallow marine settings 270
shallow sea/lake 273
Sharks Bay 117
shelf environment 156, 273, 286
shelf sequences 287
shoreface 273
shrinkage cracks 6, 7, 27, 111, 207, 214, 221, 260, 262
siderite 46, 73, 127
siliciclastic biolaminites 111
siliciclastic tidal flats 153
sinuous ridges 217
Sirbu Shale 181, 185, 186
small domes 121
small-scale load structures 143
soil formation 269
Somanpalli Group 127, 171–173
spheroidal pliable sand clasts 54–56
spindle-shaped cracks 42
spindle-shaped ridges 183
spindle-shaped sand-filled cracks 205
Spirulina 19, 20
sponge pore sand 7
storm-laid sandstone beds 181
stratiform chemical boundaries 165
stratiform iron stains 166, 169
stratiform layers of decay-related minerals 74
striped carbonaceous shales 177, 178
striped shales 44, 117, 119, 123, 127, 129, 158, 160, 161, 163, 171, 177, 197, 211, 229
stromatolites 39, 117
strongly pyritic laminae 46
subtidal shelf settings 271
sulphate-reducing bacteria 285
sulphide-oxidising bacteria 44, 285
sulphur bacteria 285
supratidal zones 233, 258, 261
synaeresis cracks 7
Synechococcus 19, 258, 261, 262
syngenetic carbonate precipitation 127
systems tracts 277, 279

Tarur Nala Formation 160, 171, 175, 177, 178
tepee-like shrinkage cracks 218
tepees 38, 150
terrigenous grains floating in a carbonate matrix 44
tidal flat hydraulics 259
tidal flats 258, 273
tidally influenced sedimentary environments 267
Tizi n-Taghatine Group 198, 199
torn/frayed edges of mats/mat fragments 46, 127
trace fossils 220
transgressive ravinement surfaces 278, 282
transgressive systems tracts 278, 281–283
transparent wrinkles 141, 156
transported mat fragments 44
tufts 6, 7, 14, 16, 42, 150, 156, 200, 217

undulating continuous organic laminae 121
upturned/overturned crack margins 42, 111, 113, 115, 150, 207, 214, 218, 234

vent systems 233
vertical chemical gradients 268
very early diagenetic dolomite 42
Vindhyan basin 271
Vindhyan Supergroup 125, 127, 129, 181, 189, 190

Waterberg Group 276
wave-dominated open shelves 181
wavy anastomosing laminae 127, 133
wavy anastomosing texture 127
wavy laminated carbonaceous oil shale 229
wavy laminated carbonaceous–pyritic layers 171
wavy lenticular laminae 197
wavy-crinkly anastomose laminae 208
wavy-crinkly anastomosing carbonaceous laminae 117, 119, 125, 129, 175, 178, 191, 193, 195, 197, 213, 229
wavy-crinkly anastomosing pyritic laminae/beds 133, 163, 197
wavy-crinkly internal laminae 111, 121, 159, 161, 171, 214, 286
wavy-crinkly laminae 44, 168, 169, 192
wavy-undulose laminae 169
Winogradsky columns 271, 272
Witwatersrand Supergroup 153, 154, 157
wrinkle marks 7, 54, 58, 60, 62, 89, 99, 135–138, 145
wrinkle structures 42, 54, 57–59, 62, 76, 97, 101, 103, 104, 135–138, 140, 141, 144, 151, 153–156, 201, 214, 276, 281, 287
wrinkled bed surface 170
wrinkles 154, 156, 169, 170, 185, 187, 188, 234, 236

This page intentionally left blank